Dysfunctional nucleocytoplasmic transport dynamics in amyotrophic lateral sclerosis and frontotemporal dementia caused by mutation in C9ORF72

Salcher-Konrad, Marie

Awarding institution:
King's College London

Dysfunctional nucleocytoplasmic transport dynamics in amyotrophic lateral sclerosis and frontotemporal dementia caused by mutation in *C9ORF72*

Marie-Thérèse Salcher-Konrad

A thesis submitted in partial fulfilment of the requirements for the degree of Doctor of Philosophy from King's College London

Department of Basic and Clinical Neuroscience
Institute of Psychiatry, Psychology and Neuroscience
King's College London

2023

Declaration

I, Marie-Thérèse Salcher-Konrad, confirm that the work presented in this thesis is my own with the following exception: Erin Hedges performed immunofluorescence staining of fixed iPSC-derived neurons and imaged these on the Opera Phenix High Content screening system. Subsequent image analyses were again conducted by me.

Acknowledgements

First and foremost, I would like to thank my supervisor, Sarah Mizielinska, for giving me the opportunity to work on this project. Thank you for your endless support, patience, responsiveness and kindness. I could not have asked for a better supervisor, thanks to you this PhD was mostly an enjoyable process.

Thank you to Agnes Nishimura from the Shaw lab for providing the iPSC lines and for teaching me iPSC work, thank you for all your support! I would also like to thank the entire Mizielinska lab for all their help and for just being great colleagues. I am especially grateful to Niamh O'Brien for providing further support during the iPSC differentiation process and for always looking at my cells. A big thank you also to Erin Hedges who helped with immunostaining and imaging of iPSC-derived neurons. I am also grateful to all my colleagues from the Ruepp, Hanger, Noble and Jimenez Sanchez labs for providing such a great working (and break) atmosphere.

I also would like to thank my friends outside of the lab. Anna-Maria, Erica, Olivier and Clarissa, you were my family in London and made my time in London unforgettable. Dawn, thank you for all the dinners and your emotional support, cannot wait to try new restaurants with you! Also thank you to Dan, Apphia and Clover for providing stress relief, especially in the final lab stages of the project.

Thank you to my friends in Vienna, thank you Clara, Clara and Anna for being my greatest cheerleaders and increasing my resilience especially during the writing phase.

The greatest of thanks to my husband, Max, I literally could not have done this without you! Thank you that I can always rely on you and for always having my back.

Finally, I would like to thank my parents for all their love and support and for always believing in me.

Abstract

A mutation in the *C9ORF72* gene is the most common genetic cause of the devastating disorders amyotrophic lateral sclerosis (ALS) and frontotemporal dementia (FTD). Currently, no effective treatments for these disorders exist. The *C9ORF72* mutation results in the production of neurotoxic dipeptide repeat proteins (DPRs). Modifier and interactome studies suggest that DPRs affect nucleocytoplasmic transport. Altered nucleocytoplasmic transport may contribute to disease pathology as this vital mechanism is the main route of information exchange between the cytoplasmic and nuclear compartments. Smaller molecules can passively diffuse through the nuclear pore, the protein complex through which transport occurs. Conversely, larger molecules need to be actively transported by receptors. We aimed to specifically study passive nucleocytoplasmic transport in the context of *C9ORF72* ALS/FTD as this yields information about nuclear pore integrity and function. In addition, passive diffusion is thought to be the main route of nuclear export of key ALS/FTD proteins TDP43 and FUS. An assay was optimised to specifically investigate passive nucleocytoplasmic transport monitoring inert fluorescent cargo of different sizes using live confocal microscopy. The influence of *C9ORF72* DPRs on passive nuclear import of reporter cargo and on passive export of TDP43 and other nuclear proteins was studied using this assay in HeLa cells. Arginine containing DPRs were shown to enhance passive nuclear translocation of reporter cargo and passive nuclear export of TDP43 and other nuclear proteins. To study potential mechanisms of action of arginine containing DPRs the localisation of various transport receptors upon DPR treatment was studied using immunofluorescence. Levels of import receptors, nucleoporins and Ran regulating factors were reduced within the nucleus and the nuclear pore in the presence of arginine containing DPRs. This might contribute to the enhancement of passive nucleocytoplasmic transport. Findings of increased passive nucleocytoplasmic transport could be recapitulated in *C9ORF72* ALS iPSC-derived neurons highlighting the disease relevance of this result. A trend of nucleocytoplasmic transport factor mislocalisation was also observed in *C9ORF72* ALS iPSC-derived neurons. In this PhD project a potential pathology mechanism of *C9ORF72* arginine containing DPRs was characterised which might contribute to cytoplasmic TDP43 mislocalisation, a pathological hallmark of ALS/FTD.

COVID-19 impact statement

The COVID-19 pandemic and resulting closure of the university campus and laboratories in March 2020 led to disruptions of this project. After the end of the first national lockdown the campus slowly re-opened in July 2020. However, building and laboratory capacity was severely reduced to a maximum of 20%, which resulted in months of working limited hours in the laboratory (e.g., 12 hours per week). This led to considerable delays in the project. As social distancing rules within the university campus did not allow for close working, I could not be taught new techniques. A planned study for this project involving super-resolution microscopy in cooperation with a postdoc of our group therefore had to be abandoned. Furthermore, iPSC studies had to be delayed by about 8 months which meant that only a limited number of differentiations could be carried out and cells could only be aged for a limited amount of time.

Table of Contents

1 Introduction

1.1 Characteristics of frontotemporal dementia and amyotrophic lateral sclerosis

Frontotemporal dementia (FTD) and amyotrophic lateral sclerosis (ALS) are both devastating neurodegenerative diseases for which no effective treatment exists to date. FTD describes a group of disorders characterised by degeneration of the frontal and/or temporal lobes of the brain (Warren et al., 2013). It is the second most common neurodegenerative dementia after Alzheimer's disease in persons under 65 years (Hogan et al., 2016) and has a prevalence of about 11 cases per 100,000 individuals (Coyle-Gilchrist et al., 2016) which is likely an underestimate predominantly due to misdiagnosis (Sivasathiaseelan et al., 2019). In ALS, both upper motor neurons, projecting from cortex to brainstem and spinal cord, and lower motor neurons, projecting from brainstem or spinal cord to muscle, degenerate (Hardiman et al., 2017). ALS has a prevalence of about 5 cases per 100,000 persons in Europe and the United States (Chiò et al., 2013; Mehta et al., 2018). Strikingly, some ALS cases additionally develop FTD (Elamin et al., 2013; Montuschi et al., 2015; Phukan et al., 2012) and a number of FTD patients also present with ALS (Burrell et al., 2011; Ringholz et al., 2005).

1.1.1 Clinical features

Frontotemporal dementia typically develops in the 6th decade of life but can develop anywhere between the 3rd to 9th decade (Hodges et al., 2003; Johnson et al., 2005; Ratnavalli et al., 2002). It can be divided into three variant syndromes depending on the main manifesting characteristic (Warren et al., 2013; Woollacott and Rohrer, 2016). **Behavioural FTD** is the most common of these variants (Sivasathiaseelan et al., 2019). Diagnostic criteria include the following changes in behaviour and personality (Rascovsky et al., 2011). For instance, patients might have lower social inhibitions and might show a lack in motivation and proactiveness. Another characteristic is reduced emotional reactivity including a loss of empathy. Compulsive behaviour such as hoarding, counting or tidying is also observed. Patients might change their eating habits and food preferences showing a tendency to gluttony or developing a sweet tooth. In addition, executive ability can be decreased while episodic memory and visuospatial skills usually remain unaffected.

Semantic variant primary progressive aphasia, the second FTD variant, affects the semantic memory which comprises understanding and recollection of words, objects and general concepts (Sivasathiaseelan et al., 2019). Patients typically have limited vocabulary, more and more forgetting the correct term for items. In the beginning of the disease course, they might still be able to relate the missing word to a group such as animals but eventually they will just refer to it as “thing”. The structure and fluency of speech are, at least initially, not affected. Face blindness and other visual or sensory recognition impairments are further characteristics of semantic variant primary progressive aphasia. Somatic symptoms including tinnitus or enhanced sensitivity towards sound or other sensations might also present in patients (Fletcher et al., 2015a, 2015b; Mahoney et al., 2011; Marshall et al., 2017). The third group of FTD syndromes, **non-fluent-agrammatic variant primary progressive aphasia**, is characterised by problems with speech production and/or sentence construction (Sivasathiaseelan et al., 2019). Speech errors include mispronunciation of words, wrong syllable usage, confusion between binary selections such as “yes/no” (Warren et al., 2016) or grammatic mistakes. Over time, patients will also make grammatic and orthography errors in their writing (Rohrer et al., 2010). General intellectual abilities are often not affected in patients. These three forms will extensively overlap in the course of the disease and patients might also develop atypical forms of parkinsonism (Sivasathiaseelan et al., 2019).

Amyotrophic lateral sclerosis is characterised by very aggressive disease progression with a median survival rate of 3 years after development of symptoms. Death is usually caused by respiratory failure (Masrori and van Damme, 2020). For sporadic ALS, describing patients without family history of disease, mean age of onset is 58-63 years while it is 40-60 years for familial ALS (Logroscino et al., 2010). The main symptom is progressive muscle weakness and loss of muscle mass, fasciculations (muscle twitching), muscle cramps and stiff muscles also occur typically. In **spinal onset ALS**, which comprises about two-thirds of cases, muscle weakness begins in the limb muscles with distal muscles (muscles further away from the body centre) more commonly affected than proximal muscles. **Bulbar onset ALS** occurring in about one-third of cases starts in bulbar muscles. This is most commonly characterised by difficulties in pronouncing words (dysarthria) or by problems with swallowing (dysphagia) and voice hoarseness. Difficulties with mouth

closing and chewing can also occur. ALS symptoms will often quite rapidly spread to different muscle groups eventually being fatal (Masrori and van Damme, 2020). ALS and FTD lie on a spectrum sharing genetic, pathological (see sections 1.1.2 and 1.1.3) and clinical features. 11-13 % of ALS patients are formally diagnosed with FTD but up to 50 % present with some form of cognitive or behavioural impairment (Elamin et al., 2013; Montuschi et al., 2015; Phukan et al., 2012). ALS(-FTD) patients might present with executive dysfunction (Štukovnik et al., 2010), language deficits (Taylor et al., 2013), problems with social cognition and emotional processing (Bora, 2017) or behavioural changes (Meier et al., 2010). Strikingly, disease progression is more rapid in patients with ALS-FTD than in patients with pure ALS or ALS with other forms of cognitive impairment (Montuschi et al., 2015). About 15 % of FTD patients also present with ALS, sometimes years after FTD development, and another 30-40% have some motor impairment (Burrell et al., 2011). Interestingly, in a cohort of pathologically confirmed FTD-ALS cases only 59 % were clinically diagnosed of FTD-ALS (Josephs et al., 2006). In addition to co-occurring within a single patient, in affected families some members might develop ALS while others might develop FTD (Abramzon et al., 2020) highlighting shared genetic causes between the two disorders.

1.1.2 Genetics

About 20 % of ALS cases are familial (hereditary) (Hardiman et al., 2017) and 10-15 % of FTD cases show a clear autosomal dominant inheritance pattern (Goldman et al., 2005; Rohrer et al., 2009) with behavioural FTD being the most heritable FTD variant and semantic variant primary progressive aphasia the least heritable (Rohrer et al., 2009). As shown in Figure 1.1 the most common genetic causes of familial ALS are mutations in *C9ORF72*, accounting for about 40 % of familial ALS, *Superoxide dismutase 1* (*SOD1*), responsible for approximately 20 % of familial ALS, with *Fused in sarcoma* (*FUS*) and *TARDBP* (encoding Transactive response DNA binding protein 43 or TDP43) each causing about 1-5 % of familial ALS cases (van Es et al., 2017). Mutations in three genes are responsible for the majority of familial FTD cases. About 25 % of familial and 5 % of sporadic FTD are caused by a mutation in *C9ORF72* (Pottier et al., 2016), *Progranulin* (*PGRN*) mutations are responsible for 5-20 % of familial and for 1-5 % of sporadic FTD (Rademakers et al.,

2012) and mutations in *Microtubule binding protein tau* (*MAPT* encoding the Tau protein) account for 5-40 % of familial FTD cases (Pickering-Brown et al., 2008; Rademakers et al., 2012; Seelaar et al., 2008). The fact that mutations in the *C9ORF72* gene are causative for both ALS and FTD further highlights that the two disorders also lie on a continuum on the genetic level. The *C9ORF72* mutation will be further detailed in section 1.3.

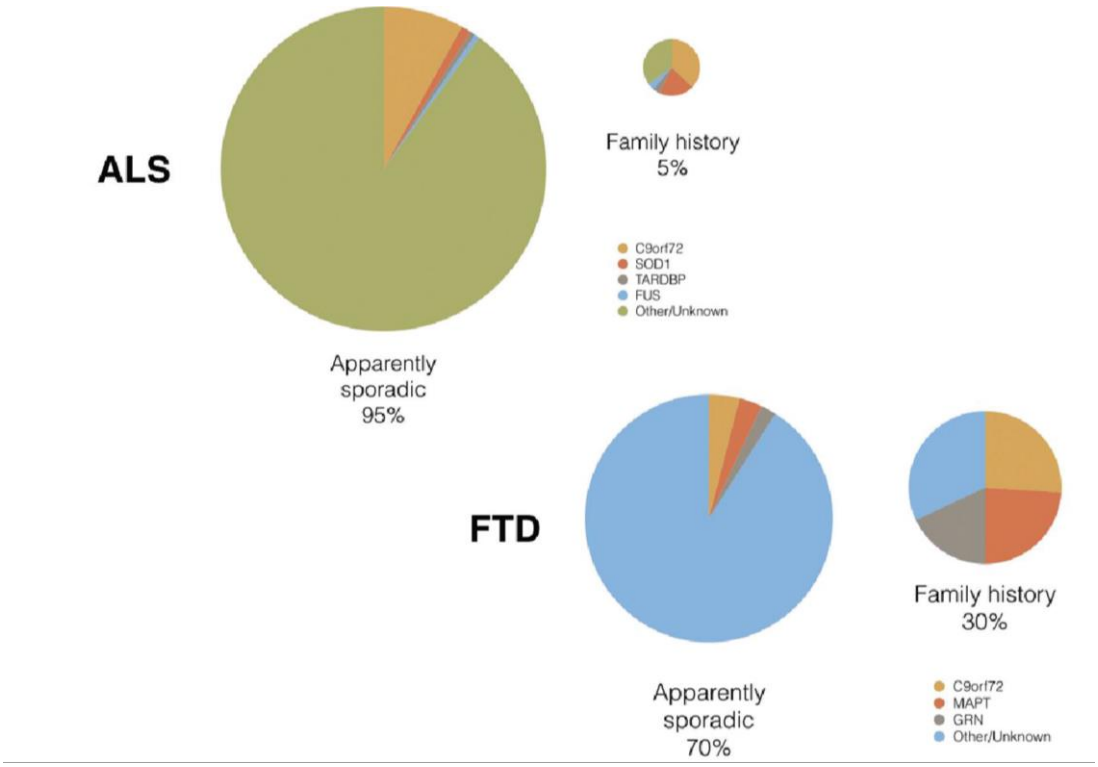

Figure 1.1: Major genetic causes of ALS and FTD (Turner et al., 2017)**.**

PGRN, *MAPT* and *SOD1* mutations

PGRN and *MAPT* mutations solely cause FTD while *SOD1* mutations are only responsible for the development of ALS. **PGRN** is a secreted growth factor. It is expressed by various cell types including neurons and has a neuroprotective function (Bateman and Bennett, 2009). Mutations in *PGRN* lead to haploinsufficiency (Baker et al., 2006; Cruts et al., 2006) meaning pathology is mediated by loss of function of the PGRN protein.

Tau (encoded by the gene *MAPT*) functions as a microtubule stabiliser thereby greatly contributing to the maintenance of neuronal integrity and axonal transport (Goedert, 2018; Hirokawa, 1994; Mackenzie and Neumann, 2016). There are over 50 *MAPT* mutations described which are linked to FTD (Katzeff et al., 2022). These

mutations reduce the binding affinity of tau to microtubules in turn leading to the formation of hyperphosphorylated tau aggregates (Olszewska et al., 2016).
SOD1 is a copper zinc superoxide dismutase and has a prominent antioxidant function in the cell (Hemerková and Vališ, 2021). However, no correlation between the enzymatic activity of SOD1 and ALS onset or disease progression in patients has been observed (Cleveland et al., 1995). Mouse models carrying ALS *SOD1* mutations show impaired mitochondrial function, SOD1 aggregation, motor neuron degeneration and paralysis which rather speaks for *SOD1* mutations causing disease via a gain of function effect than via a loss of function effect (Kim et al., 2020).

FUS and *TARDBP* mutations

Mutations in *FUS* or *TARDBP* mainly cause ALS but can also be responsible for FTD in rare cases (Huey et al., 2012; Tan et al., 2017; van Langenhove et al., 2010). **FUS** functions in DNA repair, has various roles in RNA metabolism and also plays a role in local translation at synapses (Kim et al., 2020). Many *FUS* mutations are located within its nuclear localisation signal resulting in cytoplasmic mislocalisation (Deng et al., 2014; Dormann et al., 2010; Ito et al., 2011; Lagier-Tourenne et al., 2010). *FUS* mutations could therefore lead to disease because of unusual localisation and aggregation of FUS protein in the cytoplasm or by the absence of FUS protein in the nucleus and thus resulting in DNA repair, transcription or splicing defects. Probably both a gain (in the cytoplasm) and loss of function of FUS (in the nucleus) are relevant in disease as there is reasonable evidence supporting both mechanisms (Abramzon et al., 2020). For example, mutant FUS directly impaired snRNP biogenesis in iPSC-derived motor neurons (Jutzi et al., 2020). On the other hand, mutant FUS interacted less with core paraspeckle proteins resulting in paraspeckle dysfunction in a neuroblastoma cell line (An et al., 2019).
TDP43 (encoded by *TARDBP*) has a range of functions in RNA metabolism ranging from splicing to stabilisation (Abramzon et al., 2020). It is predominantly nuclear but shuttles between the nucleus and cytoplasm (Ayala et al., 2008). Most ALS *TARDBP* mutations lie in its C-terminal disordered glycine rich region which is responsible for the recruitment of TDP43 into stress granules and aggregates (Budini et al., 2012; Freibaum et al., 2010; Prasad et al., 2019). These mutations change the characteristics of TDP43 protein including increased tendency towards aggregation,

cytoplasmic mislocalisation, enhanced protein stability, resistance to proteases or altered interactions with binding partners (Prasad et al., 2019). The most physiological knock-in mutant TDP43 mouse models exhibit motor neurodegeneration and enhanced splicing (Fratta et al., 2018) or cognitive dysfunction and disrupted TDP43 autoregulation (White et al., 2018). Similar to FUS, *TARDBP* mutations might lead to disease via a loss of function mechanism because TDP43 is absent from the nucleus and does not exert its crucial functions in the nucleus or via a gain of function mechanism by the formation of toxic cytoplasmic aggregates. However, the actual toxicity of TDP43 aggregates is still under scrutiny (Abramzon et al., 2020).

Rare mutations

A large number of mutations causing ALS, FTD and/or ALS/FTD more rarely than the ones described above have been identified (Kirola et al., 2022). Cellular pathways implicated by mutations causing ALS/FTD and/or both ALS and FTD include autophagy affected by mutations in *Sequestosome 1* (*SQSTM1*), *Vasolin-containing protein* (*VCP*), *TANK binding kinase 1* (*TBK1*) or *Ubiquilin 2* (*UBQLN2*), mitochondrial function impaired by mutations in *VCP* or *Coiled-Coil-Helix-Coiled-Coil-Helix Domain Containing 10* (*CHCHD10*), inflammation mediated by mutations in *TBK1*, the proteasome affected by mutations in *UBQLN2* (Abramzon et al., 2020), RNA processing impaired by mutations in *Matrin 3* (*MATR3*) (Malik and Barmada, 2021) or endosomal trafficking disrupted by mutations in *Charged Multivesicular Body Protein 2B* (*CHMP2B*) (Waegaert et al., 2020). Mutations in *TBK1*, *CHCHD10* and *MATR3* can also cause pure ALS in addition to ALS/FTD (Abramzon et al., 2020; Malik and Barmada, 2021). Examples of rare mutations resulting in ALS but not FTD affect autophagy by mutations in *Optineurin* (*OPTN*) or *Sigma 1 receptor* (*SIGMA1R*), ER function by mutations in *VAMP associated protein B and C* (*VAPB*), RNA metabolism by mutations in *Ataxin 2* (*ATXN2*), the cytoskeleton by mutations in *Profilin 1* (*PFN1*) or the proteasome by mutations in *SIGMA1R* (Hardiman et al., 2017). Overall, the multitude of genes affected and of cellular pathways implicated suggest that a vast range of pathology mechanisms are at play in ALS/FTD.

1.1.3 Neuropathology

Histopathologically, both ALS and FTD are characterised by protein inclusions in affected regions. Broadly, pathological features of ALS include atrophy of motor cortex and skeletal muscles, sclerosis of corticospinal and corticobulbar nerve tracts, degeneration of over 50 % of spinal motor neurons and signs of neuroinflammation in the spinal cord (Hardiman et al., 2017). Degeneration of frontal and temporal lobes is a relatively consistent feature in FTD and the term frontotemporal lobar degeneration (FTLD) is therefore commonly used in a neuropathological context. In the majority of cases, FTLD can be classified according to the major type of protein found in inclusions. About 40 % of patients present with FTLD-tau, 5-10 % with FTLD-FET (including FUS, EWS and TAF15) and about 50 % exhibit FTLD-TDP (Mackenzie and Neumann, 2016). Strikingly, 97 % of ALS cases show cytoplasmic inclusions of TDP43 (Ling et al., 2013). Furthermore, SOD1 and FUS inclusions are detected in ALS patients with *SOD1* and *FUS* mutations, respectively (Saberi et al., 2015).

ALS-SOD1

SOD1 ALS patients exhibit a greater extent of lower motor neuron degeneration than upper motor neuron degeneration. Indeed, in patients carrying *SOD1* mutations aggregates containing misfolded SOD1 are detected in spinal cord motor neurons (lower motor neurons) but are not found in Betz cells (upper motor neurons) in the motor cortex. TDP43 or FUS aggregates are not observed in these patients but ubiquitin, phosphorylated neurofilaments and chaperone proteins can be found within SOD1 inclusions (Saberi et al., 2015). Interestingly, some sporadic ALS patients also exhibit misfolded SOD1 aggregates (Forsberg et al., 2011, 2010). Mutant SOD1 has also been shown to impair mitochondrial function and axonal transport and to cause oxidative stress and ER stress (Hayashi et al., 2016).

FTLD-tau

FTLD-tau can be further classified into subtypes based on neuropathology features and the main tau isoform present in inclusions. For instance, the tau isoform containing 3 repeat domains is predominantly found in inclusions of Pick’s disease and mainly 4 repeat tau is detected in aggregates of progressive supranuclear palsy.

Hyperphosphorylated tau inclusions are found in neurons or glia cells, the latter being more or less common depending on the FTLD-tau subtype (Mackenzie and Neumann, 2016). Inclusions might be nuclear or cytoplasmic and might present as spherical or globular aggregates or as neurofibrillary tangles. Importantly, the presence of hyperphosphorylated tau aggregates is not limited to patients harbouring *MAPT* mutations but this pathology is present in cortical and subcortical grey and white matter of all patients with FTLD-tau (Mackenzie and Neumann, 2016). Tau aggregation seems to be a direct consequence of its hyperphosphorylation which impairs its binding to microtubules (Panza et al., 2020).

FTLD-FET and ALS-FUS

The FET protein family is comprised of FUS, Ewing's sarcoma (EWS), and TATA-binding protein-associated factor 15 (TAF15). These proteins are found in cytoplasmic inclusions of most FTLD cases which do not contain tau or TDP43 aggregates. Depending on the FTLD subtype different brain regions are affected in FTLD-FET but often include the frontal and temporal neocortex, the cerebral cortex, the hippocampus and the striatum. FET inclusions also contain transportin 1, which imports FET proteins into the nucleus (Mackenzie and Neumann, 2016). Often cells show a reduction or complete loss of nuclear staining for FET proteins, but nuclear levels might also be normal in some cells, especially of TAF15 (Neumann et al., 2011). ALS patients with *FUS* mutations show typical signs of degeneration for ALS including of upper and lower motor neurons, corticospinal tracts and motor nerves. These patients harbour cytoplasmic inclusions of FUS in neurons and in variable numbers of glia cells. Nuclear FUS is reduced in most but not all cells containing FUS inclusions (Mackenzie and Neumann, 2017). These inclusions might also contain proteins of the ubiquitin-proteasome system such as ubiquitin and p62 but not TDP43, the other members of the FET protein family or transportin 1 (Mackenzie and Neumann, 2017, 2016).

The mislocalisation of FUS to the cytoplasm occurs via different mechanisms in FTD and ALS. As mentioned in section 1.1.2 *FUS* mutations mainly occur with its nuclear localisation signal weakening the binding to transportin 1 and thus interfering with the nuclear import of FUS resulting in its cytoplasmic mislocalisation (Dormann et al., 2010; Neumann et al., 2011). In FTLD-FET FET proteins are hypomethylated at arginine residues adjacent to the nuclear localisation signal which results in stronger

binding of FET proteins to transportin 1 likely being the reason for transportin 1's presence in FET inclusions (Dormann et al., 2012; Suárez-Calvet et al., 2016). However, this increased interaction with transportin 1 might also be protective but ultimately does not prevent the cytoplasmic mislocalisation of FET proteins (Sternburg et al., 2022). Unmethylated FUS also shows a higher tendency to aggregate *in vitro* and increased recruitment into stress granules (Hofweber et al., 2018). In general, cytoplasmic mislocalisation of FUS and its consistent recruitment into stress granules over a longer period of time due to cellular stress occurring in disease might lead to its transition into a more solid form which eventually leads to its aggregation (Sternburg et al., 2022). The reduction of FUS in the nucleus disrupting RNA processing (Takanashi and Yamaguchi, 2014) and cytoplasmic FUS impairing translation or mitochondrial function (Birsa et al., 2021; Kamelgarn et al., 2018; López-Erauskin et al., 2018; Tsai et al., 2020) might eventually result in the observed neurodegeneration.

FTLD-TDP and ALS-TDP43

As mentioned above cytoplasmic TDP43 inclusions occur in almost all ALS cases and in about half of FTD cases showing that these two disorders also exhibit great neuropathological similarities. TDP43 inclusions are enriched for hyperphosphorylated, ubiquitinated and N-terminally truncated forms of TDP43 (Arai et al., 2006; Hasegawa et al., 2008; Neumann et al., 2009, 2006). Inclusions often also contain p62 but other disease-related proteins are absent (Mackenzie and Neumann, 2016). Importantly, different to FUS, most cells containing TDP43 inclusions exhibit a loss of nuclear TDP43 (Mackenzie and Neumann, 2016; Riku et al., 2021). FTLD-TDP can be grouped into four subtypes (A, B, C and D) according to morphological characteristics and cortical laminar distribution of inclusions (Mackenzie and Neumann, 2016). In ALS, TDP43 inclusions are mainly found in the motor cortex, spinal cord and in motor neurons in the brainstem but are also occasionally detected in the prefrontal cortex, hippocampus, temporal lobe and striatum in post-mortem tissue (Brettschneider et al., 2013; Mackenzie et al., 2007). TDP43 pathology is commonly found in patients with ALS and or FTD causing mutations including *GRN* (Cairns et al., 2007; Mackenzie et al., 2007), *C9ORF72* (Hsiung et al., 2012; Mackenzie et al., 2013; Stewart et al., 2012), *VCP* (Mackenzie and Neumann, 2016), *SQSTM1* (Kovacs et al., 2016), *UBQLN2* (Deng et al., 2011;

Fahed et al., 2014), *TBK1* (Freischmidt et al., 2015; Gijselinck et al., 2015; Pottier et al., 2015; van Mossevelde et al., 2016) and *OPTN* (Pottier et al., 2015).
Multiple mechanisms causing TDP43 to mislocalise to the cytoplasm and to aggregate have been proposed and they are likely to act in concert with each other (Tziortzouda et al., 2021). One affected pathway might be autoregulation and splicing of TDP43. For instance, disturbing TDP43 autoregulation by over-expression of a cytoplasmic TDP43 isoform or by modifying TDP43 splicing using antisense oligonucleotides resulted in reduced nuclear TDP43 levels in a human cell line or iPSC-derived neurons, respectively (D'Alton et al., 2015; Sugai et al., 2019). This splicing dysregulation also led to increased insoluble TDP43 levels and to motor neuron loss in mice (Sugai et al., 2019). The cytoplasmic TDP43 isoform was not detected in human cortex, however, which raises questions about its disease relevance (D'Alton et al., 2015). Over-expression of a cytoplasmic short N-terminal TDP43 isoform, which exhibited impaired autoregulative function for TDP43, resulted in reduced nuclear and enhanced cytoplasmic TDP43 in a human cell line and was toxic for rodent neurons. This isoform is also expressed in human spinal neurons making it more disease relevant even though no difference was observed between controls and ALS cases (Weskamp et al., 2019). On the other hand, in mutant TDP43 mouse models showing impaired autoregulation, nuclear TDP43 levels were increased but no cytoplasmic mislocalisation was observed (Fratta et al., 2018; White et al., 2018). Enhanced total levels of TDP43 were detected in an FTD patient brain with a TDP43 mutant and in patient brains with sporadic or *C9ORF72* ALS or FTD (Gitcho et al., 2009; Lee et al., 2019) suggesting that TDP43 autoregulation could be disturbed in disease.
Another mechanism rendering TDP43 permanently cytoplasmic could be via altering its tendency to aggregate. In a physiological environment TDP43 can form liquid droplets and can undergo liquid liquid phase separation, the process of demixing of two liquid phases (Mann et al., 2019), but mainly exists in a dispersed state (i.e. not locally concentrated) (Tziortzouda et al., 2021). ALS TDP43 mutations can lead to these liquid droplets becoming more prone to aggregation (Molliex et al., 2015). Furthermore, at high concentrations and over time TDP43 first forms liquid droplets and eventually aggregates *in vitro* (Babinchak et al., 2019). Stress granules, membraneless organelles formed upon cellular stress containing RNAs and proteins, are hypothesised to provide such a concentrated, aggregation promoting

environment *in vitro* (Li et al., 2013). However, many studies have shown TDP43 aggregation independent of stress granules and even propose a protective role for stress granules (Boeynaems and Gitler, 2018; Gasset-Rosa et al., 2019; Hans et al., 2020; Mann et al., 2019; McGurk et al., 2018; Zhang et al., 2020). On the other hand, incomplete dissolution or persistent or repetitive formation of stress granules have been demonstrated to cause TDP43 aggregation (P. Zhang et al., 2019). Phosphorylation of TDP43, hyperexcitability and neuronal injury are other factors shown to contribute to TDP43 aggregation or cytoplasmic mislocalisation (Goh et al., 2018; Moisse et al., 2009; Sato et al., 2009; Weskamp et al., 2019). Thus, it is still not clear what exactly causes TDP43 aggregation in ALS/FTD patients. Another mechanism leading to cytoplasmic TDP43 mislocalisation might be disturbed protein transport between the nucleus and cytoplasm which will be further investigated and discussed throughout this thesis.

What is the consequence of the loss of nuclear TDP43 and of the presence of cytoplasmic TDP43 aggregates? TDP43 knockout is embryonically lethal in mice (Kraemer et al., 2010) and conditional knockout in motor neurons results in a motor phenotype in mice (Iguchi et al., 2013; Wu et al., 2012). Depletion of TDP43 in mouse embryonic stem cells has been shown to lead to the inclusion of cryptic exons, a coding sequence within precursor mRNA usually not incorporated into mature mRNA, into mRNAs which impairs their translation and promotes their degradation (Ling et al., 2015). TDP43 knock down in a neuroblastoma cell line and in human embryonic stem cell derived motor neurons led to a reduction of stathmin 2 (STMN2), a microtubule binding protein involved in neuronal growth and maintenance, caused by altered splicing and polyadenylation. Decreased STMN2 levels have also been detected in ALS patient spinal cord and motor cortex (Klim et al., 2019; Melamed et al., 2019). Thus, loss of TDP43 leads to impairments of neuronal function.

As mentioned in section 1.1.2 studies regarding the toxicity of cytoplasmic TDP43 aggregates yield conflicting results. A mouse model pan-neuronally over-expressing TDP43 shows cytoplasmic TDP43 aggregates, motor dysfunction and severe toxicity leading to premature death (Becker et al., 2017). Over expression of TDP43 in mammalian cell lines, however, leads to cytotoxicity but TDP43 localisation was mostly nuclear (Watanabe et al., 2013; Yamashita et al., 2014). Furthermore, in rat primary neurons the formation of TDP43 inclusions was found to be unrelated to

cytotoxicity (Barmada et al., 2010). On the other hand, direct transfection of TDP43 aggregates purified from *E. coli* led to cell death without nuclear depletion of endogenous TDP43 in human and murine neuronal-like cell lines (Capitini et al., 2014; Cascella et al., 2016). In addition, light-induced aggregation of an engineered disordered TDP43 region is neurotoxic (Mann et al., 2019). TDP43 aggregates in patient tissue also contain C-terminal fragments of TDP43 of a size of 25 and 35 kDa (Neumann et al., 2006). Overexpression of these C-terminal fragments in cells caused these fragments to form cytoplasmic aggregates and led to cellular toxicity in a number of studies (Hergesheimer et al., 2019). In summary, even though the contribution of cytoplasmic TDP43 aggregates to ALS/FTD pathology has not been fully proven, cytoplasmic mislocalisation of TDP43 is clearly disadvantageous to the cell.

FTLD-UPS

Only in a small minority of FTLD cases inclusions containing proteins of the ubiquitin proteasome system (UPS) but not any other proteins are found (Mackenzie and Neumann, 2016). Cases with mutations in *CHMP2B* usually present with neuronal cytoplasmic inclusions mostly in the hippocampus with inclusions containing p62 and ubiquitin but not tau, TDP43 or FUS (Holm et al., 2009, 2007). *CHMP2B* mutation patient brains also show autofluorescent aggregates due to lysosomal storage pathology (Clayton et al., 2015).

1.2 Available treatment options

Currently no cure for ALS or FTD exists. In most European countries only one drug slowing ALS disease progression is available, named **riluzole** (Masrori and van Damme, 2020). The exact mechanism of action of riluzole is unclear but it likely reduces neurotransmitter release at the presynapse and inhibits persistent sodium currents and repetitive firing (Bellingham, 2011). Oral riluzole treatment extends mean patient survival by 3-6 months (Bensimon et al., 1994; Hinchcliffe and Smith, 2017; Lacomblez et al., 1996). Data from patient databases indicates increased survival by 6-21 months (Hinchcliffe and Smith, 2017; Miller et al., 2009). A different ALS drug **edaravone** is approved for ALS treatment in the United States, Canada, Japan, South Korea and Switzerland but not in the European Union (Masrori and van

Damme, 2020). Edaravone is a free radical scavenger and has been shown to reduce oxidative stress in ALS animal models (Kawai et al., 1997; Watanabe et al., 1994). In a clinical trial no benefits of intravenous edaravone treatment compared to placebo were detected, initially (Abe et al., 2014). However, in a post-hoc analysis a distinct patient subgroup with characteristics such as maximum disease duration of 2 years and preserved respiratory function which might benefit from edaravone treatment was identified. A phase 3 clinical trial with this patient population showed 30 % slower disease progression after 24 weeks in patients treated with edaravone compared to patients treated with placebo (Abe et al., 2017). This study received criticism about its short duration, small number of participants, patient selection and missing survival data (Al-Chalabi et al., 2017). A recent post-marketing study of real-life use showed that disease progression did not differ between patients treated with edaravone and patients treated with riluzole (Witzel et al., 2022). A third potential ALS drug, **masitinib**, is an inhibitor of the tyrosine kinase c-KIT (Dubreuil et al., 2009). It has been shown to reduce neuroinflammation in ALS mutant *SOD1* animal models (Harrison and Rafuse, 2020; Kovacs et al., 2021; Trias et al., 2020, 2018, 2017, 2016). In a randomised control trial comparing patients treated with both riluzole and masitinib with patients treated with riluzole and placebo loss of motor functions was slowed in patients treated with masitinib who were not fast progressors (Mora et al., 2020). In a follow up study lifespan was extended by two years in patients treated with masitinib if they were not fast progressor compared to patients treated with placebo (Mora et al., 2021). Very recently an application for marketing authorisation of masitinib was filed to the European Medical Agency (Press release by AB Science, 2022).

For FTD no treatments slowing disease progression are available. Certain drugs can be used for symptom management after exhausting non-pharmacological interventions (Guimet et al., 2022). Some studies showed an improvement of behavioural symptoms of FTD patients after treatment with selective serotonin reuptake inhibitors (Piguet and Hodges, 2013; Pressman and Miller, 2014; Swartz et al., 1997). The antidepressant trazodone is beneficial in treating agitation and aggression in FTD (Pressman and Miller, 2014). There is limited evidence through case reports that anticonvulsants used as mood stabilisers might improve FTD symptoms of binge eating (Cruz et al., 2008; Singam et al., 2013), alcohol misuse (Cruz et al., 2008) or hypersexuality (Poetter and Stewart, 2012). A phase 2 clinical

trial for lithium treatment, which led to some clinical improvement in case series (Arciniegas, 2006; Devanand et al., 2017), versus placebo is currently under way (ClinicalTrials.gov identifier: NCT02862210). Intranasal oxytocin has been shown to improve behavioural symptoms in FTD 8 hours after administration but not 1 week after administration due to the short half-life of oxytocin (Jesso et al., 2011). A phase 2 multicenter study investigating intranasal oxytocin effects on behavioural symptoms of FTD compared to placebo is currently active (ClinicalTrials.gov identifier: NCT03260920).

As described in this section current treatment options for ALS and FTD are extremely limited and there is an urgent need for more effective treatments based on findings from pathology mechanism studies.

1.3 The *C9ORF72* mutation

A repeat expansion of the hexanucleotide sequence GGGGCC located in the first intron of the *C9ORF72* gene is the most common genetic cause of both ALS and FTD in Europe and North America (DeJesus-Hernandez et al., 2011; Renton et al., 2011). Healthy individuals commonly have less than 11 hexanucleotide repeats within the *C9ORF72* gene (Harms et al., 2013; Rutherford et al., 2012; Zee et al., 2013) whilst patients with *C9ORF72* ALS/FTD usually carry hundreds to thousands of these repeats (Beck et al., 2013; Harms et al., 2013; Suh et al., 2015; van Blitterswijk et al., 2013). The consequences of this repeat expansion will be introduced in this section.

1.3.1 Mechanisms of *C9ORF72* pathology

The hexanucleotide G_4C_2 repeat expansion has three different immediate effects on cells which could all theoretically be causative of disease as illustrated in Figure 1.2. Firstly, epigenetic marks associated with gene silencing are found within the repeat expansion sequence and in CpG islands upstream of the repeat (Belzil et al., 2014, 2013; Gijselinck et al., 2016; Jackson et al., 2020; Xi et al., 2015, 2014) which might lead to reduced expression of *C9ORF72*. Indeed, a reduction in *C9ORF72* transcripts in comparison to control tissue is detected in patient frontal cortex, cerebellum, motor cortex and spinal cord (Belzil et al., 2013; DeJesus-Hernandez et al., 2011; Donnelly et al., 2013; Fratta et al., 2013; Gijselinck et al., 2012; Mori et al.,

2013b; van Blitterswijk et al., 2015; Waite et al., 2014) and lower C9ORF72 protein levels are found in frontal, occipital, temporal and motor cortices of *C9ORF72* repeat expansion carriers compared to non-carriers (Saberi et al., 2018; Viodé et al., 2018; Waite et al., 2014; Xiao et al., 2015). Secondly, the repeat expansion is transcribed into repetitive RNA in sense and antisense directions which clusters into RNA foci (Donnelly et al., 2013; Gendron et al., 2013; Lagier-Tourenne et al., 2013; Mizielinska et al., 2013; Zu et al., 2013) and has been shown to form different secondary structures *in vitro* (Fratta et al., 2012; Haeusler et al., 2014; Reddy et al., 2013; Su et al., 2014; Zhou et al., 2018). Thirdly, even though the repeat expansion is not located in a coding region it is translated in all reading frames via repeat associated non-ATG (RAN) translation. This results in the production of five different dipeptide repeat proteins (DPRs), namely poly-glycine-alanine (GA), poly-glycine-proline (GP), poly-glycine-arginine (GR), poly-proline-alanine and poly-proline-arginine (PR) (Ash et al., 2013; Gendron et al., 2013; Mori et al., 2013a, 2013b; Zu et al., 2013). Interestingly, two *in vitro* studies found that RAN translation occurred on unspliced, capped RNA containing the intron with the repeats starting at an upstream near cognate CUG codon (Green et al., 2017; Tabet et al., 2018). A third *in vitro* study detected RAN translation from the spliced intron containing the repeat expansion, however (Cheng et al., 2018). Possibly, RAN translation occurs from both RNA species *in vivo*.

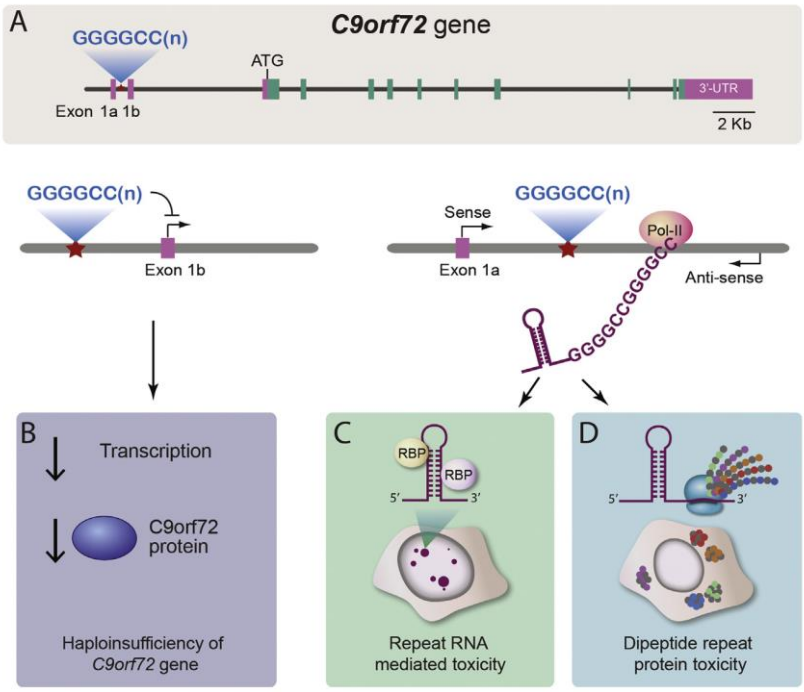

Figure 1.2: Potential mechanisms of pathology of C9ORF72 mutation (Gitler and Tsuiji, 2016)**.**

Which of these mechanisms does actually cause pathology? The C9ORF72 protein is involved in autophagy, endolysosomal trafficking and immune system regulation (Balendra and Isaacs, 2018; Smeyers et al., 2021) and a loss of C9ORF72 might affect these processes in patients and cause neurodegeneration. In fact, autophagy levels and lysosome numbers are reduced in *C9ORF72* ALS/FTD patient neurons (Aoki et al., 2017; Shi et al., 2018; Webster et al., 2016). Furthermore, ubiquitous *C9orf72* knockout mice exhibit immune system dysregulation (Atanasio et al., 2016; Burberry et al., 2016; Jiang et al., 2016; O'Rourke et al., 2016; Sudria-Lopez et al., 2016; Ugolino et al., 2016). However, these mice did not suffer from neuronal loss and only occasionally exhibited mild motor or cognitive impairments (Atanasio et al., 2016; Jiang et al., 2016). Conditional knock-down or knockout of *C9orf72* in neurons or glia did not cause motor or cognitive dysfunction in mice (Koppers et al., 2015; Lagier-Tourenne et al., 2013). Therefore, C9ORF72 haploinsufficiency is likely not the prime cause of neurodegeneration in *C9ORF72* ALS/FTD.

Repetitive RNA foci might sequester RNA binding proteins rendering them unavailable to the cell. Indeed, a number of RNA binding proteins have been found to interact with repeat expansion RNA in patient iPSC-derived neurons, cell lines, in *in vitro* studies and *in vivo*. Most commonly these were heterogeneous nuclear ribonucleoproteins (hnRNPs) such as hnRNP H, hnRNP A1 or A2. THO complex subunit 4 (ALYREF), serine/arginine- rich splicing factor 1 (SRSF1), double-stranded RNA-specific editase B2 (ADARB2), nucleolin, Pur-α, Zfp106 and SRSF2 were also detected in more than one study (Balendra and Isaacs, 2018). In *C9ORF72* ALS/FTD patient sense and antisense RNA foci colocalise with hnRNPA1, hnRNP H/F, SRSF2, and ALYREF (Cooper-Knock et al., 2014; Lee et al., 2013; Sareen et al., 2013). This colocalisation is usually found within a minority of foci, only hnRNP-H colocalises with sense foci at high frequencies (Lee et al., 2013). Furthermore, over-expression of transcriptional regulator Pur-α and zinc finger protein Zfp106 reduced neurotoxicity in *C9ORF72*-repeat expressing *Drosophila*, zebrafish or cell lines (Celona et al., 2017; Swinnen et al., 2018; Xu et al., 2013). However, in *Drosophila* models expressing the *C9ORF72* repeat expansion interspersed with stop codons so that it is not translated into DPRs but only transcribed into repetitive RNA, no neurodegeneration phenotype is detected whilst expression of the pure uninterrupted repetitive sequence does lead to neurodegeneration (Mizielinska et al., 2014; Moens et al., 2018). Another *Drosophila* model expressing *C9ORF72* repeats in an intronic

region, which only results in production of RNA and in the formation of RNA foci detectable in neurons and glia but not in the production of DPRs, did not show any signs of neurodegeneration, either (Tran et al., 2015). These studies question the potency of repetitive RNA to elicit ALS/FTD neurodegeneration. It is possible, however, that RNA foci sequester RNA binding proteins which do not occur in *Drosophila*.

Treatment with synthetic DPRs or direct expression of individual DPRs (by modifying the coding sequence which is then usually under the control of an ATG start codon) in cells and *in vivo* models is (neuro)toxic (Balendra and Isaacs, 2018). When comparing the potency of different DPR species in cell lines or primary neurons (Kanekura et al., 2016; Tao et al., 2015; Wen et al., 2014; Yamakawa et al., 2015), in *Drosophila* (Boeynaems et al., 2016a; Freibaum et al., 2015a; Lee et al., 2016; Mizielinska et al., 2014; Wen et al., 2014; Yang et al., 2015) and in zebrafish (Swaminathan et al., 2018) the arginine containing species poly-GR or -PR have been found to be the most toxic. Poly-GR or -PR are also toxic to human astrocytes and control iPSC-derived neurons (Kwon et al., 2014; Wen et al., 2014). In *Drosophila* poly-GR and -PR lead to reduced survival (Freibaum et al., 2015a; Mizielinska et al., 2014; Wen et al., 2014; Yang et al., 2015) and motor deficits (Baldwin et al., 2016; Wen et al., 2014; Yang et al., 2015). Mice expressing poly-GR or -PR postnatally in the brain exhibit neurodegenerative phenotypes (Choi et al., 2019; Y. J. Zhang et al., 2019, 2018). Poly-GA has also been shown to be toxic in cell lines (Chang et al., 2016; May et al., 2014; Zhang et al., 2014), primary neurons (Flores et al., 2016; Zhang et al., 2014), zebrafish (Ohki et al., 2017; Swaminathan et al., 2018) or mice (Schludi et al., 2017; Zhang et al., 2016). One poly-GA *Drosophila* model exhibited moderately reduced lifespans (Mizielinska et al., 2014) while poly-GA was not toxic in other *Drosophila* models (Boeynaems et al., 2016; Wen et al., 2014; Yang et al., 2015). Surprisingly, a study comparing mouse models expressing poly-PR or -GA already during embryonal development in the central nervous system found that only poly-GA mice but not poly-PR mice exhibited neuronal loss (LaClair et al., 2020).

In summary, there is clear evidence that DPRs, predominantly poly-GR and -PR and also poly-GA, are neurotoxic. However, RNA toxicity and *C9ORF72* haploinsufficiency might also contribute to disease development. For instance, toxicity in *C9ORF72* ALS/FTD patient derived induced motor neurons was

dependent on reduced C9ORF72 levels (Shi et al., 2018). Furthermore, *C9ORF72* knockout in *C9ORF72* ALS/FTD patient derived induced motor neurons enhanced axonal trafficking defects (Abo-Rady et al., 2020). In mouse models expressing *C9ORF72* repeat expansion, *C9orf72* knockout exacerbates motor impairments (Shao et al., 2019; Zhu et al., 2020), cognition defects, neurodegeneration and accumulation of DPRs (Zhu et al., 2020). These findings further highlight that *C9ORF72* mutation pathology is likely not caused via a single mechanism.

1.3.2 Neuropathology in *C9ORF72* ALS/FTD

C9ORF72 repeat expansion carriers show cytoplasmic TDP43 inclusions in multiple brain regions including frontal, temporal and primary motor cortices, hippocampus, basal ganglia, amygdala, thalamus and midbrain (Hsiung et al., 2012; Irwin et al., 2013; Mackenzie et al., 2013; Mahoney et al., 2012; Murray et al., 2011). Sense and antisense repetitive RNA foci and DPR inclusions are also present in the central nervous system of *C9ORF72* ALS/FTD patients. RNA foci are detected in neuronal nuclei in the frontal and motor cortices, hippocampus, cerebellum and spinal cord and occasionally in the cytoplasm (DeJesus-Hernandez et al., 2017; Gendron et al., 2013; Lagier-Tourenne et al., 2013; Mizielinska et al., 2013; Zu et al., 2013). DPR inclusions are most frequently found in the cerebellum, hippocampus and neocortex (including frontal cortex) and are rarely detected in the brainstem and spinal cord (Balendra and Isaacs, 2018). These inclusions stain positive for p62 but negative for TDP43 (Mori et al., 2013a) and commonly form neuronal cytoplasmic inclusions (Ash et al., 2013; Gendron et al., 2013; Mackenzie et al., 2013; Mori et al., 2013b) but can also occur within neurites (Mackenzie et al., 2013; Saberi et al., 2018) and neuronal nuclei (Ash et al., 2013; Gendron et al., 2013; Mackenzie et al., 2013; Mori et al., 2013b; Schludi et al., 2015). Poly-GA occurs most frequently, followed by poly- GP then poly-GR with poly-PA and poly-PR being the least frequent DPR species (Davidson et al., 2016; Gendron et al., 2013; Gomez-Deza et al., 2015; Liu et al., 2014; Mackenzie et al., 2015; Mann et al., 2013; Mori et al., 2013b, 2013a; Schludi et al., 2015). TDP43 pathology in patient central nervous system correlates well with ALS and FTD neurodegeneration (Davidson et al., 2016, 2014; Gendron et al., 2015; Mackenzie et al., 2013, 2015; Mann et al., 2013) whilst DPR inclusions usually do not co-localise with TDP43 inclusions (Gendron et al., 2015) and the two species are

rarely found within the same neuron (Gomez-Deza et al., 2015; Mackenzie et al., 2013; Mann et al., 2013; Mori et al., 2013b). Regional distribution of DPR inclusions is similar between FTD and ALS cases (Davidson et al., 2014; Mackenzie et al., 2013, 2015). These findings might raise doubts whether DPR inclusions contribute to neurodegeneration in patients. However, *post mortem* samples usually represent the end stage of the disease and neurons which contained DPR inclusions earlier might have died. Furthermore, it is also possible that DPRs contribute to neurodegeneration in their soluble form as soluble poly-GP, -GR and -GA was detected in patient brains (Quaegebeur et al., 2020). However, one study found specifically poly-GR inclusions to correlate well with neurodegeneration in *C9ORF72* ALS (Saberi et al., 2018) further highlighting poly-GR mediated toxicity.

1.3.3 Cellular functions implicated by the *C9ORF72* mutation

Various cellular pathways and organelles have been shown to be affected in the context of *C9ORF72* repeat expansion and a selection will be introduced here. One implicated area are membraneless organelles. Poly-GR and -PR localise to the nucleolus in cell lines, primary neurons, iPSC- derived neurons and Drosophila which results in altered nucleolus morphology (Callister et al., 2016; Mizielinska et al., 2017; Schludi et al., 2015; Tao et al., 2015; Wen et al., 2014). In human astrocytes the localisation of poly-GR and -PR to the nucleolus causes altered splicing and ribosomal RNA maturation (which occurs in the nucleolus) deficits (Kwon et al., 2014). Immunoprecipitation studies showed that poly-GR and -PR interacted with nucleolar proteins (Boeynaems et al., 2017; Lee et al., 2016; Y. Lin et al., 2016; White et al., 2019) and poly-GR and -PR changed the biophysical properties of nucleolar protein NPM1 and nucleolin (Lee et al., 2016; White et al., 2019). In *C9ORF72* ALS/FTD patient brains poly-GR and -PR rarely localise to the nucleolus (Schludi et al., 2015). However, an overall reduction in nucleolus volume is detected in *C9ORF72* FTD patient brains whilst nucleoli are enlarged in neurons exhibiting poly-GR inclusions (Mizielinska et al., 2017). *C9ORF72* ALS spinal cord motor neurons also show a shrinkage of nucleoli (Aladesuyi Arogundade et al., 2021).

Other membraneless RNA organelles are also affected by DPRs. Over-expression of poly-GR and poly-PR in cells leads to reduced numbers of cytoplasmic P bodies

(Wen et al., 2014; Xu et al., 2019), which are involved in RNA degradation and contain untranslated RNAs. Cajal bodies and gems, essential for spliceosome assembly, are also lowered in cells expressing poly-PR, -GR or -GA (Lee et al., 2016; Rossi et al., 2020). However, the formation of paraspeckles which play a role in transcriptional regulation is increased in neuronal like cells expressing poly-PR (Suzuki et al., 2019). The formation and dynamics of stress granules, cytoplasmic foci comprised of untranslated ribonucleoprotein complexes which form upon cellular stress in response to translational arrest, are also altered in *C9ORF72* ALS/FTD. Poly-GR and -PR as well as the expression of the *C9ORF72* repeat expansion enhance the number of stress granules in cells (Boeynaems et al., 2017; Lee et al., 2016; Rossi et al., 2015; Wen et al., 2014) and poly-PR induced stress granules also contain disease relevant proteins such as TDP43 and ataxin 2 (Boeynaems et al., 2017). However, mice expressing poly-GR postnatally in the brain do not form stress granules positive for the stress granule protein TIA1 in the cortex. In contrast, expression of the GGGGCC repeat expansion does lead to the formation of cytoplasmic TIA1 positive stress granules which colocalise with poly-GR (Chew et al., 2019; Y. J. Zhang et al., 2018). In *C9ORF72* ALS/FTD patient brains no colocalisation of poly-GR or -PR with stress granule markers is detected (Hartmann et al., 2018). Furthermore, disassembly of stress granules is impaired by poly-GR and -PR in cells (Boeynaems et al., 2017; Lee et al., 2016; Y. J. Zhang et al., 2018) potentially leading to mRNAs being trapped in stress granules and not being available for translation. Fittingly, poly-GR and -PR have been shown to inhibit translation in cell lines (Kanekura et al., 2016; Lee et al., 2016; Vanneste et al., 2019; Y. J. Zhang et al., 2018), *Drosophila*, control iPSC-derived motor neurons (Moens et al., 2019) and mice (Y. J. Zhang et al., 2018). Translational repression is also observed after expressing GGGGCC repeats in cells (Rossi et al., 2015) and in *C9ORF72* ALS patient iPSC-derived motor neurons (Ortega et al., 2020). Immunopreciptation and other interactome studies have found that poly-GR and -PR interact with ribosomal proteins and translation initiation and elongation factors (Boeynaems et al., 2017; Hartmann et al., 2018; Kanekura et al., 2016; Lee et al., 2016; Y. Lin et al., 2016; Lopez-Gonzalez et al., 2016; Moens et al., 2019; Radwan et al., 2020; Yin et al., 2017). Furthermore, poly-GR colocalises with ribosomal proteins and translation elongation factors in a poly-GR mouse model and poly-GR and -PR have been found to colocalise with these factors in *C9ORF72* ALS/FTD

brain (Hartmann et al., 2018; Y. J. Zhang et al., 2018). These findings might indicate that the interaction of poly-GR and -PR with translation factors makes these factors inaccessible to active translation. Furthermore, poly-GR and -PR have been shown to bind to mRNAs which might impair their translation (Kanekura et al., 2016). Another mechanism of translational repression by poly-GR and -PR might be by directly acting on the assembled ribosomal complex. Indeed, it has been shown that poly-GR and -PR cause ribosome stalling in cells (Radwan et al., 2020) and that they directly bind to the polypeptide tunnel of the ribosome *in vitro* thereby impairing the ribosome's peptidyl-transferase activity and thus protein biosynthesis (Loveland et al., 2022). Translation is also repressed as a consequence of the integrated stress response via the phosphorylation of eukaryotic translation initiation factor 2 subunit α which has been found to lead to an increase in RAN translation (Bowden and Dormann, 2016; Green et al., 2017). The resulting enhanced levels of poly-GR and -PR might then further inhibit translation and increase cellular stress in a negative feedback loop which ultimately greatly impacts cellular function as cellular protein supply is disrupted.

The *C9ORF72* repeat expansion also has an effect at the DNA level. In a mouse model expressing poly-PR in the brain, poly-PR bound to heterochromatin and cells expressing poly-PR showed decreased levels of heterochromatin protein 1α (HP1α), nuclear lamina invaginations and altered histone methylation, which in their physiological state regulate heterochromatin structure. These changes to heterochromatin led to aberrant expression of repetitive elements and double stranded RNAs which would normally be silenced (Y. J. Zhang et al., 2019). Furthermore, DNA damage is detected in primary neurons expressing *C9ORF72* repeats or poly-GR, -PR or -GA (Farg et al., 2017; Maor-Nof et al., 2021; Walker et al., 2017), human cell lines expressing *C9ORF72* repeats or poly-GR, -PR or -GA (Farg et al., 2017; Nihei et al., 2020; Walker et al., 2017), mice expressing the *C9ORF72* repeat expansion or poly-GR or -GA in the brain (Choi et al., 2019; Walker et al., 2017), *C9ORF72* ALS/FTD patient brain and spinal cord (Farg et al., 2017; Nihei et al., 2020), *C9ORF72* patient iPSC-derived motor neurons or control iPSC-derived motor neurons expressing poly-GR (Lopez-Gonzalez et al., 2016). DNA damage might be caused by impaired activation of mutated in ataxia telangiectasia (ATM), a kinase activating a DNA repair signalling pathway, because of the *C9ORF72* repeat expansion or poly-GA (Nihei et al., 2020; Walker et al., 2017). This

might be partially caused by sequestration of phosphorylated (activated) ATM and hnRNPA3, whose knockdown exacerbates DNA damage in cells expressing poly-GR, -PR or -GA and in *C9ORF72* patient iPSC-derived motor neurons, into poly-GA foci (Nihei et al., 2020). Impairment of NPM1, a nucleolar protein involved in DNA damage repair, function by poly-GR and -PR might be another factor responsible for DNA damage (Farg et al., 2017). Reduced mitochondria function correlates with DNA damage in mice expressing poly-GR in the brain and in *C9ORF72* patient iPSC-derived motor neurons as this can lead to increased oxidative stress in turn leading to DNA damage (Choi et al., 2019; Lopez-Gonzalez et al., 2016). Possibly, all of these mechanisms contribute to DNA damage in *C9ORF72* model systems. DNA damage might be partly responsible for neurodegeneration as mice expressing poly-GR or -GA show signs of DNA damage and motor phenotypes and neuronal loss or behavioural deficits and neuronal loss, respectively (Choi et al., 2019; Walker et al., 2017) and primary neurons expressing poly-PR exhibit DNA damage and axonal degeneration (Maor-Nof et al., 2021).

As mentioned above impaired mitochondria function is detected in *C9ORF72* model systems. In *C9ORF72* iPSC-derived motor neurons and mitochondria are swollen, which can trigger the release of proapoptotic factors from the mitochondria. Indeed, apoptosis markers are increased in these cells. Furthermore, the mitochondrial membrane potential is reduced in *C9ORF72* patient motor neurons compared to controls, which indicates reduced uptake of calcium necessary for the regulation of ATP production and apoptosis (Dafinca et al., 2016). As the endoplasmic reticulum (ER) acts as the cell's largest calcium storage calcium influx into mitochondria often occurs from the ER facilitated by molecular tethers between the ER and mitochondria. The number of these tethers has been found to be decreased in C9ORF72 ALS/FTD iPSC-derived neurons and in mice expressing a bacterial artificial chromosome (BAC) containing the *C9ORF72* repeat expansion. Cells expressing poly-GR, -PR or -GA also exhibited reduced ER mitochondria tethers compared to GFP expressing cells and showed reduced uptake of calcium by mitochondria (Gomez-Suaga et al., 2022). In contrast, in *C9ORF72* patient fibroblasts, grown in oxidative conditions so that cells have to solely rely on energy production via oxidative phosphorylation occurring in mitochondria, mitochondria have been found to be hyperpolarised (indicating high calcium influx) leading to enhanced ATP production and increased levels of reactive oxygen species.

However, this is not accompanied by reduced cell survival (Onesto et al., 2016). Another function of calcium uptake by mitochondria is calcium buffering after neurotransmission. Indeed, *C9ORF72* iPSC-derived motor neurons show prolonged recovery times to calcium baseline levels after glutamate depolarisation and reduced calcium uptake of mitochondria after glutamate depolarisation compared to standard and isogenic control lines. This is likely caused by the lowered expression of mitochondria calcium uniporter (MCU), responsible for calcium entry inside mitochondria, detected in *C9ORF72* motor neurons compared to isogenic controls. As *C9ORF72* motor neurons also show increased excitability upon glutamate stimulation compared to controls, the reduced calcium buffering capacity of mitochondria in these cells could contribute to glutamate excitotoxicity, the toxic overexcitement of cells due to calcium mediated excess glutamate release (Dafinca et al., 2020). Furthermore, enhanced calcium release from mitochondria upon mitochondria membrane potential breakdown (a trigger for mitochondrial calcium release) which could eventually lead to apoptosis has been observed in older but not young *C9ORF72* ALS/FTD iPSC-derived motor neurons compared to controls, but this is not accompanied by hyperexcitability (Burley et al., 2022). *C9ORF72* ALS/FTD patient iPSC-derived motor neurons also exhibit mitochondrial respiration deficits accompanied by reduced axon lengths possibly due to downregulation of electron transport chain transcripts responsible for mitochondrial respiration compared to isogenic controls. This downregulation also occurs in *C9ORF72* ALS patient spinal cord ventral horn motor neurons but not in dorsal horn sensory neurons suggesting selective vulnerability of motor neurons (Mehta et al., 2021). Poly-GR has been found to interact with ATP synthase F1 subunit alpha (ATP5A1), a part of mitochondrial complex V which synthesises ATP, in immunoprecipitation experiments using a human cell line. In addition, ATP5A1 protein levels are reduced in the cortex of mice expressing poly-GR in the brain, where *ATP5A1* RNA levels are not affected, and in frontal cortex of *C9ORF72* ALS/FTD patients. This mouse model also shows synaptic dysfunction, social behavioural deficits, neuronal cell loss and microgliosis suggesting toxicity of the mitochondrial phenotype (Choi et al., 2019). In *Drosophila* expressing poly-GR in the muscle and showing a wing phenotype poly-GR preferentially localises to mitochondria. Poly-GR is also enriched in the mitochondrial fraction of *C9ORF72* ALS/FTD patient fibroblasts exhibiting abnormal mitochondria morphology (Li et al., 2020b, 2020a). Overall, the observed

mitochondria deficits likely contribute to neurodegeneration as neurons heavily rely on ATP production by mitochondria to sustain their activity.
Lastly, axonal transport of mitochondria is impaired in *C9ORF72* ALS/FTD iPSC-derived motor neurons (Fumagalli et al., 2021; Mehta et al., 2021) or control iPSC-derived motor neurons treated with poly-GR or -PR (Fumagalli et al., 2021), in larval neuropeptidergic neurons or in adult sensory neurons in the wing of *Drosophila* models expressing *C9ORF72* repeats, poly-GR or poly-PR (Baldwin et al., 2016; Fumagalli et al., 2021) but not in larval motor neurons of a *Drosophila* model expressing *C9ORF72* repeats (Sung and Lloyd, 2022). Further regarding axonal transport deficits, poly-PR interacts with members of the axonal transport machinery from mouse spinal cord lysate. Poly-GR colocalises with motor protein kinesin-1 isoform KIF5B in *C9ORF72* ALS/FTD patient frontal cortex. In addition, KIF5B and dynein motility is impaired by poly-GR and -PR *in vitro* possibly by these DPRs binding to microtubules thereby hindering motor protein movement (Fumagalli et al., 2021). These axonal transport impairments caused by *C9ORF72* mutation likely affect neuronal function.
In summary, a variety of cellular mechanism seem to be implicated in *C9ORF72* ALS/FTD potentially all contributing to pathology possibly at different stages of disease. Another cellular mechanism affected by the *C9ORF72* mutation is nucleocytoplasmic transport which will be introduced in section 1.5.2.

1.4 Nucleocytoplasmic transport

Nucleus and cytoplasm are separate compartments divided by the two-layered nuclear membrane in eukaryotic cells. Hence, nuclear transcription and cytoplasmic translation are physically segregated. Gene expression and general information exchange between the nucleus and the cytoplasm are dependent on exchange of proteins and RNAs between the nucleus and the cytoplasm. The process ensuring this is termed nucleocytoplasmic transport (Stewart, 2007; Strambio-De-Castillia et al., 2010). 17 % of all eukaryotic proteins are estimated to be imported into the nucleus (Cokol et al., 2000). This essential mechanism is regulated by transport receptors, the GTPase Ran and by channels spanning the nuclear membrane thereby connecting nucleus and cytoplasm known as nuclear pore complexes (Eibauer et al., 2015; von Appen et al., 2015).

1.4.1 The nuclear pore

All nucleocytoplasmic transport occurs through nuclear pores with over 1000 cargoes being transported through each nuclear pore every second (Ribbeck et al., 1998). The mammalian nuclear pore is a large multi-protein complex of about 120 MDa (Beck and Hurt, 2017; Lin and Hoelz, 2019). It has eight-fold rotational symmetry and contains about 30 different proteins termed nucleoporins occurring as multiples of eight (Cronshaw et al., 2002; Lin and Hoelz, 2019). The exact composition of nucleoporins can vary between nuclear pores within the same cell (Coyne et al., 2020; Kinoshita et al., 2012) and can also differ between cell types (Ori et al., 2013; Rajoo et al., 2018). As depicted in Figure 1.3 the nuclear pore has several subcomplexes made up of multiple modules of nucleoporins with modules mostly containing the same nucleoporins within a subcomplex (Hampoelz et al., 2019; Schwartz, 2005). Each nuclear pore consists of a symmetric core surrounding the central transport channel. This symmetric core is formed by an inner ring embedded within the nuclear envelope and two outer rings, one on the inner and one on the outer nuclear membrane (Kosinski et al., 2016; D. H. Lin et al., 2016). The core acts as a scaffold anchoring asymmetric structures, namely cytoplasmic filaments on the cytoplasmic face and the nuclear basket on the nuclear side. Transmembrane nucleoporins anchor the symmetric core in the nuclear envelope (Lin and Hoelz, 2019).

The symmetric core consists of eight distinct units termed spokes. The outer rings are primarily formed by Y-shaped coat nucleoporin complexes. Each spoke contains 4 coat nucleoporin complexes, two on the nuclear outer ring and two on the cytoplasmic outer ring, with a total of 32 coat nucleoporin complexes in each human nuclear pore (Lin and Hoelz, 2019). Similarly, the inner rings are made of inner ring complexes with 4 inner ring complexes per spoke, two on the nuclear half and two on the cytoplasmic half of the inner ring. Each nuclear pore also contains a total of 32 inner ring complexes (Kosinski et al., 2016; D. H. Lin et al., 2016). Nucleoporins of the coat nucleoporin complexes connect via hydrophobic interfaces while inner ring nucleoporins are linked by short sequence motifs separated by flexible linkers allowing for greater flexibility (Lin and Hoelz, 2019).Cytoplasmic filaments act as binding sites for nucleocytoplasmic transport factors and Ran GTPase (Lin and Hoelz, 2019). On the other face of the pore, the nuclear basket nucleoporins directly

interact with the nucleocytoplasmic transport machinery, anchor RNA export factors, connect the nuclear pore with the transcriptional regulatory machinery and acts as a heterochromatin exclusion zone important for mRNA export (Köhler and Hurt, 2010; Krull et al., 2010). The central channel of the nuclear pore consists of nucleoporins containing phenylalanine-glycine (FG) domains (Lin and Hoelz, 2019) . FG-repeat regions are intrinsically disordered and are often enriched in polar amino acids and depleted of charged amino acids (Hoelz et al., 2016). These domains are found in about a third of nucleoporins also including inner ring, cytoplasmic filament and nuclear basket nucleoporins (Lin and Hoelz, 2019; Schmidt and Görlich, 2016). FG nucleoporins form the permeability barrier of the nuclear pore (Schmidt and Görlich, 2016) (see also section 1.4.2).

With this structural complexity, nuclear pore complexes play an important role in maintaining nuclear and cytoplasmic integrity by hindering macromolecules from freely moving in and out of the nucleus (see also section 1.4.2). They also greatly support cellular functionality. For instance, cargos are translocated through the nuclear pore in their natively folded state allowing them to immediately fulfil their function after transport such as transcriptional activation (Lin and Hoelz, 2019).

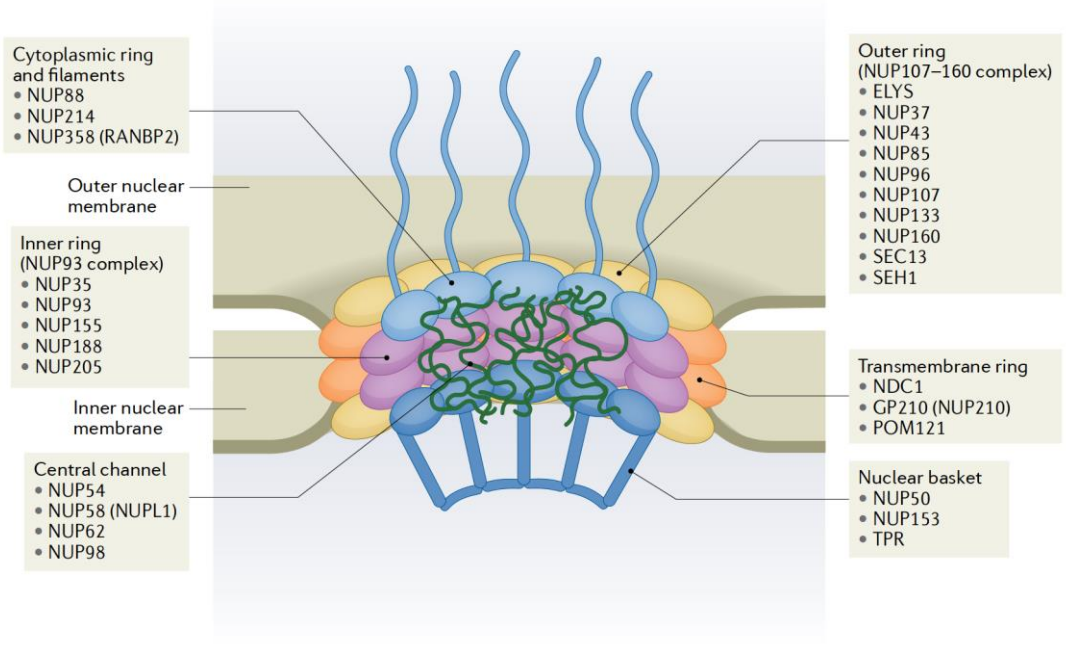

Figure 1.3: Structure and composition of the nuclear pore (Coyne and Rothstein, 2022)**.**

1.4.2 Active versus passive nucleocytoplasmic transport

Cargos are either actively transported or can passively diffuse through the nuclear pore. FG nucleoporins in the central channel region form a permeability barrier only allowing entry of molecules below a size of 40 kDa or 5 nm (Bonner, 1975; Mohr et al., 2009). This is, however, not a strict cut-off but rather an energetic barrier towards passive diffusion that rises with increasing size of macromolecules (Timney et al., 2016). In addition to size, surface properties play a role in the passive diffusion properties of protein cargos with hydrophobic surface residues being beneficial for passive translocation (Frey et al., 2018; Naim et al., 2009). Larger molecules rely on transport using transport receptors which is energy dependent (active nucleocytoplasmic transport) (Güttler and Görlich, 2011; Sloan et al., 2016). Transport receptors of the karyopherin β family (see also section 1.4.3) interact with FG repeats via hydrophobic pockets on their outer surface. The phenylalanine residue of the FG repeats can bind to this hydrophobic pocket (Bayliss et al., 2002, 2000; Koyama et al., 2017, 2014; Port et al., 2015). This interaction is weak, but each transport receptor has multiple FG binding sites which can be engaged by multiple FG repeats of the same nucleoporin in fast succession (Hough et al., 2015; Milles et al., 2015). These multivalent interactions thereby increase affinity through avidity (Kapinos et al., 2014; Schoch et al., 2012)

There are multiple hypotheses about how the permeability barrier of the nuclear pore is formed. The virtual gate model states that the nuclear pore forms an entropic barrier by decreasing the entropy of a macromolecule by restricting its movement with only small molecules being able to afford to “pay the entropy price”. The binding energy of the multiple low-affinity binding sites of FG repeats for transport receptors allows transport receptors to overcome this entropic barrier (Rout et al., 2003). The reversible collapse model is also based on an entropic barrier with transport receptor binding collapsing FG repeats into a compact conformation as opposed to the barrier conformation (Lim et al., 2007). The two gate or forest model states that FG repeats form two distinct transport zones based on their conformation with small molecules being able to diffuse through one zone and cargo loaded transport receptors translocating through the other (Yamada et al., 2010). Finally, the selective phase model, generally considered as the most plausible in the field, sees the permeability barrier as a 3D meshwork of FG repeats forming a hydrogel via reversible cohesive

interactions. This meshwork acts as a molecular sieve which can only be crossed by smaller cargo. Binding of transport receptors to FG repeats would locally break FG-FG interactions resulting in a local widening of the meshwork allowing the passage of larger cargo (Ribbeck and Görlich, 2001). Importantly, supporting this hypothesis FG repeat domains can phase-transition into hydrogels *in vitro* which replicate permeability barrier features (Frey et al., 2006; Frey and Görlich, 2007). It is also proposed that transport receptors, in particular importin β, contribute to the nuclear pore's permeability barrier (Kalita et al., 2021).

In summary, passive and active nucleocytoplasmic transport co-occur in cells (Mohr et al., 2009) and they might exist on a continuum with some cargos being actively transported and having some ability of passive diffusion (Frey et al., 2018). In any case, the permeability barrier is essential for the separation of nucleus and cytoplasm function.

1.4.3 Mechanisms of active protein import and export

Proteins not capable of passive diffusion through the nuclear pore are transported by transport receptors. The majority of macromolecules are transported by members of the transport receptor family of karyopherins β (Kimura and Imamoto, 2014). These include importins, translocating proteins from the cytoplasm into the nucleus (Boulikas, 1994; Cokol et al., 2000), exportins, passaging proteins out of the nucleus into the cytoplasm (Xu et al., 2012), and bidirectional transportins (Twyffels et al., 2014). 20 different human karyopherins β are known. Another class of transport receptors are karyopherins α with 7 members in humans (Kimura and Imamoto, 2014). These act as adaptors connecting importins β to their cargo (Goldfarb et al., 2004).

Active nucleocytoplasmic transport of proteins is regulated by the Ran gradient. The GTPase Ran can either occur in a GTP or GDP bound form. RanGTP is about 200 times more concentrated in the nucleus than in the cytoplasm (Görlich et al., 2003; Kalab et al., 2002; Smith et al., 2002). When importins transport their cargo into the nucleus, the cargo is released by RanGTP binding to importin (Jäkel and Görlich, 1998). The cargo stays in the nucleus as it cannot freely diffuse through the permeability barrier. Ran-GTP importin complexes interact with FG nucleoporins leading to the translocation of importins back to the cytoplasm. In the cytoplasm

RanGTPase-activating protein 1 (RanGAP1) hydrolyses RanGTP to RanGDP which leads to the dissociation of RanGDP from importin. Importin can now again associate with cargo (Stewart, 2007). RanGDP is recycled back to the nucleus by nuclear transport factor 2 (NTF2) (Ribbeck et al., 1998). In the nucleus, regulator of chromosome condensation 1 (RCC1) converts RanGDP into RanGTP ensuring the higher concentration of RanGTP in the nucleus compared to the cytoplasm (Klebe et al., 1995; Renault et al., 2001; Ribbeck et al., 1998). Conversely, RanGTP mediates cargo binding of exportins. After cargo translocation from the nucleus to the cytoplasm, conversion of RanGTP to RanGDP leads to the disassembly of the Ran-exportin-cargo complex (Arts et al., 1998; Fornerod et al., 1997; Kutay et al., 1998, 1997). Exportin is recycled back to the cytoplasm via FG nucleoporin interaction (Kutay and Güttinger, 2005).

Proteins usually bind to import receptors via a nuclear localisation signal (NLS) and to export receptors via a nuclear export signal (NES). Only a subset of these signals has been characterised for specific transport receptors (Fung et al., 2017; Soniat and Chook, 2015). The highly basic classical NLS binds to importin α (acting as a cargo adaptor for importin β as mentioned above) (Pumroy and Cingolani, 2015). The consensus sequence contains arginine and lysine residues (Kalderon et al., 1984; Robbins et al., 1991). Classical NLSs bind to the armadillo repeat domain of importin α (Lott et al., 2011). The N-terminal importin β binding region (IBB) of importin α contains an NLS-like sequence which binds to the major NLS binding site of importin α thereby inhibiting cargo binding (Conti et al., 1998; Kobe, 1999). Importin β binding to the IBB makes the major NLS binding site of importin α available for cargo binding thereby greatly enhancing cargo affinity (Catimel et al., 2001; Fanara et al., 2000; Hodel et al., 2006, 2001). TDP43 is a cargo imported by the importin α/β system (Nishimura et al., 2010). Another characterised NLS is the proline-tyrosine (PY) NLS which binds transportin 1 (B. J. Lee et al., 2006). These sequences have an overall positive charge and bind to a negatively charged site on transportin 1 (Chook and Süel, 2011; B. J. Lee et al., 2006; Soniat and Chook, 2016; Süel et al., 2008). FUS is imported into the nucleus by transportin 1 (Dormann 2010). The only characterised NES to date binds exportin 1. It contains hydrophobic anchor residues that bind to a hydrophobic groove on the outer surface of exportin 1 (Dong et al., 2009; Fung et al., 2017, 2015; Güttler et al., 2010; Monecke et al., 2009). Interestingly, predicted

exportin 1 NES sequences in TDP43 and FUS were shown to be non-functional (Ederle et al., 2018).

Karyopherins β use N-terminal structural motifs known as HEAT repeats to interact with the switch 1 and 2 regions (interacting with bound GTP (Vetter and Wittinghofer, 2001)) of Ran-GTP (Aksu et al., 2019, 2016; Bono et al., 2010; Chook and Blobel, 1999; Cook et al., 2009; Grünwald et al., 2013; Kobayashi and Matsuura, 2013; Lee et al., 2005; Maertens et al., 2014; Matsuura and Stewart, 2004; Monecke et al., 2009; Okada et al., 2009). Ran-GTP binds importins with very high affinity, bidirectional transport receptors with high to moderate affinity and exportins not bound to cargo with no or low affinity (Grünwald et al., 2013; Hahn and Schlenstedt, 2011; Lipowsky et al., 2000). The mutual exclusivity of cargo or Ran-GTP binding to importins is mediated by a steric clash between import cargo and Ran-GTP upon importin binding. Alternatively, it can be driven by conformational changes of importin upon Ran-GTP binding which render the cargo binding site inaccessible or by a combination of the two mechanisms (Wing et al., 2022). Exportins do not bind cargo or Ran-GTP alone but only bind them in conjunction. This cooperative binding is mediated by large conformational changes in most exportins and by direct contacts between Ran-GTP and cargo which stabilises the complex (Wing et al., 2022). Exportin 1 is the only exportin where Ran-GTP and cargo do not form direct contacts. The reason for this is that cargo binds on the outer surface and Ran-GTP on the inner surface of exportin 1. Coupled binding is therefore mediated by conformational changes of exportin 1 leading to the opening or closing of its cargo binding groove (Fung and Chook, 2014). Dissociation of the exportin 1-cargo-RanGTP complex is dependent on Ran binding protein 1 (RanBP1) which sequesters RanGTP away from the complex leading to subsequent cargo dissociation (Li et al., 2019).

In the human nuclear basket, the nucleoporin NUP50 contains a Ran binding domain and NUP153 contains a zinc finger domain both serving as binding sites for Ran (Lin and Hoelz, 2019). Ran binding of Nup153 might locally tether RanGDP for conversion into RanGTP by Rcc1. This might provide a pool of RanGTP to dissociate importin-cargo binding as Ran cannot bind Nup153 and importin β at the same time (Schrader et al., 2008). Fittingly, Nup153 depletion reduces importin α/β mediated import (Ogawa et al., 2012; Walther et al., 2001). Nup50 also plays a role in the dissociation of importin-cargo complexes (Lindsay et al., 2002; Makise et al.,

2012; Matsuura and Stewart, 2005). The cytoplasmic filament nucleoporin RANBP2 also has Ran binding domains and zinc finger domains homologous to the ones in NUP153 (Lin and Hoelz, 2019). The Ran binding domains bind both RanGTP and RanGDP with a higher affinity for RanGTP and the zinc finger domains solely bind RanGDP (Yaseen and Blobel, 1999). RanBP2 in conjunction with RanBP1 mediates efficient RanGTP hydrolysis to RanGDP by dissociating RanGTP from karyopherin complexes (Beddow et al., 1995; Bischoff et al., 1995; Vetter et al., 1999). Furthermore, RanBP2 provides an anchoring site for RanGAP1 and binding of RanGAP1 to RanBP2 is dependent on RanGAP1 SUMOylation (Mahajan et al., 1997; Reverter and Lima, 2005). Thus, RanBP2 contributes to RanGTP hydrolysis by RanGAP1. The RanGAP1-RanBP2 interaction has been shown to facilitate exportin-cargo dissociation (Ritterhoff et al., 2016).
In summary, efficiency and tight regulation of active nucleocytoplasmic transport is ensured by the interplay of transport receptors, Ran factors and nucleoporins.

1.4.4 Mechanisms of messenger RNA export

The overall mechanism of messenger RNA (mRNA) export is similar to protein export. However, it does not rely on members of the karyopherin β family and uses ATP as an energy source instead of GTP (Katahira, 2015; Natalizio and Wente, 2013; Niño et al., 2013; Stewart, 2010; Valkov et al., 2012). The nuclear RNA export factor 1:NTF2-related export protein 1 (NXF1:NXT1) complex acts as the general mRNA transport receptor (Grüter et al., 1998; Hurt et al., 2000). Upon processing and maturation mRNAs are bound by the TREX and/or TREX2 complex (Cheng et al., 2006; Ellisdon et al., 2012; Jani et al., 2012, 2009; Masuda et al., 2005; Sträßer et al., 2002; Zhou et al., 2000). TREX is recruited to mRNAs by splicing factors (Masuda et al., 2005). RNAs coupled to TREX/TREX2 and additional factors diffuse through interchromatin space or zones of heterochromatin exclusion in the nucleoplasm towards nuclear pore complexes (Ben-Ari et al., 2010; Politz et al., 1999; Shav-Tal et al., 2004). Nuclear basket nucleoporin Translocated promoter region (TPR) is involved in the formation of these heterochromatin exclusion zones (Krull et al., 2010). TREX2 interaction with the nuclear pore also requires TPR (Umlauf et al., 2013; Wickramasinghe et al., 2014). Interestingly, mRNA translocation to the nuclear pore requires several minutes whereas the passage

through the nuclear pore takes less than 500 milliseconds (Mor et al., 2010; Oeffinger and Zenklusen, 2012; Sheinberger and Shav-Tal, 2013). RNAs are transferred from the TREX/TREX2 complex to the NXF1:NXT1 complex (Wickramasinghe and Laskey, 2015). NXF1 binding to TREX components increases its affinity towards RNA (Hautbergue et al., 2008). As the NXF1:NXT1 complex binds all mRNAs, selectivity is mediated by different members of the TREX/TREX2 complex (Wickramasinghe and Laskey, 2015) . The NXF1:NXT1 complex translocates mRNAs through the nuclear pore by interacting with FG nucleoporins (Bachi et al., 2000; Fribourg et al., 2001; Grant et al., 2002) The NXF1:NXT1-RNA complex is dissociated by ATP-dependent RNA helicase Dead box protein 5 (DBP5) in the cytoplasm. This process is catalysed by DBP5's ATPase activity and is regulated by its interaction partners cytoplasmic filament nucleoporin GLE1, small signalling molecule inositol hexakisphosphate (InsP6) and cytoplasmic filament nucleoporin NUP214 (Alcázar-Román et al., 2006; Folkmann et al., 2011; Hodge et al., 2011; Montpetit et al., 2011; Noble et al., 2011; von Moeller et al., 2009; Weirich et al., 2006). The mRNAs can now be translated. Like protein transport mRNA export is a tightly regulated process ensuring that only mature mRNA molecules are transported to the translation machinery.

In summary, nucleocytoplasmic transport is of indispensable importance to the cell being the main route of information exchange between cytoplasmic and nuclear cellular activities allowing for responses to environmental changes and functional requirements. Shuttling proteins include transcription factors, hormone receptors, RNA binding proteins and cytoskeletal proteins regulating a wide range of cellular mechanisms such as differentiation, proliferation, synapse to nucleus signalling and immune response (Fu et al., 2018; Jordan and Kreutz, 2009; Korwek et al., 2016; Kumeta et al., 2012; McKinsey et al., 2000; Molenaar and Weeks, 2018).

1.5 Nucleocytoplasmic transport defects in ALS/FTD

Being such a vital part for cell function nucleocytoplasmic transport is also affected in ALS/FTD and neurodegeneration in general. As will be introduced in this section dysfunction can be related to all nucleocytoplasmic transport factor types, namely transport receptors, nucleoporins and Ran factors. A strong indication that nucleocytoplasmic transport is impaired in ALS/FTD is the cytoplasmic

mislocalisation of RNA binding proteins TDP43 and FUS observed in pathological post-mortem tissue in the majority of cases, as described above.

1.5.1 Impairments of nucleocytoplasmic transport in different types of ALS/FTD

One example of a very direct impairment of a nucleocytoplasmic transport factor in ALS is the detection of mutations in the cytoplasmic filament nucleoporin gene *GLE1* in ALS patients. A missense mutation leading to an incorporation of a premature stop codon leads to reduced RNA expression and stability. GLE1 proteins containing a splice site mutation show reduced localisation to the nuclear pore and enhanced localisation to the cytoplasm compared to wildtype proteins when transfected into a human cell line (Kaneb et al., 2015). As GLE1 plays a role in mRNA export (as described in section 1.4.4) mutations might cause disease by a loss of protein function at the nuclear pore. Cytoplasmic GLE1 is involved in translation and stress granule assembly (Aditi et al., 2015), hence enhanced cytoplasmic mutant GLE1 might also lead to pathology via toxic gain of function.

As described in sections 1.1.2 and 1.1.3 *FUS* mutations are often localised in its NLS thereby reducing binding of its import receptor transportin 1 which results in FUS being mislocalised to the cytoplasm (Dormann et al., 2010; Neumann et al., 2011). In FTD transportin 1 is found in FET (FUS, EWS, TAF15) inclusions likely due to its enhanced FET binding mediated by hypomethylation of FET proteins (Dormann et al., 2012; Suárez-Calvet et al., 2016). It is unclear, however, whether this altered transportin 1 interaction with FUS leads to its mislocalisation or is protective. Furthermore, the nuclear cytoplasmic Ran ratio was reduced in mutant *FUS* patient iPSC-derived motor neurons compared to isogenic controls. The mutant *FUS* cells also exhibited decreased staining of nucleoporins pore membrane 121 (POM121) and NUP62 at the nuclear membrane compared to controls. These findings were accompanied by lower levels of active nuclear import of a reporter cargo. Mutant FUS was also shown to interact with FG nucleoporins including NUP62 in the cytoplasm of mutant *FUS* patient iPSC-derived motor neurons. Knockdown of *Nup62* in a mutant *FUS* Drosophila model reduces toxicity indicating that mutant FUS NUP62 interactions might contribute to pathology (Lin et al., 2021). Another study found reduced nuclear membrane NUP62 also in motor neurons of mutant *FUS* ALS patient spinal cord (Aizawa et al., 2022).

In salivary glands of a mutant *TARDBP Drosophila* model decreased nuclear levels and cytoplasmic mislocalisation of importin α3 were detected (Solomon et al., 2018). Models of TDP43 aggregation showed that transport factors were recruited into these aggregates. In an immunoprecipitation experiment using a neuroblastoma cell line overexpressing TDP43 C-terminal fragment (CTF) causing the formation of CTF aggregates, transport receptors and nucleoporins (including all FG nucleoporins of the central channel) interacted with the TDP43 CTF aggregates. In primary cortical neurons over-expression of TDP43 CTF also resulted in the formation of cytoplasmic FG nucleoporin aggregates which colocalised with TDP43 CTF. These cells also showed reduced active nuclear import of a reporter cargo compared to control cells (Chou et al., 2018). In a separate study, the formation of cytoplasmic TDP43 droplets was induced by treating a neuroblastoma cell line with FUS fibrils. After 15 days to a month RanGAP1, Ran, NUP107, NUP62 and importin α formed cytoplasmic puncta and NUP62 and importin α also colocalised with cytoplasmic TDP43 droplets (Gasset-Rosa et al., 2019). Furthermore, mutant *TARDBP* ALS patient iPSC-derived motor neurons exhibited cytoplasmic mislocalisation of FG nucleoporins. Active nuclear translocation of a reporter cargo was also decreased in mutant *TARDBP* ALS patient fibroblasts. In addition, in TDP-ALS motor cortex staining of inner ring NUP205 was largely reduced compared to control cases and NUP205 formed cytoplasmic inclusions which occasionally colocalised with phospho-TDP43 (Chou et al., 2018). In FTLD-TDP frontal cortex, soluble importin α3 levels were reduced compared to control cases and importin α3 was depleted from the nucleus (Solomon et al., 2018). Furthermore, levels of importin α1 and its transport receptor Cellular apoptosis susceptibility protein (CAS) were reduced in FTLD-TDP patient brain compared to control brain (Nishimura et al., 2010).

In lumbar spinal anterior horn cells of a mutant *SOD1* mouse model, importin β and α1 showed reduced nuclear and enhanced cytoplasmic staining as well as a partial loss of NUP62 staining at the nuclear membrane compared to wildtype mice (Kinoshita et al., 2009; Nagara et al., 2013; Zhang et al., 2006). Progressive nuclear mislocalisation of RanGAP1 and nucleoporins GP210, NUP205, NUP107 and NUP50 was observed in spinal cord motor neurons of a mutant *SOD1* mouse model compared to wildtype (Shang et al., 2017). Irregular NUP62 staining was also observed in SOD1-ALS patient lumbar spinal anterior horn cells (Kinoshita et al., 2009) but this might also just be due to misshaped nuclei in patients.

Primary neurons expressing mutant *PFN1* and mutant *PFN1* ALS patient-derived lymphoblasts depicted irregular staining of FG nucleoporins and RanGAP1 at the nuclear membrane compared to controls. These cells also exhibited enhanced cytoplasmic nuclear ratios of Ran compared to controls. Active nuclear import of a reporter cargo was decreased in primary neurons expressing mutant *PFN1* in comparison to control cells (Giampetruzzi et al., 2019) This suggests that the changes in nucleoporin and Ran factor localisation detected in *PFN1* mutant cells impair active nucleocytoplasmic transport.

Widespread mislocalisation of nucleocytoplasmic transport factors was also observed in sporadic ALS. Levels of importin α7 were reduced and importin α1 was enhanced in sporadic ALS spinal cord compared to control tissue (Nishimura et al., 2010). A loss of nuclear importin β in conjunction with cytoplasmic mislocalisation was observed in spinal cord motor neurons of sporadic ALS patients compared to controls (Aizawa et al., 2019; Kinoshita et al., 2009; Nagara et al., 2013). RanGAP1 was mislocalised to the cytoplasm in sporadic ALS spinal cord motor neurons (Shang et al., 2017). Nucleoporins NUP62 and NUP153 exhibited irregular nuclear membrane staining with NUP62 staining occasionally being lost in sporadic ALS patient spinal cord (Aizawa et al., 2019; Kinoshita et al., 2009; Nagara et al., 2013; Yamashita et al., 2017). Again, the irregular staining pattern might be owed to a general misshape of nuclei in sporadic ALS patients. Nucleoporins NUP205, NUP50 and GP210 were mislocalised to the cytoplasm and NUP205 staining was reduced in sporadic ALS patient spinal cord motor neurons in comparison to control spinal cord (Chou et al., 2018; Shang et al., 2017). Sporadic ALS patient fibroblasts also showed decreased active nuclear import of reporter cargo compared to control cells (Chou et al., 2018).

Overall, a variety of transport factors are mislocalised in different types of ALS/FTD often accompanied with defects in active nucleocytoplasmic transport. This indicates that nucleocytoplasmic transport impairments are a common feature in ALS/FTD.

1.5.2 Nucleocytoplasmic transport disruptions in *C9ORF72* ALS/FTD

A substantial notion that nucleocytoplasmic transport might be implicated in *C9ORF72* ALS/FTD pathology came from modifier studies. A number of screens have been performed identifying enhancers and suppressors of pathology in yeast

expressing poly-PR, *Drosophila* expressing poly-GR, poly-PR or pure GGGGCC repeats, a human cell line treated with poly-GR or -PR peptides and mouse cortical neurons treated with poly-PR peptides or expressing poly-PR. In all these screens, genes associated with nucleocytoplasmic transport such as nucleoporins, transport receptors and factors involved in the Ran cycle have an effect on *C9ORF72* mutation mediated toxicity. Genes detected in more than one screen include transport receptors *Transportin 1*, *Importin 11*, and *Exportin 1*, FG repeat containing nuclear basket *NUP50*, outer ring *NUP107* and Ran cycle regulators *RCC1* and *RanGAP1*. *Transportin 1*, *Exportin 1* and *RanGAP1* seem to have a protective effect while reduced *NUP107* expression seems to suppress toxicity. *Importin 11*, *RCC1* and *NUP50* effects differ among studies suggesting a dual role or different roles in different organisms for these genes (Boeynaems et al., 2016; Freibaum et al., 2015; Jovičić et al., 2015; Kramer et al., 2018; Lee et al., 2016; Zhang et al., 2015). Furthermore, interactome studies showed that poly-GR and -PR interact with transport receptors, nucleoporins and components of the Ran cycle (Boeynaems et al., 2017; Hayes et al., 2020; Lee et al., 2016; Y. Lin et al., 2016).

Further studies indicated that nucleoporin localisation to the nuclear pore is affected in *C9ORF72* ALS/FTD. In salivary gland cells of a *Drosophila* model expressing the *C9ORF72* repeat expansion outer ring Nup107 formed nuclear inclusions (Freibaum et al., 2015a). The localisation of FG nucleoporins was not changed in a *Drosophila* model expressing poly-GR or -GA compared to control flies, however (Solomon et al., 2018).

In the cortex of mice expressing poly-GA in the brain, the transmembrane nucleoporin POM121 co-localised with GA in inclusions. Mice expressing the *C9ORF72* repeat expansion in the brain also showed cytoplasmic and nuclear POM121 inclusions in the cortex (Zhang et al., 2016). FG nucleoporins including NUP98 localised to GR inclusions in the cortex of a mouse model expressing poly-GR in the brain (Cook et al., 2020). In line with this, in mice ubiquitously expressing poly-GR FG repeat containing NUP62 and NUP98 nuclear membrane staining was reduced compared to control mice and the nucleoporins formed cytoplasmic punctae in the spinal cord (Gleixner et al., 2022). In the cortex of mice expressing poly-PR in the brain, FG nucleoporins localised to nuclear invaginations and occasionally colocalised with PR inclusions (Y. J. Zhang et al., 2019).

C9ORF72 ALS iPSC-derived neurons have also exhibited pathology, including reduced nuclear NUP62 staining and cytoplasmic NUP62 punctae compared to isogenic controls (Gleixner et al., 2022) . Another in-depth study investigated isolated nuclei of *C9ORF72* ALS patient iPSC-derived spinal neurons with high resolution microscopy. They found that transmembrane nucleoporins POM121, glycoprotein 210 (GP210) and Nuclear division cycle 1 (NDC1), FG repeat and nuclear basket NUP50 and TPR, FG containing NUP98 and outer ring NUP107 and NUP133 were reduced in these nuclei compared to control nuclei. The same nucleoporins, except for GP210, were also reduced in neuronal nuclear protein (NeuN) positive nuclei isolated from *C9ORF72* patient motor cortex and, except for GP210 and NUP98, in spinal cord compared to control tissue (Coyne et al., 2020). Inner ring NUP205 was also found to be mislocalised to the nucleus (instead of sole nuclear membrane localisation) in *C9ORF72* ALS patient motor cortex (Zhang et al., 2015) while NUP205 formed cytoplasmic punctae in another study in the same tissue (Chou et al., 2018). In *C9ORF72* ALS/FTD patient spinal cord and hippocampus central channel NUP62 colocalised with phospho-TDP43 in the cytoplasm (Gleixner et al., 2022) .

A number of studies give indications about the mechanism of nucleoporin mislocalisation. Poly-PR was shown to directly interact with FG domains of Nup54 and Nup98 *in vitro* (Shi et al., 2017) which might contribute to mislocalisation *in vivo*. In a human cell line over-expressing poly-GR, NUP62 localised to cytoplasmic GR inclusion. These inclusions also stained positive for TDP43, stress granule markers and RNA, a characteristic of mature stress granules (Gleixner et al., 2022) . This could indicate that nucleoporins are recruited into DPR induced stress granules. Indeed, in another study nucleoporins were shown to be recruited into stress granules upon oxidative stress (K. Zhang et al., 2018). In the iPSC nuclei study mentioned above, reduction of nucleoporins seemed to be caused by repeat RNA rather than by DPRs or *C9ORF72* haploinsufficiency as these changes could only be caused by over-expression of *C9ORF72* repetitive RNA but not of DPRs (Coyne et al., 2020). This was possibly mediated by enhanced nuclear expression of endosomal sorting complex protein Charged multivesicular body protein 7 (CHMP7) involved in nuclear pore homeostasis. Over-expression of a nuclear export deficient version of CHMP7 in control iPSC-derived neurons mimicked the nucleoporin loss observed in *C9ORF72* iPSC-derived neurons (Coyne et al., 2021).

Transporter receptor function is also impaired in *C9ORF72* ALS/FTD. Poly-GR and -PR peptides but not any other DPR species directly bind importin β1 *in vitro* (Hayes et al., 2020; Hutten et al., 2020). These DPRs also displace importin β1 from its cargo with PR showing higher relative selectivity for importin β1 than GR (Hayes et al., 2020). Furthermore, poly-GR and -PR but not poly-GP were shown to directly interact with importins 5, 7 and 9, transportins 1 and 3 and solely poly-GR bound to importins α1 and α3 (Hutten et al., 2020). These interactions might interfere with active nucleocytoplasmic transport as impairments of this pathway were detected in multiple cell models. In simple immunofluorescence experiments the localisation of reporter cargos imported via the importin α/β pathway was more cytosolic in cell lines expressing poly-GR, -PR or GGGGCC repeats, or *C9ORF72* ALS patient fibroblasts compared to control cells (Chou et al., 2018; Ortega et al., 2020; K. Zhang et al., 2018). More reporter cargo being present in the cytoplasm would suggest reduced active nuclear import of this cargo. In addition, a reporter cargo containing the NLS of TDP43 (which is also transported by importin α/β) localised more strongly to the cytoplasm in a human cell line expressing poly-GA compared to control cells. However, in another study poly-GR and -PR expression did not change the localisation of this reporter cargo in comparison to controls (Khosravi et al., 2017). In line with this finding, treatment with or expression of poly-GR or -PR in human cell lines or control iPSC-derived motor neurons had no effect on importin α/β mediated nuclear translocation of reporter cargo upon nuclear export inhibition compared to controls, whereas expression of poly-GA in control iPSC-derived motor neurons did reduce nuclear import compared to controls. Export of reporter cargo via exportin 1 was not affected either by poly-GR or -PR treatment in a human cell line compared to control cells (Vanneste et al., 2019). In a separate study, cytoplasmic poly-GA expression (via coupling to an NES) reduced cytoplasmic localisation of a reporter cargo which was solely cytoplasmic in control cells. This would suggest a decrease in nuclear export via exportin 1 upon poly-GA expression. Upon export inhibition nuclear localisation of importin α/β reporter cargo was decreased in cells cytoplasmically expressing poly-GA in comparison to controls. Conversely, nuclear expression of poly-GA had no effect on exportin 1 mediated export or importin α/β mediated import (Frottin et al., 2021). Hence, experiments investigating reporter cargo localisation in fixed cells give conflicting results upon poly-GR and -PR effects on active nuclear import. Importantly, in experiments following nuclear translocation

live, poly-GR and -PR peptides but not any other DPR species decreased importin α/β mediated nuclear import of reporter cargo in human cell lines (Hayes et al., 2020; Hutten et al., 2020; Shi et al., 2017). Also, primary cortical neurons expressing the *C9ORF72* repeat expansion and *C9ORF72* ALS iPSC-derived neurons showed reduced nuclear translocation of importin α/β reporter cargo compared to control cells (Giampetruzzi et al., 2019; Zhang et al., 2015). Importin β and transportin 1 mediated nuclear import of reporter cargo was decreased in cells treated with poly-GR or PR but not with any other DPRs compared to untreated cells (Hayes et al., 2020). Nuclear import of reporter cargo containing full length TDP43, which is also imported via importin α/β, was lowered in cells treated with poly-GR but not upon poly-GP or PR-treatment compared to controls (Hutten et al., 2020). This indicates that nuclear import inhibition of TDP43 might be mediated via poly-GR binding to importin α. Live experiments clearly support the hypothesis of active nuclear import inhibition by arginine containing DPRs. Nuclear RNA levels were also enhanced in a human cell line expressing *C9ORF72* repeat RNA or the repeat expansion, in salivary gland cells of *Drosophila* expressing *C9ORF72* repeats, and in C9ORF72 patient fibroblast or iPSC-derived cortical neurons (Chou et al., 2018; Freibaum et al., 2015a; Frottin et al., 2021). This would suggest additional RNA export reduction in *C9ORF72* ALS/FTD.

Import receptors were mislocalised in *C9ORF72* ALS/FTD models which might contribute to transport defects. In a human cell line expressing poly-GA and in salivary glands of Drosophila models expressing poly-GR or -GA importins α1 and α3 formed cytoplasmic punctae (Frottin et al., 2021; Solomon et al., 2018). Importin α1 and α5 also localised to GR inclusions in the cortex of a mouse model expressing poly-GR in the brain (Cook et al., 2020). Nuclear depletion and cytoplasmic accumulation of importin α3 was detected in *C9ORF72* FTD patient frontal cortex. This cytoplasmic importin α3 staining also occasionally overlapped with phospho-TDP43 and poly-GR, -PR and -GA staining (Solomon et al., 2018). In *C9ORF72* ALS patient spinal motor neurons staining of importin β1 was reduced compared to control cases (Xiao et al., 2015). However, in a quantitative histopathology study no difference in the importin β1 staining pattern was detected between *C9ORF72* ALS patient motor neurons in spinal cord and motor cortex and control motor neurons in the same tissues (Saberi et al., 2018). Thus, transport receptor mediated nucleocytoplasmic transport is impaired in *C9ORF72* ALS/FTD possibly by

mislocalisation of transport receptors and a reduction of their interaction capacity with the nuclear pore.

The Ran gradient is also affected by the *C9ORF72* mutation. The nuclear cytoplasmic ratio of Ran was reduced in *Drosophila* S2 cells or a human cell line expressing the *C9ORF72* repeat expansion, in human cell lines expressing poly-GR and in C9ORF72 ALS patient iPSC-derived neurons (Coyne et al., 2020; J. Lee et al., 2020; P. T. Lee et al., 2020; Zhang et al., 2015). Ran also formed cytoplasmic punctae in cells expressing poly-GR or -PR which colocalised with the stress granule marker ataxin 2 (K. Zhang et al., 2018). RCC1, which catalyses the conversion of RanGDP to RanGTP in the nucleus, was decreased in the nucleus of *C9ORF72* ALS patient induced neurons compared to control neurons. However, the localisation of RANGAP1, which catalyses RanGTP hydrolysis in the cytoplasm, was not changed in these cells (Jovičić et al., 2015). Rangap1 staining did not differ in salivary gland cells of *Drosophila* expressing poly-GR or -GA compared to control flies, either (Solomon et al., 2018). However, in the cortex of mice expressing poly-GA or GGGGCC repeats in the brain RANGAP1 formed nuclear and cytoplasmic inclusions which colocalised with poly-GA in the GA mouse model (Zhang et al., 2016). In a mouse model expressing poly-PR in the brain RANGAP1 occasionally colocalised with PR inclusions in the cortex (Y. J. Zhang et al., 2019). In contrast, cortical RANGAP1 staining did not differ between mice expressing poly-GR in the brain and control mice (Y. J. Zhang et al., 2018). Patient tissue studies showed reduced staining of RANGAP1 in *C9ORF72* ALS patient spinal motor neurons compared to control cases and nuclear mislocalisation and aggregation of RANGAP1 in *C9ORF72* ALS patient motor cortex (Zhang et al., 2015). However, RANGAP1 localisation was not altered between *C9ORF72* ALS patient motor neurons in spinal cord and motor cortex and control neurons in a quantitative study (Saberi et al., 2018). Hence, it is unclear whether RANGAP1 is affected and contributes to nucleocytoplasmic transport impairments in *C9ORF72* ALS/FTD.
In summary, there is clear evidence of active nucleocytoplasmic transport impairment in *C9ORF72* ALS/FTD with likely implications of nucleoporins, transport receptors and Ran. Due to the vital contribution of nucleocytoplasmic transport to cellular function this likely contributes to disease pathology, particularly in relation to the cytoplasmic mislocalisation of TDP-43.

1.6 Thesis aims

Active nucleocytoplasmic transport has been quite extensively studied in the context of *C9ORF72* ALS/FTD as described above. However, passive nucleocytoplasmic transport and the role of the nuclear pore and its permeability barrier in *C9ORF72* pathology has not been systematically investigated. As this permeability barrier ensures segregation and integrity of nuclear and cytoplasmic compartments, a disturbance of this system could potentially have detrimental effects to cellular function and viability. Therefore, the aims of my thesis were the following:

- **Analysis of passive nucleocytoplasmic defects in *C9ORF72* ALS/FTD**. To this end, I optimised a quantitative passive nucleocytoplasmic transport assay for live cell confocal imaging (chapter 3). This allowed for a study of passive nuclear import of fluorescent reporter cargo of different sizes in cells treated with *C9ORF72* DPRs. The effects of *C9ORF72* DPRs on passive TDP43 export were also evaluated in an immunofluorescence study (chapter 4).

- **Investigation of mechanisms of passive nucleocytoplasmic transport impairments by DPRs**. For this purpose, I compared the effects of a) a known permeability barrier modulator on passive nucleocytoplasmic transport with the effects of DPRs and b) the role of nucleic acids in nuclear cargo retention. Furthermore, I analysed the effects of *C9ORF72* DPRs on the localisation of various nucleocytoplasmic transport factors in a high-throughput immunofluorescence study (chapter 5).

- **Rescue of passive nucleocytoplasmic transport deficiency caused by DPRs**. I aimed to rescue passive nucleocytoplasmic transport deregulation, thus, studied the effects of components known to interact with FG nucleoporins on passive nucleocytoplasmic transport in the presence of DPRs (chapter 5).

- **Study of disease relevance of passive nucleocytoplasmic transport defects**. I performed live passive nucleocytoplasmic transport confocal

imaging studies in *C9ORF72* ALS iPSC-derived neurons and in control iPSC-derived neurons treated with arginine containing DPRs. Furthermore, I investigated the localisation of nucleoporins, importins and Ran in *C9ORF72* ALS iPSC-derived neurons conducting a high-throughput immunofluorescence study (chapter 6).

2 Materials and methods

2.1 HeLa cell culture

2.1.1 HeLa cell culture and passage

HeLa cells were cultured in complete media consisting of DMEM, high glucose with GlutaMAX (ThermoFisher Scientific, #61965026) which was supplemented with 10 % fetal bovine serum (Supreme, South America, Pan Biotech, #P30-3031), 1 % sodium pyruvate (100 mM, ThermoFisher Scientific, #11360039), 1 % non-essential amino acids (100x, ThermoFisher Scientific, #11140035) and 1 % penicillin-streptomycin (10,000 U/ml, ThermoFisher Scientific, #15140122). Cells were typically grown in cell culture treated 75 cm^2 flasks (Nunc™ EasYFlask™, ThermoFisher Scientific, #156499) and were incubated at 37°C, 5 % CO_2.
For passaging, cells were washed with 10 ml DPBS without calcium and magnesium (1x, ThermoFisher Scientific, #14190169) and then treated with 1 ml trypsin-EDTA (0.25 %, ThermoFisher Scientific, #25200072) for 5 minutes at 37°C, 5 % CO_2. Trypsinisation was stopped by adding 10 ml complete media. The flask was rinsed with the added media to detach any cells which still adhered to the flask and then cells were transferred into a 15 ml tube. Cells were centrifuged at 300 x *g* for 5 minutes. The supernatant was aspirated to remove the trypsin and cells were resuspended in an appropriate volume of complete media (e. g. 10 ml for a 1:10 split). The desired volume of the cell suspension was transferred to a flask containing 25 ml complete media. The flask was tilted a few times to spread the cells evenly and then incubated at 37°C, 5 % CO_2. Typically, cells were passaged every 3-4 days.

2.1.2 Cryopreservation of HeLa cells

Cells of a low passage were cryopreserved for long term storage in liquid nitrogen. Cells were trypsinised and centrifuged as described above and then resuspended in complete media containing 10 % DMSO (Hybri-Max™, Sigma-Aldrich, #D2650). Cells were transferred into cryovials and then stored in freezing containers (Nalgene® Mr. Frosty, Sigma-Aldrich, #C1562 or Corning®CoolCell™ Freezer Container, Sigma-Aldrich, #CLS432000) at -70°C. After 48 hours cells were transferred into liquid nitrogen for long term storage.

2.1.3 Thawing of HeLa cells

To revive cryopreserved cells, vials were quickly thawed at 37°C and then cells were transferred to a 15 ml tube. 8 ml complete media was added dropwise, and the tube was gently shaken during the media addition to reduce the osmotic shock to the cells. Cells were centrifuged at 300 x *g* for 5 minutes. The supernatant was aspirated, cells were resuspended in 8 ml complete media and were transferred to a 75 cm^2 flask containing 17 ml complete media (25 ml total volume). Cells were then incubated at 37°C, 5 % CO_2.

2.1.4 Poly-L-lysine coating

For cell membrane permeabilisation experiments (see below) HeLa cells were grown on poly-L-lysine (0.01 %, Sigma-Aldrich, #P4707 or #P6282) coated 8-well (ibidi, #80806) or 96-well (Perkin Elmer, #6055302) imaging plates. 8-well and 96-well plates were coated with 200 µl and 80 µl poly-L-lysine solution, respectively and incubated for 1 hour at room temperature. Plates were then washed three times with sterile dH_2O, left to dry in the tissue culture safety cabinet and were then directly used for cell plating.

2.1.5 HeLa cell plating

To plate HeLa cells for cell membrane permeabilisation experiments, cells were trypsinised and centrifuged as described above. The cell pellet was resuspended in a suitable volume (typically 5 ml per 75 cm^2 flask) of complete media. To count the cells, 100 µl of the cell suspension were transferred to an Eppendorf tube and mixed with 100 µl trypan blue stain (0.4 %, Sigma-Aldrich, #T8154 or NanoEnTek, #EBT-001) to detect dead cells. 10 µl of this solution was placed into each chamber of an EVE™ cell counting slide (NanoEnTek, #EVS-050) and cells were counted using a Countess® II FL automated cell counter (ThermoFisher Scientific). 1.5-2x10^4 cells in 400 µl complete media were plated per 8-well and 0.75-1x10^4 cells in 200 µl complete media were used per 96-well.

2.2 Induced pluripotent stem cell (iPSC) culture

2.2.1 iPSC lines

ID	ID in thesis	Sex	Genotype	Age of onset/ Age	Survival (months)	Diagnosis	Type	Number of repeats	Original sample	Reprogramming method
ORF3R1	*C9ORF72* line #1	female	C9ORF72	39	31	ALS/FTD	FALS	~760	fibroblasts	Retrovirus
M211R2	*C9ORF72* line #2	male	C9ORF72	65	68	ALS	FALS	~960	fibroblasts	Retrovirus
DN19V4	*C9ORF72* line #3	male	C9ORF72	58	N/A	ALS	SALS	~638	fibroblasts	Retrovirus
M104	Control line #1	male	-	40s	-	control	-		keratinocytes	Lentivirus
M315	Control line #2	male	-	40s	-	control	-		keratinocytes	Sendai virus
C0070	Control line #3	female	-	52	-	control	-		lymphoblasts	Sendai virus

Table 2.1: Description of iPSC lines used in this PhD project.

All iPSC lines were provided to me by Agnes Nishimura of the Shaw group in our department. Lines ORF3R1, M211R2 and DN19V4 were initially obtained from the Chandran group at the University of Edinburgh. Dermal fibroblasts from patient individuals to create these lines were obtained under full Ethical/Institutional Review Board approval at the University of Edinburgh. Lines M211R2 and DN19V4 were characterised by the Chandran group and contain RNA foci and express poly-GP, -GR and -GA (Selvaraj et al., 2018). The ORF3R1 line was characterised by Agnes Nishimura and team and contains RNA foci and expresses poly-GP. The M104 and M315 lines were created and characterised by Graham Cocks at the Price group at King's College London (Deans et al., 2017). Donors for these lines were recruited, and methods were carried out in accordance to the "Patient iPSCs for Neurodevelopmental Disorders (PiNDs) study" (REC no. 13/LO/1218). Informed consent was obtained from all subjects for participation in the PiNDs study. Ethical approval for the PiNDs study was provided by the National Health Service (NHS) Research Ethics Committee at the South London and Maudsley NHS R&D Office. The C0070 line was created and characterised by Agnes Nishimura and team. Lymphoblasts were obtained from blood donated to the European Collection of Authenticated Cell Cultures.

2.2.2 Induced pluripotent stem cell (iPSC) culture and passage

IPSCs were grown in Essential 8™ Flex (E8 Flex) media (ThermoFisher Scientific, #A2858501) with 1 % antibiotic antimycotic solution (100x, Sigma-Aldrich, #A5955) and were incubated at 37°C, 5 % CO_2, 5 % O_2. Cells were typically grown on Geltrex™ coated (see below) 6-well plates (Nunc™, ThermoFisher Scientific, #140675).

To split cells, media was aspirated and 1 ml EDTA (Versene®, 0.02 %, Lonza, #BE17-711E or GibcoTM, #15040066) was added to each well. Detachment of cells was observed under a phase contrast light microscope. Once cells sufficiently detached (not exceeding a 10-minute incubation time) EDTA was aspirated, and the well was rinsed with 3 ml E8 Flex media to detach colonies. The size of the cell clumps was observed under the microscope and if necessary, they were broken up into smaller clumps using a P1000 pipette (avoiding creating a single cell suspension). Cells were transferred to new 6-wells (0.5 ml cell suspension per well) containing 3 ml fresh E8 Flex media. Plates were moved back and forth to spread cells and were carefully transferred to the incubator. Typically, cells were split every three days, but this was dependent on cell line and confluency. Cells were fed with fresh E8 Flex media every two days.

2.2.3 Cryopreservation of iPSCs

For long term storage iPSCs were cryopreserved in liquid nitrogen. Cells were detached with EDTA as described above and wells were rinsed with E8Flex media containing 10 % DMSO (Hybri-Max™, Sigma-Aldrich, #D2650). Cell clumps were broken up as necessary and then transferred into cryovials which were incubated at -70°C in freezing containers (as described above). After 48 hours cells were moved to liquid nitrogen.

2.2.4 Thawing of iPSCs

Cells were thawed at room temperature and then transferred carefully to a 15 ml tube containing 1 ml E8 Flex media with 1x RevitaCell™ supplement (100x, ThermoFisher Scientific, #A2644501). Cells were centrifuged at 235 x *g* for 4 minutes. The supernatant was aspirated, and the bottom of the tube was gently tapped to break up the pellet but keeping the colonies intact. 1.5 ml of E8 Flex media with 1x RevitaCell™ supplement was slowly added, and cells were transferred to a

Geltrex™ coated 6-well plate containing 1 ml E8 Flex media with 1x RevitaCell™ per well. The plate was moved back and forth and side to side to disperse cells and was then carefully transferred to the incubator.
The following day media was changed to E8 Flex media (without RevitaCell™) except if confluency was very low and colonies were very small.

2.2.5 Geltrex™ coating

IPSCs and neural progenitors were grown on Geltrex™ (ThermoFisher Scientific, #A1413302) coated cell culture 6-well plates. A Geltrex™ aliquot was slowly thawed on ice and then diluted 1:100 in cold DMEM/F12 media with GlutaMAX™ supplement (ThermoFisher Scientific, # 31331028). Plates were coated with 1.5 ml Geltrex™ solution per 6-well and stored at 37°C for a minimum of 2 hours and a maximum of 2 weeks prior to cell plating. Geltrex™ solution was removed directly prior to cell plating.

2.2.6 Poly-L-ornithine and laminin coating

IPSC-derived cortical neurons were cultured on poly-L-ornithine (0.01 %, Sigma-Aldrich, #P4957) and laminin (Sigma-Aldrich, #L2020) coated 8-well (ibidi, #80806) or 96-well (Perkin Elmer, #6055302) imaging plates. 8-well and 96-well plates were coated with 200 µl and 80 µl poly-L-ornithine, respectively and then incubated over night at 37°C. The following day plates were washed three times with DPBS. Laminin was thawed slowly at 4°C. Plates were subsequently coated with 2 µg/cm^2 laminin in cold DPBS. Plates were then incubated over night at 37°C. Prior to cell plating, plates were washed once with DPBS.

2.3 Differentiating iPSCs into neural progenitor cells and cortical neurons – embryoid body method

2.3.1 Creating embryoid bodies

To make embryoid bodies, E8 Flex media was removed from iPSCs and 1 ml EDTA was added. Dissociation of cells was observed under a phase contrast light microscope. Cells were incubated in EDTA for longer compared to passaging to break up the colonies more substantially. Once cells had sufficiently dissociated EDTA was carefully aspirated and 4 ml of E8 Flex media with 1x RevitaCell™ were added. Cells were broken up into smaller clumps by triturating with a P1000 pipette

using a wet pipette tip to prevent cells from sticking inside the tip. Cells were then transferred onto an uncoated cell culture 6-well plate to form embryoid bodies and were incubated at 37°C, 5 % CO_2.

The following day neural induction was started. Embryoid bodies were transferred to a 15 ml tube and were let to sink by gravity for 2-5 minutes. The supernatant was carefully removed and 4 ml neural induction media 1 (1:1 mix of Neurobasal™ media (ThermoFisher Scientific, #21103049) and DMEM/F12 media with GlutaMAX™ supplement (ThermoFisher Scientific, #31331028) supplemented with, 0.5 % B-27 supplement (50x, ThermoFisher Scientific, #17504044), 0.5 % N-2 supplement (100 x, ThermoFisher Scientific, #17502001), 10 µM SB431542 (Tocris, #1614/1), 2 µM dorsomorphin (Tocris, #3093/10), 1 µM CHIR99021 (Tocris, #4423/10) and 200 µM L-ascorbic acid (Sigma-Aldrich, #A4403)) were added.

Two days after the start of neural induction the media was changed to 4 ml of neural induction media 2 (same components as neural induction media 1 with the addition of 100 nM EC23 (Cambridge Bioscience, #9002073)) as described above. Cells were fed with neural induction media 2 every two days using the method described above.

2.3.2 Neural progenitor cell expansion

Seven days after the start of neural induction, embryoid bodies were transferred to a 15 ml falcon, let to sink by gravity and the media was removed. 1 ml StemPro™ accutase™ (ThermoFisher Scientific, #A1110501) was added and cells were incubated for 10 minutes at room temperature. After the initial 5 minutes the tube was flicked, and cells were triturated using a P1000 pipette containing a wet pipette tip. 1 ml of basic N2B27 media (1:1 mix of Neurobasal™ media and DMEM/F12 media with GlutaMAX™ supplement supplemented with 0.5 % B-27 supplement, 0.5 % N-2 supplement and 200 µM L-ascorbic acid) with 1x RevitaCell™ was added, and cells were centrifuged at 235 x *g* for 4 minutes. The supernatant was carefully removed, cells were resuspended in 3 ml basic N2B27 media with 1x RevitaCell™ and were transferred onto a Geltrex™ coated 6-well plate. Cells were fed with 3-5 ml basic N2B27 media every two days.

2.3.3 Passaging of neural progenitors

Once cells reach 100 % confluency, they were split 1:2 into fresh 6-wells. The media was aspirated and 1 ml of accutase™ was added. Cells were incubated for 10 minutes at room temperature and then 1 ml basic N2B27 media with 1x RevitaCell™ was added. Cells were spun down at 235 x *g* for 4 minutes. The supernatant was aspirated, and cells were resuspended in an appropriate amount of basic N2B27 media with 1x RevitaCell™. Cells were then transferred onto 2 fresh Geltrex™ coated 6-wells.

2.3.4 Freezing of neural progenitors

For long term storage neural progenitors were cryopreserved in liquid nitrogen. Cells were detached using accutase™ and centrifuged as described above. Cells were resuspended in basic N2B27 media with 10 % DMSO and transferred into cryovials. Cells were incubated in freezer containers at -70°C. 48 hours later cells were transferred into liquid nitrogen.

2.3.5 Thawing of neural progenitors

Cells were thawed at room temperature and then transferred into a 15 ml tube containing 1 ml basic N2B27 media with 1x RevitaCell™. Cells were centrifuged at 235 x *g* for 4 minutes. The supernatant was aspirated, and cells were resuspended in an appropriate volume of basic N2B27 media with 1x RevitaCell™. Cells were transferred onto Geltrex™ coated 6-well, 12-well or 24-well plates depending on cell numbers.

2.3.6 Terminal differentiation of neural progenitors into cortical neurons

Cells were dissociated with accutase™ and spun down as described above. Cells were resuspended in basic N2B27 media with 10 µM DAPT (Tocris, #2634/10). Cells were passed through a 40 µm cell strainer into a 50 ml tube to avoid plating cell clumps. Cells were counted as described above. 2-3 x 10^4 cells in 400 µl basic N2B27 media with DAPT per poly-l-ornithine/laminin coated (as described above) 8-well were plated and 1x10^4 cells in 200 µl basic N2B27 media with DAPT per poly-L-ornithine/laminin coated 96-well were used. The media was changed every two days.

After three days in N2B27 media with DAPT, the media was changed to maturation media (basic N2B27 supplemented with 10 ng/ml BDNF (Peprotech, #450-02) and 10 ng/ml GDNF (Peprotech, #450-10)). Cells were fed every two days.

2.4 Differentiating iPSCs into neural progenitor cells and cortical neurons – neural induction kit method

2.4.1 Neural induction

IPSCs were passaged the day prior to neural induction and should be at 15 – 25 % confluency when starting neural induction. The E8 Flex media was aspirated, and 2.5 ml pre-warmed complete neural induction media (Neurobasal™ media supplemented with 1x neural induction supplement (50x, ThermoFisher Scientific, #A1647801) and 1 % antibiotic antimycotic solution) was added. The following day cells were checked for any non-neuronal colonies and if necessary, these colonies were removed using a 10 µl pipette tip. Two days after the start of neural induction the media was replaced with 2.5 ml pre-warmed fresh complete neural induction media. Four and six days post neural induction, cells were fed with 5 ml pre-warmed complete neural induction media. If cells were very confluent the media was also changed on day 5 of neural induction.

2.4.2 Neural progenitor expansion

Seven days after the start of neural induction neural progenitors were harvested. The media was aspirated, and cells were washed with 2 ml DPBS. 1 ml pre-warmed accutase™ was added and cells were incubated at 37°C for 4 minutes until cells were detached. To further dislodge the cells, wells were rinsed with 1 ml DPBS and cells were transferred to a 15 ml tube. The cell suspension was gently triturated to break up cell clumps and cells were passed through a 100 µm cell strainer into a 50 ml tube. Cells were centrifuged at 300 x *g* for 4 minutes. The supernatant was aspirated, and cells were resuspended in 2 ml DPBS and were centrifuged at 300 x *g* for 4 minutes. The supernatant was removed, and cells were resuspended in an appropriate volume (typically 1 ml per 6-well) of pre-warmed neural expansion media (1:1 mix of Neurobasal® media and Advanced™ DMEM/F12 media (ThermoFisher Scientific, #12634010) supplemented with neural induction supplement and 1 % antibiotic antimycotic solution) with 1x RevitaCell™. Cells were counted as described above. $1x10^6$ cells were plated onto each Geltrex™ coated 6-well. Plates were

moved back and forth and side to side to spread cells evenly. The following day the media was changed to neural expansion media (without RevitaCell™).
When cells reached 100 % confluency, they were split 1:2 into new Geltrex™ coated 6-wells. Cells were treated with accutase™ as described above. The well was rinsed with 1 ml DPBS and cells were transferred to a 15 ml tube and centrifuged at 300 x *g* for 4 minutes. The supernatant was aspirated, and cells were resuspended in 2 ml DPBS. Cells were centrifuged at 300 x *g* for 4 minutes. The supernatant was removed, and cells were resuspended in a suitable volume of neural expansion media with 1x Revitacell™ or with 5 µM ROCK inhibitor Y27632 (Sigma-Aldrich, #Y0503). Cells were transferred to Geltrex™ coated 6-well plates and incubated at 37°C, 5 % CO_2.The following day the media was replaced with neural expansion media (without RevitaCell™).

2.4.3 Terminal differentiation of neural progenitors into cortical neurons

Neural progenitors needed to be grown to a passage of 5-10 to be used for terminal differentiation. Media was aspirated and cells were washed with 2 ml DPBS. 1 ml of pre-warmed accutase™ was added and cells were incubated at 37°C for 4 minutes. Wells were rinsed with 1 ml DPBS to fully detach cells and cells were transferred to a 15 ml tube containing 10 ml DPBS. Cells were centrifuged at 200 x *g* for 4 minutes. The supernatant was aspirated, and cells were resuspended in an appropriate volume of neural expansion media. Cells were counted and $3x10^4$ cells in 200 µl neural expansion media were plated per poly-L-ornithine/laminin coated 8-well and $1.5x10^4$ cells in 100 µl neural expansion media per 96-well. The following day the same volume of Complete BrainPhys Neuronal media (BrainPhys Neuronal media (Stemcell Technologies, #05793) supplemented with 1x SM1 supplement (50x, Stemcell Technologies, #05793), 1x N2-A supplement (100x, Stemcell Technologies, #05793), 1 % antibiotic antimycotic solution, 1 mM cAMP (Sigma-Aldrich, #D0627), 0.5 % FBS, 20 ng/ml BDNF, 20 ng/ml GDNF and 200 nM L-ascorbic acid) was added. Cells were incubated at 37°C, 5 % CO2. Half the volume of media was changed every three to four days.

2.4.4 Freezing of neural progenitors

For long term storage neural progenitors were cryopreserved in liquid nitrogen. Cells were dislodged using accutase™, centrifuged and washed with DPBS as described

above (cells were not passed through a cell strainer). Cells were resuspended in neural expansion media with 10 % DMSO and transferred into cryovials. Cells were incubated in freezer containers at -70°C. After 48 hours cells were transferred into liquid nitrogen.

2.4.5 Thawing of neural progenitors

Cryovials were removed from liquid nitrogen and were thawed at 37°C. Cells were gently transferred to a 15 ml tube. The cryovial was rinsed with 1 ml DPBS and the DPBS was added dropwise to the cells in the 15 ml tube and the tube was moved back and forth to reduce osmotic shock. Cells were centrifuged at 300 x *g* for 5 minutes. The supernatant was aspirated and cells were resuspended in a suitable volume (typically 2-3 ml) of pre-warmed neural expansion media with 1x Revitacell™ or with 5 µM ROCK inhibitor Y27632. Cells were transferred onto a Geltrex™ coated 6-well plate and the plate was moved back and forth and side to side to equally disperse cells. Plates were incubated at 37°C, 5 % CO_2. The following day the media was changed to neural expansion media (without Revitacell™ or ROCK inhibitor).

2.5 Passive nucleocytoplasmic transport assay

We adapted a protocol from the Lowe laboratory at University College London as described in chapter 3.The principle of this assay is to permeabilise the cells' plasma membrane using digitonin leaving the nuclear membrane intact (semi-permeabilisation). The cytoplasm contents were then washed out. Fluorescently labelled proteins or fluorescently labelled dextrans (glucose polymers) were then added and their passive transport into the nucleus was followed live via confocal microscopy (see below).

Cells were plated 2 days prior to assay performance (see above). The assay working volume was 200 µl (8-well plates). For the assay cells were washed with 1x DPBS (Gibco, #14190094) once for 5 minutes. Half the volume of DPBS was removed and cells were washed, by adding half the volume of DPBS (to reach the total volume again), four times for 2.5 minutes. The entire volume of DPBS was removed and cells were incubated in 200 µl 1x permeabilisation buffer (50 mM HEPES pH 7.3 (VWR, #J848), 50 mM potassium acetate (Sigma-Aldrich, #P1190), 8 mM magnesium chloride (Sigma-Aldrich, #63064) for 2 minutes. Half the volume of permeabilisation buffer was removed and cells were permeabilised by adding 100 µl

1x permeabilisation buffer supplemented with 100 µg/ml digitonin (Sigma-Aldrich, #D141 or Cambridge Bioscience, #2082-1), 200 µM ATP (Roche, #10519979001), 200 µM GTP (Roche, # 10106399001), 8 mM creatine phosphate (Roche, #10621714001) and 40 U/ml creatine kinase (Roche, #10127566001) for 10 minutes. As only half the volume was added final assay concentrations were half of the values indicated here. Permeabilisation of wells was staggered as timings were critical. Subsequently, cells were washed with 1x transport buffer (20 mM HEPES pH7.3, 110 mM potassium acetate, 5 mM sodium acetate (Sigma-Aldrich, #S2889), 2 mM magnesium acetate (Sigma-Aldrich, #M5661), 2 mM dithiothreitol (Roche, #10197777001)) once for 5 minutes. Half the volume of transport buffer was removed, and cells were washed with half-volume transport buffer twice for 2.5 minutes. Cells were then stained with 2 µM DAPI (Sigma-Aldrich, #D9542) in 1x transport buffer for 15 minutes in the dark. Plates were then moved directly to the microscope (see below).

Cells were treated with the desired compounds as indicated in section 2.6 and in the results section immediately prior to imaging. To study passive import of fluorescently labelled dextrans or GFP, 180 µl transport buffer was removed from a well while the plate was under the microscope. These 180 µl were directly mixed with 20 µl 100 µg/ml FITC 20 kDa (Sigma-Aldrich, #FD20), FITC 40 kDa (Sigma-Aldrich, #FD40), FITC 70 kDa (Sigma-Aldrich, #90718) dextrans or 20 µM GFP (abcam, #ab84191) meaning the final assay concentration was tenfold lower than the values indicated here. Image acquisition was started, and the reporter cargo transport buffer mixture was placed back into the well during image acquisition. Images were taken every 2.5 seconds for 4 minutes.

2.6 Cell treatments

Cells were treated with the following compounds (dependent on experiment) subsequent to the digitonin permeabilisation assay (see section 2.5).

2.6.1 Dipeptide repeat proteins

DPRs were custom synthesised by Cambridge Research Biochemicals and by ThermoFisher Scientific. Fluorescently labelled versions of DPRs were N-terminally labelled with Alexa Fluor 647 by the same companies. Upon receipt, DPRs were

dissolved in molecular biology grade water to create stocks of 10 and 1 mM and were then stored at -80 °C. Sonication for about 5 rounds of 5 seconds was required to dissolve poly-GA. For live imaging experiments, cells were treated with 10 µM DPR in transport buffer for 30 minutes immediately prior to imaging. As only half-volume exchanges were performed as described in section 2.5 a 20 µM DPR solution was added to the cells, hence 100 µl DPR solution was added to cells in 100 µl transport buffer to yield a final assay concentration of 10 µM. Similarly, in immunofluorescence experiments half the final volume of 20 or 100 µM DPR was added to cells in transport buffer for a final assay concentration of 10 or 50 µM as indicated in the results section, respectively. Cells were treated with DPRs for 30 to 120 minutes in immunofluorescence experiments as described in the results section.

2.6.2 Cyclohexanediol

Cells were treated with a final assay concentration of 14 % w/v of 1,2-trans-cyclohexanediol (CHD; Sigma-Aldrich, #141712) in transport buffer for 15 minutes. Half of the final volume of 28 % w/v CHD was added to the cells.

2.6.3 RNAse A and DNAse I

For RNAse A treatment cells were washed once with PBS for 3 minutes after digitonin permeabilisation and transport buffer washes. Cells were then treated with half-volume 2 mg/ml RNAse A (Merck, #10109169001) in PBS for 15 minutes for a final assay concentration of 1 mg/ml. Cells were then incubated in transport buffer for a further 15 – 105 minutes before being fixed as described in section 5.3. For Pyronin Y staining cells were incubated with 10 µM Pyronin Y (Sigma-Aldrich, #P9172) in PBS for 5 minutes instead of DAPI staining within the workflow described in section 2.7.1.

For DNAse I treatment cells were washed once with 5 mM $MgCl_2$ HBSS (Gibco, #14025092) for 3 minutes after digitonin permeabilisation and transport buffer washes. Cells were then incubated with half volume 200 µg/ml DNAse I (Roche, #10104159001) in 5 mM $MgCl_2$ HBSS for 15 minutes. Cells were then kept in transport buffer for a further 15 – 105 minutes before being fixed as indicated in section 5.3.

2.6.4 Wheat germ agglutinin

Cells were treated with half-volume 2 mg/ml wheat germ agglutinin (WGA; Sigma-Aldrich, #L9640) in transport buffer to yield a final assay concentration of 1 mg/ml WGA for 30 minutes. Subsequently cells were treated with DPRs for 2 hours (see also section 5.5).

2.6.5 Importin β1

Importin β1 (Novus Biologicals, #NBP1-78815) was supplied at a concentration of 2.51 µM in 20 mM Tris-HCl buffer (pH 8.0), 1 mM DTT, 30% glycerol, 0.1 M NaCl and was stored in aliquots at -20°C. Cells were treated with 100 nM importin β1 in transport buffer for 1 hour. Importin β1 treatment was performed prior to 30-minute DPR treatment in live imaging experiments and after 1-hour DPR treatment in immunofluorescence experiments (see also section 5.6).

2.7 Immunofluorescence

2.7.1 Immunofluorescence staining

In this study, HeLa cells were always permeabilised with digitonin until the last transport buffer wash (see section 2.5) prior to immunofluorescence staining. As cells were grown on 96-well plates for immunofluorescence experiments the assay working volume was 60 µl. Cells were treated with the desired reagents as indicated in the results section and were then directly fixed with 50 µl 4 % paraformaldehyde (Generon, #04018-1) for 15 minutes. Cells were washed three times with 50 µl 1x PBS, pH 7.4 (Thermo Fisher Scientific, #10010002) for 5 minutes. Subsequently, cells were permeabilised with 50 µl 0.1 % Triton™ X-100 (Sigma-Aldrich, #T8787) for 10 minutes. Cells were washed three times with 50 µl 1x PBS for 5 minutes and then treated with blocking buffer (1 % BSA (Sigma-Aldrich, #B6917) in PBS) for 1 hour. Primary antibodies diluted in blocking buffer as indicated below were added and cells were incubated over night at 4°C. The following day cells were washed three times with 1x PBS for 5 minutes. Secondary antibodies diluted in blocking buffer as indicated below were added and cells were incubated for 1 hour in the dark. Cells were washed twice with 50 µl 1x PBS for 5 minutes and were then stained with 2 µM DAPI in PBS for 15 minutes in the dark. Cells were stored in 100 µl PBS at 4°C for a maximum of 1 week.

Neurons were not permeabilised prior to immunofluorescence staining but the media was removed, and cells were washed once for 5 minutes with 1x PBS. Half the volume of PBS was removed, and cells were fixed in half the volume of 8 % paraformaldehyde/4 % sucrose (Sigma-Aldrich, #S0389) bringing the final concentration to half of the indicated values. The remaining immunofluorescence protocol was performed as described above.

2.7.2 Primary antibodies

Target	Host	Isotype	Source	Product Code	Dilution
Histone H3	mouse	IgG3	Cell Signaling Technology	14269	1:100
hnRNP C1/C2	mouse	IgG1	Santa Cruz Biotechnology	sc-32308	1:100
Importin α1	mouse	IgG2b	Santa Cruz Biotechnology	sc-55538	1:200
Importin α3	rabbit	IgG	Sigma-Aldrich	HPA045500	1:30
Importin β1	mouse	IgG2a	abcam	ab2811	1:500
Lamin B1	rabbit	IgG	abcam	ab16048	1:500
Lamin B1	mouse	IgG1	Proteintech	66095-1	1:500
Mab414	mouse	IgG1	BioLegend	902901	1:500
Map2	chicken	IgY	abcam	ab92434	1:500
Nup98	rabbit	IgG	ThermoFisher Scientific	PA5-87449	1:100
Nup153	mouse	IgG1	BioLegend	906201	1:100
Pom121	rabbit	IgG	Novus Biologicals	NBP2-19890	1:250
Ran	mouse	IgG2a	BD Biosciences	610340	1:50
RanBP2	mouse	IgG1	Santa Cruz Biotechnology	sc-74518	1:50
RanGAP1	mouse	IgG1	Santa Cruz Biotechnology	sc-28322	1:100
RCC1	rabbit	IgG	Sigma-Aldrich	HPA027574	1:50
TDP43	rabbit	IgG	Proteintech	12892-1-AP	1:500

2.7.3 Secondary antibodies

Target	Host	Isotype	Conjugate	Source	Product Code	Dilution
Mouse	Goat	IgG	Alexa Fluor Plus 488	Invitrogen	A32723	1:500
Rabbit	Goat	IgG	Alexa Fluor Plus 488	Invitrogen	A32731	1:500
Mouse	Goat	IgG	Alexa Fluor Plus 555	Invitrogen	A32727	1:500
Rabbit	Goat	IgG	Alexa Fluor Plus 555	Invitrogen	A32732	1:500
Mouse	Goat	IgG	Alexa Fluor Plus 647	Invitrogen	A32728	1:500
Rabbit	Goat	IgG	Alexa Fluor Plus 647	Invitrogen	A32733	1:500
Chicken	Goat	IgG	Alexa Fluor 633	Invitrogen	A21103	1:500

2.8 Imaging

2.8.1 Live imaging on spinning disk confocal microscope

Cells were imaged on a Nikon Eclipse Ti Inverted spinning disk confocal System with a Yokogawa CSU-X1 spinning disk unit and an Andor iXon EMMCD camera. A Plan Apochromat 40x water immersion 1.1 NA lens was used. Samples were illuminated with 405 and 488 nm lasers. 512x512 pixel images were acquired using PMT detectors. DAPI (405 nm laser) acquisition parameters were: 150-300 ms exposure time, 25 % laser power, gain multiplier 100 and conversion gain 3. FITC or GFP (488 nm laser) acquisition parameters were: 100 ms exposure time, 10 % laser power, gain multiplier 100 and conversion gain 3. For HeLa cells, approximately 10 - 30 cells per well were imaged and 2 wells were used in each experiment. Experiments were repeated at least 3 times. For iPSCs images of around 5-20 cells per well were taken. 3 wells were imaged per experiment and experiments were repeated one to two times (one to two rounds of differentiation).

2.8.2 Imaging on Opera Phenix High Content Screening System

Immunostained cells were imaged on a Perkin Elmer Opera Phenix High Content screening system. A Plan Apochromat 40x water immersion 1.1 NA lens was used. Samples were illuminated with 375, 488, 561 and 640 nm lasers. Images were taken

in confocal mode. Exposure time and focal heights were individually determined per experiment to achieve suitable fluorescent intensities and to place the cells in focus, respectively. Laser power was always set to 100 %. Emission wavelength ranges were 435-480 nm, 500-580 nm, 570-630 nm and 650-750 nm for DAPI, Alexa Fluor 488, Alexa Fluor 555 and Alexa Fluor 647, respectively. For both HeLa cells and iPSCs, 10-13 fields of views were imaged with each field of view containing approximately 50-300 cells. 2 wells per HeLa cell experiment were used with experiments having been repeated three times. 3 wells were used per iPSC experiment and experiments were repeated one to two times (one to two rounds of differentiation).

2.8.3 Live imaging analysis

Images were analysed using the Nikon NIS-Elements AR 5.30.01 image analysis software. Nuclei were selected via thresholding DAPI intensity levels. Thresholding ranges were adjusted for individual experiments but were typically approximately 2000 – 65000. Settings were then fine-tuned using ‘smooth’ (typically 3-4 x), ‘separate’ (typically 1 x) and ‘fill holes’ (‘ON’) applications. Nuclei were further filtered by excluding small objects and objects touching borders and by setting a circularity threshold (typically 0.88-0.9) to only analyse healthy cells. GFP and DAPI intensity levels were detected in these selected nuclei over the recorded time course. Further intensity normalisations are described in section 3.5.

2.8.4 Opera Phenix imaging analysis

Images taken on the Opera Phenix High Content Screening System were analysed using the Harmony software. Within this software an image analysis sequence was created. Nuclei were defined based on DAPI thresholding using built-in methods choosing a method most suitable for variable intensities. From this nuclei population a subpopulation was created based on DAPI intensities, size and circularity to only include healthy nuclei. Where appropriate further subpopulations constituting the nucleoplasm and the nuclear membranes were created by defining image regions. Inner and outer borders of these image regions were adjusted to create subpopulations of the desired nuclear compartment. DAPI intensity levels and typically Alexa Fluor 488 and/or Alexa Fluor 647 intensity levels (based on

secondary antibody staining) were detected in the defined nuclei, nucleoplasm and nuclear membrane image regions.

For iPSC-derived neuron image analysis a cytoplasm region was also defined based on the nuclei population created as described above. Definition of the cytoplasm region was based on MAP2 staining and was also performed via built-in methods choosing a method most accurately selecting the cytoplasm. Furthermore, as our cell populations were not purely neuronal a neuron population was defined based on the nuclei population. The neuron population was defined based on MAP2 intensity levels and on nuclear size deselecting very small and very large nuclei. Neurites were also detected based on MAP2 staining using a built-in method. The neuron population was then further filtered to only consist of cells containing neurites using the software RStudio version 4.1.1. DAPI intensity levels and typically Alexa Fluor 488 and Alexa Fluor 647 intensity levels were detected in the defined nuclei, nucleoplasm and nuclear membrane and cytoplasm image regions of the neuron population using the Harmony software. Background fluorescence was also detected and was subtracted from measured nuclear, nucleoplasmic, nuclear membrane and cytoplasmic fluorescence in the subsequent analysis.

2.9 Statistical analysis

2.9.1 Averaging of data

For HeLa cell live imaging experiments (import of reporter cargo) nuclear fluorescence intensity values were averaged per experiment, thus the n numbers for statistical analysis equalled the number of experiments and not the number of cells (to not artificially drive statistical significance). The same average method was used for iPSC live imaging experiments where poly-GR treatment was compared to non-treatment in a control iPSC line. For iPSC live imaging experiments and immunofluorescence experiments comparing genotypes (control vs *C9ORF72* mutation) nuclear fluorescence intensity values were first averaged per cell line and per round of differentiation (cells from a single round of differentiation were used per experiment). These means were then averaged to obtain means per cell line (as numbers of rounds of differentiation differed between cell lines), hence n numbers used in statistical analysis equalled the number of cell lines per genotype. For plotting iPSC immunofluorescence data, individual means of each cell line were normalised to the overall mean of control lines (average of the three means of the

control lines) to represent data of individual cell lines. To represent data per genotype averages of the individual means of control lines and of *C9ORF72* lines were normalised to the overall mean of control lines. Error bars represent the standard error of the mean of individual cell line means. For HeLa cell immunofluorescence experiments data was not averaged for statistical analysis but data was analysed using a multi-level model (see section 2.9.2). To plot HeLa cell immunofluorescence data, fixed effect coefficient estimates from each individual experiment were used. Coefficients were normalised to control coefficients of the respective experiments and means of the normalised coefficients from individual experiments were plotted. Error bars represent the standard error of the mean of normalised coefficient means.

2.9.2 Statistical testing

All statistical analyses were carried out using the RStudio software version 4.1.1. For analysis of live imaging results, a two-way repeated measures ANOVA was performed. For HeLa cell results an additional Dunnett's or Tukey's post-hoc test was performed to determine effects of different treatment types. This was obsolete for iPSC live cell experiments as only two groups were compared (control vs *C9ORF72* mutation or untreated vs poly-GR treatment; see also section 6.1). For HeLa cell immunofluorescence experiments a multi-level model was fitted. The different treatments were considered as fixed effects and the different experiments (on different days) were denominated as random effects to account for variability within experiments. For random effects, random intercepts and random slopes were calculated within the model to account for potential different baseline intensity values and potential different treatment effects between experiments, respectively. This multi-level model was analysed using a type III ANOVA followed by a Dunnett's post-hoc test. For iPSC-derived neuron immunofluorescence experiments a two-sided t-test was performed. *P* values < 0.05 were considered statistically significant.

3 Optimisation of passive nucleocytoplasmic transport assay

We aimed to study passive nucleocytoplasmic transport in the context of *C9ORF72* ALS/FTD in this project as this has not been studied systematically. Passive nucleocytoplasmic transport is not dependent on transport receptors and on the Ran gradient (see also 1.4.2). Thus, studying passive nucleocytoplasmic transport dynamics in a disease context yields information about nuclear pore integrity and function and about possible changes in interactions with proteins interacting with the nuclear pore (see also 1.4.3). Mechanisms leading to any of these possible alterations have not been elucidated so far. For the investigation of passive nucleocytoplasmic transport, I used a cell permeabilisation assay. This is a classic assay and we adapted a protocol obtained from the Lowe laboratory at University College London (Lowe et al., 2015). Adaptation was necessary as we had a more pathological focus than the Lowe study. We also initially attempted to use a different cell line. Furthermore, we investigated different cargo systems with differing transport dynamics and thus imaging timings had to be adjusted. Imaging and analysis also had to be adapted on our microscope system. In addition, according to cargo fluorescence and background a fluorescence signal normalisation method had to be developed.

3.1 Basic principles of the nucleocytoplasmic transport assay

The basic principle of the transport assay is to specifically permeabilise the plasma membrane whilst leaving the nuclear membrane intact. This allows to specifically study transport into the nucleus without the need to deliver reporter cargo into a cell or to account for translocation of cargo through the plasma membrane. The assay workflow (see Figure 3.1) starts with the permeabilisation of the plasma membrane with digitonin which does not break down the nuclear membrane. After washing away the cytosol this yields intact nuclei. Nuclei are stained with DAPI to allow for nuclei definition during image analysis. Fluorescently labelled reporter cargo can then be directly added to the nuclei without having to overcome the plasma membrane. FITC-labelled dextrans, inert glucose polysaccharides, of sizes of 20, 40 and 70 kDa and GFP were used as cargo in this project. This allowed to detect differences in transport dynamics based on size and cargo type (dextran versus GFP). Furthermore, investigating transport of the 70 kDa dextran gives information

about the integrity of the nuclear pore's permeability barrier as nuclear entry of cargo of this size should be prohibited (see also section 1.4.2). The cells were grown in 8-well chamber coverslips which allowed for cargo addition directly at the microscope. This is essential to follow nuclear cargo uptake live and from the very beginning. As cargo translocation is fast capturing nuclear import from the start is necessary to investigate the transport reaction before it approaches saturation. Effects of potential passive nucleocytoplasmic transport modifiers are also easier to detect when general transport levels are high probably allowing for higher effect sizes. Therefore, the nuclear import of cargo was imaged live every 2.5 seconds over a time course of 4 minutes using a spinning disk confocal microscope as this fully captures the transport dynamics of our reporter cargo. This assay allows to measure passive nucleocytoplasmic transport quantitatively and to compare different treatment conditions.

3.2 Selection of cell type and coating agent

Initially, SH-SY5Y cells were used to perform the transport assay due to their neuronal-like characteristics as we intended to study a neurodegenerative disease. However, after permeabilisation these cells were washed away from the centre of the well only staying adherent at the edges of the well (see Figure 3.2, top panel). This was problematic for imaging as cells localised to the edge of a well tend to clump and not be attached flat onto the surface. This made it difficult to maintain focus potentially resulting in lower quality images. To overcome this problem the coating agents, poly-L-lysine, poly-D-lysine and Cell-Tak were tested to enhance cell adhesion. Unfortunately, washing away of SH-SY5Y cells could not be prevented by the usage of coating agents (see Figure 3.2, second, third and last panel).
As HeLa cells are highly adherent (Potthoff et al., 2012) this cell line was then trialled as an alternative on uncoated and plates coated with the reagents mentioned above. Whilst HeLa cells still detached from uncoated plates, they remained adherent on coated wells regardless of the type of coating agent used (see Figure 3.3). Therefore, HeLa cells were chosen for further experiments. As poly-L-lysine is the most cost effective of the coating agents tested it was selected for future transport assays.

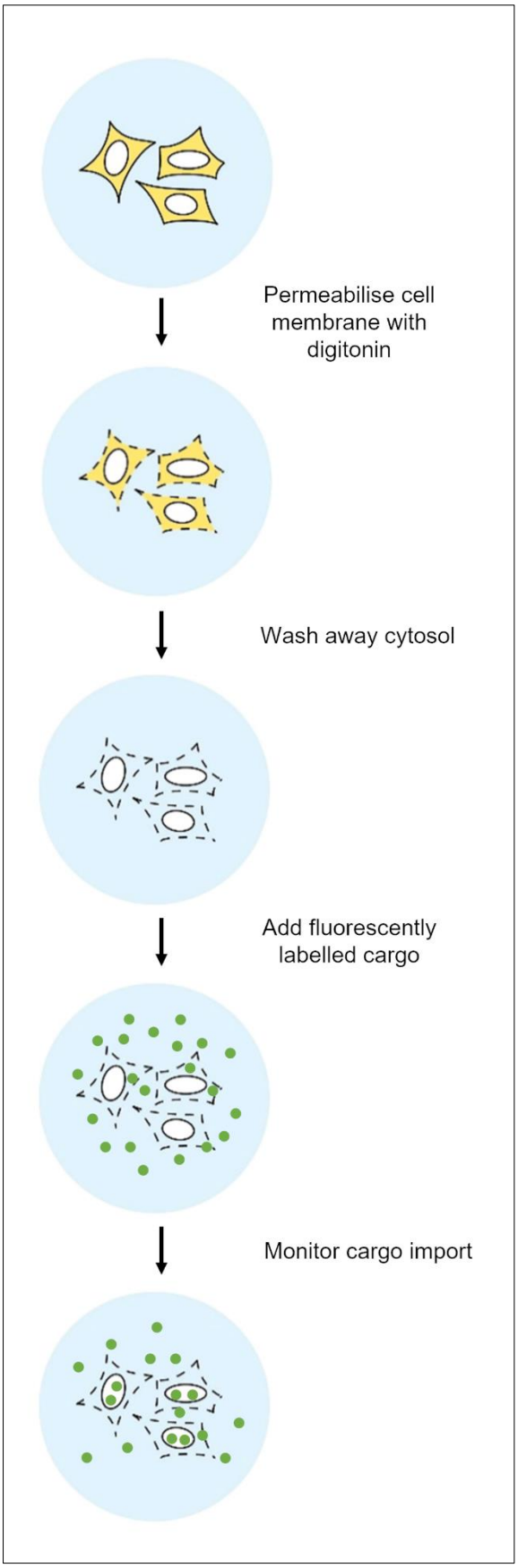

Figure 3.1: Schematic representation of nucleocytoplasmic transport assay workflow. Adapted from Andersen et al., 2013.

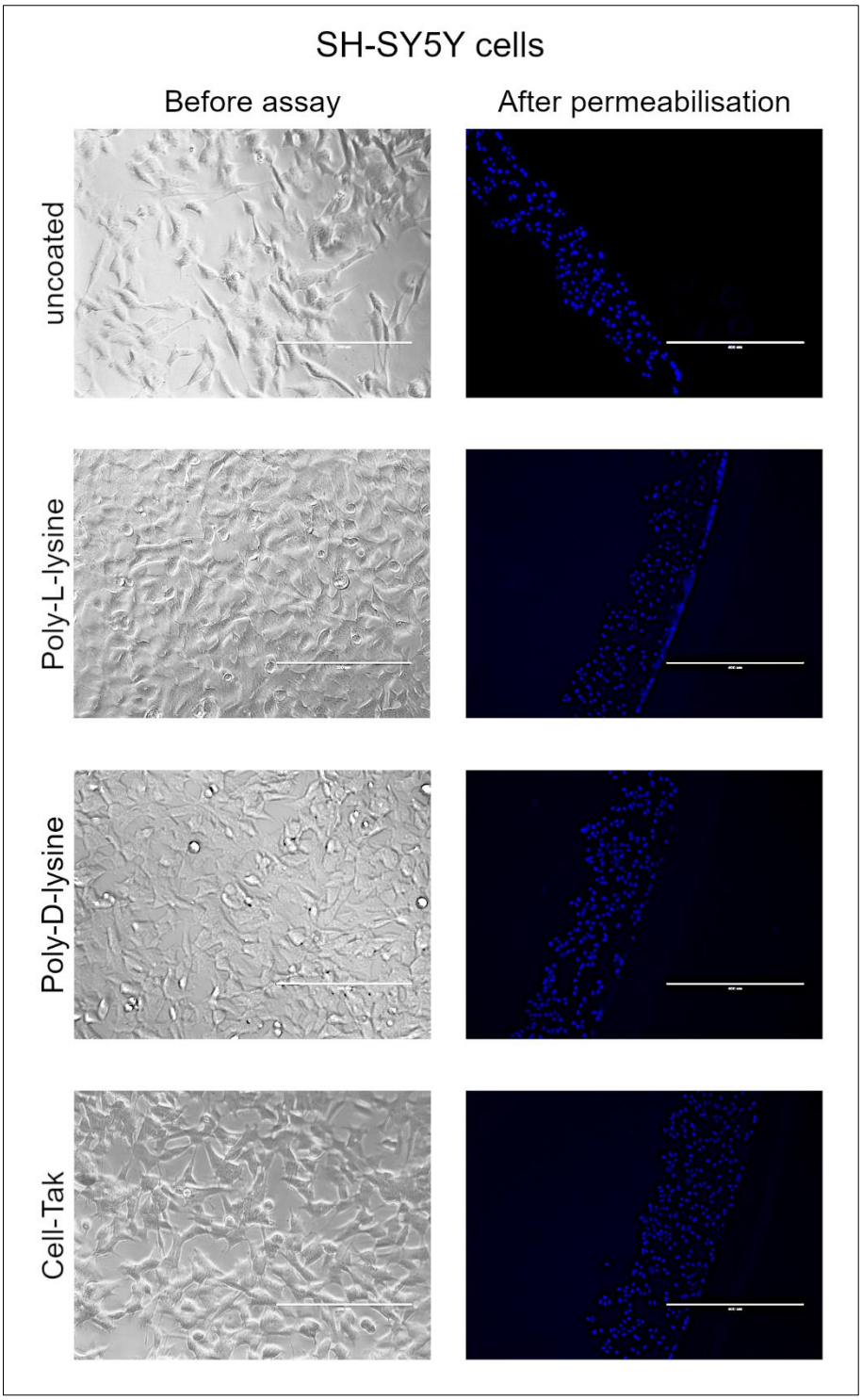

Figure 3.2: SH-SY5Y cells detach from surface upon permeabilisation. Light microscope images of SH-SY5Y cells grown on plates coated with various coating agents as indicated. Left panel shows cells prior to start of transport assay protocol. Right panel shows DAPI stained cells after permeabilisation with digitonin close to edge of well. Scale bars in left panel: 200 µm. Scale bars in right panel: 400 µm.

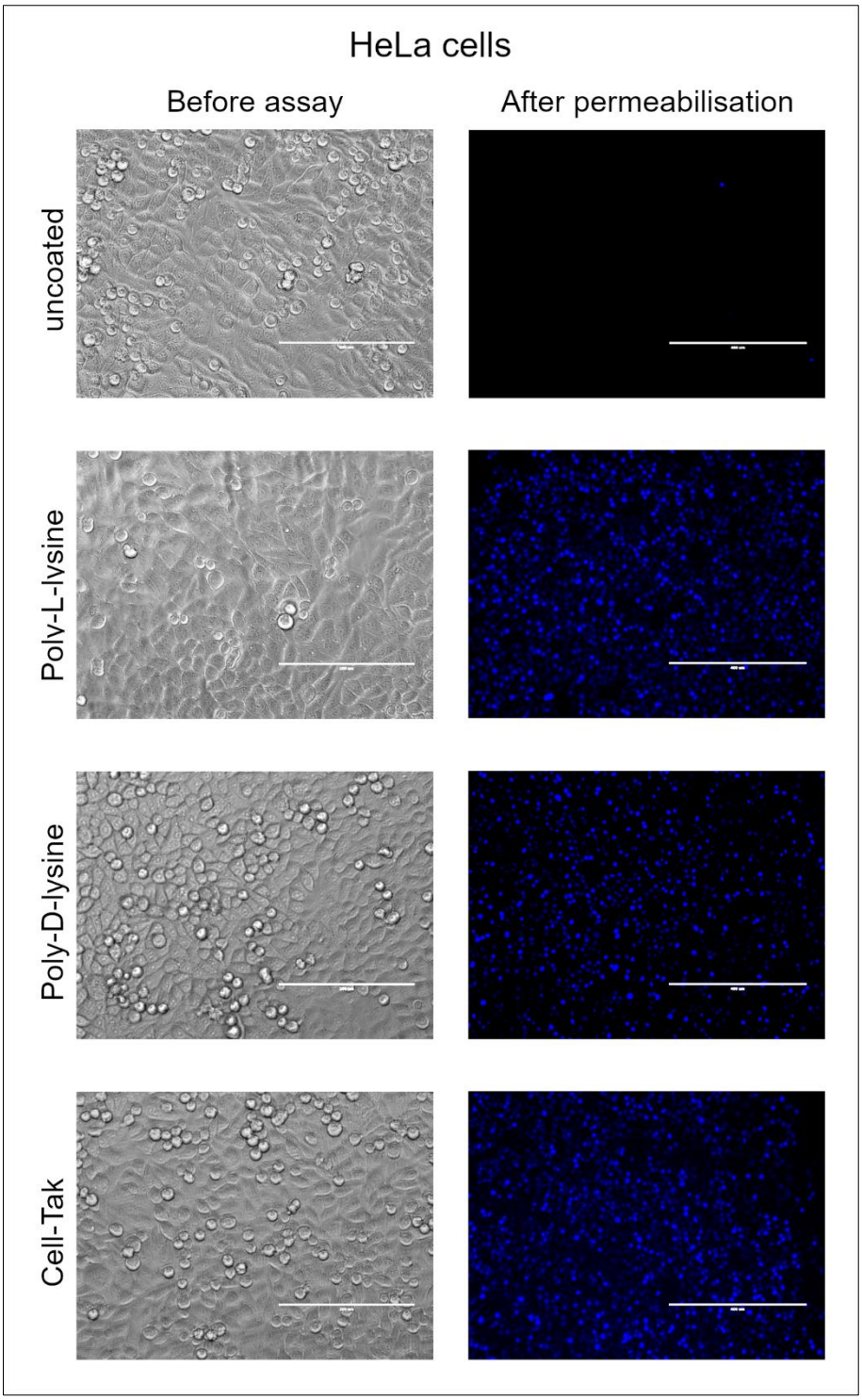

Figure 3.3: HeLa cells remain attached to coated wells after permeabilisation. Light microscope images of HeLa cells grown on plates coated with various coating agents as indicated. Left panel shows cells prior to start of transport assay protocol. Right panel shows DAPI stained cells after permeabilisation with digitonin. Scale bars in left panel: 200 µm. Scale bars in right panel: 400 µm.

3.3 Optimisation of wash steps

The nucleocytoplasmic transport assay requires several wash steps and buffer exchanges (see also section 2.5). Whilst HeLa cells remained adherent after the

permeabilisation step, considerable detachment was observed after subsequent steps. Therefore, different washing methods were tested. For this experiment cells were imaged on an Opera Phenix High Content Screening System as this allowed to conveniently image a higher proportion of the well more rapidly compared to the classic spinning disk microscope. As cells most likely detached because of the perturbation created when adding liquid directly on top of the cells, only exchanging half of the volume during a wash step was trialled. To maintain kinetics of washing away the desired solution (added during a previous step of the assay protocol), the timings of the washes were halved, and the number of washes doubled (i.e., 4 x 2.5-minute washes instead of 2 x 5-minute washes). As shown in Figure 3.4 half volume buffer exchanges significantly enhanced the adhesion of HeLa cells throughout the entire assay workflow. Thus, this method was used for all subsequent passive nucleocytoplasmic transport assays.

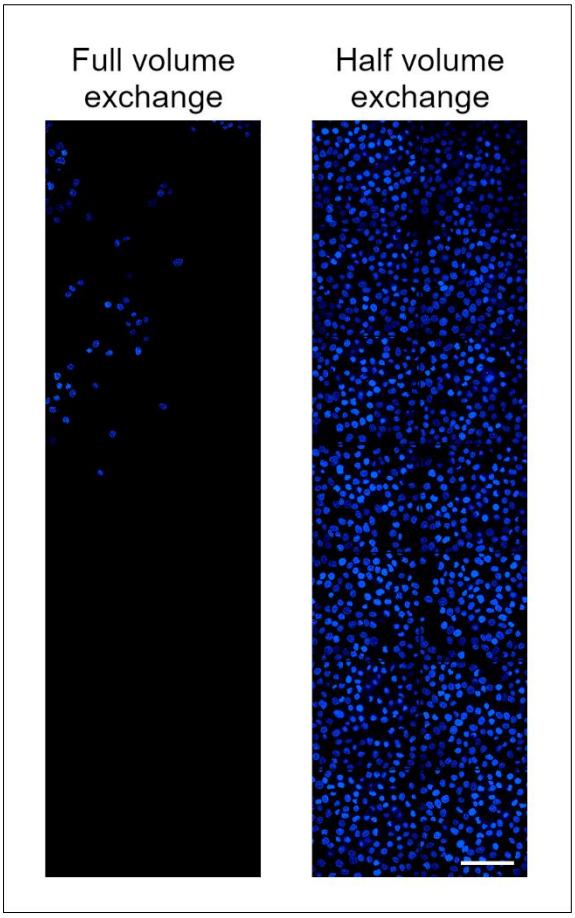

Figure 3.4: HeLa cells remain attached to well surface upon half-volume washes. Opera Phenix High Content Screening System images of HeLa cells after being subjected to the nucleocytoplasmic transport assay protocol. Left panel shows distribution of cells within the well after exchanging the entire volume of the well during wash steps. Right panel depicts distribution of cells within the well when only half the well volume is exchanged

during wash steps. Several fields of views are merged in these images depicting a section of a 96-well. Scale bar: 100 µm.

3.4 Selection of dextran concentration

After determining the optimal conditions for the permeabilisation assay monitoring of cargo import was optimised. In a first step, different concentrations of 20 kDa dextran were trialled. The optimal dextran concentration allows for imaging at a laser power that is not cell damaging whilst not exciting the fluorophores to a level that results in over-saturation of the image. In addition, the cargo should be capable of entering the nucleus at quantifiable levels within the desired timeframe. Dextran concentrations of 10 and 100 µg/ml were tested. As depicted in Figure 3.5 the 20 kDa dextran could clearly be visualised and detected within the nucleus after a 4-minute incubation period at both concentrations. The dextran seemed to have an affinity for and thus, accumulate within a nuclear structure which appeared to be the nucleolus (example indicated by arrow in Figure 3.5).

At a standard laser power of 25 % a dextran concentration of 100 µg/ml resulted in very high fluorescent signals for both the background (i.e., fluorescence of the cargo in the media surrounding the nuclei) and the nucleus (see Figure 3.6 and Figure 3.7). Values almost reached the saturation threshold of 65,000. A dextran concentration of 10 µg/ml, however, led to clearly detectable fluorescent levels which did not approach saturation. 10 µg/ml was therefore the chosen dextran concentration for further transport experiments. Fluorescence levels of the higher concentration could have been reduced by changing the image acquisition settings. However, as the more economic lower concentration yielded quantifiable results at standard imaging settings this was not deemed necessary.

It is important that dextran is not depleted from the media to avoid a premature plateau of the passive transport reaction before the end of the 4-minute imaging time period. Furthermore, there should still be scope for potential enhancement of passive nucleocytoplasmic transport levels by cell treatments. This was the case for both dextran concentrations tested as fluorescence background levels (of cargo in the media) and nuclear fluorescence levels (of cargo translocated to the nucleus) were quite similar which indicates that there was still sufficient cargo available at the end of the transport reaction.

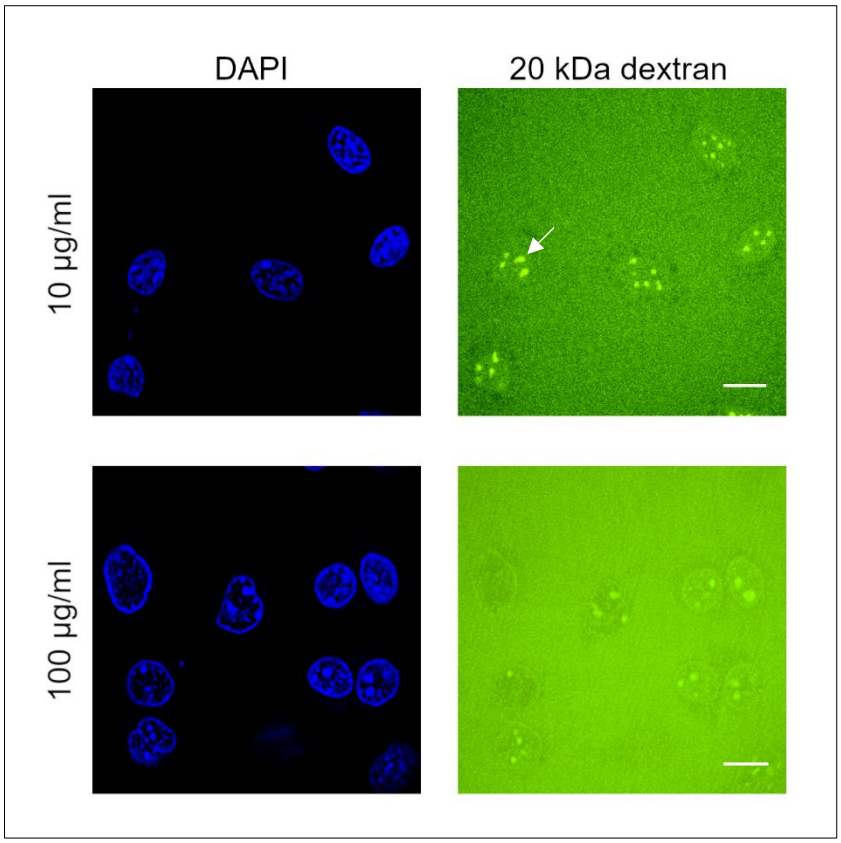

Figure 3.5: Nuclear translocation of 20 kDa dextran at different concentrations. Spinning disk confocal microscope images of semi-permeabilised HeLa cells after 4-minute incubation with 20 kDa dextran at different concentrations as indicated. Left panel: DAPI channel. Right panel: FITC 20 kDa dextran channel. Arrow depicts an example of dextran accumulation within the nucleolus. Note that brightness and contrast settings of images of different dextran concentrations are similar but not equal to allow for visualisation of dextran in the nucleus. Scale bars: 20 µm.

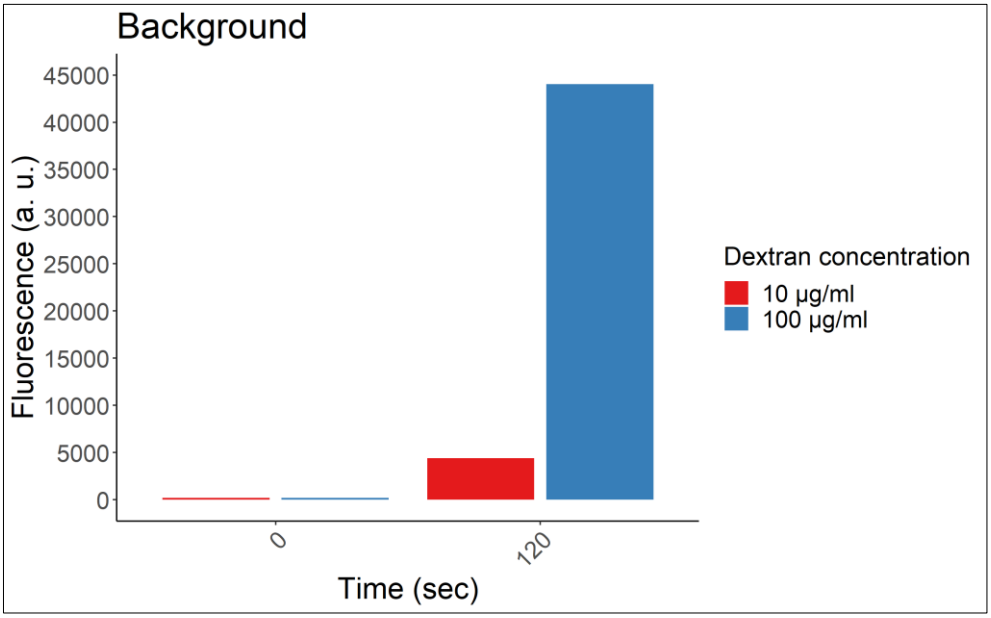

Figure 3.6: Fluorescence levels of 20 kDa dextran in the media. Quantification of raw green background fluorescence signal prior to addition of and after 4-min incubation of FITC-labelled 20 kDa dextran at concentrations as indicated to permeabilised HeLa cells. Representative values of 1 well are shown.

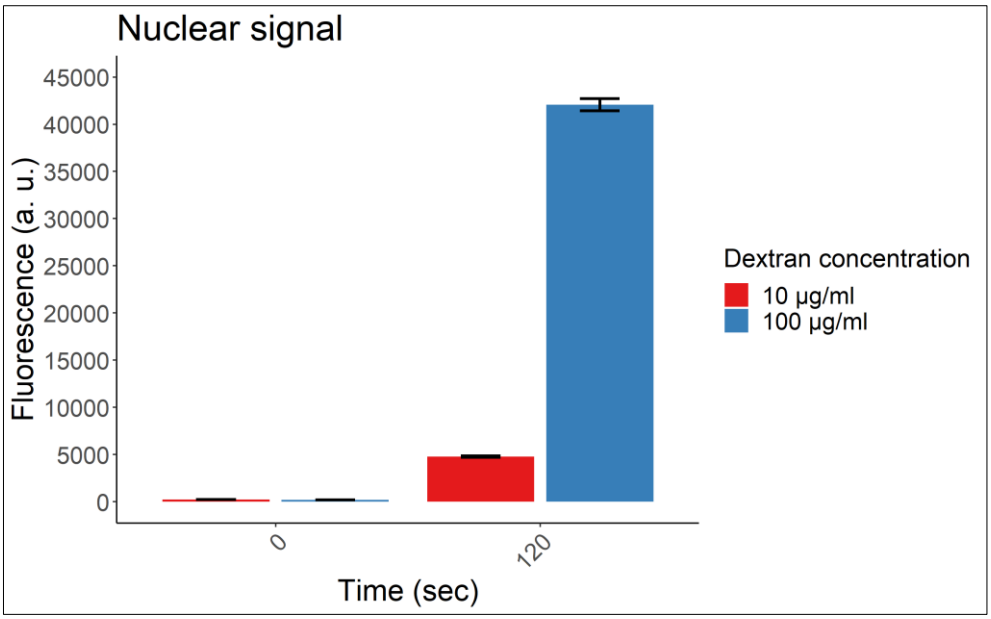

Figure 3.7: Nuclear levels of 20 kDa dextran after 4-minute passive transport reaction. Quantification of raw green nuclear fluorescence signal prior to addition of and after 4-min incubation with FITC-labelled 20 kDa dextran at concentrations as indicated with permeabilised HeLa cells. Mean values of nuclear intensities of cells of 1 well are depicted. Error bars: SEM.

3.5 Determination of image analysis and normalisation strategy

As background fluorescent signals of cargo in the media were quite high as discussed above, a normalisation strategy was required to detect and depict nuclear cargo import in a meaningful manner. Firstly, it was tested whether dextrans of different sizes and GFP could be visualised and detected under the same conditions as the 20 kDa dextran. The 40 kDa dextran could also be detected within the nucleus and accumulated at the nucleolus comparable to the 20 kDa dextran (compare Figure 3.8 and Figure 3.9). GFP which is 27 kDa entered the nucleus as well but was distributed equally throughout the nucleus (see Figure 3.10). Import into the nucleus was not seen for the 70 kDa dextran (see Figure 3.11) which was expected as it is larger than the nuclear pore permeability threshold of 40 kDa (see also section 1.4.2; (Mohr et al., 2009)). The exclusion of the 70 kDa dextran from the nucleus indicated that assay conditions mimicked physiological nucleocytoplasmic transport characteristics and did not lead to nuclear damage but maintained the permeability barrier of the nuclear pore. Import of cargo was followed and quantified over a time course of 4 minutes as this timeframe showed sufficient nuclear translocation of the 20 kDa dextran in section 3.4. Importantly, background fluorescence levels were stable over time (see Figure 3.13). Replicates, which

showed a fluctuation of background levels of more than 10 % were excluded from the analysis.

Whilst entry of cargo could clearly be detected from the microscope images it was less obvious when plotting raw nuclear fluorescence values (see Figure 3.12). Noticeably, a nuclear fluorescence signal was still detected for the 70 kDa dextran as soon as dextran was added. This was also the case for the smaller dextrans and for GFP and their nuclear fluorescence only minimally increased over time. This indicated that fluorescence bleed through from background dextran in the media in planes above or below the nuclei was occurring. To account for this phenomenon, the nuclear fluorescence levels of an early timepoint just after the cargo was added and before cargo import had a significant chance to occur (see Figure 3.8, Figure 3.9, Figure 3.10 and Figure 3.11, top panel) were subtracted from nuclear fluorescence levels of all subsequent time points (see Figure 3.14). This resulted in clearer depiction of cargo entry into the nucleus and of the exclusion of the 70 kDa dextran from the nucleus. To allow for comparison between different cargo types (as inherent fluorescence levels of cargoes differ) the adjusted nuclear fluorescence signal was then divided by the background signal of the according time point (see Figure 3.15). This was also required because of potential variation from different dextran and GFP batches, from slight differences in pipetting, from a change in microscope setup (e.g., after servicing) and from undetectable environmental perturbances (e.g. slight change in airflow). As shown in Figure 3.15 GFP showed the highest import rates after a 4-minute incubation time, followed by the 20 kDa dextran and then the 40 kDa dextran. No nuclear import of the 70 kDa dextran was detected. Entry of cargo into the nucleus occurred quickly with the slope of the curves being steepest at early time points and flattening over time. The majority of import took place within the first 2 minutes of incubation (additionally see Figure 3.8, Figure 3.9 and Figure 3.10). Interestingly, at early time points import of 20 kDa dextran was faster and occurred at higher rates than import of GFP.

Overall, this optimised passive nucleocytoplasmic transport assay led to expected and reliable results which were comparable between multiple replicates. It allowed for quantification of passive nuclear import and for the detection of differences in import rates of cargo of varying sizes. Thus, it is a suitable system to investigate nucleocytoplasmic transport in a quantitative manner in physiological and pathological conditions.

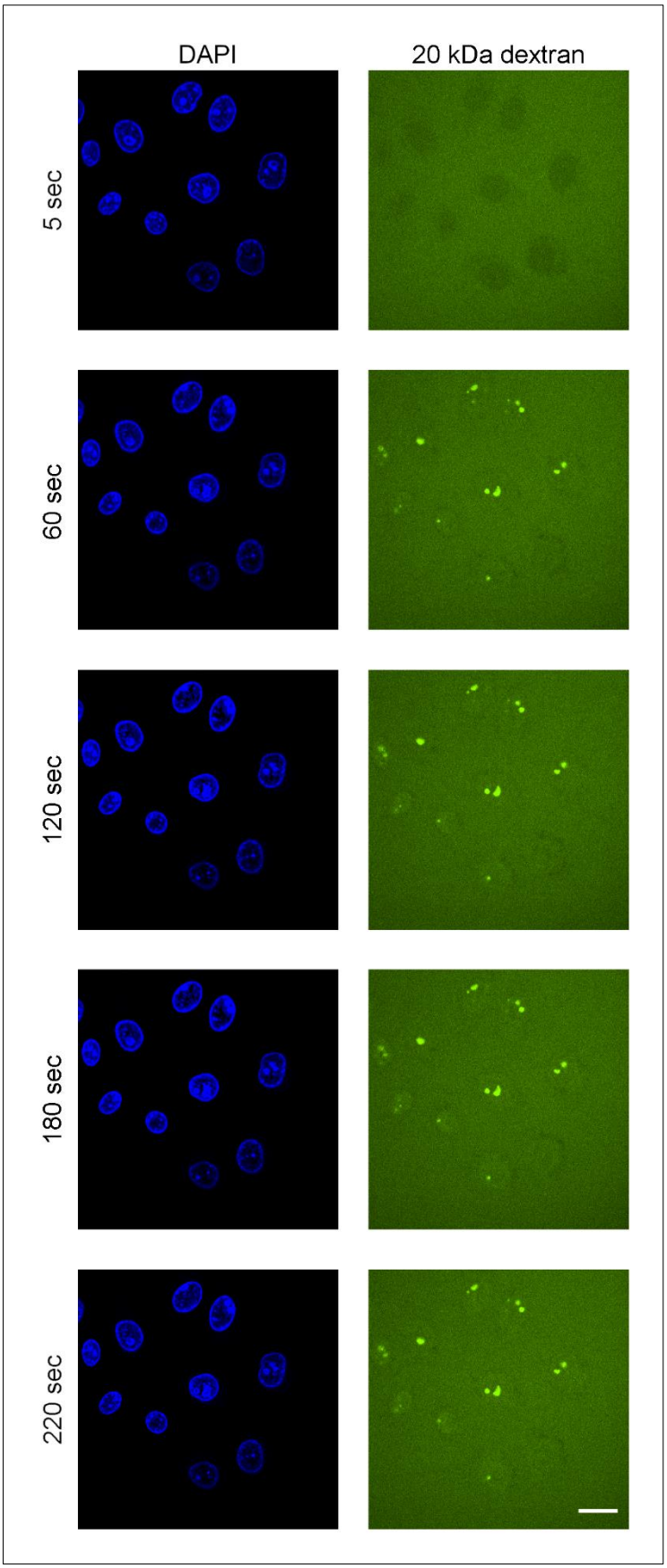

Figure 3.8: Passive nuclear import of 20 kDa dextran over time. Spinning disk confocal microscope images of semi-permeabilised HeLa cells at various timepoints as indicated after incubation with 20 kDa dextran. Left panel: DAPI channel. Right panel: FITC 20 kDa dextran channel. Scale bar: 20 µm.

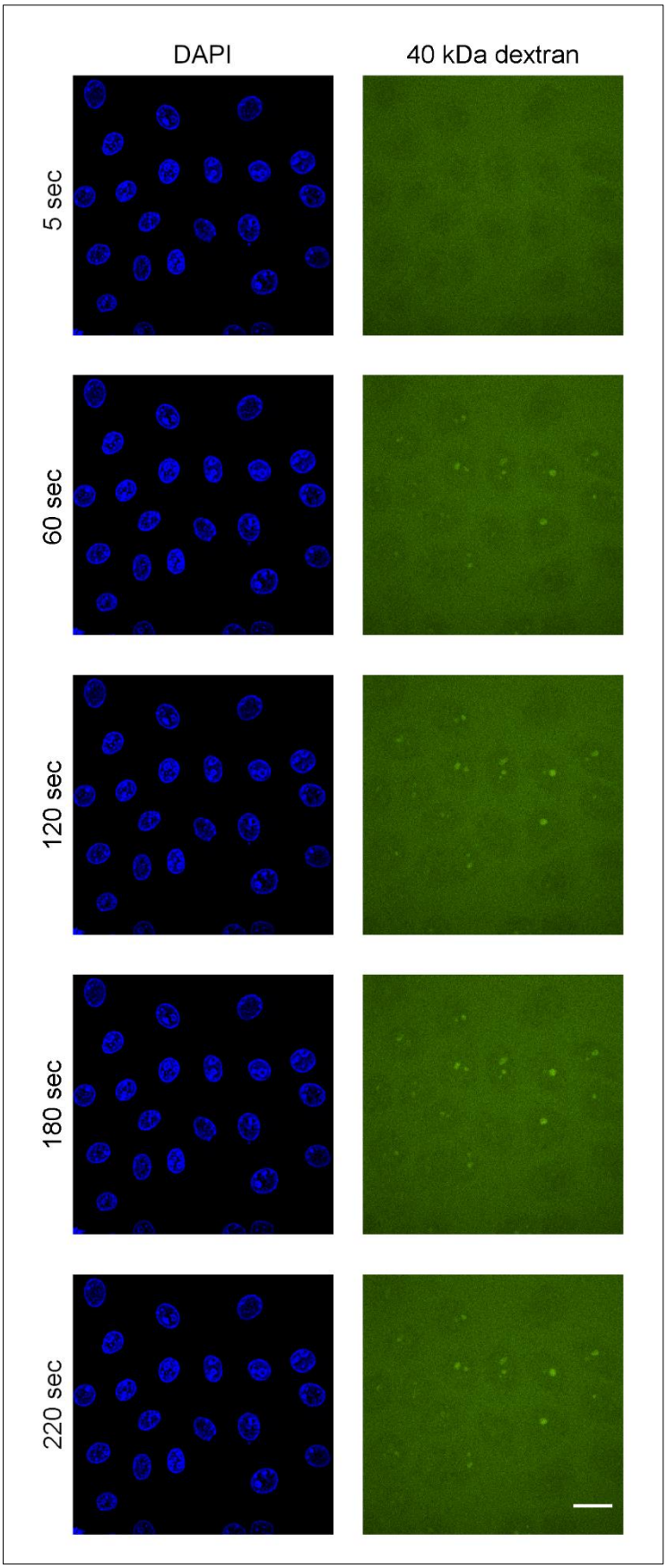

Figure 3.9: Passive nuclear import of 40 kDa dextran over time. Spinning disk confocal microscope images of semi-permeabilised HeLa cells at various timepoints as indicated after incubation with 40 kDa dextran. Left panel: DAPI channel. Right panel: FITC 40 kDa dextran channel. Scale bar: 20 µm.

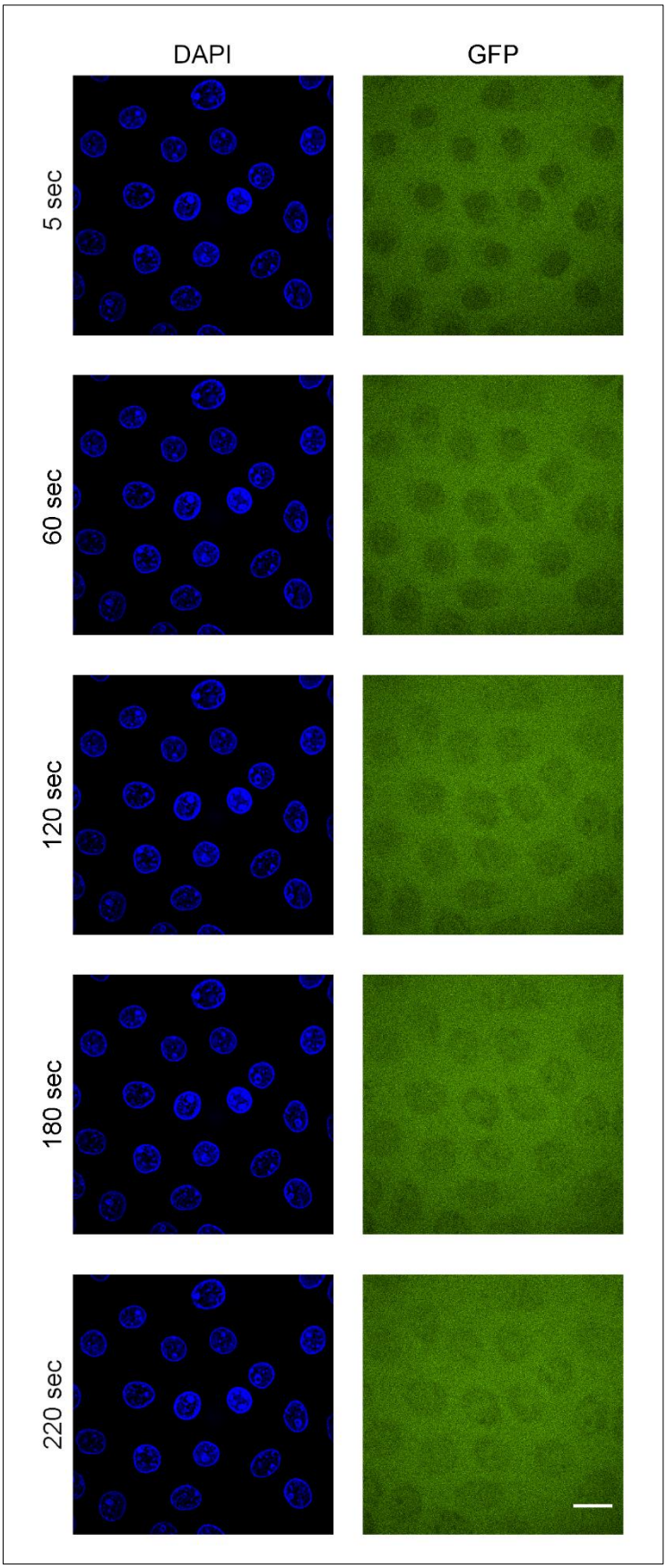

Figure 3.10: Passive nuclear import of GFP over time. Spinning disk confocal microscope images of semi-permeabilised HeLa cells at various timepoints as indicated after incubation with GFP. Left panel: DAPI channel. Right panel: GFP channel. Scale bar: 20 µm.

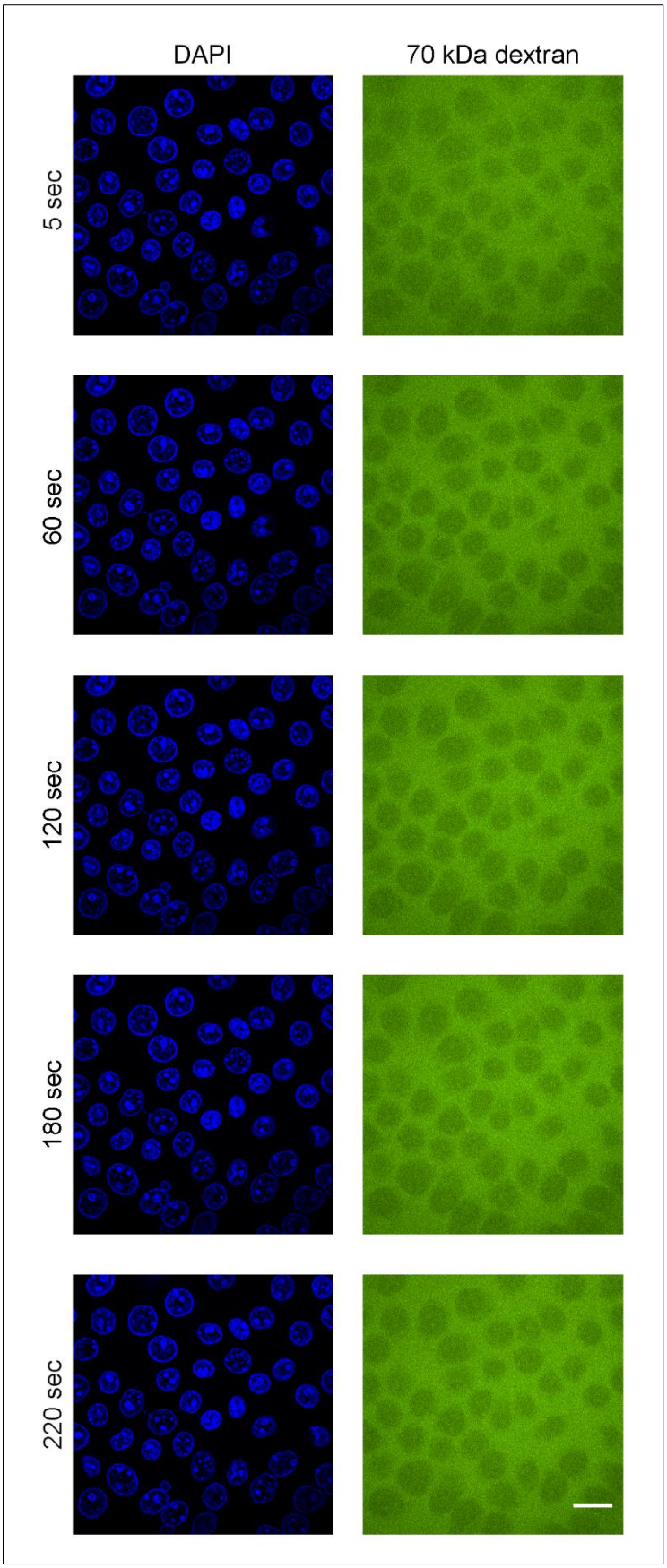

Figure 3.11: Nuclear translocation of 70 kDa dextran is prohibited. Spinning disk confocal microscope images of semi-permeabilised HeLa cells at various timepoints as indicated after incubation with 70 kDa dextran. Left panel: DAPI channel. Right panel: FITC 70 kDa dextran channel. Scale bar: 20 µm.

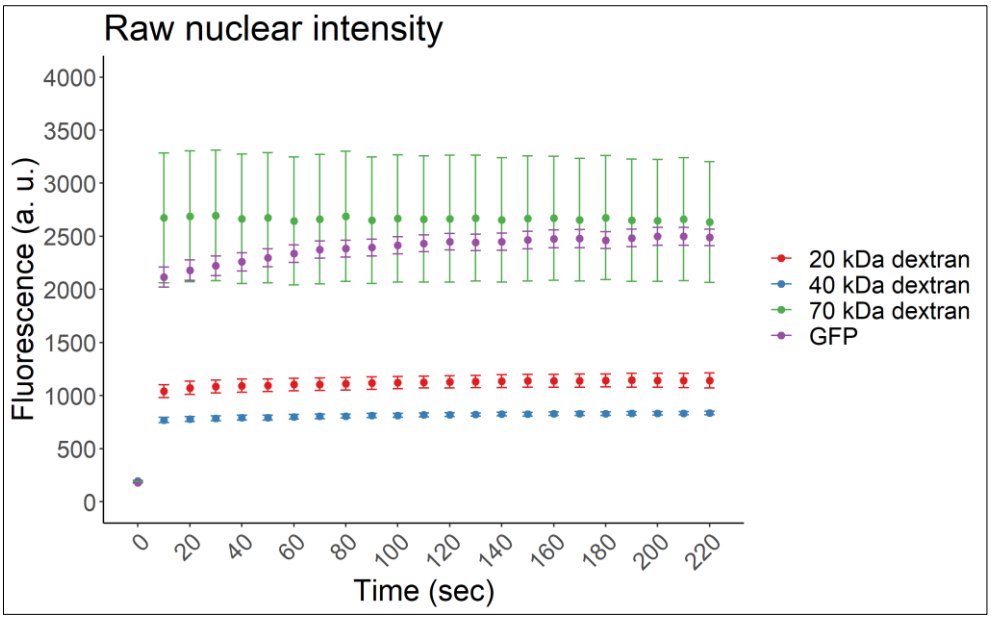

Figure 3.12: Raw nuclear fluorescence levels of cargo only slowly increase over time. Quantification of raw nuclear fluorescence depicting nuclear import of different reporter cargo species as indicated over time in permeabilised HeLa cells. 20 kDa dextran is shown in red, 40 kDa dextran in blue, 70 kDa dextran is depicted in green and GFP in purple. Means of experimental means (of individual cells) are depicted. N = min. 3. Error bars: SEM.

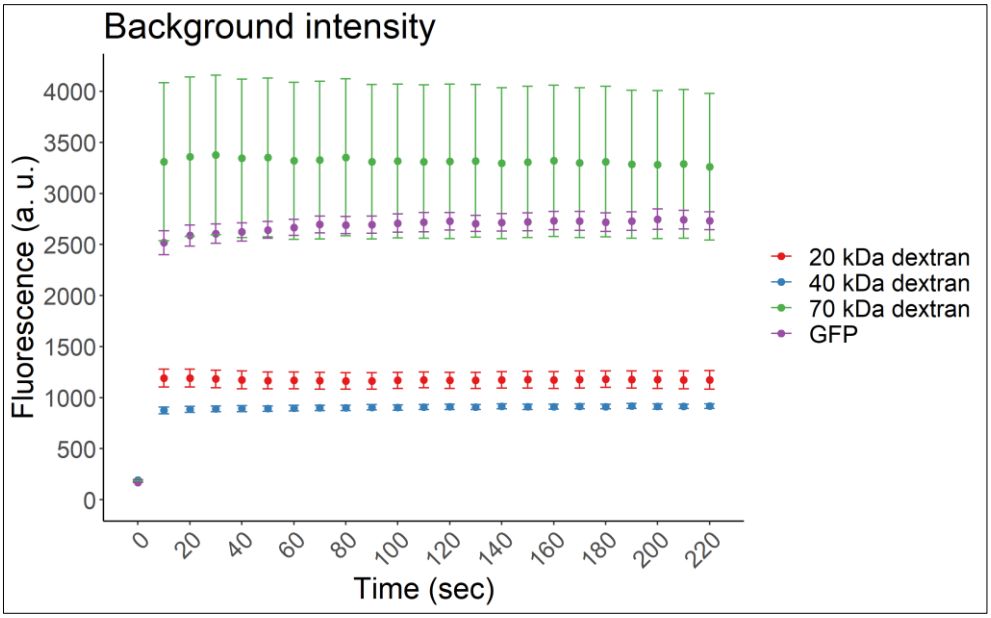

Figure 3.13: Fluorescence background levels of cargo in the media remain stable over time. Quantification of raw background fluorescence of different reporter cargo species as indicated over time after incubation with permeabilised HeLa cells. 20 kDa dextran is shown in red, 40 kDa dextran in blue, 70 kDa dextran is depicted in green and GFP in purple. Means of experimental means (of individual wells) are depicted. N = min. 3. Error bars: SEM.

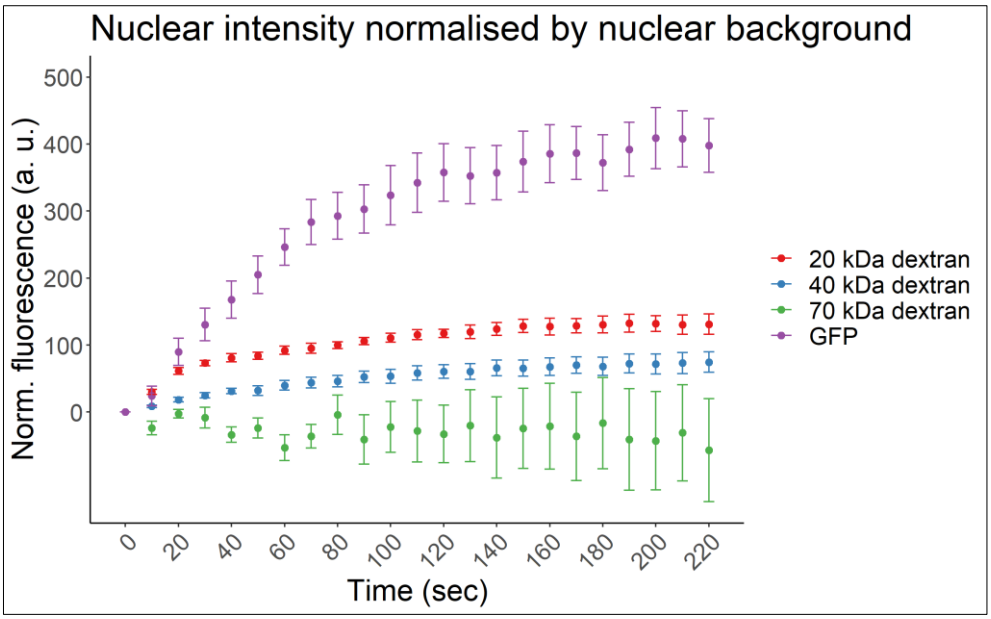

Figure 3.14: Detection of passive nuclear import of reporter cargos upon nuclear background normalisation. Quantification of nuclear fluorescence normalised to nuclear background (determined as a timepoint just after cargo addition) showing nuclear import of different reporter cargo species as indicated over time in permeabilised HeLa cells. 20 kDa dextran is shown in red, 40 kDa dextran in blue, 70 kDa dextran is depicted in green and GFP in purple. Means of experimental means (of individual cells) are depicted. N = min. 3. Error bars: SEM.

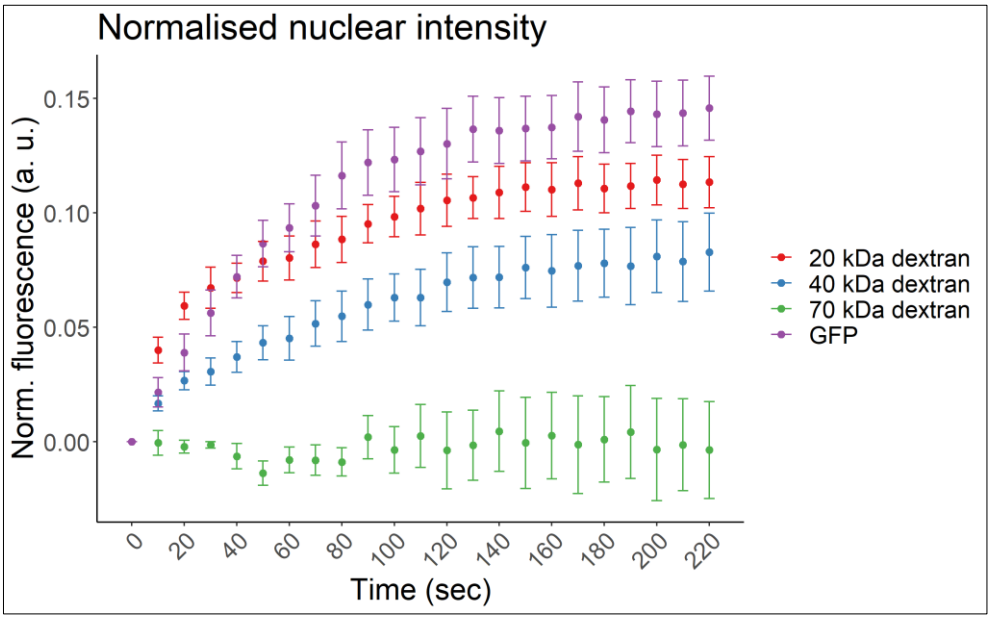

Figure 3.15: Final fluorescence signals after normalisation process determining passive nuclear import rates. Quantification of nuclear fluorescence normalised to nuclear and general background showing nuclear import of different reporter cargo species as indicated over time in permeabilised HeLa cells. 20 kDa dextran is shown in red, 40 kDa dextran in blue, 70 kDa dextran is depicted in green and GFP in purple. Means of experimental means (of individual cells) are depicted. N = min. 3. Error bars: SEM.

3.6 Discussion

In this section I determined the optimal conditions for a passive nucleocytoplasmic transport assay providing a reductionist system to determine potential changes to passive nucleocytoplasmic transport in *C9ORF72* ALS/FTD. Our cell line of choice for these experiments would have been the neuroblastoma cell line SH-SY5Y due to its neuronal-like characteristics and its potential to be differentiated into neurons. However, because of the issues regarding its adhesion to imaging plates HeLa cells had to be used instead. A potential caveat in using a less neuronal-like cell line is that the composition of the nuclear pore might differ more from those found in neurons of the human brain. Indeed, stoichiometry of nucleoporins differs between several human cancer cell lines (HeLa cells but not SH-SY5Y cells have been included in the comparison of Ori and colleagues) and between various human tissues. However, the types of nucleoporins present within the nuclear pore do not differ between cell lines and tissues investigated (Ori et al., 2013) . It seems likely that stoichiometry of nucleoporins would even differ between SH-SY5Y cells and human neurons. This highlights the importance of confirming findings of transport experiments with cell lines in a more physiological model system independent of the type of human cancer cell line used.

The cargo molecules used for the transport experiments are referred to as inert as they do not interact with the FG domains of nucleoporins (see also section 1.4.1) within the central channel of the nuclear pore (Frey et al., 2018). This allows to specifically study passive diffusion through the nuclear pore and to directly detect potential changes to nuclear pore permeability in disease. Passive diffusion becomes increasingly difficult for larger molecules (Mohr et al., 2009). This was reflected in the results of my study where the 20 kDa dextran showed higher import rates compared to the 40 kDa dextran. Interestingly, GFP which is 27 kDa entered the nucleus at increased levels compared to the 20 kDa dextran. This can potentially be explained by GFP's composition of multiple hydrophobic residues which facilitate weak interactions with FG domains which in turn results in enhanced transport rates (Frey et al., 2018). As expected, the 70 kDa dextran was not capable of entering the nucleus as it exceeds the size threshold of approximately 40 kDa of the size barrier of the nuclear pore (Mohr et al., 2009). This clearly demonstrates that permeabilisation conditions in the optimised nucleocytoplasmic transport assay are

not interfering with nuclear integrity. However, permeabilisation of the cell membrane and removal of the cytoplasm during the assay will likely interfere with ion concentrations as cytoplasmic components including ions have been removed and replaced with transport buffer. The transport buffer is designed to mimic cytoplasmic ion concentration but will unlikely constitute the perfect replacement. Thus, ion efflux from the nucleus might occur due to a change in ion concentration outside of the nucleus. This might interfere with nuclear pore function as has been shown upon calcium depletion from the perinuclear space (between inner and outer nuclear membrane) (Sarma and Yang, 2011). A change in ion concentration might also lead to a change in nuclear pH levels of semi-permeabilised cells which could affect the hydrogel within the central channel of the nuclear pore and thus nuclear pore permeability as liquid-liquid phase separation is influenced by pH (Alberti and Dormann, 2019). However, the transport buffer system should maintain physiological pH levels but slight pH fluctuations cannot be ruled out. Due to low protein concentration in the transport buffer passive export of nuclear proteins might also be enhanced and more susceptible to stressors in semi-permeabilised cells compared to intact cells. Nevertheless, even though the passive nucleocytoplasmic transport assay constitutes a reductionist system main characteristics of nuclear pore permeability (such as nuclear exclusion of 70 kDa dextran) are maintained as discussed above.

A potential caveat of accurately depicting cargo import levels was the accumulation of dextrans within the nucleolus of the cells. As dextrans became “trapped” in the nucleus and did not diffuse out of the nucleus again, levels of nuclear fluorescence might have been over-estimated. However, nuclear fluorescence levels of GFP which did not accumulate within the nucleolus were still higher at most time points compared to fluorescence of 20 and 40 kDa dextrans. In addition, investigations of this project on potential effects by cell treatments on nucleocytoplasmic transport will be compared to untreated cells separately for each cargo type. Hence, the over-estimation of maximum import levels is probably negligible.

I adapted the nucleocytoplasmic transport assay so I can quantitatively measure passive nuclear import rates. This required the development of a normalisation strategy to account for bleed-through fluorescence from the cargo pool in the media. Therefore, nuclear fluorescence levels at an early timepoint of the reaction before nuclear cargo translocation occurred were subtracted from nuclear fluorescence

levels at all subsequent timepoints. This was followed by dividing these values by the background fluorescence from cargo in the media at respective timepoints to account for potential changes in cargo fluorescence under different experimental conditions. This allows for comparison between experiments. Using this normalisation strategy passive nuclear import of cargo of different sizes can easily be detected and quantified. In summary, this transport assay reflects the physiological properties of the nuclear pore and presents a platform to quantitatively test the impact of pathological conditions on the nucleocytoplasmic transport system.

4 Effect of *C9ORF72* DPRs on passive nucleocytoplasmic transport

As outlined in the introduction (see section 1.5.2) several lines of evidence exist which indicate that nucleocytoplasmic transport is affected in the context of the *C9ORF72* mutation. With regards to active nucleocytoplasmic transport dynamics, shuttling of fluorescent reporter cargo was changed in human cell lines treated with GR polypeptides (Hutten et al., 2020), in GR- and PR-polypeptide treated primary cortical neurons (Hayes et al., 2020) and in *C9ORF72* patient iPSC-derived neurons (Zhang et al., 2015). To add on to these studies we wanted to first study the specific influence of the different *C9ORF72* DPR species on passive nucleocytoplasmic transport. Passive nucleocytoplasmic transport does not depend on transport receptors and Ran but only on the nuclear pore itself. Therefore, these experiments also give information about the functionality of the nuclear pore and about the integrity of its permeability barrier (which should restrict entry of large cargo) upon DPR treatment. To this end, we monitored nucleocytoplasmic transport of 20, 40 and 70 kDa dextrans and GFP using the optimised assay described in chapter 3 in HeLa cells treated with all five different DPR species in the form of polypeptides to test whether *C9ORF72* DPRs change the import rate and maximum import levels of reporter cargo or have an effect on the permeability barrier of the nuclear pore. It is also of note that ALS/FTD hallmark proteins TDP43 and FUS are likely to be, at least partially, passively exported from the nucleus (Archbold et al., 2018; Ederle et al., 2018; Pinarbasi et al., 2018). Therefore, we studied the nuclear export of endogenous proteins, namely the shuttling protein TDP43 and the exclusively nuclear proteins hnRNP C1/2 and histone H3, in semi permeabilised HeLa cells treated with different *C9ORF72* DPR species. This allowed us to investigate whether a change in passive nucleocytoplasmic transport may play a direct role in the cytoplasmic mislocalisation of TDP43 in ALS/FTD.

4.1 Impact of *C9ORF72* DPRs on passive nuclear import of reporter cargo

To study how *C9ORF72* DPRs affect the nucleocytoplasmic transport of fluorescent 20, 40 or 70 kDa dextran and GFP, HeLa cells were subjected to permeabilisation and then treated with 10 µM of the different *C9ORF72* DPRs for 30 minutes immediately prior to following the import of the reporter cargo for 4 minutes at the

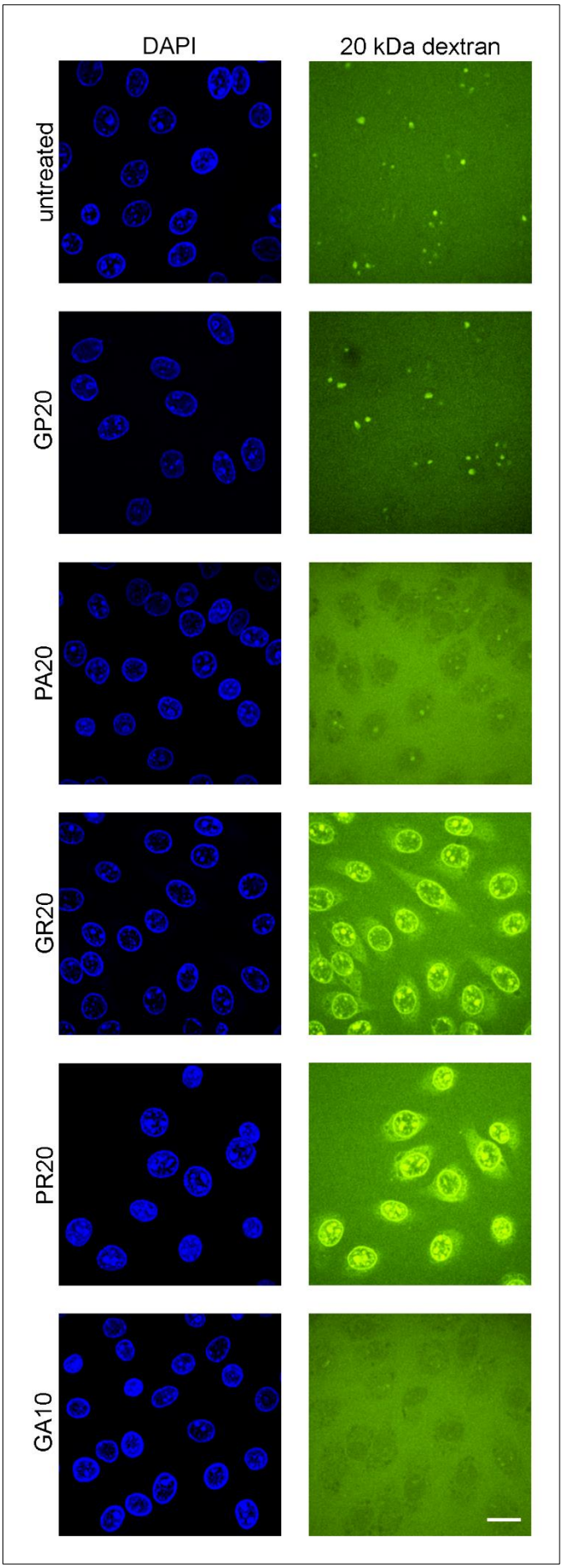
DAPI
20 kDa dextran
untreated
GP20
PA20
GR20
PR20
GA10

Figure 4.1: Effects of different *C9ORF72* DPR species on passive nuclear import of 20 kDa dextran. Spinning disk confocal microscope images of semi-permeabilised untreated HeLa cells and cells treated with 10 µM of different DPR species as indicated for 30 minutes after 4-minute incubation with 20 kDa dextran. Left panel: DAPI channel. Right panel: FITC 20 kDa dextran channel. Scale bar: 20 µm.

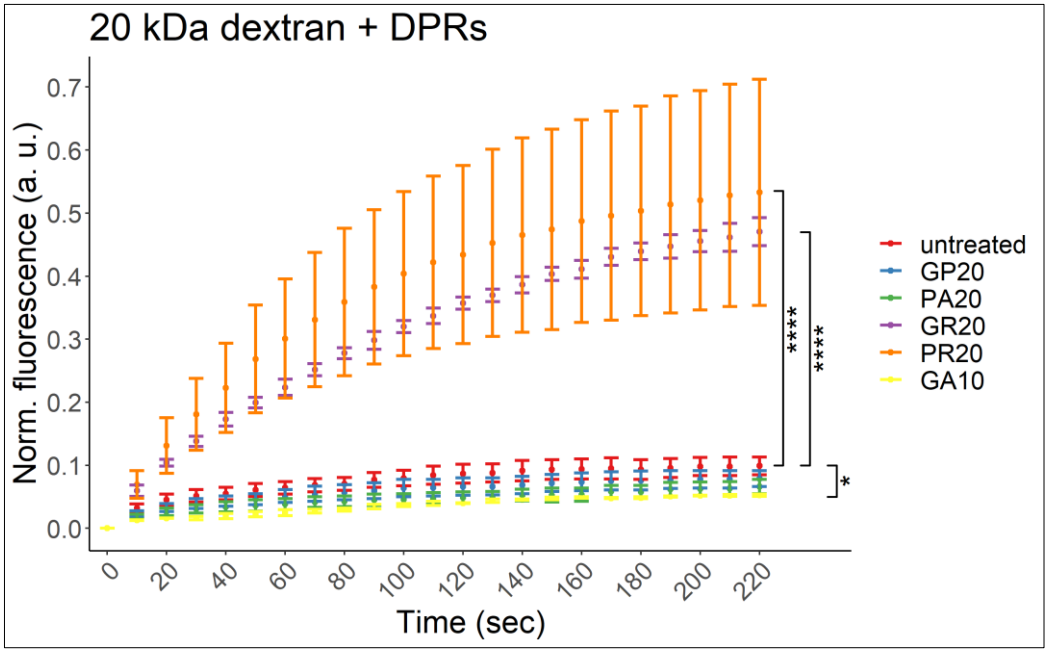

Figure 4.2: Arginine-containing *C9ORF72* DPRs increase nuclear import of 20 kDa dextran. Quantification of passive nuclear import of 20 kDa dextran (shown as nuclear fluorescence normalised to nuclear and general background) over time in semi-permeabilised untreated or DPR treated HeLa cells. Untreated condition depicted in red, GP20 treatment in blue, PA20 in green, GR20 in purple, PR20 in orange, GA10 in yellow. Means of individual experimental means are depicted. N = min. 3. Error bars: SEM. **** $p < 0.0001$ (GR20 and PR20), * $p < 0.05$ (GA10) vs untreated cells with two-way repeated measures ANOVA and Dunnett's post hoc test.

microscope. As shown in Figure 4.1 the 20 kDa dextran clearly translocated into the nucleus accumulating in nuclear structures potentially constituting nucleoli as established in chapter 3. GP20 and PA20 treated cells showed similarly bright nuclei as untreated cells suggesting similar passive import rates in these cells. Nuclei of GR20 and PR20 treated cells were distinctly brighter than those of untreated cells showing significant dextran accumulation in potential nucleolar structures and at the nuclear membrane. GA10 treatment also allowed for nuclear entry of the 20 kDa dextran but nuclei were slightly darker and exhibited less dextran accumulation in nuclear structures than those of untreated cells. This indicates potential lower levels of passive nuclear translocation in GA10 treated cells than in untreated cells. The quantification of passive nuclear import corroborated the imaging findings as depicted in Figure 4.2. The DPR peptides GP20 and PA20 did not have an effect on 20 kDa dextran import as transport curves showed a very similar slope and maximum. The arginine containing DPR species GR20 and PR20 led to a drastic

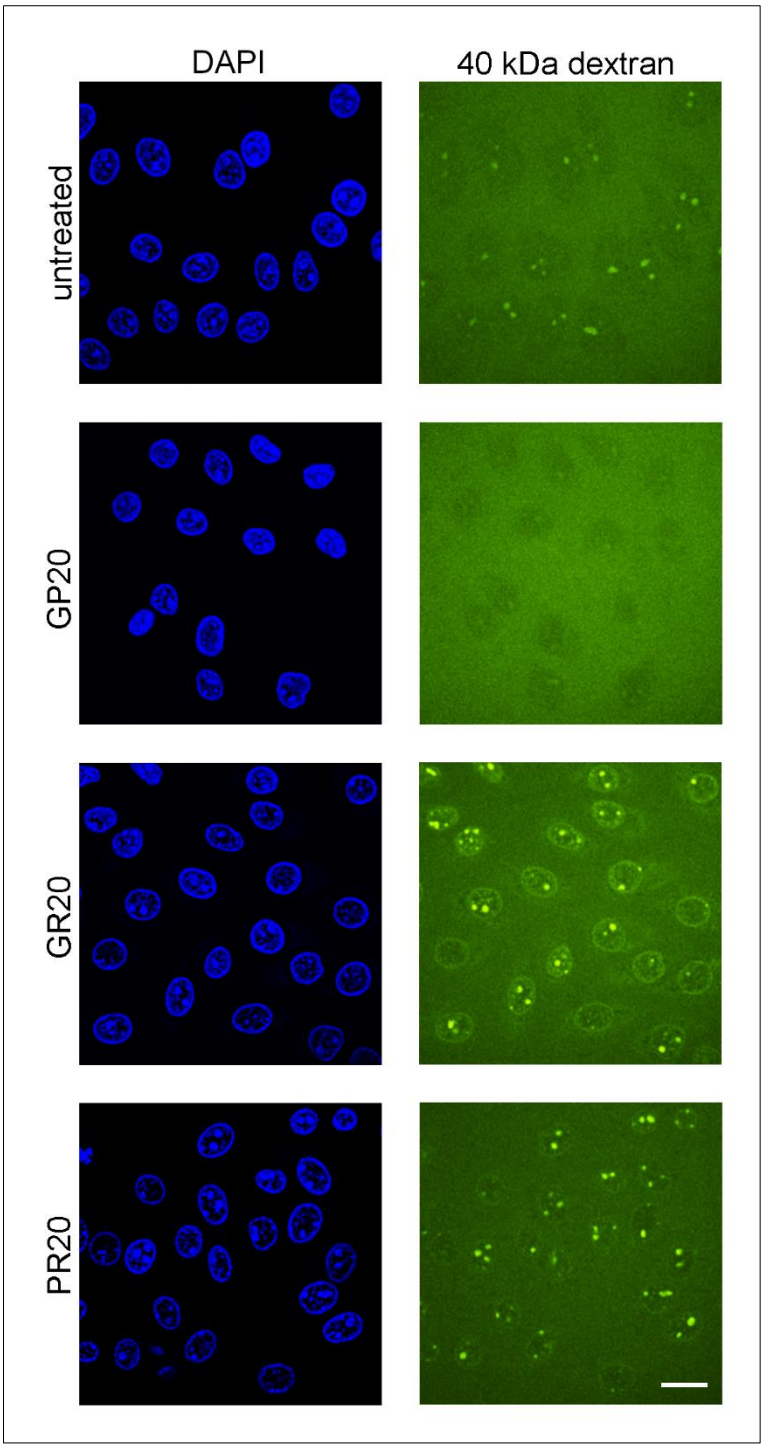

Figure 4.3: Influence of different *C9ORF72* DPR species on passive nuclear import of 40 kDa dextran. Spinning disk confocal microscope images of semi-permeabilised untreated HeLa cells and cells treated with 10 µM of different DPR species as indicated for 30 minutes after 4-minute incubation with 40 kDa dextran. Left panel: DAPI channel. Right panel: FITC 40 kDa dextran channel. Scale bar: 20 µm.

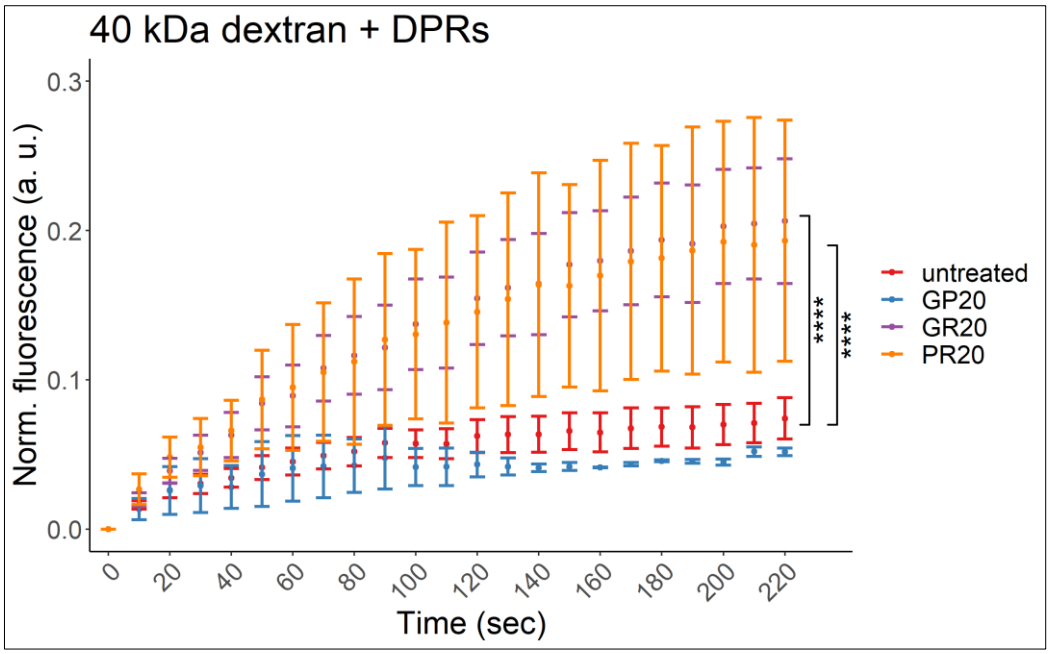

Figure 4.4: Arginine-containing *C9ORF72* DPRs enhance nuclear import of 40 kDa dextran. Quantification of passive nuclear import of 40 kDa dextran (shown as nuclear fluorescence normalised to nuclear and general background) over time in semi-permeabilised untreated or DPR treated HeLa cells. Untreated condition depicted in red, GP20 treatment in blue, GR20 in purple, PR20 in orange. Means of individual experimental means are shown. N = min. 3. Error bars: SEM. **** $p < 0.0001$ vs. untreated cells with two-way repeated measures ANOVA and Dunnett's post hoc test.

increase in import of 20 kDa dextran. The maxima of the average transport curves were 4- and 5-fold higher for GR20 and PR20, respectively, compared to the average untreated condition. These results were highly significant with a *p* value of 2.38×10^{-14} for poly-GR and a *p* value of 1.18×10^{-14} for poly-PR treatment (Dunnett's post-hoc test). Curves were steeper indicating that the transport speed was also increased by the arginine containing DPR species. Notably, the increase in 20 kDa dextran reaching the nucleus could already be seen very early after only 20 seconds. On the contrary, GA10 treatment led to a slight and significant decrease with a *p* value of 0.047 (Dunnett's post-hoc test) in nuclear import of 20 kDa dextran lowering import levels and speed.

As GR20 and PR20 treatment had the most drastic effect on passive nuclear import we decided to focus on these DPRs and to use GP20 as a control for the remaining cargos. As depicted in the images of Figure 4.3 and the quantification in Figure 4.4 GP20 did not alter the import dynamics of 40 kDa compared to the untreated condition. However, GR20 and PR20 treatment led again to a significant increase in nuclear import ($p = 2.66 \times 10^{-14}$ for poly-GR and $p = 1.21 \times 10^{-11}$ for poly-PR treatment,

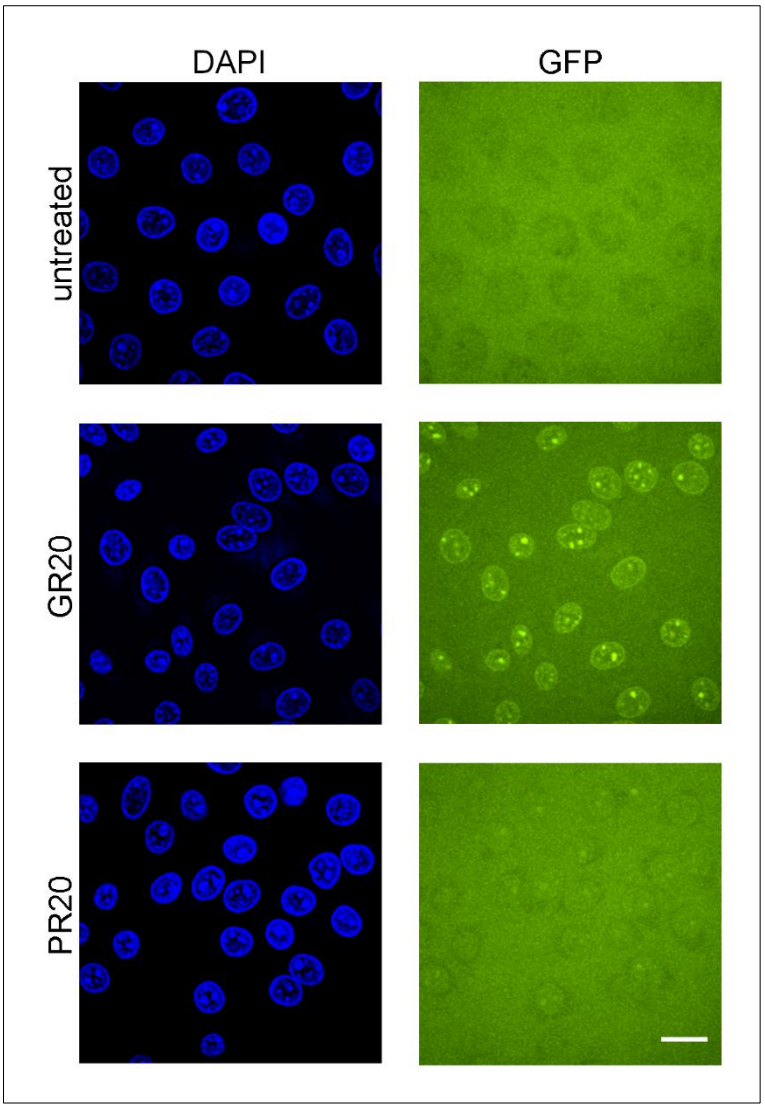

Figure 4.5: Effects of different *C9ORF72* DPR species on passive nuclear import of GFP. Spinning disk confocal microscope images of semi-permeabilised untreated HeLa cells and cells treated with 10 µM of different DPR species as indicated for 30 minutes after 4-minute incubation with GFP. Left panel: DAPI channel. Right panel: GFP channel. Scale bar: 20 µm.

Dunnett's post-hoc test). Maximum import levels were 2.5 times higher compared to untreated cells, so the transport enhancement was less distinct than for the 20 kDa dextran. Interestingly, a rise in transport efficiency only became obvious at later timepoints compared to the 20 kDa dextran. Transport speed seemed to be increased by the arginine containing DPRs, but again to a lesser extent than for the 20 kDa dextran.

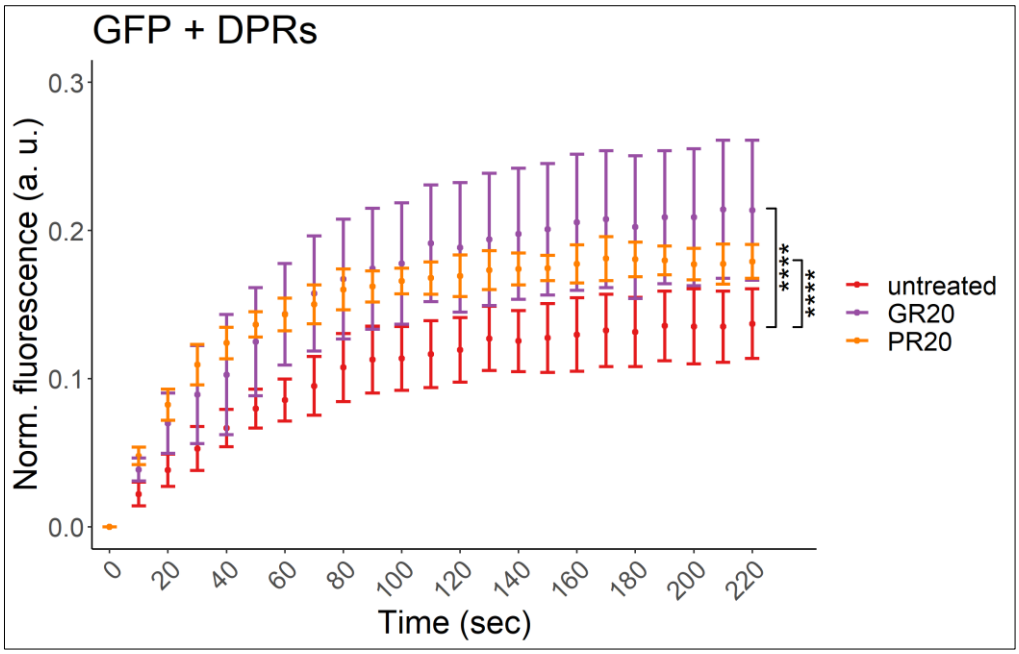

Figure 4.6: Arginine-containing *C9ORF72* DPRs lead to slightly increased nuclear import of GFP. Quantification of passive nuclear import of GFP (shown as nuclear fluorescence normalised to nuclear and general background) over time in semi-permeabilised untreated or DPR treated HeLa cells. Untreated condition depicted in red, GR20 in purple, PR20 in orange. Means of individual experimental means are plotted. N = 3. Error bars: SEM. **** $p < 0.0001$ vs untreated cells with two-way repeated measures ANOVA and Dunnett's post hoc test.

As shown in Figure 4.5 GFP passive nuclear import was increased upon PR20 and GR20 treatment compared to untreated cells with GR20 having a stronger effect than PR20. These effects were highly significant with a *p* value of 3.58×10^{-9} for poly-GR and a *p* value of 2.1×10^{-6} for poly-PR treatment (Dunnett's post-hoc test). GFP nuclear translocation rose by about 1.5-fold and 2-fold upon PR20 and GR20 treatment, respectively, as depicted in Figure 4.6. The slopes of all import curves were very similar indicating that GR20 and PR20 did not significantly change the transport speed of GFP. The effects of GR20 on GFP nuclear import varied as indicated by the large error bars. In some experiments GR20 treatment greatly enhanced nuclear brightness compared to untreated cells as depicted in Figure 4.5 while the effect was more subtle in other experiments.

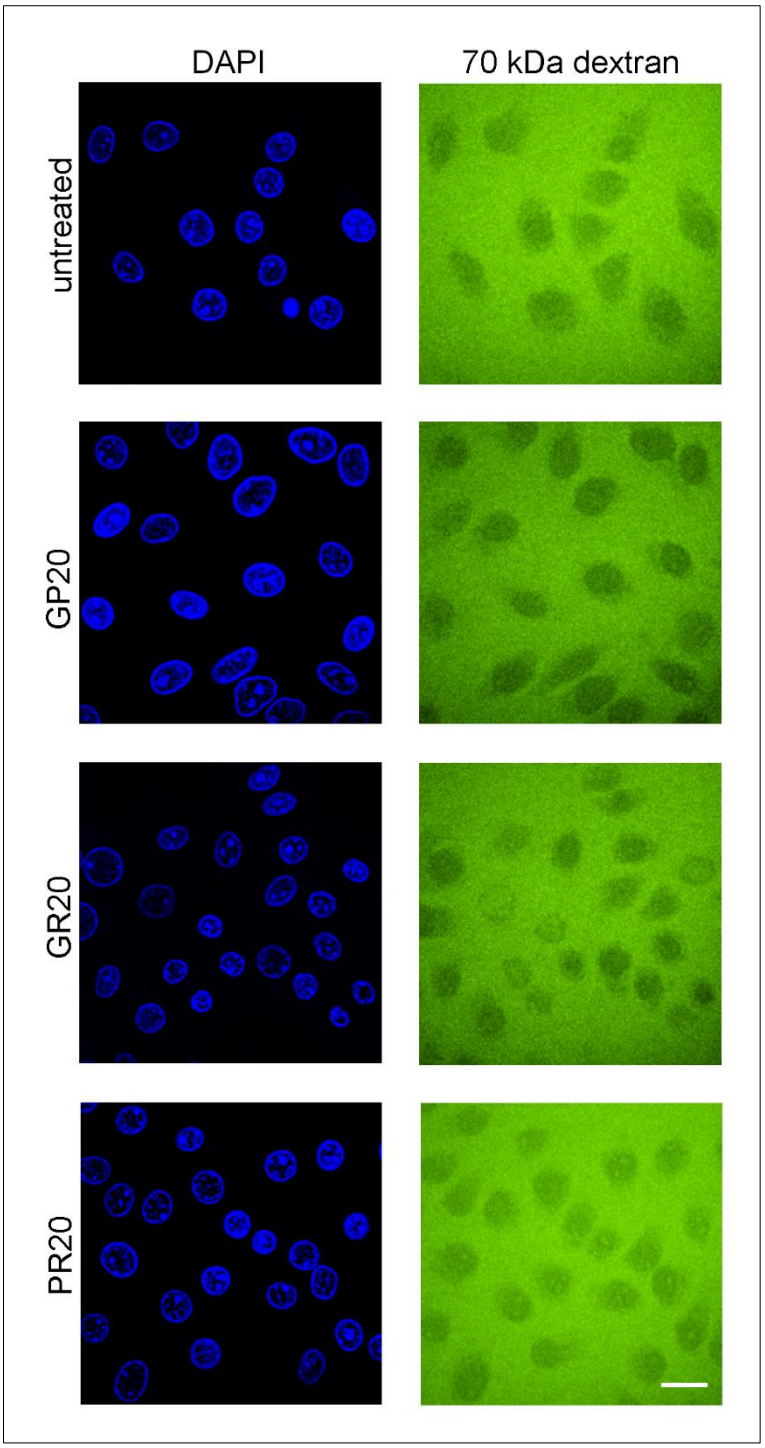

Figure 4.7: Influence of different *C9ORF72* DPR species on passive nuclear import of 70 kDa dextran. Spinning disk confocal microscope images of semi-permeabilised untreated HeLa cells and cells treated with 10 µM of different DPR species as indicated for 30 minutes after 4-minute incubation with 70 kDa dextran. Left panel: DAPI channel. Right panel: FITC 70 kDa dextran channel. Scale bar: 20 µm.

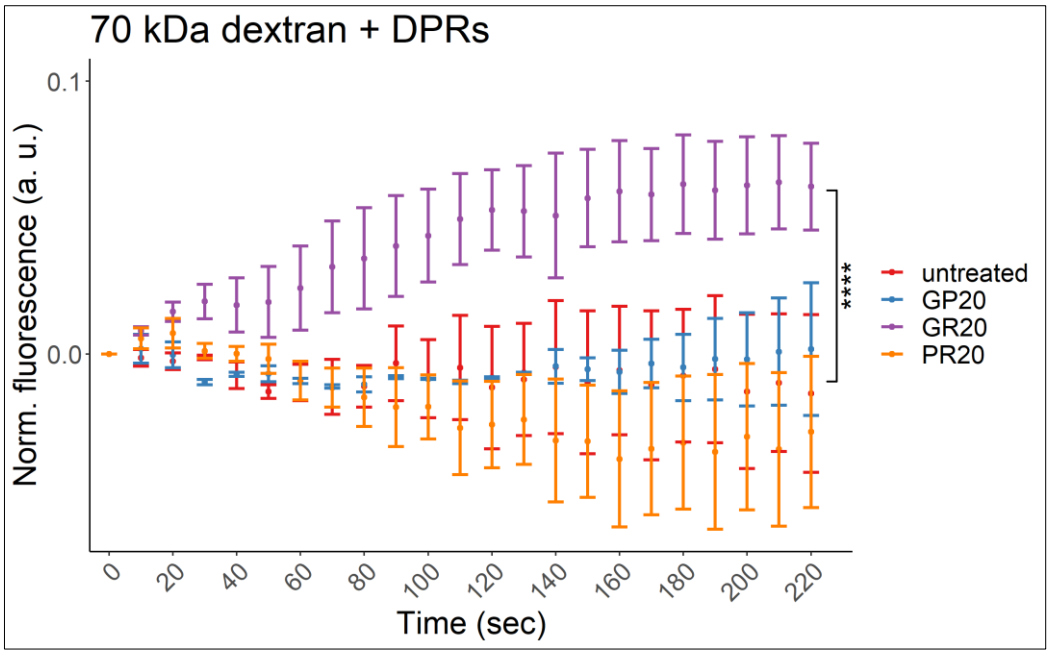

Figure 4.8: GR20 treatment leads to import of 70 kDa dextran at low levels. Quantification of passive nuclear import of 70 kDa dextran (shown as nuclear fluorescence normalised to nuclear and general background) over time in semi-permeabilised untreated or DPR treated HeLa cells. Untreated condition depicted in red, GP20 treatment in blue, GR20 in purple, PR20 in orange. Means of individual experimental means are plotted. N = 3. Error bars: SEM. **** $p < 0.0001$ vs untreated cells with two-way repeated measures ANOVA and Dunnett's post hoc test.

The 70 kDa dextran did not enter the nucleus in untreated cells due to the size-restrictive permeability barrier of the nuclear pore as depicted in the images of Figure 4.7 and the quantification of Figure 4.8. This barrier was preserved when cells were treated with GP20 or PR20. However, GR20 treatment allowed for slow (only starting after about 30 seconds) low level import of 70 kDa ($p = 1.19 \times 10^{-14}$, Dunnett's post-hoc test) indicating that the permeability barrier was slightly affected by GR20.

Overall, GR20 led to an enhancement of passive nucleocytoplasmic transport for all reporter cargo species having the highest impact on the 20 kDa dextran, the smallest cargo and the lowest on the 70 kDa dextran, the largest cargo. PR20 treatment had no effect on the import of the 70 kDa dextran. However, PR20 enhanced the transport of all other cargo species again having the largest effect on the smallest cargo, the 20 kDa dextran. GP20 and PA20 did not affect the import of any reporter cargo while GA10 led to a small reduction in nucleocytoplasmic transport of the 20 kDa dextran. Thus, arginine containing DPR species seemed to have a particularly strong effect on nucleocytoplasmic transport leading to a significant increase of passive nuclear import of several reporter cargoes.

4.2 Impact of a fluorescent tag on the effect of arginine containing *C9ORF72* DPRs on passive nucleocytoplasmic transport

As we intended to further investigate how the arginine containing *C9ORF72* DPRs caused a rise in passive nucleocytoplasmic transport we wanted to visualise the localisation of these DPRs during the transport assay experiment. To this end we used DPRs containing an N-terminal tag of the fluorescent dye Alexa Fluor 647. We again observed the import of 20, 40 and 70 kDa dextran and GFP in the presence of Alexa Flour 647-labelled GR20 and PR20. This allowed us to monitor the localisation of these DPRs within the nucleus during cargo import. As shown in Figure 4.9, Figure 4.11, Figure 4.13 and Figure 4.15 GR20 and PR20-Alexa Fluor 647 were mainly found at the nuclear membrane, nuclear structures possibly constituting nucleoli and at areas surrounding the nuclei which most likely consisted of plasma membrane residues which had not been washed away during the permeabilisation assay.

In terms of the effect on reporter cargo transport by the labelled DPRs the results were rather surprising. The nuclear import of the 20 kDa dextran was not increased by Alexa Fluor 647-tagged GR20 and PR20 but instead was slightly decreased as shown in Figure 4.9 and Figure 4.10. Thus, Alexa Fluor 647 tagged GR20 and PR20 had the exact opposite effect on 20 kDa dextran transport compared to their untagged counterparts.

The picture was very similar for the 40 kDa dextran with Alexa Fluor 647 labelled GR20 and PR20 treatment leading to a reduction in transport levels of this reporter cargo as indicated in Figure 4.11 and Figure 4.12 instead of an enhancement as we had observed for unlabelled GR20 and PR20.

Interestingly, Alexa Fluor 647-tagged GR20 still caused a mild increase in nuclear import of GFP whilst tagged PR20 had no effect as shown in Figure 4.13 and Figure 4.14. The transport enhancement of GFP by labelled GR20 was, however, lower compared to the effect of unlabelled GR20 (2-fold vs 1.3-fold; compare with Figure 4.6).

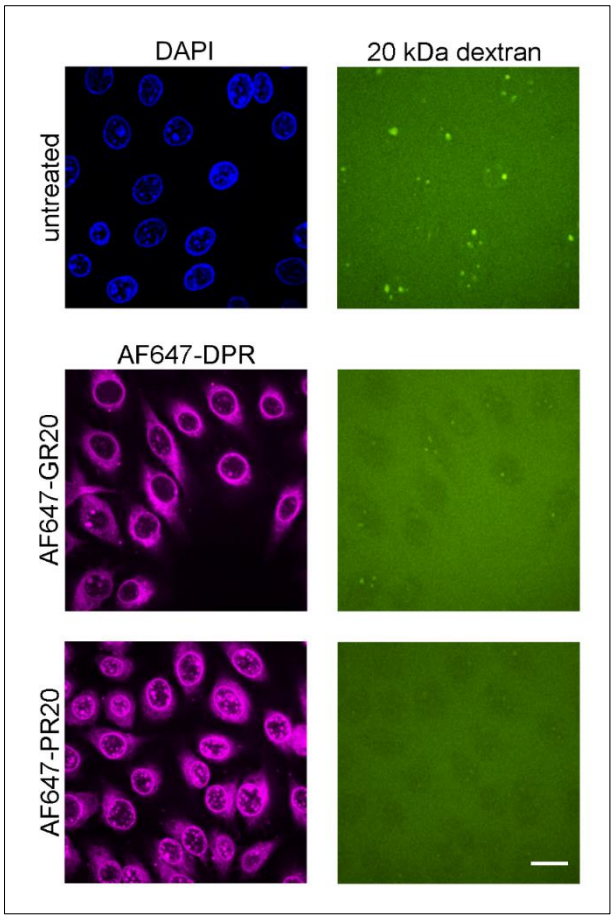

Figure 4.9: Effects of Alexa Fluor 647 labelled arginine containing *C9ORF72* DPR species on passive nuclear import of 20 kDa dextran. Spinning disk confocal microscope images of semi-permeabilised untreated HeLa cells and cells treated with 10 µM of different DPR species as indicated for 30 minutes after 4-minute incubation with 20 kDa dextran. Left panel: Alexa Fluor 647 channel. Right panel: FITC 20 kDa dextran channel. Scale bar: 20 µm.

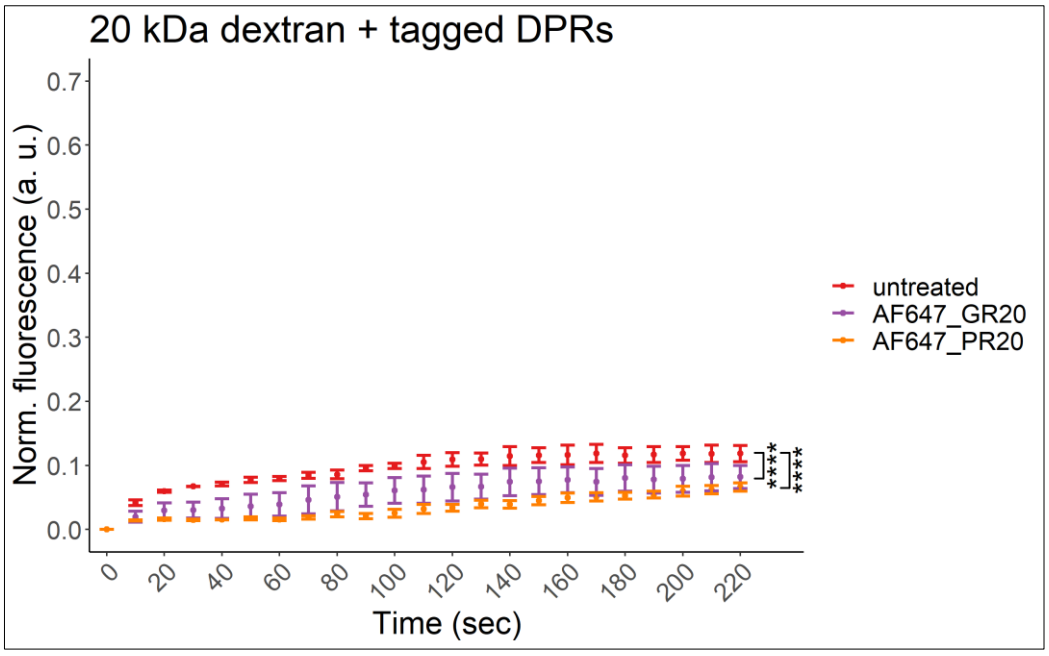

Figure 4.10: Alexa Fluor 647 labelled arginine containing *C9ORF72* DPRs decrease nuclear import of 20 kDa dextran. Quantification of passive nuclear import of 20 kDa dextran (shown as nuclear fluorescence

normalised to nuclear and general background) over time in semi-permeabilised untreated or DPR treated HeLa cells. Untreated condition depicted in red, AF647-GR20 in purple, AF647-PR20 in orange. Means of individual experimental means are shown. N = 3. Error bars: SEM. **** $p < 0.0001$ vs untreated cells with two-way repeated measures ANOVA and Dunnett's post hoc test.

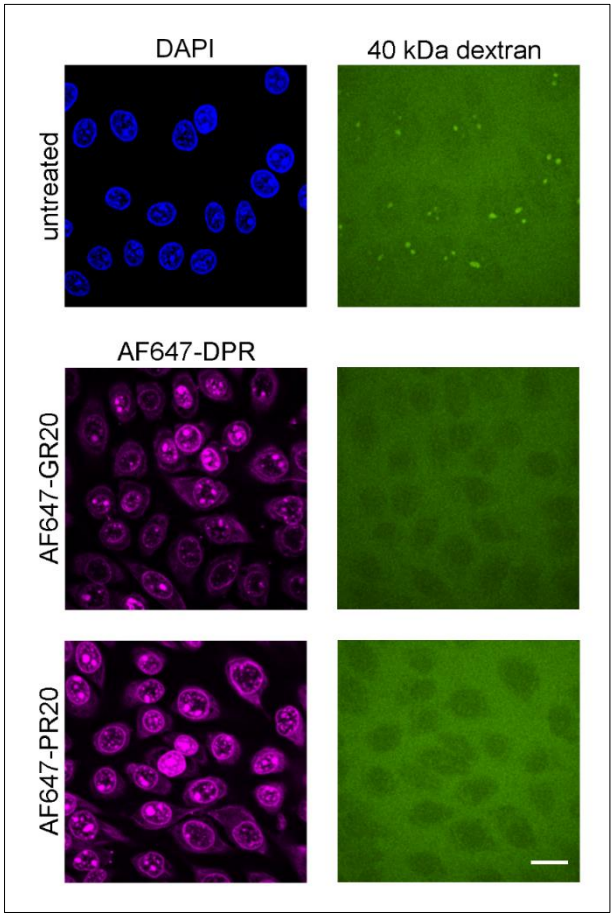

Figure 4.11: Influence of Alexa Fluor 647 labelled arginine containing *C9ORF72* DPR species on passive nuclear import of 40 kDa dextran. Spinning disk confocal microscope images of semi-permeabilised untreated HeLa cells and cells treated with 10 µM of different DPR species as indicated for 30 minutes after 4-minute incubation with 40 kDa dextran. Left panel: Alexa Fluor 647 channel. Right panel: FITC 40 kDa dextran channel. Scale bar: 20 µm.

As depicted in Figure 4.15 and Figure 4.16 Alexa Fluor 647-tagged DPRs did not change the permeability barrier of the nuclear pore thus not leading to nuclear entry of the 70 kDa dextran. This, therefore, differed from results observed with unlabelled GR20 which caused nuclear import of 70 kDa dextran at low levels (compare with Figure 4.8).

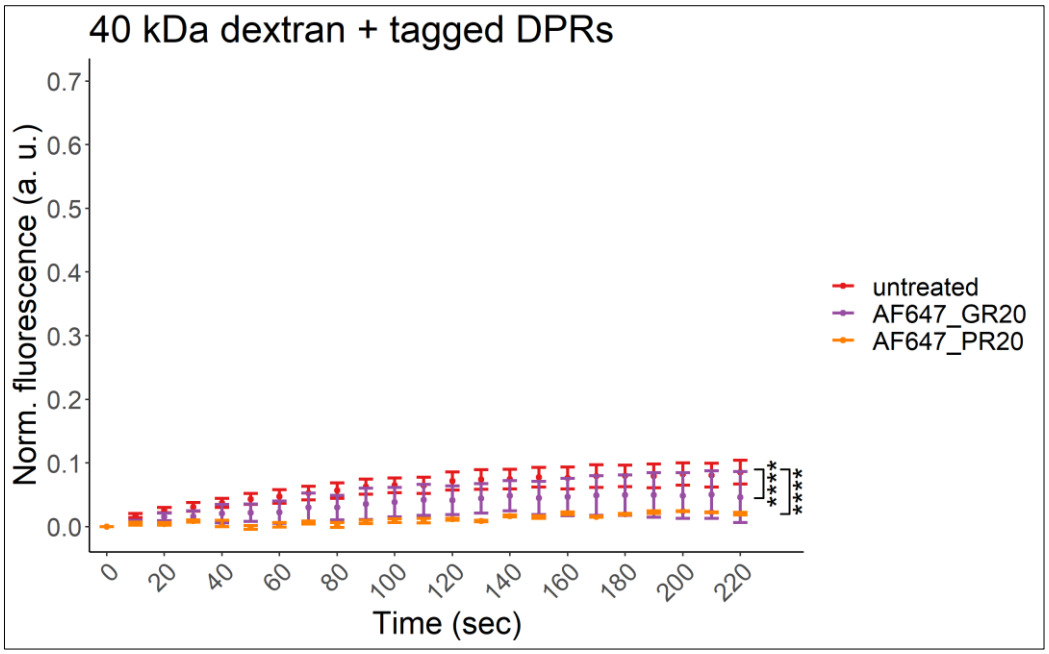

Figure 4.12: Alexa Fluor 647 labelled arginine containing *C9ORF72* DPRs reduce nuclear import of 40 kDa dextran. Quantification of passive nuclear import of 40 kDa dextran (shown as nuclear fluorescence normalised to nuclear and general background) over time in semi-permeabilised untreated or DPR treated HeLa cells. Untreated condition depicted in red, AF647-GR20 in purple, AF647-PR20 in orange. Means of individual experimental means are plotted. N = 3. Error bars: SEM. **** $p < 0.0001$ vs untreated cells with two-way repeated measures ANOVA and Dunnett's post hoc test.

Overall, Alexa Fluor 647-tagged GR20 and PR20 did not seem to be a reliable investigative tool as they led to opposite results for most reporter cargo species compared to untagged GR20 and PR20. These findings highlight the necessity for the usage of unlabelled controls to detect artefact effects when using labelled DPR species.

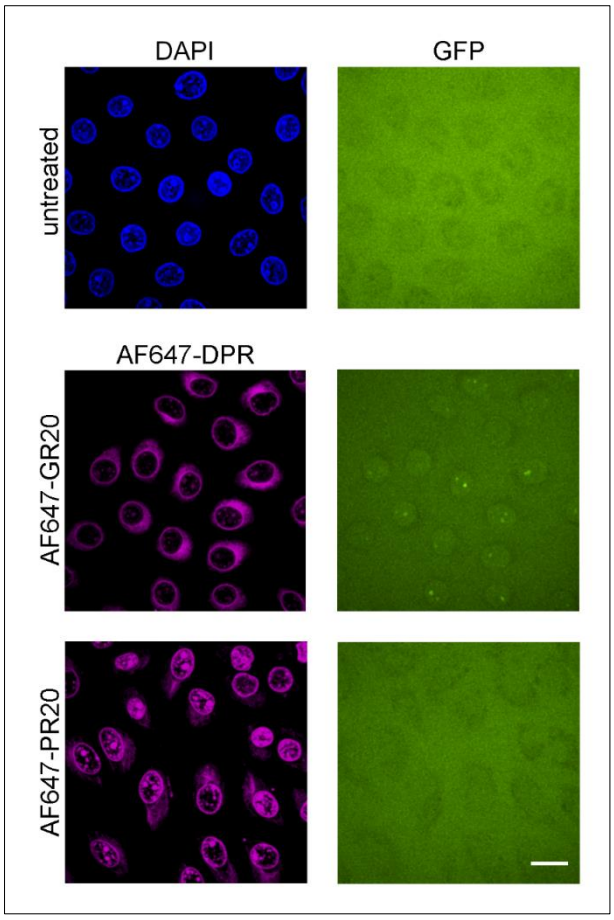

Figure 4.13: Effects of Alexa Fluor 647 labelled arginine containing *C9ORF72* DPR species on passive nuclear import of GFP. Spinning disk confocal microscope images of semi-permeabilised untreated HeLa cells and cells treated with 10 µM of different DPR species as indicated for 30 minutes after 4-minute incubation with GFP. Left panel: Alexa Fluor 647 channel. Right panel: GFP channel. Scale bar: 20 µm.

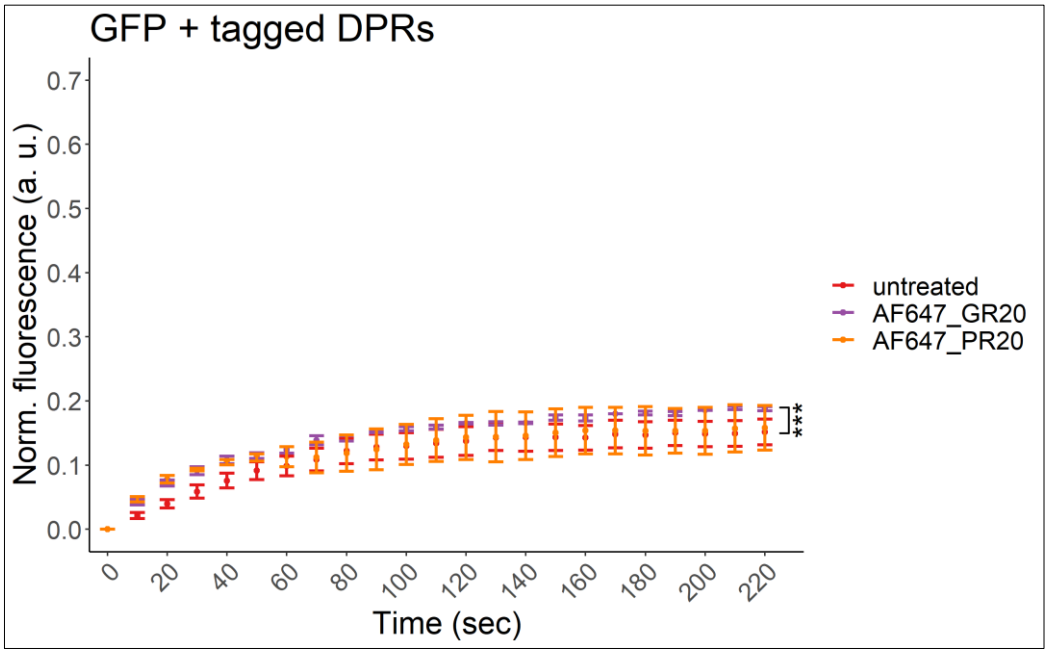

Figure 4.14: Alexa Fluor 647 labelled GR20 slightly enhances nuclear import of GFP. Quantification of passive nuclear import of GFP (shown as nuclear fluorescence normalised to nuclear and general background) over time in semi-permeabilised untreated or DPR treated HeLa cells. Untreated condition depicted in red,

AF647-GR20 in purple, AF647-PR20 in orange. Means of individual experimental means are depicted. N = 3. Error bars: SEM. *** $p < 0.001$ vs untreated cells with two-way repeated measures ANOVA and Dunnett's post hoc test.

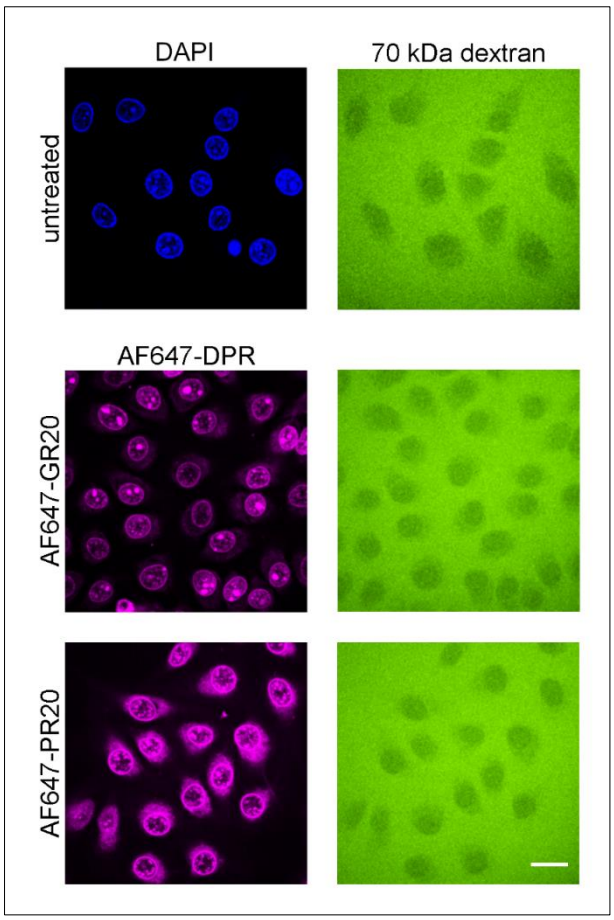

Figure 4.15: Influence of Alexa Fluor 647 labelled arginine containing *C9ORF72* DPR species on passive nuclear import of 70 kDa dextran. Spinning disk confocal microscope images of semi-permeabilised untreated HeLa cells and cells treated with 10 µM of different DPR species as indicated for 30 minutes after 4-minute incubation with 70 kDa dextran. Left panel: Alexa Fluor 647 channel. Right panel: FITC 70 kDa dextran channel. Scale bar: 20 µm.

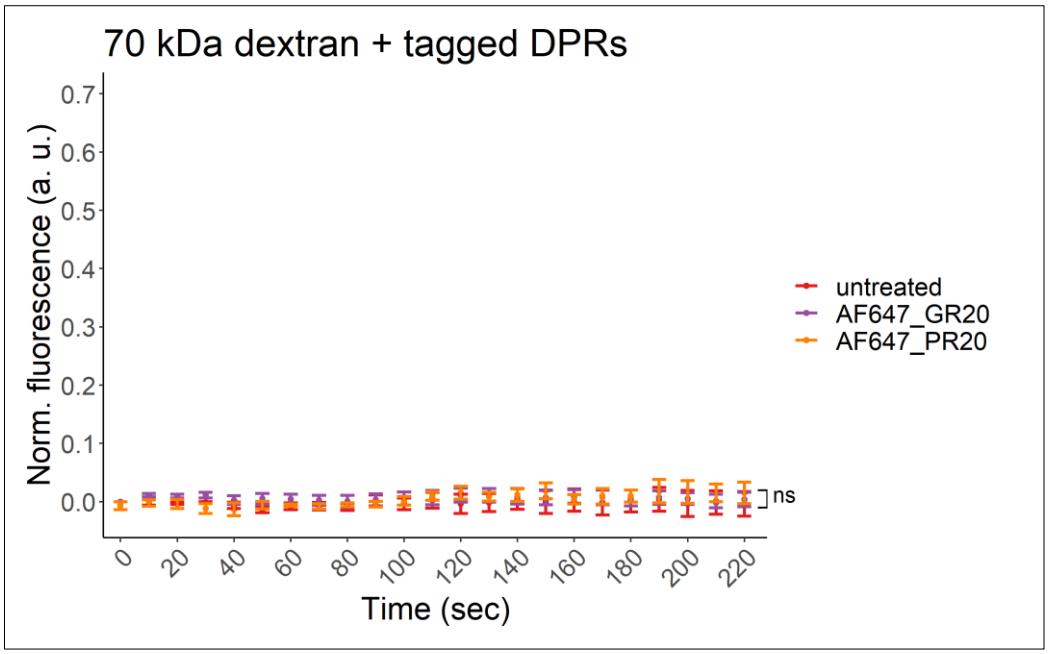

Figure 4.16: Alexa Fluor 647 labelled arginine containing *C9ORF72* DPR treatment does not result in nuclear import of 70 kDa dextran. Quantification of passive nuclear import of 70 kDa dextran (shown as nuclear fluorescence normalised to nuclear and general background) over time in semi-permeabilised untreated or DPR treated HeLa cells. Untreated condition depicted in red, AF647-GR20 in purple, AF647-PR20 in orange. Means of individual experimental means are depicted. Error bars: SEM. Ns: non-significant vs untreated cells with two-way repeated measures ANOVA and Dunnett's post hoc test.

4.3 Influence of *C9ORF72* DPRs on nuclear export of endogenous nuclear proteins

As arginine containing *C9ORF72* DPRs drastically increased import dynamics of reporter cargo we were interested to see whether they also had an effect on endogenous cargo proteins. To this end, HeLa cells were subjected to the same permeabilisation assay as described above (i.e., the plasma membrane of the tested cells was permeabilised) but fixed after 10 µM or 50 µM DPR treatment at various timepoints and immunostained for endogenous TDP43, hnRNP C1/2 and histone H3. TDP43 shuttles between the nucleus and the cytoplasm but is mainly nuclear (Ayala et al., 2008) while hnRNP C1/2 and histone H3 are exclusively located to the nucleus (Campos et al., 2010; Piñol-Roma and Dreyfuss, 1992). As TDP43 is mislocalised to the cytoplasm in *C9ORF72* ALS/FTD (Neumann et al., 2006) and can be passively exported from the nucleus (Archbold et al., 2018; Ederle et al., 2018; Pinarbasi et al., 2018) we wanted to investigate its nuclear export in the presence of *C9ORF72* DPRs.

As depicted in Figure 4.17 and Figure 4.20A after a 30-minute treatment with 10 or 50 µM GP20 TDP43 remained nuclear with nuclear TDP43 fluorescence intensities being comparable to untreated controls. A slight significant reduction in nuclear TDP43 intensity was observed after treating cells with 10 µM GP20 for 30 minutes but this decrease was not found consistently with different treatment times (see below). GR20 at a concentration of 10 µM, which led to an increase in passive nuclear import of reporter cargo, did not cause a significant reduction of nuclear TDP43 levels after a 30-minute treatment (see Figure 4.20A). The nuclear staining pattern did differ, however, compared to untreated nuclei with TDP43 looking less condensed (see Figure 4.17). Nuclear TDP43 levels were, however, significantly decreased after a 30-minute treatment with 50 µM GR20 (p = 3.88x10-^{9}, Dunnett's post-hoc test) suggesting that this DPR species has the capacity to cause a nuclear loss of TDP43. 10 µM and 50 µM PR20 both led to a significant decline in nuclear TDP43 after 30 minutes (p = 0.02 for 10 µM PR20 and p near 0 for 50 µM PR20, Dunnett's post-hoc test) with 50 µM PR20 having a more severe effect. PR20 already caused a nuclear loss of TDP43 at a concentration of 10 µM suggesting that PR20 had a stronger effect on nuclear TDP43 localisation than GR20. GA10 treatment which led to a slight reduction in nuclear import of the 20 kDa dextran (see Figure 4.2) did not change nuclear TDP43 levels at either concentration tested after 30 minutes (see Figure 4.17 and Figure 4.20A).

Results were quite similar for 60-minute DPR treatments compared to 30-minute treatments as shown in Figure 4.18 and Figure 4.20B. GP20 and GA10 at 10 µM and 50 µM did not cause a change in nuclear TDP43 levels after 60 minutes. 10 µM GR20 did not significantly decrease nuclear TDP43 but again resulted in a less condensed nuclear TDP43 staining pattern. Nuclear TDP43 levels were significantly reduced upon 50 µM GR20 treatment with a p value of 1.58x10^{-7} (Dunnett's post-hoc test). Both 10 µM and 50 µM PR20 again drastically reduced nuclear TDP43 levels after 60 minutes (p = 1.65x10-9 for 10 µM PR20 and p near 0 for 50 µM PR20, Dunnett's post-hoc test) with the higher concentration having a stronger effect.

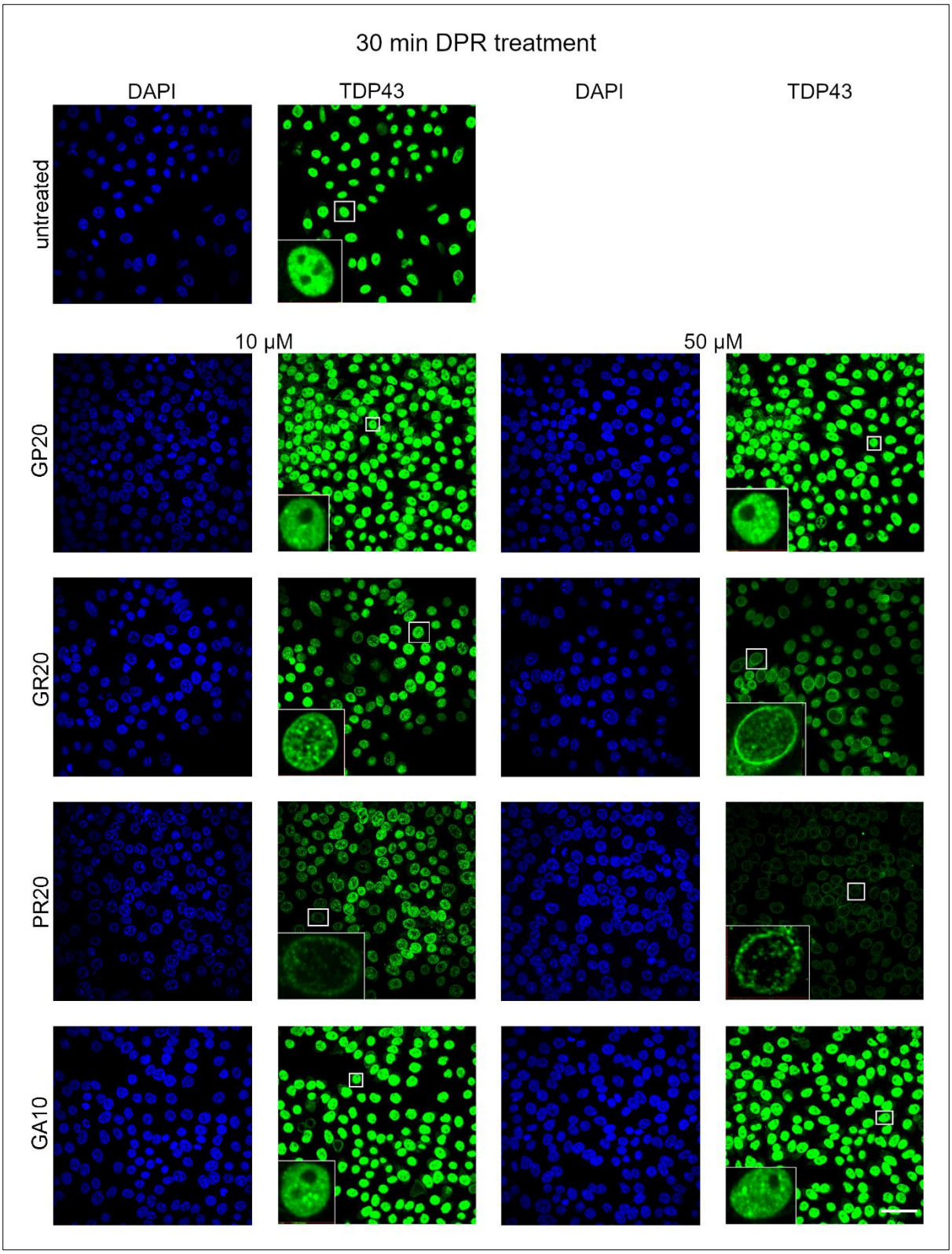

Figure 4.17: Effects of *C9ORF72*DPRs on nuclear localisation of TDP43. Opera Phenix images of immunofluorescence staining of endogenous TDP43 in semi-permeabilised untreated cells or after 30-minute treatment with different *C9ORF72* dipeptide repeat proteins at varying concentrations as indicated. Left panel: DAPI. First from left panel: TDP43. First from right panel: DAPI. Right panel: TDP43. Zoom ins are at different brightness and contrast settings as main images. Scale bar: 50 µm.

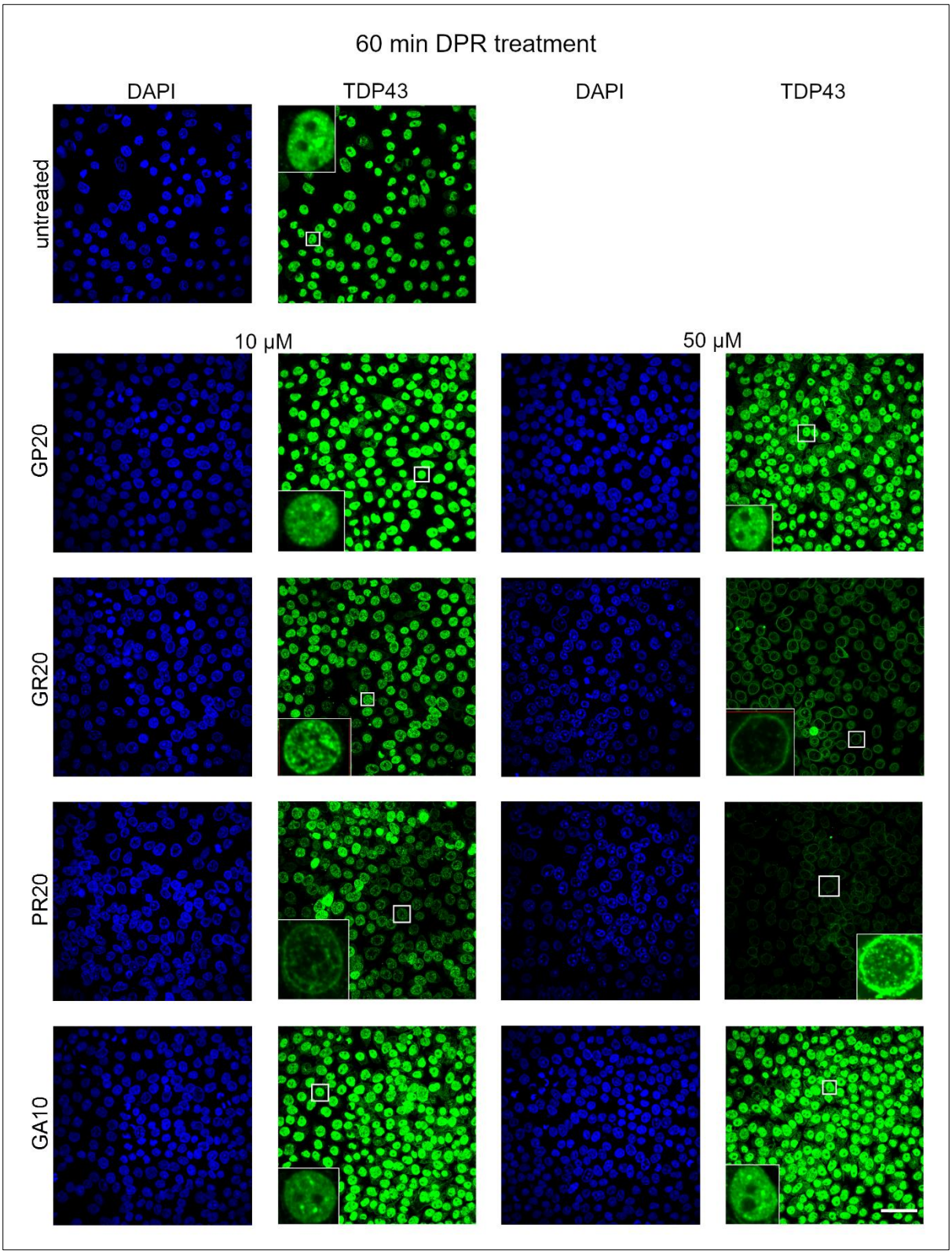

Figure 4.18: Effects of *C9ORF72* DPRs on nuclear TDP43 levels. Opera Phenix images of immunofluorescence staining of endogenous TDP43 in semi-permeabilised untreated cells or after 60-minute treatment with different *C9ORF72* dipeptide repeat proteins at varying concentrations as indicated. Left panel: DAPI. First from left panel: TDP43. First from right panel: DAPI. Right panel: TDP43. Zoom ins are at different brightness and contrast settings as main images. Scale bar: 50 µm.

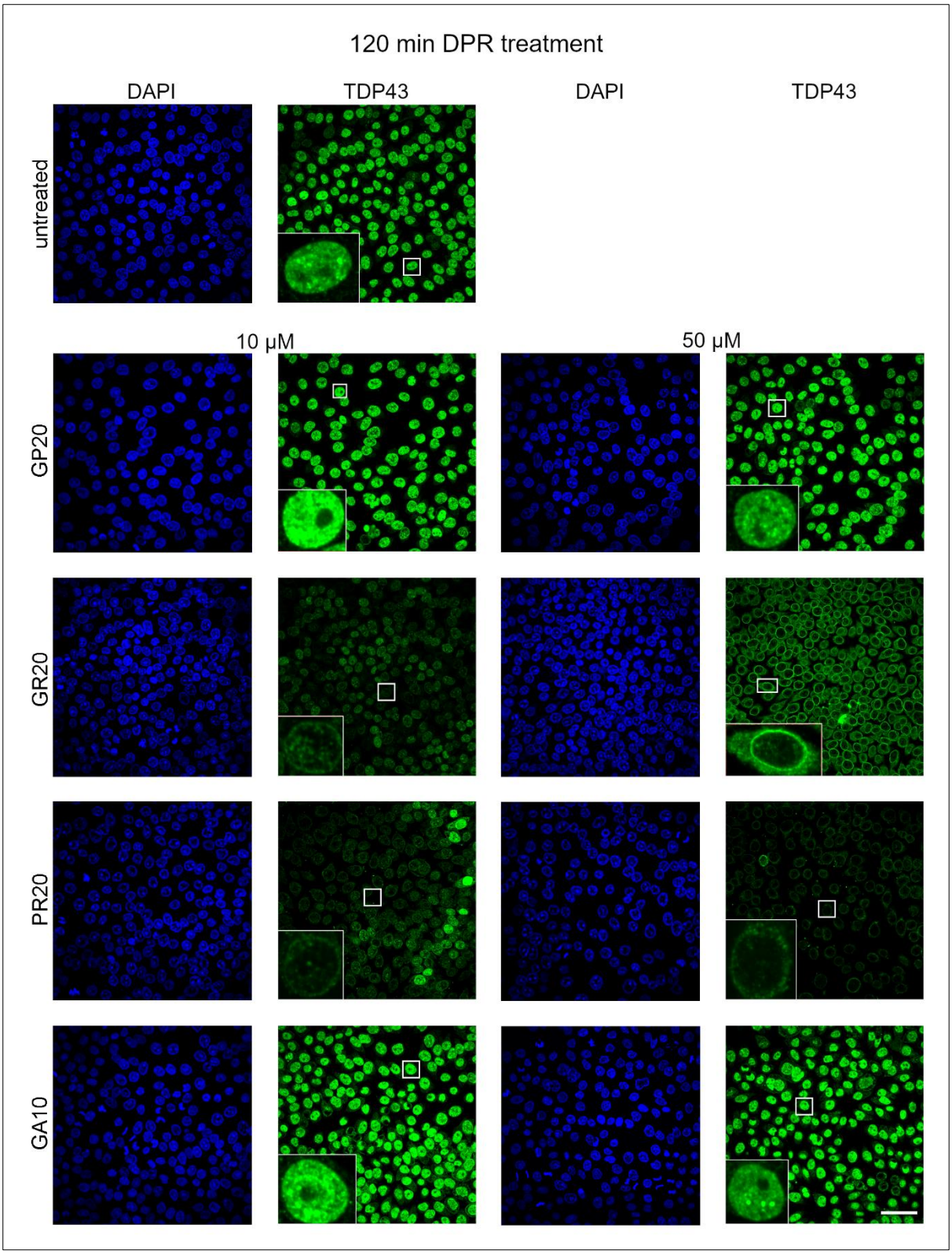

Figure 4.19: Influence of *C9ORF72* DPRs on nuclear localisation of TDP43. Opera Phenix images of immunofluorescence staining of endogenous TDP43 in semi-permeabilised untreated cells or after 120-minute treatment with different *C9ORF72* dipeptide repeat proteins at varying concentrations as indicated. Left panel: DAPI. First from left panel: TDP43. First from right panel: DAPI. Right panel: TDP43. Zoom ins are at different brightness and contrast settings as main images. Scale bar: 50 µm.

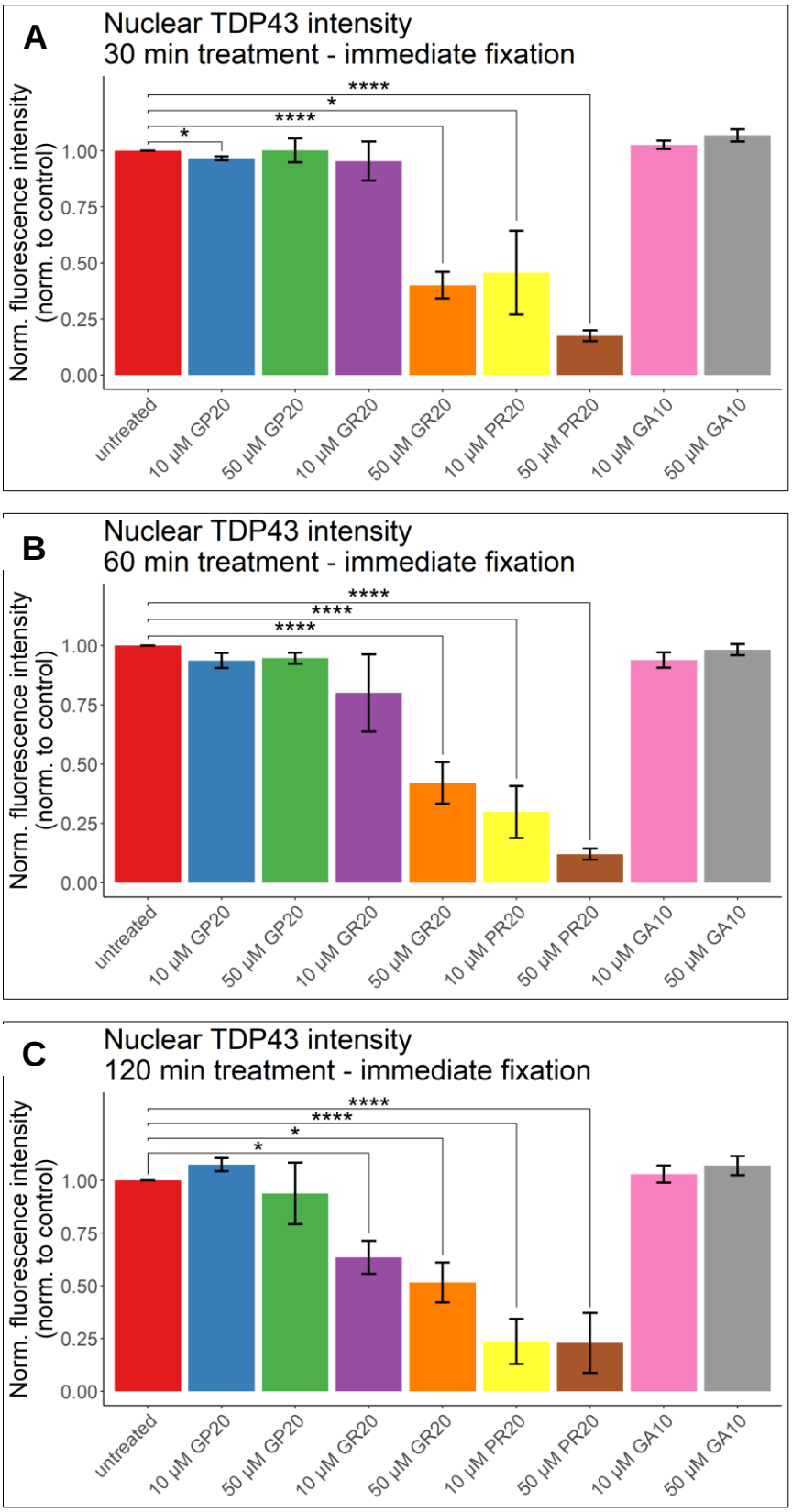

Figure 4.20: Arginine containing *C9ORF72* DPRs reduce nuclear TDP43 levels. Quantified nuclear TDP43 fluorescence signal normalised to untreated control in untreated or cells treated with varying concentrations of different DPRs as indicated. A) 30-minute DPR treatment. B) 60-minute DPR treatment. C) 120-minute DPR treatment. Means of individual experimental means are plotted. Error bars: SEM. **** $p<0.0001$, * $p < 0.05$ vs untreated cells with multi-level model one-way ANOVA and Dunnett's post hoc test.

After 120 minutes GP20 and GA10 did not affect nuclear TDP43 localisation at either concentration compared to untreated cells as depicted in Figure 4.19 and Figure 4.20C. However, nuclear staining seemed to be weaker also in the untreated cells when compared to the 30-minute timepoint (compare Figure 4.17 and Figure 4.19). This was probably owed to the longer incubation of permeabilised cells resulting in a slight loss of nuclear TDP43 irrespective of treatment. 10 µM GR20 did lead to a significant decrease in nuclear TDP43 levels after a treatment time of 120 minutes (see Figure 4.20C) with a *p* value of 0.013 (Dunnett's post-hoc test). The higher GR20 concentration again reduced nuclear TDP43 levels further. PR20 decreased nuclear TDP43 at both concentrations tested after 120 minutes. This reduction was highly significant with a *p* value of 2.86×10^{-14} for 10 µM PR20 and a *p* value of 2.79×10^{-9} for 50 µM PR20 treatment (Dunnett's post-hoc test). 50 µM PR20 had a more severe effect than 10 µM PR20 but the effect of 10 µM PR20 was also increased by the longer treatment time.

We wanted to investigate whether the increased effect of longer DPR treatment on nuclear TDP43 localisation was due to the actual treatment time or was just caused by a general longer incubation of permeabilised cells. Therefore, cells were treated with 10 and 50 µM GR20 for 30 or 60 minutes. DPRs were then washed away, and cells were still incubated for a total of up to 120 minutes.
As depicted in Figure 4.21A and Figure 4.23A 50 µM GR20 treatment led to a reduction of nuclear TDP43 compared to untreated cells when cells were treated with this DPR for 30 minutes and then incubated for 60 minutes in total. Nuclear TDP43 was not significantly decreased by 10 µM GR20 under these conditions. Similarly, 50 µM GR20 decreased nuclear TDP43 localisation upon 30-minute DPR treatment and subsequent incubation for further 90 minutes (total of 120 minutes) while 10 µM GR20 had no effect compared to untreated cells as shown in Figure 4.21B and Figure 4.23B.

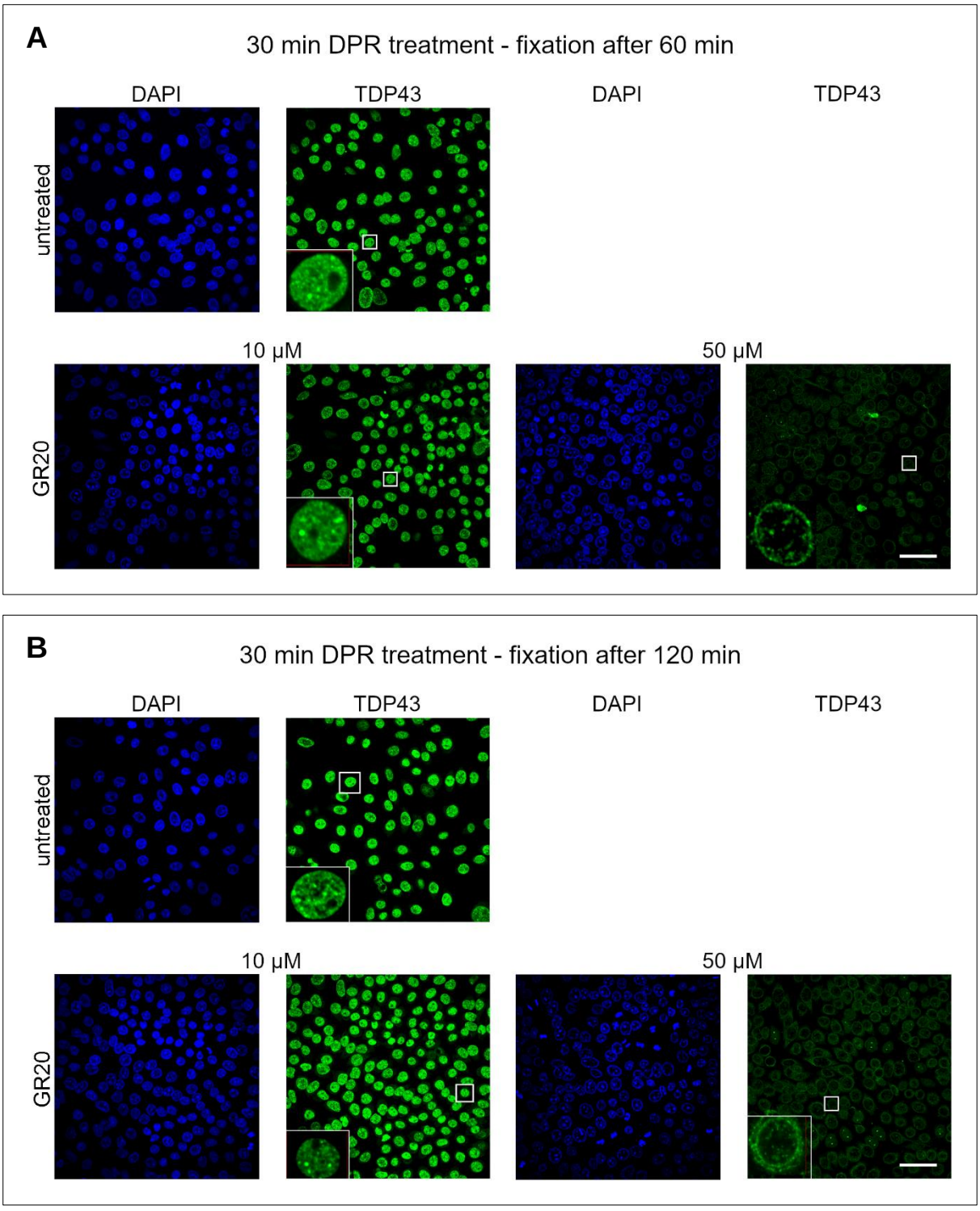

Figure 4.21: Effects of GR on nuclear TDP43 levels. Opera Phenix images of immunofluorescence staining of endogenous TDP43 in semi-permeabilised untreated cells or after 30-minute treatment with GR20 polypeptide at varying concentrations as indicated. A) 30-minute DPR treatment and fixation after further 30 minutes. B) 30-minute DPR treatment and fixation after further 90 minutes. Left panel: DAPI. First from left panel: TDP43. First from right panel: DAPI. Right panel: TDP43. Zoom ins are at different brightness and contrast settings as main images. Scale bar: 50 µm.

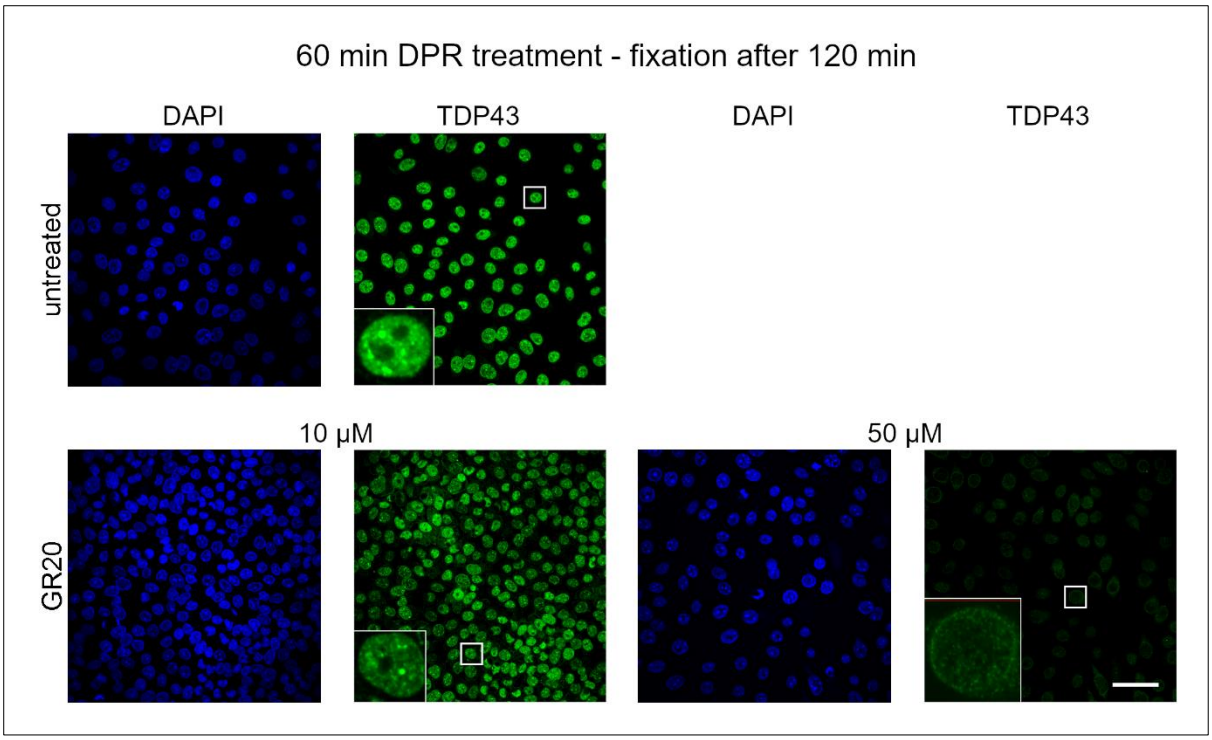

Figure 4.22: Effects of GR on nuclear TDP43 localisation. Opera Phenix images of immunofluorescence staining of endogenous TDP43 in semi-permeabilised untreated cells or after 60-minute treatment with GR20 polypeptide at varying concentrations as indicated with fixation after further 60 minutes. Left panel: DAPI. First from left panel: TDP43. First from right panel: DAPI. Right panel: TDP43. Zoom ins are at different brightness and contrast settings as main images. Scale bar: 50 µm.

Again 60-minute treatment with subsequent incubation for a total of 120 minutes with 50 µM GR20 resulted in lowered nuclear TDP43 levels compared to untreated cells as shown in Figure 4.22 and Figure 4.23C. 10 µM GR20 treatment again did not affect nuclear TDP43 levels under these conditions. This clearly indicates that the longer treatment with 10 µM GR20 was necessary to have a significant effect on nuclear TDP43 localisation. Of note, washing out of GR20 could not lead to re-import of TDP43 from the cytoplasm as cells were permeabilised and TDP43 exiting the nucleus would disperse in the media.

Overall, these experiments clearly demonstrated that arginine containing *C9ORF72* DPRs have the capacity to cause nuclear loss of TDP43 in permeabilised cells.

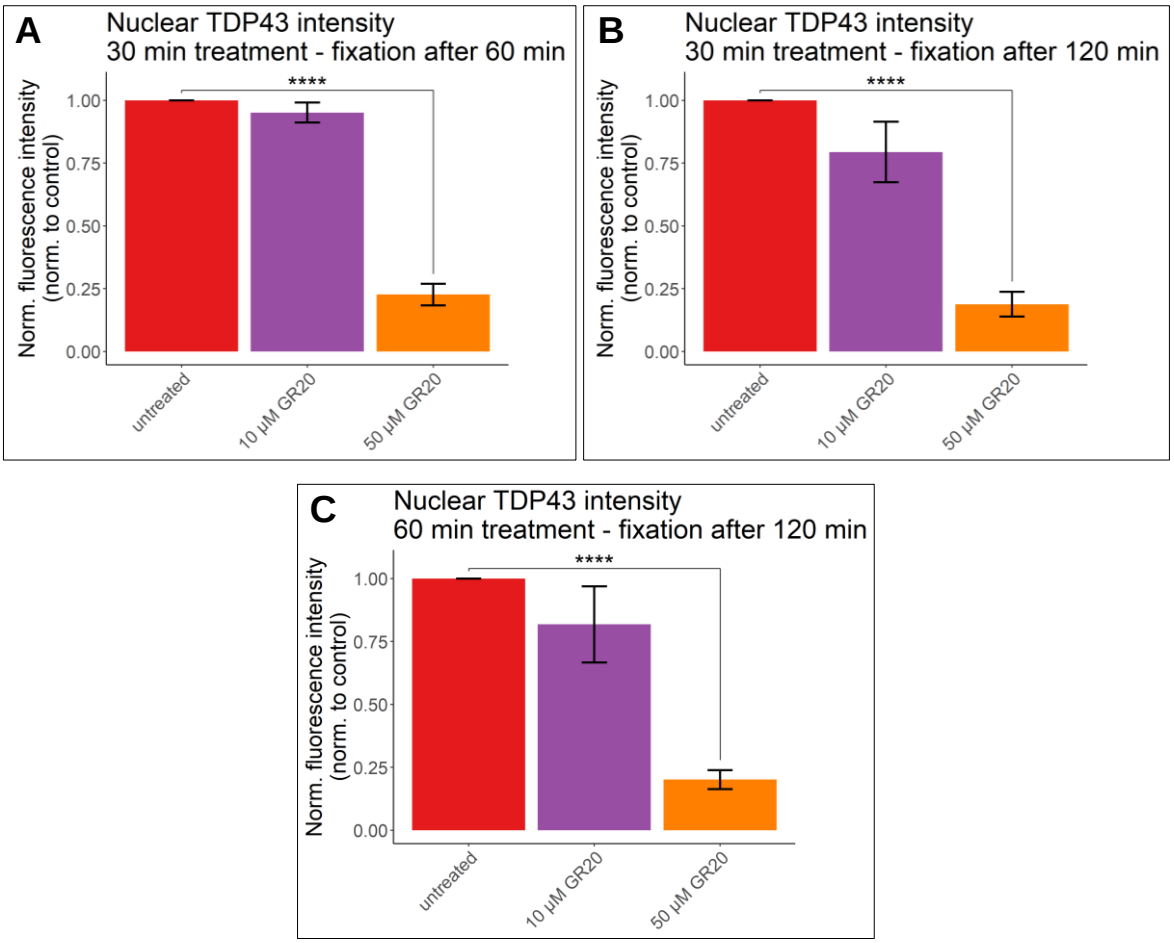

Figure 4.23: GR decreases nuclear TDP43 levels. Quantified nuclear TDP43 fluorescence signal normalised to untreated control in untreated or cells treated with varying concentrations of GR20 as indicated. A) 30-minute DPR treatment and fixation after further 30 minutes. B) 60-minute DPR treatment and fixation after further 90 minutes. C) 60-minute DPR treatment and fixation after further 60 minutes. Means of individual experimental means are shown. Error bars: SEM. **** $p<0.0001$ vs untreated cells with multi-level model one-way ANOVA and Dunnett's post hoc test.

To test if this effect was specific for TDP43 or proteins shuttling between the nucleus and the cytoplasm we immunostained permeabilised cells for the exclusively nuclear proteins hnRNP C1/2 and histone H3. Similar to TDP43, nuclear hnRNP C1/2 levels were not reduced by GP20 and GA10 at concentrations of 10 or 50 µM after 30 minutes as depicted in Figure 4.24 and Figure 4.27A. Again 10 µM GR20 treatment did not lead to a decrease in nuclear hnRNP C1/2 while 50 µM GR20 did reduce nuclear hnRNP C1/2 after 30 minutes. However, the effect of 50 µM GR20 was less drastic on nuclear hnRNP C1/2 than on nuclear TDP43 (40 % versus 65 % reduction; compare with Figure 4.20A). 10 µM PR20 did not reduce nuclear hnRNP C1/2 levels after 30 minutes (see Figure 4.24 and Figure 4.27A). HnRNP C1/2 was lost from the nucleus after a 30 minute-PR20 treatment at a concentration of 50 µM.

Again, after 60 minutes there was no change in nuclear hnRNP C1/2 levels in GP20 or GA10 treated cells compared to untreated cells as shown in Figure 4.25 and Figure 4.27B. 10 µM GR20 did not affect nuclear localisation of hnRNP C1/2 after 60 minutes either but nuclear hnRNP C1/2 was reduced at levels comparable to TDP43 after higher concentration GR20 treatment. Again 10 µM PR20 seemed to have some effect on nuclear hnRNP C1/2 after 60 minutes but this was not significant. Nuclear hnRNP C1/2 levels were drastically reduced by 50 µM PR20 after 60 minutes.

After 120 minutes nuclear hnRNP C1/2 levels still remained unchanged after GP20 and GA10 treatment compared to untreated cells as depicted in Figure 4.26 and Figure 4.27C. In contrast to its effect on TDP43, 10 µM GR20 treatment did not result in lower nuclear hnRNP C1/2 levels compared to control cells even after the longer treatment period of 120 minutes. 50 µM GR20 again reduced nuclear hnRNP C1/2 after 120 minutes with the effect being stronger compared to shorter treatment periods. The decrease of nuclear hnRNP C1/2 was significant after a 120 minute-treatment with 10 µM PR20 and 50 µM PR20 again strongly lowered nuclear hnRNP C1/2 levels. While the effects on nuclear localisation by arginine containing DPRs were not exclusive to TDP43 they were not as strong for hnRNP C1/2, with 10 µM GR20 having no effect on its localisation even after longer treatment times and 10 µM PR20 only having a significant influence after 120 minutes.

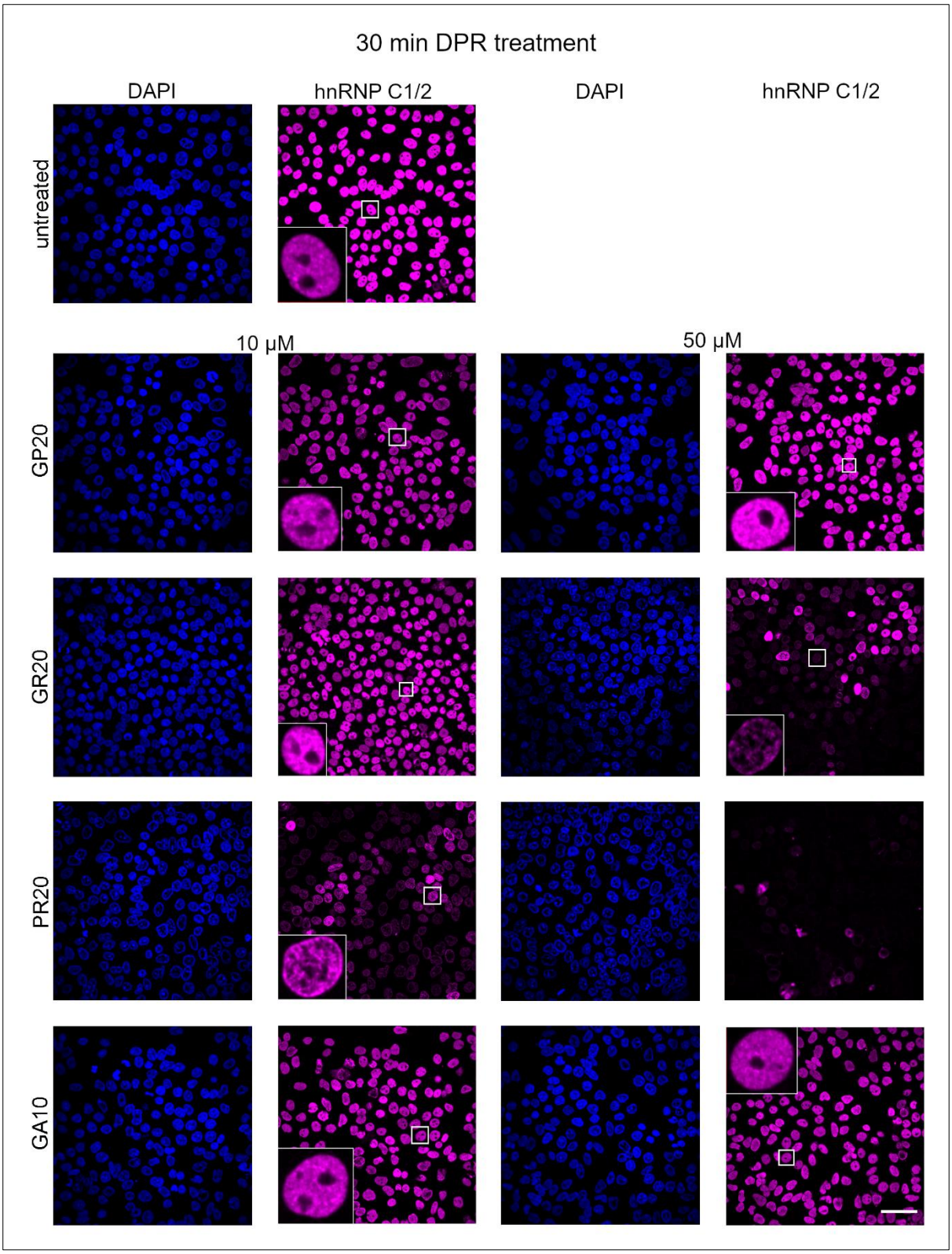

Figure 4.24: Influence of *C9ORF72* DPRs on nuclear hnRNP C1/2 levels. Opera Phenix images of immunofluorescence staining of endogenous hnRNP C1/2 in semi-permeabilised untreated cells or after 30-minute treatment with different *C9ORF72* dipeptide repeat proteins at varying concentrations as indicated. Left panel: DAPI. First from left panel: hnRNP C1/2. First from right panel: DAPI. Right panel: hnRNP C1/2. Zoom ins are at different brightness and contrast settings as main images. Scale bar: 50 µm.

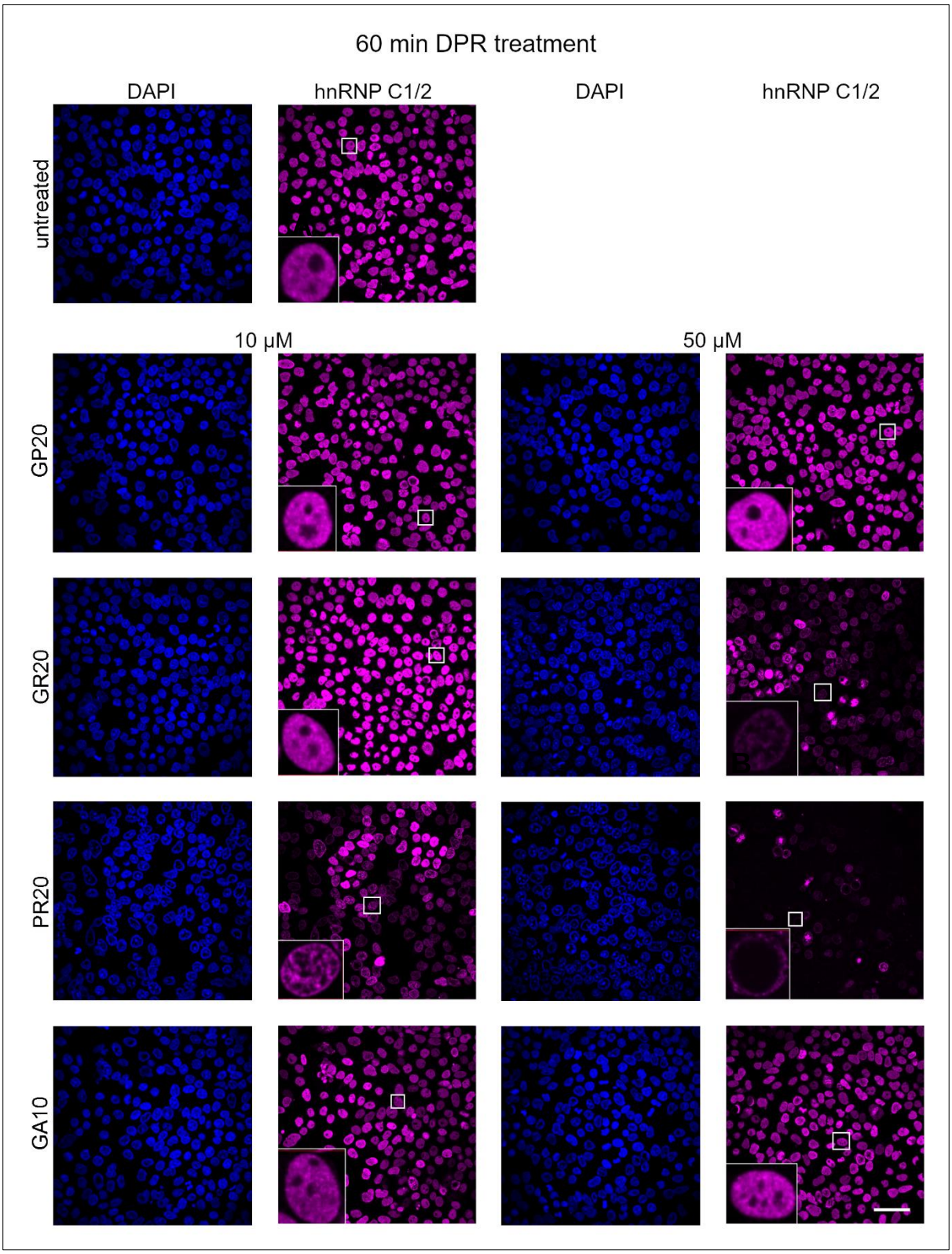

Figure 4.25: Effects of *C9ORF72* DPRs on nuclear hnRNP C1/2 levels. Opera Phenix images of immunofluorescence staining of endogenous hnRNP C1/2 in semi-permeabilised untreated cells or after 60-minute treatment with different *C9ORF72* dipeptide repeat proteins at varying concentrations as indicated. Left panel: DAPI. First from left panel: hnRNP C1/2. First from right panel: DAPI. Right panel: hnRNP C1/2. Zoom ins are at different brightness and contrast settings as main images. Scale bar: 50 µm.

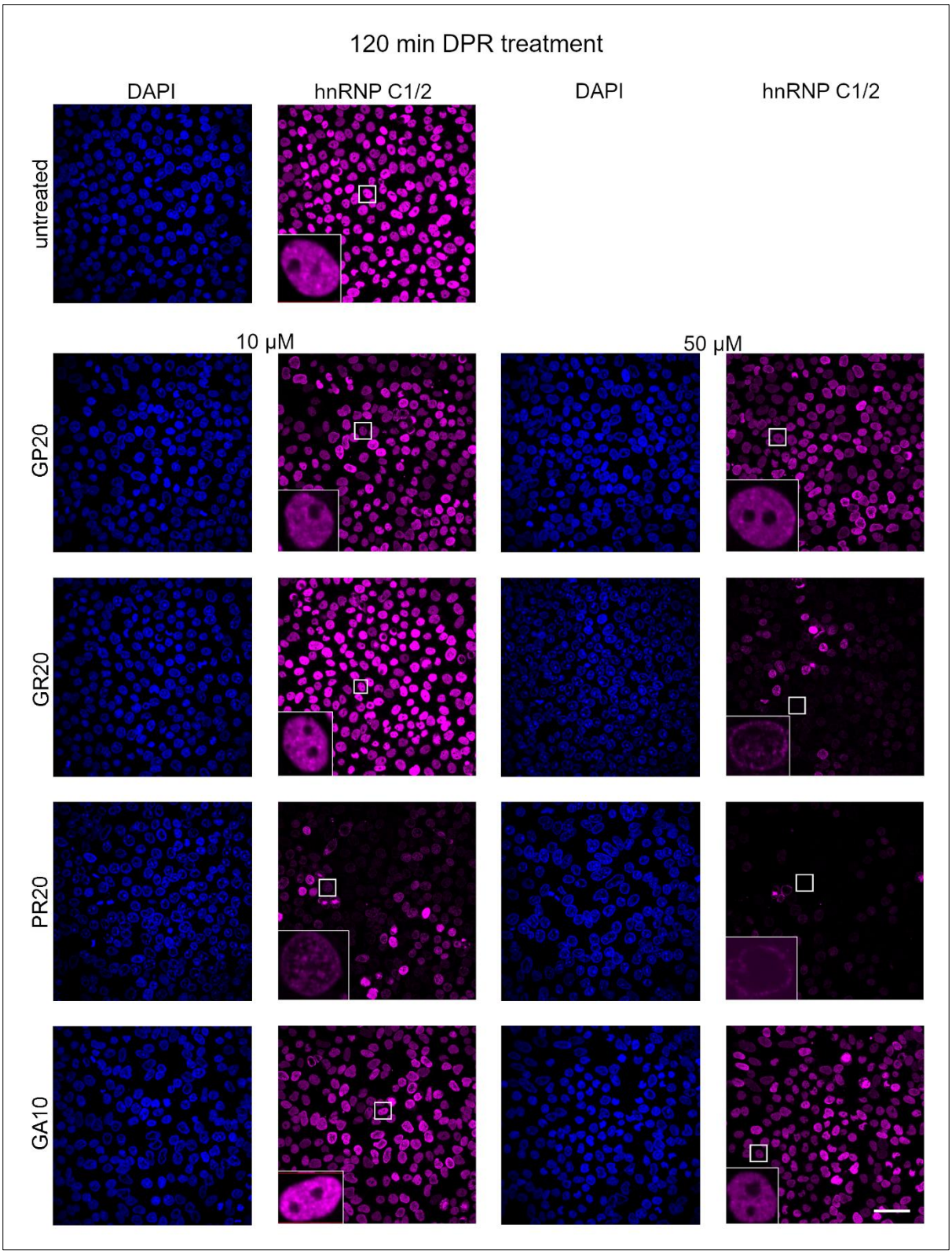

Figure 4.26: Influence of *C9ORF72* DPRs on nuclear hnRNP C1/2 localisation. Opera Phenix images of immunofluorescence staining of endogenous hnRNP C1/2 in semi-permeabilised untreated cells or after 120-minute treatment with different *C9ORF72* dipeptide repeat proteins at varying concentrations as indicated. Left panel: DAPI. First from left panel: hnRNP C1/2. First from right panel: DAPI. Right panel: hnRNP C1/2. Zoom ins are at different brightness and contrast settings as main images. Scale bar: 50 µm.

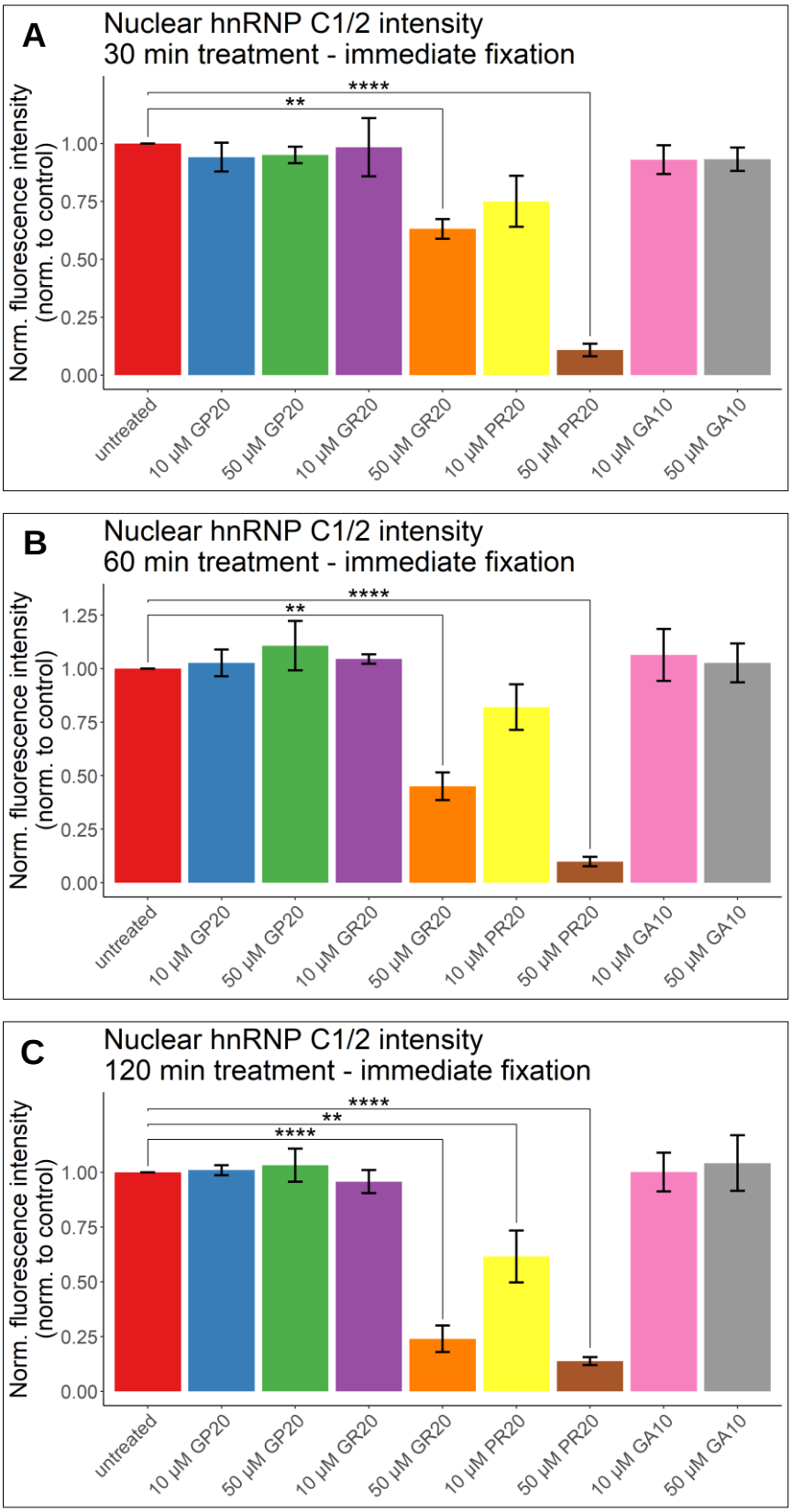

Figure 4.27: Arginine containing *C9ORF72* DPRs lower nuclear hnRNP C1/2 levels. Quantified nuclear hnRNP C1/2 fluorescence signal normalised to untreated control in untreated or cells treated with varying concentrations of different DPRs as indicated. A) 30-minute DPR treatment. B) 60-minute DPR treatment. C) 120-minute DPR treatment. Means of individual experimental means are shown. Error bars: SEM. **** $p<0.0001$, ** $p < 0.01$ vs untreated cells with multi-level model one-way ANOVA and Dunnett's post hoc test.

With regards to histone H3 GP20 and GA10 did not change its location at either concentration after 30 minutes as demonstrated in Figure 4.28 and Figure 4.31A. Contrary to TDP43, 10 µM GR20 treatment led to a significant, however small, reduction in nuclear histone H3 levels after 30 minutes. Nuclear histone H3 was highly decreased upon treatment with 50 µM GR20 after 30 minutes. PR20 treatment led to a reduction in nuclear histone H3 levels at both concentrations after 30 minutes with 50 µM PR20 having a more drastic effect compared to 10 µM. Effects of 10 µM PR20 on histone H3 localisation after 30 minutes were slightly less severe compared to its effect on TDP43 (50 % versus 65 % decrease; compare with Figure 4.20A).
After 60 minutes there was again no effect on nuclear histone H3 levels upon GP20 and GA10 treatment as shown in Figure 4.29 and Figure 4.31B. 10 µM GR20 treatment also led to a slight reduction in nuclear histone H3 levels after 60 minutes compared to controls while 50 µM GR20 resulted in a strong decrease of nuclear histone H3. Again, 60 minute-PR20 treatment reduced nuclear histone H3 levels with effect size correlating with concentration.
After 120 minutes nuclear histone H3 levels were comparable between untreated and GP20 or GA10 treated cells as depicted in Figure 4.30 and Figure 4.31C. Interestingly, 10 µM GR20 treatment did no longer lead to a decrease in nuclear histone H3 after a treatment time of 120 minutes. This could indicate that the effect of 10 µM GR20 was no longer exceeding the rate of passive diffusion of histone H3 due to incubation of permeabilised cells for an extended period of time. 50 µM GR20 still drastically lowered nuclear histone H3 levels after 120 minutes. 10 µM PR20 treatment led to a stronger decrease of nuclear histone H3 after 120 minutes compared to shorter treatment times whilst the effect of 50 µM PR20 on histone H3 localisation was still equally strong.

Notably, the DNA binding protein histone H3 seemed to be more sensitive to arginine containing *C9ORF72* DPR treatment than RNA binding protein hnRNP C1/2 with effects of these DPRs on histone H3 being comparable to their effects on TDP43. In summary, treatment with arginine containing DPRs led to a reduction of nuclear protein levels in permeabilised cells suggesting that they not only influence nuclear import of reporter cargo but also nuclear export of endogenous proteins.

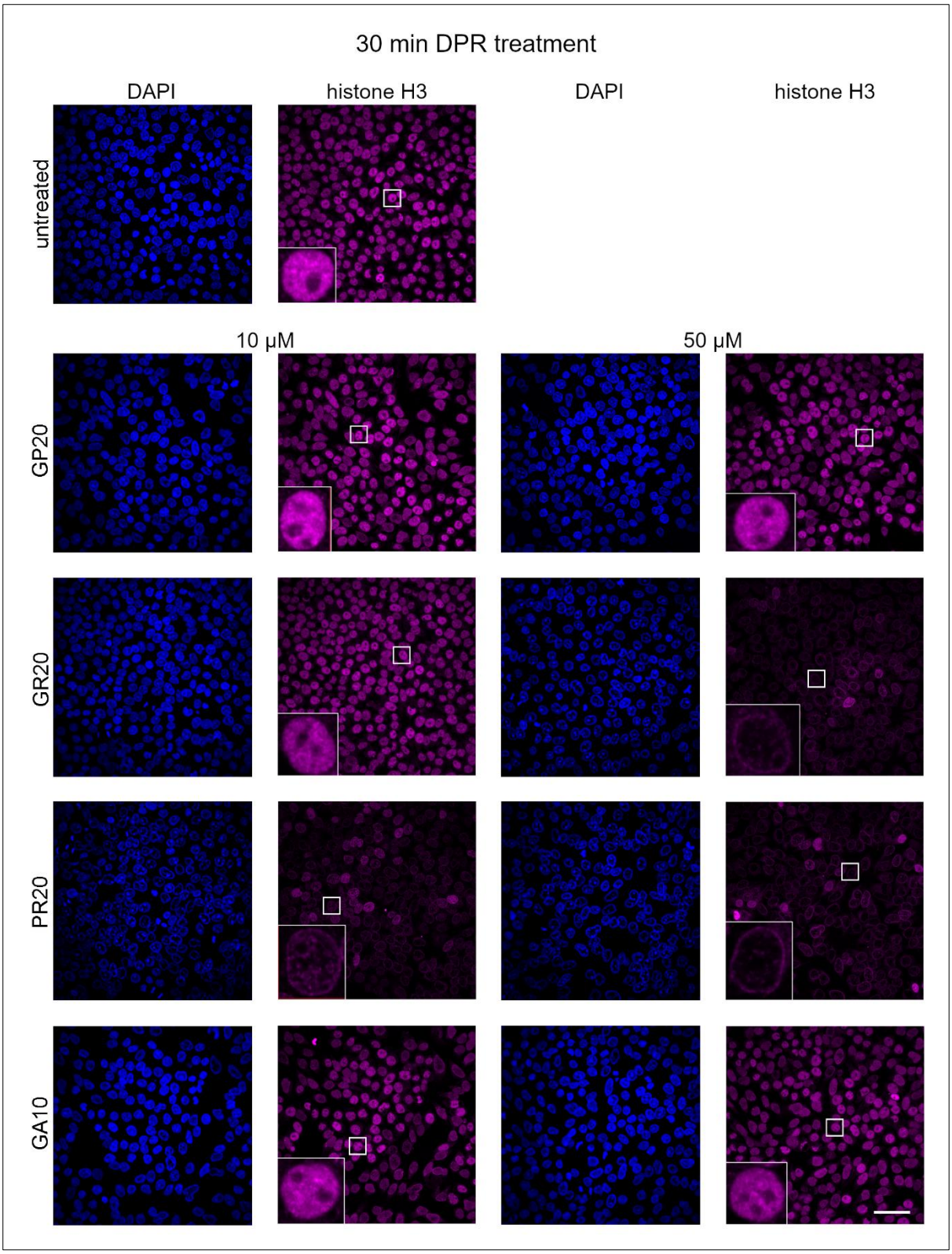

Figure 4.28: Effects of *C9ORF72* DPRs on nuclear histone H3 levels. Opera Phenix images of immunofluorescence staining of endogenous histone H3 in semi-permeabilised untreated cells or after 30-minute treatment with different *C9ORF72* dipeptide repeat proteins at varying concentrations as indicated. Left panel: DAPI. First from left panel: histone H3. First from right panel: DAPI. Right panel: histone H3. Zoom ins are at different brightness and contrast settings as main images. Scale bar: 50 µm.

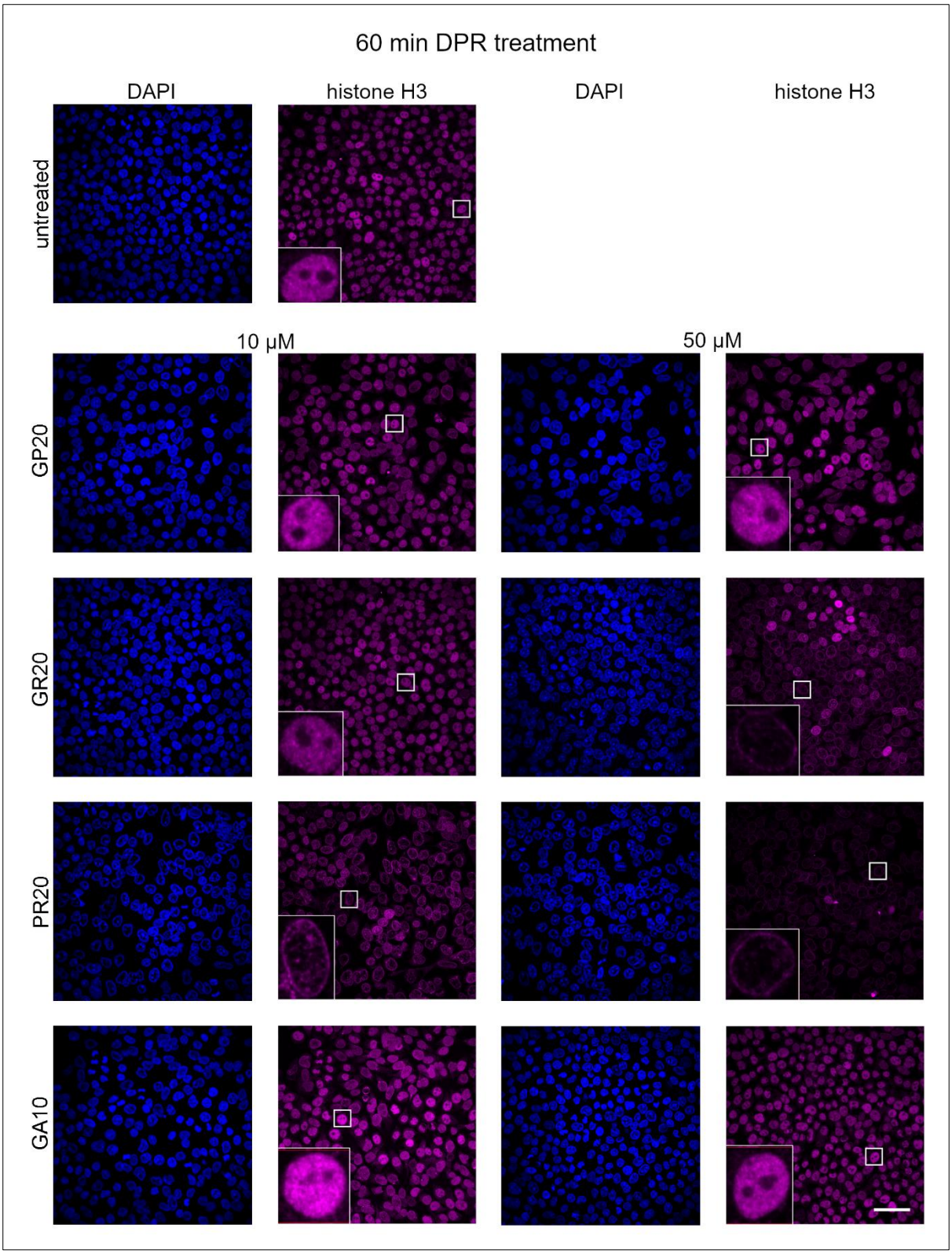

Figure 4.29: Influence of *C9ORF72* DPRs on nuclear histone H3 levels. Opera Phenix images of immunofluorescence staining of endogenous histone H3 in semi-permeabilised untreated cells or after 60-minute treatment with different *C9ORF72* dipeptide repeat proteins at varying concentrations as indicated. Left panel: DAPI. First from left panel: histone H3. First from right panel: DAPI. Right panel: histone H3. Zoom ins are at different brightness and contrast settings as main images. Scale bar: 50 µm.

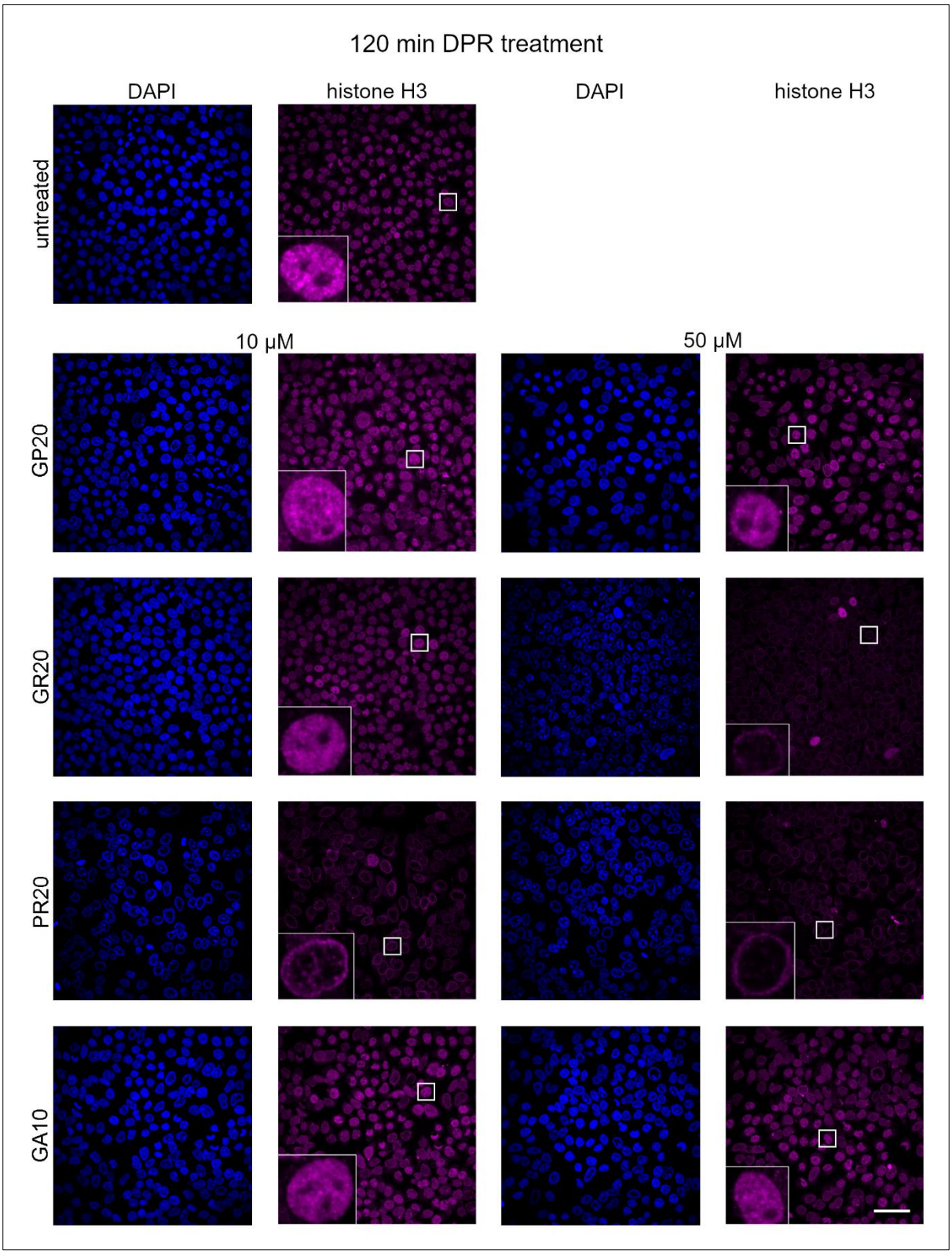

Figure 4.30: Effects of *C9ORF72* DPRs on nuclear localisation of histone H3. Opera Phenix images of immunofluorescence staining of endogenous histone H3 in semi-permeabilised untreated cells or after 120-minute treatment with different *C9ORF72* dipeptide repeat proteins at varying concentrations as indicated. Left panel: DAPI. First from left panel: histone H3. First from right panel: DAPI. Right panel: histone H3. Zoom ins are at different brightness and contrast settings as main images. Scale bar: 50 µm.

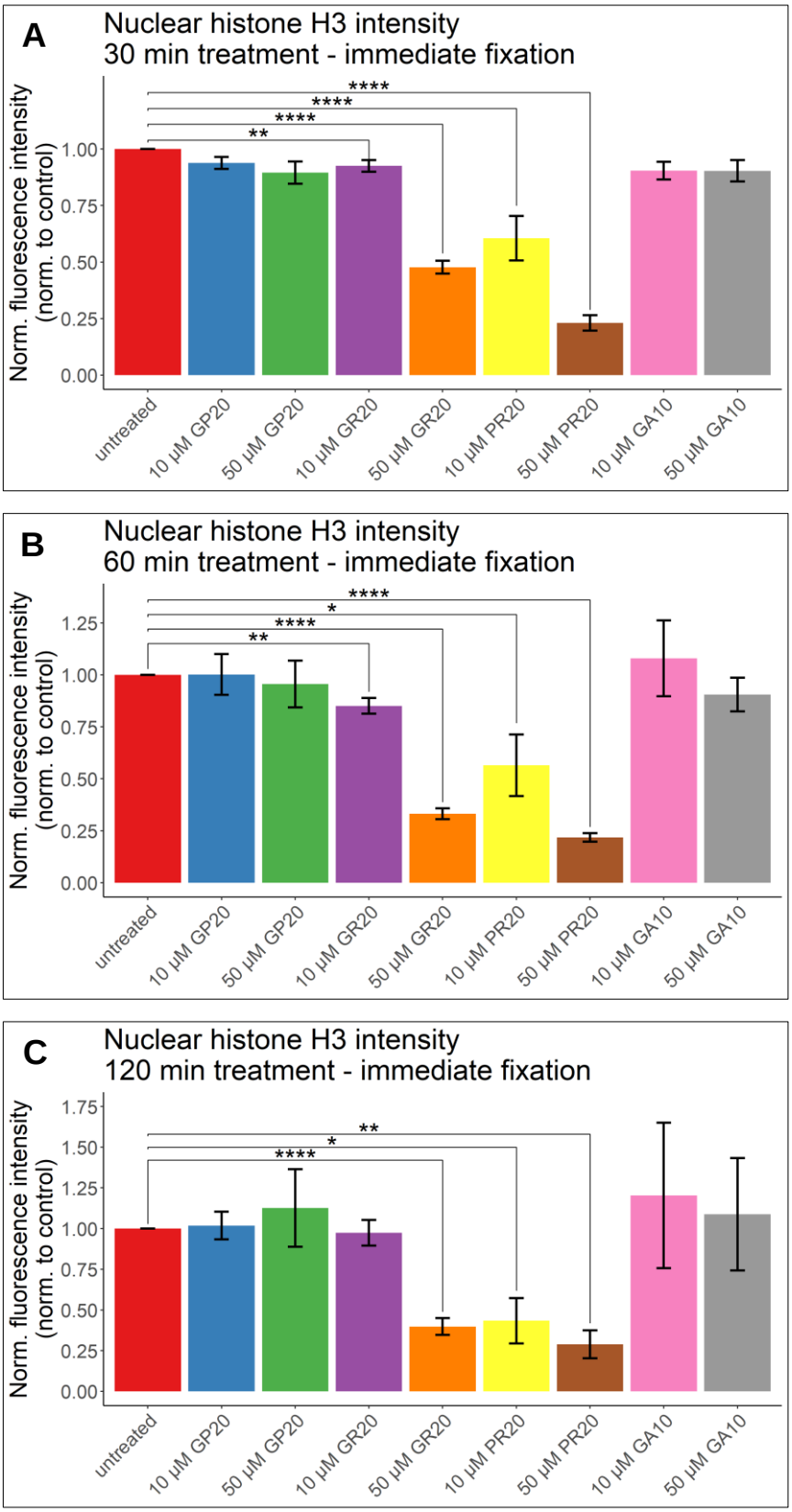

Figure 4.31: Arginine containing *C9ORF72* DPRs decrease nuclear localisation of histone H3. Quantified nuclear histone H3 fluorescence signal normalised to untreated control in untreated or cells treated with varying concentrations of different DPRs as indicated. A) 30-minute DPR treatment. B) 60-minute DPR treatment. C) 120-minute DPR treatment. Means of individual experimental means are depicted. Error bars: SEM. **** $p<0.0001$, ** $p < 0.01$, * $p < 0.05$ vs untreated cells with multi-level model one-way ANOVA and Dunnett's post hoc test.

4.4 Discussion

4.4.1 Enhancement of passive nuclear import by poly-GR and -PR

The first major finding of this chapter was that the arginine containing *C9ORF72* DPRs significantly increased passive nuclear import of fluorescent reporter cargo. This effect was more pronounced for smaller than for larger cargo with the most substantial effect being observed for the 20 kDa dextran. This suggests that these DPR species did not substantially change the size barrier of the nuclear pore as entry of larger cargo was still somewhat restricted. Importantly, PR20 did not allow for the large 70 kDa dextran to enter the nucleus indicating that the permeability barrier was still intact. Nuclear import of 70 kDa dextran upon GR20 treatment only occurred at very low levels which suggests that transport of large cargo through the nuclear pore was still partly restricted. The increase in nuclear import of 40 kDa dextran by GR20 and PR20 was less distinct than for the 20 kDa dextran but higher than for GFP. That was unexpected as GFP with a molecular weight of 27 kDa is smaller than the 40 kDa dextran. This can potentially be explained by the already very effective import of GFP (see also section 3.5) due to its hydrophobic residues promoting FG nucleoporin interaction (Frey et al., 2018) which could not be greatly improved further by the arginine containing DPRs. Poly-GR and -PR increased both the amount of cargo transported and transport speed indicating that the permeability of the nuclear pore was enhanced by poly-GR and -PR. Our findings were confirmed by a different study published during the course of this work (Hayes et al., 2020) where GR and PR polypeptides increased the passive nuclear import of 40 kDa dextran and GFP in HeLa cells. The effects on GFP by the arginine containing DPRs were more pronounced compared to our findings, however the authors used double the DPR concentration than we used.

4.4.2 Effects of poly-GR and -PR on passive versus active nucleocytoplasmic transport

Arginine containing DPRs have a different effect on active compared to passive nucleocytoplasmic transport. In a hormone induced import assay transport into the nucleus of reporter cargo containing a nuclear localisation signal specific for importin α/β was decreased by a GR polypeptide in HeLa cells (Hutten et al., 2020). Similarly, nuclear import of various reporter cargos transported by different import receptors in a permeabilised cell assay monitoring active nucleocytoplasmic transport by

providing energy and import receptors was reduced by GR and PR polypeptides in primary mouse cortical neurons or HeLa cells (Hayes et al., 2020). However, in a different study GR and PR polypeptides had no effect on active nucleocytoplasmic transport of reporter cargo binding to importin α/β or transportin 1 in HeLa cells. Interestingly, when the authors of the same study expressed longer codon-optimised PR constructs in HeLa cells this led to an increase in active nuclear import of reporter cargo (Vanneste et al., 2019). Similar to our findings that GA10 slightly decreased passive nucleocytoplasmic transport, expression of a poly-GA construct in SH-SY5Y cells or iPSC-derived motor neurons led to a decline in active nuclear import of reporter cargo (Vanneste et al., 2019). Overall, the mechanism of action of arginine containing dipeptide repeat proteins might differ between active and passive nucleocytoplasmic transport. One proposed mechanism stemming from findings that PR polypeptides bound to the central channel of nuclear pores in *Xenopus laevis* oocytes is that PR treatment leads to the blockage of the nuclear pore (Shi et al., 2017). Our findings of increased passive nuclear import contradict that suggestion.

4.4.3 Altered effects of poly-GR and -PR on passive nucleocytoplasmic transport by fluorescent labelling

Our results that Alexa Fluor 647 labelled GR20 and PR20 had the exact opposite effect on passive reporter cargo import compared to unlabelled DPRs were very surprising. As Alexa Fluor 647 is quite small with a molecular weight of about 1 kDa a change in peptide size is unlikely to be causative of the effect modulation. Alexa Flour 647 contains three unbalanced sulfate groups and thus is negatively charged (Fan et al., 2019). This could counteract the positive charge of the arginine in GR and PR polypeptides. As electrostatic interactions are thought to be one component of the binding ability of arginine containing DPRs to low complexity domain proteins including nuclear pore components (Lee et al., 2016) a reduction in positive charge could lead to modifying the effect of Alexa Fluor 647 labelled GR and PR on passive nuclear import compared to untagged GR and PR. Aromatic dyes including Alexa Fluor 647 were shown to migrate into FG domains *in vitro* (Ng et al., 2021) suggesting that Alexa Fluor 647 labelled DPRs might interact with the nuclear pore differently than unlabelled ones. In any case, caution should be exerted when performing experiments including fluorescent tagged DPR polypeptides or

expression constructs especially when these fluorophores carry a charge as results could be substantially altered compared to untagged DPR species. For instance, poly-PR shown to bind the central channel of the nuclear pore as mentioned above was coupled to a FITC fluorophore (Shi et al., 2017). Poly-GR and -PR not affecting active nucleocytoplasmic transport as introduced above were coupled to mCherry (Vanneste et al., 2019). As DPRs occurring in patients obviously are not coupled to a fluorophore we decided not to pursue further experiments using these labelled DPRs.

4.4.4 Influence of poly-GR and -PR on passive nuclear export of TDP43

Our second major finding in this chapter was that nuclear TDP43 levels were decreased upon poly-GR and -PR treatment in semi-permeabilised HeLa cells. This likely occurred via the enhancement of passive nuclear export of TDP43 as the transport buffer used in our experiments did not contain transport receptors, Ran or energy sources. Therefore, our experiments could indicate that enhanced passive TDP43 export might be at least in part responsible for the cytoplasmic mislocalisation of TDP43 in over 97 % of ALS and 45 % of FTD cases (Ling et al., 2013). This possibility is further supported by findings that TDP43 is passively rather than actively exported from the nucleus. For instance, inhibition of exportin 1, the predicted export receptor for TDP43 (Winton et al., 2008), still allowed for TDP43 export (Archbold et al., 2018; Ederle et al., 2018; Pinarbasi et al., 2018). In addition, knock down of other export receptors had no or only mild effects on TDP43 export (Archbold et al., 2018). Increasing TDP43 size by fusion to large domains diminished its export ability suggesting that exceeding the size limit of passive nucleocytoplasmic transport impaired TDP43 export (Ederle et al., 2018; Pinarbasi et al., 2018).

In addition to enhanced passive export, impairment of active TDP43 import could also contribute to its cytoplasmic mislocalisation. GR but not PR treatment reduced import of TDP43 reporter cargo in HeLa cells (Hutten et al., 2020). In contrast, in our case PR seemed to have a more potent effect than GR on nuclear TDP43 localisation with lower concentrations or treatment times required to achieve an effect. This might indicate that poly-GR has a greater effect on active nuclear import than PR possibly via interaction with transport receptors. On the other hand, poly-PR

seems to have a stronger effect on passive nuclear export possibly via interaction with nucleoporins.
Whilst GA treatment led to a small decrease in passive import of reporter cargo, it did not have an effect on nuclear export of TDP43 or other nuclear proteins in our experiments. In a different study, expression of poly-GA constructs in primary rat neurons led to an enhanced percentage of cells containing cytoplasmic TDP43 (Khosravi et al., 2020) indicating that GA might still contribute to TDP43 mislocalisation via a different mechanism possible dependent on GA aggregation. As a note of caution, we cannot fully exclude that poly-GR and -PR treatment led to nuclear degradation rather than enhanced nuclear export of TDP43.

4.4.5 Impact of poly-GR and -PR on localisation of other nuclear proteins

The exclusively nuclear proteins hnRNP C1/2 and histone H3 are not found to be mislocalised in ALS or FTD. Furthermore, in other reported transport assay experiments hnRNP C was not found to exit the nucleus upon chemical fusion of two cell types (heterokaryon assay) (Ederle et al., 2018). Semi-permeabilising the cells might have made them more sensitive to nuclear export stimuli potentially also in part due to the general low protein concentration outside of the permeabilised nuclei (unlike in physiological conditions with the cytoplasm containing proteins present). We could demonstrate that arginine containing dipeptide repeat proteins render the nuclear pore less restrictive leading to a loss of endogenous proteins from the nucleus. Interestingly, the DNA binding protein histone H3 was more vulnerable to GR and PR treatment compared to the RNA binding protein hnRNP C1/2. This could suggest that nucleic acid binding plays a role in nuclear localisation of proteins which will be explored in the next chapter. Potential influences of poly-GR and -PR on the nuclear pore will also be investigated in the next chapter.

In summary, we demonstrated in this chapter that poly-GR and -PR enhanced passive nucleocytoplasmic transport. This included increase of nuclear import of reporter cargo which could potentially lead to influx of cytoplasmic proteins into the nucleus in disease damaging nuclear integrity. Passive nuclear export of TDP43 was also enhanced by poly-GR and -PR which might contribute to cytoplasmic mislocalisation of TDP43 in *C9ORF72* ALS/FTD.

5 Potential mechanisms of action for passive nucleocytoplasmic transport enhancement by arginine containing *C9ORF72* dipeptide repeat proteins

In the previous chapter it was shown that arginine containing *C9ORF72* DPR species specifically increase the passive nuclear import of reporter cargo and the passive nuclear export of the shuttling but predominantly nuclear protein TDP43 and the exclusively nuclear proteins hnRNP C1/2 and histone H3. In this chapter we aimed to investigate how poly-GR and -PR could cause these changes in passive nucleocytoplasmic transport dynamics by studying possible routes of action and targets. We studied chemical mimics of disruption of the permeability barrier of the nuclear pore, nucleic acid anchoring of nuclear proteins and the effects of poly-GR and -PR on the localisation of transport factors. Based on these findings we investigated potential mechanisms to rescue the passive nucleocytoplasmic transport defects caused by poly-GR and -PR.

5.1 Effects of CHD treatment on passive nuclear import

To further investigate how the permeability barrier of the nuclear pore is affected by poly-GR and -PR we treated HeLa cells with the alcohol trans-1,2-cyclo-hexanediol CHD which is known to disrupt the nuclear pore's permeability barrier probably by affecting FG-FG interactions between nucleoporins forming this barrier (Ribbeck and Görlich, 2002; Schmidt and Görlich, 2015). Cells were subjected to 14 % w/v CHD for 15 minutes. We then used our optimised transport assay to investigate the nuclear import of fluorescently labelled 20, 40 and 70 kDa dextran. This allowed us to compare the impacts of CHD on passive reporter cargo import with those of arginine containing *C9ORF72* DPRs.

Import of the 20 kDa dextran was increased by CHD compared to untreated cells as shown in Figure 5.1 and Figure 5.2. However, maximum import levels were only twice as high than those in untreated cells whilst maximum import was enhanced 4- and 5-fold by poly-GR and -PR treatment, respectively compared to untreated cells (see Figure 4.2). Import enhancement by CHD in comparison to untreated cells was only observed after 80 seconds and effects by arginine containing DPRs could

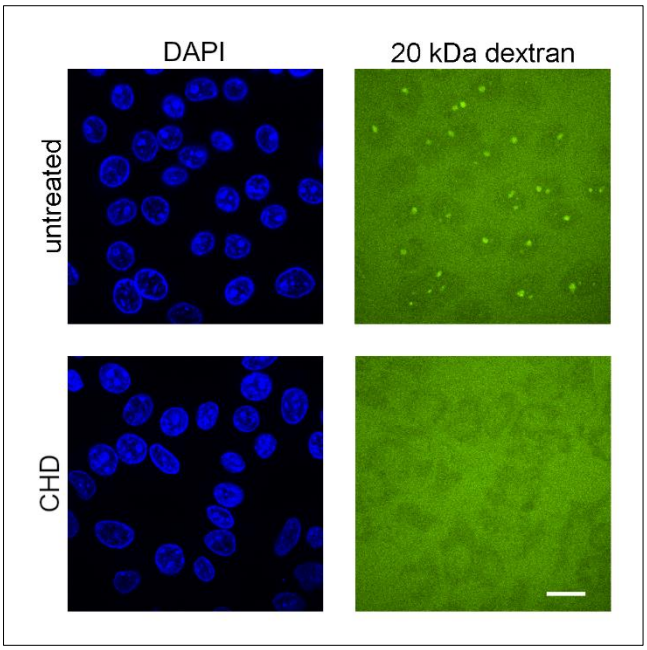

Figure 5.1: Effects of CHD on passive nuclear import of 20 kDa dextran. Spinning disk confocal microscope images of semi-permeabilised untreated HeLa cells and cells treated with 14 % w/v CHD for 15 minutes after 4-minute incubation with 20 kDa dextran. Left panel: DAPI channel. Right panel: FITC 20 kDa dextran channel. Scale bar: 20 µm.

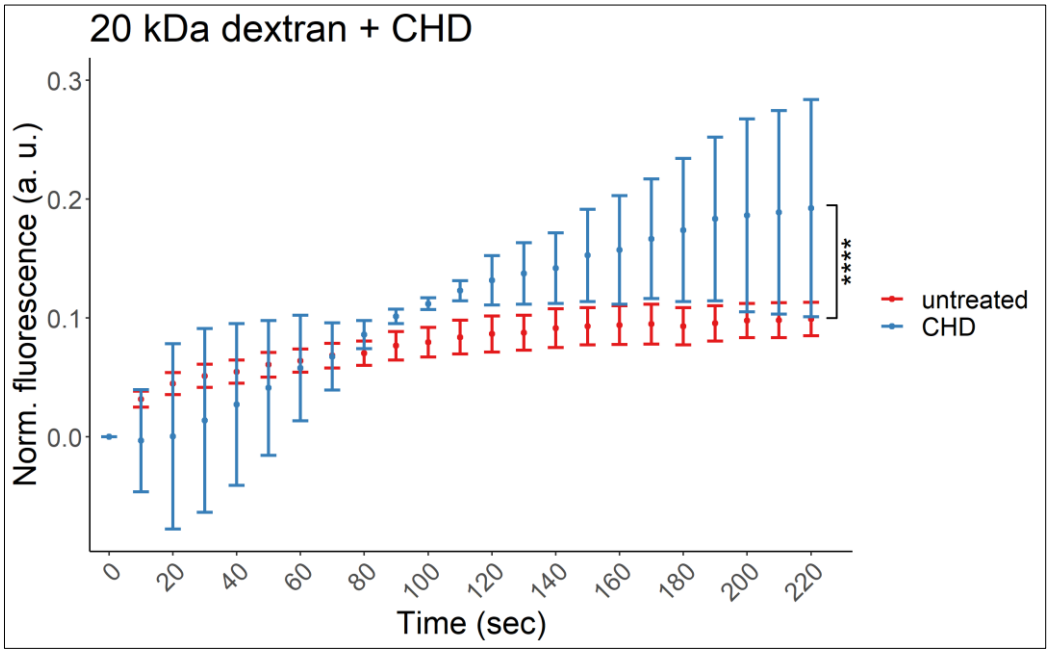

Figure 5.2: CHD increases nuclear import of 20 kDa dextran at later time points. Quantification of passive nuclear import of 20 kDa dextran (shown as nuclear fluorescence normalised to nuclear and general background) over time in semi-permeabilised untreated or CHD treated HeLa cells. Untreated condition depicted in red, CHD treatment in blue. Means of individual experimental means are shown. N = min. 3. Error bars: SEM. **** $p < 0.0001$ vs untreated cells with two-way repeated measures ANOVA and Dunnett's post hoc test.

already be observed from the earliest measured timepoints. In CHD treated cells 20 kDa dextran was evenly distributed within the nucleus whilst 20 kDa dextran accumulated in potential nucleolar structures in untreated and DPR treated cells (see

Figure 5.1 and Figure 4.1). Possibly, CHD was also disrupting these compartments allowing for broader dispersing of the 20 kDa dextran within the nucleus as it could no longer interact with these nuclear structures. CHD treatment had varying effects between experiments not consistently enhancing passive nuclear import of 20 kDa dextran.

CHD treatment resulted in 1.5-fold enhanced import of 40 kDa dextran compared to untreated cells but only at early timepoints as shown in Figure 5.3 and Figure 5.4. At later timepoints passive nuclear import of 40 kDa dextran was not changed in CHD treated cells compared to untreated cells. In contrast, poly-GR and -PR increased maximum 40 kDa dextran levels by about 2.5-fold with effects being more distinct at later than at early timepoints (see Figure 4.4). Again, the 40 kDa dextran was evenly distributed throughout the nucleus in CHD treated cells whilst it clustered in potential nucleolar locations in untreated and DPR treated cells (see Figure 5.3 and Figure 4.3).

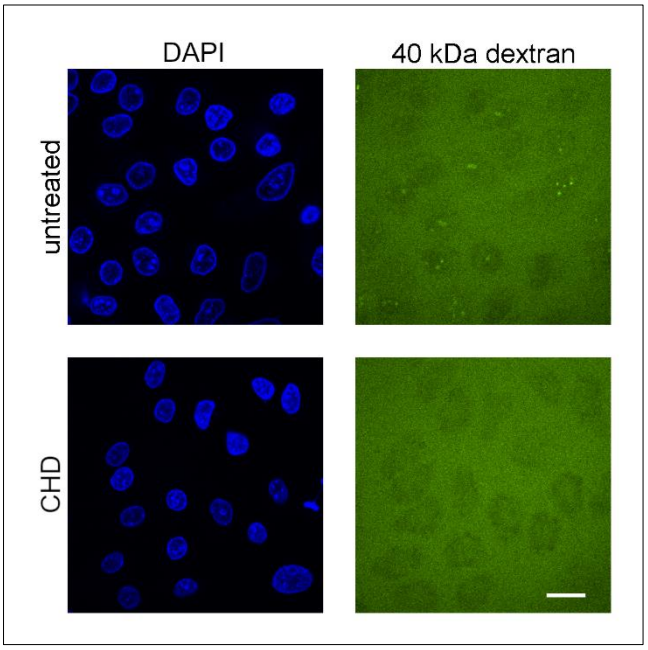

Figure 5.3: Influence of CHD on passive nuclear import of 40 kDa dextran. Spinning disk confocal microscope images of semi-permeabilised untreated HeLa cells and cells treated with 14 % w/v CHD for 15 minutes after 4-minute incubation with 40 kDa dextran. Left panel: DAPI channel. Right panel: FITC 40 kDa dextran channel. Scale bar: 20 µm.

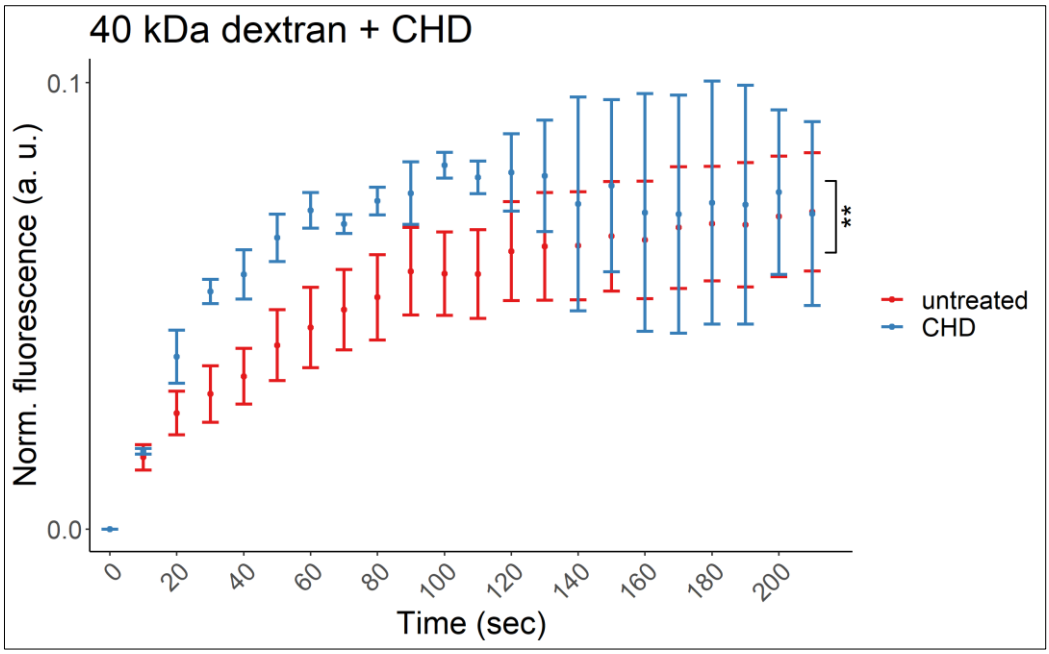

Figure 5.4: CHD enhances nuclear import of 40 kDa dextran at early time points. Quantification of passive nuclear import of 40 kDa dextran (shown as nuclear fluorescence normalised to nuclear and general background) over time in semi-permeabilised untreated or CHD treated HeLa cells. Untreated condition depicted in red, CHD treatment in blue. Means of individual experimental means are depicted. N = min. 3. Error bars: SEM. ** $p < 0.01$ vs untreated cells with two-way repeated measures ANOVA and Dunnett's post hoc test.

The 70 kDa dextran could be imported in CHD treated cells at levels similar to the 20 kDa dextran in untreated cells (see Figure 5.6 and Figure 5.2) but it did not enter the nucleus in untreated cells as it exceeds the size limit of the nuclear pore's permeability barrier (see Figure 5.5). PR treatment equally had no effect on nuclear 70 kDa dextran import whilst 70 kDa dextran was imported into the nucleus in the presence of poly-GR but at levels about 1.5-fold lower than in CHD treated cells (see Figure 4.8). Therefore, effects of CHD and poly-GR were most similar with regards to the 70 kDa dextran with poly-GR interfering with the nuclear pore's permeability barrier but not reaching CHD's potency. However, both poly-GR and -PR increased import of the smaller sized 20 and 40 kDa dextrans to much higher levels than CHD indicating that complete nuclear pore size barrier disruption was not responsible for the observed enhanced import levels by arginine containing DPRs.

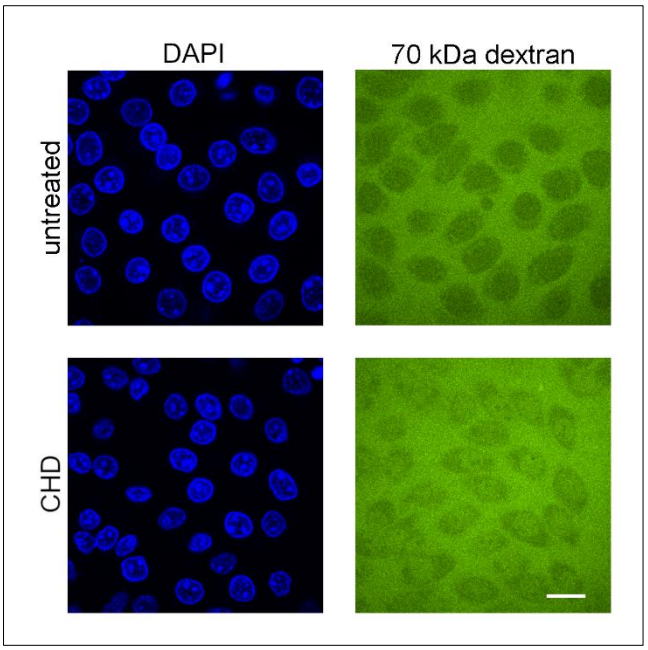

Figure 5.5: Impact of CHD on passive nuclear import of 70 kDa dextran. Spinning disk confocal microscope images of semi-permeabilised untreated HeLa cells and cells treated with 14 % w/v CHD for 15 minutes after 4-minute incubation with 70 kDa dextran. Left panel: DAPI channel. Right panel: FITC 70 kDa dextran channel. Scale bar: 20 µm.

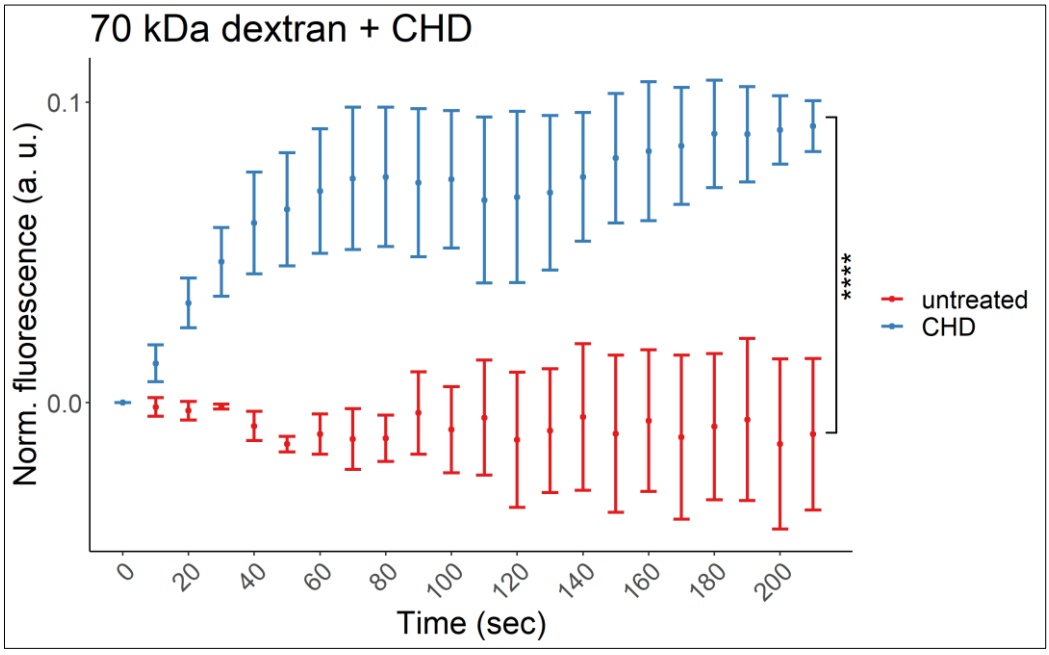

Figure 5.6: CHD treatment leads to nuclear influx of 70 kDa dextran. Quantification of passive nuclear import of 70 kDa dextran (shown as nuclear fluorescence normalised to nuclear and general background) over time in semi-permeabilised untreated or CHD treated HeLa cells. Untreated condition depicted in red, CHD treatment in blue. Means of individual experimental means are plotted. N = 3. Error bars: SEM. **** $p < 0.0001$ vs untreated cells with two-way repeated measures ANOVA and Dunnett's post hoc test.

5.2 Influence of CHD on nuclear localisation of endogenous TDP43, hnRNP C1/2 and histone H3

In this section we aimed to investigate whether a disruption of the nuclear pore's permeability barrier by impairing FG-FG interactions between nucleoporins was responsible for the nuclear loss of TDP43, hnRNP C1/2 and histone H3 caused by arginine containing C9ORF72 DPR treatment (see section 4.3). Therefore, we measured nuclear levels of the aforementioned proteins by immunofluorescence staining in semi-permeabilised HeLa cells but treated cells with CHD instead of DPRs for 30, 60 or 120 minutes. Similar to section 5.1, we could then compare the effects of CHD, which reduces permeability barrier restriction on cargo entry, on nuclear export of TDP43, hnRNP C1/2 and histone H3 to those of poly-GR and -PR.

Nuclear TDP43 levels were reduced to about 30 % of its levels in untreated cells by a 30-minute CHD treatment as shown in Figure 5.7 and Figure 5.10A. This reduction was similar in cells treated with 50 µM GR20 or 10 µM PR20 for 30 minutes whilst 10 µM GR20 had no effect (see Figure 4.20A). 30-minute 50 µM PR20 treatment decreased nuclear TDP43 localisation more strongly compared to CHD.

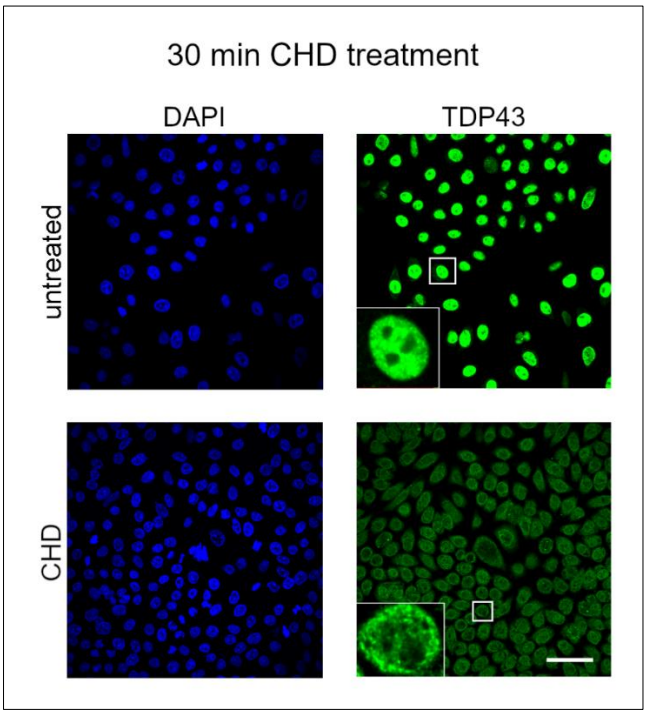

Figure 5.7: Effects of CHD on nuclear localisation of TDP43. Opera Phenix images of immunofluorescence staining of endogenous TDP43 in semi-permeabilised untreated cells or after 30-minute treatment with 14 % w/v CHD. Left panel: DAPI. Right panel: TDP43. Zoom ins are at different brightness and contrast settings as main images. Scale bar: 50 µm.

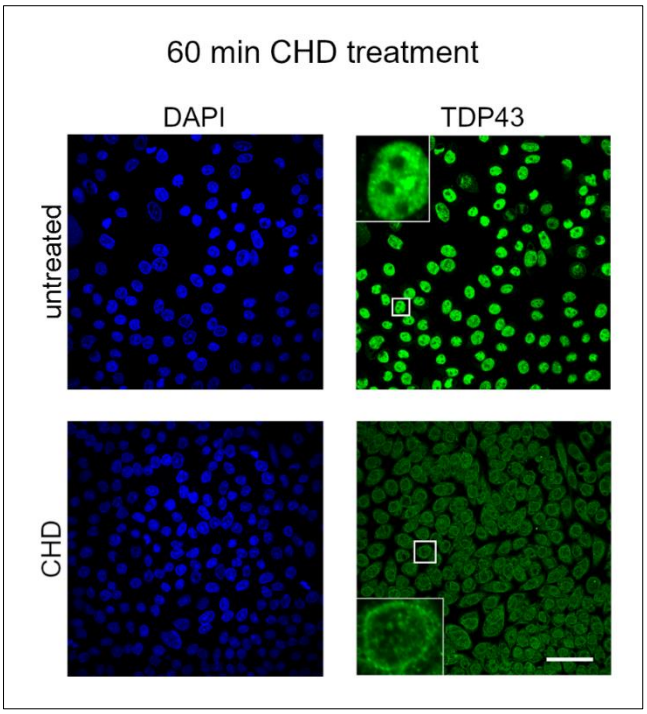

Figure 5.8: Influence of CHD on nuclear localisation of TDP43. Opera Phenix images of immunofluorescence staining of endogenous TDP43 in semi-permeabilised untreated cells or after 60-minute treatment with 14 % w/v CHD. Left panel: DAPI. Right panel: TDP43. Zoom ins are at different brightness and contrast settings as main images. Scale bar: 50 µm.

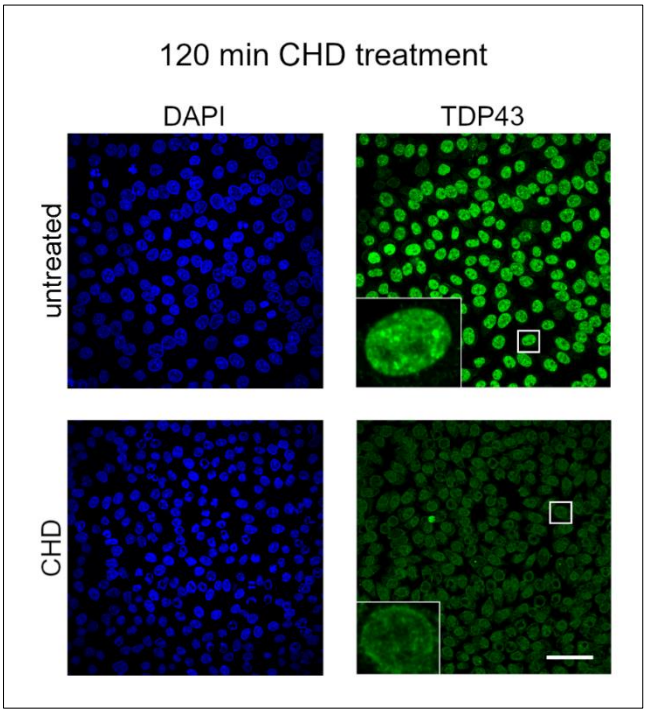

Figure 5.9: Impact of CHD on nuclear localisation of TDP43. Opera Phenix images of immunofluorescence staining of endogenous TDP43 in semi-permeabilised untreated cells or after 120-minute treatment with 14 % w/v CHD. Left panel: DAPI. Right panel: TDP43. Zoom ins are at different brightness and contrast settings as main images. Scale bar: 50 µm.

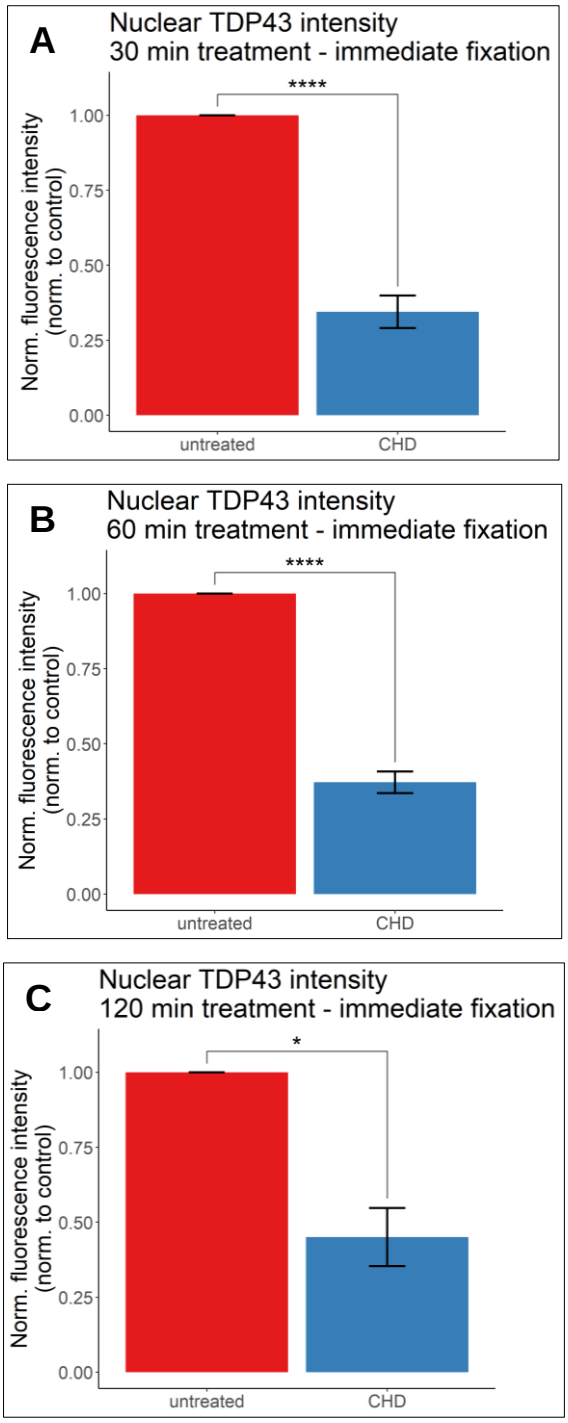

Figure 5.10: CHD reduces nuclear TDP43 levels. Quantified nuclear TDP43 fluorescence signal normalised to untreated control in untreated or cells treated with 14 % w/v CHD. A) 30-minute CHD treatment. B) 60-minute CHD treatment. C) 120-minute CHD treatment. Means of individual experimental means are shown. Error bars: SEM. **** $p < 0.0001$, * $p < 0.05$ vs untreated cells with multi-level model one-way ANOVA and Dunnett's post hoc test.

60-minute CHD treatment again decreased nuclear TDP43 by about 70 % compared to untreated cells (see Figure 5.8 and Figure 5.10B) which was similar to 30-minute CHD treatment (see Figure 5.10A). This was also comparable to the effect of 60-minute 50 µM GR20 treatment on nuclear TDP43 (see Figure 4.20B). 10 µM GR20

was less potent than CHD as it did not decrease nuclear TDP43 levels. 60-minute PR20 treatment showed a stronger effect than CHD with 10 µM and 50 µM PR20 lowering nuclear TDP43 localisation 1.5-fold and 3-fold more, respectively, than CHD.

TDP43 levels were reduced by 50 % in cells treated with CHD for 120 minutes compared to untreated cells (see Figure 5.9 and Figure 5.10B). This was a lower reduction compared to shorter CHD treatment times (see Figure 5.10A and B) which could be explained by some nuclear TDP43 also diffusing out of untreated nuclei after a 120-minute incubation time. 120 minute 50 µM GR20 treatment decreased nuclear TDP43 levels to a similar extent than CHD while 10 µM GR20 was slightly less potent with reducing nuclear TDP43 by about 40 % (see Figure 4.20C). Nuclear TDP43 localisation was reduced twice as much by low and high PR20 concentrations than by CHD after 120 minutes.

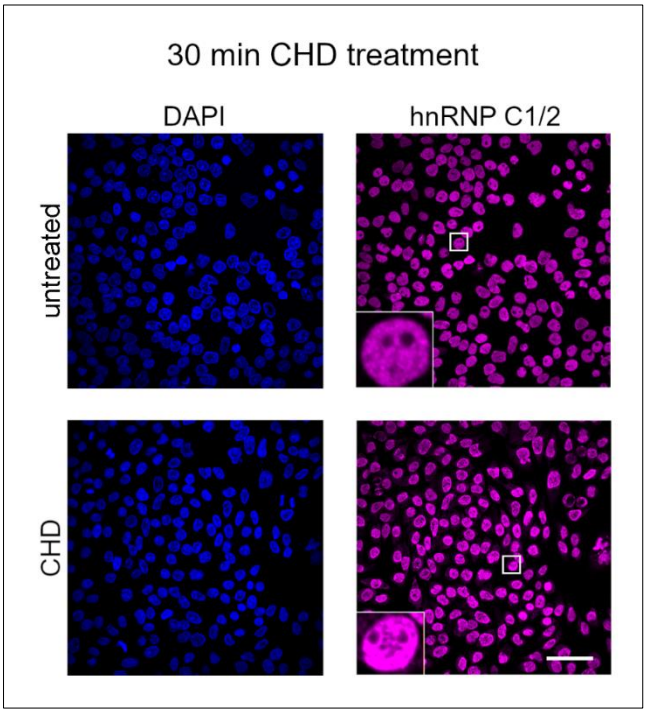

Figure 5.11: Influence of CHD on nuclear levels of hnRNP C1/2. Opera Phenix images of immunofluorescence staining of endogenous hnRNP C1/2 in semi-permeabilised untreated cells or after 30-minute treatment with 14 % w/v CHD. Left panel: DAPI. Right panel: hnRNP C1/2. Zoom ins are at different brightness and contrast settings as main images. Scale bar: 50 µm.

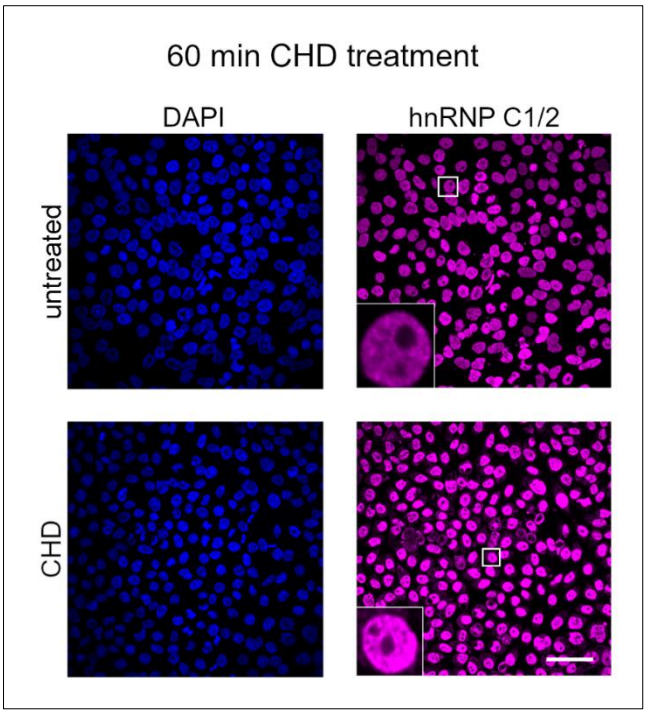

Figure 5.12: Effects of CHD on nuclear localisation of hnRNP C1/2. Opera Phenix images of immunofluorescence staining of endogenous hnRNP C1/2 in semi-permeabilised untreated cells or after 60-minute treatment with 14 % w/v CHD. Left panel: DAPI. Right panel: hnRNP C1/2. Zoom ins are at different brightness and contrast settings as main images. Scale bar: 50 µm.

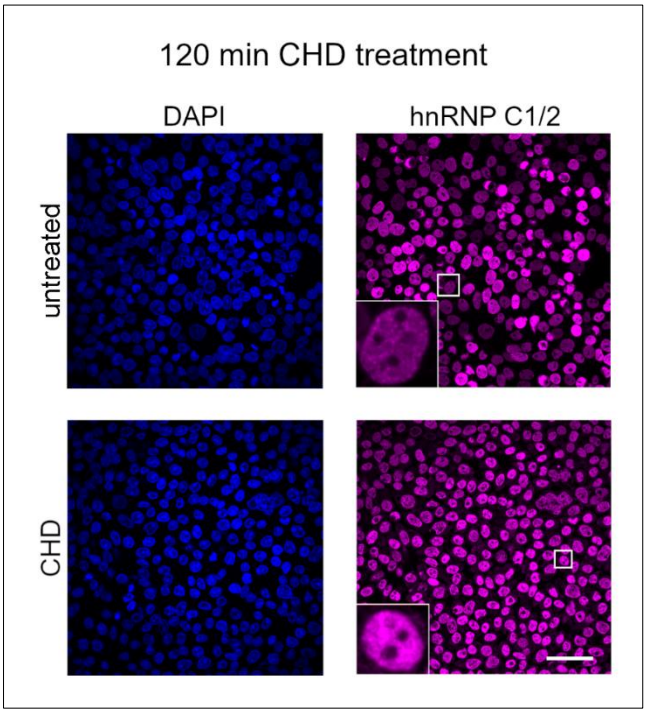

Figure 5.13: Influence of CHD on nuclear localisation of hnRNP C1/2. Opera Phenix images of immunofluorescence staining of endogenous hnRNP C1/2 in semi-permeabilised untreated cells or after 120-minute treatment with 14 % w/v CHD. Left panel: DAPI. Right panel: hnRNP C1/2. Zoom ins are at different brightness and contrast settings as main images. Scale bar: 50 µm.

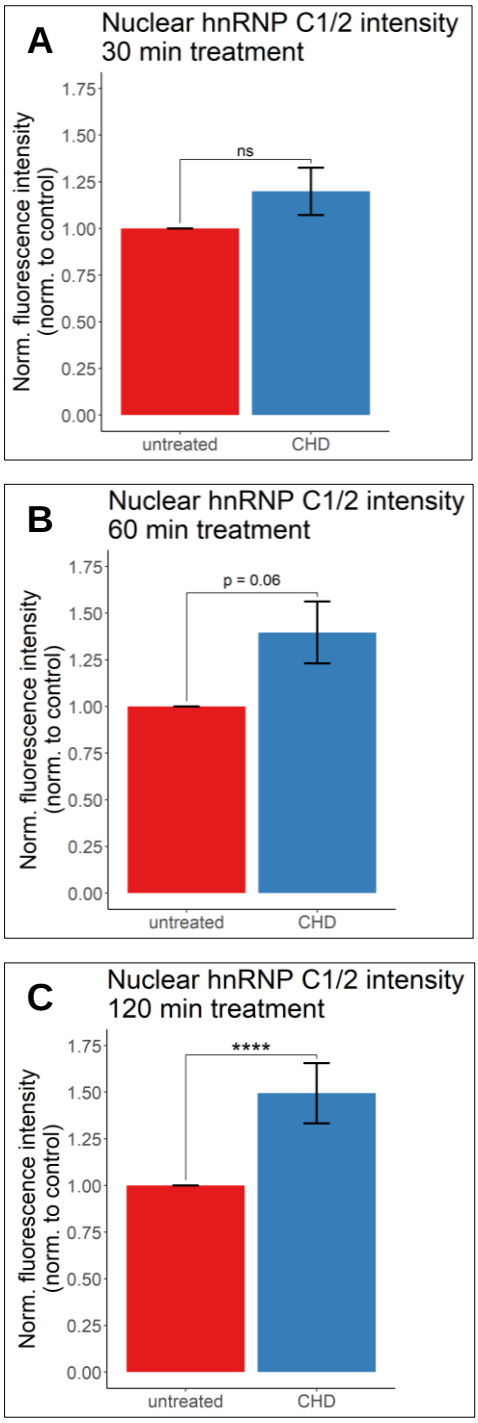

Figure 5.14: CHD does not affect or increases nuclear hnRNP C1/2 levels. Quantified nuclear hnRNP C1/2 fluorescence signal normalised to untreated control in untreated or cells treated with 14 % w/v CHD. A) 30-minute CHD treatment. B) 60-minute CHD treatment. C) 120-minute CHD treatment. Means of individual experimental means are plotted. Error bars: SEM. **** $p < 0.0001$, ns not significant vs untreated cells with multi-level model one-way ANOVA and Dunnett's post hoc test.

Nuclear hnRNP C1/2 levels were not changed by 30-minute CHD treatment compared to untreated cells (see Figure 5.11 and Figure 5.14A) but were reduced by arginine containing DPRs at 50 µM after 30 minutes (see Figure 4.27A). After 60-minute CHD treatment a trend to increased nuclear hnRNP C1/2 levels compared to

untreated cells was observed (see Figure 5.12 and Figure 5.14B). In contrast, high concentration poly-GR and -PR treatment did lead to a reduction in nuclear hnRNP C1/2 localisation after 60 minutes compared to untreated cells (see Figure 4.27B). Surprisingly, nuclear hnRNP C1/2 levels were enhanced 1.5-fold after 120-minute CHD treatment compared to untreated cells (see Figure 5.13 and Figure 5.14C). In contrast, 50 µM GR20 and PR20 at both concentrations significantly lowered nuclear hnRNP C1/2 intensities after 120 minutes compared to untreated cells (see Figure 4.27C).

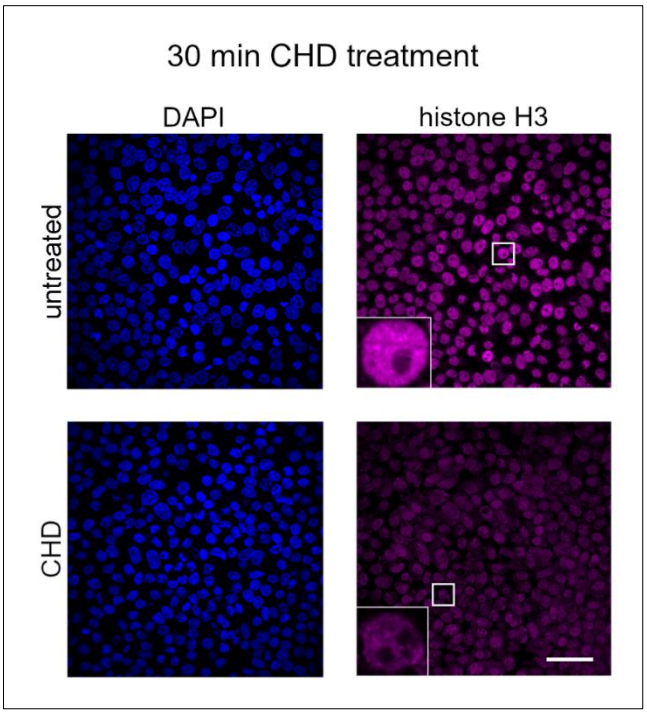

Figure 5.15: Influence of CHD on nuclear localisation of histone H3. Opera Phenix images of immunofluorescence staining of endogenous histone H3 in semi-permeabilised untreated cells or after 30-minute treatment with 14 % w/v CHD. Left panel: DAPI. Right panel: histone H3. Zoom ins are at different brightness and contrast settings as main images. Scale bar: 50 µm.

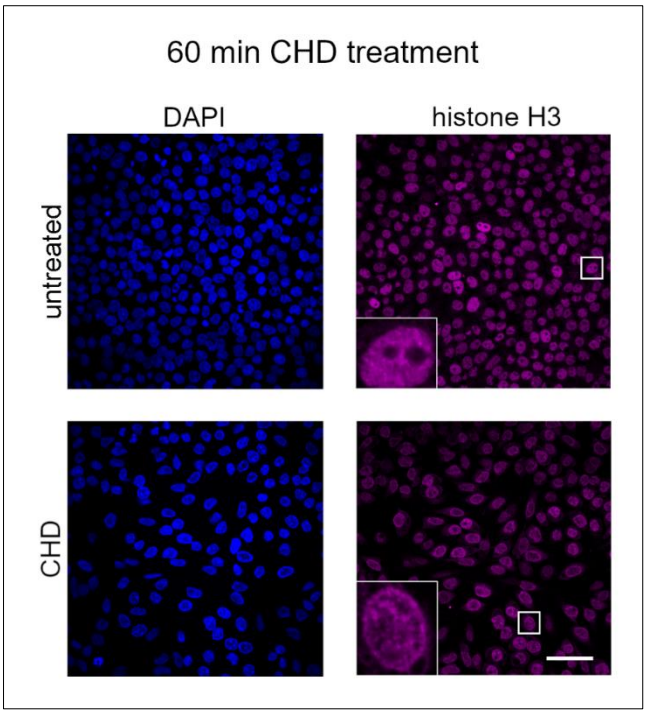

Figure 5.16: Impact of CHD on nuclear localisation of histone H3. Opera Phenix images of immunofluorescence staining of endogenous histone H3 in semi-permeabilised untreated cells or after 60-minute treatment with 14 % w/v CHD. Left panel: DAPI. Right panel: histone H3. Zoom ins are at different brightness and contrast settings as main images. Scale bar: 50 µm.

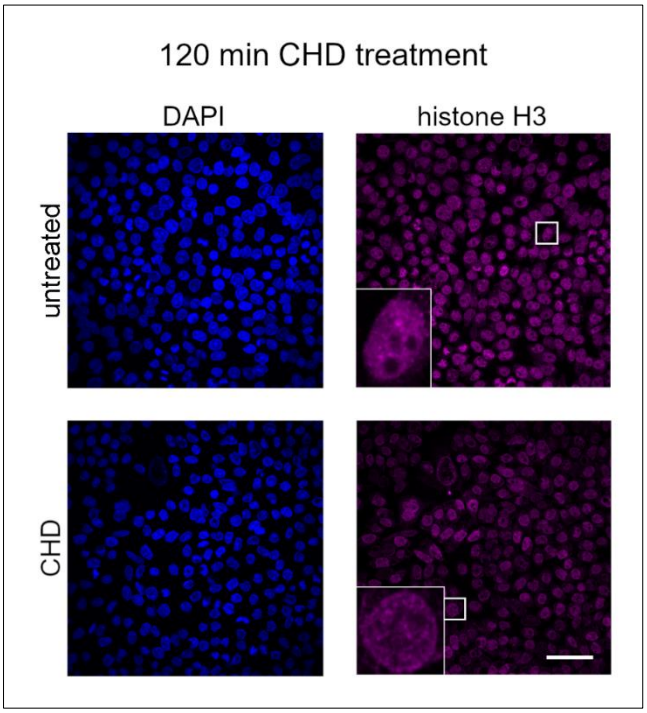

Figure 5.17: Effects of CHD on nuclear localisation of histone H3. Opera Phenix images of immunofluorescence staining of endogenous histone H3 in semi-permeabilised untreated cells or after 120-minute treatment with 14 % w/v CHD. Left panel: DAPI. Right panel: histone H3. Zoom ins are at different brightness and contrast settings as main images. Scale bar: 50 µm.

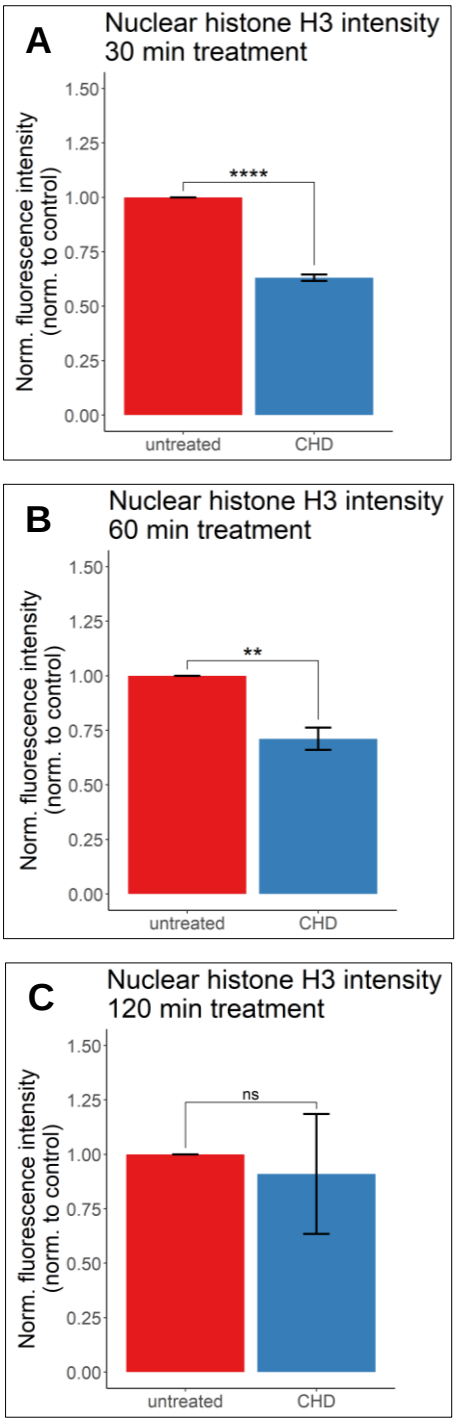

Figure 5.18: CHD decreases or does not change nuclear histone H3 levels. Quantified nuclear histone H3 fluorescence signal normalised to untreated control in untreated or cells treated with 14 % w/v CHD. A) 30-minute CHD treatment. B) 60-minute CHD treatment. C) 120-minute CHD treatment. Means of individual experimental means are shown. Error bars: SEM. **** $p < 0.0001$, ** $p < 0.01$, ns not significant vs untreated cells with multi-level model one-way ANOVA and Dunnett's post hoc test.

Nuclear histone H3 intensities were reduced by about 40 % compared to untreated cells after 30-minute CHD treatment (see Figure 5.15 and Figure 5.18A). This was comparable to the reduction observed after 30-minute 10 µM PR20 treatment (see Figure 4.31A). 50 µM GR20 and PR20 led to a higher decrease in nuclear histone

H3 levels after 30 minutes compared to CHD with PR showing the strongest effect. After 60-minute CHD treatment nuclear histone levels were lowered to levels of about 75 % of those of untreated cells as indicated in Figure 5.16 and Figure 5.18B. This was 2-fold more effective than 10 µM GR20 treatment and similar to 10 µM PR20 after 60 minutes (see Figure 4.31B). 50 µM GR20 and 50 µM PR20 60-minute treatment led to a 1.5-fold and 2-fold higher reduction of histone H3 levels, respectively, in comparison to 60-minute CHD treatment.

120-minute CHD treatment did not lead to a significant reduction in nuclear histone H3 levels compared to untreated cells (see Figure 5.17 and Figure 5.18C) with nuclear histone H3 levels varying between cells. However, 50 µM GR20 and PR20 at both used concentrations did significantly lower nuclear histone H3 intensities after 120 minutes (see Figure 4.31C).

Overall, CHD treatment reduced nuclear TDP43 levels to a similar degree as 50 µM GR20 and 10 µM PR20. 14 % w/v CHD was more potent in decreasing nuclear TDP43 intensities than 10 µM GR20 as this only showed an effect after 120 minutes. 50 µM PR20 lowered nuclear TDP43 to a higher extent than CHD. Especially at higher concentrations arginine containing *C9ORF72* DPRs reduced nuclear histone H3 levels more strongly than CHD. Surprisingly, CHD seemed to have the opposite effect on hnRNP C1/2 localisation than poly-GR and -PR as it led to an increase in nuclear hnRNP C1/2 intensities with longer incubation times whilst hnRNP C1/2 intensities were reduced upon poly-GR and -PR treatment. Especially these last observations would not suggest that the reduction in nuclear levels of the nuclear proteins tested by poly-GR and -PR were caused by a disruption in the nuclear pore's permeability barrier by interfering with FG-FG interactions.

5.3 Influence of RNAse A and DNAse I treatment on nuclear TDP43, hnRNP C1/2 and histone H3 levels

In this section we tested whether poly-GR and -PR interfered with the binding of TDP43, hnRNP C1/2 or histone H3 to RNA or DNA, causing enhanced nuclear export of these proteins. We treated semi-permeabilised HeLa cells with RNAse A or DNAse I for 15 minutes to remove nucleic acids and hence binding partners of

TDP43, hnRNP C1/2 or histone H3. Cells were then fixed after a total of 30, 60 or 120 minutes and immunofluorescently stained for TDP43, hnRNP C1/2 or histone H3. We could then again compare these findings with results from the same experimental workflow obtained by treating cells with poly-GR and -PR.

To ensure that RNAse A treatment efficiently degraded RNA molecules we fixed semi-permeabilised and RNAse A treated cells after 120 minutes and stained cells with the RNA intercalating dye Pyronin Y (Kim and Sederstrom, 2015). Pyronin Y intensity levels were significantly reduced after RNAse A treatment compared to untreated cells as shown in Figure 5.19 and Figure 5.20. Therefore, RNAse A treatment was effective and could be used in the subsequent experiments.

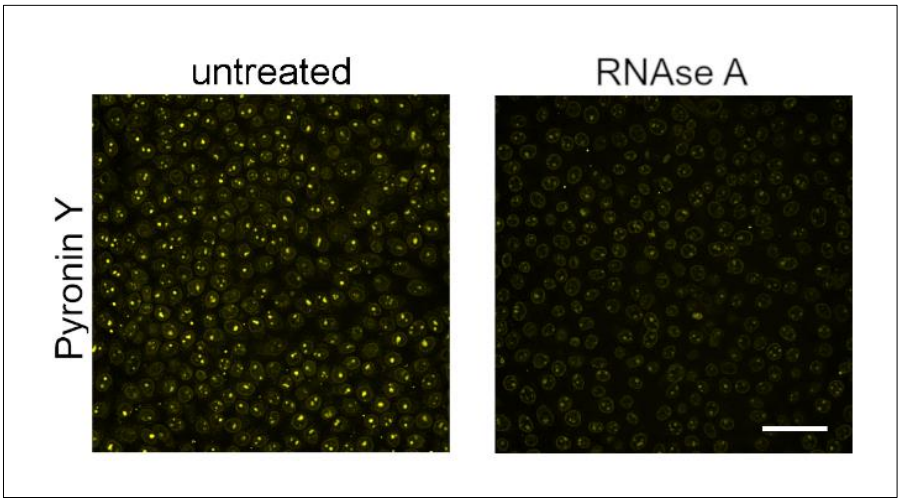

Figure 5.19: Effects of RNAse A treatment on RNA levels. Opera Phenix images of Pyronin Y (RNA dye) staining in semi-permeabilised untreated cells or after 15 min RNAse A treatment and fixation after 120 min. Scale bar: 50 µm.

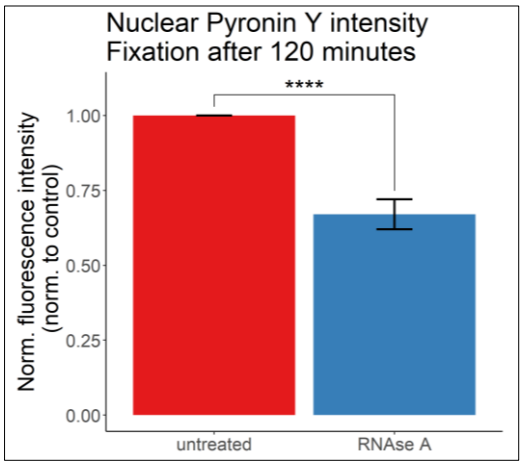

Figure 5.20: RNAse A reduces RNA levels. Quantified nuclear Pyronin Y fluorescence signal normalised to untreated control in untreated or cells treated with RNAse A for 15 min, fixation after 120 min. Means of individual

experimental means are depicted. N = 3. Error bars: SEM. **** p < 0.0001 vs untreated cells with multi-level model one-way ANOVA and Dunnett's post hoc test.

To also establish that DNAse I treatment led to sufficient degradation of DNA molecules, cells were treated as described above and stained with the DNA intercalating dye DAPI (Kapuscinski, 1995) post-fixation. DNAse I treatment led to a significant decrease in DAPI intensity compared to untreated cells (see Figure 5.21 and Figure 5.22) and thus effectively reduced DNA levels. We therefore considered it suitable for the next experiments. As lower DAPI levels made nuclear detection using the DAPI channel more difficult cells were also stained for the nuclear membrane protein Lamin B1 which was then used as the nucleus detection channel.

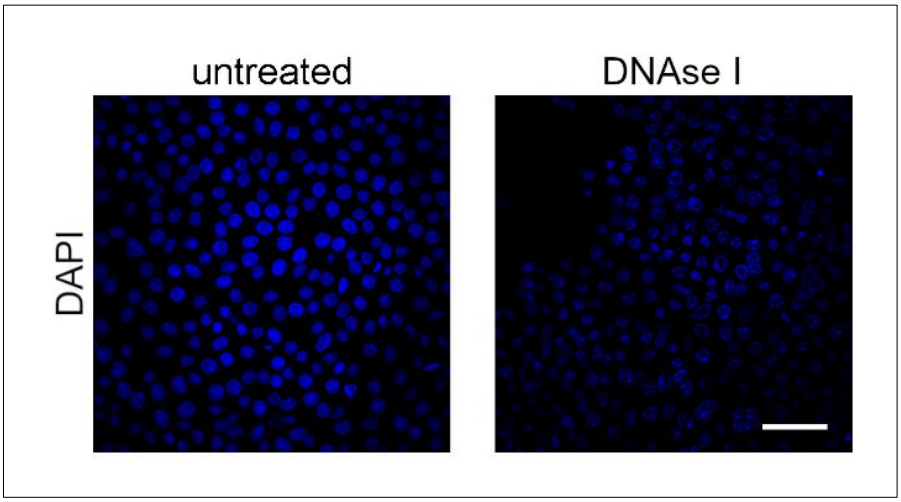

Figure 5.21: Effects of DNAse I treatment on DNA levels. Opera Phenix images of DAPI (DNA dye) staining in semi-permeabilised untreated cells or after 15 min DNAse I treatment and fixation after 120 min. Scale bar: 50 µm.

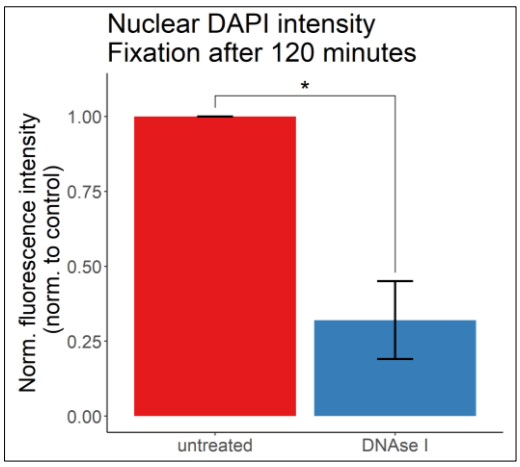

Figure 5.22: DNAse I decreases DNA levels. Quantified nuclear DAPI fluorescence signal normalised to untreated control in untreated or cells treated with DNAse I for 15 min, fixation after 120 min. Means of individual experimental means are shown. N = 3. Error bars: SEM. * p < 0.05 vs untreated cells with multi-level model one-way ANOVA and Dunnett's post hoc test.

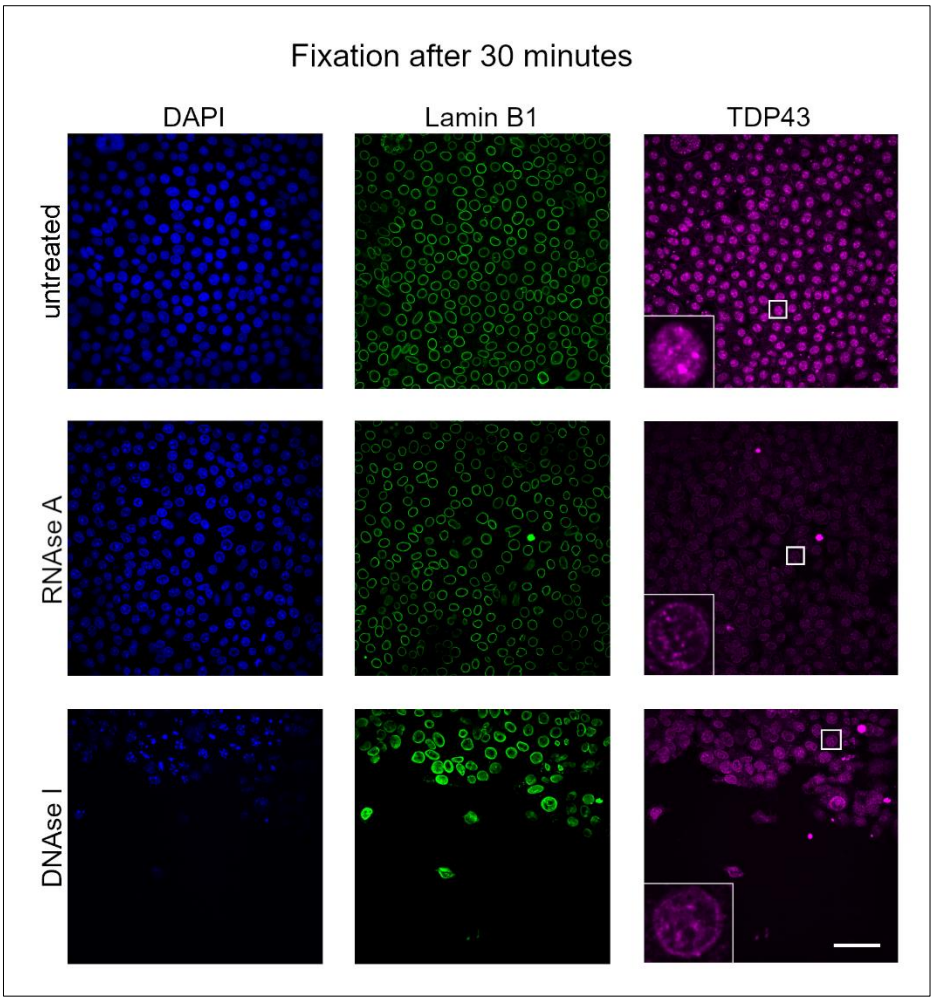

Figure 5.23: Influence of RNAse A or DNAse I on nuclear levels of TDP43. Opera Phenix images of immunofluorescence staining of endogenous TDP43 in semi-permeabilised untreated cells or after 15-minute treatment with RNAse A or DNAse I as indicated, fixation after 30 min. Left panel: DAPI. Middle panel: Lamin B1. Right panel: TDP43. Zoom ins are at different brightness and contrast settings as main images. Scale bar: 50 µm.

As depicted in Figure 5.23 and Figure 5.26A nuclear TDP43 levels were reduced by RNAse A treatment after 30 minutes to about 25 % of the same levels in untreated cells (p = 1.54x10^{-7}, Dunnett's post-hoc test). DNAse I did not lead to a significant reduction of nuclear TDP43 after 30 minutes but TDP43 appeared to be differently distributed within the nucleus compared to untreated cells (see Figure 5.23). Nuclear membrane levels of TDP43 which include TDP43 present within nuclear pores were halved by RNAse A treatment compared to non-treatment with a p value of 3.11x10^{-15} (Dunnett's post-hoc test; see Figure 5.26B). DNAse I treatment had no effect on nuclear membrane TDP43 levels. With the exception of 10 µM GR20 (which showed no effect) RNAse A and poly-GR and -PR treatment reduced nuclear TDP43 levels in a similar manner (compare Figure 4.20A).

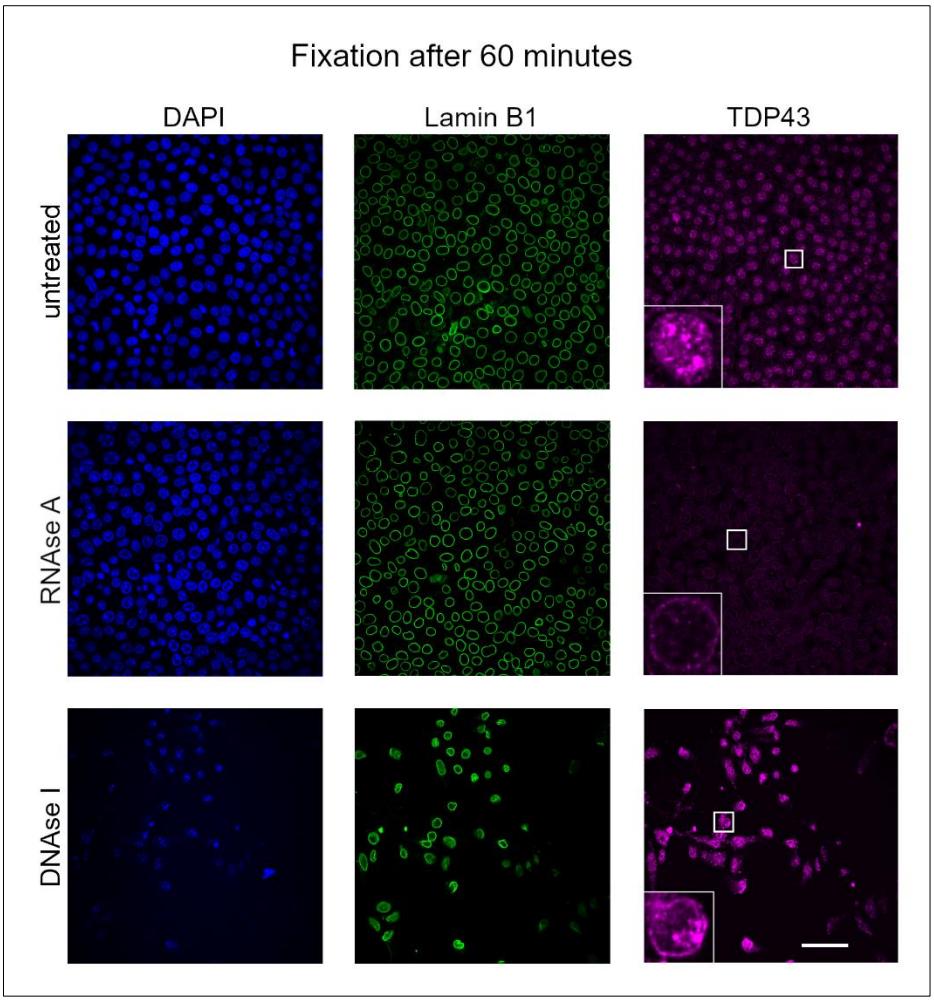

Figure 5.24: Effects of RNAse A or DNAse I on nuclear levels of TDP43. Opera Phenix images of immunofluorescence staining of endogenous TDP43 in semi-permeabilised untreated cells or after 15-minute treatment with RNAse A or DNAse I as indicated, fixation after 60 min. Left panel: DAPI. Middle panel: Lamin B1. Right panel: TDP43. Zoom ins are at different brightness and contrast settings as main images. Scale bar: 50 µm.

After 60 minutes RNAse A treatment decreased nuclear TDP43 levels by about 70 % compared to untreated cells (see Figure 5.24 and Figure 5.26C) with a *p* value of 4.31×10^{-4} (Dunnett's post-hoc test). Nuclear membrane TDP43 levels were also decreased by RNAse A treatment compared to untreated cells after 60-minute incubation ($p = 0.002$, Dunnett's post-hoc test; see Figure 5.26D). DNAse I treatment did not change nuclear or nuclear membrane TDP43 levels after 60 minutes (see Figure 5.26C and D). Effects on nuclear TDP43 localisation were quite similar between RNAse A and arginine containing DPR treatment, except for 10 µM GR20 (compare Figure 4.20B).

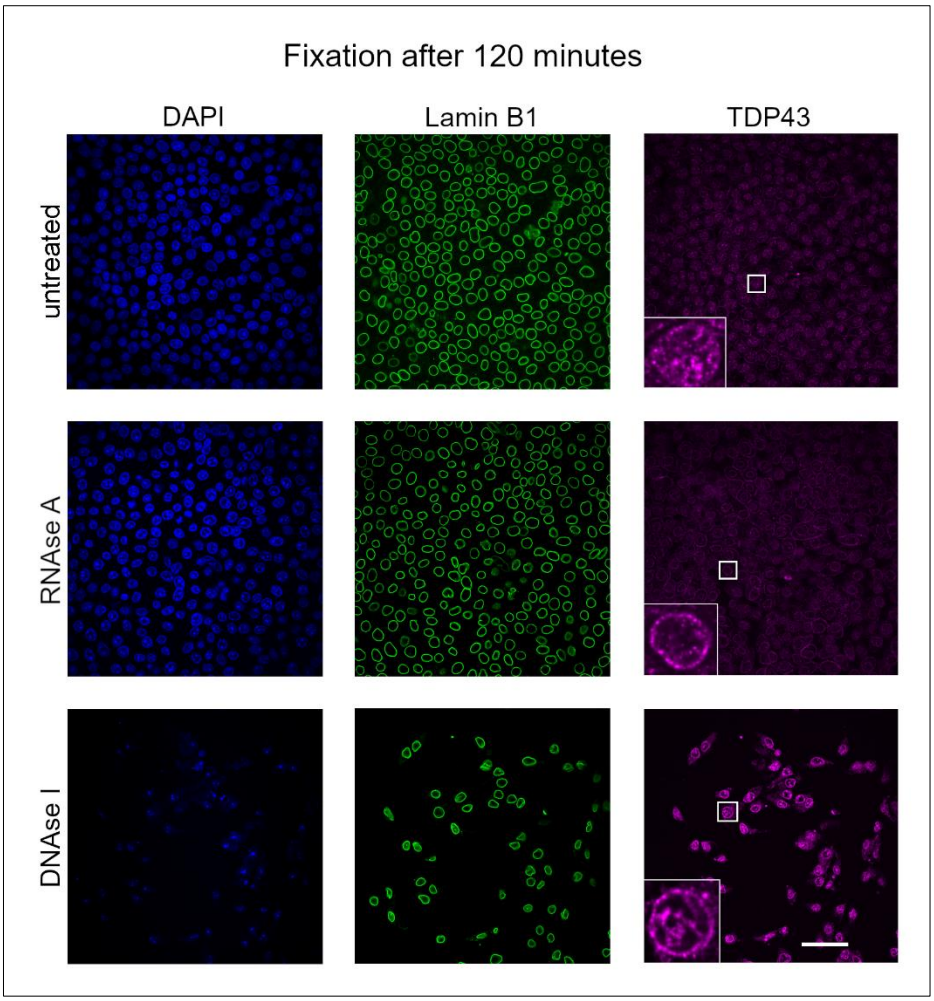

Figure 5.25: Impact of RNAse A or DNAse I on nuclear levels of TDP43. Opera Phenix images of immunofluorescence staining of endogenous TDP43 in semi-permeabilised untreated cells or after 15-minute treatment with RNAse A or DNAse I as indicated, fixation after 120 min. Left panel: DAPI. Middle panel: Lamin B1. Right panel: TDP43. Zoom ins are at different brightness and contrast settings as main images. Scale bar: 50 µm.

Nuclear TDP43 levels were again reduced to about 25 % of the same levels in untreated cells by RNAse A treatment after 120 minutes with a *p* value of 0.007 (Dunnett's post-hoc test) as shown in Figure 5.25 and Figure 5.26E. DNAse I treatment did not significantly affect nuclear TDP43 localisation compared to untreated cells after 120 minutes. Nuclear membrane levels were decreased by about 40 % by RNAse A treatment ($p = 0.016$, Dunnett's post-hoc test) whilst DNAse I treatment showed no effect compared to non-treatment after 120 minutes (see Figure 5.26F). Compared to poly-GR/PR treatment RNAse A reduced nuclear TDP43 levels to a similar extent after 120 minutes (compare Figure 4.20C).

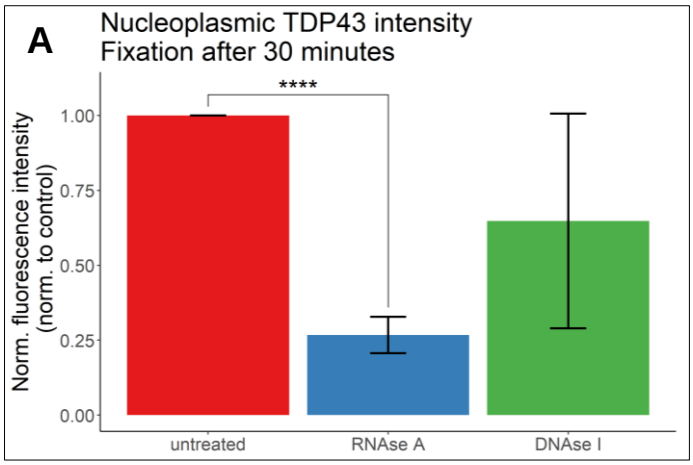
A
Nucleoplasmic TDP43 intensity
Fixation after 30 minutes
****
Norm. fluorescence intensity
(norm. to control)
1.00
0.75
0.50
0.25
0.00
untreated
RNAse A
DNAse I

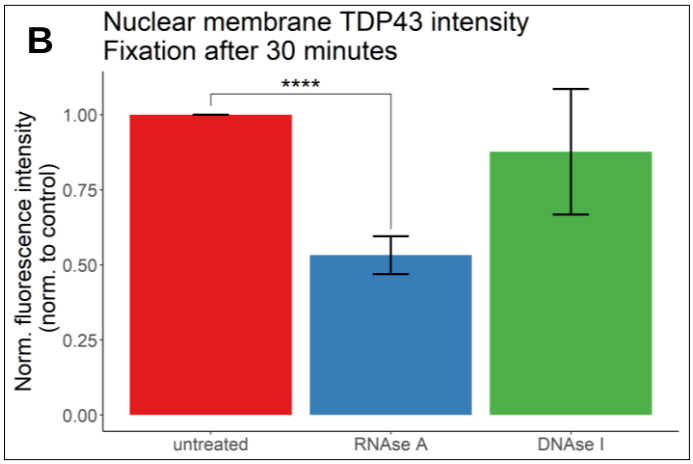
B
Nuclear membrane TDP43 intensity
Fixation after 30 minutes
****
Norm. fluorescence intensity
(norm. to control)
1.00
0.75
0.50
0.25
0.00
untreated
RNAse A
DNAse I

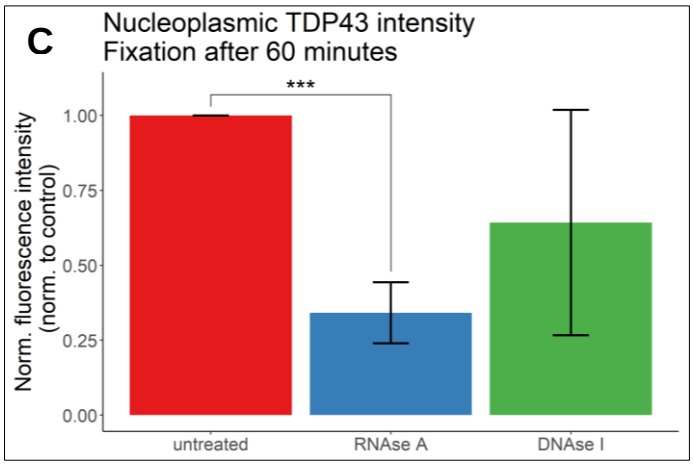
C
Nucleoplasmic TDP43 intensity
Fixation after 60 minutes
***
Norm. fluorescence intensity
(norm. to control)
1.00
0.75
0.50
0.25
0.00
untreated
RNAse A
DNAse I

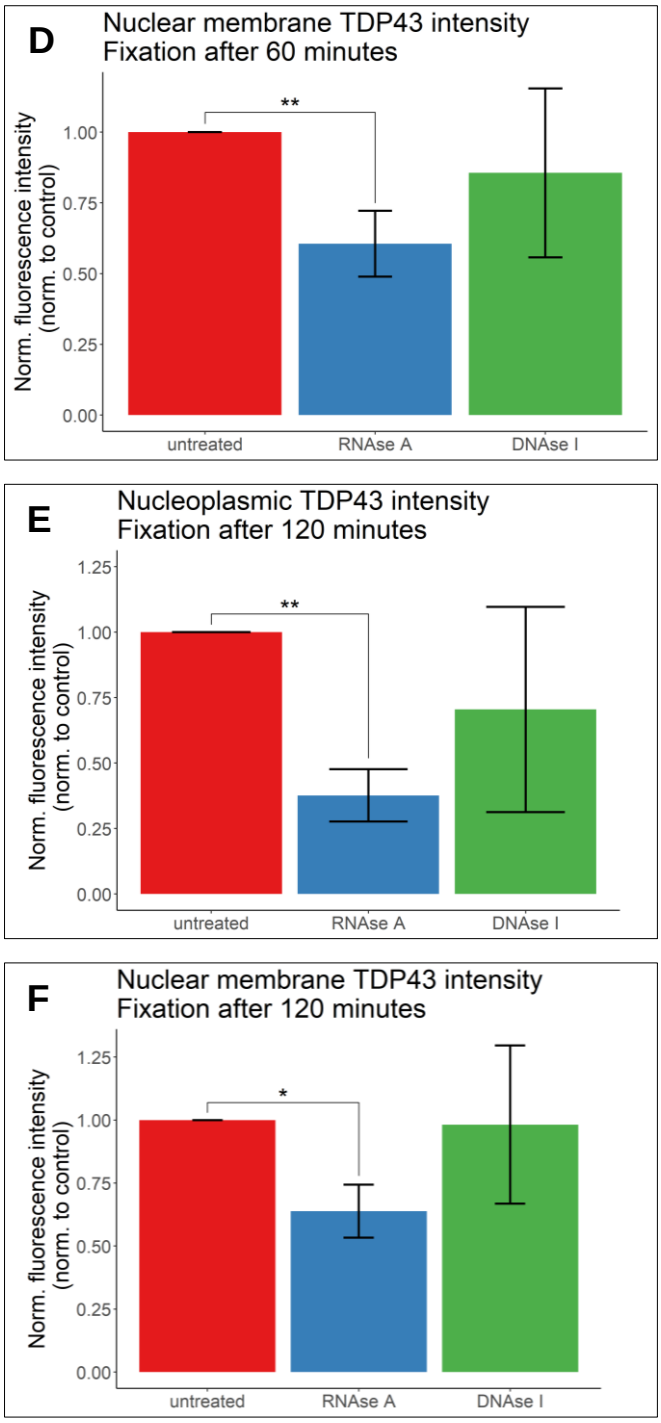

Figure 5.26: RNAse A reduces nuclear TDP43 levels. Quantified nuclear TDP43 fluorescence signal normalised to untreated control in untreated or cells treated with RNAse A or DNAse I. A) Nucleoplasmic TDP43 levels with fixation after 30 minutes. B) Nuclear membrane TDP43 levels with fixation after 30 minutes. C) Nucleoplasmic TDP43 levels with fixation after 60 minutes. D) Nuclear membrane TDP43 levels with fixation after 60 minutes. E) Nucleoplasmic TDP43 levels with fixation after 120 minutes. F) Nuclear membrane TDP43 levels with fixation after 120 minutes. Means of individual experimental means are plotted. N = 3. Error bars: SEM. ** $p < 0.01$, * $p < 0.05$ vs untreated cells with multi-level model one-way ANOVA and Dunnett's post hoc test.

Overall, DNAse I treatment had no significant effect on nuclear TDP43 levels but seemed to change its nuclear distribution. Effects of DNAse I on nuclear TDP43 localisation varied between experiments which explains the detected variability (see

Figure 5.23, Figure 5.24 and Figure 5.25). Reduction of nuclear TDP43 localisation by RNAse A treatment was independent of the incubation time with the decrease occurring to similar extents at all tested time spans indicating that nuclear TDP43 decreased relatively fast. Effects of arginine containing *C9ORF72* DPRs on nuclear TDP43 levels were similar to those of RNAse A.

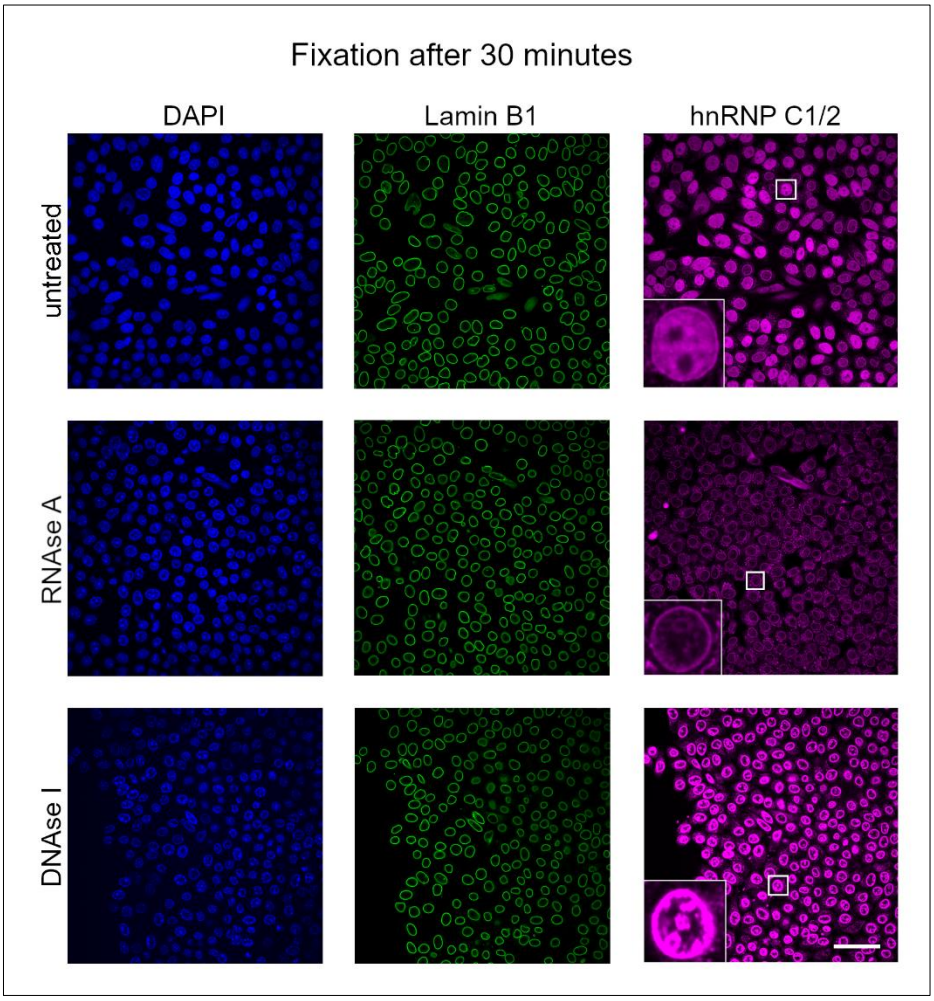

Figure 5.27: Influence of RNAse A or DNAse I on nuclear localisation of hnRNP C1/2. Opera Phenix images of immunofluorescence staining of endogenous hnRNP C1/2 in semi-permeabilised untreated cells or after 15-minute treatment with RNAse A or DNAse I as indicated, fixation after 30 min. Left panel: DAPI. Middle panel: Lamin B1. Right panel: hnRNP C1/2. Zoom ins are at different brightness and contrast settings as main images. Scale bar: 50 µm.

Nuclear hnRNP C1/2 levels were reduced to about a quarter of levels observed in untreated cells after 30-minute incubation as depicted in Figure 5.27 and Figure 5.30A. DNAse I had no significant effect on nuclear hnRNP C1/2 levels after 30 minutes but seemed to lead to a different nuclear distribution compared to untreated cells. Nuclear membrane hnRNP C1/2 levels were reduced by RNAse A whilst they

were increased by DNAse I treatment (see Figure 5.30B) possibly owing to the nuclear redistribution of hnRNP C1/2.

After 60 minutes RNAse A lowered nuclear hnRNP C1/2 intensities by about 75 % compared to untreated cells (see Figure 5.28 and Figure 5.30C). Again, DNAse I showed no significant effect on nuclear hnRNP C1/2 levels but hnRNP C1/2 seemed to be differently distributed compared to untreated cells. Nuclear membrane hnRNP C1/2 levels were reduced to about 40 % of the same levels in untreated cells by RNAse A after 60 minutes whilst DNAse I increased these levels compared to non-treatment (see Figure 5.30D).

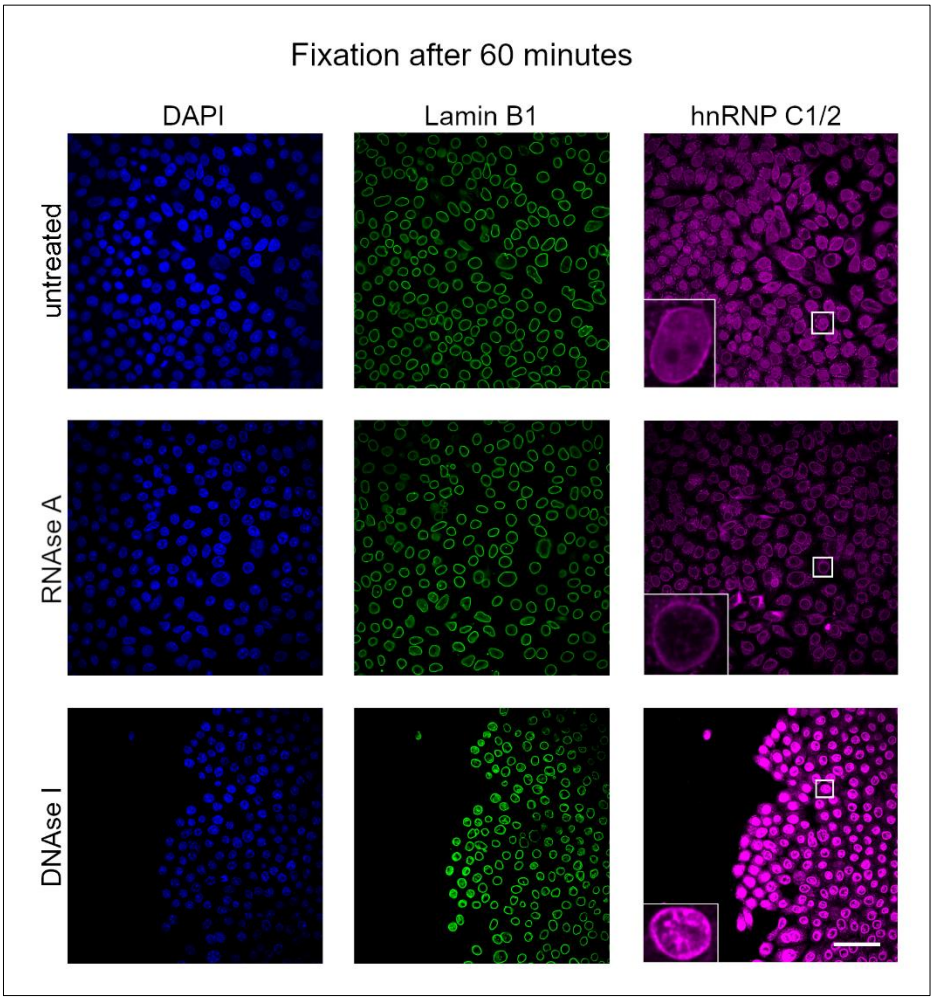

Figure 5.28: Impact of RNAse A or DNAse I on nuclear localisation of hnRNP C1/2. Opera Phenix images of immunofluorescence staining of endogenous hnRNP C1/2 in semi-permeabilised untreated cells or after 15-minute treatment with RNAse A or DNAse I as indicated, fixation after 60 min. Left panel: DAPI. Middle panel: Lamin B1. Right panel: hnRNP C1/2. Zoom ins are at different brightness and contrast settings as main images. Scale bar: 50 µm.

As depicted in Figure 5.29 and Figure 5.30E RNAse A treatment led to a 60 % decline of hnRNP C1/2 levels after 120 minutes compared to untreated cells. DNAse I showed no significant effect on nuclear hnRNP C1/2 levels compared to untreated cells after 120 minutes but nuclear hnRNP C1/2 distribution seemed to have changed. Nuclear membrane levels were not significantly reduced by RNAse A after 120 minutes whilst they were significantly enhanced by DNAse I treatment (see Figure 5.30F).

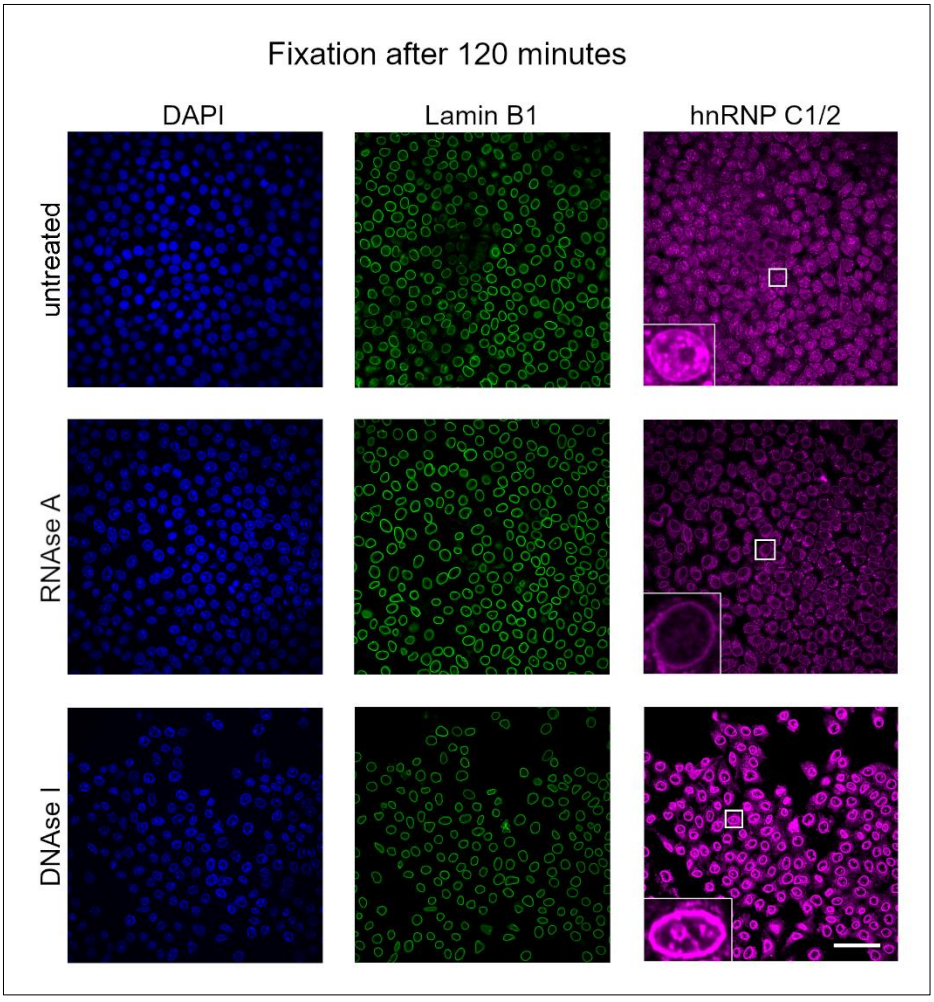

Figure 5.29: Effects of RNAse A or DNAse I on nuclear localisation of hnRNP C1/2. Opera Phenix images of immunofluorescence staining of endogenous hnRNP C1/2 in semi-permeabilised untreated cells or after 15-minute treatment with RNAse A or DNAse I as indicated, fixation after 120 min. Left panel: DAPI. Middle panel: Lamin B1. Right panel: hnRNP C1/2. Zoom ins are at different brightness and contrast settings as main images. Scale bar: 50 µm.

Overall, RNAse A had similar effects on nuclear hnRNP C1/2 at different timepoints indicating that hnRNP C1/2 is lost from the nucleus already after a short treatment time. DNAse I treatment led to a different nuclear distribution of hnRNP C1/2 with it being predominantly located at the nuclear membrane. RNAse A treatment seemed

to lower nuclear hnRNP C1/2 to a greater extent than arginine containing DPRs especially when the latter were used at 10 µM but the direction of the observed effect was the same between the two treatment types (compare section 4.3).

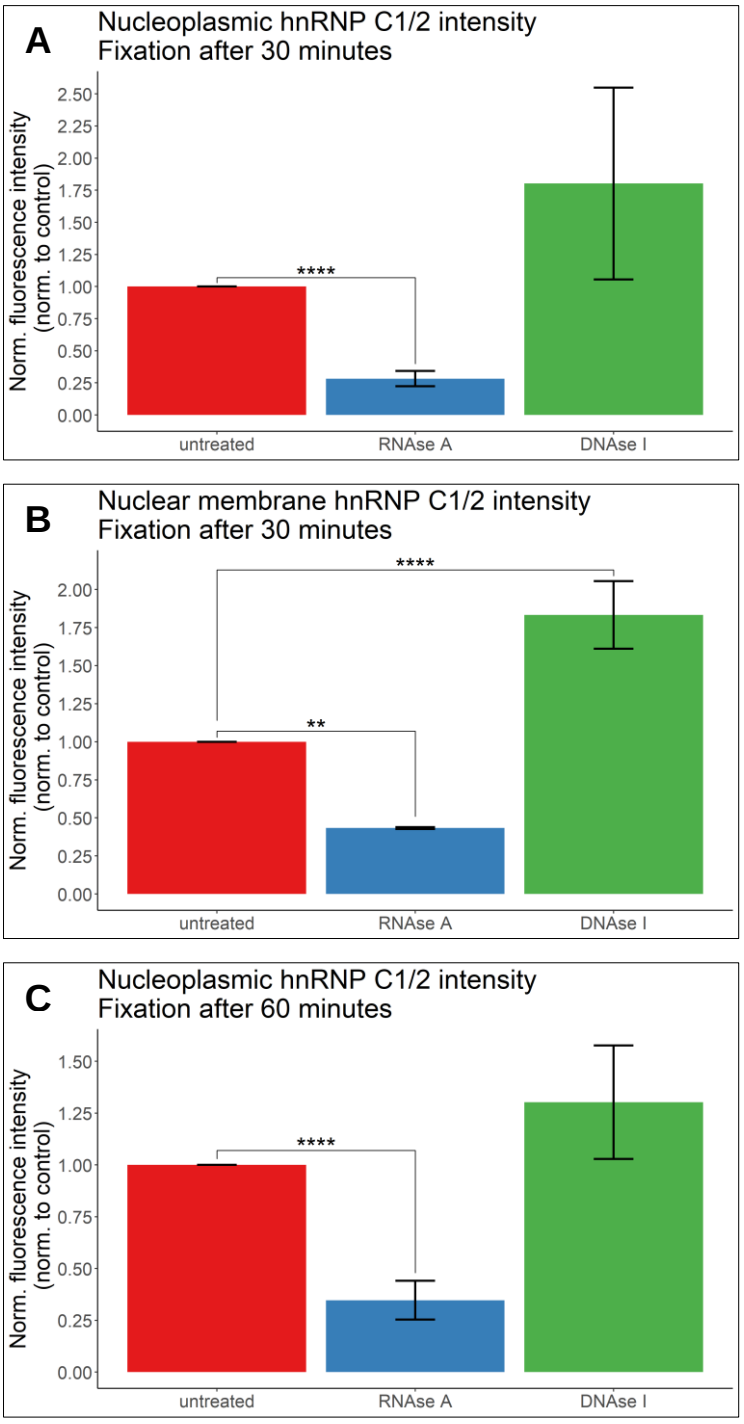

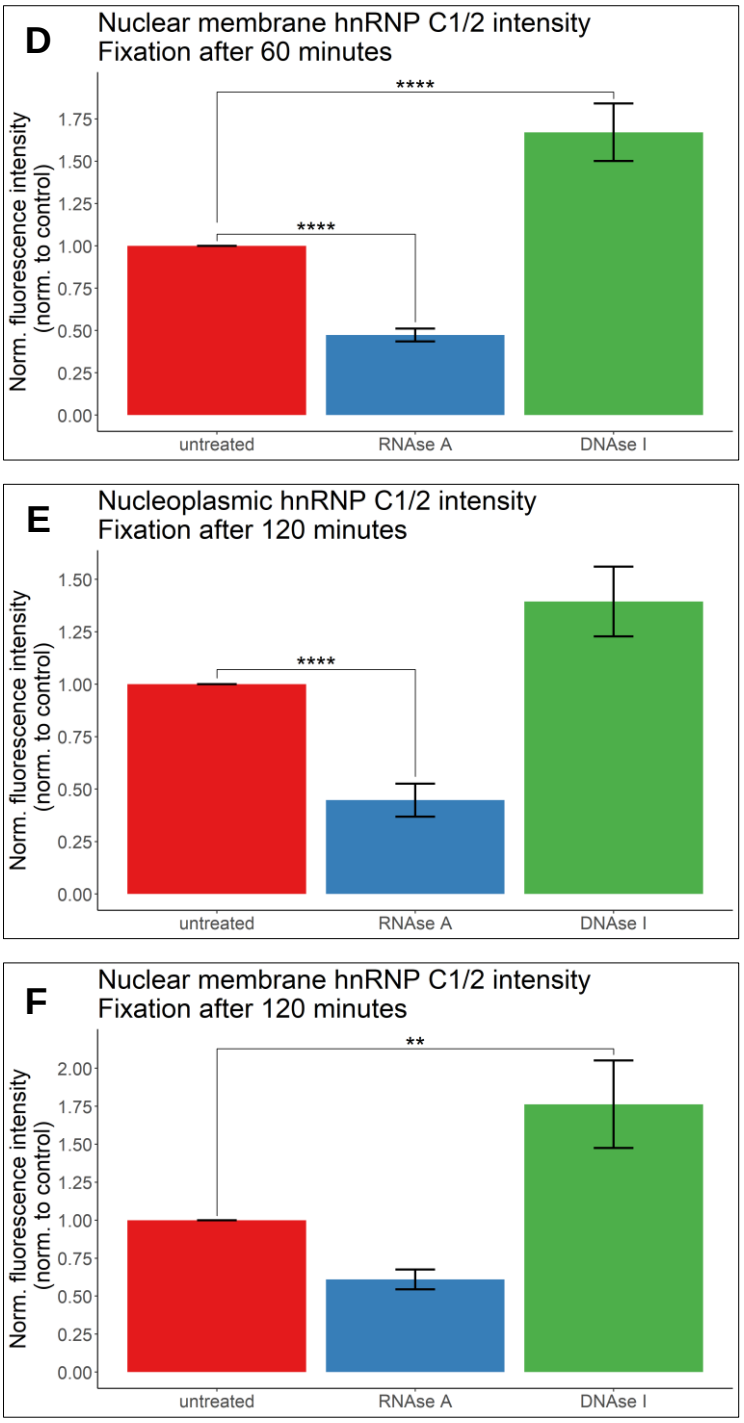

Figure 5.30: RNAse A decreases whilst DNAse I increases nuclear hnRNP C1/2 levels. Quantified nuclear hnRNP C1/2 fluorescence signal normalised to untreated control in untreated or cells treated with RNAse A or DNAse I. A) Nucleoplasmic hnRNP C1/2 levels with fixation after 30 minutes. B) Nuclear membrane hnRNP C1/2 levels with fixation after 30 minutes. C) Nucleoplasmic hnRNP C1/2 levels with fixation after 60 minutes. D) Nuclear membrane hnRNP C1/2 levels with fixation after 60 minutes. E) Nucleoplasmic hnRNP C1/2 levels with fixation after 120 minutes. F) Nuclear membrane hnRNP C1/2 levels with fixation after 120 minutes. Means of individual experimental means are depicted. N =3. Error bars: SEM. **** $p < 0.0001$, ** $p < 0.01$vs untreated cells with multi-level model one-way ANOVA and Dunnett's post hoc test.

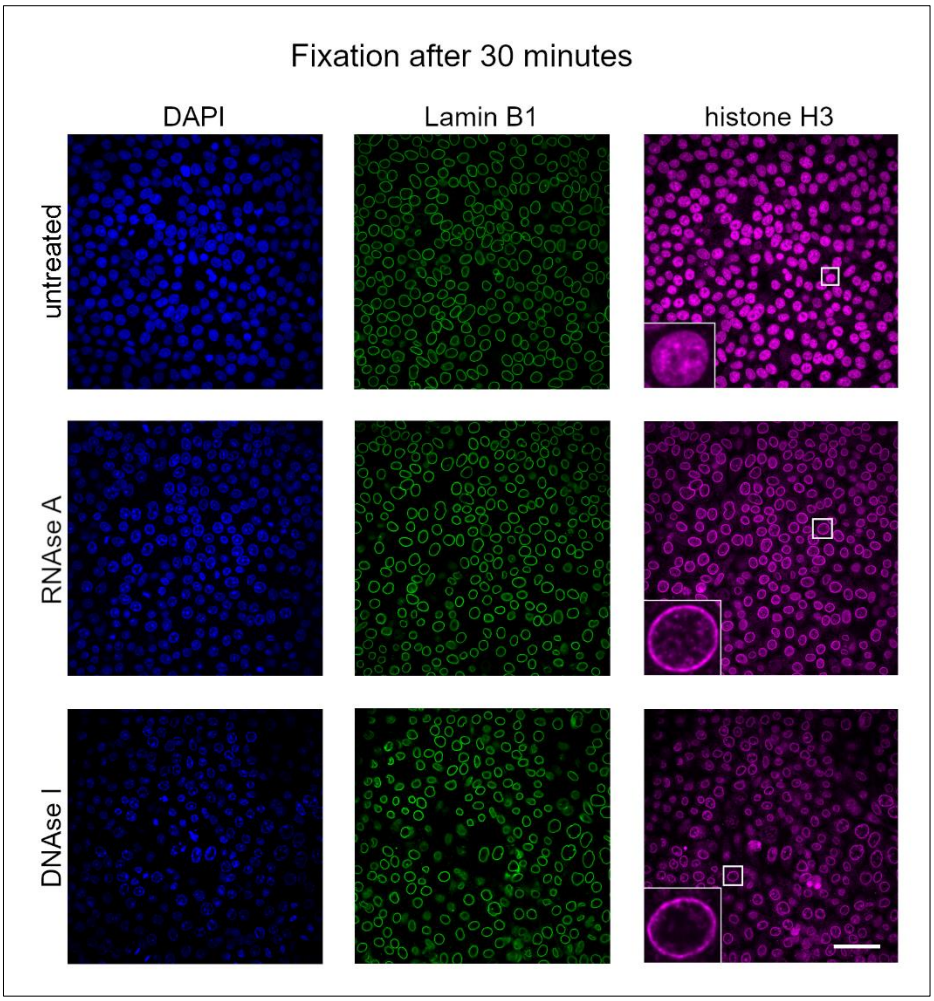

Figure 5.31: Influence of RNAse A or DNAse I on nuclear levels of histone H3. Opera Phenix images of immunofluorescence staining of endogenous histone H3 in semi-permeabilised untreated cells or after 15-minute treatment with RNAse A or DNAse I as indicated, fixation after 30 min. Left panel: DAPI. Middle panel: Lamin B1. Right panel: histone H3. Zoom ins are at different brightness and contrast settings as main images. Scale bar: 50 µm.

As depicted in Figure 5.31 and Figure 5.34A nuclear histone H3 levels were reduced by about 70 and 60 % by 30-minute RNAse A and DNAse I treatment, respectively, in comparison to untreated cells. Nuclear membrane histone H3 levels were also reduced by both RNAse A and DNAse I after 30 minutes but only by about 25 - 30 % (see Figure 5.34B).

After 60 minutes nuclear histone H3 levels were again decreased by 70 and 60 % by RNAse A and DNAse I treatment, respectively, compared to untreated cells (see Figure 5.32 and Figure 5.34C). Nuclear membrane levels of histone H3 were only lowered upon RNAse A treatment after 60 minutes to about 75 % of the levels of untreated cells (see Figure 5.34D).

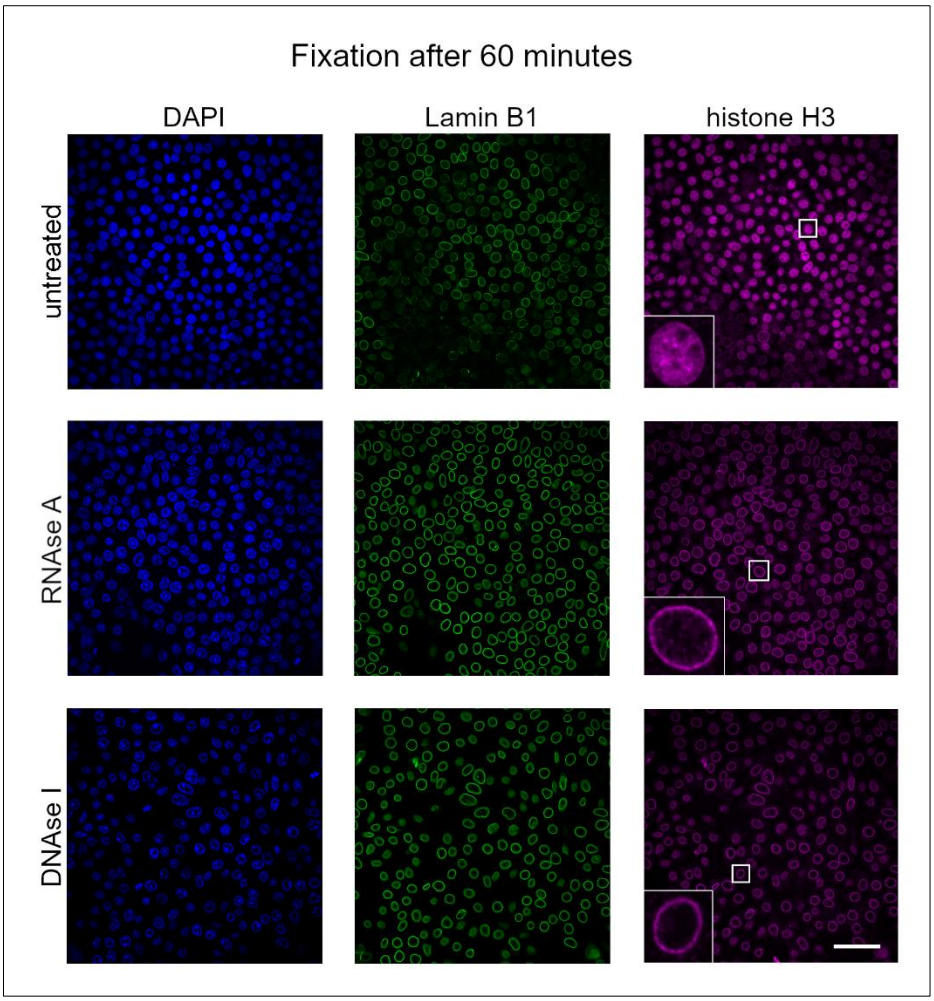

Figure 5.32: Impact of RNAse A or DNAse I on nuclear levels of histone H3. Opera Phenix images of immunofluorescence staining of endogenous histone H3 in semi-permeabilised untreated cells or after 15-minute treatment with RNAse A or DNAse I as indicated, fixation after 60 min. Left panel: DAPI. Middle panel: Lamin B1. Right panel: histone H3. Zoom ins are at different brightness and contrast settings as main images. Scale bar: 50 µm.

RNAse A and DNAse I decreased nuclear histone H3 levels by about 60 % compared to untreated cells after 120 minutes (see Figure 5.33 and Figure 5.34E). DNAse I treatment but not RNAse A treatment resulted in a 25 % reduction of nuclear membrane histone H3 levels after 120 minutes (see Figure 5.34F). Overall, the influence of nuclease treatment and arginine containing DPRs on nuclear histone H3 levels seemed to go in the same direction (compare section 4.3).

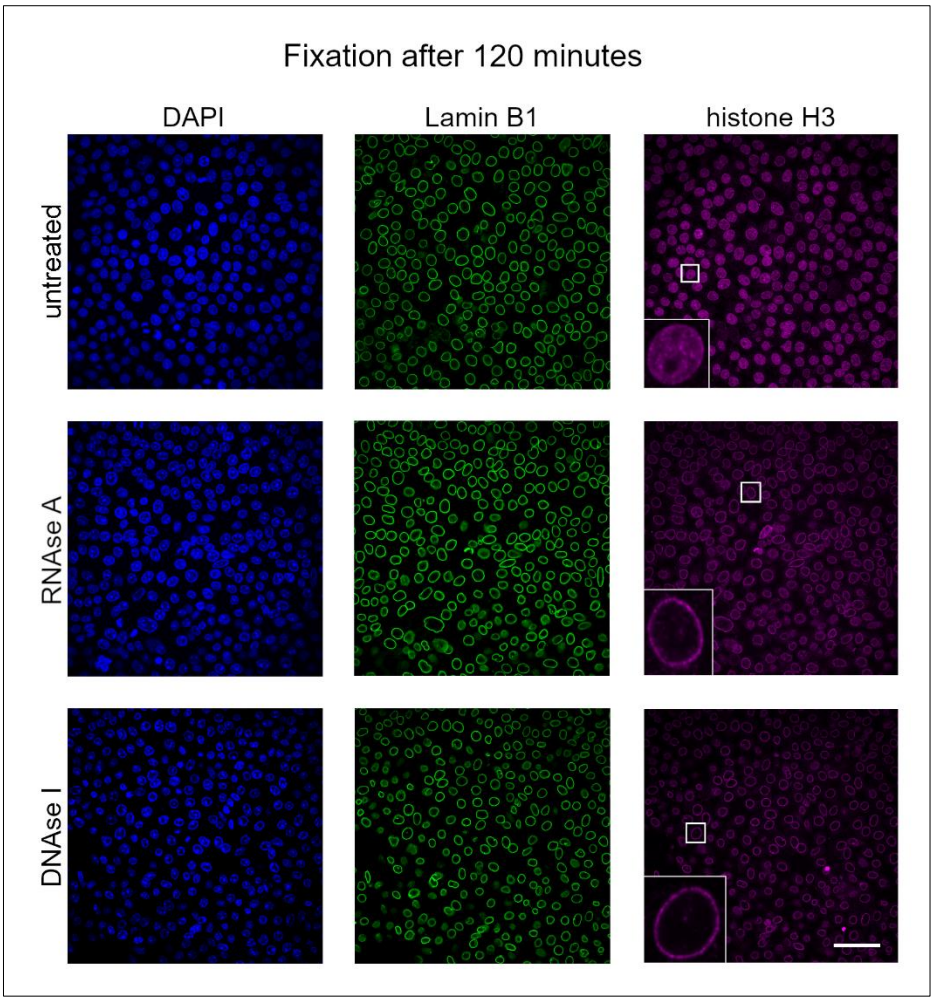

Figure 5.33: Effects of RNAse A or DNAse I on nuclear levels of histone H3. Opera Phenix images of immunofluorescence staining of endogenous histone H3 in semi-permeabilised untreated cells or after 15-minute treatment with RNAse A or DNAse I as indicated, fixation after 120 min. Left panel: DAPI. Middle panel: Lamin B1. Right panel: histone H3. Zoom ins are at different brightness and contrast settings as main images. Scale bar: 50 µm.

Nuclear levels of TDP43, hnRNP C1/2 and histone H3 were reduced in the same manner by nuclease and poly-GR/PR treatment. This suggests that nuclear localisation of nucleic acid binding proteins could be promoted by their interaction with RNA and DNA. Furthermore, poly-GR and -PR might have disturbed this interaction with RNA/DNA of TDP43, hnRNP C1/2 and histone which potentially led to their enhanced export from the nucleus.

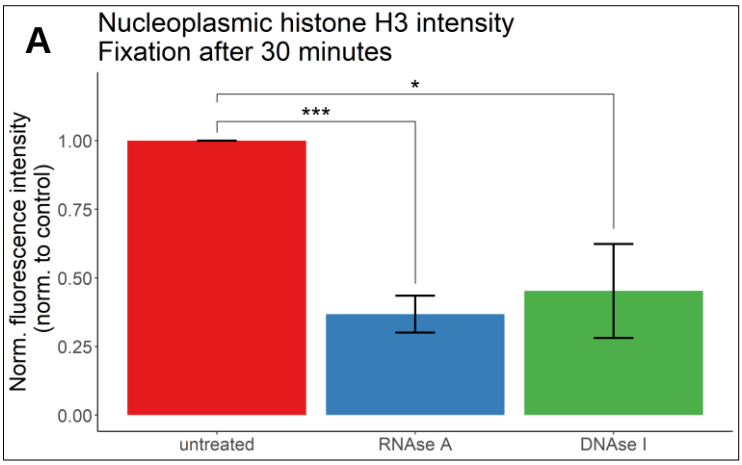
A
Nucleoplasmic histone H3 intensity
Fixation after 30 minutes
Norm. fluorescence intensity
(norm. to control)
1.00
0.75
0.50
0.25
0.00
***
*
untreated
RNAse A
DNAse I

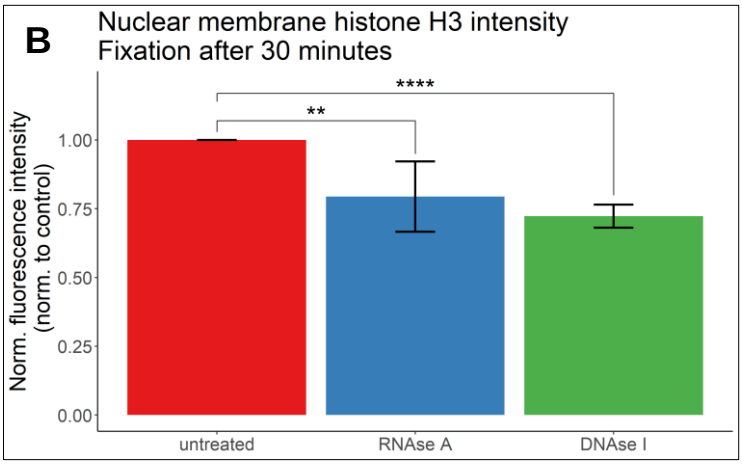
B
Nuclear membrane histone H3 intensity
Fixation after 30 minutes
Norm. fluorescence intensity
(norm. to control)
1.00
0.75
0.50
0.25
0.00
**
****
untreated
RNAse A
DNAse I

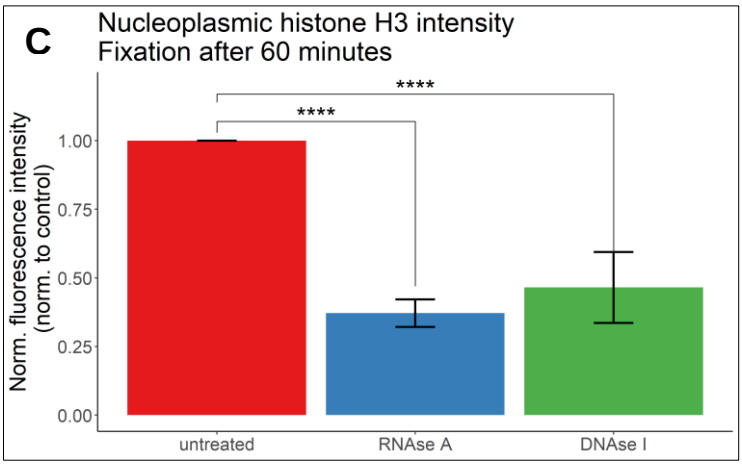
C
Nucleoplasmic histone H3 intensity
Fixation after 60 minutes
Norm. fluorescence intensity
(norm. to control)
1.00
0.75
0.50
0.25
0.00
****
****
untreated
RNAse A
DNAse I

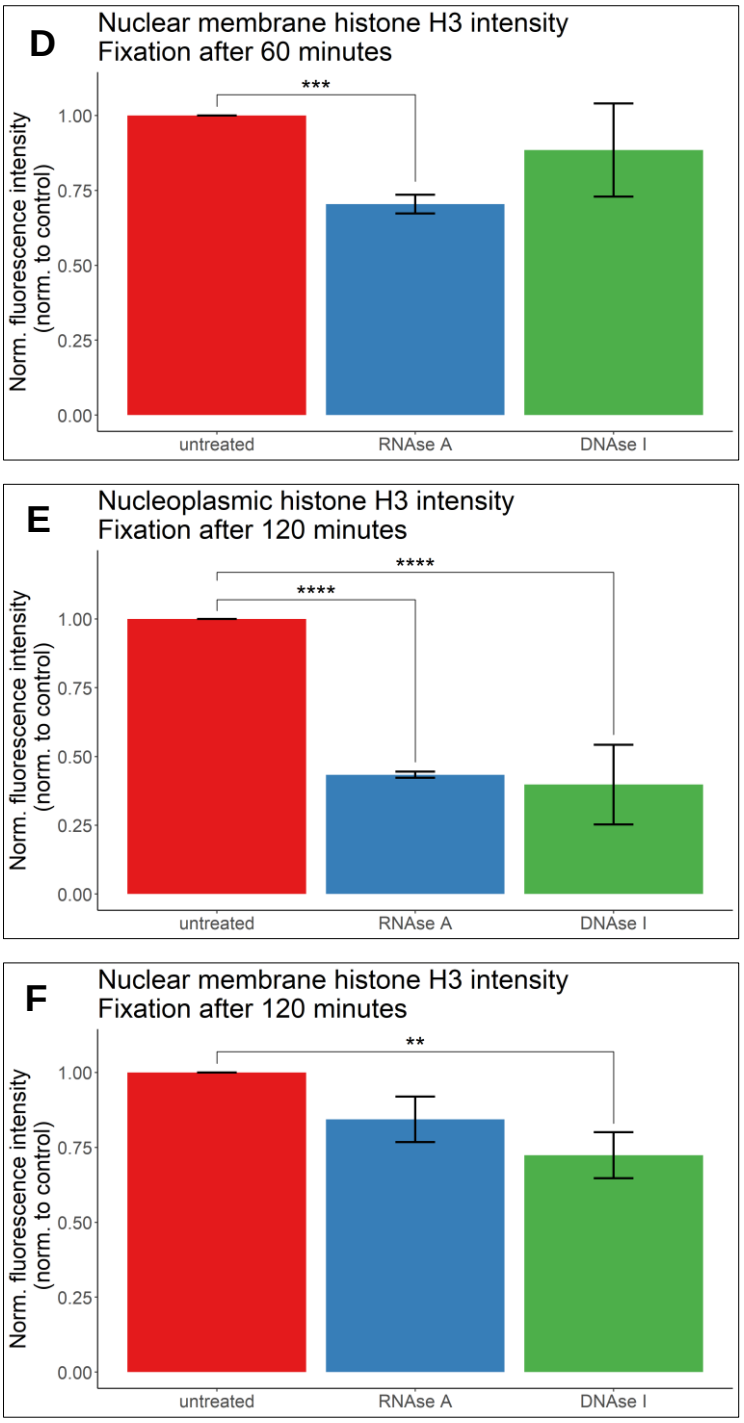

Figure 5.34: RNAse A and DNAse I lower nuclear histone H3 levels. Quantified nuclear histone H3 fluorescence signal normalised to untreated control in untreated or cells treated with RNAse A or DNAse I. A) Nucleoplasmic histone H3 levels with fixation after 30 minutes. B) Nuclear membrane histone H3 levels with fixation after 30 minutes. C) Nucleoplasmic histone H3 levels with fixation after 60 minutes. D) Nuclear membrane histone H3 levels with fixation after 60 minutes. E) Nucleoplasmic histone H3 levels with fixation after 120 minutes. F) Nuclear membrane histone H3 levels with fixation after 120 minutes. Means of individual experimental means are plotted. N = 3. Error bars: SEM. **** $p < 0.0001$, *** $p < 0.001$, ** $p < 0.01$, * $p < 0.05$, vs untreated cells with multi-level model one-way ANOVA and Dunnett's post hoc test.

5.4 Impact of *C9ORF72* DPRs on nucleocytoplasmic transport factors

To test whether the passive nucleocytoplasmic transport enhancement by poly-GR and -PR was caused by the interference of these DPRs with the localisation of nucleocytoplasmic transport factors we subjected HeLa cells to the permeabilisation assay, treated them with 10 µM *C9ORF72* DPRs for 2 hours (treatment time where also 10 µM GR20 affected nuclear TDP43 localisation as described in section 4.3) and immunostained cells for various nucleocytoplasmic transport proteins. As FG nucleoporins (nuclear pore proteins) are forming the permeability barrier of the nuclear pore (Schmidt and Görlich, 2016) we investigated a selection of human FG nucleoporins namely, NUP98, POM121, NUP153, NUP54 and RanBP2 (Lyngdoh et al., 2021). We also studied the localisation of Ran and its regulating factors RanGAP1 and RCC1, and of import receptors importin β1, α1 and α3. We aimed to investigate the influence of poly-GR and -PR on all these transport factors in our semi-permeabilised cell system and thus the contribution of these effects on the increase of passive nucleocytoplasmic transport.

Nucleoporins

We investigated the localisation of a range of FG nucleoporins upon *C9ORF72* DPR treatment as a change in their localisation might affect the permeability barrier of the nuclear pore. The cytoplasmic filament nucleoporin RanBP2 also plays a role in hydrolysis of RanGTP to RanGDP (Beddow et al., 1995; Vetter et al., 1999). As shown in Figure 5.35 in untreated cells, NUP98 was found predominantly at the nuclear membrane, where nuclear pores reside, as would be expected. However, it also showed some nucleoplasmic staining in cells. We therefore quantified both nucleoplasmic and nuclear membrane levels of NUP98 (and of all other transport factors localising to these compartments in untreated cells). Nucleoplasmic nucleoporin NUP98 levels were not changed by GP20 treatment compared to untreated cells (see Figure 5.35 and Figure 5.36A). PR20 significantly lowered nucleoplasmic NUP98 by about 80 % compared to non-treatment with a *p* value of 3.82×10^{-13} (Dunnett's post-hoc test). A trend to a decrease in nucleoplasmic NUP98 levels was observed after poly-GR and a trend to an increase in the same levels was detected after poly-GA treatment compared to untreated cells. Nuclear membrane levels (and thus levels within the nuclear pore) of NUP98 were significantly reduced

by PR treatment by about 25 % compared to untreated cells (p = 8.37x10^{-9}, Dunnett's post-hoc test) whilst no significant change was detected with any other DPR treatment (see Figure 5.36B).

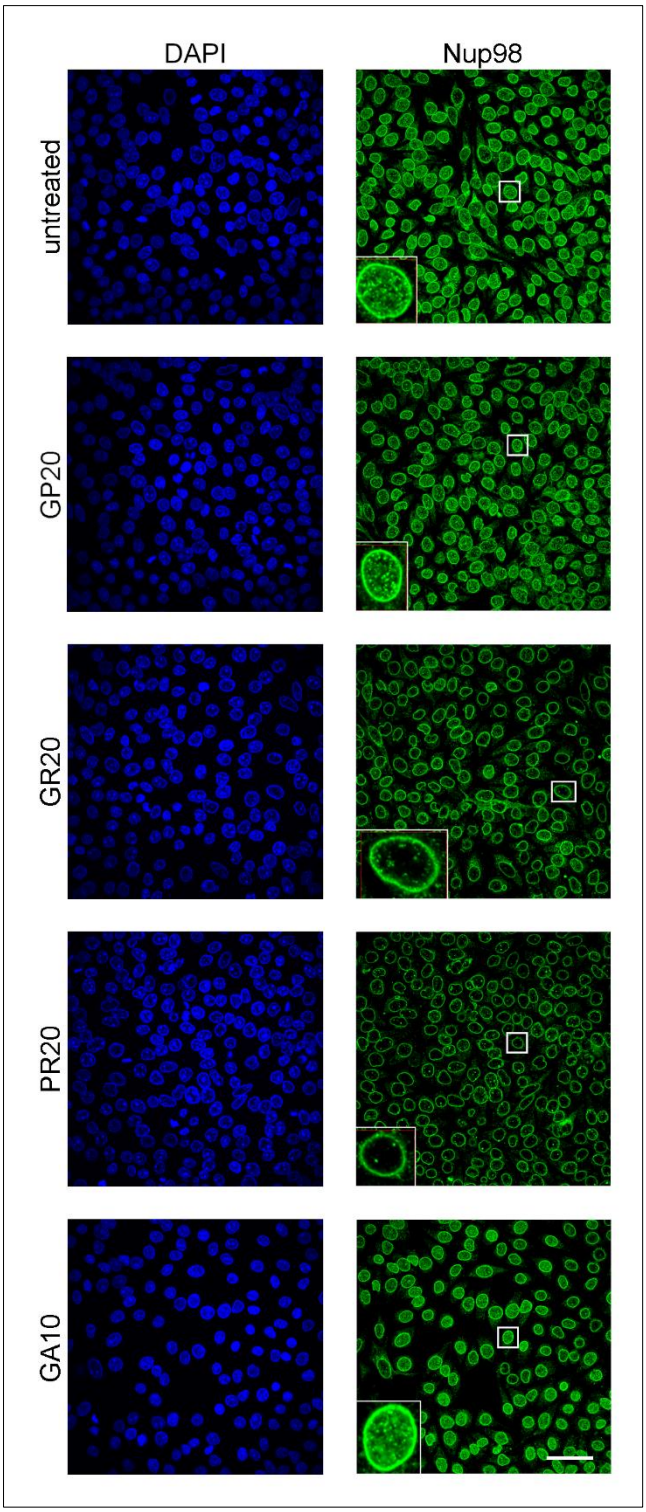

Figure 5.35: Effects of *C9ORF72* DPRs on nuclear NUP98 levels. Opera Phenix images of immunofluorescence staining of endogenous NUP98 in semi-permeabilised untreated cells or after 120-minute treatment with 10 µM of different *C9ORF72* dipeptide repeat proteins as indicated. Left panel: DAPI. Right panel: NUP98. Zoom ins are at different brightness and contrast settings as main images. Scale bar: 50 µm.

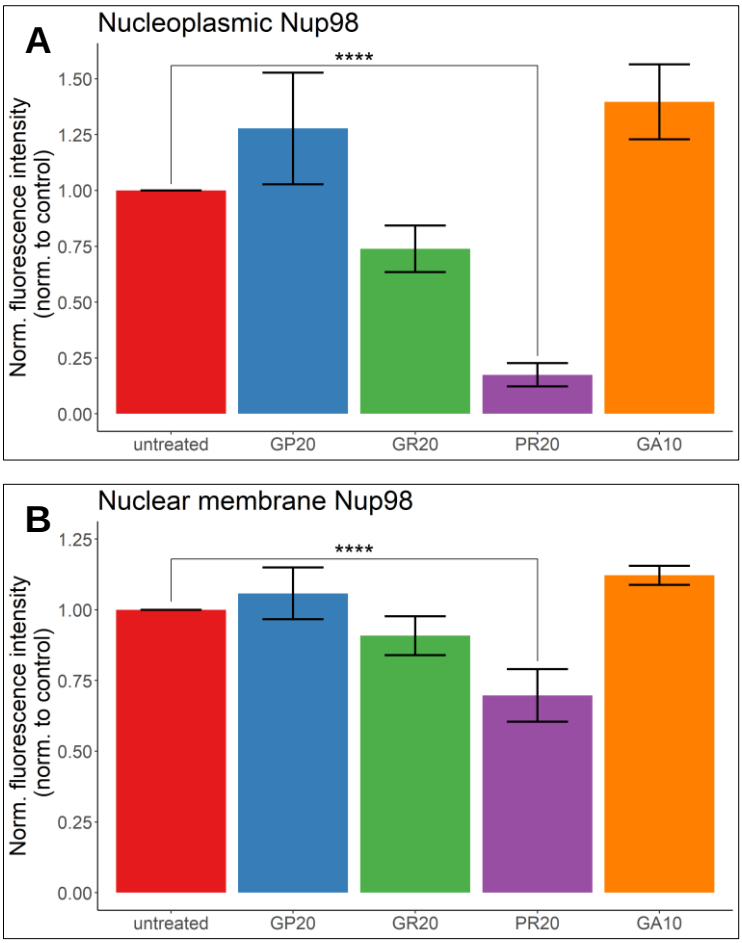

Figure 5.36: Poly-PR decreases nuclear NUP98 levels. Quantified nuclear NUP98 fluorescence signal normalised to untreated control in untreated cells or after 120-minute treatment with 10 µM of different *C9ORF72* dipeptide repeat proteins as indicated. A) Nucleoplasmic NUP98 levels. B) Nuclear membrane NUP98 levels. Means of individual experimental means are plotted. N = 3. Error bars: SEM. **** $p < 0.0001$ vs untreated cells with multi-level model one-way ANOVA and Dunnett's post hoc test.

FG and transmembrane nucleoporin POM121 also showed staining at both the nuclear membrane/nuclear pore and in the nucleoplasm in untreated cells as depicted in Figure 5.37. GP20 and GA10 treatment did not significantly alter nucleoplasmic levels of nucleoporin POM121 compared to untreated cells (see Figure 5.37 and Figure 5.38A). Nucleoplasmic POM121 was significantly decreased by about 80 % by poly-PR ($p = 3.38 \times 10^{-6}$, Dunnett's post-hoc test) and trended to decrease upon poly-GR treatment compared to untreated cells. Nuclear membrane or nuclear pore POM121 levels were only significantly changed by PR20 which led to a 40 % reduction of these levels compared to non-treatment with a p value of 2.2×10^{-7} (Dunnett's post-hoc test; see Figure 5.38B).

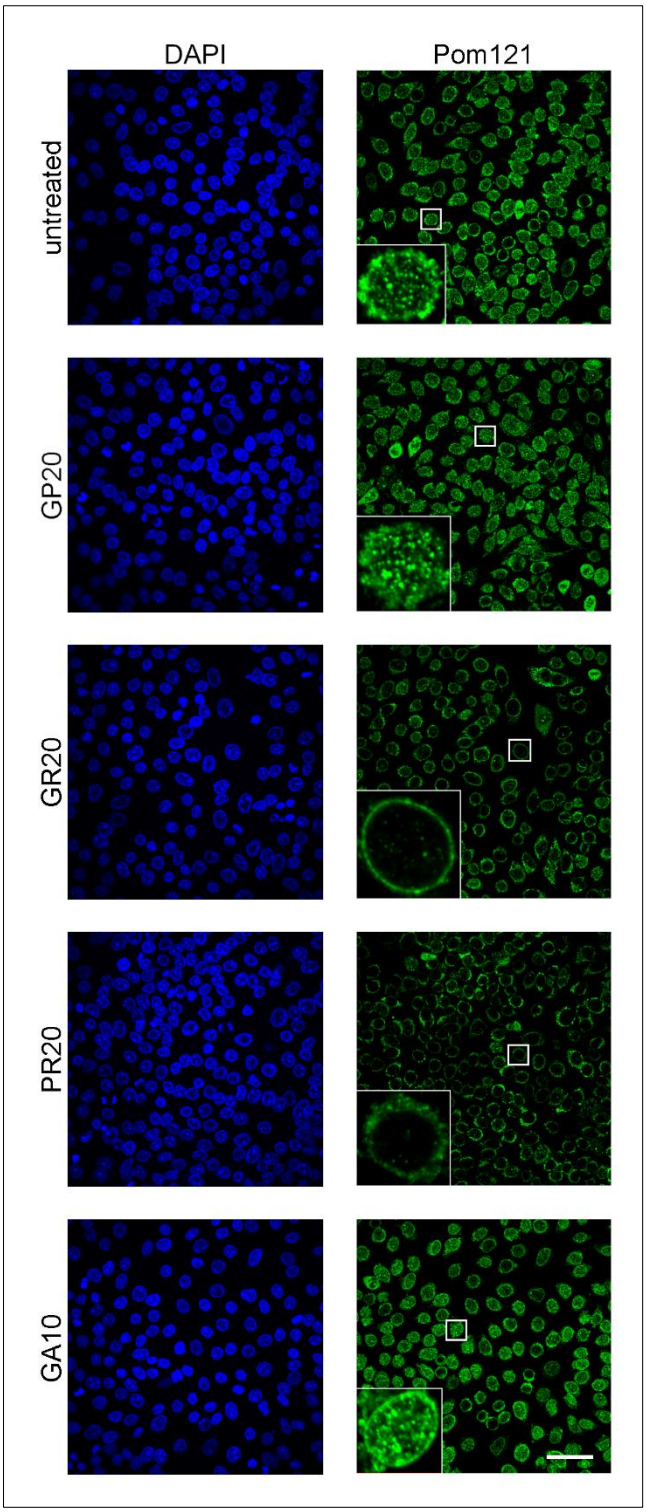

Figure 5.37: Influence of *C9ORF72* DPRs on nuclear POM121 levels. Opera Phenix images of immunofluorescence staining of endogenous POM121 in semi-permeabilised untreated cells or after 120-minute treatment with 10 µM of different *C9ORF72* dipeptide repeat proteins as indicated. Left panel: DAPI. Right panel: POM121. Zoom ins are at different brightness and contrast settings as main images. Scale bar: 50 µm.

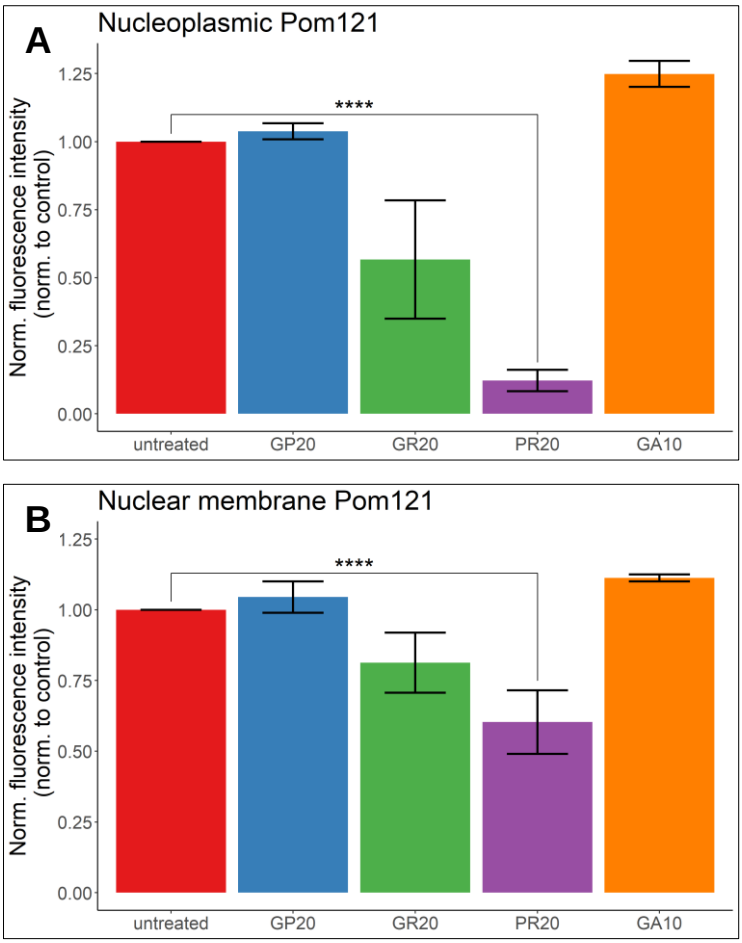

Figure 5.38: Poly-PR reduces nuclear POM121 levels. Quantified nuclear POM121 fluorescence signal normalised to untreated control in untreated cells or after 120-minute treatment with 10 µM of different *C9ORF72* dipeptide repeat proteins as indicated. A) Nucleoplasmic POM121 levels. B) Nuclear membrane POM121 levels. Means of individual experimental means are shown. N = 3. Error bars: SEM. **** $p < 0.0001$ vs untreated cells with multi-level model one-way ANOVA and Dunnett's post hoc test.

Nuclear basket FG nucleoporin NUP153 only localised to the nuclear membrane, hence nuclear pore, in untreated cells as shown in Figure 5.39. Nuclear membrane/pore NUP153 was not influenced by *C9ORF72* DPR treatment as depicted in Figure 5.39 and Figure 5.40.

Central channel FG nucleoporin NUP54 staining was detected at the nuclear membrane/nuclear pore and in the nucleoplasm in untreated cells as illustrated in Figure 5.41. GR20 and PR20 treatment halved nucleoplasmic levels of nucleoporin NUP54 compared to untreated cells with a *p* value of 1.17×10^{-17} and 1.73×10^{-12}, respectively (Dunnett's post-hoc test; see Figure 5.41 and Figure 5.42A) whilst nuclear membrane/pore levels were increased about 1.4-fold by poly-GR (*p* near 0, Dunnett's post-hoc test) potentially indicating a redistribution of NUP54 and were not changed by poly-PR compared to untreated cells (see Figure 5.42B).

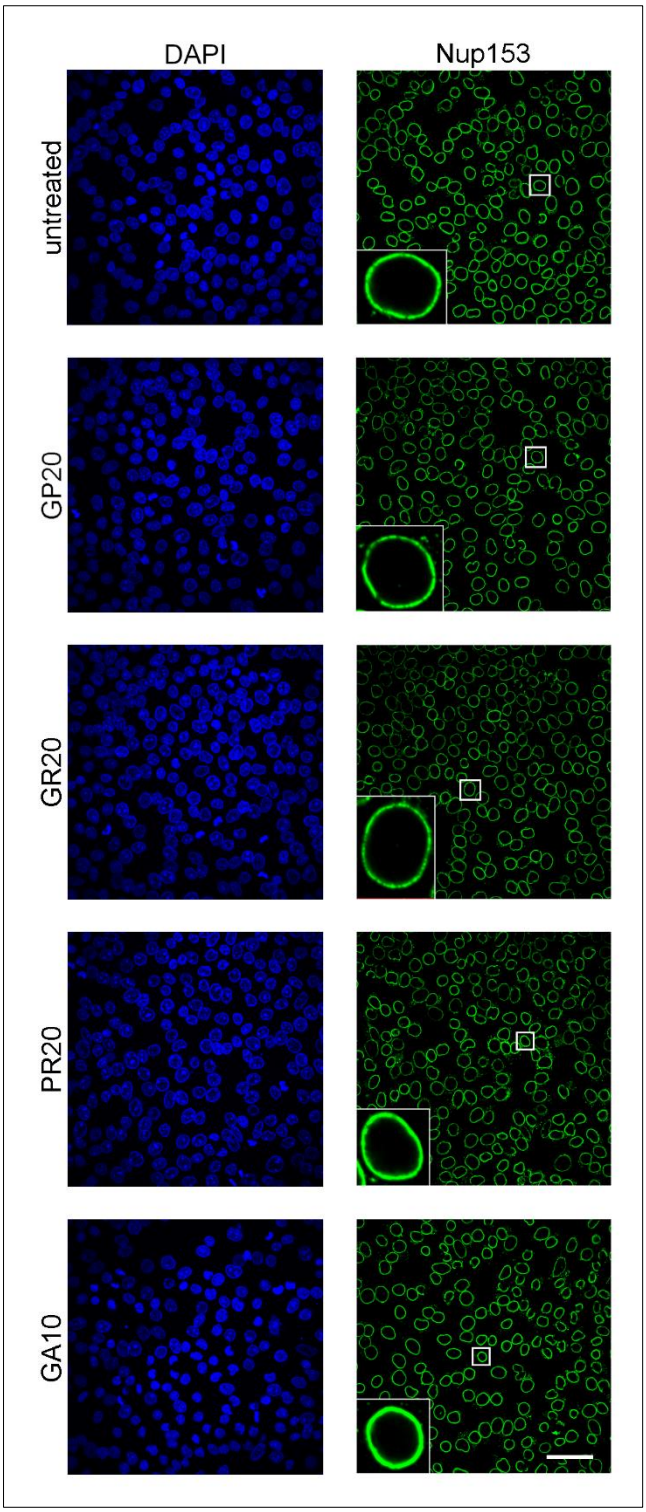

Figure 5.39: Impact of *C9ORF72* DPRs on nuclear membrane NUP153 levels. Opera Phenix images of immunofluorescence staining of endogenous NUP153 in semi-permeabilised untreated cells or after 120-minute treatment with 10 µM of different *C9ORF72* dipeptide repeat proteins as indicated. Left panel: DAPI. Right panel: NUP153. Zoom ins are at different brightness and contrast settings as main images. Scale bar: 50 µm.

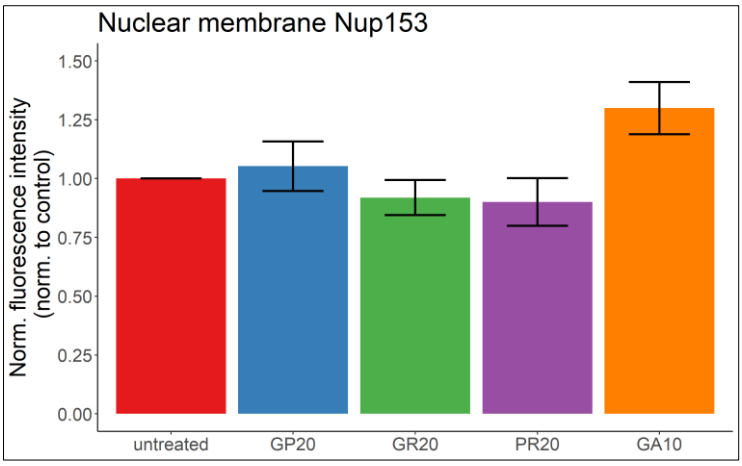

Figure 5.40: Nuclear membrane NUP153 levels are not changed upon *C9ORF72* DPR treatment. Quantified nuclear NUP153 fluorescence signal normalised to untreated control in untreated cells or after 120-minute treatment with 10 µM of different *C9ORF72* dipeptide repeat proteins as indicated. A) Nucleoplasmic NUP153 levels. B) Nuclear membrane NUP153 levels. Means of individual experimental means are depicted. N = 3. Error bars: SEM. Treated vs untreated cells with multi-level model one-way ANOVA and Dunnett's post hoc test.

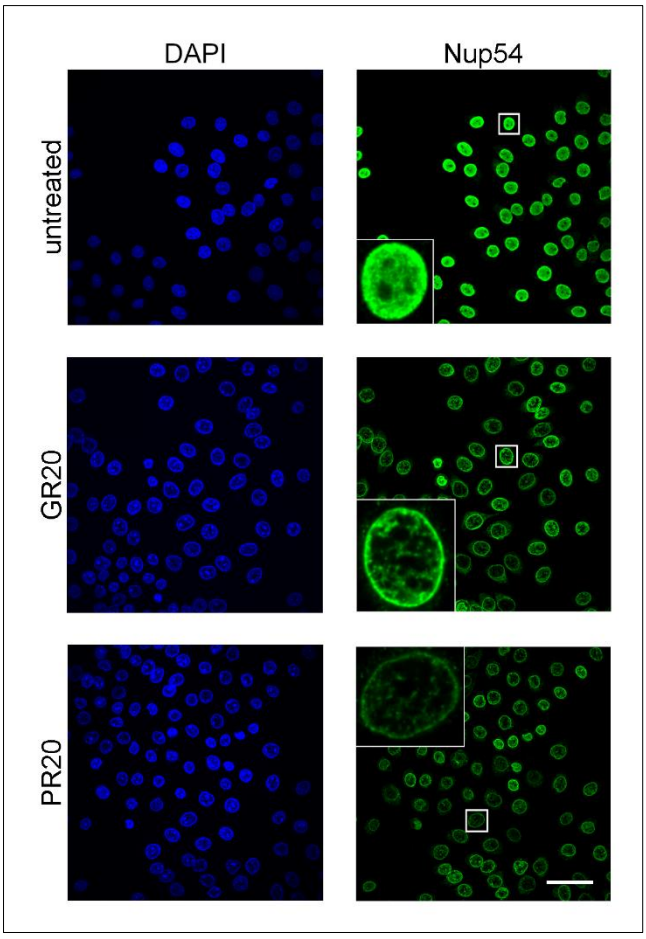

Figure 5.41: Effects of *C9ORF72* DPRs on nuclear NUP54 localisation. Opera Phenix images of immunofluorescence staining of endogenous NUP54 in semi-permeabilised untreated cells or after 120-minute treatment with 10 µM of different *C9ORF72* dipeptide repeat proteins as indicated. Left panel: DAPI. Right panel: NUP54. Zoom ins are at different brightness and contrast settings as main images. Scale bar: 50 µm.

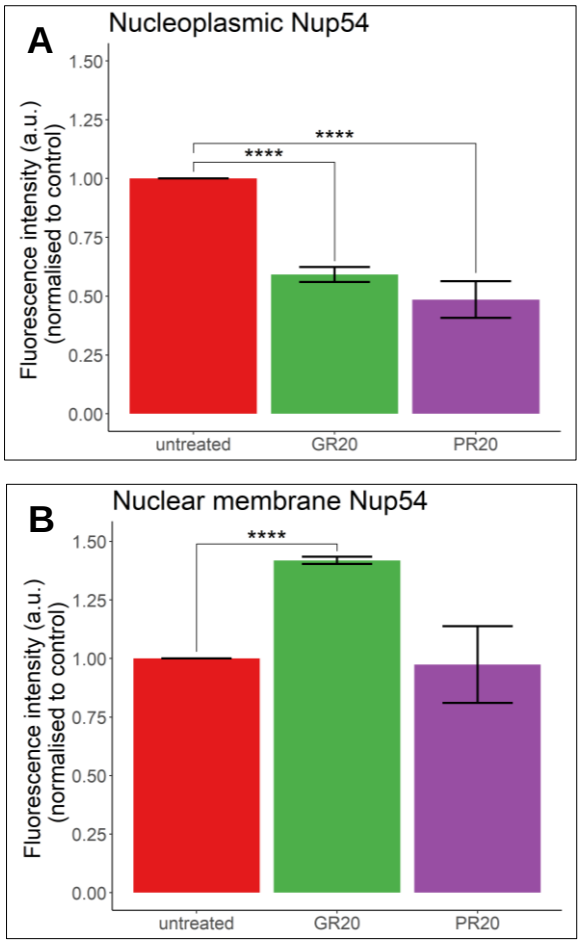

Figure 5.42: Poly-GR and -PR lower nuclear NUP54 levels. Quantified nuclear NUP54 fluorescence signal normalised to untreated control in untreated cells or after 120-minute treatment with 10 µM of different *C9ORF72* dipeptide repeat proteins as indicated. A) Nucleoplasmic NUP54 levels. B) Nuclear membrane NUP54 levels. Means of individual experimental means are plotted. N = 3. Error bars: SEM. **** $p < 0.0001$ vs untreated cells with multi-level model one-way ANOVA and Dunnett's post hoc test.

As depicted in Figure 5.43 cytoplasmic filament FG nucleoporin RANBP2 is exclusively located to the nuclear pore/membrane in untreated cells. Nuclear membrane and pore levels of nucleoporin RANBP2 were not significantly changed by GP20, GR20 or GA10 treatment whilst PR20 treatment caused a 25 % decrease compared to untreated cells with a *p* value of 0.04 (Dunnett's post-hoc test; see Figure 5.43 and Figure 5.44).

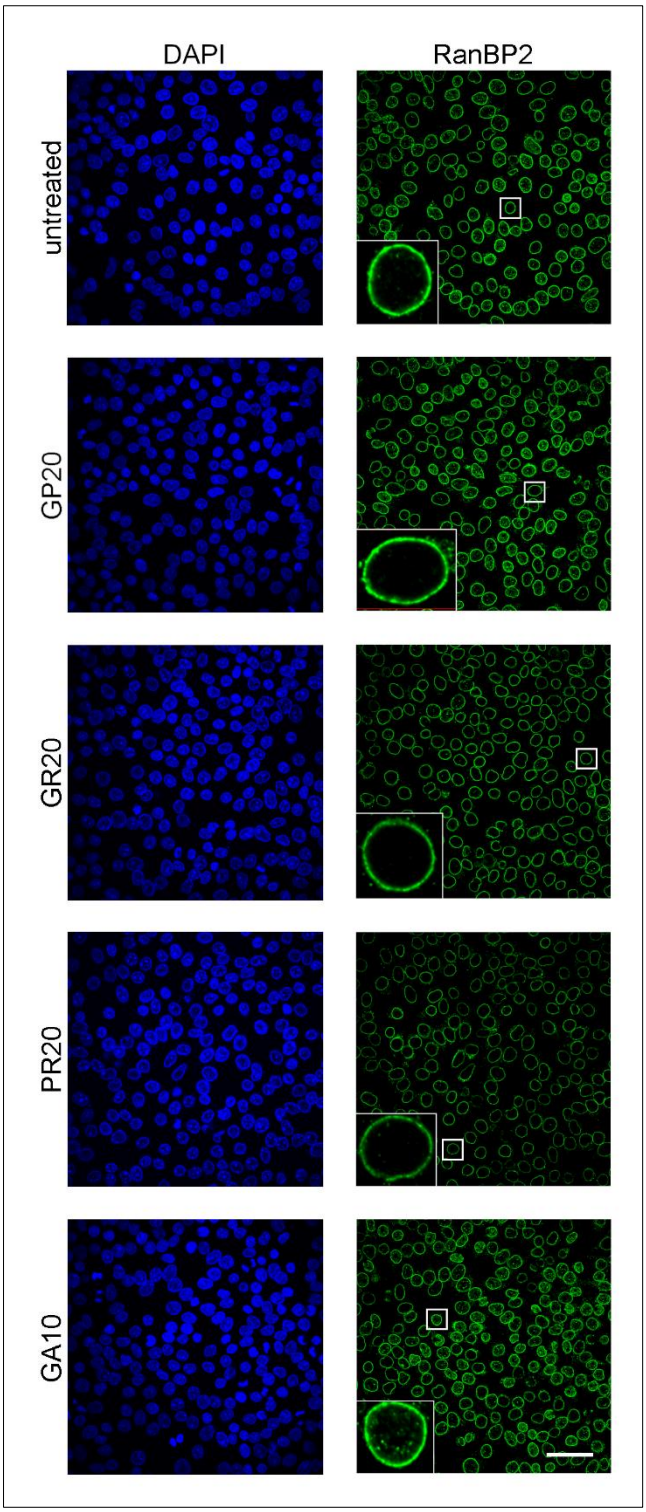

Figure 5.43: Impact of *C9ORF72* DPRs on nuclear membrane RANBP2 localisation. Opera Phenix images of immunofluorescence staining of endogenous RANBP2 in semi-permeabilised untreated cells or after 120-minute treatment with 10 µM of different *C9ORF72* dipeptide repeat proteins as indicated. Left panel: DAPI. Right panel: RANBP2. Zoom ins are at different brightness and contrast settings as main images. Scale bar: 50 µm.

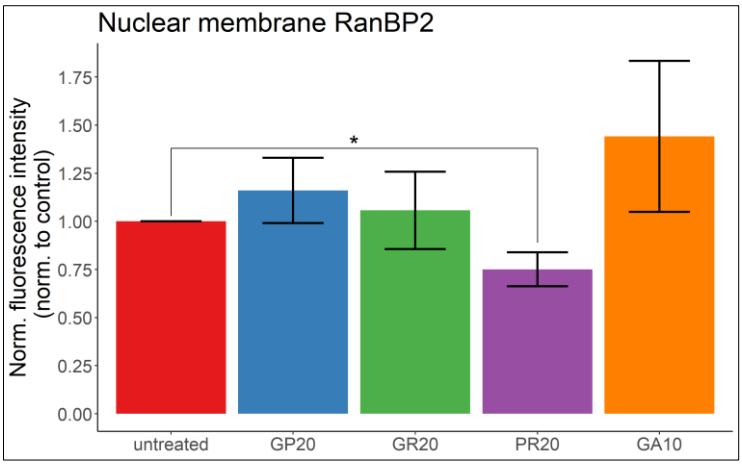

Figure 5.44: Nuclear membrane RANBP2 levels are decreased upon poly-PR treatment. Quantified nuclear membrane RANBP2 fluorescence signal normalised to untreated control in untreated cells or after 120-minute treatment with 10 µM of different *C9ORF72* dipeptide repeat proteins as indicated. Means of individual experimental means are depicted. N = 3. Error bars: SEM. * $p < 0.05$ vs untreated cells with multi-level model one-way ANOVA and Dunnett's post hoc test.

The antibody mAb414 broadly recognises FG nucleoporins. As depicted in Figure 5.45 mAb414 staining was found at the nuclear membrane, thus within nuclear pores in untreated cells. Staining with the antibody mAb414, was not significant altered by DPR treatment but a trend to reduction could be observed after PR20 treatment compared to untreated cells (see Figure 5.45 and Figure 5.46).

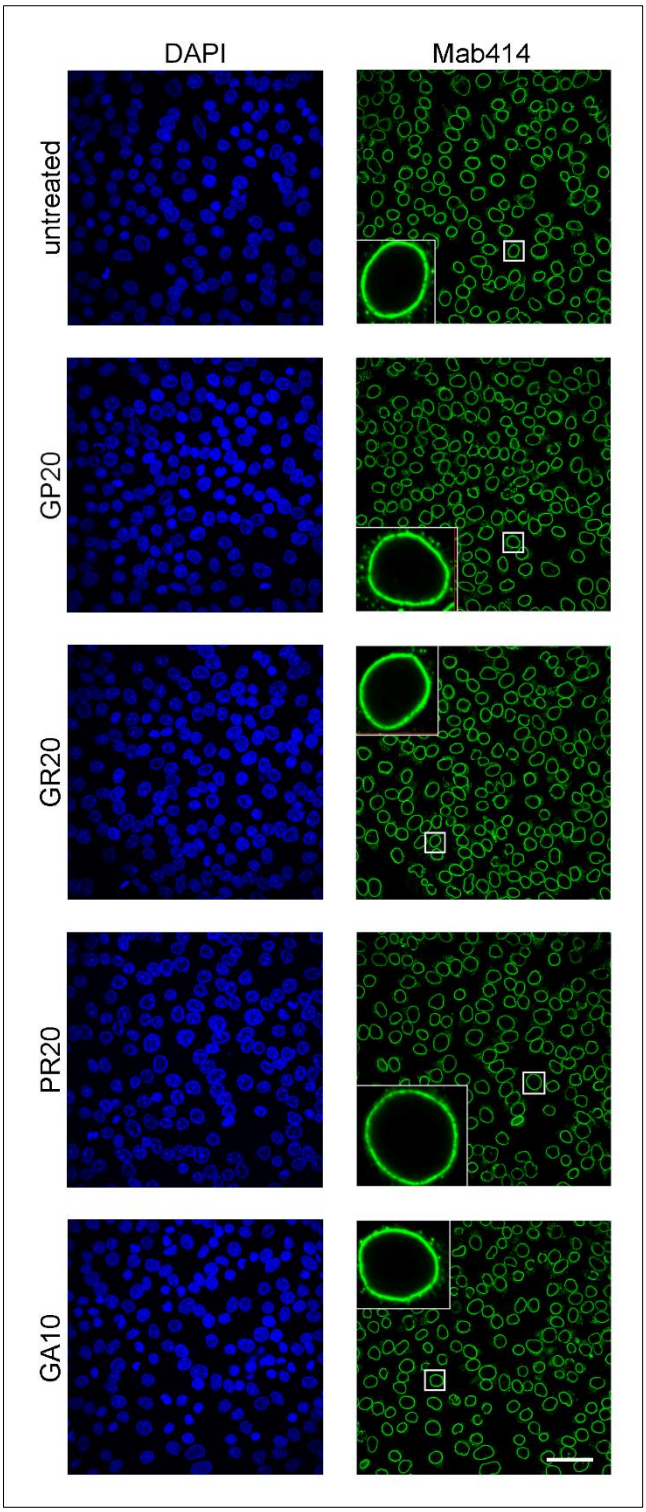

Figure 5.45: Influence of *C9ORF72* DPRs on nuclear membrane mAb414 staining. Opera Phenix images of immunofluorescence mAb414 staining in semi-permeabilised untreated cells or after 120-minute treatment with 10 µM of different *C9ORF72* dipeptide repeat proteins as indicated. Left panel: DAPI. Right panel: MAb414. Zoom ins are at different brightness and contrast settings as main images. Scale bar: 50 µm.

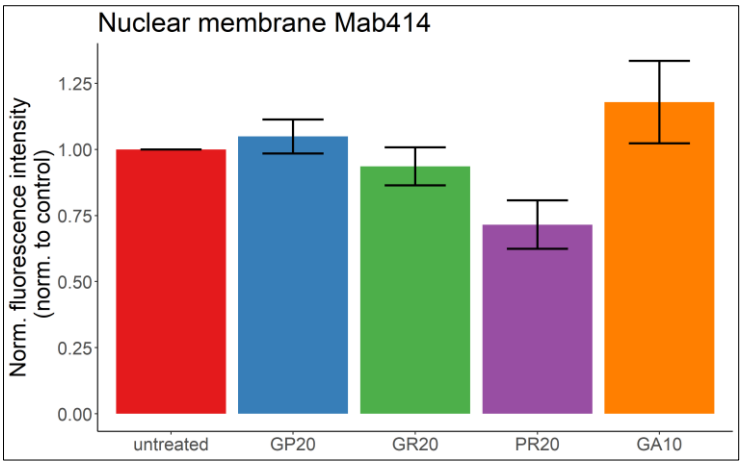

Figure 5.46: MAb414 nuclear membrane staining is not affected by *C9ORF72* DPRs. Quantified nuclear membrane mAb414 fluorescence signal normalised to untreated control in untreated cells or after 120-minute treatment with 10 µM of different *C9ORF72* dipeptide repeat proteins as indicated. Means of individual experimental means are shown. N = 3. Error bars: SEM. Treated vs untreated cells vs untreated cells with multi-level model one-way ANOVA and Dunnett's post hoc test.

Ran and Ran regulating factors

We also studied potential changes in localisation of Ran, RCC1 and RanGAP1 upon *C9ORF72* DPR treatment. RCC1 catalyses conversion of RanGDP to RanGTP in the nucleus (Klebe et al., 1995; Renault et al., 2001). RanGAP1 mediates hydrolysis of RanGTP to RanGDP in the cytoplasm (Stewart, 2007). This Ran gradient is essential for active nucleocytoplasmic transport (Stewart, 2007). However, as these factors localise to the nuclear pore their localisation could potentially also interfere with passive nucleocytoplasmic transport.

Ran was found to localise to the nucleoplasm and to the nuclear membrane as expected in untreated cells as depicted in Figure 5.47. Levels of nucleoplasmic Ran were not changed by poly-GP and -GA but were reduced by about 90 % by poly-PR (p = 0.04, Dunnett's post-hoc test; see Figure 5.47 and Figure 5.48A). A trend towards a decrease of nucleoplasmic Ran was observed after GR treatment compared to non-treatment. Nuclear membrane Ran levels which also comprise of Ran within the nuclear pore were not altered by DPRs, but levels trended towards a decrease after poly-PR treatment (see Figure 5.48B).

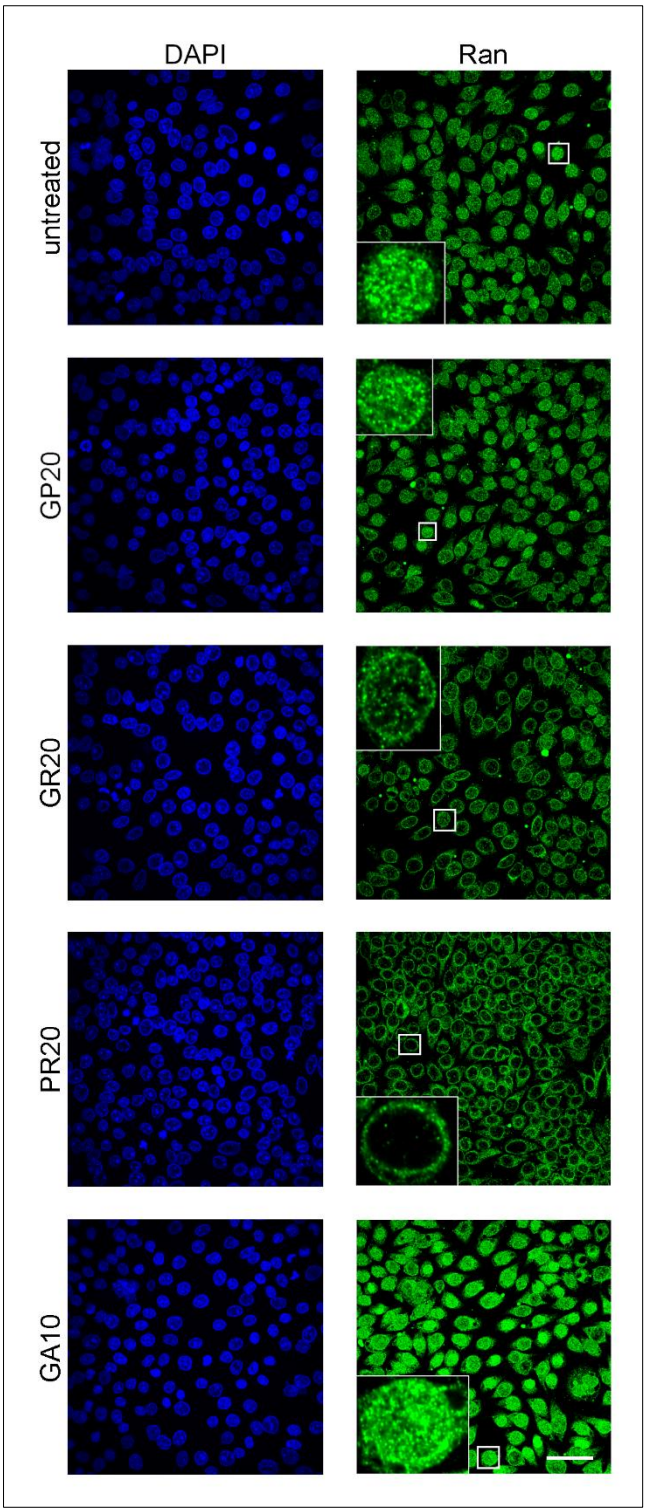

Figure 5.47: Effects of *C9ORF72* DPRs on nuclear RAN localisation. Opera Phenix images of immunofluorescence staining of endogenous RAN in semi-permeabilised untreated cells or after 120-minute treatment with 10 µM of different *C9ORF72* dipeptide repeat proteins as indicated. Left panel: DAPI. Right panel: RAN. Zoom ins are at different brightness and contrast settings as main images. Scale bar: 50 µm.

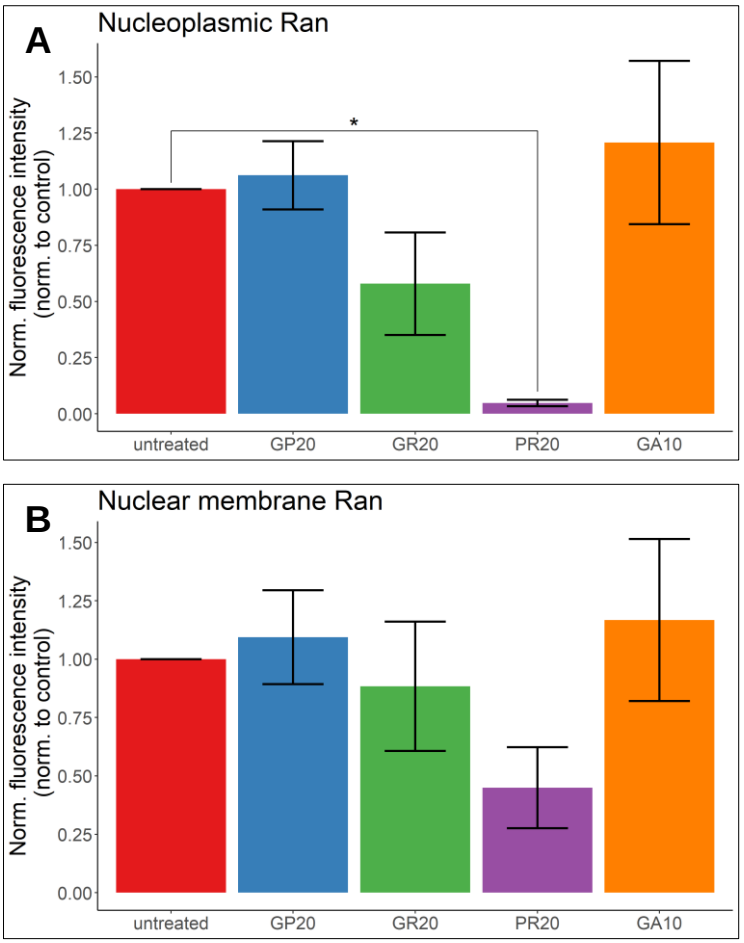

Figure 5.48: Poly-PR decreases nuclear RAN levels. Quantified nuclear RAN fluorescence signal normalised to untreated control in untreated cells or after 120-minute treatment with 10 µM of different *C9ORF72* dipeptide repeat proteins as indicated. A) Nucleoplasmic RAN levels. B) Nuclear membrane RAN levels. Means of individual experimental means are depicted. N = 3. Error bars: SEM. * $p < 0.05$ vs untreated cells with multi-level model one-way ANOVA and Dunnett's post hoc test.

As shown in Figure 5.49 RanGAP1 purely localised to the nuclear membrane in untreated cells as expected due to its function. Nuclear membrane and pore levels of RanGAP1 did not show a significant change upon *C9ORF72* DPR treatment, however a trend to reduction was observed after PR20 treatment compared to untreated cells (see Figure 5.49 and Figure 5.50).

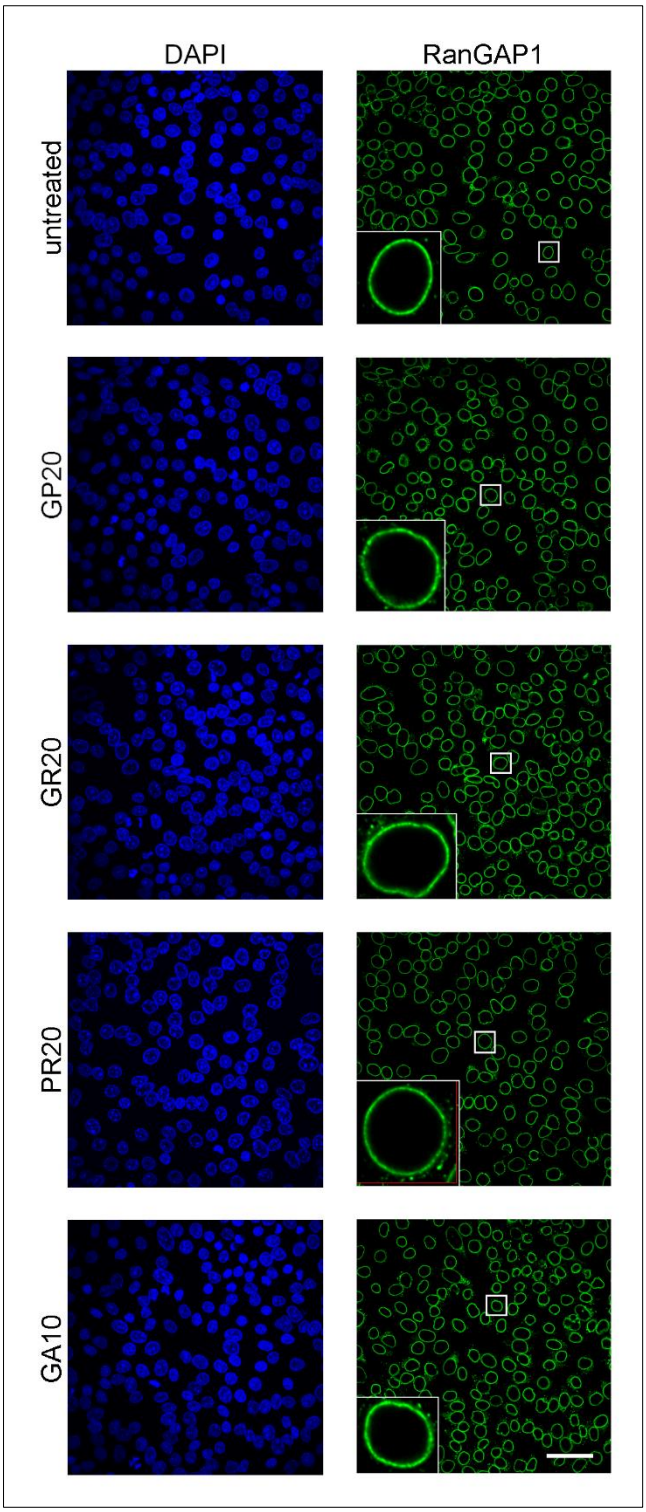

Figure 5.49: Influence of *C9ORF72* DPRs on nuclear membrane RANGAP1 levels. Opera Phenix images of immunofluorescence staining of endogenous RANGAP1 in semi-permeabilised untreated cells or after 120-minute treatment with 10 µM of different *C9ORF72* dipeptide repeat proteins as indicated. Left panel: DAPI. Right panel: RANGAP1. Zoom ins are at different brightness and contrast settings as main images. Scale bar: 50 µm.

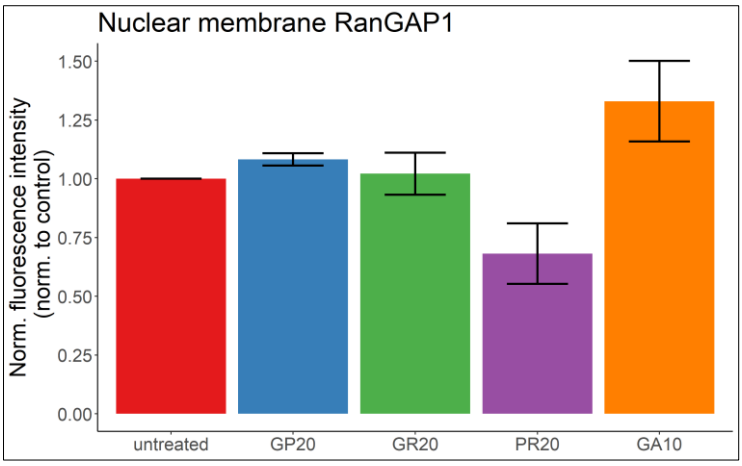

Figure 5.50: *C9ORF72* DPRs do not change nuclear membrane RANGAP1 levels. Quantified nuclear membrane RANGAP1 fluorescence signal normalised to untreated control in untreated cells or after 120-minute treatment with 10 µM of different *C9ORF72* dipeptide repeat proteins as indicated. Means of individual experimental means are plotted. N = 3. Error bars: SEM. Treated vs untreated cells with multi-level model one-way ANOVA and Dunnett's post hoc test.

RCC1 localisation was detected within the nucleoplasm and at the nuclear membrane in untreated cells as shown in Figure 5.51. GR20 halved nucleoplasmic levels of Ran regulator RCC1 (p = 0.039, Dunnett's post-hoc test) and PR20 decreased these levels by 90 % compared to untreated cells with a p value of 3.02×10^{-10} (Dunnett's post-hoc test; see Figure 5.51 and Figure 5.52A). GP20 did not alter nucleoplasmic RCC1 whilst GA10 led to a trend in increased nucleoplasmic RCC1 levels compared to untreated cells. Nuclear membrane RCC1 levels, which also reflect RCC1 associated with the nuclear pore, were reduced by 50 % by poly-PR ($p = 6.13 \times 10^{-8}$, Dunnett's post-hoc test) whilst a trend to enhanced nuclear membrane RCC1 levels was observed again after poly-GA treatment compared to untreated cells (see Figure 5.52B). GR20 and GP20 did not significantly influence nuclear membrane RCC1 levels compared to untreated cells.

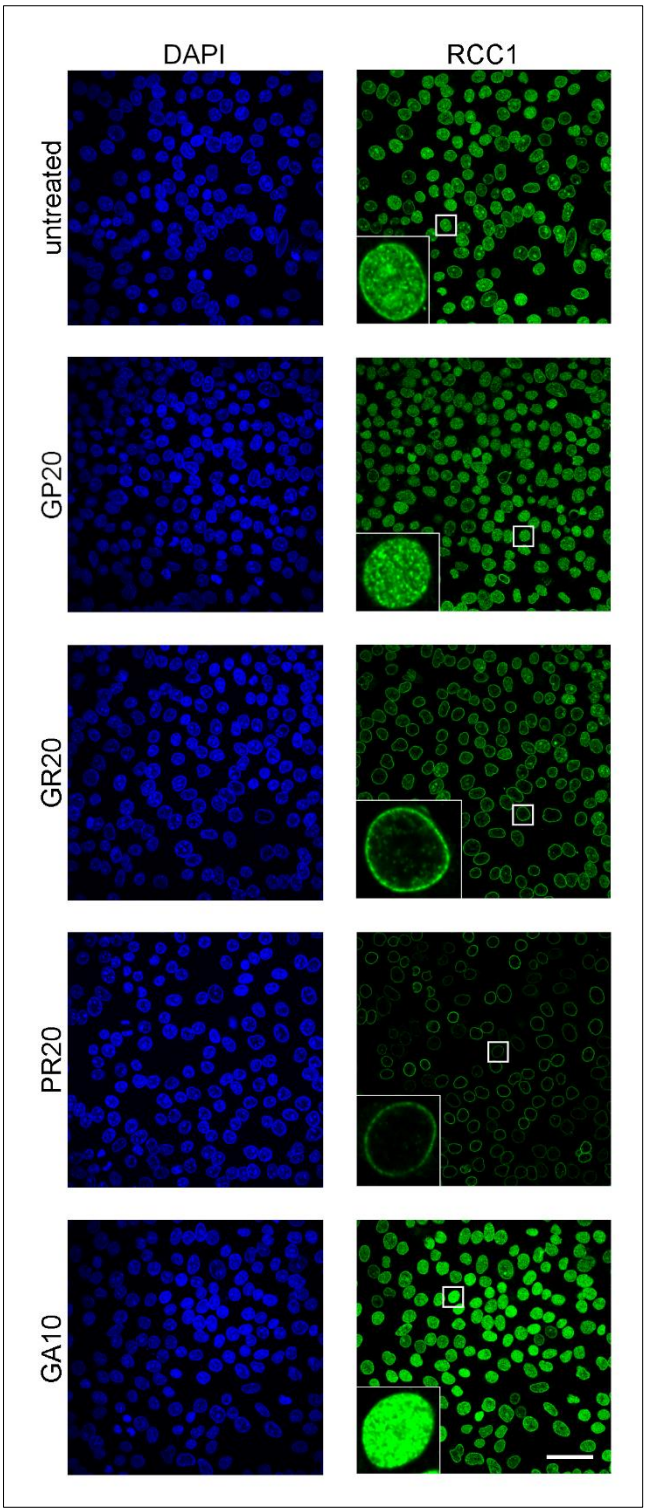

Figure 5.51: Impact of *C9ORF72* DPRs on nuclear RCC1 localisation. Opera Phenix images of immunofluorescence staining of endogenous RCC1 in semi-permeabilised untreated cells or after 120-minute treatment with 10 µM of different *C9ORF72* dipeptide repeat proteins as indicated. Left panel: DAPI. Right panel: RCC1. Zoom ins are at different brightness and contrast settings as main images. Scale bar: 50 µm.

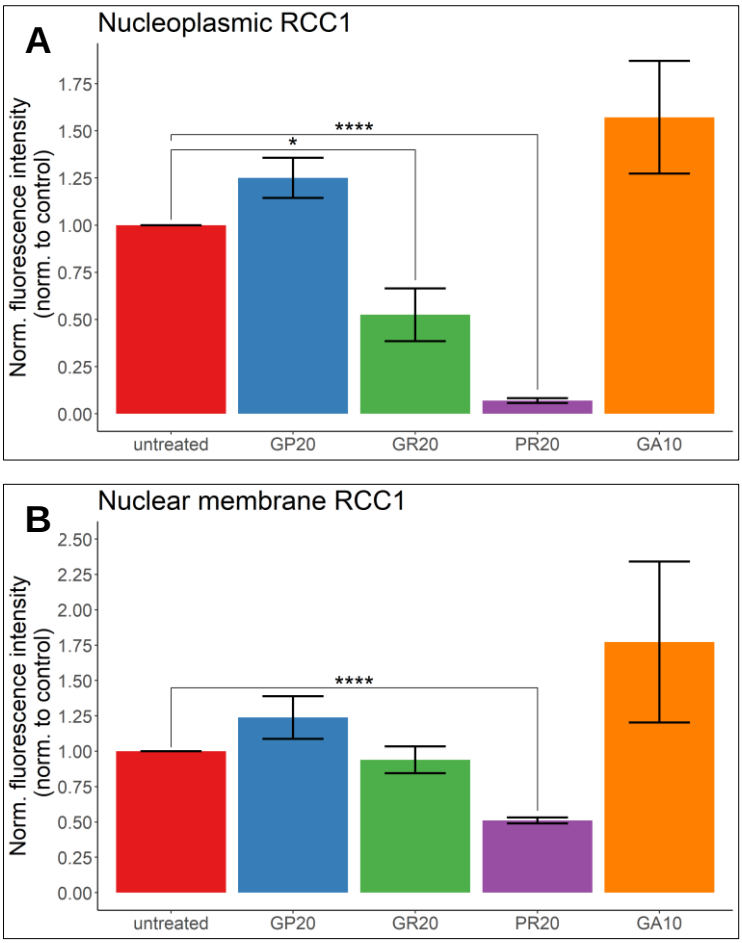

Figure 5.52: Poly-GR and -PR decrease nuclear RCC1 levels. Quantified nuclear RCC1 fluorescence signal normalised to untreated control in untreated cells or after 120-minute treatment with 10 µM of different *C9ORF72* dipeptide repeat proteins as indicated. A) Nucleoplasmic RCC1 levels. B) Nuclear membrane RCC1 levels. Means of individual experimental means are depicted. N = 3. Error bars: SEM. **** $p < 0.0001$, * $p < 0.05$ vs untreated cells with multi-level model one-way ANOVA and Dunnett's post hoc test.

Import receptors

Actively transported cargo is translocated from the cytoplasm to the nucleus by import receptors (Kimura and Imamoto, 2014). However, studies suggest that import receptors, especially importin β1, might contribute to the permeability barrier of the nuclear pore (Kapinos et al., 2017; Lowe et al., 2015). We, therefore, investigated localisation of importin β1, α1 and α3 upon DPR treatment.

As depicted in Figure 5.53 importin β1 mainly localised to the nuclear membrane and at low levels to the nucleoplasm in untreated cells. This was also observed in another study using semi-permeabilised cells (Kapinos et al., 2017). Nucleoplasmic levels of transport receptor Importin β1 were decreased by 20 % by poly-GR and by 50 % by poly-PR with *p* values of 0.018 and 2.11×10^{-7}, respectively (Dunnett's post-hoc test) whilst not significantly changed by poly-GP and -GA compared to untreated cells (see Figure 5.53 and Figure 5.54A). As shown in Figure 5.54B nuclear

membrane importin β1 levels, also comprised of importin β1 at the nuclear pore, were slightly increased after GP20 treatment and trended to decrease after PR20 treatment. GR20 and GA10 treatment did not significantly alter nuclear membrane importin β1 levels.

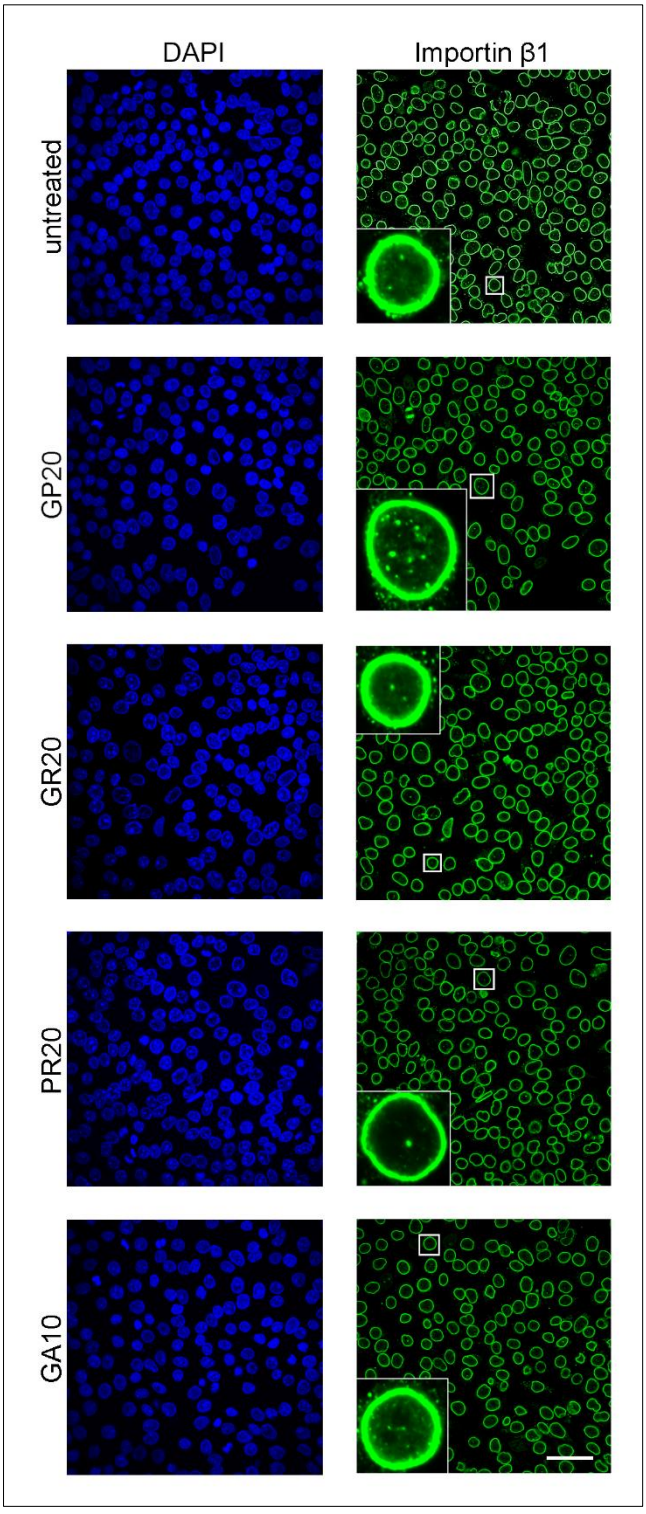

Figure 5.53: Effects of *C9ORF72* DPRs on nuclear importin β1 levels. Opera Phenix images of immunofluorescence staining of endogenous importin β1 in semi-permeabilised untreated cells or after 120-

minute treatment with 10 µM of different *C9ORF72* dipeptide repeat proteins as indicated. Left panel: DAPI. Right panel: Importin β1. Zoom ins are at different brightness and contrast settings as main images. Scale bar: 50 µm.

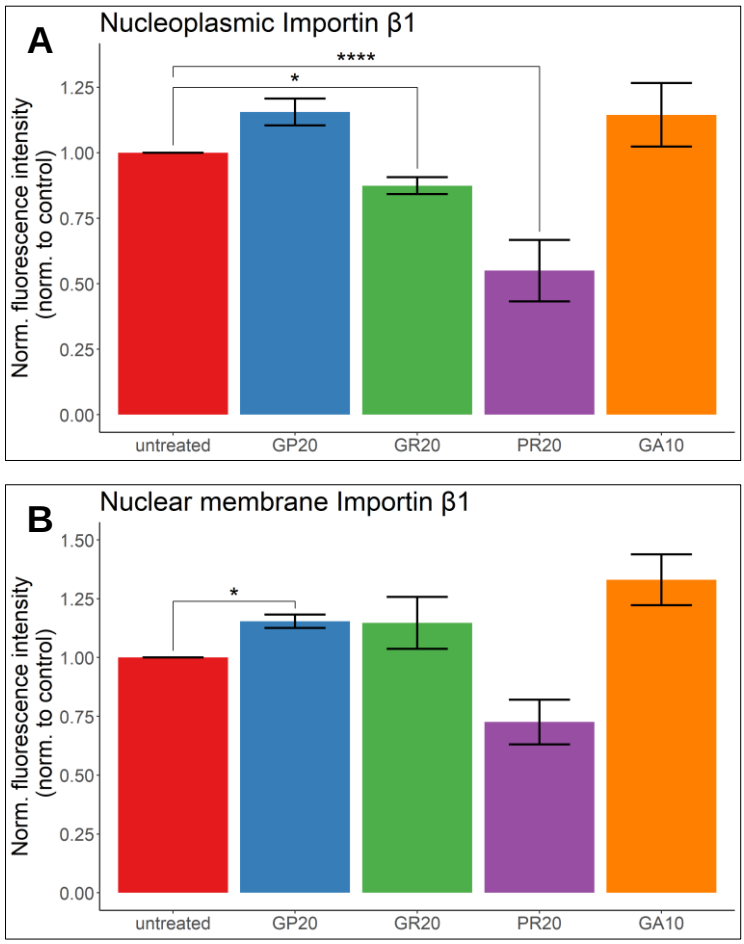

Figure 5.54: Poly-GR and -PR reduce nuclear importin β1 levels. Quantified nuclear importin β1 fluorescence signal normalised to untreated control in untreated cells or after 120-minute treatment with 10 µM of different *C9ORF72* dipeptide repeat proteins as indicated. A) Nucleoplasmic importin β1 levels. B) Nuclear membrane importin β1 levels. Means of individual experimental means are shown. N = 3. Error bars: SEM. **** $p < 0.0001$, * $p < 0.05$ vs untreated cells with multi-level model one-way ANOVA and Dunnett's post hoc test.

Importin α1 was detected in the nucleoplasm and at the nuclear membrane in untreated cells as depicted in Figure 5.55. Nucleoplasmic levels of transport receptor importin α1 were not significantly altered by DPR treatment but a trend towards a decrease was detected after poly-GR and -PR treatment compared to untreated cells as depicted in Figure 5.55 and Figure 5.56A. Nuclear membrane importin α1 was not significantly changed by *C9ORF72* DPRs either but levels trended towards a reduction after PR20 treatment (see Figure 5.56B).

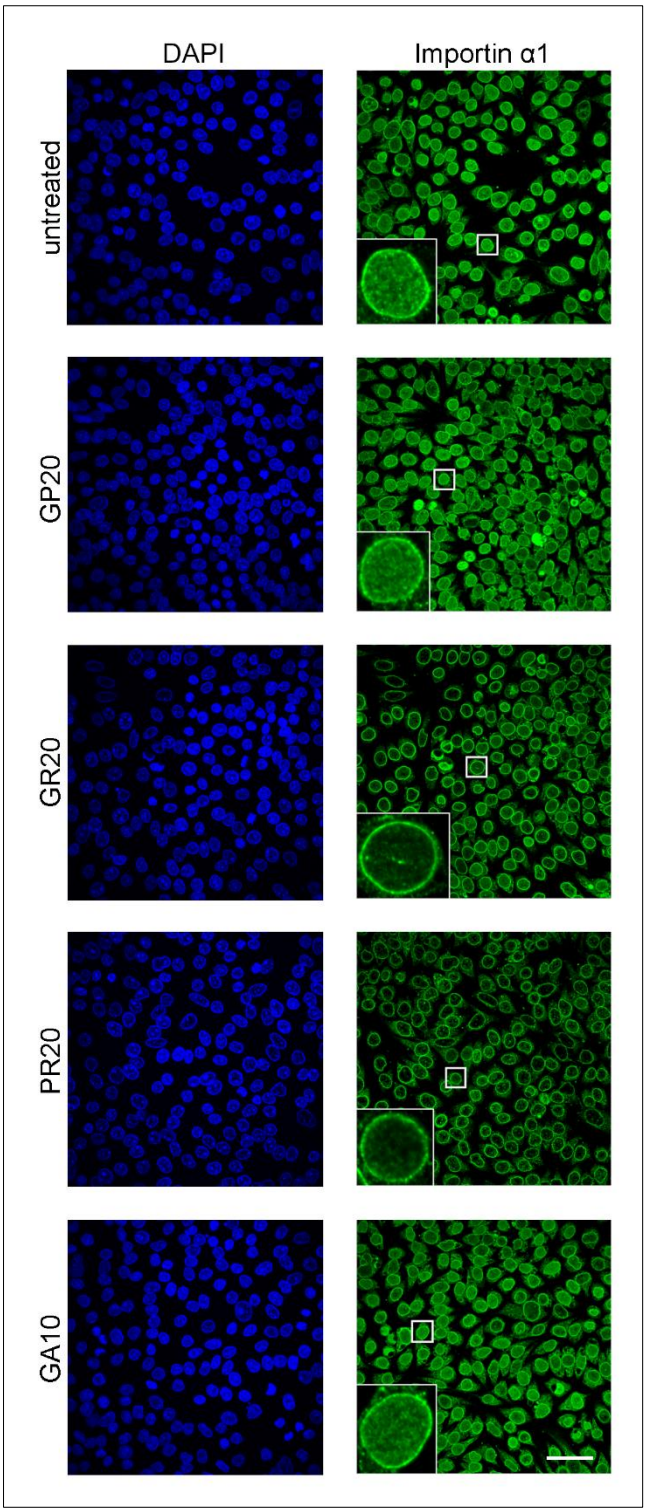

Figure 5.55: Influence of *C9ORF72* DPRs on nuclear importin α1 levels. Opera Phenix images of immunofluorescence staining of endogenous importin α1 in semi-permeabilised untreated cells or after 120-minute treatment with 10 µM of different *C9ORF72* dipeptide repeat proteins as indicated. Left panel: DAPI. Right panel: Importin α1. Zoom ins are at different brightness and contrast settings as main images. Scale bar: 50 µm.

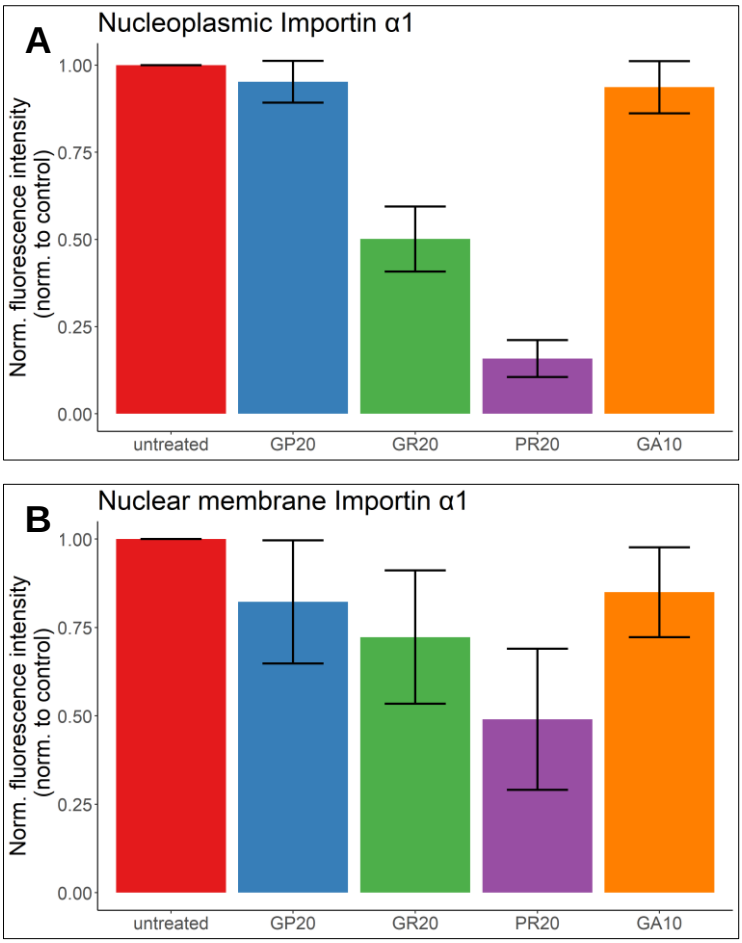

Figure 5.56: Nuclear importin α1 localisation is not affected by poly-GR and -PR. Quantified nuclear importin α1 fluorescence signal normalised to untreated control in untreated cells or after 120-minute treatment with 10 µM of different *C9ORF72* dipeptide repeat proteins as indicated. Means of individual experimental means are plotted. N = 3. A) Nucleoplasmic importin α1 levels. B) Nuclear membrane importin α1 levels. Error bars: Treated vs untreated cells with multi-level model one-way ANOVA and Dunnett's post hoc test.

As illustrated in Figure 5.57 importin α3 localised to the nuclear membrane and to the nucleoplasm. Transport receptor importin α3's nucleoplasmic levels were decreased by 70 % and 90 % by poly-GR and -PR, respectively (p near 0, Dunnett's post-hoc test) whilst poly-GP and -GA did not influence these levels compared to non-treatment as shown in Figure 5.57 and Figure 5.58B. Nuclear membrane comprising nuclear pore levels of importin α3 were reduced by 25 % by GR20 and by 60 % by PR20 (p = 0.046 for poly-GR and $p = 2x10^{-5}$ for poly-PR treatment, Dunnett's post-hoc test) whilst they were increased 1.2-fold by GP20 ($p = 2.4x10^{-4}$, Dunnett's post-hoc test) and not changed by GA10 compared to untreated cells (see Figure 5.58B).

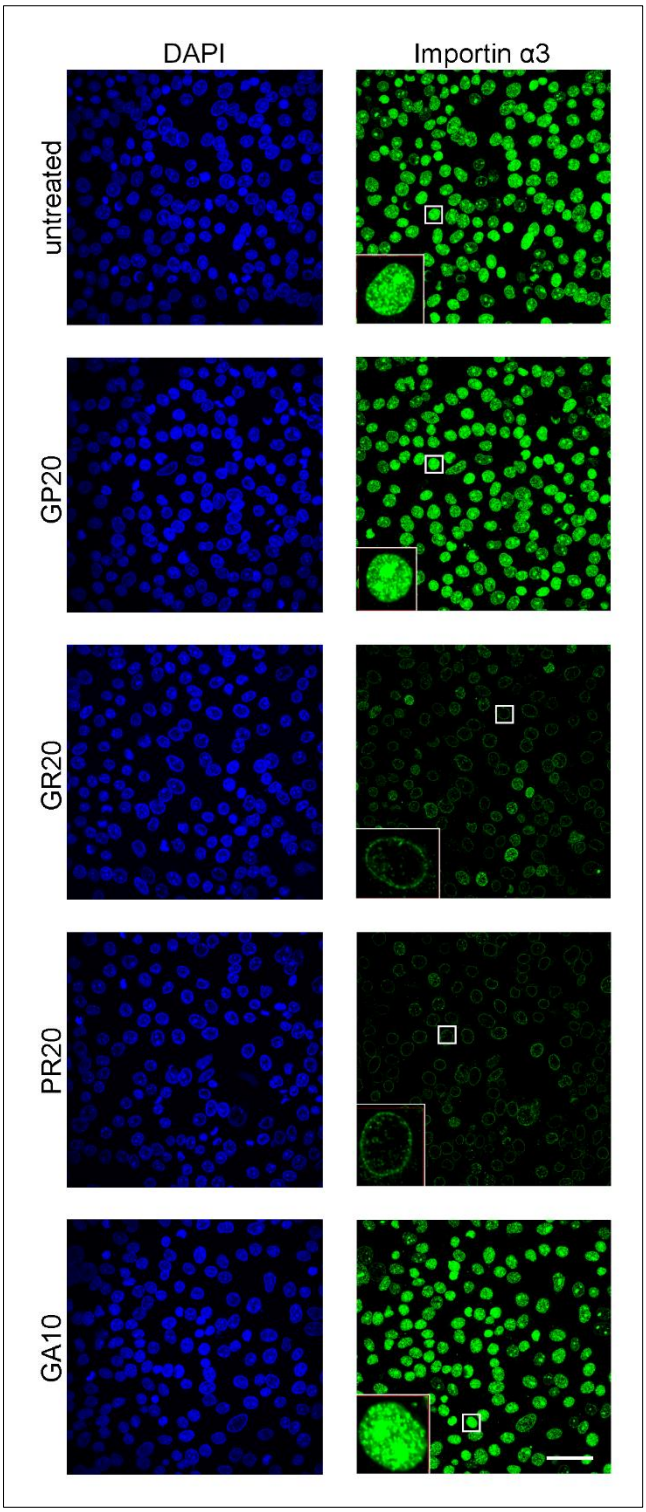

Figure 5.57: Impact of *C9ORF72* DPRs on nuclear importin α3 levels. Opera Phenix images of immunofluorescence staining of endogenous importin α3 in semi-permeabilised untreated cells or after 120-minute treatment with 10 µM of different *C9ORF72* dipeptide repeat proteins as indicated. Left panel: DAPI. Right panel: Importin α3. Zoom ins are at different brightness and contrast settings as main images. Scale bar: 50 µm.

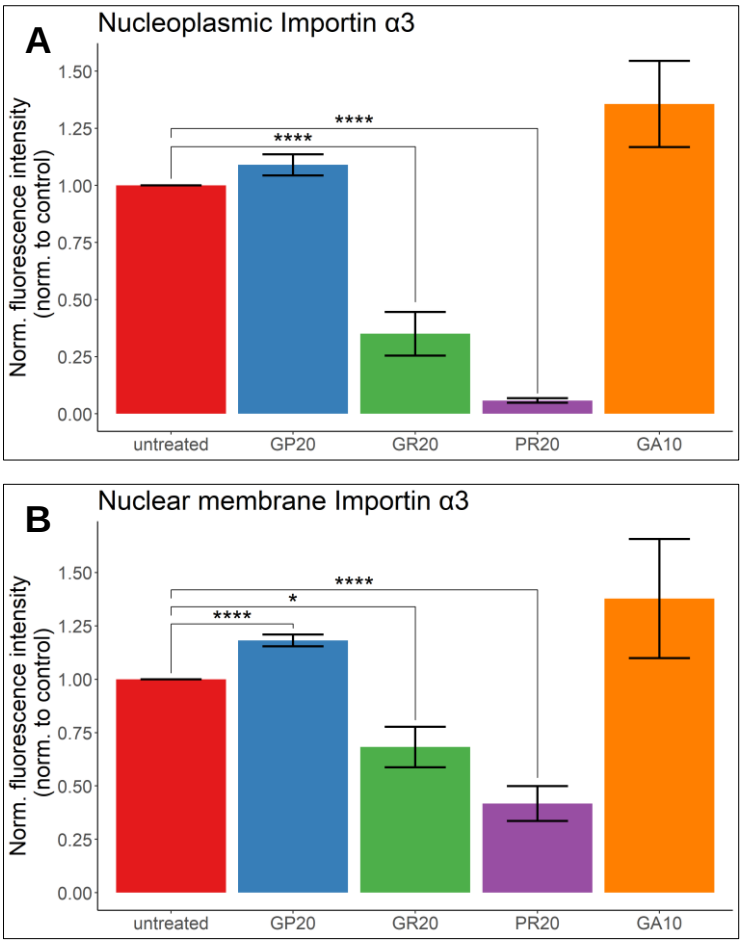

Figure 5.58: Poly-GR and -PR lower nuclear importin α3 levels. Quantified nuclear importin α3 fluorescence signal normalised to untreated control in untreated cells or after 120-minute treatment with 10 µM of different *C9ORF72* dipeptide repeat proteins as indicated. A) Nucleoplasmic importin α3 levels. B) Nuclear membrane importin α3 levels. Means of individual experimental means are shown. N = 3. Error bars: SEM. **** $p < 0.0001$, * $p < 0.05$ vs untreated cells with multi-level model one-way ANOVA and Dunnett's post hoc test.

In summary (as depicted in Table 5.1), levels at the nuclear pore (as opposed to nucleoplasmic levels) of FG nucleoporins NUP98, POM121 and RANBP2 were significantly lowered by PR20. Nucleoplasmic RAN and RCC1 levels were reduced by poly-PR and both poly-GR and -PR, respectively. PR20 also lowered nuclear membrane RCC1 levels. In terms of transport receptors, nucleoplasmic levels of importin β1 and α3 as well as nuclear membrane importin α3 levels were significantly decreased upon treatment with poly-GR and -PR. Therefore, nucleocytoplasmic transport factor localisation was substantially affected by arginine containing *C9ORF72* DPRs. These DPRs led to a change in nuclear pore composition and potentially to altered interactions of nuclear pore binding partners such as importins with nucleoporins. This probably contributed to the enhancement of passive nucleocytoplasmic transport by poly-GR and -PR we detected as these changes likely affected the permeability barrier of the nuclear pore.

Transport factor	Change nucleoplasm	Change nuclear membrane
Nucleoporins		
NUP98	↓ PR	↓ PR
POM121	↓ PR	↓ PR
NUP153	--	no change
NUP54	↓ GR, PR	↑ GR
RANBP2	--	↓ PR
MAB414	--	no change
Ran regulating factors		
RAN	↓ PR	no change
RANGAP1	--	no change
RCC1	↓ GR, PR	↓ PR
Import receptors		
Impβ1	↓ GR, PR	no change
Impα1	no change	no change
Impα3	↓ GR, PR	↓ GR, PR

Table 5.1: Summary of changes in transport factor localisation in semi-permeabilised HeLa cells upon poly-GR and -PR treatment.

5.5 Reversing effects of poly-GR and -PR on passive nuclear TDP43 export by WGA treatment

Another aim of this chapter was to find ways to counteract the enhancement of passive nucleocytoplasmic transport by poly-GR and -PR. To this end, we first made use of the lectin wheat germ agglutinin (WGA), which is known to inhibit active nucleocytoplasmic transport by binding to *N*-acetylglucosamine residues on nucleoporins (Finlay et al., 1987; Ribbeck and Görlich, 2002) and thus "blocking" the nuclear pore, hence making it less permeable for cargo translocation. We intended to establish whether "blocking" the nuclear pore could prevent the enhanced passive nuclear export of TDP43 in semi-permeabilised HeLa cells resulting from arginine containing *C9ORF72* DPR treatment. To this end, we treated semi-permeabilised

HeLa cells with 1 mg/ml WGA for 1 hour and subsequently with 10 or 50 µM GR20 and PR20 for 2 hours and then immunostained cells for TDP43.

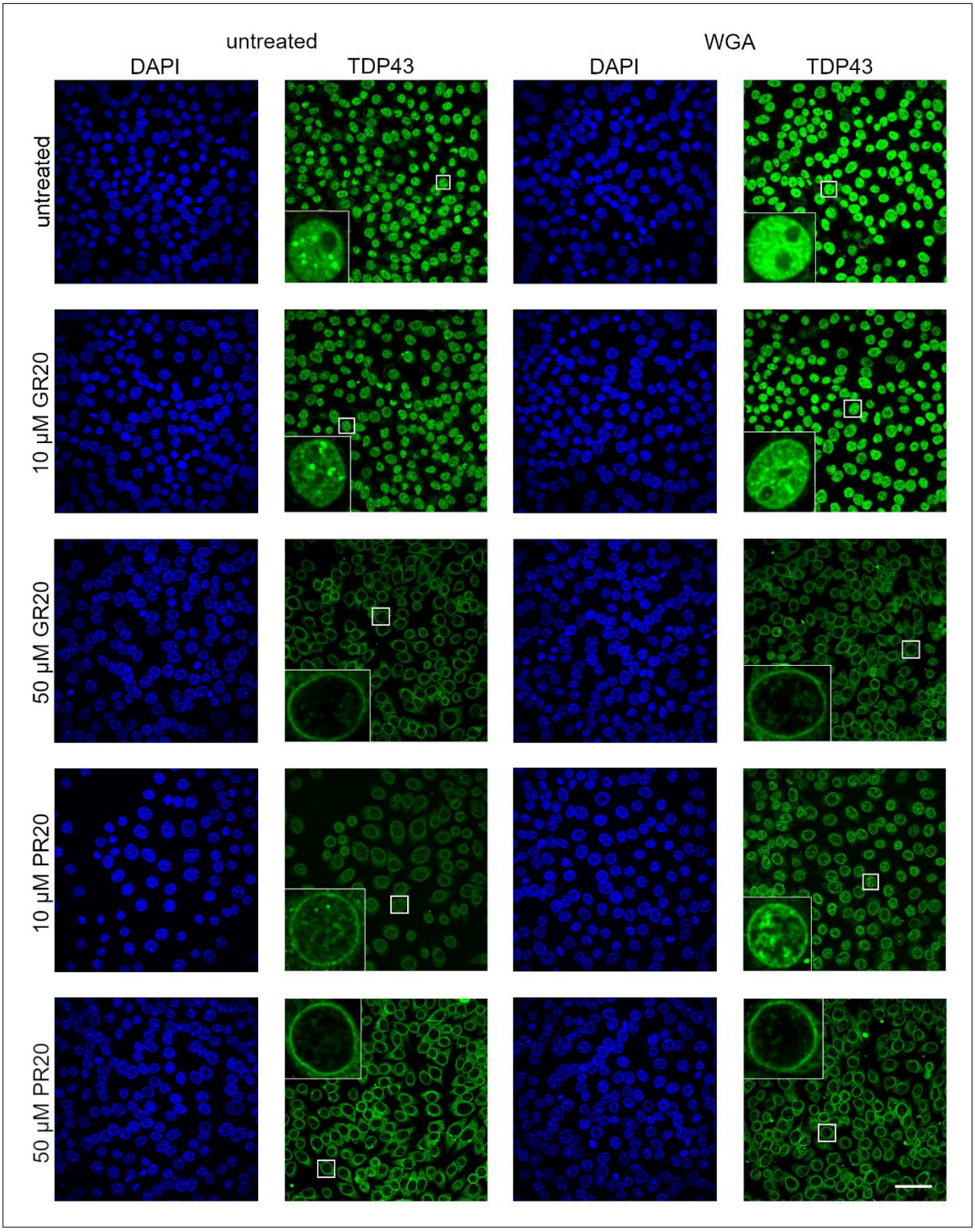

Figure 5.59: Reversal of influence of *C9ORF72* arginine containing DPRs on nuclear localisation of TDP43 by WGA. Opera Phenix images of immunofluorescence staining of endogenous TDP43 in semi-permeabilised untreated cells or after 1-hour treatment with 1 mg/ml WGA for 1 hour as indicated. Subsequently, cells were either treated with different *C9ORF72* dipeptide repeat proteins at varying concentrations or left untreated as indicated. Far-left panel: DAPI. Second from left panel: TDP43. Second from right panel: DAPI. Far-right panel:

TDP43. First two panels from the left: Cells not treated with WGA. Third and fourth panel from the left: WGA-treated cells. Zoom ins are at different brightness and contrast settings as main images. Scale bar: 50 µm.

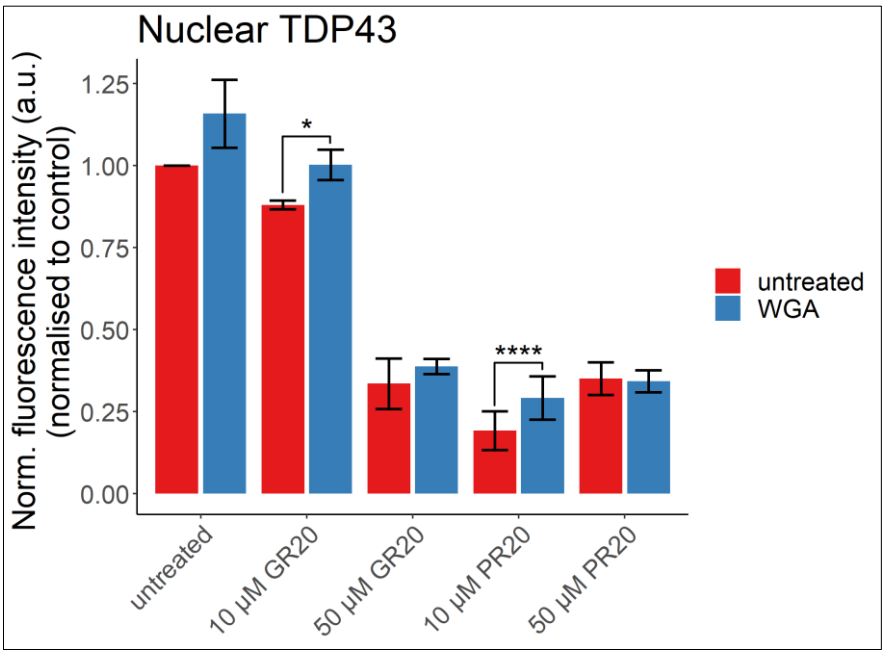

Figure 5.60: WGA treatment counteracts reduction of nuclear TDP43 by poly-GR and -PR. Quantified nuclear TDP43 fluorescence signal normalised to untreated control in untreated (red) or cells treated with 1 mg/ml WGA (blue). Subsequently cells were either left untreated or treated with varying concentrations of arginine containing DPRs as indicated N = 3. Error bars: SEM. **** p<0.0001, * p < 0.05 with multi-level model two-way ANOVA and Tukey's post hoc test.

As we observed previously (see section 4.3) a 2-hour treatment with GR20 and PR20 at concentrations of 10 and 50 µM led to a significant reduction in nuclear TDP43 levels as depicted in Figure 5.59 and Figure 5.60. Nuclear levels of TDP43 were slightly higher (although not significantly) in WGA treated cells which did not receive DPR treatment than in completely untreated cells. This suggests that low levels of TDP43 passively diffused out of the nucleus even in untreated cells. This could be prevented by WGA treatment. Effects of high concentration (50 µM) DPR treatments on nuclear TDP43 localisation could not be reversed by WGA treatment. However, the substantial decrease of nuclear TDP43 upon 10 µM PR20 could be significantly increased by 1.5-fold upon WGA treatment (*p* near 0, Tukey's post-hoc test). The milder lowering of nuclear TDP43 levels by 10 µM GR20 treatment could be brought back to levels observed in untreated controls upon WGA treatment (*p* = 0.014, Tukey's post-hoc test). Thus, WGA treatment resulted in a full or partial rescue of the enhanced nuclear export of TDP43 caused by 10 µM poly-GR or -PR, respectively.

5.6 Investigating the potential to rescue increased passive nucleocytoplasmic transport caused by poly-GR and -PR with importin β1 treatment

A second rescue strategy we developed was to treat cells with exogenous importin β1 as we found that nuclear importin β1 was reduced in poly-GR and -PR treated cells and also reduced at the nuclear membrane in poly-PR treated cells compared to untreated cells (see section 5.4). Furthermore, it was previously shown that decreased importin β1 levels at the nuclear pore led to increased permeability of the nuclear pore (Kapinos et al., 2017; Lowe et al., 2015). We therefore reasoned that resupplying importin β1 might revert the reduction of importin β1 caused by arginine containing *C9ORF72* DPRs and at the same time the reduced restrictiveness of the nuclear pore. Hence, we subjected HeLa cells to the same transport assay as in previous chapters and treated cells for 30 minutes with 10 µM GR20 and subsequently for 1 hour with 100 nM importin β1. We then followed the nuclear uptake of FITC labelled 20 kDa dextran by live confocal microscopy.

As observed previously (see section 4.1) and as depicted in Figure 5.61 and Figure 5.62 20 kDa dextran readily entered the nucleus in untreated cells and its nuclear import was significantly increased upon GR20 treatment. Importin β1 treatment alone did not alter the import dynamics of 20 kDa dextran in non-DPR treated cells (see Figure 5.62) compared to cells not treated with importin β1 nor with GR20. Importin β1 treatment, therefore, did not allow for enhanced passive diffusion of 20 kDa dextran under physiological conditions. Cells treated with both importin β1 and poly-GR still exhibited enhanced nuclear import of 20 kDa dextran to the same extent as cells treated with GR20 but not importin β1. Therefore, supplementation of importin β1 could not revert the effects of poly-GR on passive nuclear import of reporter cargo.

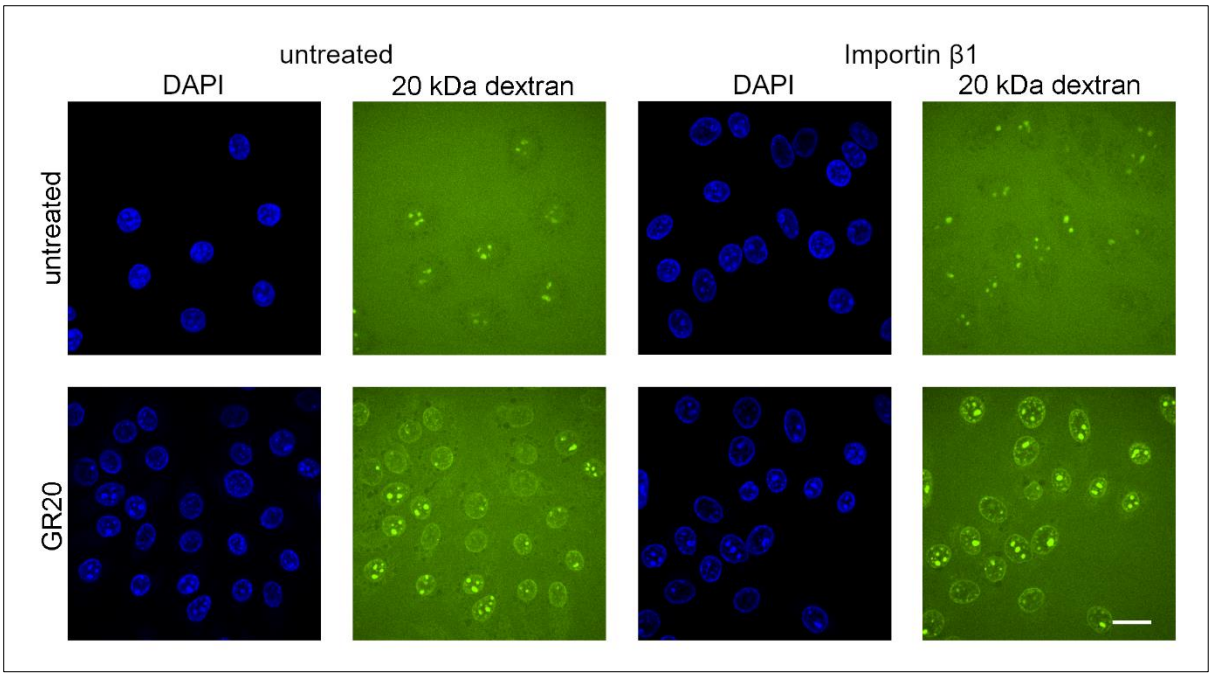

Figure 5.61: Influence of importin β1 on enhancement of passive nuclear import of 20 kDa dextran by poly-GR. Spinning disk confocal microscope images of semi-permeabilised untreated HeLa cells and cells treated with 10 µM of poly-GR for 30 minutes as indicated. Subsequently cells were either left untreated or treated with 100 nM importin β1 for 1 hour as indicated. Images depict 4-minute incubation with 20 kDa dextran. Far-left panel: DAPI channel. Second from left panel: FITC 20 kDa dextran channel. Second from right panel: DAPI channel. Far-right panel: FITC 20 kDa dextran channel. First two panels from the left: Cells not treated with importin β1. Third and fourth panel from the left: Importin β1-treated cells. Scale bar: 20 µm.

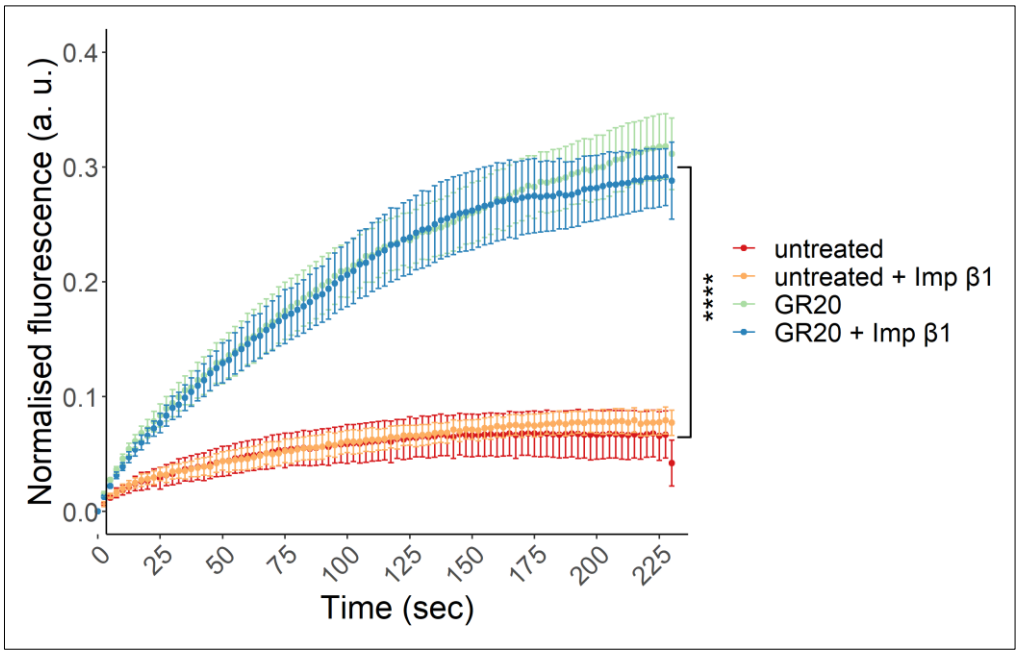

Figure 5.62: Importin β1 treatment does not reverse passive nuclear import increase of 20 kDa dextran by poly-GR. Quantification of passive nuclear import of 20 kDa dextran (shown as nuclear fluorescence normalised to nuclear and general background) over time in semi-permeabilised untreated or poly-GR treated HeLa cells. Subsequently cells were either left untreated or treated with importin β1. Untreated condition depicted in red, importin β1 treatment without poly-GR treatment in orange, GR20 treatment in green, GR20 treatment in combination with importin β1 treatment in blue. Means of individual experimental means are depicted. N = 3. Error bars: SEM. **** $p < 0.0001$ with two-way repeated measures ANOVA and Tukey's post hoc test.

Furthermore, we analysed whether the increase in nuclear export of TDP43 resulting from poly-GR or -PR treatment could be inhibited by importin β1 treatment. Therefore, we treated semi-permeabilised HeLa cells for 1 hour with 100 nM importin β1 and subsequently with 10 µM GR20 or PR20 for another hour. We then fixed the cells and immunostained them for TDP43. As shown in Figure 5.63 and Figure 5.64 nuclear TDP43 levels were depleted in cells treated with GR20 or PR20 compared to untreated cells. Effects of poly-PR treatment on nuclear TDP43 localisation were comparable to previous observations while poly-GR treatment resulted in a higher decrease of nuclear TDP43 levels as seen previously (compare section 4.3). Cells treated with both importin β1 and poly-GR or -PR exhibited similar nuclear TDP43 levels as cells solely treated with poly-GR or -PR (see Figure 5.64). As observed in previous experiments (compare section 5.4) nuclear importin β1 levels were reduced upon poly-GR or -PR treatment (see Figure 5.65). Surprisingly, nuclear importin β1 levels were even lower in cells supplemented with importin β1 than in cells not treated with importin β1. In any case, importin β1 treatment did not alleviate the reduction of nuclear TDP43 upon arginine after *C9ORF72* DPR treatment.

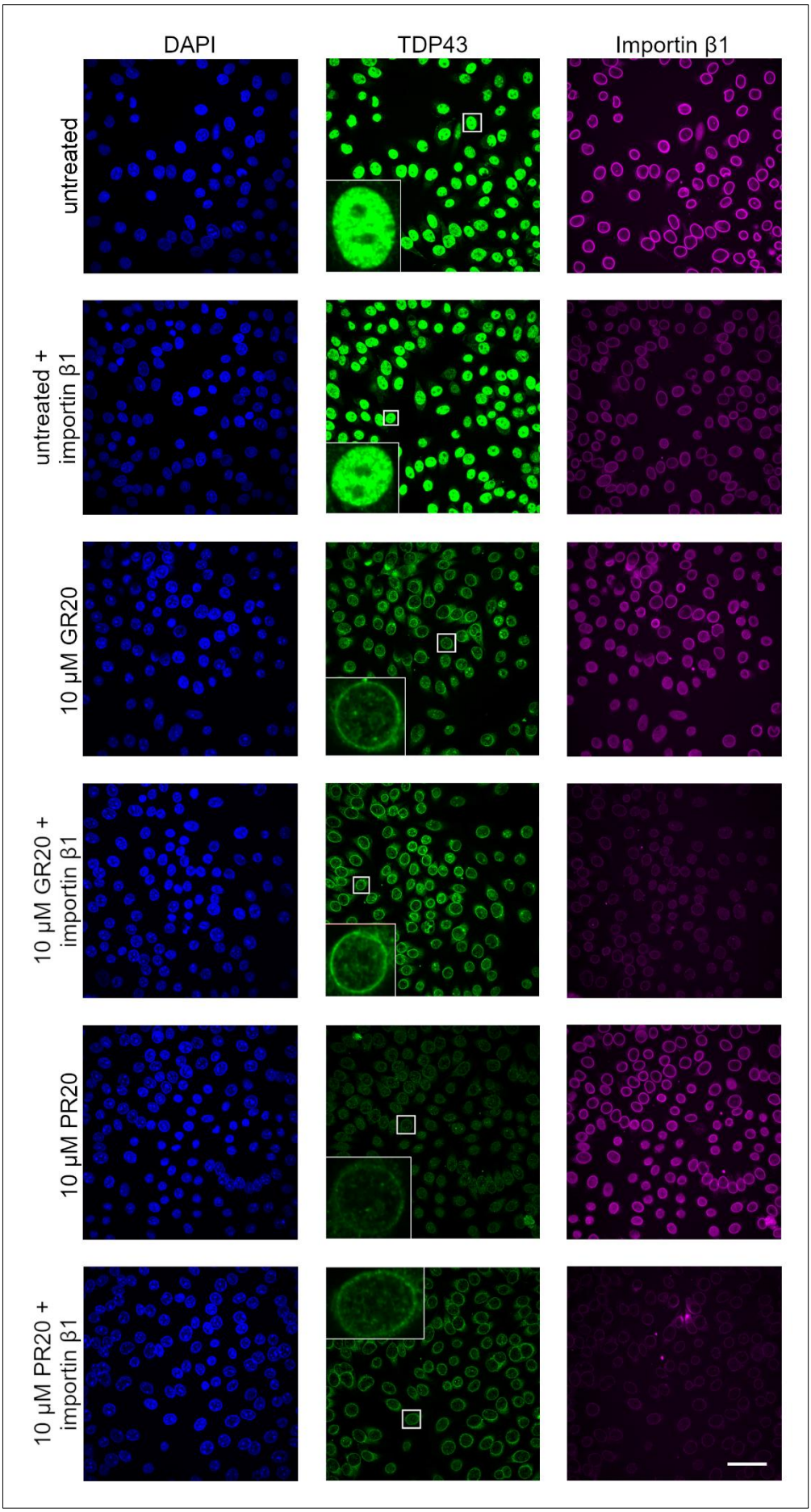
DAPI
TDP43
Importin β1
untreated
untreated + importin β1
10 μM GR20
10 μM GR20 + importin β1
10 μM PR20
10 μM PR20 + importin β1

Figure 5.63: Effect of importin β1 on increase of passive nuclear export of TDP43 by poly-GR or -PR. Opera Phenix images of immunofluorescence staining of endogenous TDP43 in semi-permeabilised untreated cells or after 1 hour treatment with 100 nM importin β1 as indicated. Subsequently cells were either left untreated or treated with 10 µM arginine containing *C9ORF72* DPRs for 1 hour as indicated. Left panel: DAPI. Middle panel: TDP43. Right panel: Importin β1. Zoom ins are at different brightness and contrast settings as main images. Scale bar: 50 µm.

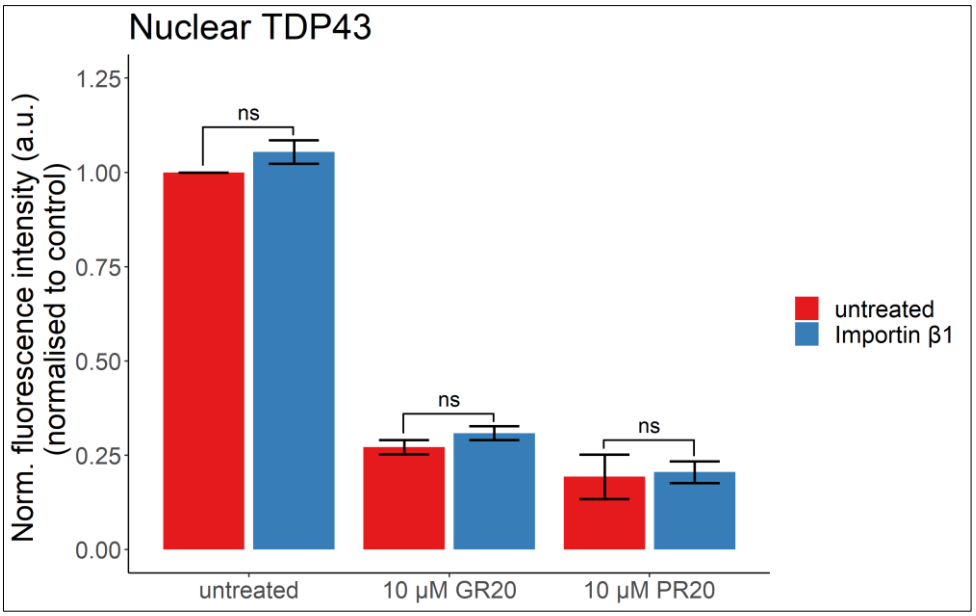

Figure 5.64: Importin β1 treatment does not reverse passive nuclear export enhancement of TDP43 by poly-GR or -PR. Quantified nuclear TDP43 fluorescence signal normalised to untreated control in untreated (red) or cells treated with 100 nM importin β1 (blue). Subsequently cells were either left untreated or treated with 10 µM of arginine containing DPRs as indicated. Means of individual experimental means are shown. N = 3. Error bars: SEM. ns: non-significant with multi-level model two-way ANOVA and Tukey's post hoc test.

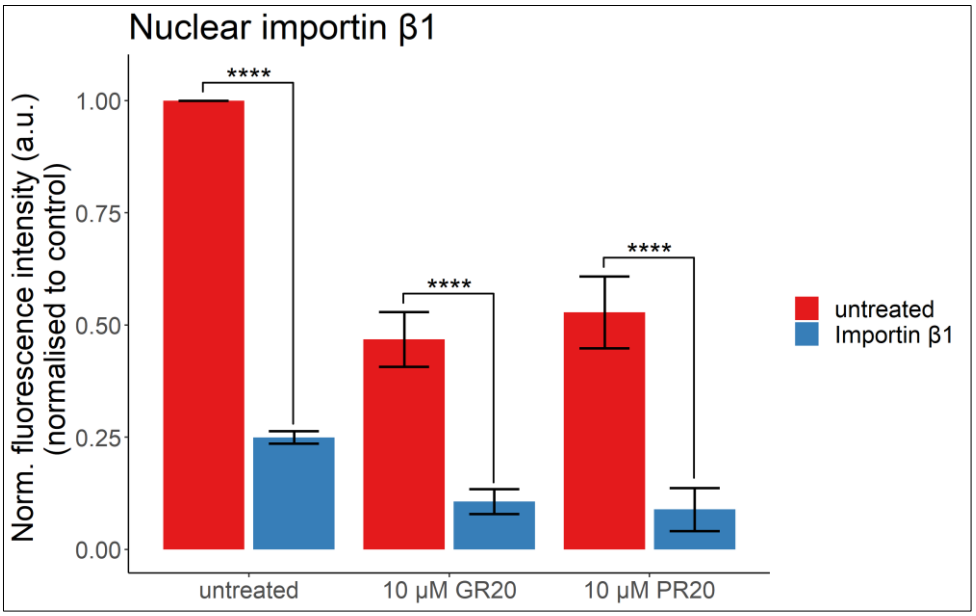

Figure 5.65: Nuclear importin β1 signal is not increased upon addition of exogenous importin β1. Quantified nuclear importin β1 fluorescence signal normalised to untreated control in untreated (red) or cells treated with 100 nM importin β1 (blue). Subsequently cells were either left untreated or treated with 10 µM of arginine containing DPRs as indicated. Means of individual experimental means are plotted. N = 3. Error bars: SEM. **** $p < 0.0001$ with multi-level model two-way ANOVA and Tukey's post hoc test.

5.7 Discussion

In the previous chapter we established that poly-GR and -PR increased passive nuclear import of reporter cargo and passive nuclear export of endogenous TDP43 and other nuclear proteins. Possible mechanisms of action were elucidated in this chapter.

5.7.1 CHD treatment differs from poly-GR and -PR treatment

To investigate potential modes of action of arginine containing DPRs on passive nucleocytoplasmic transport we compared DPR effects on this pathway with effects of compounds with known mode of action. CHD treatment led to enhanced passive nuclear import of reporter cargo having the most pronounced effect on the large 70 kDa dextran whilst only exhibiting a mild effect on the smaller 20 and 40 kDa dextrans. The opposite was observed for poly-GR and -PR which had the largest influence on nuclear entry of the 20 kDa dextran and only a minor effect on 70 kDa dextran influx. In accordance with our findings, in another study CHD treatment caused rapid influx of fluorescent maltose binding protein (40 kDa) in semi-permeabilised HeLa cells whilst this protein showed no visible nuclear influx in untreated cells. The authors of this study also mentioned (but did not show data) that nuclear entry of proteins already effectively entering the nucleus such as NTF2 or transportin was not enhanced by CHD (Ribbeck and Görlich, 2002). We found that nuclear TDP43 and histone H3 were reduced whilst nuclear intensities of hnRNP C1/2 were enhanced upon CHD treatment compared to untreated cells. Similarly, in a different study treatment with the aliphatic alcohol 1,6-hexanediol, which exhibited similar effects on the permeability barrier of the nuclear pore as CHD (Ribbeck and Görlich, 2002), led to a decrease of nuclear TDP43 levels in semi-permeabilised HeLa cells (Duan et al., 2022). In contrast, poly-GR and -PR treatment overall caused a decrease in nuclear levels of all three of these proteins (as shown in section 4.3). CHD likely acts by interrupting weak hydrophobic interactions between phenylalanine residues in FG domains of FG nucleoporins thereby breaking down the permeability barrier meshwork (Ribbeck and Görlich, 2002). This was further evidenced by CHD treatment leading to the dispersal of Nup116 FG domains expressed in yeast cells (Patel et al., 2007) and by CHD inhibiting the formation of *S. cerevisiae* Nup116 FG and *Tetrahymena* Mac98A FG particles *in vitro* (Schmidt and

Görlich, 2015). How these effects of CHD on FG nucleoporins led to an enhancement in nuclear signal of hnRNP C1/2 in my data is unclear. It is unlikely that this was caused by an increase in translation of hnRNP C1/2 protein as cells lacked a functional cytoplasm in our assay system. Potentially, the changed permeability barrier of the nuclear pore impeded nuclear exit of hnRNP C1/2 whilst some hnRNP C1/2 molecules were diffusing out of the nucleus in untreated cells as seemed to be the case for TDP43 in section 5.5. HnRNP C1/2 also possesses a nuclear retention signal (Nakielny and Dreyfuss, 1996) which possibly counteracted the effects of CHD. Importantly, poly-GR and -PR probably did not exert their effects on passive nuclear import and export by the same mechanism as CHD, namely by disrupting FG domain interactions between nucleoporins, as we found that their impact on these pathways differed to CHD's impact.

5.7.2 Nuclease treatment has the same effects as poly-GR and -PR

RNAse A treatment caused a reduction in nuclear TDP43 levels indicating that TDP43's interaction with RNA is important for its nuclear localisation. This interaction via TDP43's RNA recognition motif has previously been shown for both RNA and DNA (Kuo et al., 2014; Lukavsky et al., 2013). In agreement with our findings, in a recent study RNAse A treatment in semi-permeabilised HeLa cells also reduced nuclear TDP43. The authors further confirmed that this was probably due to TDP43 losing its RNA binding partners as addition of GU-rich RNA oligomers which would compete with endogenous nuclear RNA also reduced the nuclear signal of TDP43. This nuclear retention of TDP43 by RNA was transcription dependent as inhibition of RNA polymerase II led to a decreased nuclear/cytoplasmic TDP43 ratio (Duan et al., 2022). Treatment with the broader transcription suppressor and DNA intercalator actinomycin D also resulted in enhanced cytoplasmic TDP43 in HeLa cells (Ayala et al., 2008; Ederle et al., 2018) indicating that broader transcription and not only polymerase II mediated transcription contributes to TDP43's nuclear localisation. Additionally, we found RNAse A treatment to reduce nuclear levels of another RNA binding protein hnRNP C1/2 indicating that RNA binding also contributes to hnRNP C1/2's nuclear localisation. This effect is probably not transcription dependent as RNA polymerase II inhibition can enhance nuclear hnRNP C1/2 levels (Duan et al., 2022). HnRNP C1/2 nuclear levels were also increased upon DNAse I treatment in

our experiments possibly due to the observed redistribution of hnRNP C1/2 to more concentrated clusters. These clusters might be nuclear stress bodies although these have not been described in response to DNA damage (Campos-Melo et al., 2021) and the cytoplasmic stress granule response to DNA damage was shown to be very slow (Kedersha et al., 2002; Moutaoufik et al., 2014). As a general observation, however, nuclear hnRNP C1/2 levels seem to be increased upon cellular stress as we found after CHD and DNAse I treatment, and it also occurs after polymerase II inhibition (Duan et al., 2022).

In the case of the DNA binding protein histone H3, DNAse I treatment resulted in the reduction of its nuclear localisation in our experiments suggesting that DNA binding tethers histone H3 to the nucleus. Surprisingly, RNAse A treatment also reduced nuclear levels of histone H3. A possible link between histone H3 and RNA molecules exists as histone H3's interaction with several RNA binding proteins has been demonstrated (Huang et al., 2019; Kim et al., 2018). Overall, the effects on localisation of nuclear proteins by RNAse/DNAse and poly-GR/-PR treatment were the same indicating that poly-GR and -PR may disrupt the interaction of certain RNA or DNA binding proteins with their nucleic acid binding partners resulting in the loss of these proteins from the nucleus.

5.7.3 Poly-GR and -PR change localisation of FG nucleoporins

We found that arginine containing *C9ORF72* DPRs affected the localisation of various nucleocytoplasmic transport factors. With regards to FG nucleoporins (as summarised in Table 5.1), poly-GR and -PR reduced nucleoplasmic levels of NUP54 and poly-PR treatment resulted in a decrease of both nucleoplasmic and nuclear membrane NUP98 and POM121 as well as of RANBP2 nuclear membrane levels. NUP153 localisation was not affected by DPR treatment. Partially in line with our results, NUP98 and POM121 levels were reduced in nuclei of 32-day-old *C9ORF72* iPSC-derived spinal neurons and in nuclei extracted from *C9ORF72* patient motor cortex compared to healthy controls, and NUP153 was not changed in these models. However, NUP54 and RANBP2 levels were not changed in *C9ORF72* iPSC-derived neuron nuclei (Coyne et al., 2020). Furthermore, overexpression of GA_{50}-, GR_{50}, or PR_{50}-GFP constructs did not result in loss of POM121 in nuclei of 20-25-day-old iPSC-derived neurons but expression of G_4C_2 repeat RNA in the same cells did

(Coyne et al., 2020) suggesting that POM121 loss from the nuclear pore was caused by repeat RNA rather than by DPRs, contrary to what we observed. However, DPRs were tested in younger neurons than the investigated *C9ORF72* neurons which could potentially still show an effect at a later stage.

Localisation of NUP153 was normal upon DPR treatment in our experiments. In a different study knockdown of *NUP153* led to an enhancement of passive import of reporter cargo in semi-permeabilised HeLa cells (Lowe et al., 2015). However, changed NUP153 localisation did not contribute to the enhanced passive nucleocytoplasmic transport we observed in the presence of poly-GR and -PR.

In addition to nuclear membrane loss, we also detected nucleoplasmic loss of NUP98, POM121 and NUP54 upon poly-GR and -PR treatment. This might still have effects on nuclear pore levels as these nucleoporins could be recruited from the nucleoplasm to the pore. This recruitment has been shown for NUP98 in HEK cells (Griffis et al., 2002). In addition, nucleoporins might have functions besides nucleocytoplasmic transport within the nucleus which could be affected by poly-GR and -PR. For instance, NUP98 acts as a transcriptional regulator in embryonic stem cells, neuronal progenitors (Liang et al., 2013) and hematopoietic progenitors (Franks et al., 2017).

The mislocalisation of FG nucleoporins is potentially mediated by direct interaction of poly-GR and -PR with these nucleoporins. For example, poly-PR was shown to directly bind to NUP98 and NUP54 FG polymers *in vitro* (Shi et al., 2017) and these proteins were also found within poly-GR and -PR aggregates in HEK cell lysates (Hayes et al., 2020). Interestingly, it was demonstrated in our group that this interaction changed the permeability characteristics of FG domains which led to increased influx of reporter cargo in NUP98 FG particles *in vitro* (unpublished results). Therefore, my findings of passive nucleocytoplasmic transport enhancement by poly-GR and -PR might also be mediated by direct interactions of these DPRs with FG nucleoporins within the nuclear pore.

5.7.4 Poly-GR and -PR alter nuclear levels of Ran and Ran regulators

We also found nuclear Ran levels to be lowered upon poly-PR treatment in comparison to no treatment as depicted in Table 5.1. This was also detected in other C9ORF72 ALS/FTD models such as S2 cells expressing 30 *C9ORF72* repeats

(Zhang et al., 2015), HeLa cells expressing 31 *C9ORF72* repeats (P. T. Lee et al., 2020), GFP-GR100 expressing SH-SY5Y cells (J. Lee et al., 2020) and *C9ORF72* ALS iPSC-derived neurons (Coyne et al., 2020; J. Lee et al., 2020; Zhang et al., 2015). Furthermore, expression of a dominant negative version of Ran in a *Drosophila* model expressing 58 *C9ORF72* repeats led to an enhancement of the rough eye phenotype associated with neuronal toxicity (Freibaum et al., 2015) which might be explained by Ran's essential role in active nucleocytoplasmic transport. Furthermore, changed nuclear localisation of Ran might also change its interaction with nucleoporins. This could alter the restrictiveness of the permeability barrier potentially contributing to the enhancement of passive nucleocytoplasmic transport by arginine containing *C9ORF72* DPRs.

We also observed a decrease in nucleoplasmic and nuclear membrane levels of Ran regulator RCC1 upon poly-GR and -PR treatment and poly-PR reduced nuclear membrane levels of Ran regulator RanBP2 which could further disturb the regulation of the Ran cycle. A reduced nuclear cytoplasmic ratio of RCC1 was also observed in *C9ORF72* induced neurons (Jovičić et al., 2015) suggesting that this localisation might be disease relevant. On the other hand, localisation of dRCC1 (*Drosophila* homologue of RCC1) was normal in salivary gland cells of a *Drosophila* model expressing GR 64-mers (Solomon et al., 2018) indicating that poly-GR mediated mislocalisation of RCC1 might be model dependent.

RANGAP1, another Ran regulator, was not significantly changed upon DPR treatment in our experiments. In *C9ORF72* ALS iPSC-derived neurons and in *C9ORF72* ALS patient motor cortex nuclear aggregation of RANGAP1, which is normally localised to the cytoplasm or the nuclear membrane (Cha et al., 2015), was detected (Zhang et al., 2015). In these models RanGAP1 mislocalisation might be mediated by repetitive *C9ORF72* RNA. Indeed, RanGAP1 and *C9ORF72* repeat RNA were shown to interact *in vitro* and RanGAP1 localised to RNA foci in *C9ORF72* ALS iPSC-derived neurons (Zhang et al., 2015). In agreement with our results RanGAP1 localisation was normal in poly-GR models, namely in *Drosophila* expressing 64-mers of GR (Solomon et al., 2018) and in the cortex of 6-month-old GFP-GR100 mice (Y. J. Zhang et al., 2018). Additionally, a quantitative histopathology study did not detect differences in RanGAP1 localisation in *C9ORF72* ALS patient motor cortex and spinal cord (Saberi et al., 2018). This suggests that RanGAP1 mislocalisation might not contribute to *C9ORF72* ALS/FTD pathology at

least at later stages of disease. Therefore, results regarding components of the Ran cycle in *C9ORF72* ALS/FTD are not unanimous but there is some evidence that Ran localisation and its regulation is disturbed in the presence of arginine containing *C9ORF72* DPRs and in *C9ORF72* ALS/FTD in general.

5.7.5 Altered import receptor localisation upon poly-GR and -PR treatment

We found nucleoplasmic levels of importin β1 and nucleoplasmic and nuclear membrane levels of importin α3 to be decreased upon poly-GR and -PR treatment. In addition, there was a trend of a reduction of nuclear membrane levels of importin β1 by poly-PR as summarised in Table 5.1. Hence, enhancement of passive nucleocytoplasmic transport might be caused by the reduction of nuclear importin α/β levels by poly-GR and -PR. GR and PR polymers most likely have the ability to interact with these importins as they were shown to directly bind to importin β1 (Hayes et al., 2020; Hutten et al., 2020) and poly-GR also directly interacted with importin α3 (Hutten et al., 2020) *in vitro*. Thus, similarly to mislocalisation of FG nucleoporins direct interaction of poly-GR and -PR with these importins might tether the import receptors away from the nuclear pore.

5.7.6 Different impacts on cellular mechanisms between poly-GR and -PR

Overall, PR20 treatment seemed to have a stronger effect on nucleocytoplasmic transport factor localisation than GR20 treatment. Differing effects of poly-GR and PR have also been reported elsewhere. For instance, poly-PR was found to bind importin β more selectively than GR20 (Hayes et al., 2020). PR20 but not GR20 treatment resulted in proteasome inhibition in rat primary neurons (Gupta et al., 2017). This suggests that poly-PR and -GR have different interaction partners within the cell. Indeed, the interactome of GR50 and PR50 differed to a substantial degree not exhibiting a full overlap (Lee et al., 2016). Finally, PR exhibited greater stability than GR when analysing cell lysates of U2OS cells treated with either peptide (Kwon et al., 2014). Therefore, poly-GR and -PR concentrations might have differed to some extent in our studies as some GR peptides had already been degraded. This might be one reason for the greater potency of poly-PR than poly-GR we observed in our transport factor experiments.

In summary, even though the influence of poly-PR was greater both poly-GR and -PR treatment affected the localisation of a subset of FG nucleoporins, members of the Ran cycle and importins which could all contribute to the changes in passive nucleocytoplasmic transport dynamics we observed.

5.7.7 Rescuing passive nucleocytoplasmic transport increase

In our attempts to reverse the effects of poly-GR and -PR on passive nucleocytoplasmic transport dynamics we found that WGA treatment could inhibit the enhanced export of TDP43 upon treatment with 10 µM poly-GR and -PR (see section 5.5). WGA binds to *N*-acetylglucosamine in nucleoporins including the Nup62 complex within the central channel of the nuclear pore (Davis and Blobel, 1986; Finlay et al., 1987; Hanover et al., 1987) and was shown to inhibit active nucleocytoplasmic transport (Finlay et al., 1987; Mohr et al., 2009). It also prohibited passive nuclear translocation but this effect was size-dependent with the import of larger molecules being more greatly affected than the import of smaller molecules. The authors investigating WGA's influence on passive translocation speculated that WGA's binding to nucleoporins created additional links between these proteins and thereby introduced additional mesh structures into the "central channel mesh" (see also 1.4.2) resulting in a narrower nuclear pore central channel structure. Indeed, radius estimation calculations concluded lower radii of nuclear pore channels in WGA treated cells compared to untreated cells (Mohr et al., 2009). However, cargo properties also seemed to influence the effect of WGA as passive nuclear import of 40 kDa dextran was not inhibited while the import of the smaller GFP (27 kDa) was impaired by WGA (Hayes et al., 2020). The fact that WGA, which acts at the nuclear pore, at least partly inhibited export of TDP43 indicates that the reduced nuclear signal of TDP43 upon poly-GR and -PR treatment was due increased nuclear export of TDP43 rather than degradation of TDP43 in the nucleus. As the rescue by WGA was not complete in poly-PR treated cells even at a lower concentration PR might still be able to bind to and influence nuclear pore structures even in the presence of WGA. It would be interesting to further investigate whether WGA and poly-GR/PR compete for binding sites at the nuclear pore and whether these DPRs have the capacity to displace WGA from the nuclear pore and vice versa.

Even though we found nuclear importin β1 to be reduced in HeLa cells upon poly-GR and -PR treatment, addition of importin β1 did not decrease the increased passive nucleocytoplasmic import rates of 20 kDa dextran and the enhanced export rates of TDP43 caused by poly-GR and -PR. In a different study the reduction of nuclear membrane importin β1 by addition of Ran to semi-permeabilised HeLa cells resulted in passive nuclear influx of reporter cargo which otherwise did not enter the nucleus as it exceeds the size limit of the nuclear pore's permeability barrier. In contrast to our findings, the nuclear influx of reporter cargo was prohibited by the addition of importin β1 (Kapinos et al., 2017). It is possible that, in contrast to a reduction in importin β1 levels by Ran, a decrease in nuclear importin β1 levels by poly-GR or -PR is not responsible for the heightened passive nucleocytoplasmic rates we observed. Another possibility would be that the 100 nM concentration of importin β 1 we used (due to limited availability) was not sufficient for a rescue of the increase in passive translocation caused by arginine containing *C9ORF72* DPRs which were used at concentrations 100 times higher. However, 100 nM was enough to restore importin β1 in the study mentioned above (Kapinos et al., 2017). It is unclear whether nuclear importin β1 levels were restored in our experiments as immunostaining yielded surprising results. Nuclear importin β1 levels were lower in cells treated with importin β1 than in cells to which importin β1 was not added (see Figure 5.65). A possible explanation for this unexpected finding would be that there was still excess importin β1 protein present in the media upon addition of the antibody against importin β1 and this excess importin β1 titrated the antibody out of the staining reaction. Another reason for the failed rescue could be that a fully functional form of importin β1 is needed to reduce passive nucleocytoplasmic transport levels in poly-GR or -PR treated cells to levels observed in untreated cells while we used a denatured form. Kapinos and colleagues used a physiologically folded form of importin β1 (Kapinos et al., 2017) which might also explain the difference with our results. As nuclear importin β1 levels were again clearly reduced upon poly-GR/PR treatment in our rescue experiments follow-up experiments using higher importin β1 concentrations and/or native forms of importin β1 seem to be warranted.
Overall, enhanced passive nuclear import and export upon poly-GR and -PR treatment might be caused by mislocalisation of transport factors. In addition, increased nuclear export by poly-GR and -PR might also be due to interference of these DPRs with the interaction of DNA/RNA binding proteins with DNA/RNA.

6 Confirmation of key results in *C9ORF2* iPSC-derived neuronal model

In this chapter we aimed to confirm our main findings from the previous chapters in the immortalised human HeLa cell line in the more disease relevant system of *C9ORF72* patient iPSC-derived neurons. These main findings were the increase in passive nucleocytoplasmic transport upon poly-GR and -PR treatment and the change in localisation of various transport factors by these DPR species. We, therefore, subjected three control and three *C9ORF72* ALS patient lines to the same passive transport assay as the HeLa cells. We then measured passive nuclear translocation of 20 kDa dextran to test if the presence of the *C9ORF72* mutation also led to enhancement of passive nucleocytoplasmic transport. We also treated one control iPSC line with poly-GR and assessed the effects on nuclear import of 20 kDa dextran to investigate whether poly-GR increased passive nuclear import in human neurons. Furthermore, we wanted to test whether the presence of the *C9ORF72* mutation resulted in mislocalisation of transport factors in human neurons. Therefore, we immunostained the same three control and patient lines for TDP43 and for transport factors we previously found to be changed upon arginine containing *C9ORF72* DPR treatment (see section 5.4) or which are key players in the nucleocytoplasmic transport system. Thus, in this chapter we intended to further establish that nucleocytoplasmic transport dynamics were changed in *C9ORF72* ALS/FTD in a very disease relevant system.

6.1 Examining passive nucleocytoplasmic transport in *C9ORF72* ALS iPSC-derived neurons

To analyse whether our findings of enhanced passive nuclear import upon arginine containing *C9ORF72* DPR treatment in HeLa cells were also occurring in a more disease relevant system we differentiated three control and three *C9ORF72* ALS iPSC lines into cortical neurons. After 14 days of terminal differentiation, we subjected the cells to our optimised transport assay and observed the nuclear influx of FITC labelled 20 kDa dextran via live confocal microscopy. As our cell populations were not purely neuronal fields of view containing neurons were selected using the brightfield channel.

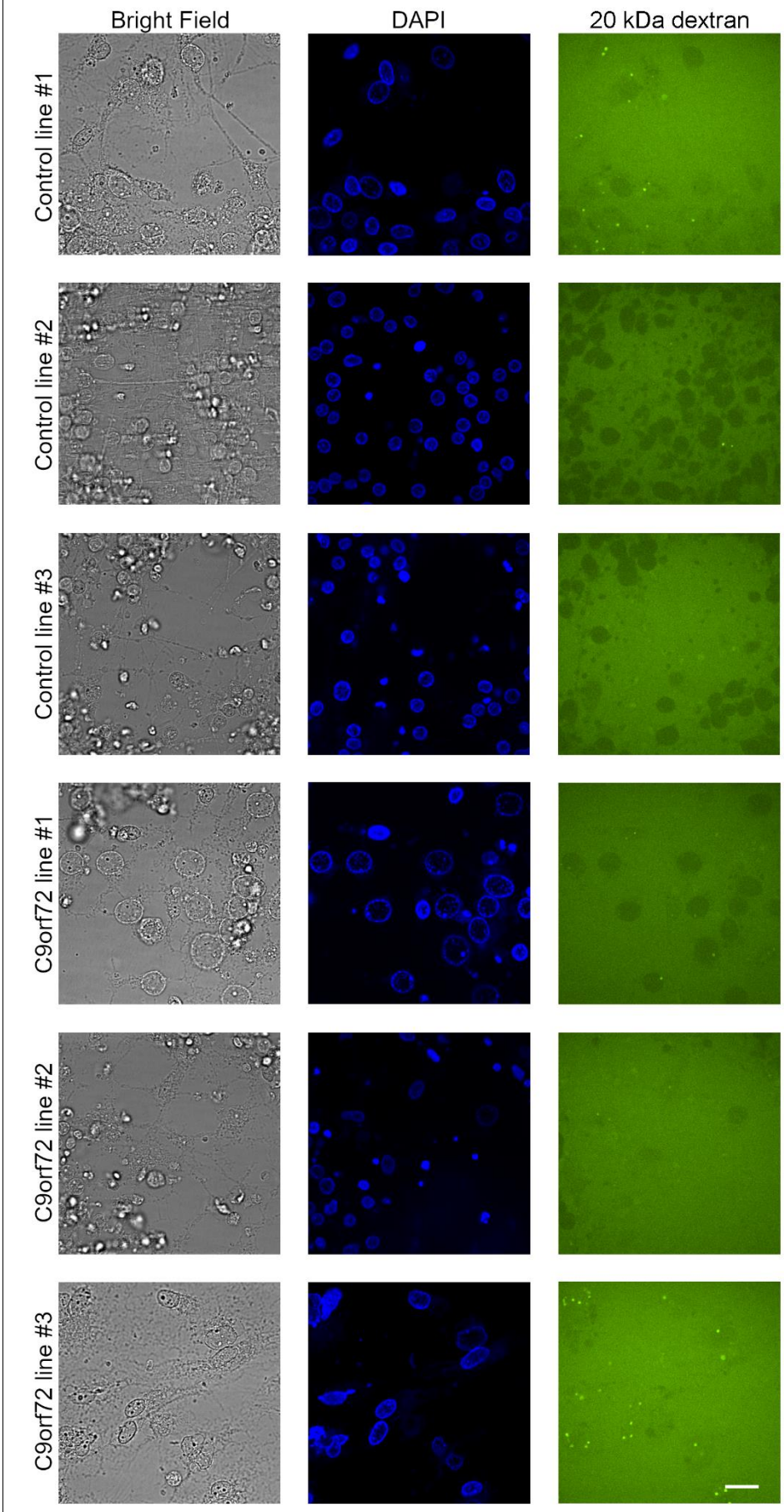
Bright Field
DAPI
20 kDa dextran
Control line #1
Control line #2
Control line #3
C9orf72 line #1
C9orf72 line #2
C9orf72 line #3

Figure 6.1: Effect of *C9ORF72* mutation on passive nuclear import of 20 kDa dextran. Spinning disk confocal microscope images of semi-permeabilised control or *C9ORF72* ALS iPSC-derived neurons as indicated after 4-minute incubation with 20 kDa dextran. Left panel: Bright field channel. Middle panel: DAPI channel. Right panel: FITC 20 kDa dextran channel. Scale bar: 20 µm.

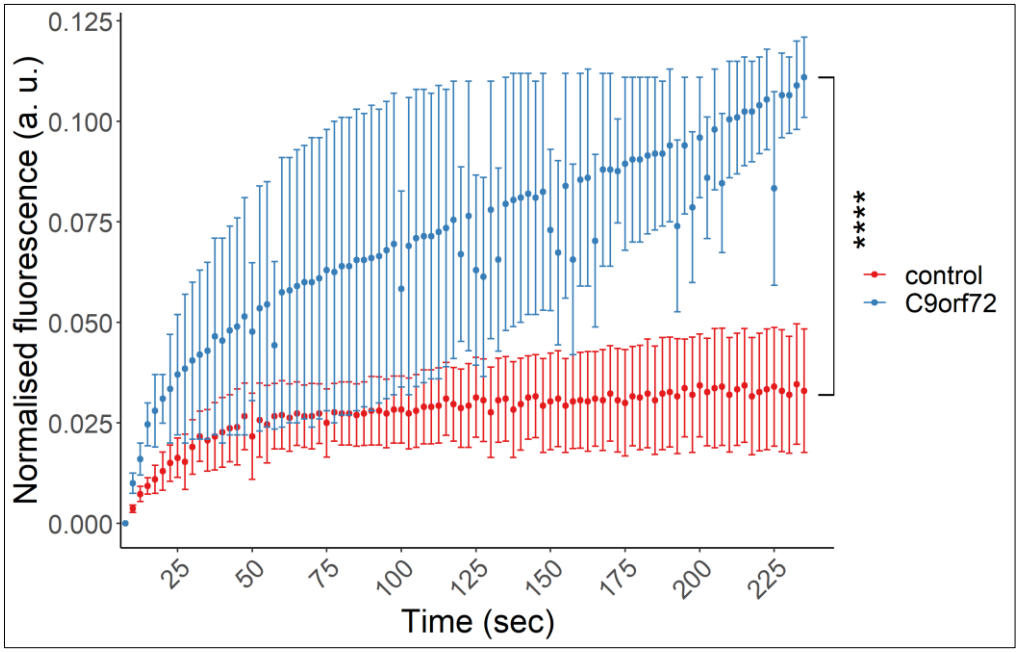

Figure 6.2: *C9ORF72* mutation enhances passive nuclear translocation of 20 kDa dextran. Quantification of passive nuclear import of 20 kDa dextran (shown as nuclear fluorescence normalised to nuclear and general background) over time in semi-permeabilised control or *C9ORF72* ALS iPSC-derived neurons. Controls depicted in red, *C9ORF72* lines in blue. N = 3 control and 3 *C9ORF72* ALS lines with 1 control line differentiated once and all other lines differentiated twice. Means of individual cell line means are plotted. Error bars: SEM. **** $p < 0.0001$ vs control with two-way repeated measures ANOVA.

As depicted in Figure 6.1 and Figure 6.2, 20 kDa dextran could enter control neurons at low levels. Levels of passive nuclear import of 20 kDa dextran were higher in *C9ORF72* ALS cells compared to control lines. These levels were comparable to levels observed in untreated HeLa cells (see sections 3.5 and 4.1) suggesting that nucleocytoplasmic transport occurred at higher levels in untreated HeLa cells compared to untreated control iPSC-derived neurons. The amount of passive nuclear import was variable between cell lines (see Figure 6.1) but was on average greater in *C9ORF72* ALS compared to control neurons ($p = 5.58 \times 10^{-10}$, repeated measures ANOVA; see Figure 6.2). This finding is similar to our previous results of increased passive nucleocytoplasmic import of reporter cargo in poly-GR or -PR treated HeLa cells. The enhancement of passive nucleocytoplasmic transport by poly-GR and -PR might therefore be disease relevant as we could also detect it in *C9ORF72* ALS patient cells.

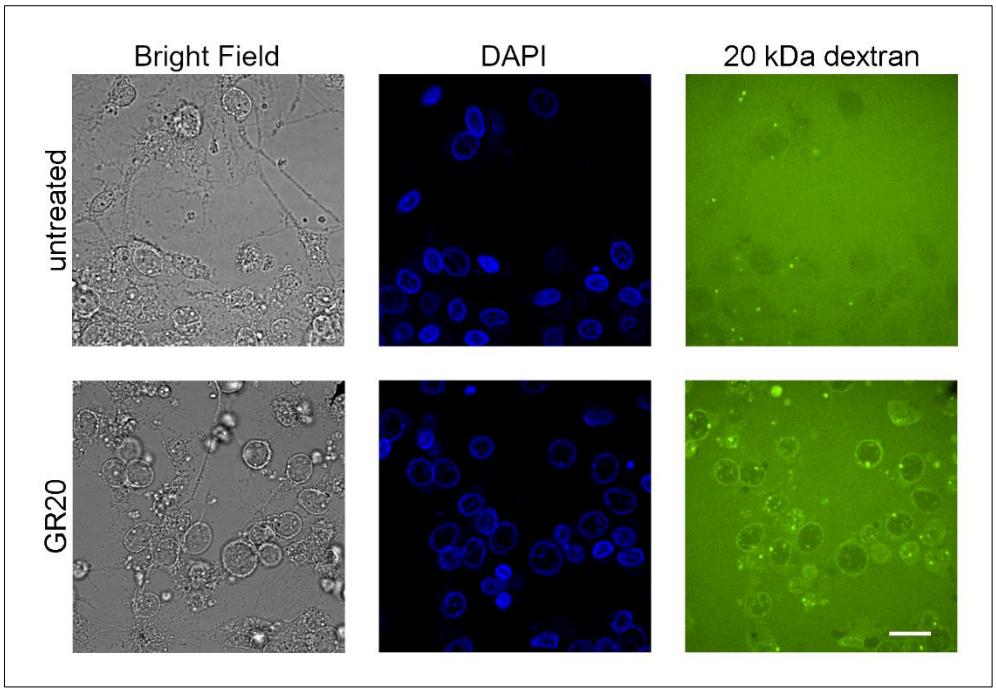

Figure 6.3: Influence of poly-GR on passive nuclear import of 20 kDa dextran in iPSC-derived neurons. Spinning disk confocal microscope images of semi-permeabilised untreated control iPSC-derived neurons and control iPSC-derived neurons treated with 10 µM poly-GR as indicated for 30 minutes after 4-minute incubation with 20 kDa dextran. Left panel: Bright field channel. Middle panel: DAPI channel. Right panel: FITC 20 kDa dextran channel. Scale bar: 20 µm.

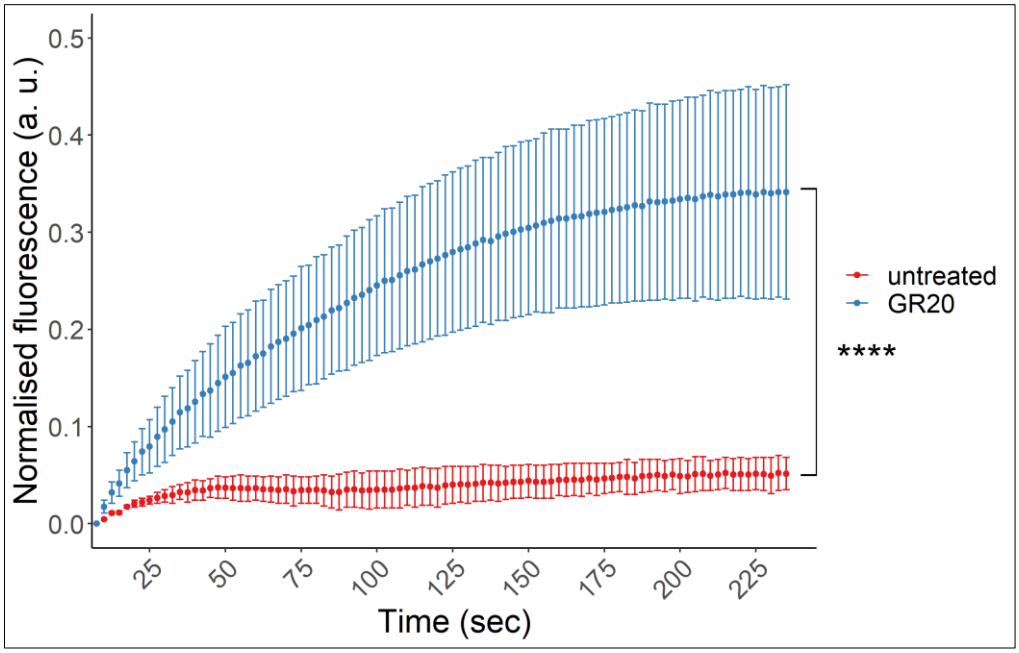

Figure 6.4: Nuclear import of 20 kDa dextran is increased upon poly-GR treatment in iPSC-derived neurons. Quantification of passive nuclear import of 20 kDa dextran (shown as nuclear fluorescence normalised to nuclear and general background) over time in semi-permeabilised untreated control iPSC-derived neurons and control iPSC-derived neurons treated with poly-GR. Untreated condition depicted in red, GR20 treatment in blue. N = 3 wells per condition and differentiation of 1 control line with 2 rounds of differentiation. Means of individual experimental (differentiation) means are depicted. Error bars: SEM. **** $p < 0.0001$ vs untreated cells with two-way repeated measures ANOVA.

We also wanted to check whether poly-GR treatment led to enhanced passive nuclear import of 20 kDa dextran in human neurons equally to HeLa cells. We therefore performed the transport assay on neurons derived from an iPSC control line (control line #1 from above) and treated these cells with 10 µM GR20 for 30 minutes. Subsequently, the passive nuclear translocation of FITC labelled 20 kDa dextran was followed live using confocal microscopy. Again 20 kDa dextran entered untreated cells at low levels (see Figure 6.3 and Figure 6.4) which were lower than in untreated HeLa cells (see sections 3.5 and 4.1). GR20 treatment led to a significant increase in passive nuclear transport of 20 kDa dextran in the control line compared to untreated cells of the same line with a *p* value of 4.79×10^{-59} (repeated measures ANOVA) as shown in Figure 6.3 and Figure 6.4. Import levels of 20 kDa dextran upon poly-GR treatment were higher in HeLa cells than in iPSC-derived neurons (compare Figure 4.2) but the extent of the increase compared to non-treatment was greater in the iPSC line compared to Hela cells (12-fold increase vs 4-fold increase of maximum import levels). In summary, poly-GR treatment also led to a rise in passive nuclear import in iPSC-derived neurons compared to untreated neurons. This shows that our previous finding was not specific to HeLa cells. Therefore, poly-GR might also lead to enhanced passive nucleocytoplasmic transport in *C9ORF72* ALS/FTD patients.

6.2 Localisation of nucleocytoplasmic transport factors and TDP43 in *C9ORF72* ALS iPSC-derived neurons

In section 5.4 we found that poly-GR and -PR treatment led to a reduction in nuclear levels of the nucleoporins NUP98 and POM121, of RAN and of the transport receptors importin β1 and importin α3. As these might contribute to the increase of passive nucleocytoplasmic transport levels caused by poly-GR and -PR we investigated whether these were also decreased in *C9ORF72* ALS iPSC-derived neurons. Furthermore, we determined whether there was a difference in the localisation of TDP43 between control and *C9ORF72* neurons to check if TDP43 also mislocalised in this system. To this end, we differentiated three control and two *C9ORF72* ALS iPSC cell lines into cortical neurons (the third ALS line could not be successfully differentiated) and fixed the neurons at day 14 of terminal differentiation. Subsequently, we immunostained the cells against the proteins mentioned above. Of

note, for this analysis cells were not semi-permeabilised with digitonin, hence the entire cell not just the nucleus was investigated. As cell populations were not purely neuronal, neurons were defined with the neuronal marker MAP2 (see 2.8.4) and only this population was used in the image analysis.

TDP43

As shown in Figure 6.5 TDP43 predominantly localised to the nucleus in control lines. As depicted in Figure 6.5 and Figure 6.6A there was a trend (defined as p value of maximum of 0.25) of decreased nuclear TDP43 levels in *C9ORF72* neurons compared to control neurons with two of the three control lines showing higher nuclear TDP43 levels than *C9ORF72* lines. However, cytoplasmic TDP43 levels and nuclear cytoplasmic ratios of TDP43 did not differ between *C9ORF72* and control cells (see Figure 6.6B and C).

Nucleoporins

As depicted in Figure 6.7 NUP98 localised to the nucleoplasm and to the nuclear membrane/pore in control neurons. It also showed staining in the cytoplasm to a lower extent than in the nucleus and surprisingly quite strong staining within the neurites. To separate nuclear localisation of transport factors between the nucleoplasm and the nuclear pore we detected nucleoplasmic and nuclear membrane levels separately. Nucleoplasmic localisation of NUP98 was similar between control and *C9ORF72* cell lines as shown in Figure 6.7 and Figure 6.8A. However, there was a clear trend of decreased nuclear membrane levels and thus levels at the nuclear pore of NUP98 in *C9ORF72* neurons compared to all three control neuron lines (see Figure 6.8B). A reduction in NUP98 nuclear membrane levels was also observed upon poly-PR treatment in HeLa cells compared to untreated cells (see Figure 5.36B) and in contrast to *C9ORF72* iPSC-derived neurons poly-PR treated semi-permeabilised HeLa cells also exhibited lowered nuclear NUP98 levels (see Figure 5.36A). Cytoplasmic NUP98 levels were also trending towards a decrease in *C9ORF72* cells compared to control cells as illustrated in Figure 6.8C.

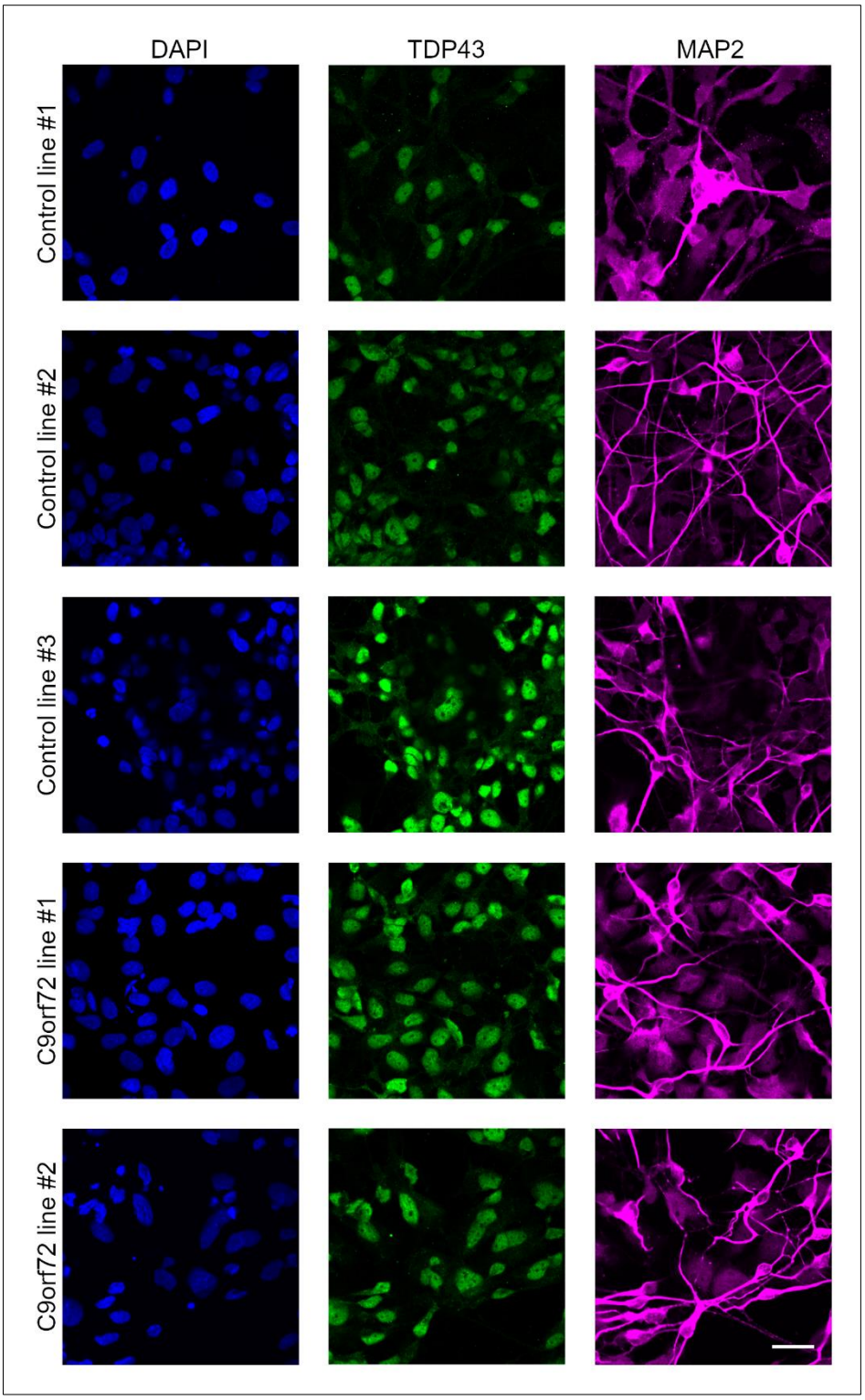

Figure 6.5: Effects of *C9ORF72* mutation on TDP43 localisation. Opera Phenix images of immunofluorescence staining of endogenous TDP43 in control or *C9ORF72* ALS cells as indicated. Left panel: DAPI. Middle panel: TDP43. Right panel: MAP2. Scale bar: 25 µm.

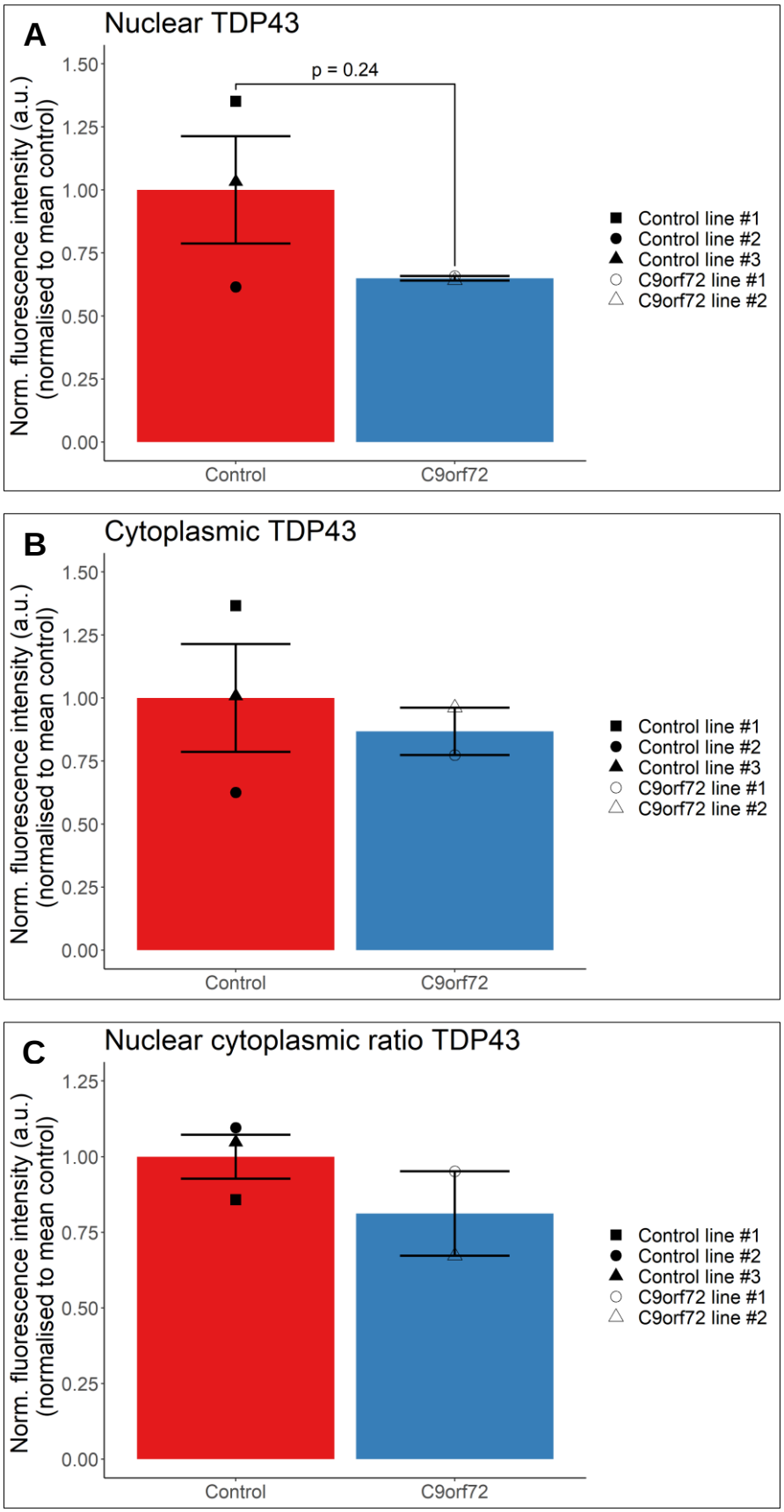

Figure 6.6: Nuclear TDP43 levels trend to decrease in *C9ORF72* iPSC lines. Quantified TDP43 fluorescence signal normalised to mean of control lines in control or *C9ORF72* ALS iPSC-derived neurons as indicated. A) Nuclear TDP43 levels. B) Cytoplasmic TDP43 levels. C) Nuclear cytoplasmic ratio of TDP43. N = 3 control and 2

C9ORF72 iPSC lines with 1 - 2 differentiations. Means of individual cell line means are shown in bar chart. Error bars: SEM. Two-sided t-test.

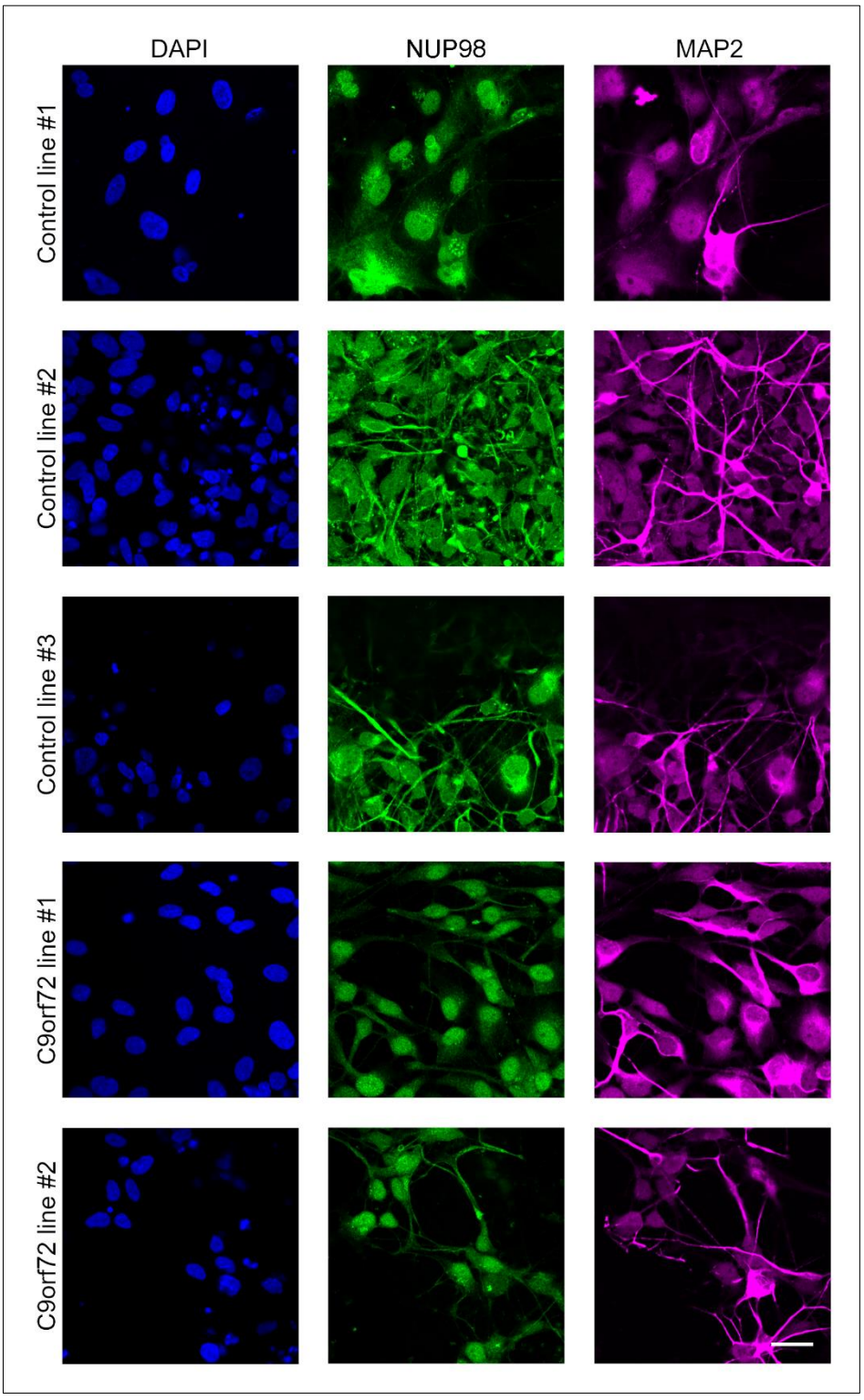

Figure 6.7: Influence of *C9ORF72* mutation on NUP98 localisation. Opera Phenix images of immunofluorescence staining of endogenous NUP98 in control or *C9ORF72* ALS cells as indicated. Left panel: DAPI. Middle panel: NUP98. Right panel: MAP2. Scale bar: 25 µm.

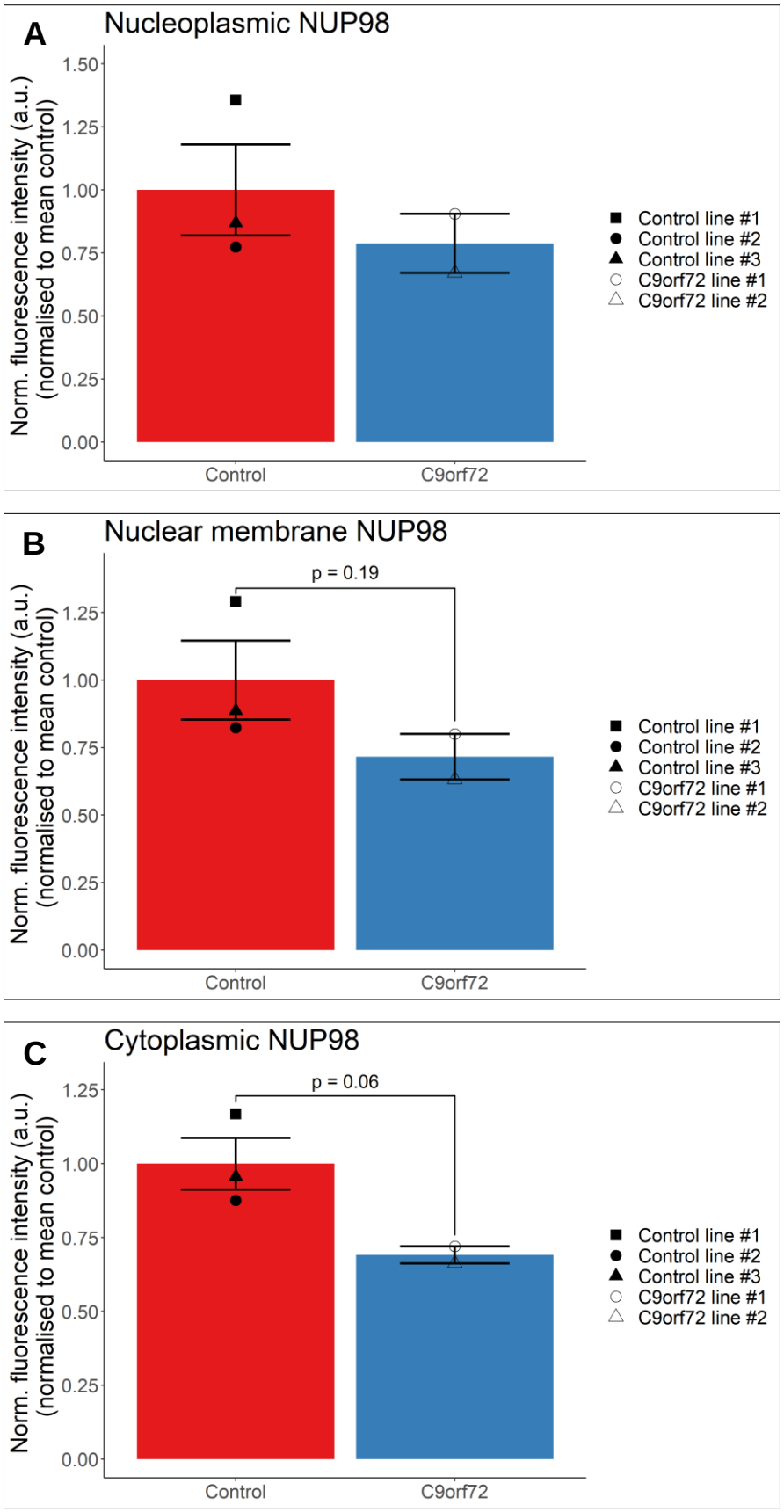

Figure 6.8: Nuclear membrane and cytoplasmic NUP98 levels exhibit trend to reduction in *C9ORF72* iPSC lines. Quantified NUP98 fluorescence signal normalised to mean of control lines in control or *C9ORF72* ALS iPSC-derived neurons as indicated. A) Nucleoplasmic NUP98 levels. B) Nuclear membrane NUP98 levels. C)

Cytoplasmic NUP98 levels. N = 3 control and 2 *C9ORF72* iPSC lines with 1 - 2 differentiations. Means of individual cell line means are plotted in bar chart. Error bars: SEM. Two-sided t-test.

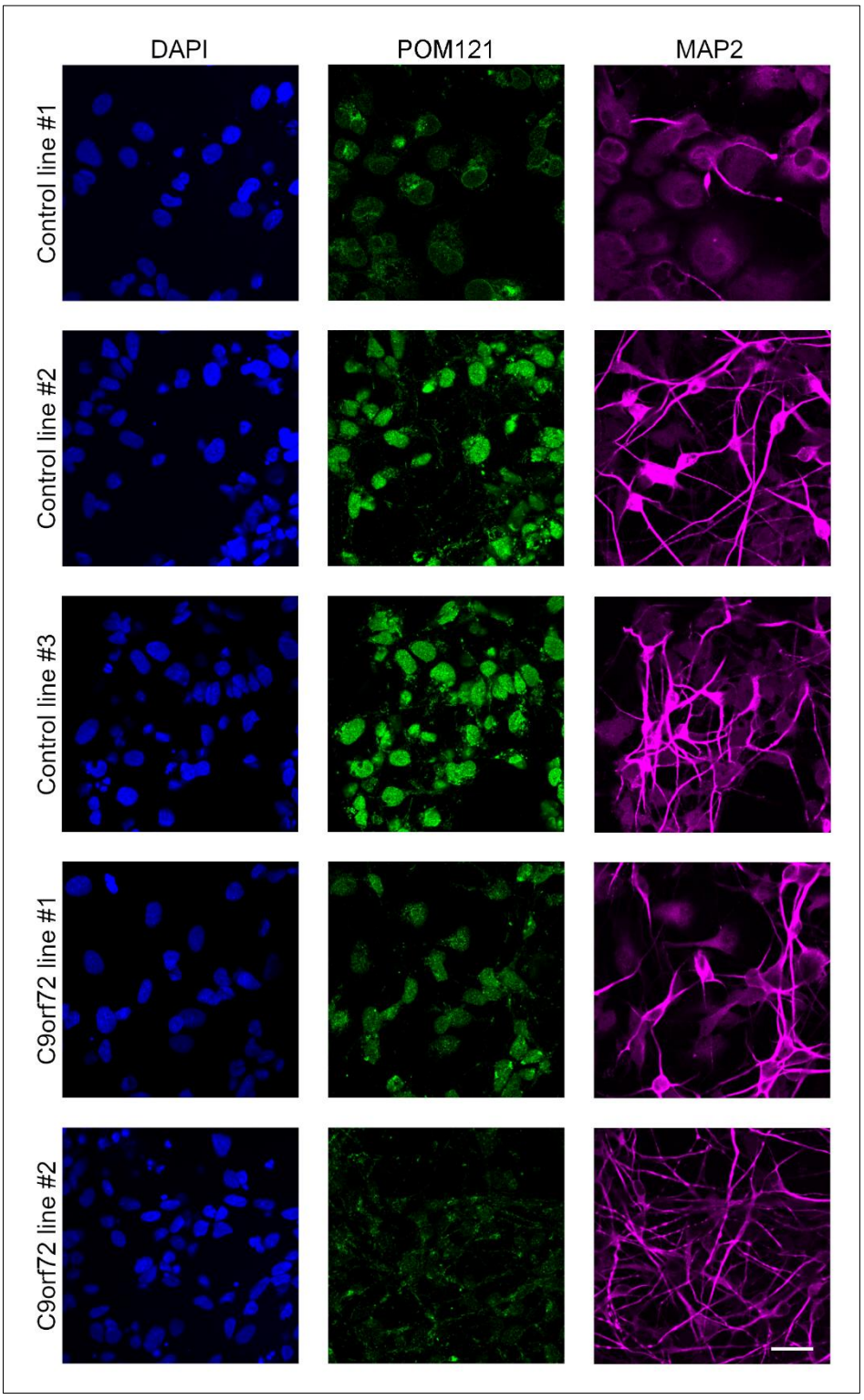

Figure 6.9: Impact of *C9ORF72* mutation on POM121 levels. Opera Phenix images of immunofluorescence staining of endogenous POM121 in control or *C9ORF72* ALS cells as indicated. Left panel: DAPI. Middle panel: POM121. Right panel: MAP2. Scale bar: 25 µm.

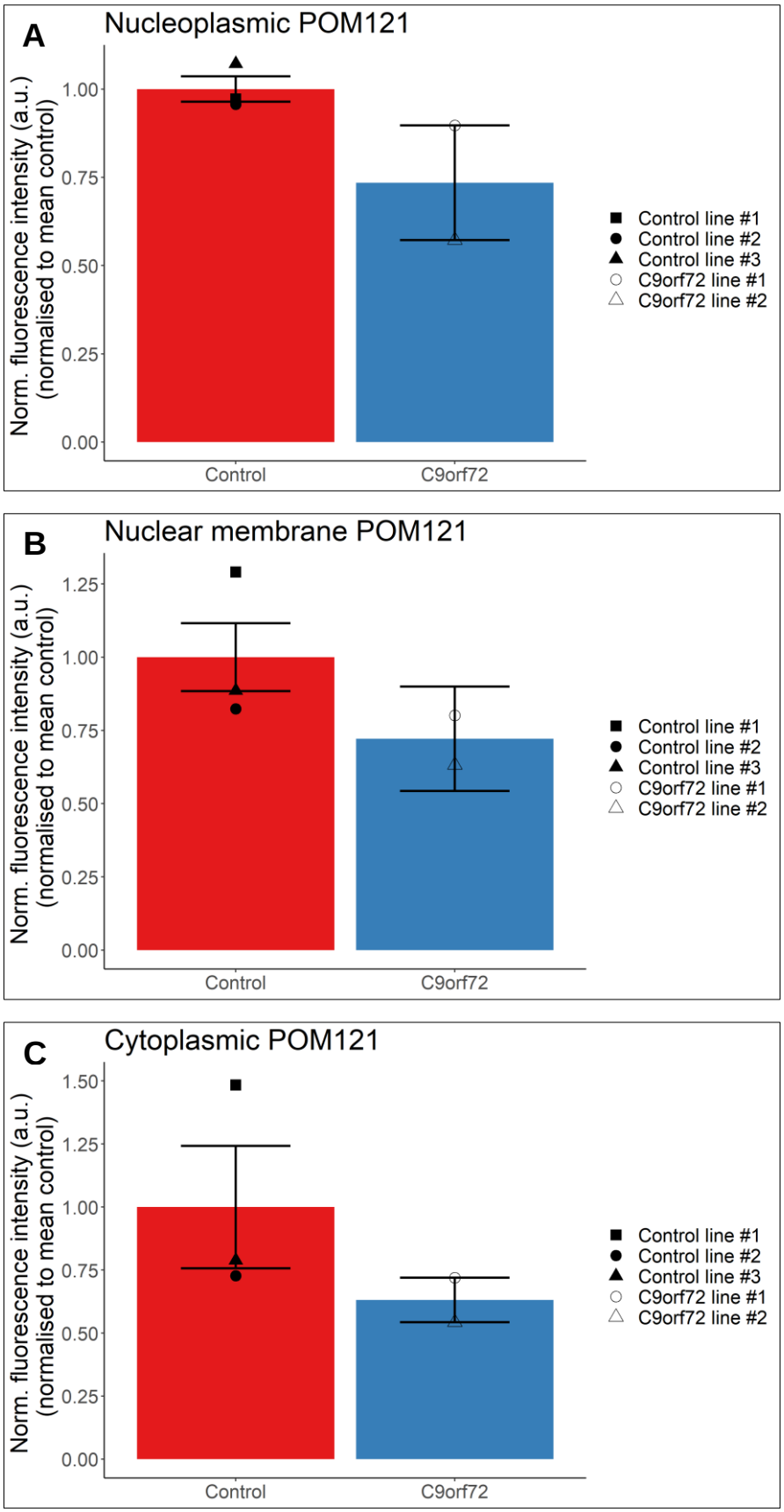

Figure 6.10: POM121 signal is not changed between control and *C9ORF72* iPSC lines. Quantified POM121 fluorescence signal normalised to mean of control lines in control or *C9ORF72* ALS iPSC-derived neurons as indicated. A) Nucleoplasmic POM121 levels. B) Nuclear membrane POM121 levels. C) Cytoplasmic POM121

levels. N = 3 control and 2 *C9ORF72* iPSC lines with 1 - 2 differentiations. Means of individual cell line means are depicted in bar chart. Error bars: SEM. Two-sided t-test.

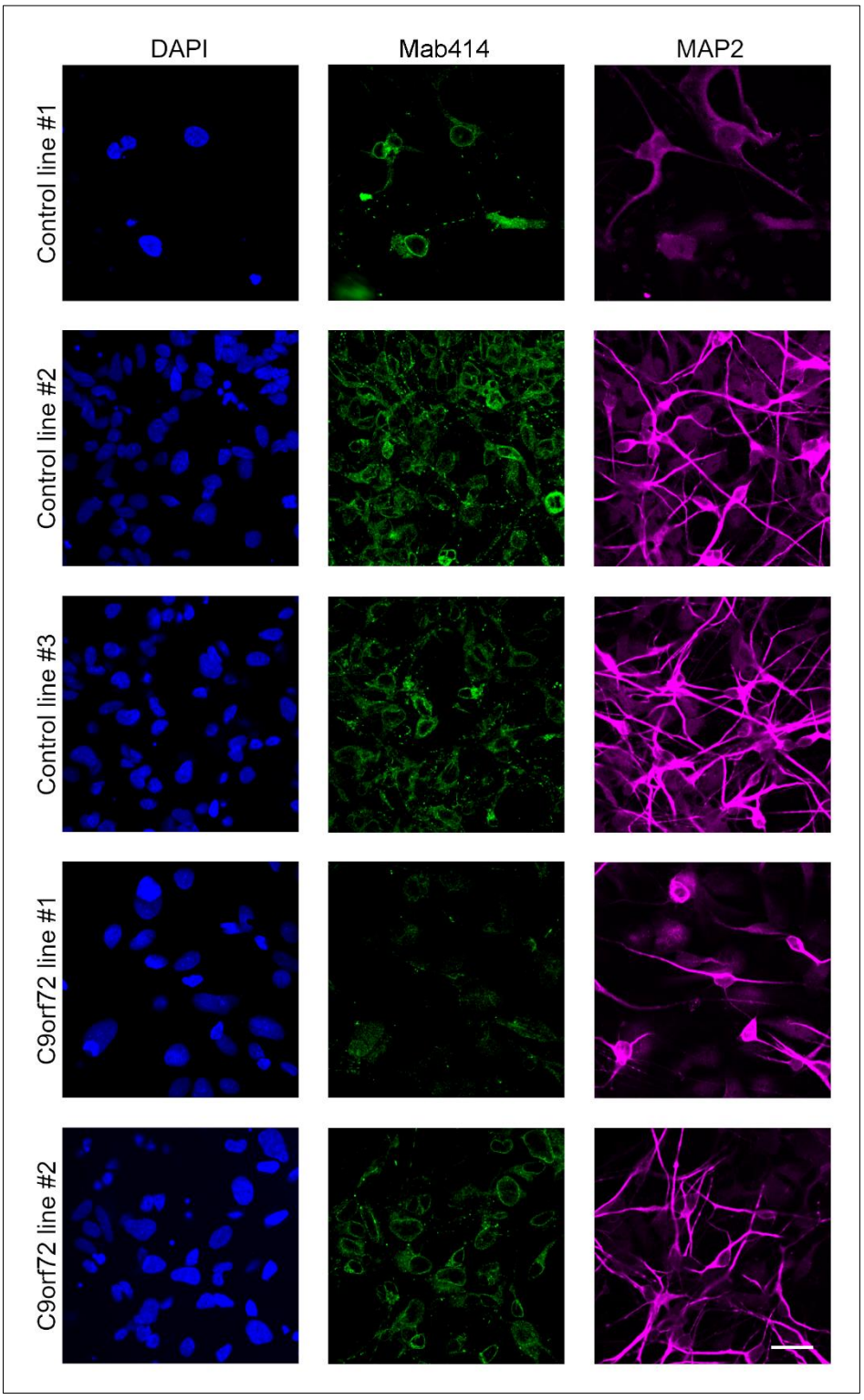

Figure 6.11: Effects of *C9ORF72* mutation on mAb414 staining. Opera Phenix images of immunofluorescence mAb414 staining in control or *C9ORF72* ALS cells as indicated. Left panel: DAPI. Middle panel: mAb414. Right panel: MAP2. Scale bar: 25 µm.

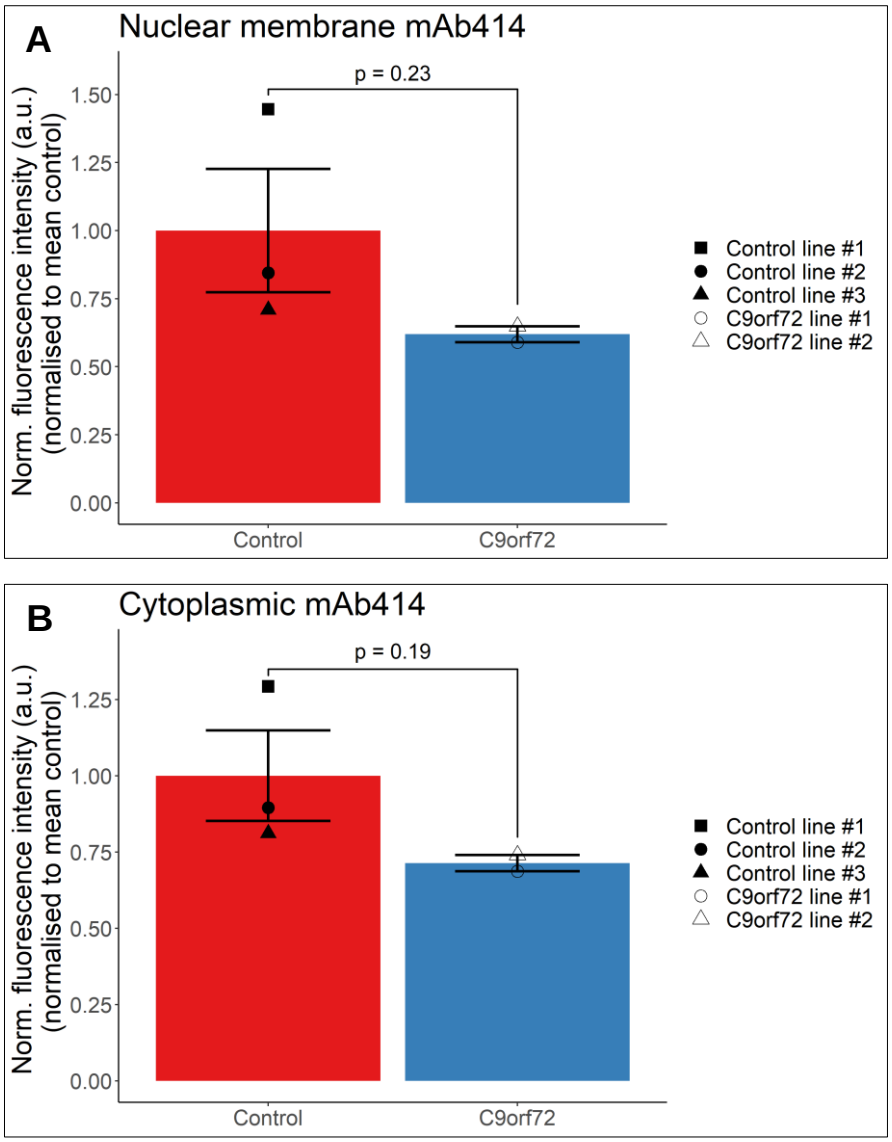

Figure 6.12: Trend of lower nuclear membrane and cytoplasmic mAb414 staining in *C9ORF72* iPSC lines. Quantified mAb414 fluorescence signal normalised to mean of control lines in control or *C9ORF72* ALS iPSC-derived neurons as indicated. A) Nuclear membrane NUP98 levels. B) Cytoplasmic NUP98 levels. N = 3 control and 2 *C9ORF72* iPSC lines with 1 - 2 differentiations. Means of individual cell line means are plotted in bar chart. Error bars: SEM. Two-sided t-test.

As depicted in Figure 6.9 POM121 localised to the nuclear membrane and the cytoplasm in control line #1 while it showed additional staining in the nucleoplasm in control lines #2 and #3. Nucleoplasmic POM121 levels were not significantly altered between control and *C9ORF72* iPSC-derived neurons with only one *C9ORF72* cell line exhibiting lower nucleoplasmic POM121 levels compared to control lines as shown in Figure 6.9 and Figure 6.10A. Nuclear membrane POM121 levels were also similar between control and *C9ORF72* cells again with lower levels in the same *C9ORF72* line compared to all other lines used (see Figure 6.10B). Similarly, no difference in cytoplasmic POM121 localisation was detected when comparing control

and *C9ORF72* neurons (see Figure 6.10C). In contrast, nucleoplasmic and nuclear membrane POM121 levels were decreased in PR20 treated semi-permeabilised HeLa cells compared to control cells (see Figure 5.38).

The general FG nucleoporin antibody mAb414 stained the nuclear membrane and the cytoplasm in control neurons as shown in Figure 6.11. Nuclear membrane staining using the mAb414 antibody showed a trend towards decline in *C9ORF72* lines compared to control lines as detailed in Figure 6.11 and Figure 6.12A. In addition, cytoplasmic mAb414 levels trended towards a decrease in *C9ORF72* cells in comparison to control cells (see Figure 6.12B). However, in HeLa cells no change in mAb414 staining was observed in poly-GR or -PR treated cells compared to untreated cells (see Figure 5.46).

Ran

Ran provides the energy required for active nucleocytoplasmic transport and regulates the direction of active nucleocytoplasmic transport by establishing a RanGTP gradient between the nucleus and the cytoplasm (Stewart, 2007). Due to its interaction with the nuclear pore it might also influence passive nucleocytoplasmic transport. As shown in Figure 6.13 Ran localised to the nucleus, nuclear membrane and cytoplasm at relatively equal levels and also to neurites at lower levels than in the other compartments in control lines. As depicted in Figure 6.13 and Figure 6.14A and B nucleoplasmic and nuclear membrane levels of Ran did not significantly differ between control and *C9ORF72* neurons. Furthermore, cytoplasmic Ran localisation (see Figure 6.14C) and the nuclear cytoplasmic ratio of RAN levels (see Figure 6.14D) were similar in *C9ORF72* and control neurons. In contrast, in semi-permeabilised HeLa cells poly-PR treatment did lead to a significant reduction of nuclear RAN levels compared to untreated cells (see Figure 5.48).

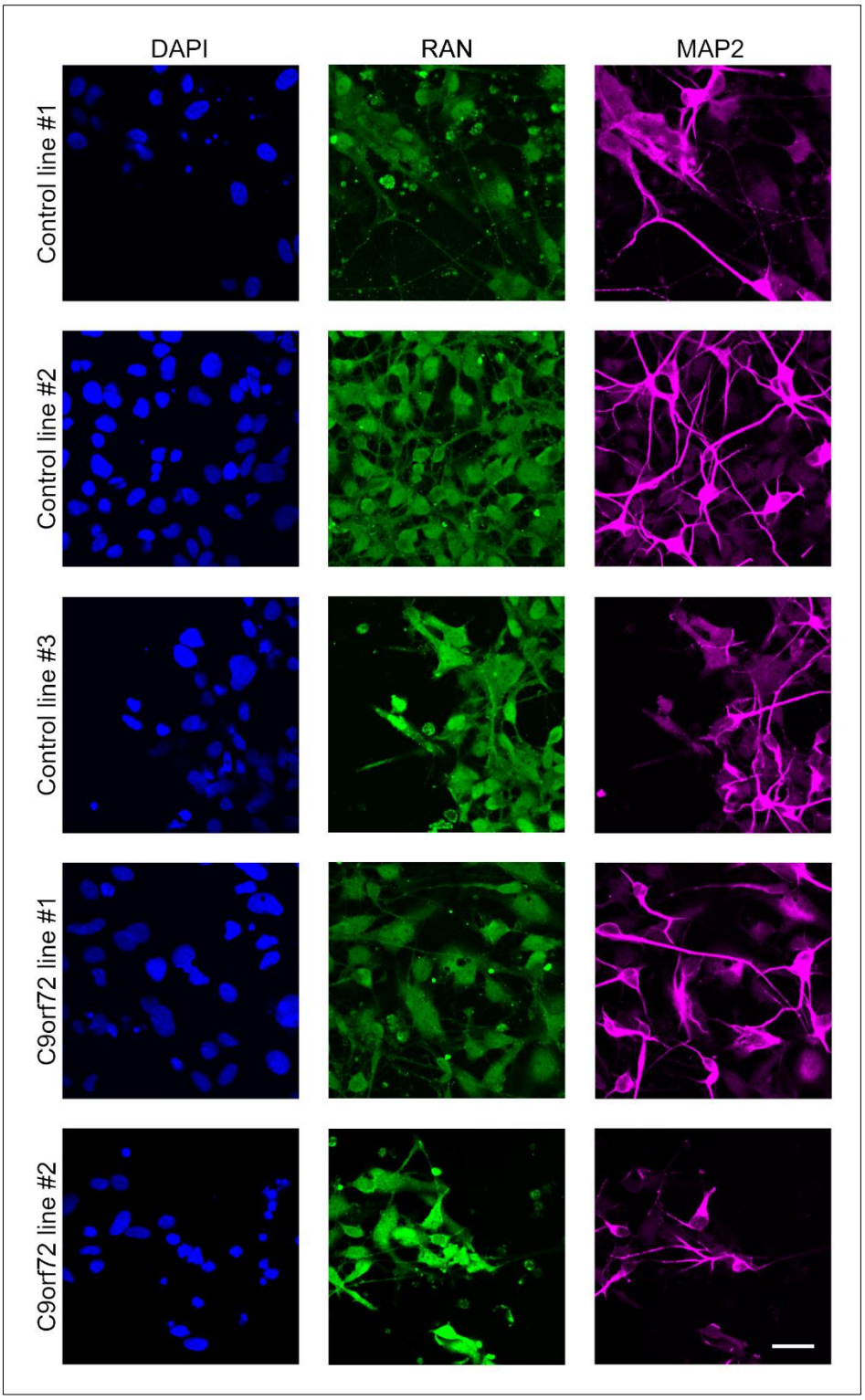

Figure 6.13: Influence of *C9ORF72* mutation on RAN levels. Opera Phenix images of immunofluorescence staining of endogenous RAN in control or *C9ORF72* ALS cells as indicated. Left panel: DAPI. Middle panel: RAN. Right panel: MAP2. Scale bar: 25 µm.

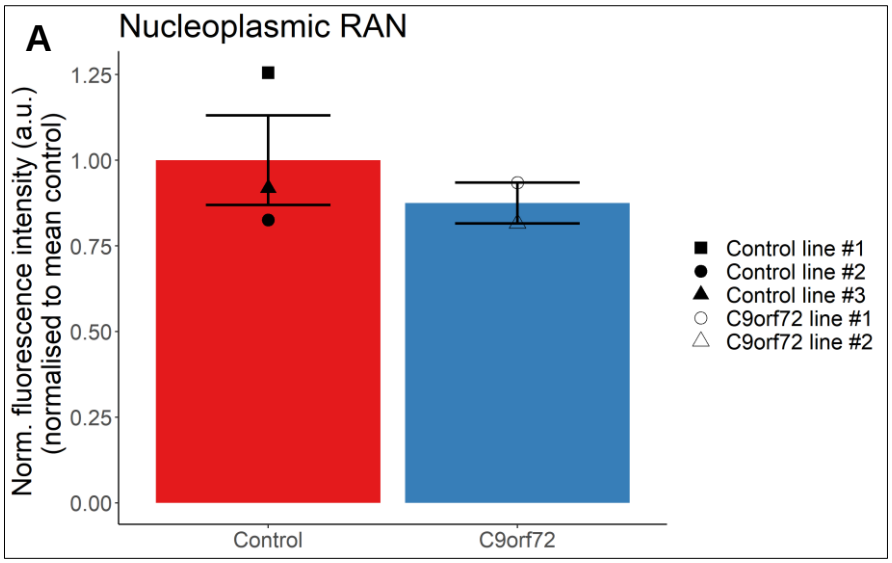
A
Nucleoplasmic RAN
Norm. fluorescence intensity (a.u.)
(normalised to mean control)
1.25
1.00
0.75
0.50
0.25
0.00
Control
C9orf72
Control line #1
Control line #2
Control line #3
C9orf72 line #1
C9orf72 line #2

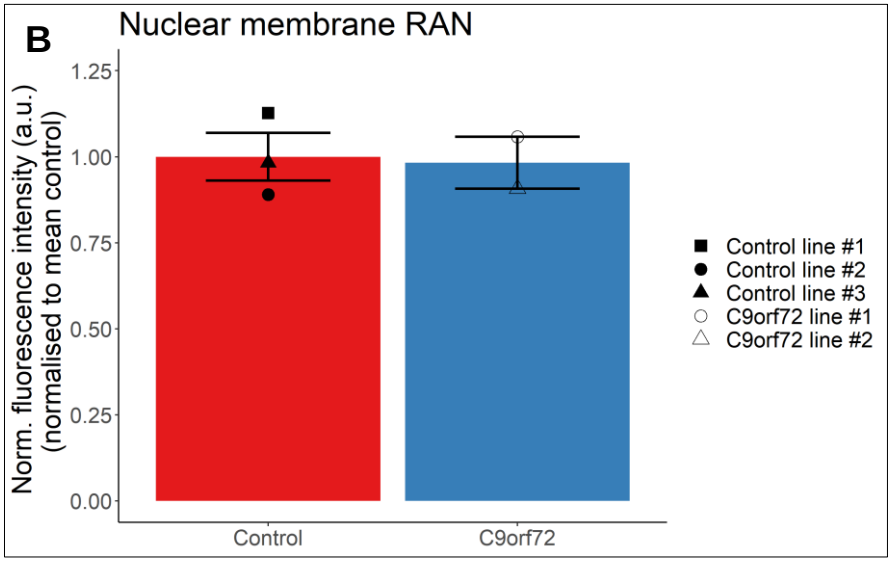
B
Nuclear membrane RAN
Norm. fluorescence intensity (a.u.)
(normalised to mean control)
1.25
1.00
0.75
0.50
0.25
0.00
Control
C9orf72
Control line #1
Control line #2
Control line #3
C9orf72 line #1
C9orf72 line #2

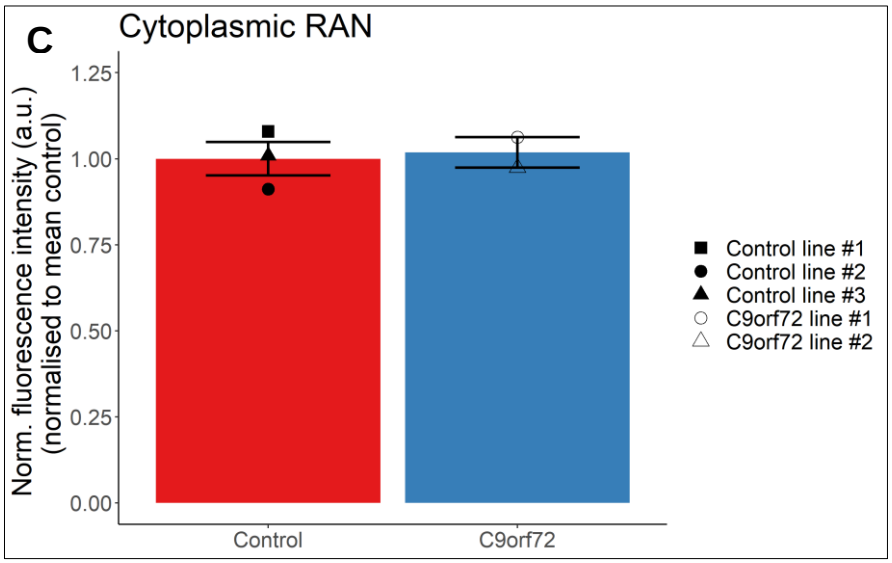
C
Cytoplasmic RAN
Norm. fluorescence intensity (a.u.)
(normalised to mean control)
1.25
1.00
0.75
0.50
0.25
0.00
Control
C9orf72
Control line #1
Control line #2
Control line #3
C9orf72 line #1
C9orf72 line #2

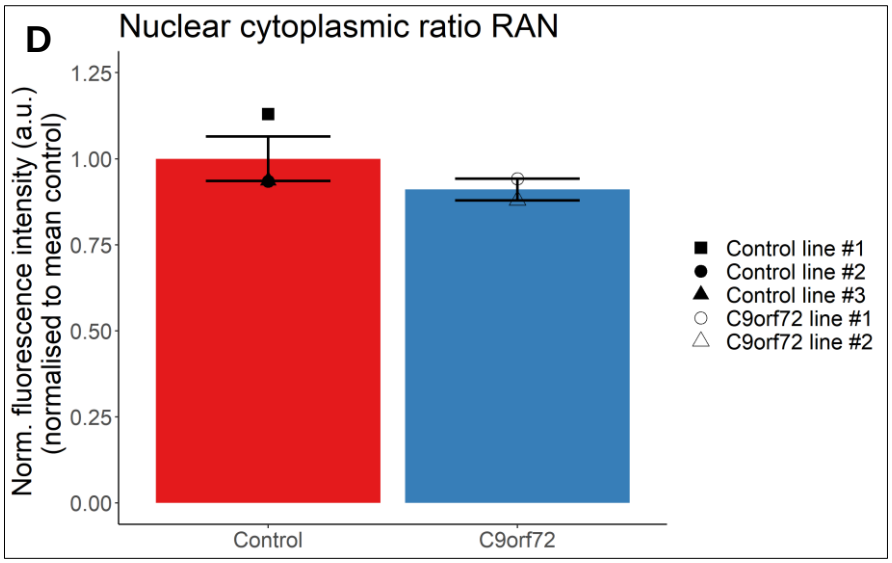

Figure 6.14: Ran levels do not differ between control and *C9ORF72* iPSC-derived neurons. Quantified RAN fluorescence signal normalised to mean of control lines in control or *C9ORF72* ALS iPSC-derived neurons as indicated. A) Nucleoplasmic RAN levels. B) Nuclear membrane RAN levels. C) Cytoplasmic Ran levels. D) Nuclear cytoplasmic Ran ratio. N = 3 control and 2 *C9ORF72* iPSC lines with 1 - 2 differentiations. Means of individual cell line means are depicted in bar chart. Error bars: SEM. Two-sided t-test.

Import receptors

Importin β1 showed localisation to the nucleoplasm, nuclear membrane and cytoplasm in control iPSC lines as depicted in Figure 6.15. Nucleoplasmic importin β1 levels showed a trend towards reduction in *C9ORF72* cell lines compared to control lines with two control lines exhibiting higher nucleoplasmic importin β1 levels than all *C9ORF72* lines as depicted in Figure 6.15 and Figure 6.16A. Nuclear membrane importin β1 levels were trending even more clearly towards a decrease in *C9ORF72* neurons compared to control neurons with all control lines showing increased nuclear membrane importin β1 levels compared to *C9ORF72* lines (see Figure 6.16B). Cytoplasmic importin β1 levels were also lower in *C9ORF72* cells compared to control cells (see Figure 6.16C). In line with these results, poly-PR treated HeLa cells presented with significantly lowered nuclear importin β1 levels compared to untreated cells (see Figure 5.54).

As shown in Figure 6.17 importin α3 was detected in the nucleoplasm and at the nuclear membrane and, at lower levels than in the nucleus, in the cytoplasm. Similarly to importin β1, nucleoplasmic levels of transport receptor importin α3 were trending towards a decrease in *C9ORF72* neurons compared to control neurons as shown in Figure 6.17 and Figure 6.18A. Nuclear membrane and cytoplasmic importin α3 levels were not changed, however, between control and *C9ORF72* cells (see

Figure 6.18B and C). In contrast, both nuclear and nuclear membrane importin α3 levels were decreased in poly-GR and -PR treated HeLa cells (see Figure 5.58).

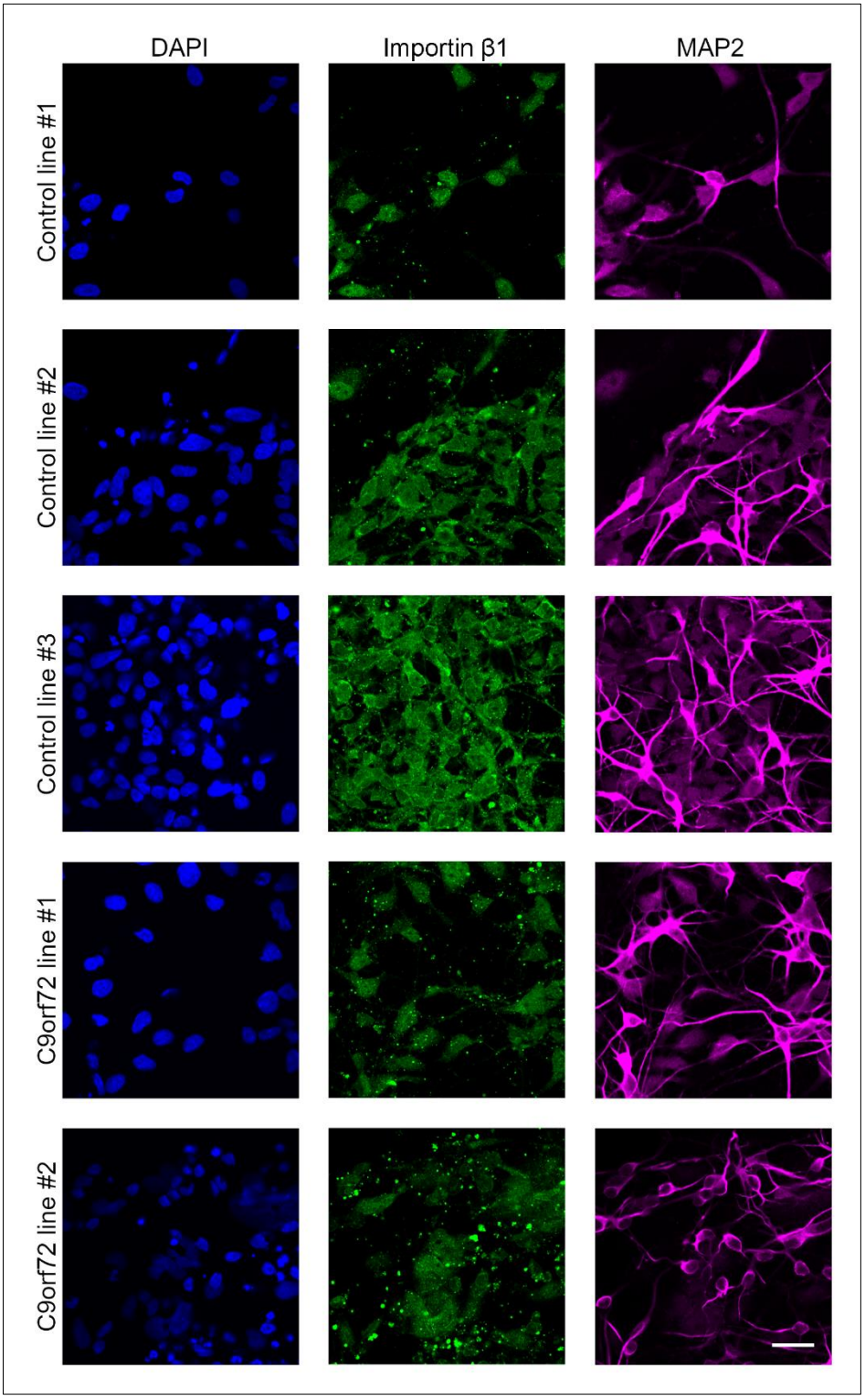

Figure 6.15: Influence of *C9ORF72* mutation on importin β1 localisation. Opera Phenix images of immunofluorescence staining of endogenous importin β1 in control or *C9ORF72* ALS cells as indicated. Left panel: DAPI. Middle panel: importin β1. Right panel: MAP2. Scale bar: 25 µm.

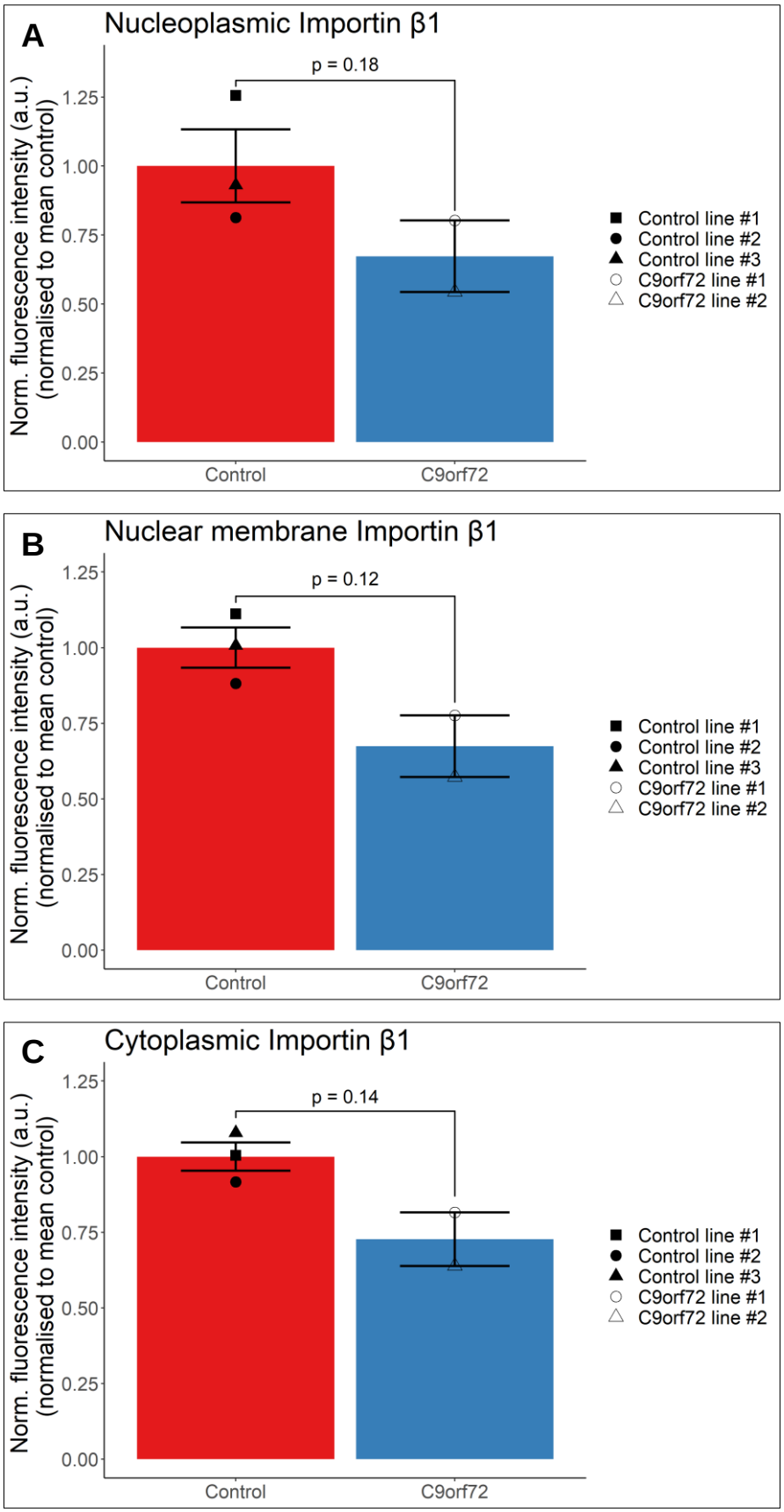

Figure 6.16: Importin β1 levels show trend to decrease in *C9ORF72* iPSC lines. Quantified importin β1 fluorescence signal normalised to mean of control lines in control or *C9ORF72* ALS iPSC-derived neurons as indicated. A) Nucleoplasmic importin β1 levels. B) Nuclear membrane importin β1 levels. C) Cytoplasmic importin

β1 levels. N = 3 control and 2 *C9ORF72* iPSC lines with 1 - 2 differentiations. Means of individual cell line means are shown in bar chart. Error bars: SEM. Two-sided t-test.

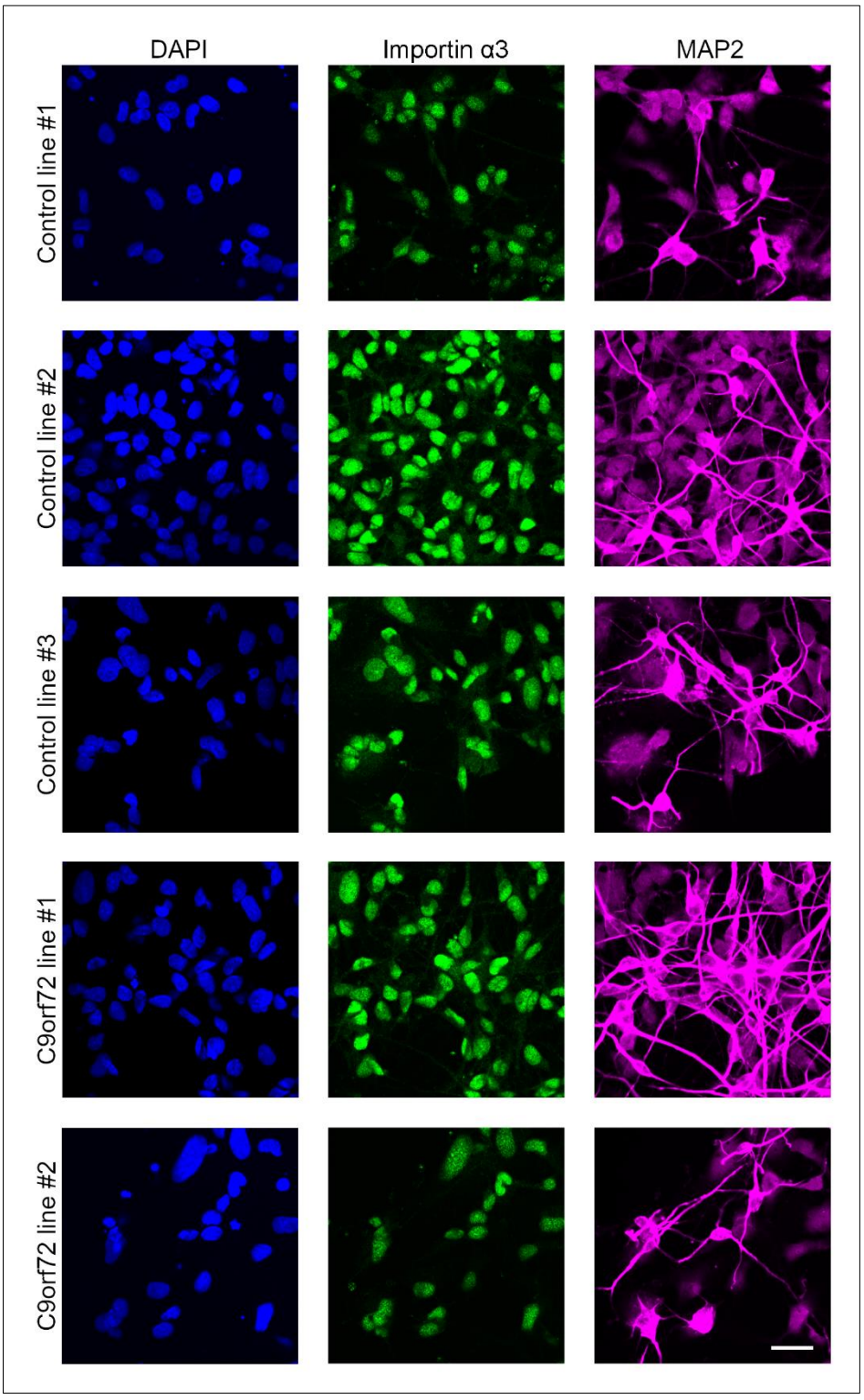

Figure 6.17: Effects of *C9ORF72* mutation on importin α3 localisation. Opera Phenix images of immunofluorescence staining of endogenous importin α3 in control or *C9ORF72* cells as indicated. Left panel: DAPI. Middle panel: Importin α3. Right panel: MAP2. Scale bar: 25 μm.

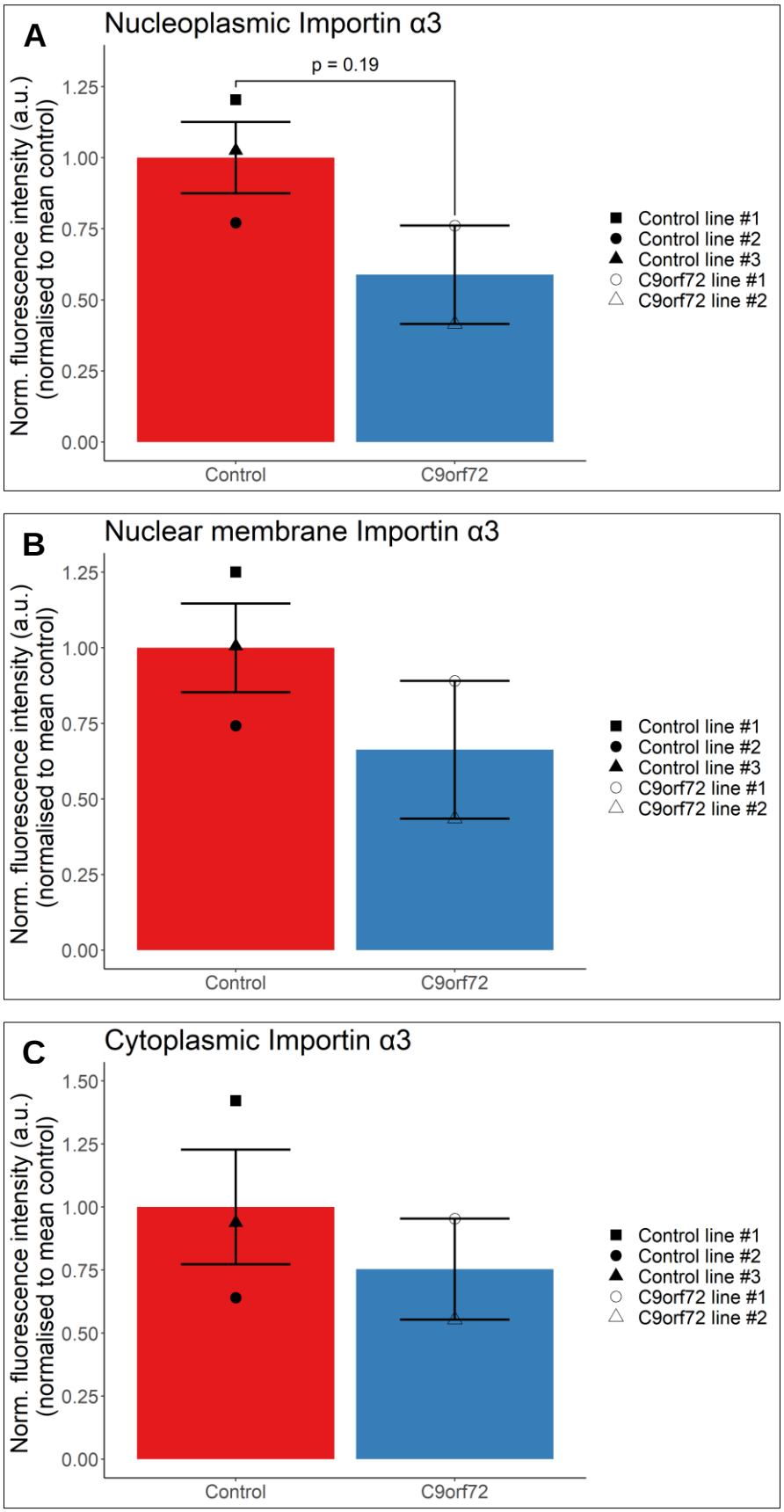

Figure 6.18: Nucleoplasmic importin α3 signal displays trend towards reduction in *C9ORF72* iPSC lines. Quantified importin α3 fluorescence signal normalised to mean of control lines in control or *C9ORF72* ALS iPSC-derived neurons as indicated. A) Nucleoplasmic importin α3 levels. B) Nuclear membrane importin α3 levels. C)

Cytoplasmic importin α3 levels. N = 3 control and 2 *C9ORF72* iPSC lines with 1 - 2 differentiations. Means of individual cell line means are plotted in bar chart. Error bars: SEM. Two-sided t-test.

In summary (as shown in Table 6.1), most tested nucleocytoplasmic transport factors showed a trend towards reduced nuclear localisation in *C9ORF72* neurons compared to control neurons. This was observed for nucleoporin NUP98, FG nucleoporin recognising antibody mAb414, for transport receptors importin β1 and importin α3 and for TDP43. On the other hand, POM121 and Ran levels were not changed between control and *C9ORF72* neurons. Overall, *C9ORF72* mutation did seem to influence the localisation of different nucleoporins and import receptors in iPSC-derived neurons although this did not reach a 95 % confidence level normally defined as an appropriate cut off in statistics.

Transport factor	**Change nucleoplasm**		**Change nuclear membrane**	
	HeLa	iPSC neurons	HeLa	iPSC neurons
Nucleoporins				
NUP98	↓ PR	no change	↓ PR	↓
POM121	↓ PR	no change	↓ PR	no change
MAB414	--	--	no change	↓
Ran regulating factors				
RAN	↓ PR	no change	no change	no change
Import receptors				
Impβ1	↓GR, PR	↓	no change	↓
Impα3	↓GR, PR	↓	↓GR, PR	no change

Table 6.1: Summary of changes in nucleocytoplasmic factor localisation in the presence of *C9ORF72* mutation in iPSC-derived neurons. Comparison with results in poly-GR and -PR treated semi-permeabilised HeLa cells.

6.3 Discussion

6.3.1 Caveats of *C9ORF72* iPSCs

We used *C9ORF72* iPSC-derived cortical neurons to test whether our main findings from the experiments with HeLa cells also occurred in a more disease relevant model. However, there is some debate around the suitability of the *C9ORF72* iPSC model as an accurate model of *C9ORF72* ALS/FTD. One issue is that *C9ORF72* repeat RNA foci were usually detected in these cells (Hawrot et al., 2020) while there was more variability around DPR detection. In most cases only GP was measured (probably for technical reasons) in *C9ORF72* iPSC-derived neurons (Almeida et al., 2013; Coyne et al., 2020; Donnelly et al., 2013; Simone et al., 2018) or no *C9ORF72* DPRs could be detected when using an antibody recognising poly-GP, -GA and -GR (Sareen et al., 2013). When other DPR species such as poly-GR were found levels of these peptide were only slightly higher than in controls (Dafinca et al., 2016; Lopez-Gonzalez et al., 2016). The *C9ORF72* ALS iPSC lines #2 and #3 used in this project showed expression of poly-GA, -GP and -GR although GR levels were rather low (Selvaraj et al., 2018). Poly-GP expression was detected in *C9ORF72* ALS iPSC line #1 (unpublished results).

6.3.2 Potential bias due to different iPSC generation methods used for different cell lines

The iPSC lines used in this project were not all generated using the same methodology. As shown in Table 2.1 *C9ORF72* lines were reprogrammed using retrovirus while one control line was reprogrammed using lentivirus and the remaining two control lines using Sendai virus. Retro- and lentiviruses integrate their genome into the host genome which might lead to mutations while Sendai virus does not integrate into the host genome. As *C9ORF72* lines were all reprogrammed via retrovirus it cannot be excluded that effects observed in this study with these cell lines were caused by additional mutations acquired in the reprogramming process. This would likely not have occurred in control lines reprogrammed by Sendai virus but mutations might also have been introduced in the control line reprogrammed by lentivirus. Thus, the reprogramming bias should be reduced to some extent. Additionally, different cell types were used to create the different iPSC lines. As indicated in Table 2.1 all *C9ORF72* lines were generated from fibroblasts which only divide infrequently. Two control lines were created from keratinocytes and the

remaining control line from lymphoblasts. Keratinocytes and particularly lymphoblasts proliferate at higher rates than fibroblasts which increases the risk of acquiring mutations. These potentially developed mutations in the control lines might also influence nucleocytoplasmic transport or differentiation behaviour and thus results observed might have been caused by unknown mutations. However, as mutations might have been introduced in both control lines and *C9ORF72* lines by different means the overall bias should be balanced out. Reprogrammed stem cells should show the same characteristics, for instance epigenetic stem cell signature, independent of the cell type they have been generated from. However, it cannot be completely ruled out that the original cell type has an influence on cellular mechanisms such as nucleocytoplasmic transport on the iPSCs and differentiated cells generated from it.

6.3.3 Passive nucleocytoplasmic transport in *C9ORF72* iPSC-derived neurons

We found that passive nuclear import of a reporter cargo was significantly increased in *C9ORF72* iPSC lines compared to control lines (see section 6.1) which to our knowledge has not been shown previously and emphasises the disease relevance our findings in poly-GR and -PR treated HeLa cells (see section 4.1). While we cannot determine whether these DPR species were responsible for our results in *C9ORF72* iPSC-derived neurons, poly-GR treatment of a control iPSC line led to increased nuclear translocation of 20 kDa dextran compared to untreated controls (see section 6.1) indicating that poly-GR also influences passive nucleocytoplasmic transport in this cell type.

6.3.4 TDP43 and transport factor localisation in *C9ORF72* iPSC-derived neurons

As we found nucleocytoplasmic transport defects in *C9ORF72* iPSC-derived neurons we wanted to investigate whether these were accompanied by mislocalisation of TDP43 and transport factors (results summarised in Table 6.1). With regards to cytoplasmic TDP43 mislocalisation we found a trend of lower nuclear TDP43 levels but no change in cytoplasmic levels or in the nuclear cytoplasmic ratio (see Figure 6.6). This major pathological characteristic of *C9ORF72* ALS/FTD (Mackenzie and Neumann, 2016) was neither detected in some other *C9ORF72* iPSC-derived neuron studies (Almeida et al., 2013; Coyne et al., 2020; Donnelly et al., 2013).

However, some studies showed reduced nuclear to cytoplasmic ratios of TDP43 in *C9ORF72* ALS iPSC-derived neurons compared to controls (Zhang et al., 2015) or enhanced insoluble TDP43 levels in *C9ORF72* ALS iPSC-derived motor neurons compared to control lines (Seminary et al., 2020).

The nucleoporin NUP98 was trending towards a reduction at nuclear membrane and cytoplasmic levels in *C9ORF72* lines compared to control lines (see Figure 6.8) as was the case for the more general FG nucleoporin marker mAb414 (see Figure 6.12). Levels of the nucleoporin POM121 did not differ between *C9ORF72* and control cells (see Figure 6.10). In a different study NUP98 and POM121 levels were reduced while mAb414 staining was not changed in isolated nuclei of *C9ORF72* ALS iPSC-derived motor neurons (Coyne et al., 2020). This discrepancy in results might be explained by the fact that our neurons were only kept in culture for 14 days due to project time constraints while the neurons of the Coyne study were 32-days old. The authors did not detect any differences in nucleoporin levels in 18-day old neurons either. A caveat of studying age related diseases such as neurodegeneration in iPSC-derived cells is that the reprogramming of somatic cells into stem cells rejuvenates them, for instance at the epigenetic or cellular functionality level (Mertens et al., 2018). Culturing cells for longer time periods might counteract this phenomenon to some extent (Chen et al., 2020) and it is possible that we might have found a significant effect in older neurons.

We did not identify a change in Ran levels between *C9ORF72* iPSC-derived cortical neurons and control neurons (see Figure 6.14). Other investigations observed reduced nuclear cytoplasmic ratios of Ran in *C9ORF72* ALS iPSC-derived motor neurons compared to control cells seemingly due to increased cytoplasmic localisation of RAN (Coyne et al., 2020; J. Lee et al., 2020; Zhang et al., 2015). Again, these neurons were older than ours and had been differentiated into motor neurons while ours were cortical neurons. In *C9ORF72* patient tissue reduced Ran levels have only been detected in spinal motor neurons so far (Vatsavayai et al., 2018; Xiao et al., 2015).

Looking at transport receptors, we found nucleoplasmic, nuclear membrane and cytoplasmic importin β1 (see Figure 6.16) and nucleoplasmic importin α3 (see Figure 6.18) levels trending towards reduction in *C9ORF72* iPSC-derived neurons compared to control neurons. A loss of importin β1 staining was detected in *C9ORF72* ALS spinal cord tissue (Xiao et al., 2015) but this could not be confirmed

in a quantitative histopathology study (Saberi et al., 2018). As previously mentioned, importin α3 was shown to be lost from the nucleus and to concentrate in the cytoplasm of *C9ORF72* ALS/FTD frontal cortex (Solomon et al., 2018).
As at least a trend in nucleocytoplasmic factor mislocalisation was detected in both *C9ORF72* iPSC-derived neurons and in poly-GR/PR treated HeLa cells (see Table 6.1) it might be causative for enhanced passive nucleocytoplasmic transport in *C9ORF72* ALS/FTD.

6.3.5 Differentiation issues

As our cortical neuron differentiation yielded a mixed cellular population one might be concerned that our findings might stem from a difference in differentiation behaviour between control and *C9ORF72* iPSC lines. However, mixed populations were detected in all cell lines used. For example, as depicted in Figure 6.19 levels of the neuroprogenitor marker SOX2 were not significantly different between differentiated *C9ORF72* and control cell populations. Nuclear SOX2 levels varied between cell lines but this variation was not dependent on genotype.

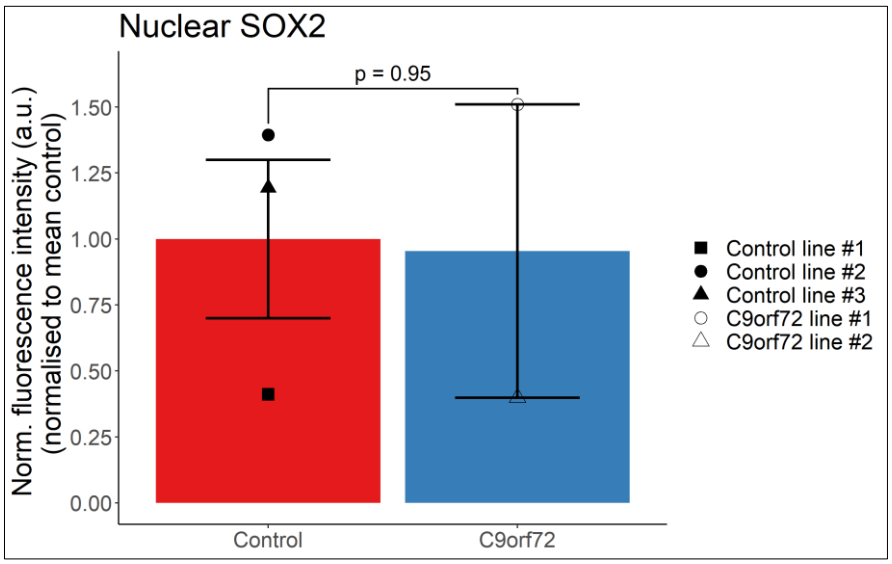

Figure 6.19: Nuclear SOX2 levels are not changed between control and *C9ORF72* iPSC lines. Quantified nuclear SOX2 fluorescence signal normalised to mean of control lines in control or *C9ORF72* ALS cells as indicated. N = 3 control and 2 *C9ORF72* iPSC lines with 1 - 2 differentiations. Means of individual cell line means are shown in bar chart. Error bars: SEM. Two-sided t-test.

Overall, even though we used quite young neurons in our experiments we could observe a significant difference in passive nucleocytoplasmic transport dynamics between *C9ORF72* and control cells. We could also detect trends of changed localisation of nucleoporins and importins between control and *C9ORF72* iPSC lines. These results in iPSC-derived neurons corroborate the disease relevance of our findings regarding affected passive nucleocytoplasmic transport in the context of *C9ORF72* ALS/FTD.

7 Discussion

7.1 Summary of thesis results

In this thesis, I specifically studied the effects of *C9ORF72* dipeptide repeat proteins on passive nucleocytoplasmic transport and on the permeability barrier of the nuclear pore. The main findings are summarised in Figure 7.1. I found that the arginine containing DPRs enhanced passive nuclear import of reporter cargo in HeLa cells. Poly-GR treatment allowed for the passive nuclear entry of cargo above the passive diffusion size limit suggesting that the permeability barrier became less exclusive. Increased passive nuclear import of small reporter cargo was also detected in *C9ORF72* ALS patient iPSC-derived neurons and in control iPSC-derived neurons treated with poly-GR. This confirms that the effects of arginine containing DPRs on passive nucleocytoplasmic transport also occur in human neurons. In addition, the passive diffusion enhancement is not only caused by treatment with exogenous DPR peptides but also by the presence of the *C9ORF72* repat expansion in patient neurons. Furthermore, treatment with poly-GR and -PR resulted in increased passive nuclear export of TDP43 and other nuclear proteins leading to a significant reduction of their nuclear levels in HeLa cells.

Poly-GR and -PR treatment also led to a reduction in nuclear and nuclear membrane localisation of import receptors (including importin β1), FG nucleoporins and regulators of the Ran cycle in HeLa cells which might lead to the observed passive translocation dysfunction. *C9ORF72* ALS patient iPSC-derived neurons showed a trend towards decreased nuclear/nuclear membrane levels of these transport factors. The increased nuclear export of TDP43 might also be caused in part by interference of its binding to RNA by poly-GR and -PR as treatment with RNAse A led to decreased nuclear TDP43 levels.

Enhancement of nuclear TDP43 export by poly-GR or -PR could be partially prohibited by treatment with the FG nucleoporin interactor WGA. This corroborates that reduced nuclear TDP43 levels upon poly-GR and -PR treatment were caused by increased translocation of TDP43 from the nucleus to the cytoplasm and not by increased degeneration of TDP43. It also suggests that poly-GR and -PR interaction with the nuclear pore contributed to these effects. Furthermore, I tested whether importin β1 treatment could inhibit the influence of poly-GR on passive nucleocytoplasmic transport as this was previously shown to reduce passive

diffusion (Kapinos et al., 2017; Lowe et al., 2015). However, in our experimental system addition of importin β1 did not change passive nuclear import of reporter cargo or nuclear export of TDP43 in poly-GR/PR treated cells. Thus, I established in this PhD project that passive nucleocytoplasmic transport is affected in *C9ORF72* ALS/FTD and shed light on possible mechanisms causing this passive nucleocytoplasmic transport deregulation.

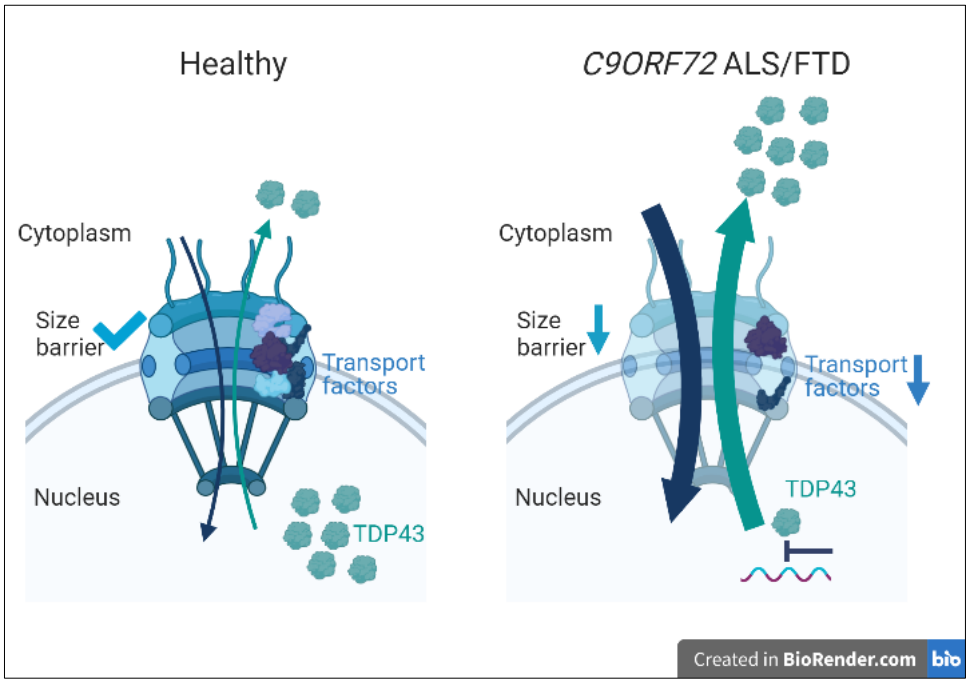

Figure 7.1: Summary of main thesis results. Passive nuclear import and export are increased in *C9ORF72* ALS/FTD models. This might be caused by mislocalisation of nucleocytoplasmic transport factors and reduced RNA binding of nuclear RNA binding proteins (such as TDP43) in the presence of arginine containing DPRs. Created with BioRender.com.

7.2 Effects of poly-GR and -PR on active versus passive nucleocytoplasmic transport

As discussed in section 1.4.2 macromolecules of a size ≤ 40 kDa can passively diffuse through the nuclear pore while this diffusion is restricted for larger molecules by the permeability barrier formed by FG nucleoporins (Mohr et al., 2009; Timney et al., 2016). According to the selective phase model the permeability barrier is created by a 3D meshwork hydrogel of FG nucleoporins which can only be traversed by small cargo (Ribbeck and Görlich, 2001). Larger molecules therefore have to be actively transported through the nuclear pore. As described in section 1.4.3 active nucleocytoplasmic transport is mediated by transport receptors such as importins, exportins or transportins binding their cargo via a nuclear localisation signal (NLS) or

a nuclear export signal (NES) (Wing et al., 2022). Transport receptor interaction with FG nucleoporins locally interrupt FG-FG connections thereby allowing passage of larger cargo (Schmidt and Görlich, 2016). Direction of nucleocytoplasmic transport is regulated via the Ran gradient. A higher concentration of RanGTP in the nucleus than in the cytoplasm promotes cargo binding of exportins and cargo release from importins (Stewart, 2007).

Arginine containing *C9ORF72* DPRs have opposite effects on active and passive nucleocytoplasmic transport. A number of studies have shown poly-GR and -PR to inhibit active nucleocytoplasmic transport including importin α/β, importin β1 and transportin mediated transport (Hayes et al., 2020; Hutten et al., 2020; Shi et al., 2017; K. Zhang et al., 2018). On the other hand, my PhD study together with another study (Hayes et al., 2020) have found passive nucleocytoplasmic transport to be enhanced by poly-GR and -PR. Mechanisms resulting in these opposing effects are discussed in this section.

7.2.1 Interaction of poly-GR and -PR with transport receptors

Poly-GR and/or -PR have been shown to directly bind to importin β1, importins α1 and α3 and transportin 1 *in vitro* (Hayes et al., 2020; Hutten et al., 2020). It is proposed that this interaction interferes with the binding of import receptors to their cargo, as has been shown for importin β1 (Hayes et al., 2020), and thereby leads to an impairment of active nucleocytoplasmic transport. Furthermore, this interaction might also hinder binding of import receptors to nucleoporins. I have shown in this thesis that nuclear and nuclear membrane levels of importin β1, importin α1 and α3 are reduced in HeLa cells upon poly-GR and -PR treatment. This reduction might be mediated by direct binding of poly-GR and -PR to these importins. It would be interesting to conduct double immunofluorescence studies for arginine containing DPRs and importins to detect potential co-localisation. *C9ORF72* ALS iPSC-derived neurons also exhibited a trend towards a decrease of nuclear and nuclear membrane levels of importin β1 and nuclear levels of importin α3. Reduced importin β1 levels are also found in *C9ORF72* ALS patient spinal motor neurons compared to controls (Xiao et al., 2015). However, in a different study no change in importin β1 localisation is detected between *C9ORF72* ALS patient motor neurons in spinal cord and motor cortex and control motor neurons (Saberi et al., 2018). Importin β1

reduction may vary between patients or may be dynamic which might not always be detectable in end stage tissue. Mislocalisation of importins α1 and α3 is detected in a *Drosophila* model expressing poly-GR where these importins aggregate into cytoplasmic punctae. GR does not localise to these punctae. However, in the cortex of a poly-GR mouse model importin α1 and α5 are present in GR inclusions (Cook et al., 2020). In *C9ORF72* FTD patient frontal cortex importin α3 is reduced in the nucleus and increased in the cytoplasm with cytoplasmic importin α3 occasionally colocalising with GR aggregates (Solomon et al., 2018). It is, therefore, possible that importins are recruited into poly-GR aggregates or that GR-importin interactions promote their co-aggregation. In summary, poly-GR/-PR interaction with importins might hinder their interaction with cargo and with the nuclear pore which might lead to their mislocalisation and active nucleocytoplasmic transport defects. Importin mislocalisation and reduced interaction with FG nucleoporins might also be the reason for the observed enhancement of passive nucleocytoplasmic transport upon poly-GR and -PR treatment. Reduction of importin β1 from the nuclear pore by RanGTP treatment increases passive diffusion through the nuclear pore in cells (Kapinos et al., 2017). Importin β1 might thus contribute to the permeability barrier when bound to FG nucleoporins. In my PhD project however, exogenous importin β1 treatment has not changed passive nucleocytoplasmic transport dynamics in poly-GR/PR treated cells. It is possible that importin β1 has not been successfully replenished in my experiments because of the low concentration used (see also section 5.6) or because arginine containing DPRs have not been sufficiently washed away and interact with importin β1 inhibiting its binding to the nuclear pore. Further studies are therefore needed to investigate whether reduced importin β1 interaction with FG nucleoporins contributes to passive nucleocytoplasmic transport enhancement by poly-GR and -PR.

7.2.2 Interaction of poly-GR and -PR with nucleoporins

Poly-PR directly binds to the FG domains of Nup54 and Nup98 *in vitro* (Shi et al., 2017). Mass spectrometry studies also identify nucleoporins including FG nucleoporins 54, 98 and 153 as interactors of poly-GR or-PR (Boeynaems et al., 2017; Hayes et al., 2020; Y. Lin et al., 2016). I have found nuclear pore levels of NUP98, POM121 and RanBP2 but not NUP54 or NUP153 to be reduced upon poly-

PR treatment in HeLa cells. NUP98 nuclear pore levels have also shown a trend towards reduction in *C9ORF72* ALS iPSC-derived neurons in my study. Again, it is unclear whether a direct interaction of poly-PR with these nucleoporins leads to their removal from the nuclear pore and further co-immunofluorescence studies are warranted. However, in a poly-GR mouse model NUP98 localises to GR inclusions (Cook et al., 2020) and staining with a general FG nucleoporin antibody colocalises with PR inclusion staining in a PR mouse model (Y. J. Zhang et al., 2019). Furthermore, NUP62 is present in GR aggregates in cells over-expressing GR (Gleixner et al., 2022). Poly-GR/PR interaction with nucleoporins might therefore lead to nucleoporin mislocalisation. In the poly-GR mouse model TDP43 is mislocalised to the cytoplasm (Cook et al., 2020) and TDP43 is also found in the NUP62-GR inclusions in cells suggesting that these mislocalisations interfere with nucleocytoplasmic transport (Gleixner et al., 2022). Active nucleocytoplasmic transport might be impaired by the loss of FG nucleoporin binding partners for transport receptors. Passive nucleocytoplasmic transport might be enhanced as mislocalisation of FG nucleoporins could reduce the restrictiveness of the permeability barrier. For instance, Nup98 has been shown to be essential for the nuclear pore's permeability barrier (Hülsmann et al., 2012). Nucleoporin mislocalisation might also directly contribute to *C9ORF72* toxicity as Nup62 overexpression recues a neurodegenerative eye phenotype in a *Drosophila* model expressing GGGGCC repeats (Gleixner et al., 2022).

7.2.3 Influence of poly-GR and -PR on liquid-liquid phase separation of transport factors

Liquid-liquid phase separation in cells describes the process of demixing of two liquid phases. In cells, proteins or RNAs might separate into concentrated liquid droplets with the surrounding liquid phase (such as the cytoplasm) now devoid of the separated proteins or RNAs (Alberti and Dormann, 2019). This allows for the formation of membraneless organelles, for example (Aguzzi and Altmeyer, 2016). Most proteins undergoing liquid-liquid phase separation contain disordered domains (Brangwynne et al., 2015; Taylor et al., 2016). Aberrant liquid-liquid phase separation or liquid to solid phase transition can lead to protein aggregation (Alberti and Dormann, 2019) which might be cytotoxic. Poly-GR and -PR have been shown to induce aberrant liquid-liquid phase separation of RNA binding proteins such as

hnRNP-A1, TIA-1, NPM1 and FUS (Boeynaems et al., 2017; Lee et al., 2016; Odeh and Shorter, 2020; White et al., 2019). They also have this effect on transportin 1, importin α3 and the importin α3/β1 complex. This leads to reduced solubility and enhanced condensation of these import receptors. Transportin 1 also shows decreased recovery after photobleaching upon poly-GR treatment indicating reduced mobility (Hutten et al., 2020). These changes might further interfere with the interaction of import receptors with their cargo and with FG nucleoporins. Restricted mobility might also impede transport receptor translocation through the nuclear pore. Interaction of poly-PR with Nup54 and Nup98 FG domains might stabilise these in a more rigid polymeric state compared to a monomeric state (Shi et al., 2017). The higher rigidity might favour passive translocation of small molecules through the nuclear pore as the meshwork is less flexible constantly allowing for the passage of small molecules. Melting of this meshwork by transport receptors might be impaired, however. A different study has created synthetic FG hydrogels modelling those within the nuclear pore. Poly-GR and -PR have shown strong binding to these hydrogels. Furthermore, binding of poly-PR to the FG hydrogel has inhibited binding of importin β1 to the FG hydrogel. In addition, the poly-PR-FG hydrogel interaction has rendered importin β1 more immobile not allowing for translocation through the gel (Friedman et al., 2022). These findings indicate that poly-GR and -PR can also bind FG nucleoporins when in a hydrogel state and that this binding interferes with importin β1 binding to FG domains. This is likely to counteract active translocation through the nuclear pore but might also enhance passive diffusion as discussed above. The interaction of poly-GR/PR with FG nucleoporins might also interfere with FG-FG domain binding weakening the permeability barrier of the nuclear pore which might lead to enhanced passive diffusion.

7.2.4 Impact of poly-GR and -PR on nucleocytoplasmic transport of TDP43

Nuclear import of reporter cargo containing full length TDP43 has been shown to be reduced upon poly-GR treatment in cells (Hutten et al., 2020). TDP43 is imported by the importin α/β complex (Nishimura et al., 2010). Poly-GR interaction with this complex likely interferes with FG nucleoporin binding of the importin complex and might also lead to aberrant liquid-liquid phase separation of these importins as discussed in sections 7.2.1 and 7.2.3. TDP43 likely exits the nucleus via passive

diffusion (Archbold et al., 2018; Ederle et al., 2018; Pinarbasi et al., 2018). I have found that the passive nuclear export of TDP43 is increased upon poly-GR or -PR treatment. This is likely mediated by poly-GR/PR interaction with nucleoporins and potentially transport receptors changing the characteristics of the nuclear pore's permeability barrier as discussed in sections 7.2.1, 7.2.2 and 7.2.3. Thus, TDP43 is exported from the nucleus at increased levels in the presence of arginine containing DPRs compared to physiological conditions but is also re-imported into the nucleus at reduced levels. This likely results in the cytoplasmic mislocalisation of TDP43 which is the pathology hallmark of *C9ORF72* ALS/FTD (Mackenzie and Neumann, 2016). Poly-GR and -PR promote aberrant phase separation of TDP43 leading to its condensation and reducing its solubility (Cook et al., 2020; Hutten et al., 2020) which might contribute to aggregation of mislocalised cytoplasmic TDP43. It might also reduce TDP43 interaction with RNA in the nucleus possibly making it more prone to be exported from the nucleus. Thus, impairment of nucleocytoplasmic transport of TDP43 by poly-GR and -PR likely contributes to TDP43's cytoplasmic mislocalisation and aggregation in *C9ORF72* ALS/FTD.

In summary, arginine containing *C9ORF72* DPRs inhibit active and enhance passive nucleocytoplasmic transport, but these effects are likely linked and caused by the same mechanisms possibly simultaneously.

7.3 Further factors involved in nucleocytoplasmic transport defects

Nucleocytoplasmic transport dysfunction is a common phenomenon in cells exposed to stressors. In this discussion section it will be discussed in the context of neurodegeneration outside of *C9ORF72* ALS/FTD, ageing and cellar stress such as oxidative stress.

7.3.1 Nucleocytoplasmic transport defects in neurodegeneration

Alzheimer's disease (AD) and FTLD-tau

Both of these diseases constitute a form of dementia and share the pathological characteristic of cytoplasmic accumulations of phosphorylated tau known as neurofibrillary tangles (Deture and Dickson, 2019; Mackenzie and Neumann, 2016). In early electron microscopy studies of AD patient frontal lobes, these neurofibrillary tangles have been shown to associate with the nuclear lamina and with nuclear

pores (Metuzals et al., 1988). This raises the possibility that these tangles interfere with nucleocytoplasmic transport. Indeed, Ran transport receptor NTF2 accumulates in the cytoplasm of AD patient hippocampus. However, this is observed both in neurons containing neurofibrillary tangles and in neurons without them (Sheffield et al., 2006). Importin α1 also mislocalises to the cytoplasm in AD hippocampus but this similarly does not correlate with neurofibrillary tangles (H. gon Lee et al., 2006). On the other hand, NUP62 and NUP98 are detected within perinuclear tau aggregates in AD patient brain and in the hippocampus of an FTD-tau mouse model. NUP98 and recombinant human phospho-tau directly interact in *in vitro* experiments which could mediate this co-aggregation. In fact, NUP98 induces tau aggregation *in vitro* (Eftekharzadeh et al., 2018). In addition to nucleoporin mislocalisation, a reduction in nuclear Ran levels is detected in AD patient and FTD-tau mouse model hippocampus. This decrease in the nuclear cytoplasmic ratio of Ran can be induced in primary neurons by addition of phosphorylated tau isolated from AD brain. This treatment also reduces active nuclear import of reporter cargo in these cells in live experiments (Eftekharzadeh et al., 2018). This indicates that the Ran deficit might impair active nucleocytoplasmic transport and is directly caused by pathological tau. In line with this, repression of pathological tau expression restores the Ran gradient in an FTD-tau mouse model. Furthermore, knockdown of *Nup98* in the primary neuron model treated with pathological tau also normalises the Ran gradient (Eftekharzadeh et al., 2018). This suggests that NUP98 aggregates cause nucleocytoplasmic transport defects via toxic gain of function. In summary, pathological tau seems to be the mediator of nucleocytoplasmic transport impairments in AD and FTLD-tau.

Huntington’s disease (HD)

Huntington’s disease is an inherited neurodegenerative disease characterised by motor dysfunction, cognitive decline and psychiatric symptoms. This is mediated by degeneration in the striatum and basal ganglia. The cause of HD is a CAG repeat expansion in the *Huntingtin* gene which leads to the production of a Huntingtin (HTT) protein with an N-terminal poly-glutamine (polyQ) expansion which is prone to aggregation (McColgan and Tabrizi, 2018; Ross and Tabrizi, 2011).

PolyQ aggregates in cells have been shown to contain NUP62 in a proteomics study indicating that a polyQ tract might lead to mislocalisation of nucleoporins (Suhr et al.,

2001). Indeed, in HD mouse models nucleoporins NUP62, NUP88 and GLE1 as well as RANGAP1 are found in mutant HTT inclusions. NUP62 and RANGAP1 are also mislocalised in cortex and striatum of HD patients (Gasset-Rosa et al., 2017; Grima et al., 2017) and in HD patient iPSC-derived neurons (Grima et al., 2017). In addition, an HD mouse model shows increased levels of nuclear mRNA compared to controls (Gasset-Rosa et al., 2017) indicating an mRNA export defect. A reporter cargo shows enhanced cytoplasmic localisation in HD iPSC-derived neurons compared to controls indicative of reduced active nuclear import. This is also accompanied by a reduction in the nuclear cytoplasmic ratio of Ran. These deficits also occur in primary neurons expressing mutant HTT (Grima et al., 2017) which suggests that they are mediated by mutant HTT. Nucleoporin, Ran and RANGAP1 mislocalisation in HD, therefore, seems to cause impaired nucleocytoplasmic transport. Further contributors to these deficits might be the identification of RANGAP1 and RNA export factor RAE 1 as interaction partners of mutant HTT, and not physiological HTT, in a mass spectrometry screen (Hosp et al., 2015). In addition, non-mutant HTT binds to nuclear basket nucleoporin TPR (Cornett et al., 2005) which is important for protein and mRNA export (see also section 1.4.4). This interaction is lost with mutant HTT as shown in an HD mouse model (Havel et al., 2011) which might lead to reduced mRNA export and nuclear accumulation of mutant HTT. These studies clearly show that nucleocytoplasmic transport deficits are a part of HD pathology. Overall, these deficits are a common theme across neurodegeneration suggesting that neurons might be particularly susceptible to these.

7.3.2 Impairments of nucleocytoplasmic transport in physiological ageing

In differentiated non-dividing cells (such as neurons) nuclear pores are highly stable complexes (D'Angelo et al., 2009; Savas et al., 2012; Toyama et al., 2013) with some nucleoporins only being exchanged in the time frame of months or years (Toyama et al., 2019). This means that any damage to nuclear pores can easily accumulate over time and makes ageing a risk factor for this damage (D'Angelo et al., 2009). Nuclear pore composition does change with age in rat brains and *C. elegans* myotubes (D'Angelo et al., 2009; Savas et al., 2012; Toyama et al., 2013) which might influence nuclear pore function. In the ageing rat dentate gyrus nuclear

pores are lost (Fifková et al., 1987) while nuclear pore numbers are not changed in the ageing rat hippocampus (Topple et al., 1990). This suggests that there might be regional vulnerability for age related nuclear pore function impairments. Nuclei isolated from brains of ageing rats or mice more frequently allow for the entry of 70 kDa dextran, which exceeds the size limit of the permeability barrier of the nuclear pore, than nuclei from younger animals (D'Angelo et al., 2009; Gillon et al., 2020). Cytoplasmic proteins also mislocalise to the nucleus in aged nuclei (D'Angelo et al., 2009). This suggests that the permeability barrier becomes less restrictive with age which might compromise nuclear integrity and function. FG nucleoporin staining is reduced in leaky nuclei compared to restrictive nuclei (D'Angelo et al., 2009) which might increase permeability of the nuclear pore. Expression of transport receptors including CAS, importin α2, RanBP1 and RanBP17 is reduced in human neurons or fibroblasts upon ageing (Mertens et al., 2015; Pujol et al., 2002). In line with this, reporter cargo transported by importin α/β shows less nuclear localisation upon export inhibition in old fibroblasts compared to young ones (Pujol et al., 2002). This suggests that reduced expression of import receptors correlates with decreased nuclear import rates which might further affect nuclear composition and function. As ageing is a risk factor for neurodegeneration age related nucleocytoplasmic defects might be exacerbated in neurodegenerative disorders (Coyne and Rothstein, 2022).

7.3.3 Cellular stress related nucleocytoplasmic transport dysfunction

As introduced in section 1.3.3 cellular stress mediated translation arrest leads to the formation of cytoplasmic stress granules. These contain untranslated ribonucleoprotein complexes and other proteins involved in stress granule formation. Several transport factors have been found to localise to stress granules in human cell lines upon oxidative stress, heat shock or hyperosmosis. These include transport receptors importins α1 and β1, transportin 1 and exportin 1, Ran, and nucleoporins POM121, NUP205, NUP50 and NUP88 (Chang and Tarn, 2009; Fujimura et al., 2010; Jain et al., 2016; Kodiha et al., 2008, 2004; Mahboubi et al., 2013; Markmiller et al., 2018; Vanneste et al., 2022; K. Zhang et al., 2018). This can also be accompanied by a disruption of the Ran gradient or the nuclear retention of importins (Kodiha et al., 2008, 2004; Miyamoto et al., 2004; K. Zhang et al., 2018). These mislocalisations likely cause nucleocytoplasmic transport defects as importin α/β

mediated nuclear import and exportin 1 mediated nuclear export are reduced upon cellular stress (Crampton et al., 2009; Kodiha et al., 2008, 2004; Vanneste et al., 2022; K. Zhang et al., 2018). Localisation of transport factors to stress granules might also be protective, however. Transportin 1 localisation to stress granules supports the cellular stress response (Chang and Tarn, 2009). In addition, importin α1 localisation to stress granules improves cellular survival (Fujimura et al., 2010). On the other hand, inhibition of stress granule formation restores the Ran gradient and importin α/β mediated nuclear import in a human cell line (K. Zhang et al., 2018). However, a different study shows that repression of stress granule formation does not rescue importin α/β mediated nuclear import in a human cell line (Vanneste et al., 2022). The differing results between the two studies are surprising because both used very similar approaches to inhibit stress granule formation. Potentially, the effects are cell line or cargo dependent but even though different fluorescent proteins were used for the reporter cargo the NLS was the same. In any case, cellular stress (possibly via the formation of stress granules) can cause nucleocytoplasmic transport defects. Interestingly, nucleoporins from “leaky” nuclei of ageing rat brains show signs of oxidative damage (D’Angelo et al., 2009) linking age related and cellular stress related nucleocytoplasmic transport defects. Stress granules formed upon expression of poly-GR or -PR in human cell lines have been shown to contain Ran or NUP62 (Gleixner et al., 2022; K. Zhang et al., 2018). Inhibition of stress granule formation restores the Ran gradient in *C9ORF72* ALS iPSC-derived neurons and rescues a neurodegenerative eye phenotype in a *Drosophila* model expressing the *C9ORF72* repeat expansion (K. Zhang et al., 2018). Thus, *C9ORF72* ALS/FTD nucleocytoplasmic transport defects might therefore be partly mediated via stress granules.

In summary, nucleocytoplasmic transport impairments occur upon several cellular insults such as neurodegeneration, ageing and cellular stress. Mechanisms leading to these impairments can be shared and linked defects might be exacerbated if several insults occur simultaneously such as neurodegeneration coupled with general ageing phenotypes.

7.4 Therapeutics targeting nucleocytoplasmic transport

The current main strategy for future *C9ORF72* ALS/FTD treatment is the usage of antisense oligonucleotides (ASOs). These target sequences adjacent to the GGGGCC repeat in the *C9ORF72* pre-mRNA. This leads to the degradation of repetitive RNA while maintaining physiological C9ORF72 protein levels. A phase 1a/2b clinical trial testing an ASO compound (FOCUS-C9) is currently under way (ClinicalTrials.gov Identifier: NCT04931862). Biogen has recently completed a phase 1 trial of a different ASO agent in *C9ORF72* ALS patients (ClinicalTrials.gov Identifier: NCT03626012). However, Biogen has stated that no clinical benefit could be detected (Press release by Biogen, 2022). As the development of different ALS/FTD therapeutics is still required therapeutic strategies in the context of nucleocytoplasmic transport are discussed here.

7.4.1 Nuclear export inhibitors

Several compounds inhibiting exportin 1 mediated nuclear export have been described as anticancer agents (Kosyna and Depping, 2018). They might also have potential for the treatment of ALS. The exportin 1 inhibitor KPT 335 rescues aberrant nuclear morphology in primary cortical neurons overexpressing ALS mutant TDP43 or the C terminal fragment of TDP43 often present in TDP43 aggregates. It also increases the cell viability of these cells. Furthermore, motor deficits in *Drosophila* larvae expressing ALS mutant TDP43 are ameliorated by KPT 335 and another exportin 1 inhibitor KPT 276 (Chou et al., 2018). In primary motor neurons expressing ALS mutant *PFN1* KPT 276 rescues cytoplasmic mislocalisation of TDP43 and axonal growth defects (Giampetruzzi et al., 2019). Furthermore, KPT 276 reduces nuclear import defects in salivary gland cells of *Drosophila* larvae expressing *C9ORF72* repeat. In addition, it alleviates neurodegeneration in the eye of a *Drosophila* model expressing the *C9ORF72* repeat expansion (Zhang et al., 2015). Therefore, inhibition of exportin 1 might be beneficial in different types of ALS. A phase 1 clinical trial of oral exportin KPT 350 (BIIB100) in ALS patients has been completed by Biogen (ClinicalTrials.gov Identifier: NCT03945279). However, Biogen has recently announced the termination of a development agreement with Karyopharm (Alzforum, 2022) suggesting a negative outcome.

7.4.2 Inhibition of *C9ORF72* repeat RNA export

In addition to targeted degradation of *C9ORF72* repeat RNA, another potential therapeutic strategy is to inhibit the nuclear export of *C9ORF72* repeat RNA. A study has found that nuclear export of *C9ORF72* repeat RNA is dependent on serine/arginine- rich splicing factor 1 (SRSF1) in a mouse neuroblastoma cell line expressing sense or antisense repeats and in *C9ORF72* ALS induced motor neurons. SRSF1 mediates *C9ORF72* repeat RNA export by interaction with the RNA export NXF1 complex which translocates through the nuclear pore (see also 1.4.4). Partial knockdown of *SRSF1* reduces *C9ORF72* repeat containing RNA export, but not export of RNA where the repeat has been spliced out, in a mouse neuroblastoma cell line expressing *C9ORF72* repeats and in *C9ORF72* ALS induced motor neurons. Depletion of SRSF1 further leads to a reduction of poly-GP and -GA levels in a mouse neuroblastoma cell line expressing sense or antisense repeats and of poly-GP in *C9ORF72* motor neurons and in *Drosophila* expressing *C9ORF72* repeats. Levels of other DPR species have not been assessed in this study. Partial *SRSF1* knockdown has been found to be neuroprotective. It enhances survival of *C9ORF72* induced neurons co-cultured with *C9ORF72* induced astrocytes. Furthermore, knockdown of *Srsf1* in *Drosophila* expressing *C9ORF72* repeats ameliorates motor impairments and eye neurodegeneration (Hautbergue et al., 2017). Additionally, partial *SRSF1* knockdown in *C9ORF72* ALS induced motor neurons changes their transcriptome signature. Expression of 90 transcripts, whose expression has been increased or decreased compared to control induced motor neurons, is reverted back (or near) to physiological levels by SRSF1 depletion in *C9ORF72* neurons (Castelli et al., 2021). This suggests that *SRSF1* knockdown interferes directly and indirectly with *C9ORF72* toxicity. Interestingly, reduction in DPR levels seems to be sufficient for the neuroprotective effects mediated by SRSF1 depletion as cells still display nuclear *C9ORF72* RNA foci (Hautbergue et al., 2017).

7.4.3 Use of import receptors as therapeutics

Import receptors have been shown to not only interact with cargo for translocation through the nuclear pore but to also act as chaperones and disaggregases for them (Odeh et al., 2022). For instance, transportin 1 can inhibit and reverse fibrillisation of its import cargo FUS and ALS related FUS mutants *in vitro* (Guo et al., 2018).

Transportin 1 also impedes and reverts liquid-liquid phase separation of FUS which possibly functions as an early prevention of FUS aggregation *in vitro* and in cells (Guo et al., 2018; Hofweber et al., 2018; Nanaura et al., 2021; Qamar et al., 2018; Yoshizawa et al., 2018). This is probably achieved by transportin 1 not only interacting with the NLS of FUS but also with other regions mediating phase separation (Yoshizawa et al., 2018). TDP43's import receptor complex importin α/β1 also inhibits and reverses its condensation and fibrillisation *in vitro* including TDP43 ALS mutants (Guo et al., 2018; Hutten et al., 2020).

As arginine containing DPRs interact with several import receptors and impede their function as discussed in section 7.2.1 it might be possible that import receptors can convey their chaperone function on these DPRs. Arginine containing DPRs can themselves undergo liquid-liquid phase separation (Solomon et al., 2021). Importin β1 and transportin 1 but not importin α3 inhibit RNA mediated poly-GR condensation *in vitro* when GR and import receptor levels are equimolar. When poly-GR is in excess relative to import receptor levels it promotes their condensation and inhibits nuclear import of TDP43 (Hutten et al., 2020). Similarly, poly-PR does not interfere with inhibition of FUS condensation by transportin 1 when at equimolar levels with transportin 1. However, poly-PR does repress the chaperone function of transportin 1 for FUS when at a higher concentration than transportin 1 (Nanaura et al., 2021). The increase of TDP43 condensation and insolubility by poly-GR can also be inhibited by equimolar concentrations (relative to GR) of importin β1, transportin 1 and importin α3/β1 but not by importin α3 alone (Hutten et al., 2020). At elevated levels import receptors can thereby shield arginine containing DPRs from damaging interactions. As import receptors are reduced or present in inclusions in *C9ORF72* ALS/FTD raising their cellular levels might be therapeutic (Pasha et al., 2021). Compounds acting at several levels to enhance import receptor could be developed. They could trigger RanGTP-importin disassembly in the nucleus to promote importin turnover or directly increase import receptor activity. Agents raising the affinity of import receptors towards their cargo or cargo of therapeutic interest might also be beneficial. Increasing import receptor expression via small molecules or gene therapy could also be a therapeutic strategy. It remains to be seen whether any of these approaches will prove beneficial in ALS/FTD or other neurodegenerative diseases. However, as nucleocytoplasmic transport defects likely contribute to

toxicity in (*C9ORF72*) ALS/FTD and neurodegeneration in general, targeting this indispensable cellular pathway could have therapeutic potential.

7.5 Conclusion

Nucleocytoplasmic transport is dysregulated in *C9ORF72* ALS/FTD. Active nucleocytoplasmic transport is inhibited while passive nucleocytoplasmic transport is increased as I have shown in this thesis. Arginine containing *C9ORF72* dipeptide repeats can mediate this enhancement of passive nucleocytoplasmic transport likely by interfering with the localisation and/or function of a variety transport factors including FG nucleoporins and transport receptors. The increase of passive nuclear export of TDP43 by poly-GR and -PR could be the cause of its cytoplasmic mislocalisation in conjunction with its impaired nuclear import in *C9ORF72* ALS/FTD. This suggests a direct contribution of enhanced passive nucleocytoplasmic transport to disease pathology. A less restrictive permeability barrier of the nuclear pore could also lead to general mislocalisation of nuclear proteins to the cytoplasm and vice versa affecting nuclear and cytoplasmic function and integrity. This might also be involved in *C9ORF72* toxicity. Targeting nucleocytoplasmic transport defects could therefore have therapeutic potential, possibly including the re-establishment of physiological passive nucleocytoplasmic transport rates.

References

Abe, K., Aoki, M., Tsuji, S., Itoyama, Y., Sobue, G., Togo, M., Hamada, C., Tanaka, M., Akimoto, M., Nakamura, K., Takahashi, F., Kondo, K., Yoshino, H., Abe, K., Tsuji, S., Itoyama, Y., Sobue, G., Togo, M., Hamada, C., Sasaki, H., Yabe, I., Doi, S., Warita, H., Imai, T., Ito, H., Fukuchi, M., Osumi, E., Wada, M., Nakano, I., Morita, M., Ogata, K., Maruki, Y., Ito, K., Kano, O., Yamazaki, M., Takahashi, Y., Ishiura, H., Ogino, M., Koike, R., Ishida, C., Uchiyama, T., Mizoguchi, K., Obi, T., Watanabe, H., Atsuta, N., Aiba, I., Taniguchi, A., Sawada, H., Hazama, T., Fujimura, H., Kusaka, H., Kunieda, T., Kikuchi, H., Matsuo, H., Ueyama, H., Uekawa, K., Tanaka, M., Akimoto, M., Ueda, M., Murakami, A., Sumii, R., Kudou, T., Nakamura, K., Morimoto, K., Yoneoka, T., Hirai, M., Sasaki, K., Terai, H., Natori, T., Matsui, H., Kotani, K., Yoshida, K., Iwasaki, T., Takahashi, F., Kondo, K., Yoshino, H., 2017. Safety and efficacy of edaravone in well defined patients with amyotrophic lateral sclerosis: a randomised, double-blind, placebo-controlled trial. Lancet Neurol 16, 505–512. https://doi.org/10.1016/S1474-4422(17)30115-1

Abe, K., Itoyama, Y., Sobue, G., Tsuji, S., Aoki, M., Doyu, M., Hamada, C., Kondo, K., Yoneoka, T., Akimoto, M., Yoshino, H., 2014. Confirmatory double-blind, parallel-group, placebo-controlled study of efficacy and safety of edaravone (MCI-186) in amyotrophic lateral sclerosis patients. Amyotroph Lateral Scler Frontotemporal Degener 15, 610–617. https://doi.org/10.3109/21678421.2014.959024

Abo-Rady, M., Kalmbach, N., Pal, A., Schludi, C., Janosch, A., Richter, T., Freitag, P., Bickle, M., Kahlert, A.K., Petri, S., Stefanov, S., Glass, H., Staege, S., Just, W., Bhatnagar, R., Edbauer, D., Hermann, A., Wegner, F., Sterneckert, J.L., 2020. Knocking out C9ORF72 Exacerbates Axonal Trafficking Defects Associated with Hexanucleotide Repeat Expansion and Reduces Levels of Heat Shock Proteins. Stem Cell Reports 14, 390–405. https://doi.org/10.1016/j.stemcr.2020.01.010

Abramzon, Y.A., Fratta, P., Traynor, B.J., Chia, R., 2020. The Overlapping Genetics of Amyotrophic Lateral Sclerosis and Frontotemporal Dementia. Front Neurosci 14. https://doi.org/10.3389/FNINS.2020.00042

Aditi, Folkmann, A.W., Wente, S.R., 2015. Cytoplasmic hGle1A regulates stress granules by modulation of translation. Mol Biol Cell 26, 1476. https://doi.org/10.1091/MBC.E14-11-1523

Aguzzi, A., Altmeyer, M., 2016. Phase Separation: Linking Cellular Compartmentalization to Disease. Trends Cell Biol 26, 547–558. https://doi.org/10.1016/J.TCB.2016.03.004

Aizawa, H., Teramoto, S., Hideyama, T., Kato, H., Terashi, H., Suzuki, Y., Kimura, T., Kwak, S., 2022. Nuclear pore destruction and loss of nuclear TDP-43 in FUS mutation-related amyotrophic lateral sclerosis motor neurons. J Neurol Sci 436, 120187. https://doi.org/10.1016/J.JNS.2022.120187

Aizawa, H., Yamashita, T., Kato, H., Kimura, T., Kwak, S., 2019. Impaired Nucleoporins Are Present in Sporadic Amyotrophic Lateral Sclerosis Motor Neurons that Exhibit Mislocalization of the 43-kDa TAR DNA-Binding Protein. Journal of Clinical Neurology 15, 62–67. https://doi.org/10.3988/JCN.2019.15.1.62

Aksu, M., Trakhanov, S., Görlich, D., 2016. Structure of the exportin Xpo4 in complex with RanGTP and the hypusine-containing translation factor eIF5A. Nat Commun 7. https://doi.org/10.1038/NCOMMS11952

Aksu, M., Trakhanov, S., Rodriguez, A.V., Görlich, D., 2019. Structural basis for the nuclear import and export functions of the biportin Pdr6/Kap122. J Cell Biol 218, 1839–1852. https://doi.org/10.1083/JCB.201812093

Aladesuyi Arogundade, O., Nguyen, S., Leung, R., Wainio, D., Rodriguez, M., Ravits, J., 2021. Nucleolar stress in C9orf72 and sporadic ALS spinal motor neurons precedes TDP-43 mislocalization. Acta Neuropathol Commun 9, 26. https://doi.org/10.1186/s40478-021-01125-6

Alberti, S., Dormann, D., 2019. Liquid–Liquid Phase Separation in Disease. https://doi.org/10.1146/annurev-genet-112618-043527 53, 171–194. https://doi.org/10.1146/ANNUREV-GENET-112618-043527

Alcázar-Román, A.R., Tran, E.J., Guo, S., Wente, S.R., 2006. Inositol hexakisphosphate and Gle1 activate the DEAD-box protein Dbp5 for nuclear mRNA export. Nat Cell Biol 8, 711–716. https://doi.org/10.1038/NCB1427

Al-Chalabi, A., Andersen, P.M., Chandran, S., Chio, A., Corcia, P., Couratier, P., Danielsson, O., de Carvalho, M., Desnuelle, C., Grehl, T., Grosskreutz, J., Holmøy, T., Ingre, C., Karlsborg, M., Kleveland, G., Christoph Koch, J., Koritnik,

B., KuzmaKozakiewicz, M., Laaksovirta, H., Ludolph, A., McDermott, C., Meyer, T., Mitre Ropero, B., Mora Pardina, J., Nygren, I., Petri, S., Povedano Panades, M., Salachas, F., Shaw, P., Silani, V., Staaf, G., Svenstrup, K., Talbot, K., Tysnes, O.B., van Damme, P., van der Kooi, A., Weber, M., Weydt, P., Wolf, J., Hardiman, O., van den Berg, L.H., 2017. July 2017 ENCALS statement on edaravone. Amyotroph Lateral Scler Frontotemporal Degener 18, 471–474. https://doi.org/10.1080/21678421.2017.1369125

Almeida, S., Gascon, E., Tran, H., Chou, H.J., Gendron, T.F., DeGroot, S., Tapper, A.R., Sellier, C., Charlet-Berguerand, N., Karydas, A., Seeley, W.W., Boxer, A.L., Petrucelli, L., Miller, B.L., Gao, F.-B., 2013. Modeling key pathological features of frontotemporal dementia with C9ORF72 repeat expansion in iPSC-derived human neurons. Acta Neuropathol 126, 385–399. https://doi.org/10.1007/s00401-013-1149-y

An, H., Skelt, L., Notaro, A., Highley, J.R., Fox, A.H., Bella, V. la, Buchman, V.L., Buchman, V.L., Shelkovnikova, T.A., Shelkovnikova, T.A., Shelkovnikova, T.A., 2019. ALS-linked FUS mutations confer loss and gain of function in the nucleus by promoting excessive formation of dysfunctional paraspeckles. Acta Neuropathol Commun 7, 1–14. https://doi.org/10.1186/S40478-019-0658-X/FIGURES/5

Andersen, K.R., Onischenko, E., Tang, J.H., Kumar, P., Chen, J.Z., Ulrich, A., Liphardt, J.T., Weis, K., Schwartz, T.U., 2013. Scaffold nucleoporins Nup188 and Nup192 share structural and functional properties with nuclear transport receptors. Elife 2013. https://doi.org/10.7554/ELIFE.00745

Aoki, Y., Manzano, R., Lee, Y., Dafinca, R., Aoki, M., Douglas, A.G.L., Varela, M.A., Sathyaprakash, C., Scaber, J., Barbagallo, P., Vader, P., Mäger, I., Ezzat, K., Turner, M.R., Ito, N., Gasco, S., Ohbayashi, N., el Andaloussi, S., Takeda, S., Fukuda, M., Talbot, K., Wood, M.J.A., 2017. C9orf72 and RAB7L1 regulate vesicle trafficking in amyotrophic lateral sclerosis and frontotemporal dementia. Brain 140, 887–897. https://doi.org/10.1093/brain/awx024

Arai, T., Hasegawa, M., Akiyama, H., Ikeda, K., Nonaka, T., Mori, H., Mann, D., Tsuchiya, K., Yoshida, M., Hashizume, Y., Oda, T., 2006. TDP-43 is a component of ubiquitin-positive tau-negative inclusions in frontotemporal lobar degeneration and amyotrophic lateral sclerosis. Biochem Biophys Res Commun 351, 602–611. https://doi.org/10.1016/J.BBRC.2006.10.093

Archbold, H.C., Jackson, K.L., Arora, A., Weskamp, K., Tank, E.M.-H., Li, X., Miguez, R., Dayton, R.D., Tamir, S., Klein, R.L., Barmada, S.J., 2018. TDP43 nuclear export and neurodegeneration in models of amyotrophic lateral sclerosis and frontotemporal dementia. Sci Rep 8, 4606. https://doi.org/10.1038/s41598-018-22858-w

Arciniegas, D.B., 2006. New-onset bipolar disorder in late life: A case of mistaken identity. American Journal of Psychiatry 163, 198–203. https://doi.org/10.1176/APPI.AJP.163.2.198/ASSET/IMAGES/LARGE/Q18F1.JPEG

Arts, G.J., Fornerod, M., Mattaj, I.W., 1998. Identification of a nuclear export receptor for tRNA. Curr Biol 8, 305–314. https://doi.org/10.1016/S0960-9822(98)70130-7

Ash, P.E.A., Bieniek, K.F., Gendron, T.F., Caulfield, T., Lin, W.L., DeJesus-Hernandez, M., van Blitterswijk, M.M., Jansen-West, K., Paul, J.W., Rademakers, R., Boylan, K.B., Dickson, D.W., Petrucelli, L., 2013. Unconventional Translation of C9ORF72 GGGGCC Expansion Generates Insoluble Polypeptides Specific to c9FTD/ALS. Neuron 77, 639–646. https://doi.org/10.1016/J.NEURON.2013.02.004

Atanasio, A., Decman, V., White, D., Ramos, M., Ikiz, B., Lee, H.-C., Siao, C.-J., Brydges, S., LaRosa, E., Bai, Y., Fury, W., Burfeind, P., Zamfirova, R., Warshaw, G., Orengo, J., Oyejide, A., Fralish, M., Auerbach, W., Poueymirou, W., Freudenberg, J., Gong, G., Zambrowicz, B., Valenzuela, D., Yancopoulos, G., Murphy, A., Thurston, G., Lai, K.-M.V., 2016. C9orf72 ablation causes immune dysregulation characterized by leukocyte expansion, autoantibody production and glomerulonephropathy in mice. Sci Rep 6, 23204. https://doi.org/10.1038/srep23204

Ayala, Y.M., Zago, P., D'Ambrogio, A., Xu, Y.-F., Petrucelli, L., Buratti, E., Baralle, F.E., 2008. Structural determinants of the cellular localization and shuttling of TDP-43. J Cell Sci 121, 3778–85. https://doi.org/10.1242/jcs.038950

Babinchak, W.M., Haider, R., Dumm, B.K., Sarkar, P., Surewicz, K., Choi, J.K., Surewicz, W.K., 2019. The role of liquid-liquid phase separation in aggregation of the TDP-43 low-complexity domain. Journal of Biological Chemistry 294, 6306–6317. https://doi.org/10.1074/JBC.RA118.007222/ATTACHMENT/E9E1A18D-8AF4-4AC4-8577-DC1BD8A68396/MMC1.PDF

Bachi, A., Braun, I.C., Rodrigues, J.P., Panté, N., Ribbeck, K., von Kobbe, C., Kutay, U., Wilm, M., Görlich, D., Carmo-Fonseca, M., Izaurralde, E., 2000. The C-terminal domain of TAP interacts with the nuclear pore complex and promotes export of specific CTE-bearing RNA substrates. RNA 6, 136–158. https://doi.org/10.1017/S1355838200991994

Baker, M., Mackenzie, I.R., Pickering-Brown, S.M., Gass, J., Rademakers, R., Lindholm, C., Snowden, J., Adamson, J., Sadovnick, A.D., Rollinson, S., Cannon, A., Dwosh, E., Neary, D., Melquist, S., Richardson, A., Dickson, D., Berger, Z., Eriksen, J., Robinson, T., Zehr, C., Dickey, C.A., Crook, R., McGowan, E., Mann, D., Boeve, B., Feldman, H., Hutton, M., 2006. Mutations in progranulin cause tau-negative frontotemporal dementia linked to chromosome 17. Nature 2006 442:7105 442, 916–919. https://doi.org/10.1038/nature05016

Baldwin, K.R., Godena, V.K., Hewitt, V.L., Whitworth, A.J., 2016. Axonal transport defects are a common phenotype in Drosophila models of ALS. Hum Mol Genet 25, 2378–2392. https://doi.org/10.1093/HMG/DDW105

Balendra, R., Isaacs, A.M., 2018. C9orf72-mediated ALS and FTD: multiple pathways to disease. Nat Rev Neurol 1. https://doi.org/10.1038/s41582-018-0047-2

Barmada, S.J., Skibinski, G., Korb, E., Rao, E.J., Wu, J.Y., Finkbeiner, S., 2010. Cytoplasmic Mislocalization of TDP-43 Is Toxic to Neurons and Enhanced by a Mutation Associated with Familial Amyotrophic Lateral Sclerosis. Journal of Neuroscience 30, 639–649. https://doi.org/10.1523/JNEUROSCI.4988-09.2010

Bateman, A., Bennett, H.P.J., 2009. The granulin gene family: from cancer to dementia. BioEssays 31, 1245–1254. https://doi.org/10.1002/BIES.200900086

Bayliss, R., Littlewood, T., Stewart, M., 2000. Structural basis for the interaction between FxFG nucleoporin repeats and importin-beta in nuclear trafficking. Cell 102, 99–108. https://doi.org/10.1016/S0092-8674(00)00014-3

Bayliss, R., Littlewood, T., Strawn, L.A., Wente, S.R., Stewart, M., 2002. GLFG and FxFG Nucleoporins Bind to Overlapping Sites on Importin-β. Journal of Biological Chemistry 277, 50597–50606. https://doi.org/10.1074/JBC.M209037200

Beck, J., Poulter, M., Hensman, D., Rohrer, J.D., Mahoney, C.J., Adamson, G., Campbell, T., Uphill, J., Borg, A., Fratta, P., Orrell, R.W., Malaspina, A., Rowe, J., Brown, J., Hodges, J., Sidle, K., Polke, J.M., Houlden, H., Schott, J.M., Fox,

N.C., Rossor, M.N., Tabrizi, S.J., Isaacs, A.M., Hardy, J., Warren, J.D., Collinge, J., Mead, S., 2013. Large C9orf72 hexanucleotide repeat expansions are seen in multiple neurodegenerative syndromes and are more frequent than expected in the UK population. Am J Hum Genet 92, 345–353. https://doi.org/10.1016/j.ajhg.2013.01.011

Beck, M., Hurt, E., 2017. The nuclear pore complex: understanding its function through structural insight. Nat Rev Mol Cell Biol 18, 73–89. https://doi.org/10.1038/NRM.2016.147

Becker, L.A., Huang, B., Bieri, G., Ma, R., Knowles, D.A., Jafar-Nejad, P., Messing, J., Kim, H.J., Soriano, A., Auburger, G., Pulst, S.M., Taylor, J.P., Rigo, F., Gitler, A.D., 2017. Therapeutic reduction of ataxin-2 extends lifespan and reduces pathology in TDP-43 mice. Nature 2017 544:7650 544, 367–371. https://doi.org/10.1038/nature22038

Beddow, A.L., Richards, S.A., Orem, N.R., Macara, I.G., 1995. The Ran/TC4 GTPase-binding domain: identification by expression cloning and characterization of a conserved sequence motif. Proc Natl Acad Sci U S A 92, 3328–3332. https://doi.org/10.1073/PNAS.92.8.3328

Bellingham, M.C., 2011. A Review of the Neural Mechanisms of Action and Clinical Efficiency of Riluzole in Treating Amyotrophic Lateral Sclerosis: What have we Learned in the Last Decade? CNS Neurosci Ther 17, 4–31. https://doi.org/10.1111/J.1755-5949.2009.00116.X

Belzil, V. v., Bauer, P.O., Gendron, T.F., Murray, M.E., Dickson, D., Petrucelli, L., 2014. Characterization of DNA hypermethylation in the cerebellum of c9FTD/ALS patients. Brain Res 1584, 15–21. https://doi.org/10.1016/J.BRAINRES.2014.02.015

Belzil, V. v., Bauer, P.O., Prudencio, M., Gendron, T.F., Stetler, C.T., Yan, I.K., Pregent, L., Daughrity, L., Baker, M.C., Rademakers, R., Boylan, K., Patel, T.C., Dickson, D.W., Petrucelli, L., 2013. Reduced C9orf72 gene expression in c9FTD/ALS is caused by histone trimethylation, an epigenetic event detectable in blood. Acta Neuropathol 126, 895–905. https://doi.org/10.1007/s00401-013-1199-1

Ben-Ari, Y., Brody, Y., Kinor, N., Mor, A., Tsukamoto, T., Spector, D.L., Singer, R.H., Shav-Tal, Y., 2010. The life of an mRNA in space and time. J Cell Sci 123, 1761. https://doi.org/10.1242/JCS.062638

Bensimon, G., Lacomblez, L., Meininger, V., 1994. A controlled trial of riluzole in amyotrophic lateral sclerosis. ALS/Riluzole Study Group. N Engl J Med 330, 585–591. https://doi.org/10.1056/NEJM199403033300901

Birsa, N., Ule, A.M., Garone, M.G., Tsang, B., Mattedi, F., Andrew Chong, P., Humphrey, J., Jarvis, S., Pisiren, M., Wilkins, O.G., Nosella, M.L., Devoy, A., Bodo, C., de la Fuente, R.F., Fisher, E.M.C., Rosa, A., Viero, G., Forman-Kay, J.D., Schiavo, G., Fratta, P., 2021. FUS-ALS mutants alter FMRP phase separation equilibrium and impair protein translation. Sci Adv 7, 8660–8681. https://doi.org/10.1126/SCIADV.ABF8660/SUPPL_FILE/SCIADV.ABF8660_TABLES_S1_TO_S3.ZIP

Bischoff, F.R., Krebber, H., Smirnova, E., Dong, W., Ponstingl, H., 1995. Co-activation of RanGTPase and inhibition of GTP dissociation by Ran-GTP binding protein RanBP1. EMBO J 14, 705–715. https://doi.org/10.1002/J.1460-2075.1995.TB07049.X

Boeynaems, S., Bogaert, E., Kovacs, D., Konijnenberg, A., Timmerman, E., Volkov, A., Guharoy, M., de Decker, M., Jaspers, T., Ryan, V.H., Janke, A.M., Baatsen, P., Vercruysse, T., Kolaitis, R.-M., Daelemans, D., Taylor, J.P., Kedersha, N., Anderson, P., Impens, F., Sobott, F., Schymkowitz, J., Rousseau, F., Fawzi, N.L., Robberecht, W., van Damme, P., Tompa, P., van den Bosch, L., 2017. Phase Separation of C9orf72 Dipeptide Repeats Perturbs Stress Granule Dynamics. Mol Cell 65, 1044-1055.e5. https://doi.org/10.1016/J.MOLCEL.2017.02.013

Boeynaems, S., Bogaert, E., Michiels, E., Gijselinck, I., Sieben, A., Jovičić, A., de Baets, G., Scheveneels, W., Steyaert, J., Cuijt, I., Verstrepen, K.J., Callaerts, P., Rousseau, F., Schymkowitz, J., Cruts, M., van Broeckhoven, C., van Damme, P., Gitler, A.D., Robberecht, W., van den Bosch, L., 2016. Drosophila screen connects nuclear transport genes to DPR pathology in c9ALS/FTD. Sci Rep 6, 20877. https://doi.org/10.1038/srep20877

Boeynaems, S., Gitler, A.D., 2018. Pour Some Sugar on TDP(-43). Mol Cell 71, 649–651. https://doi.org/10.1016/J.MOLCEL.2018.08.032

Bonner, W.M., 1975. Protein migration into nuclei. I. Frog oocyte nuclei in vivo accumulate microinjected histones, allow entry to small proteins, and exclude large proteins. J Cell Biol 64, 421–430. https://doi.org/10.1083/JCB.64.2.421

Bono, F., Cook, A.G., Grünwald, M., Ebert, J., Conti, E., 2010. Nuclear import mechanism of the EJC component Mago-Y14 revealed by structural studies of importin 13. Mol Cell 37, 211–222. https://doi.org/10.1016/J.MOLCEL.2010.01.007

Bora, E., 2017. Meta-analysis of social cognition in amyotrophic lateral sclerosis. Cortex 88, 1–7. https://doi.org/10.1016/J.CORTEX.2016.11.012

Boulikas, T., 1994. Putative nuclear localization signals (NLS) in protein transcription factors. J Cell Biochem 55, 32–58. https://doi.org/10.1002/JCB.240550106

Bowden, H.A., Dormann, D., 2016. Altered mRNP granule dynamics in FTLD pathogenesis. J Neurochem 138 Suppl 1, 112–133. https://doi.org/10.1111/JNC.13601

Brangwynne, C.P., Tompa, P., Pappu, R. v., 2015. Polymer physics of intracellular phase transitions. Nature Physics 2015 11:11 11, 899–904. https://doi.org/10.1038/nphys3532

Brettschneider, J., del Tredici, K., Toledo, J.B., Robinson, J.L., Irwin, D.J., Grossman, M., Suh, E., van Deerlin, V.M., Wood, E.M., Baek, Y., Kwong, L., Lee, E.B., Elman, L., McCluskey, L., Fang, L., Feldengut, S., Ludolph, A.C., Lee, V.M.Y., Braak, H., Trojanowski, J.Q., 2013. Stages of pTDP-43 pathology in amyotrophic lateral sclerosis. Ann Neurol 74, 20. https://doi.org/10.1002/ANA.23937

Budini, M., Romano, V., Avendaño-Vázquez, S.E., Bembich, S., Buratti, E., Baralle, F.E., 2012. Role of selected mutations in the Q/N rich region of TDP-43 in EGFP-12xQ/N-induced aggregate formation. Brain Res 1462, 139–150. https://doi.org/10.1016/J.BRAINRES.2012.02.031

Burberry, A., Suzuki, N., Wang, J.-Y., Moccia, R., Mordes, D.A., Stewart, M.H., Suzuki-Uematsu, S., Ghosh, S., Singh, A., Merkle, F.T., Koszka, K., Li, Q.-Z., Zon, L., Rossi, D.J., Trowbridge, J.J., Notarangelo, L.D., Eggan, K., 2016. Loss-of-function mutations in the C9ORF72 mouse ortholog cause fatal autoimmune disease. Sci Transl Med 8, 347ra93. https://doi.org/10.1126/scitranslmed.aaf6038

Burley, S., Beccano-Kelly, D.A., Talbot, K., Llana, O.C., Wade-Martins, R., 2022. Hyperexcitability in young iPSC-derived C9ORF72 mutant motor neurons is associated with increased intracellular calcium release. Sci Rep 12, 7378. https://doi.org/10.1038/S41598-022-09751-3

Burrell, J.R., Kiernan, M.C., Vucic, S., Hodges, J.R., 2011. Motor Neuron dysfunction in frontotemporal dementia. Brain 134, 2582–2594. https://doi.org/10.1093/BRAIN/AWR195

Cairns, N.J., Neumann, M., Bigio, E.H., Holm, I.E., Troost, D., Hatanpaa, K.J., Foong, C., White, C.L., Schneider, J.A., Kretzschmar, H.A., Carter, D., Taylor-Reinwald, L., Paulsmeyer, K., Strider, J., Gitcho, M., Goate, A.M., Morris, J.C., Mishra, M., Kwong, L.K., Stieber, A., Xu, Y., Forman, M.S., Trojanowski, J.Q., Lee, V.M.Y., Mackenzie, I.R.A., 2007. TDP-43 in familial and sporadic frontotemporal lobar degeneration with ubiquitin inclusions. American Journal of Pathology 171, 227–240. https://doi.org/10.2353/ajpath.2007.070182

Callister, J.B., Ryan, S., Sim, J., Rollinson, S., Pickering-Brown, S.M., 2016. Modelling C9orf72 dipeptide repeat proteins of a physiologically relevant size. Hum Mol Genet 25, 5069–5082. https://doi.org/10.1093/hmg/ddw327

Campos, E.I., Fillingham, J., Li, G., Zheng, H., Voigt, P., Kuo, W.H.W., Seepany, H., Gao, Z., Day, L.A., Greenblatt, J.F., Reinberg, D., 2010. The program for processing newly synthesized histones H3.1 and H4. Nat Struct Mol Biol 17, 1343–1351. https://doi.org/10.1038/NSMB.1911

Campos-Melo, D., Hawley, Z.C.E., Droppelmann, C.A., Strong, M.J., 2021. The Integral Role of RNA in Stress Granule Formation and Function. Front Cell Dev Biol 9. https://doi.org/10.3389/FCELL.2021.621779

Capitini, C., Conti, S., Perni, M., Guidi, F., Cascella, R., de Poli, A., Penco, A., Relini, A., Cecchi, C., Chiti, F., 2014. TDP-43 Inclusion Bodies Formed in Bacteria Are Structurally Amorphous, Non-Amyloid and Inherently Toxic to Neuroblastoma Cells. PLoS One 9, e86720. https://doi.org/10.1371/JOURNAL.PONE.0086720

Cascella, R., Capitini, C., Fani, G., Dobson, C.M., Cecchi, C., Chiti, F., 2016. Quantification of the Relative Contributions of Loss-offunction and Gain-of-function Mechanisms in TAR DNA-binding Protein 43 (TDP-43) Proteinopathies. Journal of Biological Chemistry 291, 19437–19448. https://doi.org/10.1074/jbc.M116.737726

Castelli, L.M., Cutillo, L., Souza, C.D.S., Sanchez-Martinez, A., Granata, I., Lin, Y.H., Myszczynska, M.A., Heath, P.R., Livesey, M.R., Ning, K., Azzouz, M., Shaw, P.J., Guarracino, M.R., Whitworth, A.J., Ferraiuolo, L., Milo, M., Hautbergue, G.M., 2021. SRSF1-dependent inhibition of C9ORF72-repeat RNA nuclear export: genome-wide mechanisms for neuroprotection in amyotrophic lateral

sclerosis. Mol Neurodegener 16, 1–24. https://doi.org/10.1186/S13024-021-00475-Y/FIGURES/6

Catimel, B., Teh, T., Fontes, M.R.M., Jennings, I.G., Jans, D.A., Howlett, G.J., Nice, E.C., Kobe, B., 2001. Biophysical characterization of interactions involving importin-alpha during nuclear import. J Biol Chem 276, 34189–34198. https://doi.org/10.1074/JBC.M103531200

Celona, B., von Dollen, J., Vatsavayai, S.C., Kashima, R., Johnson, J.R., Tang, A.A., Hata, A., Miller, B.L., Huang, E.J., Krogan, N.J., Seeley, W.W., Black, B.L., 2017. Suppression of c9orf72 RNA repeat-induced neurotoxicity by the ALS-associated RNA-binding protein Zfp106. Elife 6. https://doi.org/10.7554/ELIFE.19032

Cha, K., Sen, P., Raghunayakula, S., Zhang, X.D., 2015. The Cellular Distribution of RanGAP1 Is Regulated by CRM1-Mediated Nuclear Export in Mammalian Cells. PLoS One 10, e0141309. https://doi.org/10.1371/JOURNAL.PONE.0141309

Chang, W.L., Tarn, W.Y., 2009. A role for transportin in deposition of TTP to cytoplasmic RNA granules and mRNA decay. Nucleic Acids Res 37, 6600–6612. https://doi.org/10.1093/NAR/GKP717

Chang, Y.-J., Jeng, U.-S., Chiang, Y.-L., Hwang, I.-S., Chen, Y.-R., 2016. The Glycine-Alanine Dipeptide Repeat from C9orf72 Hexanucleotide Expansions Forms Toxic Amyloids Possessing Cell-to-Cell Transmission Properties. J Biol Chem 291, 4903–11. https://doi.org/10.1074/jbc.M115.694273

Chen, S.D., Li, H.Q., Cui, M., Dong, Q., Yu, J.T., 2020. Pluripotent stem cells for neurodegenerative disease modeling: an expert view on their value to drug discovery. https://doi.org/10.1080/17460441.2020.1767579 15, 1081–1094. https://doi.org/10.1080/17460441.2020.1767579

Cheng, H., Dufu, K., Lee, C.S., Hsu, J.L., Dias, A., Reed, R., 2006. Human mRNA export machinery recruited to the 5’ end of mRNA. Cell 127, 1389–1400. https://doi.org/10.1016/J.CELL.2006.10.044

Cheng, W., Wang, S., Mestre, A.A., Fu, C., Makarem, A., Xian, F., Hayes, L.R., Lopez-Gonzalez, R., Drenner, K., Jiang, J., Cleveland, D.W., Sun, S., 2018. C9ORF72 GGGGCC repeat-associated non-AUG translation is upregulated by stress through eIF2α phosphorylation. Nature Communications 2017 9:1 9, 1–12. https://doi.org/10.1038/s41467-017-02495-z

Chew, J., Cook, C., Gendron, T.F., Jansen-West, K., del Rosso, G., Daughrity, L.M., Castanedes-Casey, M., Kurti, A., Stankowski, J.N., Disney, M.D., Rothstein, J.D., Dickson, D.W., Fryer, J.D., Zhang, Y.J., Petrucelli, L., 2019. Aberrant deposition of stress granule-resident proteins linked to C9orf72-associated TDP-43 proteinopathy. Mol Neurodegener 14. https://doi.org/10.1186/s13024-019-0310-z

Chiò, A., Logroscino, G., Traynor, B.J., Collins, J., Simeone, J.C., Goldstein, L.A., White, L.A., 2013. Global epidemiology of amyotrophic lateral sclerosis: a systematic review of the published literature. Neuroepidemiology 41, 118–30. https://doi.org/10.1159/000351153

Choi, S.Y., Lopez-Gonzalez, R., Krishnan, G., Phillips, H.L., Li, A.N., Seeley, W.W., Yao, W.-D., Almeida, S., Gao, F.-B., 2019. C9ORF72-ALS/FTD-associated poly(GR) binds Atp5a1 and compromises mitochondrial function in vivo. Nat Neurosci 22, 851–862. https://doi.org/10.1038/s41593-019-0397-0

Chook, Y.M., Blobel, G., 1999. Structure of the nuclear transport complex karyopherin-beta2-Ran x GppNHp. Nature 399, 230–237. https://doi.org/10.1038/20375

Chook, Y.M., Süel, K.E., 2011. Nuclear import by karyopherin-βs: recognition and inhibition. Biochim Biophys Acta 1813, 1593–1606. https://doi.org/10.1016/J.BBAMCR.2010.10.014

Chou, C.-C., Zhang, Y., Umoh, M.E., Vaughan, S.W., Lorenzini, I., Liu, F., Sayegh, M., Donlin-Asp, P.G., Chen, Y.H., Duong, D.M., Seyfried, N.T., Powers, M.A., Kukar, T., Hales, C.M., Gearing, M., Cairns, N.J., Boylan, K.B., Dickson, D.W., Rademakers, R., Zhang, Y.-J., Petrucelli, L., Sattler, R., Zarnescu, D.C., Glass, J.D., Rossoll, W., 2018. TDP-43 pathology disrupts nuclear pore complexes and nucleocytoplasmic transport in ALS/FTD. Nat Neurosci 21, 228–239. https://doi.org/10.1038/s41593-017-0047-3

Clayton, E.L., Mizielinska, S., Edgar, J.R., Nielsen, T.T., Marshall, S., Norona, F.E., Robbins, M., Damirji, H., Holm, I.E., Johannsen, P., Nielsen, J.E., Asante, E.A., Collinge, J., Isaacs, A.M., 2015. Frontotemporal dementia caused by CHMP2B mutation is characterised by neuronal lysosomal storage pathology. Acta Neuropathol 130, 511–523. https://doi.org/10.1007/S00401-015-1475-3/FIGURES/7

Cleveland, D.W., Laing, N., Brown, R.H., 1995. Toxic mutants in Charcot's sclerosis. Nature 1995 378:6555 378, 342–343. https://doi.org/10.1038/378342a0

Cokol, M., Nair, R., Rost, B., 2000. Finding nuclear localization signals. EMBO Rep 1, 411–415. https://doi.org/10.1093/EMBO-REPORTS/KVD092

Conti, E., Uy, M., Leighton, L., Blobel, G., Kuriyan, J., 1998. Crystallographic analysis of the recognition of a nuclear localization signal by the nuclear import factor karyopherin alpha. Cell 94, 193–204. https://doi.org/10.1016/S0092-8674(00)81419-1

Cook, A.G., Fukuhara, N., Jinek, M., Conti, E., 2009. Structures of the tRNA export factor in the nuclear and cytosolic states. Nature 461, 60–65. https://doi.org/10.1038/NATURE08394

Cook, C.N., Wu, Y., Odeh, H.M., Gendron, T.F., Jansen-West, K., del Rosso, G., Yue, M., Jiang, P., Gomes, E., Tong, J., Daughrity, L.M., Avendano, N.M., Castanedes-Casey, M., Shao, W., Oskarsson, B., Tomassy, G.S., McCampbell, A., Rigo, F., Dickson, D.W., Shorter, J., Zhang, Y.-J., Petrucelli, L., 2020. C9orf72 poly(GR) aggregation induces TDP-43 proteinopathy. Sci Transl Med 12. https://doi.org/10.1126/scitranslmed.abb3774

Cooper-Knock, J., Walsh, M.J., Higginbottom, A., Highley, J.R., Dickman, M.J., Edbauer, D., Ince, P.G., Wharton, S.B., Wilson, S.A., Kirby, J., Hautbergue, G.M., Shaw, P.J., 2014. Sequestration of multiple RNA recognition motif-containing proteins by C9orf72 repeat expansions. Brain 137, 2040–2051. https://doi.org/10.1093/BRAIN/AWU120

Cornett, J., Cao, F., Wang, C.E., Ross, C.A., Bates, G.P., Li, S.H., Li, X.J., 2005. Polyglutamine expansion of huntingtin impairs its nuclear export. Nat Genet 37, 198–204. https://doi.org/10.1038/NG1503

Coyle-Gilchrist, I.T.S., Dick, K.M., Patterson, K., Rodríquez, P.V., Wehmann, E., Wilcox, A., Lansdall, C.J., Dawson, K.E., Wiggins, J., Mead, S., Brayne, C., Rowe, J.B., 2016. Prevalence, characteristics, and survival of frontotemporal lobar degeneration syndromes. Neurology 86, 1736–1743. https://doi.org/10.1212/WNL.0000000000002638

Coyne, A.N., Baskerville, V., Zaepfel, B.L., Dickson, D.W., Rigo, F., Bennett, F., Lusk, C.P., Rothstein, J.D., 2021. Nuclear accumulation of CHMP7 initiates nuclear pore complex injury and subsequent TDP-43 dysfunction in sporadic

and familial ALS. Sci Transl Med 13, eabe1923. https://doi.org/10.1126/SCITRANSLMED.ABE1923

Coyne, A.N., Rothstein, J.D., 2022. Nuclear pore complexes — a doorway to neural injury in neurodegeneration. Nature Reviews Neurology 2022 1–15. https://doi.org/10.1038/s41582-022-00653-6

Coyne, A.N., Zaepfel, B.L., Hayes, L., Fitchman, B., Salzberg, Y., Luo, E.-C., Bowen, K., Trost, H., Aigner, S., Rigo, F., Yeo, G.W., Harel, A., Svendsen, C.N., Sareen, D., Rothstein, J.D., 2020. G4C2 Repeat RNA Initiates a POM121-Mediated Reduction in Specific Nucleoporins in C9orf72 ALS/FTD. Neuron. https://doi.org/10.1016/J.NEURON.2020.06.027

Crampton, N., Kodiha, M., Shrivastava, S., Umar, R., Stochaj, U., 2009. Oxidative stress inhibits nuclear protein export by multiple mechanisms that target FG nucleoporins and Crm1. Mol Biol Cell 20, 5106–5116. https://doi.org/10.1091/MBC.E09-05-0397/ASSET/IMAGES/LARGE/ZMK0240992760009.JPEG

Cronshaw, J.M., Krutchinsky, A.N., Zhang, W., Chait, B.T., Matunis, M.L.J., 2002. Proteomic analysis of the mammalian nuclear pore complex. Journal of Cell Biology 158, 915–927. https://doi.org/10.1083/JCB.200206106

Cruts, M., Gijselinck, I., van der Zee, J., Engelborghs, S., Wils, H., Pirici, D., Rademakers, R., Vandenberghe, R., Dermaut, B., Martin, J.J., van Duijn, C., Peeters, K., Sciot, R., Santens, P., de Pooter, T., Mattheijssens, M., van den Broeck, M., Cuijt, I., Vennekens, K., de Deyn, P.P., Kumar-Singh, S., van Broeckhoven, C., 2006. Null mutations in progranulin cause ubiquitin-positive frontotemporal dementia linked to chromosome 17q21. Nature 2006 442:7105 442, 920–924. https://doi.org/10.1038/nature05017

Cruz, M., Marinho, V., Fontenelle, L.F., Engelhardt, E., Laks, J., 2008. Topiramate may modulate alcohol abuse but not other compulsive behaviors in frontotemporal dementia. Cognitive and Behavioral Neurology 21, 104–106. https://doi.org/10.1097/WNN.0B013E31816BDF73

Dafinca, R., Barbagallo, P., Farrimond, L., Candalija, A., Scaber, J., Ababneh, A., Sathyaprakash, C., Vowles, J., Cowley, S.A., Talbot, K., 2020. Stem Cell Reports Article Impairment of Mitochondrial Calcium Buffering Links Mutations in C9ORF72 and TARDBP in iPS-Derived Motor Neurons from Patients with ALS/FTD. https://doi.org/10.1016/j.stemcr.2020.03.023

Dafinca, R., Scaber, J., Ababneh, N., Lalic, T., Weir, G., Christian, H., Vowles, J., Douglas, A.G.L., Fletcher-Jones, A., Browne, C., Nakanishi, M., Turner, M.R., Wade-Martins, R., Cowley, S.A., Talbot, K., 2016. C9orf72 Hexanucleotide Expansions Are Associated with Altered Endoplasmic Reticulum Calcium Homeostasis and Stress Granule Formation in Induced Pluripotent Stem Cell-Derived Neurons from Patients with Amyotrophic Lateral Sclerosis and Frontotemporal Demen. Stem Cells 34, 2063–2078. https://doi.org/10.1002/stem.2388

D'Alton, S., Altshuler, M., Lewis, J., 2015. Studies of alternative isoforms provide insight into TDP-43 autoregulation and pathogenesis. RNA 21, 1419–1432. https://doi.org/10.1261/RNA.047647.114

D'Angelo, M.A., Raices, M., Panowski, S.H., Hetzer, M.W., 2009. Age-Dependent Deterioration of Nuclear Pore Complexes Causes a Loss of Nuclear Integrity in Postmitotic Cells. Cell 136, 284–295. https://doi.org/10.1016/J.CELL.2008.11.037

Davidson, Y., Robinson, A.C., Liu, X., Wu, D., Troakes, C., Rollinson, S., Masuda-Suzukake, M., Suzuki, G., Nonaka, T., Shi, J., Tian, J., Hamdalla, H., Ealing, J., Richardson, A., Jones, M., Pickering-Brown, S., Snowden, J.S., Hasegawa, M., Mann, D.M.A., 2016. Neurodegeneration in frontotemporal lobar degeneration and motor neurone disease associated with expansions in C9orf72 is linked to TDP-43 pathology and not associated with aggregated forms of dipeptide repeat proteins. Neuropathol Appl Neurobiol 42, 242–254. https://doi.org/10.1111/NAN.12292

Davidson, Y.S., Barker, H., Robinson, A.C., Thompson, J.C., Harris, J., Troakes, C., Smith, B., Al-Saraj, S., Shaw, C., Rollinson, S., Masuda-Suzukake, M., Hasegawa, M., Pickering-Brown, S., Snowden, J.S., Mann, D.M., 2014. Brain distribution of dipeptide repeat proteins in frontotemporal lobar degeneration and motor neurone disease associated with expansions in C9ORF72. Acta Neuropathol Commun 2. https://doi.org/10.1186/2051-5960-2-70

Davis, L.I., Blobel, G., 1986. Identification and characterization of a nuclear pore complex protein. Cell 45, 699–709. https://doi.org/10.1016/0092-8674(86)90784-1

Deans, P.J.M., Raval, P., Sellers, K.J., Gatford, N.J.F., Halai, S., Duarte, R.R.R., Shum, C., Warre-Cornish, K., Kaplun, V.E., Cocks, G., Hill, M., Bray, N.J., Price,

J., Srivastava, D.P., 2017. Psychosis Risk Candidate ZNF804A Localizes to Synapses and Regulates Neurite Formation and Dendritic Spine Structure. Biol Psychiatry 82, 49–61. https://doi.org/10.1016/J.BIOPSYCH.2016.08.038

DeJesus-Hernandez, M., Finch, N.A., Wang, X., Gendron, T.F., Bieniek, K.F., Heckman, M.G., Vasilevich, A., Murray, M.E., Rousseau, L., Weesner, R., Lucido, A., Parsons, M., Chew, J., Josephs, K.A., Parisi, J.E., Knopman, D.S., Petersen, R.C., Boeve, B.F., Graff-Radford, N.R., de Boer, J., Asmann, Y.W., Petrucelli, L., Boylan, K.B., Dickson, D.W., van Blitterswijk, M., Rademakers, R., 2017. In-depth clinico-pathological examination of RNA foci in a large cohort of C9ORF72 expansion carriers. Acta Neuropathol 134, 255–269. https://doi.org/10.1007/s00401-017-1725-7

DeJesus-Hernandez, M., Mackenzie, I.R., Boeve, B.F., Boxer, A.L., Baker, M., Rutherford, N.J., Nicholson, A.M., Finch, N.A., Flynn, H., Adamson, J., Kouri, N., Wojtas, A., Sengdy, P., Hsiung, G.-Y.R., Karydas, A., Seeley, W.W., Josephs, K.A., Coppola, G., Geschwind, D.H., Wszolek, Z.K., Feldman, H., Knopman, D.S., Petersen, R.C., Miller, B.L., Dickson, D.W., Boylan, K.B., Graff-Radford, N.R., Rademakers, R., 2011. Expanded GGGGCC Hexanucleotide Repeat in Noncoding Region of C9ORF72 Causes Chromosome 9p-Linked FTD and ALS. Neuron 72, 245–256. https://doi.org/10.1016/J.NEURON.2011.09.011

Deng, H., Gao, K., Jankovic, J., 2014. The role of FUS gene variants in neurodegenerative diseases. Nature Reviews Neurology 2014 10:6 10, 337–348. https://doi.org/10.1038/nrneurol.2014.78

Deng, H.X., Chen, W., Hong, S.T., Boycott, K.M., Gorrie, G.H., Siddique, N., Yang, Y., Fecto, F., Shi, Y., Zhai, H., Jiang, H., Hirano, M., Rampersaud, E., Jansen, G.H., Donkervoort, S., Bigio, E.H., Brooks, B.R., Ajroud, K., Sufit, R.L., Haines, J.L., Mugnaini, E., Pericak-Vance, M.A., Siddique, T., 2011. Mutations in UBQLN2 cause dominant X-linked juvenile and adult-onset ALS and ALS/dementia. Nature 2011 477:7363 477, 211–215. https://doi.org/10.1038/nature10353

Deture, M.A., Dickson, D.W., 2019. The neuropathological diagnosis of Alzheimer's disease. Molecular Neurodegeneration 2019 14:1 14, 1–18. https://doi.org/10.1186/S13024-019-0333-5

Devanand, D.P., Pelton, G.H., D'Antonio, K., Strickler, J.G., Kreisl, W.C., Noble, J., Marder, K., Skomorowsky, A., Huey, E.D., 2017. Low-dose Lithium treatment for

agitation and psychosis in Alzheimer's disease and Frontotemporal dementia: A case series. Alzheimer Dis Assoc Disord 31, 73. https://doi.org/10.1097/WAD.0000000000000161

Dong, X., Biswas, A., Süel, K.E., Jackson, L.K., Martinez, R., Gu, H., Chook, Y.M., 2009. Structural basis for leucine-rich nuclear export signal recognition by CRM1. Nature 458, 1136–1141. https://doi.org/10.1038/NATURE07975

Donnelly, C.J., Zhang, P.-W., Pham, J.T., Haeusler, A.R., Mistry, N.A., Vidensky, S., Daley, E.L., Poth, E.M., Hoover, B., Fines, D.M., Maragakis, N., Tienari, P.J., Petrucelli, L., Traynor, B.J., Wang, J., Rigo, F., Bennett, C.F., Blackshaw, S., Sattler, R., Rothstein, J.D., 2013. RNA Toxicity from the ALS/FTD C9ORF72 Expansion Is Mitigated by Antisense Intervention. Neuron 80, 415–428. https://doi.org/10.1016/J.NEURON.2013.10.015

Dormann, D., Madl, T., Valori, C.F., Bentmann, E., Tahirovic, S., Abou-Ajram, C., Kremmer, E., Ansorge, O., MacKenzie, I.R.A., Neumann, M., Haass, C., 2012. Arginine methylation next to the PY-NLS modulates Transportin binding and nuclear import of FUS. EMBO J 31, 4258–4275. https://doi.org/10.1038/EMBOJ.2012.261

Dormann, D., Rodde, R., Edbauer, D., Bentmann, E., Fischer, I., Hruscha, A., Than, M.E., Mackenzie, I.R.A., Capell, A., Schmid, B., Neumann, M., Haass, C., 2010. ALS-associated fused in sarcoma (FUS) mutations disrupt Transportin-mediated nuclear import. EMBO J 29, 2841–57. https://doi.org/10.1038/emboj.2010.143

Duan, L., Zaepfel, B.L., Aksenova, V., Dasso, M., Rothstein, J.D., Kalab, P., Correspondence, L.R.H., Hayes, L.R., 2022. Nuclear RNA binding regulates TDP-43 nuclear localization and passive nuclear export. Cell Rep 40. https://doi.org/10.1016/j.celrep.2022.111106

Dubreuil, P., Letard, S., Ciufolini, M., Gros, L., Humbert, M., Castéran, N., Borge, L., Hajem, B., Lermet, A., Sippl, W., Voisset, E., Arock, M., Auclair, C., Leventhal, P.S., Mansfield, C.D., Moussy, A., Hermine, O., 2009. Masitinib (AB1010), a Potent and Selective Tyrosine Kinase Inhibitor Targeting KIT. PLoS One 4, e7258. https://doi.org/10.1371/JOURNAL.PONE.0007258

Ederle, H., Funk, C., Abou-Ajram, C., Hutten, S., Funk, E.B.E., Kehlenbach, R.H., Bailer, S.M., Dormann, D., 2018. Nuclear egress of TDP-43 and FUS occurs independently of Exportin-1/CRM1. Sci Rep 8, 7084. https://doi.org/10.1038/s41598-018-25007-5

Eftekharzadeh, B., Daigle, J.G., Kapinos, L.E., Coyne, A., Schiantarelli, J., Carlomagno, Y., Cook, C., Miller, S.J., Dujardin, S., Amaral, A.S., Grima, J.C., Bennett, R.E., Tepper, K., DeTure, M., Vanderburgh, C.R., Corjuc, B.T., DeVos, S.L., Gonzalez, J.A., Chew, J., Vidensky, S., Gage, F.H., Mertens, J., Troncoso, J., Mandelkow, E., Salvatella, X., Lim, R.Y.H., Petrucelli, L., Wegmann, S., Rothstein, J.D., Hyman, B.T., 2018. Tau Protein Disrupts Nucleocytoplasmic Transport in Alzheimer's Disease. Neuron 99, 925-940.e7. https://doi.org/10.1016/j.neuron.2018.07.039

Eibauer, M., Pellanda, M., Turgay, Y., Dubrovsky, A., Wild, A., Medalia, O., 2015. Structure and gating of the nuclear pore complex. Nature Communications 2015 6:1 6, 1–9. https://doi.org/10.1038/ncomms8532

Elamin, M., Bede, P., Byrne, S., Jordan, N., Gallagher, L., Wynne, B., O'Brien, C., Phukan, J., Lynch, C., Pender, N., Hardiman, O., 2013. Cognitive changes predict functional decline in ALS: a population-based longitudinal study. Neurology 80, 1590–7. https://doi.org/10.1212/WNL.0b013e31828f18ac

Ellisdon, A.M., Dimitrova, L., Hurt, E., Stewart, M., 2012. Structural basis for the assembly and nucleic acid binding of the TREX-2 transcription-export complex. Nat Struct Mol Biol 19, 328–336. https://doi.org/10.1038/NSMB.2235

Fahed, A.C., McDonough, B., Gouvion, C.M., Newell, K.L., Dure, L.S., Bebin, M., Bick, A.G., Seidman, J.G., Harter, D.H., Seidman, C.E., 2014. UBQLN2 mutation causing heterogeneous X-linked dominant neurodegeneration. Ann Neurol 75, 793–798. https://doi.org/10.1002/ANA.24164

Fan, S., Webb, J.E.A., Yang, Y., Nieves, D.J., Gonçales, V.R., Tran, J., Hilzenrat, G., Kahram, M., Tilley, R.D., Gaus, K., Gooding, J.J., 2019. Observing the Reversible Single Molecule Electrochemistry of Alexa Fluor 647 Dyes by Total Internal Reflection Fluorescence Microscopy. Angewandte Chemie International Edition 58, 14495–14498. https://doi.org/10.1002/ANIE.201907298

Fanara, P., Hodel, M.R., Corbett, A.H., Hodel, A.E., 2000. Quantitative analysis of nuclear localization signal (NLS)-importin alpha interaction through fluorescence depolarization. Evidence for auto-inhibitory regulation of NLS binding. J Biol Chem 275, 21218–21223. https://doi.org/10.1074/JBC.M002217200

Farg, M.A., Konopka, A., Soo, K.Y., Ito, D., Atkin, J.D., 2017. The DNA damage response (DDR) is induced by the C9orf72 repeat expansion in amyotrophic

lateral sclerosis. Hum Mol Genet 26, 2882–2896. https://doi.org/10.1093/HMG/DDX170

Fifková, E., Tonks, M., Cullen-Dockstader, K., 1987. Changes in the nuclear pore complexes of the dentate granule cells in aged rats. Exp Neurol 95, 755–762. https://doi.org/10.1016/0014-4886(87)90314-1

Finlay, D.R., Newmeyer, D.D., Price, T.M., Forbes, D.J., 1987. Inhibition of in vitro nuclear transport by a lectin that binds to nuclear pores. Journal of Cell Biology 104, 189–200. https://doi.org/10.1083/JCB.104.2.189

Fletcher, P.D., Downey, L.E., Golden, H.L., Clark, C.N., Slattery, C.F., Paterson, R.W., Rohrer, J.D., Schott, J.M., Rossor, M.N., Warren, J.D., 2015a. Pain and temperature processing in dementia: a clinical and neuroanatomical analysis. Brain 138, 3360. https://doi.org/10.1093/BRAIN/AWV276

Fletcher, P.D., Downey, L.E., Golden, H.L., Clark, C.N., Slattery, C.F., Paterson, R.W., Schott, J.M., Rohrer, J.D., Rossor, M.N., Warren, J.D., 2015b. Auditory hedonic phenotypes in dementia: A behavioural and neuroanatomical analysis. Cortex 67, 95–105. https://doi.org/10.1016/J.CORTEX.2015.03.021

Flores, B.N., Dulchavsky, M.E., Krans, A., Sawaya, M.R., Paulson, H.L., Todd, P.K., Barmada, S.J., Ivanova, M.I., 2016. Distinct C9orf72-Associated Dipeptide Repeat Structures Correlate with Neuronal Toxicity. PLoS One 11, e0165084. https://doi.org/10.1371/journal.pone.0165084

Folkmann, A.W., Noble, K.N., Cole, C.N., Wente, S.R., 2011. Dbp5, Gle1-IP6 and Nup159: a working model for mRNP export. Nucleus 2, 540–548. https://doi.org/10.4161/NUCL.2.6.17881

Fornerod, M., Ohno, M., Yoshida, M., Mattaj, I.W., 1997. CRM1 is an export receptor for leucine-rich nuclear export signals. Cell 90, 1051–1060. https://doi.org/10.1016/S0092-8674(00)80371-2

Forsberg, K., Andersen, P.M., Marklund, S.L., Brännström, T., 2011. Glial nuclear aggregates of superoxide dismutase-1 are regularly present in patients with amyotrophic lateral sclerosis. Acta Neuropathol 121, 623–634. https://doi.org/10.1007/S00401-011-0805-3/FIGURES/4

Forsberg, K., Jonsson, P.A., Andersen, P.M., Bergemalm, D., Graffmo, K.S., Hultdin, M., Jacobsson, J., Rosquist, R., Marklund, S.L., Brännström, T., 2010. Novel Antibodies Reveal Inclusions Containing Non-Native SOD1 in Sporadic ALS

Patients. PLoS One 5, e11552. https://doi.org/10.1371/JOURNAL.PONE.0011552

Franks, T.M., McCloskey, A., Shokirev, M., Benner, C., Rathore, A., Hetzer, M.W., 2017. Nup98 recruits the Wdr82–Set1A/COMPASS complex to promoters to regulate H3K4 trimethylation in hematopoietic progenitor cells. Genes Dev 31, 2222–2234. https://doi.org/10.1101/GAD.306753.117

Fratta, P., Mizielinska, S., Nicoll, A.J., Zloh, M., Fisher, E.M.C., Parkinson, G., Isaacs, A.M., 2012. C9orf72 hexanucleotide repeat associated with amyotrophic lateral sclerosis and frontotemporal dementia forms RNA G-quadruplexes. Sci Rep 2. https://doi.org/10.1038/SREP01016

Fratta, P., Poulter, M., Lashley, T., Rohrer, J.D., Polke, J.M., Beck, J., Ryan, N., Hensman, D., Mizielinska, S., Waite, A.J., Lai, M.-C., Gendron, T.F., Petrucelli, L., Fisher, E.M.C., Revesz, T., Warren, J.D., Collinge, J., Isaacs, A.M., Mead, S., 2013. Homozygosity for the C9orf72 GGGGCC repeat expansion in frontotemporal dementia. Acta Neuropathol 126, 401–409. https://doi.org/10.1007/s00401-013-1147-0

Fratta, P., Sivakumar, P., Humphrey, J., Lo, K., Ricketts, T., Oliveira, H., Brito-Armas, J.M., Kalmar, B., Ule, A., Yu, Y., Birsa, N., Bodo, C., Collins, T., Conicella, A.E., Maza, A.M., Marrero-Gagliardi, A., Stewart, M., Mianne, J., Corrochano, S., Emmett, W., Codner, G., Groves, M., Fukumura, R., Gondo, Y., Lythgoe, M., Pauws, E., Peskett, E., Stanier, P., Teboul, L., Hallegger, M., Calvo, A., Chiò, A., Isaacs, A.M., Fawzi, N.L., Wang, E., Housman, D.E., Baralle, F., Greensmith, L., Buratti, E., Plagnol, V., Fisher, E.M., Acevedo-Arozena, A., 2018. Mice with endogenous TDP-43 mutations exhibit gain of splicing function and characteristics of amyotrophic lateral sclerosis. EMBO J 37, e98684. https://doi.org/10.15252/EMBJ.201798684

Freibaum, B.D., Chitta, R.K., High, A.A., Taylor, J.P., 2010. Global analysis of TDP-43 interacting proteins reveals strong association with RNA splicing and translation machinery. J Proteome Res 9, 1104–1120. https://doi.org/10.1021/PR901076Y

Freibaum, B.D., Lu, Y., Lopez-Gonzalez, R., Kim, N.C., Almeida, S., Lee, K.-H., Badders, N., Valentine, M., Miller, B.L., Wong, P.C., Petrucelli, L., Kim, H.J., Gao, F.-B., Taylor, J.P., 2015a. GGGGCC repeat expansion in C9orf72

compromises nucleocytoplasmic transport. Nature 525, 129–133. https://doi.org/10.1038/nature14974

Freibaum, B.D., Lu, Y., Lopez-Gonzalez, R., Kim, N.C., Almeida, S., Lee, K.-H., Badders, N., Valentine, M., Miller, B.L., Wong, P.C., Petrucelli, L., Kim, H.J., Gao, F.-B., Taylor, J.P., 2015b. GGGGCC repeat expansion in C9orf72 compromises nucleocytoplasmic transport. Nature 525, 129–133. https://doi.org/10.1038/nature14974

Freischmidt, A., Wieland, T., Richter, B., Ruf, W., Schaeffer, V., Müller, K., Marroquin, N., Nordin, F., Hübers, A., Weydt, P., Pinto, S., Press, R., Millecamps, S., Molko, N., Bernard, E., Desnuelle, C., Soriani, M.H., Dorst, J., Graf, E., Nordström, U., Feiler, M.S., Putz, S., Boeckers, T.M., Meyer, T., Winkler, A.S., Winkelman, J., de Carvalho, M., Thal, D.R., Otto, M., Brännström, T., Volk, A.E., Kursula, P., Danzer, K.M., Lichtner, P., Dikic, I., Meitinger, T., Ludolph, A.C., Strom, T.M., Andersen, P.M., Weishaupt, J.H., 2015. Haploinsufficiency of TBK1 causes familial ALS and fronto-temporal dementia. Nature Neuroscience 2015 18:5 18, 631–636. https://doi.org/10.1038/nn.4000

Frey, S., Görlich, D., 2007. A Saturated FG-Repeat Hydrogel Can Reproduce the Permeability Properties of Nuclear Pore Complexes. Cell 130, 512–523. https://doi.org/10.1016/J.CELL.2007.06.024

Frey, S., Rees, R., Rgen, J., Nemann, S., Ng, C., Huyton, T., Ng, S.C., Fü Nfgeld, K., Gö Rlich, D., 2018. Surface Properties Determining Passage Rates of Proteins through Nuclear Pores Article Surface Properties Determining Passage Rates of Proteins through Nuclear Pores. Cell 174, 202–217. https://doi.org/10.1016/j.cell.2018.05.045

Frey, S., Richter, R.P., Görlich, D., 2006. FG-rich repeats of nuclear pore proteins form a three-dimensional meshwork with hydrogel-like properties. Science 314, 815–7. https://doi.org/10.1126/science.1132516

Fribourg, S., Braun, I.C., Izaurralde, E., Conti, E., 2001. Structural basis for the recognition of a nucleoporin FG repeat by the NTF2-like domain of the TAP/p15 mRNA nuclear export factor. Mol Cell 8, 645–656. https://doi.org/10.1016/S1097-2765(01)00348-3

Friedman, A.K., Boeynaems, S., Baker, L.A., 2022. Synthetic hydrogel mimics of the nuclear pore complex for the study of nucleocytoplasmic transport defects in

C9orf72 ALS/FTD. Anal Bioanal Chem 414, 525–532. https://doi.org/10.1007/S00216-021-03478-2/FIGURES/5

Frottin, F., Pérez-Berlanga, M., Hartl, F.U., Hipp, M.S., 2021. Multiple pathways of toxicity induced by c9orf72 dipeptide repeat aggregates and g4c2 rna in a cellular model. Elife 10. https://doi.org/10.7554/ELIFE.62718

Fu, X., Liang, C., Li, F., Wang, L., Wu, X., Lu, A., Xiao, G., Zhang, G., Fu, X., Liang, C., Li, F., Wang, L., Wu, X., Lu, A., Xiao, G., Zhang, G., 2018. The Rules and Functions of Nucleocytoplasmic Shuttling Proteins. Int J Mol Sci 19, 1445. https://doi.org/10.3390/ijms19051445

Fujimura, K., Suzuki, T., Yasuda, Y., Murata, M., Katahira, J., Yoneda, Y., 2010. Identification of importin α1 as a novel constituent of RNA stress granules. Biochimica et Biophysica Acta (BBA) - Molecular Cell Research 1803, 865–871. https://doi.org/10.1016/J.BBAMCR.2010.03.020

Fumagalli, L., Young, F.L., Boeynaems, S., de Decker, M., Mehta, A.R., Swijsen, A., Fazal, R., Guo, W., Moisse, M., Beckers, J., Dedeene, L., Selvaraj, B.T., Vandoorne, T., Madan, V., van Blitterswijk, M., Raitcheva, D., McCampbell, A., Poesen, K., Gitler, A.D., Koch, P., Berghe, P. vanden, Thal, D.R., Verfaillie, C., Chandran, S., van den Bosch, L., Bullock, S.L., van Damme, P., 2021. C9orf72-derived arginine-containing dipeptide repeats associate with axonal transport machinery and impede microtubule-based motility. Sci Adv 7. https://doi.org/10.1126/SCIADV.ABG3013/SUPPL_FILE/ABG3013_TABLE_S7.XLSX

Fung, H.Y.J., Chook, Y.M., 2014. Atomic basis of CRM1-cargo recognition, release and inhibition. Semin Cancer Biol 27, 52–61. https://doi.org/10.1016/J.SEMCANCER.2014.03.002

Fung, H.Y.J., Fu, S.C., Brautigam, C.A., Chook, Y.M., 2015. Structural determinants of nuclear export signal orientation in binding to exportin CRM1. Elife 4. https://doi.org/10.7554/ELIFE.10034

Fung, H.Y.J., Fu, S.C., Chook, Y.M., 2017. Nuclear export receptor CRM1 recognizes diverse conformations in nuclear export signals. Elife 6. https://doi.org/10.7554/ELIFE.23961

Gasset-Rosa, F., Chillon-Marinas, C., Goginashvili, A., Atwal, R.S., Artates, J.W., Tabet, R., Wheeler, V.C., Bang, A.G., Cleveland, D.W., Lagier-Tourenne, C., 2017. Polyglutamine-Expanded Huntingtin Exacerbates Age-Related Disruption

of Nuclear Integrity and Nucleocytoplasmic Transport. Neuron 94, 48-57.e4. https://doi.org/10.1016/j.neuron.2017.03.027

Gasset-Rosa, F., Lu, S., Yu, H., Chen, C., Melamed, Z., Guo, L., Shorter, J., da Cruz, S., Cleveland, D.W., 2019. Cytoplasmic TDP-43 De-mixing Independent of Stress Granules Drives Inhibition of Nuclear Import, Loss of Nuclear TDP-43, and Cell Death. Neuron. https://doi.org/10.1016/J.NEURON.2019.02.038

Gendron, T.F., Bieniek, K.F., Zhang, Y.-J., Jansen-West, K., Ash, P.E.A., Caulfield, T., Daughrity, L., Dunmore, J.H., Castanedes-Casey, M., Chew, J., Cosio, D.M., van Blitterswijk, M., Lee, W.C., Rademakers, R., Boylan, K.B., Dickson, D.W., Petrucelli, L., 2013. Antisense transcripts of the expanded C9ORF72 hexanucleotide repeat form nuclear RNA foci and undergo repeat-associated non-ATG translation in c9FTD/ALS. Acta Neuropathol 126, 829–844. https://doi.org/10.1007/s00401-013-1192-8

Gendron, T.F., van Blitterswijk, M., Bieniek, K.F., Daughrity, L.M., Jiang, J., Rush, B.K., Pedraza, O., Lucas, J.A., Murray, M.E., Desaro, P., Robertson, A., Overstreet, K., Thomas, C.S., Crook, J.E., Castanedes-Casey, M., Rousseau, L., Josephs, K.A., Parisi, J.E., Knopman, D.S., Petersen, R.C., Boeve, B.F., Graff-Radford, N.R., Rademakers, R., Lagier-Tourenne, C., Edbauer, D., Cleveland, D.W., Dickson, D.W., Petrucelli, L., Boylan, K.B., 2015. Cerebellar c9RAN proteins associate with clinical and neuropathological characteristics of C9ORF72 repeat expansion carriers. Acta Neuropathol 130, 559–573. https://doi.org/10.1007/S00401-015-1474-4

Giampetruzzi, A., Danielson, E.W., Gumina, V., Jeon, M., Boopathy, S., Brown, R.H., Ratti, A., Landers, J.E., Fallini, C., 2019. Modulation of actin polymerization affects nucleocytoplasmic transport in multiple forms of amyotrophic lateral sclerosis. Nat Commun 10, 3827. https://doi.org/10.1038/s41467-019-11837-y

Gijselinck, I., van Langenhove, T., van der Zee, J., Sleegers, K., Philtjens, S., Kleinberger, G., Janssens, J., Bettens, K., van Cauwenberghe, C., Pereson, S., Engelborghs, S., Sieben, A., de Jonghe, P., Vandenberghe, R., Santens, P., de Bleecker, J., Maes, G., Bäumer, V., Dillen, L., Joris, G., Cuijt, I., Corsmit, E., Elinck, E., van Dongen, J., Vermeulen, S., van den Broeck, M., Vaerenberg, C., Mattheijssens, M., Peeters, K., Robberecht, W., Cras, P., Martin, J.-J., de Deyn, P.P., Cruts, M., van Broeckhoven, C., 2012. A C9orf72 promoter repeat expansion in a Flanders-Belgian cohort with disorders of the frontotemporal

lobar degeneration-amyotrophic lateral sclerosis spectrum: a gene identification study. Lancet Neurol 11, 54–65. https://doi.org/10.1016/S1474-4422(11)70261-7

Gijselinck, I., van Mossevelde, S., van der Zee, J., Sieben, A., Engelborghs, S., de Bleecker, J., Ivanoiu, A., Deryck, O., Edbauer, D., Zhang, M., Heeman, B., Bäumer, V., van den Broeck, M., Mattheijssens, M., Peeters, K., Rogaeva, E., de Jonghe, P., Cras, P., Martin, J.J., de Deyn, P.P., Cruts, M., van Broeckhoven, C., 2016. The C9orf72 repeat size correlates with onset age of disease, DNA methylation and transcriptional downregulation of the promoter. Mol Psychiatry 21, 1112–1124. https://doi.org/10.1038/MP.2015.159

Gijselinck, I., van Mossevelde, S., van der Zee, J., Sieben, A., Philtjens, S., Heeman, B., Engelborghs, S., Vandenbulcke, M., de Baets, G., Bäumer, V., Cuijt, I., van den Broeck, M., Peeters, K., Mattheijssens, M., Rousseau, F., Vandenberghe, R., de Jonghe, P., Cras, P., de Deyn, P.P., Martin, J.J., Cruts, M., van Broeckhoven, C., 2015. Loss of TBK1 is a frequent cause of frontotemporal dementia in a Belgian cohort. Neurology 85, 2116. https://doi.org/10.1212/WNL.0000000000002220

Gillon, A., Steel, C., Cornwall, J., Sheard, P., 2020. Increased nuclear permeability is a driver for age-related motoneuron loss. Geroscience. https://doi.org/10.1007/s11357-020-00155-7

Gitcho, M.A., Bigio, E.H., Mishra, M., Johnson, N., Weintraub, S., Mesulam, M., Rademakers, R., Chakraverty, S., Cruchaga, C., Morris, J.C., Goate, A.M., Cairns, N.J., 2009. TARDBP 3′-UTR variant in autopsy-confirmed frontotemporal lobar degeneration with TDP-43 proteinopathy. Acta Neuropathol 118, 633. https://doi.org/10.1007/S00401-009-0571-7

Gitler, A.D., Tsuiji, H., 2016. There has been an awakening: Emerging mechanisms of C9orf72 mutations in FTD/ALS. Brain Res 1647, 19–29. https://doi.org/10.1016/J.BRAINRES.2016.04.004

Gleixner, A.M., Verdone, B.M., Otte, C.G., Anderson, E.N., Ramesh, N., Shapiro, O.R., Gale, J.R., Mauna, J.C., Mann, J.R., Copley, K.E., Daley, E.L., Ortega, J.A., Cicardi, M.E., Kiskinis, E., Kofler, J., Pandey, U.B., Trotti, D., Donnelly, C.J., 2022. NUP62 localizes to ALS/FTLD pathological assemblies and contributes to TDP-43 insolubility. Nature Communications 2022 13:1 13, 1–17. https://doi.org/10.1038/s41467-022-31098-6

Goedert, M., 2018. Tau filaments in neurodegenerative diseases. FEBS Lett 592, 2383–2391. https://doi.org/10.1002/1873-3468.13108

Goh, C.W., Lee, I.C., Sundaram, J.R., George, S.E., Yusoff, P., Brush, M.H., Sze, N.S.K., Shenolikar, S., 2018. Chronic oxidative stress promotes GADD34-mediated phosphorylation of the TAR DNA-binding protein TDP-43, a modification linked to neurodegeneration. Journal of Biological Chemistry 293, 163–176. https://doi.org/10.1074/JBC.M117.814111/ATTACHMENT/4BBF70D7-1850-49C6-B137-3ED96927466D/MMC1.PDF

Goldfarb, D.S., Corbett, A.H., Mason, D.A., Harreman, M.T., Adam, S.A., 2004. Importin alpha: a multipurpose nuclear-transport receptor. Trends Cell Biol 14, 505–514. https://doi.org/10.1016/J.TCB.2004.07.016

Goldman, J.S., Farmer, J.M., Wood, E.M., Johnson, J.K., Boxer, A., Neuhaus, J., Lomen-Hoerth, C., Wilhelmsen, K.C., Lee, V.M.Y., Grossman, M., Miller, B.L., 2005. Comparison of family histories in FTLD subtypes and related tauopathies. Neurology 65, 1817–1819. https://doi.org/10.1212/01.WNL.0000187068.92184.63

Gomez-Deza, J., Lee, Y.B., Troakes, C., Nolan, M., Al-Sarraj, S., Gallo, J.M., Shaw, C.E., 2015. Dipeptide repeat protein inclusions are rare in the spinal cord and almost absent from motor neurons in C9ORF72 mutant amyotrophic lateral sclerosis and are unlikely to cause their degeneration. Acta Neuropathol Commun 3, 38. https://doi.org/10.1186/S40478-015-0218-Y

Gomez-Suaga, P., Gábor, |, Mórotz, M., Markovinovic, A., Martín-Guerrero, S.M., Preza, E., Arias, N., Mayl, | Keith, Aabdien, A., Gesheva, V., Nishimura, A., Annibali, A., Lee, Y., Mitchell, J.C., Wray, S., Shaw, | Christopher, Noble, W., Christopher, |, Miller, C.J., Mórotz, G.M., Martín, S.M., Miller, C.C.J., 2022. Disruption of ER-mitochondria tethering and signalling in C9orf72-associated amyotrophic lateral sclerosis and frontotemporal dementia. Aging Cell 00, e13549. https://doi.org/10.1111/ACEL.13549

Görlich, D., Seewald, M.J., Ribbeck, K., 2003. Characterization of Ran-driven cargo transport and the RanGTPase system by kinetic measurements and computer simulation. EMBO J 22, 1088–1100. https://doi.org/10.1093/EMBOJ/CDG113

Grant, R.P., Hurt, E., Neuhaus, D., Stewart, M., 2002. Structure of the C-terminal FG-nucleoporin binding domain of Tap/NXF1. Nat Struct Biol 9, 247–251. https://doi.org/10.1038/NSB773

Green, K.M., Glineburg, M.R., Kearse, M.G., Flores, B.N., Linsalata, A.E., Fedak, S.J., Goldstrohm, A.C., Barmada, S.J., Todd, P.K., 2017. RAN translation at C9orf72-associated repeat expansions is selectively enhanced by the integrated stress response. Nature Communications 2017 8:1 8, 1–13. https://doi.org/10.1038/s41467-017-02200-0

Griffis, E.R., Altan, N., Lippincott-Schwartz, J., Powers, M.A., 2002. Nup98 Is a Mobile Nucleoporin with Transcription-dependent Dynamics. Mol Biol Cell 13, 1282. https://doi.org/10.1091/MBC.01-11-0538

Grima, J.C., Daigle, J.G., Arbez, N., Cunningham, K.C., Zhang, K., Ochaba, J., Geater, C., Morozko, E., Stocksdale, J., Glatzer, J.C., Pham, J.T., Ahmed, I., Peng, Q., Wadhwa, H., Pletnikova, O., Troncoso, J.C., Duan, W., Snyder, S.H., Ranum, L.P.W., Thompson, L.M., Lloyd, T.E., Ross, C.A., Rothstein, J.D., 2017. Mutant Huntingtin Disrupts the Nuclear Pore Complex. Neuron 94, 93-107.e6. https://doi.org/10.1016/J.NEURON.2017.03.023

Grünwald, M., Lazzaretti, D., Bono, F., 2013. Structural basis for the nuclear export activity of Importin13. EMBO J 32, 899. https://doi.org/10.1038/EMBOJ.2013.29

Grüter, P., Tabernero, C., von Kobbe, C., Schmitt, C., Saavedra, C., Bachi, A., Wilm, M., Felber, B.K., Izaurralde, E., 1998. TAP, the human homolog of Mex67p, mediates CTE-dependent RNA export from the nucleus. Mol Cell 1, 649–659. https://doi.org/10.1016/S1097-2765(00)80065-9

Guimet, N.M., Zapata-Restrepo, L.M., Miller, B.L., 2022. Advances in Treatment of Frontotemporal Dementia. https://doi.org/10.1176/appi.neuropsych.21060166. https://doi.org/10.1176/APPI.NEUROPSYCH.21060166

Guo, L., Kim, H.J., Wang, H., Monaghan, J., Freyermuth, F., Sung, J.C., O'Donovan, K., Fare, C.M., Diaz, Z., Singh, N., Zhang, Z.C., Coughlin, M., Sweeny, E.A., DeSantis, M.E., Jackrel, M.E., Rodell, C.B., Burdick, J.A., King, O.D., Gitler, A.D., Lagier-Tourenne, C., Pandey, U.B., Chook, Y.M., Taylor, J.P., Shorter, J., 2018. Nuclear-Import Receptors Reverse Aberrant Phase Transitions of RNA-Binding Proteins with Prion-like Domains. Cell 173, 677-692.e20. https://doi.org/10.1016/j.cell.2018.03.002

Gupta, R., Lan, M., Mojsilovic-Petrovic, J., Choi, W.H., Safren, N., Barmada, S., Lee, M.J., Kalb, R., 2017. The Proline/Arginine Dipeptide from Hexanucleotide Repeat Expanded C9ORF72 Inhibits the Proteasome. eNeuro 4, 249–265. https://doi.org/10.1523/ENEURO.0249-16.2017

Güttler, T., Görlich, D., 2011. Ran-dependent nuclear export mediators: a structural perspective. EMBO J 30, 3457. https://doi.org/10.1038/EMBOJ.2011.287

Güttler, T., Madl, T., Neumann, P., Deichsel, D., Corsini, L., Monecke, T., Ficner, R., Sattler, M., Görlich, D., 2010. NES consensus redefined by structures of PKI-type and Rev-type nuclear export signals bound to CRM1. Nat Struct Mol Biol 17, 1367–1376. https://doi.org/10.1038/NSMB.1931

Haeusler, A.R., Donnelly, C.J., Periz, G., Simko, E.A.J., Shaw, P.G., Kim, M.S., Maragakis, N.J., Troncoso, J.C., Pandey, A., Sattler, R., Rothstein, J.D., Wang, J., 2014. C9orf72 nucleotide repeat structures initiate molecular cascades of disease. Nature 507, 195–200. https://doi.org/10.1038/NATURE13124

Hahn, S., Schlenstedt, G., 2011. Importin β-type nuclear transport receptors have distinct binding affinities for Ran-GTP. Biochem Biophys Res Commun 406, 383–388. https://doi.org/10.1016/J.BBRC.2011.02.051

Hampoelz, B., Andres-Pons, A., Kastritis, P., Beck, M., 2019. Structure and Assembly of the Nuclear Pore Complex. https://doi.org/10.1146/annurev-biophys-052118

Hanover, J.A., Cohen, C.K., Willingham, M.C., Park, M.K., 1987. O-linked N-acetylglucosamine is attached to proteins of the nuclear pore. Evidence for cytoplasmic and nucleoplasmic glycoproteins. Journal of Biological Chemistry 262, 9887–9894. https://doi.org/10.1016/S0021-9258(18)48017-9

Hans, F., Glasebach, H., Kahle, P.J., 2020. Multiple distinct pathways lead to hyperubiquitylated insoluble TDP-43 protein independent of its translocation into stress granules. Journal of Biological Chemistry 295, 673–689. https://doi.org/10.1016/S0021-9258(17)49926-1

Hardiman, O., Al-Chalabi, A., Chio, A., Corr, E.M., Logroscino, G., Robberecht, W., Shaw, P.J., Simmons, Z., van den Berg, L.H., 2017. Amyotrophic lateral sclerosis. Nat Rev Dis Primers 3, 17071. https://doi.org/10.1038/nrdp.2017.71

Harms, M.B., Cady, J., Zaidman, C., Cooper, P., Bali, T., Allred, P., Cruchaga, C., Baughn, M., Libby, R.T., Pestronk, A., Goate, A., Ravits, J., Baloh, R.H., 2013. Lack of C9ORF72 coding mutations supports a gain of function for repeat expansions in ALS. Neurobiol Aging 34, 2234.e13. https://doi.org/10.1016/J.NEUROBIOLAGING.2013.03.006

Harrison, J.M., Rafuse, V.F., 2020. Muscle fiber-type specific terminal Schwann cell pathology leads to sprouting deficits following partial denervation in SOD1G93A mice. Neurobiol Dis 145. https://doi.org/10.1016/J.NBD.2020.105052

Hartmann, H., Hornburg, D., Czuppa, M., Bader, J., Michaelsen, M., Farny, D., Arzberger, T., Mann, M., Meissner, F., Edbauer, D., 2018. Proteomics and C9orf72 neuropathology identify ribosomes as poly-GR/PR interactors driving toxicity. Life Sci Alliance 1. https://doi.org/10.26508/LSA.201800070

Hasegawa, M., Arai, T., Nonaka, T., Kametani, F., Yoshida, M., Hashizume, Y., Beach, T.G., Buratti, E., Baralle, F., Morita, M., Nakano, I., Oda, T., Tsuchiya, K., Akiyama, H., 2008. Phosphorylated TDP-43 in frontotemporal lobar degeneration and amyotrophic lateral sclerosis. Ann Neurol 64, 60–70. https://doi.org/10.1002/ANA.21425

Hautbergue, G.M., Castelli, L.M., Ferraiuolo, L., Sanchez-Martinez, A., Cooper-Knock, J., Higginbottom, A., Lin, Y.H., Bauer, C.S., Dodd, J.E., Myszczynska, M.A., Alam, S.M., Garneret, P., Chandran, J.S., Karyka, E., Stopford, M.J., Smith, E.F., Kirby, J., Meyer, K., Kaspar, B.K., Isaacs, A.M., El-Khamisy, S.F., de Vos, K.J., Ning, K., Azzouz, M., Whitworth, A.J., Shaw, P.J., 2017. SRSF1-dependent nuclear export inhibition of C9ORF72 repeat transcripts prevents neurodegeneration and associated motor deficits. Nature Communications 2017 8:1 8, 1–18. https://doi.org/10.1038/ncomms16063

Hautbergue, G.M., Hung, M.L., Golovanov, A.P., Lian, L.Y., Wilson, S.A., 2008. Mutually exclusive interactions drive handover of mRNA from export adaptors to TAP. Proc Natl Acad Sci U S A 105, 5154–5159. https://doi.org/10.1073/PNAS.0709167105

Havel, L.S., Wang, C.E., Wade, B., Huang, B., Li, S., Li, X.J., 2011. Preferential accumulation of N-terminal mutant huntingtin in the nuclei of striatal neurons is regulated by phosphorylation. Hum Mol Genet 20, 1424–1437. https://doi.org/10.1093/HMG/DDR023

Hawrot, J., Imhof, S., Wainger, B.J., 2020. Modeling cell-autonomous motor neuron phenotypes in ALS using iPSCs. Neurobiol Dis 134, 104680. https://doi.org/10.1016/J.NBD.2019.104680

Hayashi, Y., Homma, K., Ichijo, H., 2016. SOD1 in neurotoxicity and its controversial roles in SOD1 mutation-negative ALS. Adv Biol Regul 60, 95–104. https://doi.org/10.1016/J.JBIOR.2015.10.006

Hayes, L.R., Duan, L., Bowen, K., Kalab, P., Rothstein, J.D., 2020. C9orf72 arginine-rich dipeptide repeat proteins disrupt karyopherin-mediated nuclear import. Elife 9. https://doi.org/10.7554/eLife.51685

Hemerková, P., Vališ, M., 2021. Role of Oxidative Stress in the Pathogenesis of Amyotrophic Lateral Sclerosis: Antioxidant Metalloenzymes and Therapeutic Strategies. Biomolecules 2021, Vol. 11, Page 437 11, 437. https://doi.org/10.3390/BIOM11030437

Hergesheimer, R.C., Chami, A.A., de Assis, D.R., Vourc'h, P., Andres, C.R., Corcia, P., Lanznaster, D., Blasco, H., 2019. The debated toxic role of aggregated TDP-43 in amyotrophic lateral sclerosis: a resolution in sight? Brain 142, 1176–1194. https://doi.org/10.1093/BRAIN/AWZ078

Hinchcliffe, M., Smith, A., 2017. Riluzole: real-world evidence supports significant extension of median survival times in patients with amyotrophic lateral sclerosis. Degener Neurol Neuromuscul Dis 7, 61–70. https://doi.org/10.2147/DNND.S135748

Hirokawa, N., 1994. Microtubule organization and dynamics dependent on microtubule-associated proteins. Curr Opin Cell Biol 6, 74–81. https://doi.org/10.1016/0955-0674(94)90119-8

Hodel, A.E., Harreman, M.T., Pulliam, K.F., Harben, M.E., Holmes, J.S., Hodel, M.R., Berland, K.M., Corbett, A.H., 2006. Nuclear localization signal receptor affinity correlates with in vivo localization in Saccharomyces cerevisiae. J Biol Chem 281, 23545–23556. https://doi.org/10.1074/JBC.M601718200

Hodel, M.R., Corbett, A.H., Hodel, A.E., 2001. Dissection of a nuclear localization signal. J Biol Chem 276, 1317–1325. https://doi.org/10.1074/JBC.M008522200

Hodge, C.A., Tran, E.J., Noble, K.N., Alcazar-Roman, A.R., Ben-Yishay, R., Scarcelli, J.J., Folkmann, A.W., Shav-Tal, Y., Wente, S.R., Cole, C.N., 2011. The Dbp5 cycle at the nuclear pore complex during mRNA export I: dbp5 mutants with defects in RNA binding and ATP hydrolysis define key steps for Nup159 and Gle1. Genes Dev 25, 1052–1064. https://doi.org/10.1101/GAD.2041611

Hodges, J.R., Davies, R., Xuereb, J., Kril, J., Halliday, G., 2003. Survival in frontotemporal dementia. Neurology 61, 349–354. https://doi.org/10.1212/01.WNL.0000078928.20107.52

Hoelz, A., Glavy, J.S., Beck, M., 2016. Toward the atomic structure of the nuclear pore complex: when top down meets bottom up. Nature Structural & Molecular Biology 2016 23:7 23, 624–630. https://doi.org/10.1038/nsmb.3244

Hofweber, M., Hutten, S., Bourgeois, B., Spreitzer, E., Niedner-Boblenz, A., Schifferer, M., Ruepp, M.-D., Simons, M., Niessing, D., Madl, T., Dormann, D., 2018. Phase Separation of FUS Is Suppressed by Its Nuclear Import Receptor and Arginine Methylation. Cell 173, 706-719.e13. https://doi.org/10.1016/j.cell.2018.03.004

Hogan, D.B., Jetté, N., Fiest, K.M., Roberts, J.I., Pearson, D., Smith, E.E., Roach, P., Kirk, A., Pringsheim, T., Maxwell, C.J., 2016. The Prevalence and Incidence of Frontotemporal Dementia: a Systematic Review. Canadian Journal of Neurological Sciences / Journal Canadien des Sciences Neurologiques 43, S96–S109. https://doi.org/10.1017/cjn.2016.25

Holm, I.E., Englund, E., Mackenzie, I.R.A., Johannsen, P., Isaacs, A.M., 2007. A Reassessment of the Neuropathology of Frontotemporal Dementia Linked to Chromosome 3. J Neuropathol Exp Neurol 66, 884–891. https://doi.org/10.1097/NEN.0B013E3181567F02

Holm, I.E., Isaacs, A.M., MacKenzie, I.R.A., 2009. Absence of FUS-immunoreactive pathology in frontotemporal dementia linked to chromosome 3 (FTD-3) caused by mutation in the CHMP2B gene. Acta Neuropathologica 2009 118:5 118, 719–720. https://doi.org/10.1007/S00401-009-0593-1

Hosp, F., Vossfeldt, H., Heinig, M., Vasiljevic, D., Arumughan, A., Wyler, E., Landthaler, M., Hubner, N., Wanker, E.E., Lannfelt, L., Ingelsson, M., Lalowski, M., Voigt, A., Selbach, M., Harold, D., Abraham, R., Hollingworth, P., Sims, R., Gerrish, A., Chapman, J., Russo, G., Hamshere, M., Singh Pahwa, J., Escott-Price, V., Dowzell, K., Williams, A., Jones, N., Thomas, C., Stretton, A., Morgan, A., Lovestone, S., Powell, J., Proitsi, P., Lupton, M.K., Brayne, C., Rubinsztein, D.C., Gill, M., Lawlor, B., Lynch, A., Morgan, K., Brown, K., Passmore, P., Craig, D., McGuinness, B., Todd, S., Johnston, J., Holmes, C., Mann, D., David Smith, A., Love, S., Kehoe, P.G., Hardy, J., Mead, S., Fox, N., Rossor, M., Collinge, J., Maier, W., Jessen, F., Heun, R., Schürmann, B., Ramirez, A., Becker, T., Herold, C., Lacour, A., Drichel, D., van den Bussche, H., Heuser, I., Kornhuber, J., Wiltfang, J., Dichgans, M., Frölich, L., Hampel, H., Hüll, M., Rujescu, D., Goate, A., Kauwe, J.S.K., Cruchaga, C., Nowotny, P., Morris, J.C., Mayo, K.,

Livingston, G., Bass, N.J., Gurling, H., McQuillin, A., Gwilliam, R., Deloukas, P., Al-Chalabi, A., Shaw, C.E., Singleton, A.B., Guerreiro, R., Mühleisen, T.W., Nöthen, M.M., Moebus, S., Jöckel, K.H., Klopp, N., Wichmann, H.E., Carrasquillo, M.M., Shane Pankratz, V., Younkin, S.G., Holmans, P., O'Donovan, M., Owen, M.J., Williams, J., 2015. Quantitative Interaction Proteomics of Neurodegenerative Disease Proteins. Cell Rep 11, 1134–1146. https://doi.org/10.1016/j.celrep.2015.04.030

Hough, L.E., Dutta, K., Sparks, S., Temel, D.B., Kamal, A., Tetenbaum-Novatt, J., Rout, M.P., Cowburn, D., 2015. The molecular mechanism of nuclear transport revealed by atomic-scale measurements. Elife 4. https://doi.org/10.7554/ELIFE.10027

Hsiung, G.Y.R., Dejesus-Hernandez, M., Feldman, H.H., Sengdy, P., Bouchard-Kerr, P., Dwosh, E., Butler, R., Leung, B., Fok, A., Rutherford, N.J., Baker, M., Rademakers, R., Mackenzie, I.R.A., 2012. Clinical and pathological features of familial frontotemporal dementia caused by C9ORF72 mutation on chromosome 9p. Brain 135, 709–722. https://doi.org/10.1093/BRAIN/AWR354

Huang, H., Weng, H., Zhou, K., Wu, T., Zhao, B.S., Sun, Mingli, Chen, Z., Deng, X., Xiao, G., Auer, F., Klemm, L., Wu, H., Zuo, Z., Qin, X., Dong, Y., Zhou, Y., Qin, H., Tao, S., Du, J., Liu, J., Lu, Z., Yin, H., Mesquita, A., Yuan, C.L., Hu, Y.C., Sun, W., Su, R., Dong, L., Shen, C., Li, C., Qing, Y., Jiang, X., Wu, X., Sun, Miao, Guan, J.L., Qu, L., Wei, M., Müschen, M., Huang, G., He, C., Yang, J., Chen, J., 2019. Histone H3 trimethylation at lysine 36 guides m6A RNA modification co-transcriptionally. Nature 2019 567:7748 567, 414–419. https://doi.org/10.1038/s41586-019-1016-7

Huey, E.D., Ferrari, R., Moreno, J.H., Jensen, C., Morris, C.M., Potocnik, F., Kalaria, R.N., Tierney, M., Wassermann, E.M., Hardy, J., Grafman, J., Momeni, P., 2012. FUS and TDP43 genetic variability in FTD and CBS. Neurobiol Aging 33, 1016.e9-1016.e17. https://doi.org/10.1016/J.NEUROBIOLAGING.2011.08.004

Hülsmann, B.B., Labokha, A.A., Görlich, D., 2012. The Permeability of Reconstituted Nuclear Pores Provides Direct Evidence for the Selective Phase Model. Cell 150, 738–751. https://doi.org/10.1016/J.CELL.2012.07.019

Hurt, E., Sträßer, K., Segref, A., Bailer, S., Schlaich, N., Presutti, C., Tollervey, D., Jansen, R., 2000. Mex67p mediates nuclear export of a variety of RNA

polymerase II transcripts. J Biol Chem 275, 8361–8368. https://doi.org/10.1074/JBC.275.12.8361

Hutten, S., Usluer, S., Bourgeois, B., Simonetti, F., Odeh, H.M., Fare, C.M., Czuppa, M., Hruska-Plochan, M., Hofweber, M., Polymenidou, M., Shorter, J., Edbauer, D., Madl, T., Dormann, D., 2020. Nuclear Import Receptors Directly Bind to Arginine-Rich Dipeptide Repeat Proteins and Suppress Their Pathological Interactions. Cell Rep 33. https://doi.org/10.1016/j.celrep.2020.108538

Iguchi, Y., Katsuno, M., Niwa, J.I., Takagi, S., Ishigaki, S., Ikenaka, K., Kawai, K., Watanabe, H., Yamanaka, K., Takahashi, R., Misawa, H., Sasaki, S., Tanaka, F., Sobue, G., 2013. Loss of TDP-43 causes age-dependent progressive motor neuron degeneration. Brain 136, 1371–1382. https://doi.org/10.1093/BRAIN/AWT029

Irwin, D.J., McMillan, C.T., Brettschneider, J., Libon, D.J., Powers, J., Rascovsky, K., Toledo, J.B., Boller, A., Bekisz, J., Chandrasekaran, K., Wood, E.M.C., Shaw, L.M., Woo, J.H., Cook, P.A., Wolk, D.A., Arnold, S.E., van Deerlin, V.M., McCluskey, L.F., Elman, L., Lee, V.M.Y., Trojanowski, J.Q., Grossman, M., 2013. Cognitive decline and reduced survival in C9orf72 expansion frontotemporal degeneration and amyotrophic lateral sclerosis. J Neurol Neurosurg Psychiatry 84, 163–169. https://doi.org/10.1136/JNNP-2012-303507

Ito, D., Seki, M., Tsunoda, Y., Uchiyama, H., Suzuki, N., 2011. Nuclear transport impairment of amyotrophic lateral sclerosis-linked mutations in FUS/TLS. Ann Neurol 69, 152–162. https://doi.org/10.1002/ANA.22246

Jackson, J.L., Finch, N.A., Baker, M.C., Kachergus, J.M., DeJesus-Hernandez, M., Pereira, K., Christopher, E., Prudencio, M., Heckman, M.G., Thompson, E.A., Dickson, D.W., Shah, J., Oskarsson, B., Petrucelli, L., Rademakers, R., van Blitterswijk, M., 2020. Elevated methylation levels, reduced expression levels, and frequent contractions in a clinical cohort of C9orf72 expansion carriers. Mol Neurodegener 15, 7. https://doi.org/10.1186/s13024-020-0359-8

Jain, S., Wheeler, J.R., Walters, R.W., Agrawal, A., Barsic, A., Parker, R., 2016. ATPase-Modulated Stress Granules Contain a Diverse Proteome and Substructure. Cell 164, 487–498. https://doi.org/10.1016/j.cell.2015.12.038

Jäkel, S., Görlich, D., 1998. Importin β, transportin, RanBP5 and RanBP7 mediate nuclear import of ribosomal proteins in mammalian cells. EMBO J 17, 4491–4502. https://doi.org/10.1093/EMBOJ/17.15.4491

Jani, D., Lutz, S., Hurt, E., Laskey, R.A., Stewart, M., Wickramasinghe, V.O., 2012. Functional and structural characterization of the mammalian TREX-2 complex that links transcription with nuclear messenger RNA export. Nucleic Acids Res 40, 4562–4573. https://doi.org/10.1093/NAR/GKS059

Jani, D., Lutz, S., Marshall, N.J., Fischer, T., Köhler, A., Ellisdon, A.M., Hurt, E., Stewart, M., 2009. Sus1, Cdc31, and the Sac3 CID Region Form a Conserved Interaction Platform that Promotes Nuclear Pore Association and mRNA Export. Mol Cell 33, 727. https://doi.org/10.1016/J.MOLCEL.2009.01.033

Jesso, S., Morlog, D., Ross, S., Pell, M.D., Pasternak, S.H., Mitchell, D.G.V., Kertesz, A., Finger, E.C., 2011. The effects of oxytocin on social cognition and behaviour in frontotemporal dementia. Brain 134, 2493–2501. https://doi.org/10.1093/BRAIN/AWR171

Jiang, J., Zhu, Q., Gendron, T.F., Saberi, S., McAlonis-Downes, M., Seelman, A., Stauffer, J.E., Jafar-nejad, P., Drenner, K., Schulte, D., Chun, S., Sun, S., Ling, S.-C., Myers, B., Engelhardt, J., Katz, M., Baughn, M., Platoshyn, O., Marsala, M., Watt, A., Heyser, C.J., Ard, M.C., De Muynck, L., Daughrity, L.M., Swing, D.A., Tessarollo, L., Jung, C.J., Delpoux, A., Utzschneider, D.T., Hedrick, S.M., de Jong, P.J., Edbauer, D., Van Damme, P., Petrucelli, L., Shaw, C.E., Bennett, C.F., Da Cruz, S., Ravits, J., Rigo, F., Cleveland, D.W., Lagier-Tourenne, C., 2016. Gain of Toxicity from ALS/FTD-Linked Repeat Expansions in C9ORF72 Is Alleviated by Antisense Oligonucleotides Targeting GGGGCC-Containing RNAs. Neuron 90, 535–550. https://doi.org/10.1016/J.NEURON.2016.04.006

Johnson, J.K., Diehl, J., Mendez, M.F., Neuhaus, J., Shapira, J.S., Forman, M., Chute, D.J., Roberson, E.D., Pace-Savitsky, C., Neumann, M., Chow, T.W., Rosen, H.J., Forstl, H., Kurz, A., Miller, B.L., 2005. Frontotemporal Lobar Degeneration: Demographic Characteristics of 353 Patients. Arch Neurol 62, 925–930. https://doi.org/10.1001/ARCHNEUR.62.6.925

Jordan, B.A., Kreutz, M.R., 2009. Nucleocytoplasmic protein shuttling: the direct route in synapse-to-nucleus signaling. Trends Neurosci 32, 392–401. https://doi.org/10.1016/j.tins.2009.04.001

Josephs, K.A., Parisi, J.E., Knopman, D.S., Boeve, B.F., Petersen, R.C., Dickson, D.W., 2006. Clinically Undetected Motor Neuron Disease in Pathologically Proven Frontotemporal Lobar Degeneration With Motor Neuron Disease. Arch Neurol 63, 506–512. https://doi.org/10.1001/ARCHNEUR.63.4.506

Jovičić, A., Mertens, J., Boeynaems, S., Bogaert, E., Chai, N., Yamada, S.B., Paul, J.W., Sun, S., Herdy, J.R., Bieri, G., Kramer, N.J., Gage, F.H., van den Bosch, L., Robberecht, W., Gitler, A.D., 2015. Modifiers of C9orf72 dipeptide repeat toxicity connect nucleocytoplasmic transport defects to FTD/ALS. Nat Neurosci 18, 1226–1229. https://doi.org/10.1038/nn.4085

Jutzi, D., Campagne, S., Schmidt, R., Reber, S., Mechtersheimer, J., Gypas, F., Schweingruber, C., Colombo, M., von Schroetter, C., Loughlin, F.E., Devoy, A., Hedlund, E., Zavolan, M., Allain, F.H.T., Ruepp, M.D., 2020. Aberrant interaction of FUS with the U1 snRNA provides a molecular mechanism of FUS induced amyotrophic lateral sclerosis. Nature Communications 2020 11:1 11, 1–14. https://doi.org/10.1038/s41467-020-20191-3

Kalab, P., Weis, K., Heald, R., 2002. Visualization of a Ran-GTP gradient in interphase and mitotic Xenopus egg extracts. Science (1979) 295, 2452–2456. https://doi.org/10.1126/SCIENCE.1068798/SUPPL_FILE/1068798S5_THUMB.GIF

Kalderon, D., Richardson, W.D., Markham, A.F., Smith, A.E., 1984. Sequence requirements for nuclear location of simian virus 40 large-T antigen. Nature 311, 33–38. https://doi.org/10.1038/311033A0

Kalita, J., Kapinos, L.E., Lim, R.Y.H., 2021. On the asymmetric partitioning of nucleocytoplasmic transport – recent insights and open questions. J Cell Sci 134. https://doi.org/10.1242/jcs.240382

Kamelgarn, M., Chen, J., Kuang, L., Jin, H., Kasarskis, E.J., Zhu, H., 2018. ALS mutations of FUS suppress protein translation and disrupt the regulation of nonsense-mediated decay. Proc Natl Acad Sci U S A 115, E11904–E11913. https://doi.org/10.1073/PNAS.1810413115/SUPPL_FILE/PNAS.1810413115.SD03.XLSX

Kaneb, H.M., Folkmann, A.W., Belzil, V. v., Jao, L.E., Leblond, C.S., Girard, S.L., Daoud, H., Noreau, A., Rochefort, D., Hince, P., Szuto, A., Levert, A., Vidal, S., André-Guimont, C., Camu, W., Bouchard, J.P., Dupré, N., Rouleau, G.A., Wente, S.R., Dion, P.A., 2015. Deleterious mutations in the essential mRNA metabolism factor, hGle1, in amyotrophic lateral sclerosis. Hum Mol Genet 24, 1363–1373. https://doi.org/10.1093/HMG/DDU545

Kanekura, K., Yagi, T., Cammack, A.J., Mahadevan, J., Kuroda, M., Harms, M.B., Miller, T.M., Urano, F., 2016. Poly-dipeptides encoded by the C9ORF72 repeats

block global protein translation. Hum Mol Genet 25, 1803–1813. https://doi.org/10.1093/hmg/ddw052

Kapinos, L.E., Huang, B., Rencurel, C., Lim, R.Y.H., 2017. Karyopherins regulate nuclear pore complex barrier and transport function. Journal of Cell Biology 216, 3609–3624. https://doi.org/10.1083/jcb.201702092

Kapinos, L.E., Schoch, R.L., Wagner, R.S., Schleicher, K.D., Lim, R.Y.H., 2014. Karyopherin-centric control of nuclear pores based on molecular occupancy and kinetic analysis of multivalent binding with FG nucleoporins. Biophys J 106, 1751–1762. https://doi.org/10.1016/J.BPJ.2014.02.021

Kapuscinski, J., 1995. DAPI: a DNA-Specific Fluorescent Probe. Biotechnic & Histochemistry 70, 220–233. https://doi.org/10.3109/10520299509108199

Katahira, J., 2015. Nuclear export of messenger RNA. Genes (Basel) 6, 163–84. https://doi.org/10.3390/genes6020163

Katzeff, J.S., Bright, F., Phan, K., Kril, J.J., Ittner, L.M., Kassiou, M., Hodges, J.R., Piguet, O., Kiernan, M.C., Halliday, G.M., Kim, W.S., 2022. Biomarker discovery and development for frontotemporal dementia and amyotrophic lateral sclerosis. Brain 139, 16–17. https://doi.org/10.1093/BRAIN/AWAC077

Kawai, H., Nakai, H., Suga, M., Yuki, S., Watanabe, T., Saito, K.-I., 1997. Effects of a Novel Free Radical Scavenger, MCI-186, on Ischemic Brain Damage in the Rat Distal Middle Cerebral Artery Occlusion Model. Journal of Pharmacology and Experimental Therapeutics 281.

Kedersha, N., Chen, S., Gilks, N., Li, W., Miller, I.J., Stahl, J., Anderson, P., 2002. Evidence that ternary complex (eIF2-GTP-tRNAiMet)-Deficient preinitiation complexes are core constituents of mammalian stress granules. Mol Biol Cell 13, 195–210. https://doi.org/10.1091/MBC.01-05-0221/ASSET/IMAGES/LARGE/MK0121717009.JPEG

Khosravi, B., Hartmann, H., May, S., Möhl, C., Ederle, H., Michaelsen, M., Schludi, M.H., Dormann, D., Edbauer, D., 2017. Cytoplasmic poly-GA aggregates impair nuclear import of TDP-43 in C9orf72 ALS/FTLD. Hum Mol Genet 26, ddw432. https://doi.org/10.1093/hmg/ddw432

Khosravi, B., LaClair, K.D., Riemenschneider, H., Zhou, Q., Frottin, F., Mareljic, N., Czuppa, M., Farny, D., Hartmann, H., Michaelsen, M., Arzberger, T., Hartl, F.U., Hipp, M.S., Edbauer, D., 2020. Cell-to-cell transmission of C9orf72 poly-(Gly-

Ala) triggers key features of ALS / FTD. EMBO J 39. https://doi.org/10.15252/embj.2019102811

Kim, G., Gautier, O., Tassoni-Tsuchida, E., Ma, X.R., Gitler, A.D., 2020. ALS Genetics: Gains, Losses, and Implications for Future Therapies. Neuron 108, 822–842. https://doi.org/10.1016/J.NEURON.2020.08.022

Kim, K.H., Sederstrom, J.M., 2015. Assaying cell cycle status using flow cytometry. Current protocols in molecular biology / edited by Frederick M. Ausubel ... [et al.] 111, 28.6.1. https://doi.org/10.1002/0471142727.MB2806S111

Kim, Y.E., Park, C., Kim, K.E., Kim, K.K., 2018. Histone and RNA-binding protein interaction creates crosstalk network for regulation of alternative splicing. Biochem Biophys Res Commun 499, 30–36. https://doi.org/10.1016/J.BBRC.2018.03.101

Kimura, M., Imamoto, N., 2014. Biological Significance of the Importin-β Family-Dependent Nucleocytoplasmic Transport Pathways. Traffic 15, 727–748. https://doi.org/10.1111/TRA.12174

Kinoshita, Y., Ito, H., Hirano, A., Fujita, K., Wate, R., Nakamura, M., Kaneko, S., Nakano, S., Kusaka, H., 2009. Nuclear Contour Irregularity and Abnormal Transporter Protein Distribution in Anterior Horn Cells in Amyotrophic Lateral Sclerosis. J Neuropathol Exp Neurol 68, 1184–1192. https://doi.org/10.1097/NEN.0B013E3181BC3BEC

Kinoshita, Y., Kalir, T., Dottino, P., Kohtz, D.S., 2012. Nuclear Distributions of NUP62 and NUP214 Suggest Architectural Diversity and Spatial Patterning among Nuclear Pore Complexes. PLoS One 7, e36137. https://doi.org/10.1371/JOURNAL.PONE.0036137

Kirola, L., Mukherjee, A., Mutsuddi, · Mousumi, 2022. Recent Updates on the Genetics of Amyotrophic Lateral Sclerosis and Frontotemporal Dementia. Molecular Neurobiology 2022 59:9 59, 5673–5694. https://doi.org/10.1007/S12035-022-02934-Z

Klebe, C., Prinz, H., Wittinghofer, A., Goody, R.S., 1995. The Kinetic Mechanism of Ran-Nucleotide Exchange Catalyzed by RCC1. Biochemistry 34, 12543–12552. https://doi.org/10.1021/BI00039A008/ASSET/BI00039A008.FP.PNG_V03

Klim, J.R., Williams, L.A., Limone, F., Guerra San Juan, I., Davis-Dusenbery, B.N., Mordes, D.A., Burberry, A., Steinbaugh, M.J., Gamage, K.K., Kirchner, R., Moccia, R., Cassel, S.H., Chen, K., Wainger, B.J., Woolf, C.J., Eggan, K., 2019.

ALS-implicated protein TDP-43 sustains levels of STMN2, a mediator of motor neuron growth and repair. Nat Neurosci. https://doi.org/10.1038/s41593-018-0300-4

Kobayashi, J., Matsuura, Y., 2013. Structural basis for cell-cycle-dependent nuclear import mediated by the karyopherin Kap121p. J Mol Biol 425, 1852–1868. https://doi.org/10.1016/J.JMB.2013.02.035

Kobe, B., 1999. Autoinhibition by an internal nuclear localization signal revealed by the crystal structure of mammalian importin alpha. Nat Struct Biol 6, 388–397. https://doi.org/10.1038/7625

Kodiha, M., Chu, A., Matusiewicz, N., Stochaj, U., 2004. Multiple mechanisms promote the inhibition of classical nuclear import upon exposure to severe oxidative stress. Cell Death & Differentiation 2004 11:8 11, 862–874. https://doi.org/10.1038/sj.cdd.4401432

Kodiha, M., Tran, D., Qian, C., Morogan, A., Presley, J.F., Brown, C.M., Stochaj, U., 2008. Oxidative stress mislocalizes and retains transport factor importin-α and nucleoporins Nup153 and Nup88 in nuclei where they generate high molecular mass complexes. Biochimica et Biophysica Acta (BBA) - Molecular Cell Research 1783, 405–418. https://doi.org/10.1016/J.BBAMCR.2007.10.022

Köhler, A., Hurt, E., 2010. Gene regulation by nucleoporins and links to cancer. Mol Cell 38, 6–15. https://doi.org/10.1016/J.MOLCEL.2010.01.040

Koppers, M., Blokhuis, A.M., Westeneng, H.-J., Terpstra, M.L., Zundel, C.A.C., Vieira de Sá, R., Schellevis, R.D., Waite, A.J., Blake, D.J., Veldink, J.H., van den Berg, L.H., Pasterkamp, R.J., 2015. C9orf72 ablation in mice does not cause motor neuron degeneration or motor deficits. Ann Neurol 78, 426–438. https://doi.org/10.1002/ana.24453

Korwek, Z., Tudelska, K., Nałęcz-Jawecki, P., Czerkies, M., Prus, W., Markiewicz, J., Kochańczyk, M., Lipniacki, T., 2016. Importins promote high-frequency NF-κB oscillations increasing information channel capacity. Biol Direct 11, 61. https://doi.org/10.1186/s13062-016-0164-z

Kosinski, J., Mosalaganti, S., von Appen, A., Teimer, R., DiGuilio, A.L., Wan, W., Bui, K.H., Hagen, W.J.H., Briggs, J.A.G., Glavy, J.S., Hurt, E., Beck, M., 2016. Molecular architecture of the inner ring scaffold of the human nuclear pore complex. Science (1979) 352, 363–365. https://doi.org/10.1126/science.aaf0643

Kosyna, F.K., Depping, R., 2018. Controlling the Gatekeeper: Therapeutic Targeting of Nuclear Transport. Cells 2018, Vol. 7, Page 221 7, 221. https://doi.org/10.3390/CELLS7110221

Kovacs, G.G., van der Zee, J., Hort, J., Kristoferitsch, W., Leitha, T., Höftberger, R., Ströbel, T., van Broeckhoven, C., Matej, R., 2016. Clinicopathological description of two cases with SQSTM1 gene mutation associated with frontotemporal dementia. Neuropathology 36, 27–38. https://doi.org/10.1111/NEUP.12233

Kovacs, M., Alamón, C., Maciel, C., Varela, V., Ibarburu, S., Tarragó, L., King, P.H., Si, Y., Kwon, Y., Hermine, O., Barbeito, L., Trias, E., 2021. The pathogenic role of c-Kit+ mast cells in the spinal motor neuron-vascular niche in ALS. Acta Neuropathol Commun 9, 1–18. https://doi.org/10.1186/S40478-021-01241-3/FIGURES/8

Koyama, M., Hirano, H., Shirai, N., Matsuura, Y., 2017. Crystal structure of the Xpo1p nuclear export complex bound to the SxFG/PxFG repeats of the nucleoporin Nup42p. Genes to Cells 22, 861–875. https://doi.org/10.1111/GTC.12520

Koyama, M., Shirai, N., Matsuura, Y., 2014. Structural insights into how Yrb2p accelerates the assembly of the Xpo1p nuclear export complex. Cell Rep 9, 983–995. https://doi.org/10.1016/J.CELREP.2014.09.052

Kraemer, B.C., Schuck, T., Wheeler, J.M., Robinson, L.C., Trojanowski, J.Q., Lee, V.M.Y., Schellenberg, G.D., 2010. Loss of Murine TDP-43 disrupts motor function and plays an essential role in embryogenesis. Acta Neuropathol 119, 409–419. https://doi.org/10.1007/S00401-010-0659-0/FIGURES/5

Kramer, N.J., Haney, M.S., Morgens, D.W., Jovičić, A., Couthouis, J., Li, A., Ousey, J., Ma, R., Bieri, G., Tsui, C.K., Shi, Y., Hertz, N.T., Tessier-Lavigne, M., Ichida, J.K., Bassik, M.C., Gitler, A.D., 2018. CRISPR–Cas9 screens in human cells and primary neurons identify modifiers of C9ORF72 dipeptide-repeat-protein toxicity. Nat Genet 50, 603–612. https://doi.org/10.1038/s41588-018-0070-7

Krull, S., Dörries, J., Boysen, B., Reidenbach, S., Magnius, L., Norder, H., Thyberg, J., Cordes, V.C., 2010. Protein Tpr is required for establishing nuclear pore-associated zones of heterochromatin exclusion. EMBO J 29, 1659–1673. https://doi.org/10.1038/EMBOJ.2010.54

Kumeta, M., Yoshimura, S.H., Hejna, J., Takeyasu, K., 2012. Nucleocytoplasmic shuttling of cytoskeletal proteins: molecular mechanism and biological significance. Int J Cell Biol 2012, 494902. https://doi.org/10.1155/2012/494902

Kuo, P.H., Chiang, C.H., Wang, Y.T., Doudeva, L.G., Yuan, H.S., 2014. The crystal structure of TDP-43 RRM1-DNA complex reveals the specific recognition for UG- and TG-rich nucleic acids. Nucleic Acids Res 42, 4712. https://doi.org/10.1093/NAR/GKT1407

Kutay, U., Güttinger, S., 2005. Leucine-rich nuclear-export signals: born to be weak. Trends Cell Biol 15, 121–124. https://doi.org/10.1016/J.TCB.2005.01.005

Kutay, U., Lipowsky, G., Izaurralde, E., Bischoff, F.R., Schwarzmaier, P., Hartmann, E., Görlich, D., 1998. Identification of a tRNA-specific nuclear export receptor. Mol Cell 1, 359–369. https://doi.org/10.1016/S1097-2765(00)80036-2

Kutay, U., Ralf Bischoff, F., Kostka, S., Kraft, R., Görlich, D., 1997. Export of importin alpha from the nucleus is mediated by a specific nuclear transport factor. Cell 90, 1061–1071. https://doi.org/10.1016/S0092-8674(00)80372-4

Kwon, I., Xiang, S., Kato, M., Wu, L., Theodoropoulos, P., Wang, T., Kim, J., Yun, J., Xie, Y., McKnight, S.L., 2014. Poly-dipeptides encoded by the C9orf72 repeats bind nucleoli, impede RNA biogenesis, and kill cells. Science 345, 1139–45. https://doi.org/10.1126/science.1254917

LaClair, K.D., Zhou, Q., Michaelsen, M., Wefers, B., Brill, M.S., Janjic, A., Rathkolb, B., Farny, D., Cygan, M., de Angelis, M.H., Wurst, W., Neumann, M., Enard, W., Misgeld, T., Arzberger, T., Edbauer, D., 2020. Congenic expression of poly-GA but not poly-PR in mice triggers selective neuron loss and interferon responses found in C9orf72 ALS. Acta Neuropathol 1–22. https://doi.org/10.1007/s00401-020-02176-0

Lacomblez, L., Bensimon, G., Leigh, P.N., Guillet, P., Meininger, V., 1996. Dose-ranging study of riluzole in amyotrophic lateral sclerosis. Amyotrophic Lateral Sclerosis/Riluzole Study Group II. Lancet 347, 1425–1431. https://doi.org/10.1016/S0140-6736(96)91680-3

Lagier-Tourenne, C., Baughn, M., Rigo, F., Sun, S., Liu, P., Li, H.-R., Jiang, J., Watt, A.T., Chun, S., Katz, M., Qiu, J., Sun, Y., Ling, S.-C., Zhu, Q., Polymenidou, M., Drenner, K., Artates, J.W., McAlonis-Downes, M., Markmiller, S., Hutt, K.R., Pizzo, D.P., Cady, J., Harms, M.B., Baloh, R.H., Vandenberg, S.R., Yeo, G.W., Fu, X.-D., Bennett, C.F., Cleveland, D.W., Ravits, J., 2013. Targeted

degradation of sense and antisense C9orf72 RNA foci as therapy for ALS and frontotemporal degeneration. Proc Natl Acad Sci U S A 110, E4530-9. https://doi.org/10.1073/pnas.1318835110

Lagier-Tourenne, C., Polymenidou, M., Cleveland, D.W., 2010. TDP-43 and FUS/TLS: emerging roles in RNA processing and neurodegeneration. Hum Mol Genet 19, R46–R64. https://doi.org/10.1093/HMG/DDQ137

Lee, B.J., Cansizoglu, A.E., Süel, K.E., Louis, T.H., Zhang, Z., Chook, Y.M., 2006. Rules for Nuclear Localization Sequence Recognition by Karyopherinβ2. Cell 126, 543–558. https://doi.org/10.1016/j.cell.2006.05.049

Lee, H. gon, Ueda, M., Miyamoto, Y., Yoneda, Y., Perry, G., Smith, M.A., Zhu, X., 2006. Aberrant localization of importin α1 in hippocampal neurons in Alzheimer disease. Brain Res 1124, 1–4. https://doi.org/10.1016/J.BRAINRES.2006.09.084

Lee, J., Park, J., Kim, J., Lee, G., Park, T.-E., Yoon, K.-J., Kim, Y.K., Lim, C., 2020. LSM12-EPAC1 defines a neuroprotective pathway that sustains the nucleocytoplasmic RAN gradient. PLoS Biol 18, e3001002. https://doi.org/10.1371/journal.pbio.3001002

Lee, K.-H., Zhang, P., Kim, H.J., Mitrea, D.M., Sarkar, M., Freibaum, B.D., Cika, J., Coughlin, M., Messing, J., Molliex, A., Maxwell, B.A., Kim, N.C., Temirov, J., Moore, J., Kolaitis, R.-M., Shaw, T.I., Bai, B., Peng, J., Kriwacki, R.W., Taylor, J.P., 2016. C9orf72 Dipeptide Repeats Impair the Assembly, Dynamics, and Function of Membrane-Less Organelles. Cell 167, 774-788.e17. https://doi.org/10.1016/J.CELL.2016.10.002

Lee, P.T., Liévens, J.C., Wang, S.M., Chuang, J.Y., Khalil, B., Wu, H. en, Chang, W.C., Maurice, T., Su, T.P., 2020. Sigma-1 receptor chaperones rescue nucleocytoplasmic transport deficit seen in cellular and Drosophila ALS/FTD models. Nat Commun 11, 1–14. https://doi.org/10.1038/s41467-020-19396-3

Lee, S.J., Matsuura, Y., Liu, S.M., Stewart, M., 2005. Structural basis for nuclear import complex dissociation by RanGTP. Nature 435, 693–696. https://doi.org/10.1038/NATURE03578

Lee, S.M., Asress, S., Hales, C.M., Gearing, M., Vizcarra, J.C., Fournier, C.N., Gutman, D.A., Chin, L.-S., Li, L., Glass, J.D., 2019. TDP-43 cytoplasmic inclusion formation is disrupted in C9orf72-associated amyotrophic lateral

sclerosis/frontotemporal lobar degeneration. Brain Commun 1. https://doi.org/10.1093/BRAINCOMMS/FCZ014

Lee, Y.-B., Chen, H.-J., Peres, J.N., Gomez-Deza, J., Attig, J., Štalekar, M., Troakes, C., Nishimura, A.L., Scotter, E.L., Vance, C., Adachi, Y., Sardone, V., Miller, J.W., Smith, B.N., Gallo, J.-M., Ule, J., Hirth, F., Rogelj, B., Houart, C., Shaw, C.E., 2013. Hexanucleotide Repeats in ALS/FTD Form Length-Dependent RNA Foci, Sequester RNA Binding Proteins, and Are Neurotoxic. Cell Rep 5, 1178–1186. https://doi.org/10.1016/J.CELREP.2013.10.049

Li, S., Wu, Z., Li, Y., Tantray, I., de Stefani, D., Mattarei, A., Krishnan, G., Gao, F.-B., Vogel, H., Lu, B., 2020a. Altered MICOS Morphology and Mitochondrial Ion Homeostasis Contribute to Poly(GR) Toxicity Associated with C9-ALS/FTD. Cell Rep 32, 107989. https://doi.org/10.1016/j.celrep.2020.107989

Li, S., Wu, Z., Tantray, I., Li, Y., Chen, S., Dong, J., Glynn, S., Vogel, H., 2020b. Quality-control mechanisms targeting translationally stalled and C-terminally extended poly (GR) associated with ALS / FTD. Proceedings of the National Academy of Sciences 1–12. https://doi.org/10.1073/pnas.2005506117

Li, Y., Zhou, J., Min, S., Zhang, Yang, Zhang, Yuqing, Zhou, Q., Shen, X., Jia, D., Han, J., Sun, Q., 2019. Distinct RanBP1 nuclear export and cargo dissociation mechanisms between fungi and animals. Elife 8. https://doi.org/10.7554/ELIFE.41331

Li, Y.R., King, O.D., Shorter, J., Gitler, A.D., 2013. Stress granules as crucibles of ALS pathogenesis. Journal of Cell Biology 201, 361–372. https://doi.org/10.1083/JCB.201302044

Liang, Y., Franks, T.M., Marchetto, M.C., Gage, F.H., Hetzer, M.W., 2013. Dynamic Association of NUP98 with the Human Genome. PLoS Genet 9, e1003308. https://doi.org/10.1371/JOURNAL.PGEN.1003308

Lim, R.Y.H., Fahrenkrog, B., Köser, J., Schwarz-Herion, K., Deng, J., Aebi, U., 2007. Nanomechanical basis of selective gating by the nuclear pore complex. Science 318, 640–643. https://doi.org/10.1126/SCIENCE.1145980

Lin, D.H., Hoelz, A., 2019. The Structure of the Nuclear Pore Complex (An Update). https://doi.org/10.1146/annurev-biochem-062917-011901 88, 725–783. https://doi.org/10.1146/ANNUREV-BIOCHEM-062917-011901

Lin, D.H., Stuwe, T., Schilbach, S., Rundlet, E.J., Perriches, T., Mobbs, G., Fan, Y., Thierbach, K., Huber, F.M., Collins, L.N., Davenport, A.M., Jeon, Y.E., Hoelz, A.,

2016. Architecture of the symmetric core of the nuclear pore. Science 352. https://doi.org/10.1126/SCIENCE.AAF1015

Lin, Y., Mori, E., Kato, M., Xiang, S., Wu, L., Kwon, I., McKnight, S.L., 2016. Toxic PR Poly-Dipeptides Encoded by the C9orf72 Repeat Expansion Target LC Domain Polymers. Cell 167, 789-802.e12. https://doi.org/10.1016/J.CELL.2016.10.003

Lin, Y.-C., Kumar, M.S., Ramesh, N., Anderson, E.N., Nguyen, A.T., Kim, B., Cheung, S., McDonough, J.A., Skarnes, W.C., Lopez-Gonzalez, R., Landers, J.E., Fawzi, N.L., Mackenzie, I.R.A., Lee, E.B., Nickerson, J.A., Grunwald, D., Pandey, U.B., Bosco, D.A., 2021. Interactions between ALS-linked FUS and nucleoporins are associated with defects in the nucleocytoplasmic transport pathway. Nat Neurosci 1–12. https://doi.org/10.1038/s41593-021-00859-9

Lindsay, M.E., Plafker, K., Smith, A.E., Clurman, B.E., Macara, I.G., 2002. Npap60/Nup50 is a tri-stable switch that stimulates importin-α:β-mediated nuclear protein import. Cell 110, 349–360. https://doi.org/10.1016/S0092-8674(02)00836-X

Ling, J.P., Pletnikova, O., Troncoso, J.C., Wong, P.C., 2015. TDP-43 repression of nonconserved cryptic exons is compromised in ALS-FTD. Science (1979) 349, 650–655. https://doi.org/10.1126/SCIENCE.AAB0983/SUPPL_FILE/LING-SM.PDF

Ling, S.-C., Polymenidou, M., Cleveland, D.W., 2013. Converging Mechanisms in ALS and FTD: Disrupted RNA and Protein Homeostasis. Neuron 79, 416–438. https://doi.org/10.1016/J.NEURON.2013.07.033

Lipowsky, G., Bischoff, F.R., Schwarzmaier, P., Kraft, R., Kostka, S., Hartmann, E., Kutay, U., Görlich, D., 2000. Exportin 4: a mediator of a novel nuclear export pathway in higher eukaryotes. EMBO J 19, 4362. https://doi.org/10.1093/EMBOJ/19.16.4362

Liu, E.Y., Russ, J., Wu, K., Neal, D., Suh, E., McNally, A.G., Irwin, D.J., van Deerlin, V.M., Lee, E.B., 2014. C9orf72 hypermethylation protects against repeat expansion-associated pathology in ALS/FTD. Acta Neuropathol 128, 525–541. https://doi.org/10.1007/S00401-014-1286-Y

Logroscino, G., Traynor, B.J., Hardiman, O., Chió, A., Mitchell, D., Swingler, R.J., Millul, A., Benn, E., Beghi, E., 2010. Incidence of amyotrophic lateral sclerosis in

Europe. J Neurol Neurosurg Psychiatry 81, 385–390. https://doi.org/10.1136/JNNP.2009.183525

López-Erauskin, J., Tadokoro, T., Baughn, M.W., Myers, B., McAlonis-Downes, M., Chillon-Marinas, C., Asiaban, J.N., Artates, J., Bui, A.T., Vetto, A.P., Lee, S.K., Le, A.V., Sun, Y., Jambeau, M., Boubaker, J., Swing, D., Qiu, J., Hicks, G.G., Ouyang, Z., Fu, X.D., Tessarollo, L., Ling, S.C., Parone, P.A., Shaw, C.E., Marsala, M., Lagier-Tourenne, C., Cleveland, D.W., da Cruz, S., 2018. ALS/FTD-Linked Mutation in FUS Suppresses Intra-axonal Protein Synthesis and Drives Disease Without Nuclear Loss-of-Function of FUS. Neuron 100, 816-830.e7. https://doi.org/10.1016/J.NEURON.2018.09.044/ATTACHMENT/551C5DB9-5B57-419F-B087-C88DE31A9E6E/MMC2.XLSX

Lopez-Gonzalez, R., Lu, Y., Gendron, T.F., Karydas, A., Tran, H., Yang, D., Petrucelli, L., Miller, B.L., Almeida, S., Gao, F.-B., 2016. Poly(GR) in C9ORF72-Related ALS/FTD Compromises Mitochondrial Function and Increases Oxidative Stress and DNA Damage in iPSC-Derived Motor Neurons. Neuron 92, 383–391. https://doi.org/10.1016/J.NEURON.2016.09.015

Lott, K., Bhardwaj, A., Sims, P.J., Cingolani, G., 2011. A Minimal Nuclear Localization Signal (NLS) in Human Phospholipid Scramblase 4 That Binds Only the Minor NLS-binding Site of Importin α1. J Biol Chem 286, 28160. https://doi.org/10.1074/JBC.M111.228007

Loveland, A.B., Svidritskiy, E., Susorov, D., Lee, S., Park, A., Zvornicanin, S., Demo, G., Gao, F.B., Korostelev, A.A., 2022. Ribosome inhibition by C9ORF72-ALS/FTD-associated poly-PR and poly-GR proteins revealed by cryo-EM. Nature Communications 2022 13:1 13, 1–13. https://doi.org/10.1038/s41467-022-30418-0

Lowe, A.R., Tang, J.H., Yassif, J., Graf, M., Huang, W.Y., Groves, J.T., Weis, K., Liphardt, J.T., 2015. Importin-β modulates the permeability of the nuclear pore complex in a Ran-dependent manner. Elife 4, e04052. https://doi.org/10.7554/eLife.04052

Lukavsky, P.J., Daujotyte, D., Tollervey, J.R., Ule, J., Stuani, C., Buratti, E., Baralle, F.E., Damberger, F.F., Allain, F.H.T., 2013. Molecular basis of UG-rich RNA recognition by the human splicing factor TDP-43. Nature Structural & Molecular Biology 2013 20:12 20, 1443–1449. https://doi.org/10.1038/nsmb.2698

Lyngdoh, D.L., Nag, N., Uversky, V.N., Tripathi, T., 2021. Prevalence and functionality of intrinsic disorder in human FG-nucleoporins. Int J Biol Macromol 175, 156–170. https://doi.org/10.1016/J.IJBIOMAC.2021.01.218

Mackenzie, I.R., Arzberger, T., Kremmer, E., Troost, D., Lorenzl, S., Mori, K., Weng, S.-M., Haass, C., Kretzschmar, H.A., Edbauer, D., Neumann, M., 2013. Dipeptide repeat protein pathology in C9ORF72 mutation cases: clinico-pathological correlations. Acta Neuropathol 126, 859–879. https://doi.org/10.1007/s00401-013-1181-y

Mackenzie, I.R.A., Bigio, E.H., Ince, P.G., Geser, F., Neumann, M., Cairns, N.J., Kwong, L.K., Forman, M.S., Ravits, J., Stewart, H., Eisen, A., McClusky, L., Kretzschmar, H.A., Monoranu, C.M., Highley, J.R., Kirby, J., Siddique, T., Shaw, P.J., Lee, V.M.-Y., Trojanowski, J.Q., 2007. Pathological TDP-43 distinguishes sporadic amyotrophic lateral sclerosis from amyotrophic lateral sclerosis withSOD1 mutations. Ann Neurol 61, 427–434. https://doi.org/10.1002/ana.21147

Mackenzie, I.R.A., Frick, P., Grässer, F.A., Gendron, T.F., Petrucelli, L., Cashman, N.R., Edbauer, D., Kremmer, E., Prudlo, J., Troost, D., Neumann, M., 2015. Quantitative analysis and clinico-pathological correlations of different dipeptide repeat protein pathologies in C9ORF72 mutation carriers. Acta Neuropathol 130, 845–861. https://doi.org/10.1007/S00401-015-1476-2

Mackenzie, I.R.A., Neumann, M., 2017. Fused in Sarcoma Neuropathology in Neurodegenerative Disease. Cold Spring Harb Perspect Med 7, a024299. https://doi.org/10.1101/CSHPERSPECT.A024299

Mackenzie, I.R.A., Neumann, M., 2016. Molecular neuropathology of frontotemporal dementia: insights into disease mechanisms from postmortem studies. J Neurochem 138, 54–70. https://doi.org/10.1111/jnc.13588

Maertens, G.N., Cook, N.J., Wang, W., Hare, S., Gupta, S.S., Öztop, I., Lee, K.E., Pye, V.E., Cosnefroy, O., Snijders, A.P., Ramani, V.N.K., Fassati, A., Engelman, A., Cherepanov, P., 2014. Structural basis for nuclear import of splicing factors by human Transportin 3. Proc Natl Acad Sci U S A 111, 2728–2733. https://doi.org/10.1073/PNAS.1320755111

Mahajan, R., Delphin, C., Guan, T., Gerace, L., Melchior, F., 1997. A Small Ubiquitin-Related Polypeptide Involved in Targeting RanGAP1 to Nuclear Pore

Complex Protein RanBP2. Cell 88, 97–107. https://doi.org/10.1016/S0092-8674(00)81862-0

Mahboubi, H., Seganathy, E., Kong, D., Stochaj, U., 2013. Identification of Novel Stress Granule Components That Are Involved in Nuclear Transport. PLoS One 8, e68356. https://doi.org/10.1371/JOURNAL.PONE.0068356

Mahoney, C.J., Beck, J., Rohrer, J.D., Lashley, T., Mok, K., Shakespeare, T., Yeatman, T., Warrington, E.K., Schott, J.M., Fox, N.C., Rossor, M.N., Hardy, J., Collinge, J., Revesz, T., Mead, S., Warren, J.D., 2012. Frontotemporal dementia with the C9ORF72 hexanucleotide repeat expansion: clinical, neuroanatomical and neuropathological features. Brain 135, 736–750. https://doi.org/10.1093/BRAIN/AWR361

Mahoney, C.J., Rohrer, J.D., Goll, J.C., Fox, N.C., Rossor, M.N., Warren, J.D., 2011. Structural neuroanatomy of tinnitus and hyperacusis in semantic dementia. J Neurol Neurosurg Psychiatry 82, 1274–1278. https://doi.org/10.1136/JNNP.2010.235473

Makise, M., Mackay, D.R., Elgort, S., Shankaran, S.S., Adam, S.A., Ullman, K.S., 2012. The Nup153-Nup50 protein interface and its role in nuclear import. J Biol Chem 287, 38515–22. https://doi.org/10.1074/jbc.M112.378893

Malik, A.M., Barmada, S.J., 2021. Matrin 3 in neuromuscular disease: physiology and pathophysiology. JCI Insight 6. https://doi.org/10.1172/JCI.INSIGHT.143948

Mann, D.M., Rollinson, S., Robinson, A., Bennion Callister, J., Thompson, J.C., Snowden, J.S., Gendron, T., Petrucelli, L., Masuda-Suzukake, M., Hasegawa, M., Davidson, Y., Pickering-Brown, S., 2013. Dipeptide repeat proteins are present in the p62 positive inclusions in patients with frontotemporal lobar degeneration and motor neurone disease associated with expansions in C9ORF72. Acta Neuropathol Commun 1, 68. https://doi.org/10.1186/2051-5960-1-68

Mann, J.R., Gleixner, A.M., Mauna, J.C., Gomes, E., DeChellis-Marks, M.R., Needham, P.G., Copley, K.E., Hurtle, B., Portz, B., Pyles, N.J., Guo, L., Calder, C.B., Wills, Z.P., Pandey, U.B., Kofler, J.K., Brodsky, J.L., Thathiah, A., Shorter, J., Donnelly, C.J., 2019. RNA Binding Antagonizes Neurotoxic Phase Transitions of TDP-43. Neuron 102, 321-338.e8. https://doi.org/10.1016/j.neuron.2019.01.048

Maor-Nof, M., Shipony, Z., Lopez-Gonzalez, R., Nakayama, L., Zhang, Y.-J., Couthouis, J., Blum, J.A., Castruita, P.A., Linares, G.R., Ruan, K., Ramaswami, G., Simon, D.J., Nof, A., Santana, M., Han, K., Sinnott-Armstrong, N., Bassik, M.C., Geschwind, D.H., Tessier-Lavigne, M., Attardi, L.D., Lloyd, T.E., Ichida, J.K., Gao, F.-B., Greenleaf, W.J., Yokoyama, J.S., Petrucelli, L., Gitler, A.D., 2021. p53 is a central regulator driving neurodegeneration caused by C9orf72 poly(PR). Cell. https://doi.org/10.1016/j.cell.2020.12.025

Markmiller, S., Soltanieh, S., Server, K.L., Mak, R., Jin, W., Fang, M.Y., Luo, E.C., Krach, F., Yang, D., Sen, A., Fulzele, A., Wozniak, J.M., Gonzalez, D.J., Kankel, M.W., Gao, F.B., Bennett, E.J., Lécuyer, E., Yeo, G.W., 2018. Context-Dependent and Disease-Specific Diversity in Protein Interactions within Stress Granules. Cell 172, 590-604.e13. https://doi.org/10.1016/j.cell.2017.12.032

Marshall, C.R., Hardy, C.J.D., Russell, L.L., Clark, C.N., Dick, K.M., Brotherhood, E. v., Bond, R.L., Mummery, C.J., Schott, J.M., Rohrer, J.D., Kilner, J.M., Warren, J.D., 2017. Impaired interoceptive accuracy in semantic variant primary progressive aphasia. Front Neurol 8, 610. https://doi.org/10.3389/FNEUR.2017.00610/XML/NLM

Masrori, P., van Damme, P., 2020. Amyotrophic lateral sclerosis: a clinical review. Eur J Neurol 27, 1918–1929. https://doi.org/10.1111/ENE.14393

Masuda, S., Das, R., Cheng, H., Hurt, E., Dorman, N., Reed, R., 2005. Recruitment of the human TREX complex to mRNA during splicing. Genes Dev 19, 1512–1517. https://doi.org/10.1101/GAD.1302205

Matsuura, Y., Stewart, M., 2005. Nup50/Npap60 function in nuclear protein import complex disassembly and importin recycling. EMBO J 24, 3681. https://doi.org/10.1038/SJ.EMBOJ.7600843

Matsuura, Y., Stewart, M., 2004. Structural basis for the assembly of a nuclear export complex. Nature 432, 872–877. https://doi.org/10.1038/NATURE03144

May, S., Hornburg, D., Schludi, M.H., Arzberger, T., Rentzsch, K., Schwenk, B.M., Grässer, F.A., Mori, K., Kremmer, E., Banzhaf-Strathmann, J., Mann, M., Meissner, F., Edbauer, D., 2014. C9orf72 FTLD/ALS-associated Gly-Ala dipeptide repeat proteins cause neuronal toxicity and Unc119 sequestration. Acta Neuropathol 128, 485–503. https://doi.org/10.1007/s00401-014-1329-4

McColgan, P., Tabrizi, S.J., 2018. Huntington's disease: a clinical review. Eur J Neurol 25, 24–34. https://doi.org/10.1111/ENE.13413

McGurk, L., Gomes, E., Guo, L., Mojsilovic-Petrovic, J., Tran, V., Kalb, R.G., Shorter, J., Bonini, N.M., 2018. Poly(ADP-Ribose) Prevents Pathological Phase Separation of TDP-43 by Promoting Liquid Demixing and Stress Granule Localization. Mol Cell 71, 703-717.e9. https://doi.org/10.1016/J.MOLCEL.2018.07.002

McKinsey, T.A., Zhang, C.L., Lu, J., Olson, E.N., 2000. Signal-dependent nuclear export of a histone deacetylase regulates muscle differentiation. Nature 408, 106–11. https://doi.org/10.1038/35040593

Mehta, A.R., Gregory, J.M., Dando, O., Carter, R.N., Burr, K., Nanda, J., Story, D., McDade, K., Smith, C., Morton, N.M., Mahad, D.J., Hardingham, G.E., Chandran, S., Selvaraj, B.T., 2021. Mitochondrial bioenergetic deficits in C9orf72 amyotrophic lateral sclerosis motor neurons cause dysfunctional axonal homeostasis. Acta Neuropathol 1, 3. https://doi.org/10.1007/s00401-020-02252-5

Mehta, P., Kaye, W., Raymond, J., Wu, R., Larson, T., Punjani, R., Heller, D., Cohen, J., Peters, T., Muravov, O., Horton, K., 2018. Prevalence of Amyotrophic Lateral Sclerosis — United States, 2014. MMWR Morb Mortal Wkly Rep 67, 216–218. https://doi.org/10.15585/mmwr.mm6707a3

Meier, S.L., Charleston, A.J., Tippett, L.J., 2010. Cognitive and behavioural deficits associated with the orbitomedial prefrontal cortex in amyotrophic lateral sclerosis. Brain 133, 3444–3457. https://doi.org/10.1093/BRAIN/AWQ254

Melamed, Z., López-Erauskin, J., Baughn, M.W., Zhang, O., Drenner, K., Sun, Y., Freyermuth, F., McMahon, M.A., Beccari, M.S., Artates, J.W., Ohkubo, T., Rodriguez, M., Lin, N., Wu, D., Bennett, C.F., Rigo, F., da Cruz, S., Ravits, J., Lagier-Tourenne, C., Cleveland, D.W., 2019. Premature polyadenylation-mediated loss of stathmin-2 is a hallmark of TDP-43-dependent neurodegeneration. Nature Neuroscience 2019 22:2 22, 180–190. https://doi.org/10.1038/s41593-018-0293-z

Mertens, J., Paquola, A.C.M., Ku, M., Hatch, E., Böhnke, L., Ladjevardi, S., McGrath, S., Campbell, B., Lee, H., Herdy, J.R., Gonçalves, J.T., Toda, T., Kim, Y., Winkler, J., Yao, J., Hetzer, M.W., Gage, F.H., 2015. Directly Reprogrammed Human Neurons Retain Aging-Associated Transcriptomic Signatures and Reveal Age-Related Nucleocytoplasmic Defects. Cell Stem Cell 17, 705–718. https://doi.org/10.1016/J.STEM.2015.09.001

Mertens, J., Reid, D., Lau, S., Kim, Y., Gage, F.H., 2018. Aging in a Dish: iPSC-Derived and Directly Induced Neurons for Studying Brain Aging and Age-Related Neurodegenerative Diseases. https://doi.org/10.1146/annurev-genet-120417-031534 52, 271–293. https://doi.org/10.1146/ANNUREV-GENET-120417-031534

Metuzals, J., Robitaille, Y., Houghton, S., Gauthier, S., Leblanc, R., 1988. Paired helical filaments and the cytoplasmic-nuclear interface in Alzheimer's disease. J Neurocytol 17, 827–833. https://doi.org/10.1007/BF01216709

Miller, R.G., Jackson, C.E., Kasarskis, E.J., England, J.D., Forshew, D., Johnston, W., Kalra, S., Katz, J.S., Mitsumoto, H., Rosenfeld, J., Shoesmith, C., Strong, M.J., Woolley, S.C., 2009. Practice parameter update: the care of the patient with amyotrophic lateral sclerosis: drug, nutritional, and respiratory therapies (an evidence-based review): report of the Quality Standards Subcommittee of the American Academy of Neurology. Neurology 73, 1218–1226. https://doi.org/10.1212/WNL.0B013E3181BC0141

Milles, S., Mercadante, D., Aramburu, I.V., Jensen, M.R., Banterle, N., Koehler, C., Tyagi, S., Clarke, J., Shammas, S.L., Blackledge, M., Gräter, F., Lemke, E.A., 2015. Plasticity of an ultrafast interaction between nucleoporins and nuclear transport receptors. Cell 163, 734–745. https://doi.org/10.1016/J.CELL.2015.09.047

Miyamoto, Y., Saiwaki, T., Yamashita, J., Yasuda, Y., Kotera, I., Shibata, S., Shigeta, M., Hiraoka, Y., Haraguchi, T., Yoneda, Y., 2004. Cellular stresses induce the nuclear accumulation of importin α and cause a conventional nuclear import block. Journal of Cell Biology 165, 617–623. https://doi.org/10.1083/JCB.200312008/VIDEO-4

Mizielinska, S., Grönke, S., Niccoli, T., Ridler, C.E., Clayton, E.L., Devoy, A., Moens, T., Norona, F.E., Woollacott, I.O.C., Pietrzyk, J., Cleverley, K., Nicoll, A.J., Pickering-Brown, S., Dols, J., Cabecinha, M., Hendrich, O., Fratta, P., Fisher, E.M.C., Partridge, L., Isaacs, A.M., 2014. C9orf72 repeat expansions cause neurodegeneration in Drosophila through arginine-rich proteins. Science 345, 1192–1194. https://doi.org/10.1126/science.1256800

Mizielinska, S., Lashley, T., Norona, F.E., Clayton, E.L., Ridler, C.E., Fratta, P., Isaacs, A.M., 2013. C9orf72 frontotemporal lobar degeneration is characterised

by frequent neuronal sense and antisense RNA foci. Acta Neuropathol 126, 845–857. https://doi.org/10.1007/s00401-013-1200-z

Mizielinska, S., Ridler, C.E., Balendra, R., Thoeng, A., Woodling, N.S., Grässer, F.A., Plagnol, V., Lashley, T., Partridge, L., Isaacs, A.M., 2017. Bidirectional nucleolar dysfunction in C9orf72 frontotemporal lobar degeneration. Acta Neuropathol Commun 5, 29. https://doi.org/10.1186/s40478-017-0432-x

Moens, T.G., Mizielinska, S., Niccoli, T., Mitchell, J.S., Thoeng, A., Ridler, C.E., Grönke, S., Esser, J., Heslegrave, A., Zetterberg, H., Partridge, L., Isaacs, A.M., 2018. Sense and antisense RNA are not toxic in Drosophila models of C9orf72-associated ALS/FTD. Acta Neuropathol 135, 445–457. https://doi.org/10.1007/s00401-017-1798-3

Moens, T.G., Niccoli, T., Wilson, K.M., Atilano, M.L., Birsa, N., Gittings, L.M., Holbling, B. v., Dyson, M.C., Thoeng, A., Neeves, J., Glaria, I., Yu, L., Bussmann, J., Storkebaum, E., Pardo, M., Choudhary, J.S., Fratta, P., Partridge, L., Isaacs, A.M., 2019. C9orf72 arginine-rich dipeptide proteins interact with ribosomal proteins in vivo to induce a toxic translational arrest that is rescued by eIF1A. Acta Neuropathol 137, 487–500. https://doi.org/10.1007/S00401-018-1946-4/FIGURES/5

Mohr, D., Frey, S., Fischer, T., Güttler, T., Görlich, D., 2009. Characterisation of the passive permeability barrier of nuclear pore complexes. EMBO J 28, 2541–2553. https://doi.org/10.1038/EMBOJ.2009.200

Moisse, K., Mepham, J., Volkening, K., Welch, I., Hill, T., Strong, M.J., 2009. Cytosolic TDP-43 expression following axotomy is associated with caspase 3 activation in NFL−/− mice: Support for a role for TDP-43 in the physiological response to neuronal injury. Brain Res 1296, 176–186. https://doi.org/10.1016/J.BRAINRES.2009.07.023

Molenaar, C., Weeks, K.L., 2018. Nucleocytoplasmic shuttling: the ins and outs of quantitative imaging. Clin Exp Pharmacol Physiol. https://doi.org/10.1111/1440-1681.12969

Molliex, A., Temirov, J., Lee, J., Coughlin, M., Kanagaraj, A.P., Kim, H.J., Mittag, T., Taylor, J.P., 2015. Phase Separation by Low Complexity Domains Promotes Stress Granule Assembly and Drives Pathological Fibrillization. Cell 163, 123–133. https://doi.org/10.1016/j.cell.2015.09.015

Monecke, T., Güttler, T., Neumann, P., Dickmanns, A., Görlich, D., Ficner, R., 2009. Crystal structure of the nuclear export receptor CRM1 in complex with Snurportin1 and RanGTP. Science 324, 1087–1091. https://doi.org/10.1126/SCIENCE.1173388

Montpetit, B., Thomsen, N.D., Helmke, K.J., Seeliger, M.A., Berger, J.M., Weis, K., 2011. A conserved mechanism of DEAD-box ATPase activation by nucleoporins and InsP6 in mRNA export. Nature 472, 238–244. https://doi.org/10.1038/NATURE09862

Montuschi, A., Iazzolino, B., Calvo, A., Moglia, C., Lopiano, L., Restagno, G., Brunetti, M., Ossola, I., lo Presti, A., Cammarosano, S., Canosa, A., Chiò, A., 2015. Cognitive correlates in amyotrophic lateral sclerosis: a population-based study in Italy. J Neurol Neurosurg Psychiatry 86, 168–173. https://doi.org/10.1136/JNNP-2013-307223

Mor, A., Suliman, S., Ben-Yishay, R., Yunger, S., Brody, Y., Shav-Tal, Y., 2010. Dynamics of single mRNP nucleocytoplasmic transport and export through the nuclear pore in living cells. Nat Cell Biol 12, 543–552. https://doi.org/10.1038/NCB2056

Mora, J.S., Bradley, W.G., Chaverri, D., Hernández-Barral, M., Mascias, J., Gamez, J., Gargiulo-Monachelli, G.M., Moussy, A., Mansfield, C.D., Hermine, O., Ludolph, A.C., 2021. Long-term survival analysis of masitinib in amyotrophic lateral sclerosis. Ther Adv Neurol Disord 14. https://doi.org/10.1177/17562864211030365

Mora, J.S., Genge, A., Chio, A., Estol, C.J., Chaverri, D., Hernández, M., Marín, S., Mascias, J., Rodriguez, G.E., Povedano, M., Paipa, A., Dominguez, R., Gamez, J., Salvado, M., Lunetta, C., Ballario, C., Riva, N., Mandrioli, J., Moussy, A., Kinet, J.P., Auclair, C., Dubreuil, P., Arnold, V., Mansfield, C.D., Hermine, O., 2020. Masitinib as an add-on therapy to riluzole in patients with amyotrophic lateral sclerosis: a randomized clinical trial. Amyotroph Lateral Scler Frontotemporal Degener 21, 5–14. https://doi.org/10.1080/21678421.2019.1632346

Mori, K., Arzberger, T., Grässer, F.A., Gijselinck, I., May, S., Rentzsch, K., Weng, S.-M., Schludi, M.H., van der Zee, J., Cruts, M., van Broeckhoven, C., Kremmer, E., Kretzschmar, H.A., Haass, C., Edbauer, D., 2013a. Bidirectional transcripts of the expanded C9orf72 hexanucleotide repeat are translated into aggregating

dipeptide repeat proteins. Acta Neuropathol 126, 881–893. https://doi.org/10.1007/s00401-013-1189-3

Mori, K., Weng, S.-M., Arzberger, T., May, S., Rentzsch, K., Kremmer, E., Schmid, B., Kretzschmar, H.A., Cruts, M., van Broeckhoven, C., Haass, C., Edbauer, D., 2013b. The C9orf72 GGGGCC repeat is translated into aggregating dipeptide-repeat proteins in FTLD/ALS. Science 339, 1335–8. https://doi.org/10.1126/science.1232927

Moutaoufik, M.T., el Fatimy, R., Nassour, H., Gareau, C., Lang, J., Tanguay, R.M., Mazroui, R., Khandjian, E.W., 2014. UVC-Induced Stress Granules in Mammalian Cells. PLoS One 9, e112742. https://doi.org/10.1371/JOURNAL.PONE.0112742

Murray, M.E., DeJesus-Hernandez, M., Rutherford, N.J., Baker, M., Duara, R., Graff-Radford, N.R., Wszolek, Z.K., Ferman, T.J., Josephs, K.A., Boylan, K.B., Rademakers, R., Dickson, D.W., 2011. Clinical and neuropathologic heterogeneity of c9FTD/ALS associated with hexanucleotide repeat expansion in C9ORF72. Acta Neuropathol 122, 673–690. https://doi.org/10.1007/s00401-011-0907-y

Nagara, Y., Tateishi, T., Yamasaki, R., Hayashi, S., Kawamura, M., Kikuchi, H., Iinuma, K.M., Tanaka, M., Iwaki, T., Matsushita, T., Ohyagi, Y., Kira, J.I., 2013. Impaired cytoplasmic-nuclear transport of hypoxia-inducible factor-1α in amyotrophic lateral sclerosis. Brain Pathology 23, 534–546. https://doi.org/10.1111/BPA.12040

Naim, B., Zbaida, D., Dagan, S., Kapon, R., Reich, Z., 2009. Cargo surface hydrophobicity is sufficient to overcome the nuclear pore complex selectivity barrier. EMBO J 28, 2697–2705. https://doi.org/10.1038/EMBOJ.2009.225

Nakielny, S., Dreyfuss, G., 1996. The hnRNP C proteins contain a nuclear retention sequence that can override nuclear export signals. Journal of Cell Biology 134, 1365–1373. https://doi.org/10.1083/JCB.134.6.1365

Nanaura, H., Kawamukai, H., Fujiwara, A., Uehara, T., Aiba, Y., Nakanishi, M., Shiota, T., Hibino, M., Wiriyasermkul, P., Kikuchi, S., Nagata, R., Matsubayashi, M., Shinkai, Y., Niwa, T., Mannen, T., Morikawa, N., Iguchi, N., Kiriyama, T., Morishima, K., Inoue, R., Sugiyama, M., Oda, T., Kodera, N., Toma-Fukai, S., Sato, M., Taguchi, H., Nagamori, S., Shoji, O., Ishimori, K., Matsumura, H., Sugie, K., Saio, T., Yoshizawa, T., Mori, E., 2021. C9orf72-derived arginine-rich

poly-dipeptides impede phase modifiers. Nature Communications 2021 12:1 12, 1–12. https://doi.org/10.1038/s41467-021-25560-0

Natalizio, B.J., Wente, S.R., 2013. Postage for the messenger: Designating routes for nuclear mRNA export. Trends Cell Biol 23, 365–373. https://doi.org/10.1016/j.tcb.2013.03.006

Neumann, M., Bentmann, E., Dormann, D., Jawaid, A., Dejesus-Hernandez, M., Ansorge, O., Roeber, S., Kretzschmar, H.A., Munoz, D.G., Kusaka, H., Yokota, O., Ang, L.C., Bilbao, J., Rademakers, R., Haass, C., MacKenzie, I.R.A., 2011. FET proteins TAF15 and EWS are selective markers that distinguish FTLD with FUS pathology from amyotrophic lateral sclerosis with FUS mutations. Brain 134, 2595–2609. https://doi.org/10.1093/BRAIN/AWR201

Neumann, M., Kwong, L.K., Lee, E.B., Kremmer, E., Flatley, A., Xu, Y., Forman, M.S., Troost, D., Kretzschmar, H.A., Trojanowski, J.Q., Lee, V.M.Y., 2009. Phosphorylation of S409/410 of TDP-43 is a consistent feature in all sporadic and familial forms of TDP-43 proteinopathies. Acta Neuropathol 117, 137–149. https://doi.org/10.1007/S00401-008-0477-9/FIGURES/5

Neumann, M., Sampathu, D.M., Kwong, L.K., Truax, A.C., Micsenyi, M.C., Chou, T.T., Bruce, J., Schuck, T., Grossman, M., Clark, C.M., McCluskey, L.F., Miller, B.L., Masliah, E., Mackenzie, I.R., Feldman, H., Feiden, W., Kretzschmar, H.A., Trojanowski, J.Q., Lee, V.M.-Y., 2006. Ubiquitinated TDP-43 in frontotemporal lobar degeneration and amyotrophic lateral sclerosis. Science 314, 130–3. https://doi.org/10.1126/science.1134108

Ng, S.C., Güttler, T., Görlich, D., 2021. Recapitulation of selective nuclear import and export with a perfectly repeated 12mer GLFG peptide. Nature Communications 2021 12:1 12, 1–17. https://doi.org/10.1038/s41467-021-24292-5

Nihei, Y., Mori, K., Werner, G., Arzberger, T., Zhou, Q., Khosravi, B., Japtok, J., Hermann, A., Sommacal, A., Weber, M., Kamp, F., Nuscher, B., Edbauer, D., Haass, C., 2020. Poly-glycine-alanine exacerbates C9orf72 repeat expansion-mediated DNA damage via sequestration of phosphorylated ATM and loss of nuclear hnRNPA3. Acta Neuropathol 139, 99–118. https://doi.org/10.1007/S00401-019-02082-0

Niño, C.A., Hérissant, L., Babour, A., Dargemont, C., 2013. MRNA nuclear export in yeast. Chem Rev 113, 8523–8545.

https://doi.org/10.1021/CR400002G/ASSET/IMAGES/CR400002G.SOCIAL.JPEG_V03

Nishimura, A.L., Župunski, V., Troakes, C., Kathe, C., Fratta, P., Howell, M., Gallo, J., Hortobágyi, T., Shaw, C.E., Rogelj, B., 2010. Nuclear import impairment causes cytoplasmic trans-activation response DNA-binding protein accumulation and is associated with frontotemporal lobar degeneration. Brain 133, 1763–1771. https://doi.org/10.1093/BRAIN/AWQ111

Noble, K.N., Tran, E.J., Alcázar-Román, A.R., Hodge, C.A., Cole, C.N., Wente, S.R., 2011. The Dbp5 cycle at the nuclear pore complex during mRNA export II: nucleotide cycling and mRNP remodeling by Dbp5 are controlled by Nup159 and Gle1. Genes Dev 25, 4065–1077. https://doi.org/10.1101/GAD.2040611

Odeh, H.M., Fare, C.M., Shorter, J., 2022. Nuclear-Import Receptors Counter Deleterious Phase Transitions in Neurodegenerative Disease. J Mol Biol 434, 167220. https://doi.org/10.1016/J.JMB.2021.167220

Odeh, H.M., Shorter, J., 2020. Arginine-rich dipeptide-repeat proteins as phase disruptors in C9-ALS/FTD. Emerg Top Life Sci 4, 293–305. https://doi.org/10.1042/ETLS20190167

Oeffinger, M., Zenklusen, D., 2012. To the pore and through the pore: a story of mRNA export kinetics. Biochim Biophys Acta 1819, 494–506. https://doi.org/10.1016/J.BBAGRM.2012.02.011

Ogawa, Y., Miyamoto, Y., Oka, M., Yoneda, Y., 2012. The interaction between importin-α and Nup153 promotes importin-α/β-mediated nuclear import. Traffic 13, 934–946. https://doi.org/10.1111/J.1600-0854.2012.01367.X

Ohki, Y., Wenninger-Weinzierl, A., Hruscha, A., Asakawa, K., Kawakami, K., Haass, C., Edbauer, D., Schmid, B., 2017. Glycine-alanine dipeptide repeat protein contributes to toxicity in a zebrafish model of C9orf72 associated neurodegeneration. Mol Neurodegener 12, 6. https://doi.org/10.1186/s13024-016-0146-8

Okada, C., Yamashita, E., Lee, S.J., Shibata, S., Katahira, J., Nakagawa, A., Yoneda, Y., Tsukihara, T., 2009. A high-resolution structure of the pre-microRNA nuclear export machinery. Science 326, 1275–1279. https://doi.org/10.1126/SCIENCE.1178705

Olszewska, D.A., Lonergan, R., Fallon, E.M., Lynch, T., 2016. Genetics of Frontotemporal Dementia. Curr Neurol Neurosci Rep 16, 1–15. https://doi.org/10.1007/S11910-016-0707-9/FIGURES/3

Onesto, E., Colombrita, C., Gumina, V., Borghi, M.O., Dusi, S., Doretti, A., Fagiolari, G., Invernizzi, F., Moggio, M., Tiranti, V., Silani, V., Ratti, A., 2016. Gene-specific mitochondria dysfunctions in human TARDBP and C9ORF72 fibroblasts. Acta Neuropathol Commun 4, 47. https://doi.org/10.1186/S40478-016-0316-5

Ori, A., Banterle, N., Iskar, M., Andrés-Pons, A., Escher, C., Khanh Bui, H., Sparks, L., Solis-Mezarino, V., Rinner, O., Bork, P., Lemke, E.A., Beck, M., 2013. Cell type-specific nuclear pores: a case in point for context-dependent stoichiometry of molecular machines. Mol Syst Biol 9, 648. https://doi.org/10.1038/msb.2013.4

O'Rourke, J.G., Bogdanik, L., Yáñez, A., Lall, D., Wolf, A.J., Muhammad, A.K.M.G., Ho, R., Carmona, S., Vit, J.P., Zarrow, J., Kim, K.J., Bell, S., Harms, M.B., Miller, T.M., Dangler, C.A., Underhill, D.M., Goodridge, H.S., Lutz, C.M., Baloh, R.H., 2016. C9orf72 is required for proper macrophage and microglial function in mice. Science 351, 1324–1329. https://doi.org/10.1126/SCIENCE.AAF1064

Ortega, J.A., Daley, E.L., Kour, S., Samani, M., Tellez, L., Smith, H.S., Hall, E.A., Esengul, Y.T., Tsai, Y.-H., Gendron, T.F., Donnelly, C.J., Siddique, T., Savas, J.N., Pandey, U.B., Kiskinis, E., 2020. Nucleocytoplasmic Proteomic Analysis Uncovers eRF1 and Nonsense-Mediated Decay as Modifiers of ALS/FTD C9orf72 Toxicity. Neuron. https://doi.org/10.1016/j.neuron.2020.01.020

Panza, F., Lozupone, M., Seripa, D., Daniele, A., Watling, M., Giannelli, G., Imbimbo, B.P., 2020. Development of disease-modifying drugs for frontotemporal dementia spectrum disorders. Nature Reviews Neurology 2020 16:4 16, 213–228. https://doi.org/10.1038/s41582-020-0330-x

Pasha, T., Zatorska, A., Sharipov, D., Rogelj, B., Hortobágyi, T., Hirth, F., 2021. Karyopherin abnormalities in neurodegenerative proteinopathies. Brain 144, 2915–2932. https://doi.org/10.1093/BRAIN/AWAB201

Patel, S.S., Belmont, B.J., Sante, J.M., Rexach, M.F., 2007. Natively Unfolded Nucleoporins Gate Protein Diffusion across the Nuclear Pore Complex. Cell 129, 83–96. https://doi.org/10.1016/J.CELL.2007.01.044

Phukan, J., Elamin, M., Bede, P., Jordan, N., Gallagher, L., Byrne, S., Lynch, C., Pender, N., Hardiman, O., 2012. The syndrome of cognitive impairment in

amyotrophic lateral sclerosis: a population-based study. J Neurol Neurosurg Psychiatry 83, 102–8. https://doi.org/10.1136/jnnp-2011-300188

Pickering-Brown, S.M., Rollinson, S., du Plessis, D., Morrison, K.E., Varma, A., Richardson, A.M.T., Neary, D., Snowden, J.S., Mann, D.M.A., 2008. Frequency and clinical characteristics of progranulin mutation carriers in the Manchester frontotemporal lobar degeneration cohort: comparison with patients with MAPT and no known mutations. Brain 131, 721–731. https://doi.org/10.1093/BRAIN/AWM331

Piguet, O., Hodges, J.R., 2013. Behavioural-variant frontotemporal dementia: an update. Dement Neuropsychol 7, 10. https://doi.org/10.1590/S1980-57642013DN70100003

Pinarbasi, E.S., Cağatay, T., Fung, H.Y.J., Li, Y.C., Chook, Y.M., Thomas, P.J., 2018. Active nuclear import and passive nuclear export are the primary determinants of TDP-43 localization. Sci Rep 8, 7083. https://doi.org/10.1038/s41598-018-25008-4

Piñol-Roma, S., Dreyfuss, G., 1992. Shuttling of pre-mRNA binding proteins between nucleus and cytoplasm. Nature 1992 355:6362 355, 730–732. https://doi.org/10.1038/355730a0

Poetter, C.E., Stewart, J.T., 2012. Treatment of indiscriminate, inappropriate sexual behavior in frontotemporal dementia with carbamazepine. J Clin Psychopharmacol 32, 137–138. https://doi.org/10.1097/JCP.0B013E31823F91B9

Politz, J.C., Tuft, R.A., Pederson, T., Singer, R.H., 1999. Movement of nuclear poly(A) RNA throughout the interchromatin space in living cells. Curr Biol 9, 285–291. https://doi.org/10.1016/S0960-9822(99)80136-5

Port, S.A., Monecke, T., Dickmanns, A., Spillner, C., Hofele, R., Urlaub, H., Ficner, R., Kehlenbach, R.H., 2015. Structural and Functional Characterization of CRM1-Nup214 Interactions Reveals Multiple FG-Binding Sites Involved in Nuclear Export. Cell Rep 13, 690–702. https://doi.org/10.1016/J.CELREP.2015.09.042

Potthoff, E., Guillaume-Gentil, O., Ossola, D., Polesel-Maris, J., LeibundGut-Landmann, S., Zambelli, T., Vorholt, J.A., 2012. Rapid and Serial Quantification of Adhesion Forces of Yeast and Mammalian Cells. PLoS One 7, 52712. https://doi.org/10.1371/JOURNAL.PONE.0052712

Pottier, C., Bieniek, K.F., Finch, N.C., van de Vorst, M., Baker, M., Perkersen, R., Brown, P., Ravenscroft, T., van Blitterswijk, M., Nicholson, A.M., DeTure, M., Knopman, D.S., Josephs, K.A., Parisi, J.E., Petersen, R.C., Boylan, K.B., Boeve, B.F., Graff-Radford, N.R., Veltman, J.A., Gilissen, C., Murray, M.E., Dickson, D.W., Rademakers, R., 2015. Whole-genome sequencing reveals important role for TBK1 and OPTN mutations in frontotemporal lobar degeneration without motor neuron disease. Acta Neuropathol 130, 77–92. https://doi.org/10.1007/S00401-015-1436-X/FIGURES/4

Pottier, C., Ravenscroft, T.A., Sanchez-Contreras, M., Rademakers, R., 2016. Genetics of FTLD: overview and what else we can expect from genetic studies. J Neurochem 138, 32–53. https://doi.org/10.1111/jnc.13622

Prasad, A., Bharathi, V., Sivalingam, V., Girdhar, A., Patel, B.K., 2019. Molecular mechanisms of TDP-43 misfolding and pathology in amyotrophic lateral sclerosis. Front Mol Neurosci 12, 25. https://doi.org/10.3389/FNMOL.2019.00025/BIBTEX

Pressman, P.S., Miller, B.L., 2014. Diagnosis and Management of Behavioral Variant Frontotemporal Dementia. Biol Psychiatry 75, 574–581. https://doi.org/10.1016/J.BIOPSYCH.2013.11.006

Pujol, G., Söderqvist, H., Radu, A., 2002. Age-associated reduction of nuclear protein import in human fibroblasts. Biochem Biophys Res Commun 294, 354–358. https://doi.org/10.1016/S0006-291X(02)00492-8

Pumroy, R.A., Cingolani, G., 2015. Diversification of importin-α isoforms in cellular trafficking and disease states. Biochem J 466, 13–28. https://doi.org/10.1042/BJ20141186

Qamar, S., Wang, G., Randle, S.J., Ruggeri, F.S., Varela, J.A., Lin, J.Q., Phillips, E.C., Miyashita, A., Williams, D., Ströhl, F., Meadows, W., Ferry, R., Dardov, V.J., Tartaglia, G.G., Farrer, L.A., Kaminski Schierle, G.S., Kaminski, C.F., Holt, C.E., Fraser, P.E., Schmitt-Ulms, G., Klenerman, D., Knowles, T., Vendruscolo, M., St George-Hyslop, P., 2018. FUS Phase Separation Is Modulated by a Molecular Chaperone and Methylation of Arginine Cation-π Interactions. Cell 173, 720-734.e15. https://doi.org/10.1016/j.cell.2018.03.056

Quaegebeur, A., Glaria, I., Lashley, T., Isaacs, A.M., 2020. Soluble and insoluble dipeptide repeat protein measurements in C9orf72-frontotemporal dementia brains show regional differential solubility and correlation of poly-GR with clinical

severity. Acta Neuropathol Commun 8, 184. https://doi.org/10.1186/s40478-020-01036-y

Rademakers, R., Neumann, M., MacKenzie, I.R., 2012. Advances in understanding the molecular basis of frontotemporal dementia. Nature Reviews Neurology 2012 8:8 8, 423–434. https://doi.org/10.1038/nrneurol.2012.117

Radwan, M., Ang, C.S., Ormsby, A.R., Cox, D., Daly, J.C., Reid, G.E., Hatters, D.M., 2020. Arginine in C9ORF72 dipolypeptides mediates promiscuous proteome binding and multiple modes of toxicity. Molecular and Cellular Proteomics 19. https://doi.org/10.1074/mcp.RA119.001888

Rajoo, S., Vallotton, P., Onischenko, E., Weis, K., 2018. Stoichiometry and compositional plasticity of the yeast nuclear pore complex revealed by quantitative fluorescence microscopy. Proc Natl Acad Sci U S A 115, E3969–E3977. https://doi.org/10.1073/PNAS.1719398115

Rascovsky, K., Hodges, J.R., Knopman, D., Mendez, M.F., Kramer, J.H., Neuhaus, J., van Swieten, J.C., Seelaar, H., Dopper, E.G.P., Onyike, C.U., Hillis, A.E., Josephs, K.A., Boeve, B.F., Kertesz, A., Seeley, W.W., Rankin, K.P., Johnson, J.K., Gorno-Tempini, M.L., Rosen, H., Prioleau-Latham, C.E., Lee, A., Kipps, C.M., Lillo, P., Piguet, O., Rohrer, J.D., Rossor, M.N., Warren, J.D., Fox, N.C., Galasko, D., Salmon, D.P., Black, S.E., Mesulam, M., Weintraub, S., Dickerson, B.C., Diehl-Schmid, J., Pasquier, F., Deramecourt, V., Lebert, F., Pijnenburg, Y., Chow, T.W., Manes, F., Grafman, J., Cappa, S.F., Freedman, M., Grossman, M., Miller, B.L., 2011. Sensitivity of revised diagnostic criteria for the behavioural variant of frontotemporal dementia. Brain 134, 2456–2477. https://doi.org/10.1093/BRAIN/AWR179

Ratnavalli, E., Brayne, C., Dawson, K., Hodges, J.R., 2002. The prevalence of frontotemporal dementia. Neurology 58, 1615–1621. https://doi.org/10.1212/WNL.58.11.1615

Reddy, K., Zamiri, B., Stanley, S.Y.R., Macgregor, R.B., Pearson, C.E., 2013. The disease-associated r(GGGGCC)n repeat from the C9orf72 gene forms tract length-dependent uni- and multimolecular RNA G-quadruplex structures. J Biol Chem 288, 9860–9866. https://doi.org/10.1074/JBC.C113.452532

Renault, L., Kuhlmann, J., Henkel, A., Wittinghofer, A., 2001. Structural basis for guanine nucleotide exchange on Ran by the regulator of chromosome

condensation (RCC1). Cell 105, 245–255. https://doi.org/10.1016/S0092-8674(01)00315-4

Renton, A.E., Majounie, E., Waite, A., Simón-Sánchez, J., Rollinson, S., Gibbs, J.R., Schymick, J.C., Laaksovirta, H., van Swieten, J.C., Myllykangas, L., Kalimo, H., Paetau, A., Abramzon, Y., Remes, A.M., Kaganovich, A., Scholz, S.W., Duckworth, J., Ding, J., Harmer, D.W., Hernandez, D.G., Johnson, J.O., Mok, K., Ryten, M., Trabzuni, D., Guerreiro, R.J., Orrell, R.W., Neal, J., Murray, A., Pearson, J., Jansen, I.E., Sondervan, D., Seelaar, H., Blake, D., Young, K., Halliwell, N., Callister, J.B., Toulson, G., Richardson, A., Gerhard, A., Snowden, J., Mann, D., Neary, D., Nalls, M.A., Peuralinna, T., Jansson, L., Isoviita, V.-M., Kaivorinne, A.-L., Hölttä-Vuori, M., Ikonen, E., Sulkava, R., Benatar, M., Wuu, J., Chiò, A., Restagno, G., Borghero, G., Sabatelli, M., Heckerman, D., Rogaeva, E., Zinman, L., Rothstein, J.D., Sendtner, M., Drepper, C., Eichler, E.E., Alkan, C., Abdullaev, Z., Pack, S.D., Dutra, A., Pak, E., Hardy, J., Singleton, A., Williams, N.M., Heutink, P., Pickering-Brown, S., Morris, H.R., Tienari, P.J., Traynor, B.J., 2011. A Hexanucleotide Repeat Expansion in C9ORF72 Is the Cause of Chromosome 9p21-Linked ALS-FTD. Neuron 72, 257–268. https://doi.org/10.1016/J.NEURON.2011.09.010

Reverter, D., Lima, C.D., 2005. Insights into E3 ligase activity revealed by a SUMO-RanGAP1-Ubc9-Nup358 complex. Nature 435, 687–692. https://doi.org/10.1038/NATURE03588

Ribbeck, K., Görlich, D., 2002. The permeability barrier of nuclear pore complexes appears to operate via hydrophobic exclusion. EMBO J 21, 2664–71. https://doi.org/10.1093/emboj/21.11.2664

Ribbeck, K., Görlich, D., 2001. Kinetic analysis of translocation through nuclear pore complexes. EMBO J 20, 1320–30. https://doi.org/10.1093/emboj/20.6.1320

Ribbeck, K., Lipowsky, G., Kent, H.M., Stewart, M., Görlich, D., 1998. NTF2 mediates nuclear import of Ran. EMBO J 17, 6587–6598. https://doi.org/10.1093/EMBOJ/17.22.6587

Riku, Y., Seilhean, D., Duyckaerts, C., Boluda, S., Iguchi, Y., Ishigaki, S., Iwasaki, Y., Yoshida, M., Sobue, G., Katsuno, M., 2021. Pathway from TDP-43-Related Pathology to Neuronal Dysfunction in Amyotrophic Lateral Sclerosis and Frontotemporal Lobar Degeneration. Int J Mol Sci 22, 3843. https://doi.org/10.3390/IJMS22083843

Ringholz, G.M., Appel, S.H., Bradshaw, M., Cooke, N.A., Mosnik, D.M., Schulz, P.E., Yanagihara, T., 2005. Prevalence and patterns of cognitive impairment in sporadic ALS. Neurology 65, 586–90. https://doi.org/10.1212/01.wnl.0000172911.39167.b6

Ritterhoff, T., Das, H., Hofhaus, G., Schröder, R.R., Flotho, A., Melchior, F., 2016. The RanBP2/RanGAP1*SUMO1/Ubc9 SUMO E3 ligase is a disassembly machine for Crm1-dependent nuclear export complexes. Nature Communications 2016 7:1 7, 1–13. https://doi.org/10.1038/ncomms11482

Robbins, J., Dilwortht, S.M., Laskey, R.A., Dingwall, C., 1991. Two interdependent basic domains in nucleoplasmin nuclear targeting sequence: identification of a class of bipartite nuclear targeting sequence. Cell 64, 615–623. https://doi.org/10.1016/0092-8674(91)90245-T

Rohrer, J.D., Guerreiro, R., Vandrovcova, J., Uphill, J., Reiman, D., Beck, J., Isaacs, A.M., Authier, A., Ferrari, R., Fox, N.C., MacKenzie, I.R.A., Warren, J.D., de Silva, R., Holton, J., Revesz, T., Hardy, J., Mead, S., Rossor, M.N., 2009. The heritability and genetics of frontotemporal lobar degeneration. Neurology 73, 1451–1456. https://doi.org/10.1212/WNL.0B013E3181BF997A

Rohrer, J.D., Rossor, M.N., Warren, J.D., 2010. Syndromes of nonfluent primary progressive aphasia: A clinical and neurolinguistic analysis. Neurology 75, 603. https://doi.org/10.1212/WNL.0B013E3181ED9C6B

Ross, C.A., Tabrizi, S.J., 2011. Huntington's disease: from molecular pathogenesis to clinical treatment. Lancet Neurol 10, 83–98. https://doi.org/10.1016/S1474-4422(10)70245-3

Rossi, S., Rompietti, V., Antonucci, Y., Giovannini, D., Scopa, C., Scaricamazza, S., Scardigli, R., Cestra, G., Serafino, A., Carrì, M.T., D'Ambrosi, N., Cozzolino, M., 2020. UsnRNP trafficking is regulated by stress granules and compromised by mutant ALS proteins. Neurobiol Dis 104792. https://doi.org/10.1016/j.nbd.2020.104792

Rossi, S., Serrano, A., Gerbino, V., Giorgi, A., di Francesco, L., Nencini, M., Bozzo, F., Schininà, M.E., Bagni, C., Cestra, G., Carrì, M.T., Achsel, T., Cozzolino, M., 2015. Nuclear accumulation of mRNAs underlies G4C2-repeat-induced translational repression in a cellular model of C9orf72 ALS. J Cell Sci 128, 1787–1799. https://doi.org/10.1242/JCS.165332/260408/AM/NUCLEAR-ACCUMULATION-OF-MRNAS-UNDERLIES-G4C2

Rout, M.P., Aitchison, J.D., Magnasco, M.O., Chait, B.T., 2003. Virtual gating and nuclear transport: The hole picture. Trends Cell Biol 13, 622–628. https://doi.org/10.1016/j.tcb.2003.10.007

Rutherford, N.J., Heckman, M.G., DeJesus-Hernandez, M., Baker, M.C., Soto-Ortolaza, A.I., Rayaprolu, S., Stewart, H., Finger, E., Volkening, K., Seeley, W.W., Hatanpaa, K.J., Lomen-Hoerth, C., Kertesz, A., Bigio, E.H., Lippa, C., Knopman, D.S., Kretzschmar, H.A., Neumann, M., Caselli, R.J., White, C.L., Mackenzie, I.R., Petersen, R.C., Strong, M.J., Miller, B.L., Boeve, B.F., Uitti, R.J., Boylan, K.B., Wszolek, Z.K., Graff-Radford, N.R., Dickson, D.W., Ross, O.A., Rademakers, R., 2012. Length of normal alleles of C9ORF72 GGGGCC repeat do not influence disease phenotype. Neurobiol Aging 33, 2950.e5-2950.e7. https://doi.org/10.1016/J.NEUROBIOLAGING.2012.07.005

Saberi, S., Stauffer, J.E., Jiang, J., Garcia, S.D., Taylor, A.E., Schulte, D., Ohkubo, T., Schloffman, C.L., Maldonado, M., Baughn, M., Rodriguez, M.J., Pizzo, D., Cleveland, D., Ravits, J., 2018. Sense-encoded poly-GR dipeptide repeat proteins correlate to neurodegeneration and uniquely co-localize with TDP-43 in dendrites of repeat-expanded C9orf72 amyotrophic lateral sclerosis. Acta Neuropathol 135, 459–474. https://doi.org/10.1007/s00401-017-1793-8

Saberi, S., Stauffer, J.E., Schulte, D.J., Ravits, J., 2015. “Neuropathology of amyotrophic lateral sclerosis and its variants.” Neurol Clin 33, 855. https://doi.org/10.1016/J.NCL.2015.07.012

Sareen, D., O’Rourke, J.G., Meera, P., Muhammad, A.K.M.G., Grant, S., Simpkinson, M., Bell, S., Carmona, S., Ornelas, L., Sahabian, A., Gendron, T., Petrucelli, L., Baughn, M., Ravits, J., Harms, M.B., Rigo, F., Bennett, C.F., Otis, T.S., Svendsen, C.N., Baloh, R.H., 2013. Targeting RNA foci in iPSC-derived motor neurons from ALS patients with a C9ORF72 repeat expansion. Sci Transl Med 5, 208ra149. https://doi.org/10.1126/scitranslmed.3007529

Sarma, A., Yang, W., 2011. Calcium regulation of nucleocytoplasmic transport. Protein Cell 2, 291–302. https://doi.org/10.1007/S13238-011-1038-X

Sato, T., Takeuchi, S., Saito, A., Ding, W., Bamba, H., Matsuura, H., Hisa, Y., Tooyama, I., Urushitani, M., 2009. Axonal ligation induces transient redistribution of TDP-43 in brainstem motor neurons. Neuroscience 164, 1565–1578. https://doi.org/10.1016/J.NEUROSCIENCE.2009.09.050

Savas, J.N., Toyama, B.H., Xu, T., Yates, J.R., Hetzer, M.W., 2012. Extremely long-lived nuclear pore proteins in the rat brain. Science (1979) 335, 942. https://doi.org/10.1126/SCIENCE.1217421/SUPPL_FILE/SAVAS.SOM.PDF

Schludi, M.H., Becker, L., Garrett, L., Gendron, T.F., Zhou, Q., Schreiber, F., Popper, B., Dimou, L., Strom, T.M., Winkelmann, J., von Thaden, A., Rentzsch, K., May, S., Michaelsen, M., Schwenk, B.M., Tan, J., Schoser, B., Dieterich, M., Petrucelli, L., Hölter, S.M., Wurst, W., Fuchs, H., Gailus-Durner, V., de Angelis, M.H., Klopstock, T., Arzberger, T., Edbauer, D., 2017. Spinal poly-GA inclusions in a C9orf72 mouse model trigger motor deficits and inflammation without neuron loss. Acta Neuropathol 134, 241–254. https://doi.org/10.1007/s00401-017-1711-0

Schludi, M.H., May, S., Grässer, F.A., Rentzsch, K., Kremmer, E., Küpper, C., Klopstock, T., Arzberger, T., Edbauer, D., Arzberger, T., Edbauer, D., 2015. Distribution of dipeptide repeat proteins in cellular models and C9orf72 mutation cases suggests link to transcriptional silencing. Acta Neuropathol 130, 537–555. https://doi.org/10.1007/s00401-015-1450-z

Schmidt, H.B., Görlich, D., 2016. Transport Selectivity of Nuclear Pores, Phase Separation, and Membraneless Organelles. Trends Biochem Sci 41. https://doi.org/10.1016/j.tibs.2015.11.001

Schmidt, H.B., Görlich, D., 2015. Nup98 FG domains from diverse species spontaneously phase-separate into particles with nuclear pore-like permselectivity. Elife 2015. https://doi.org/10.7554/ELIFE.04251.001

Schoch, R.L., Kapinos, L.E., Lim, R.Y.H., 2012. Nuclear transport receptor binding avidity triggers a self-healing collapse transition in FG-nucleoporin molecular brushes. Proc Natl Acad Sci U S A 109, 16911–16916. https://doi.org/10.1073/PNAS.1208440109/SUPPL_FILE/PNAS.1208440109_SI.PDF

Schrader, N., Koerner, C., Koessmeier, K., Bangert, J.A., Wittinghofer, A., Stoll, R., Vetter, I.R., 2008. The Crystal Structure of the Ran-Nup153ZnF2 Complex: a General Ran Docking Site at the Nuclear Pore Complex. Structure 16, 1116–1125. https://doi.org/10.1016/j.str.2008.03.014

Schwartz, T.U., 2005. Modularity within the architecture of the nuclear pore complex. Curr Opin Struct Biol 15, 221–226. https://doi.org/10.1016/J.SBI.2005.03.003

Seelaar, H., Kamphorst, W., Rosso, S.M., Azmani, A., Masdjedi, R., de Koning, I., Maat-Kievit, J.A., Anar, B., Kaat, L.D., Breedveld, G.J., Dooijes, D., Rozemuller, J.M., Bronner, I.F., Rizzu, P., van Swieten, J.C., 2008. Distinct genetic forms of frontotemporal dementia. Neurology 71, 1220–1226. https://doi.org/10.1212/01.WNL.0000319702.37497.72

Selvaraj, B.T., Livesey, M.R., Zhao, C., Gregory, J.M., James, O.T., Cleary, E.M., Chouhan, A.K., Gane, A.B., Perkins, E.M., Dando, O., Lillico, S.G., Lee, Y.-B., Nishimura, A.L., Poreci, U., Thankamony, S., Pray, M., Vasistha, N.A., Magnani, D., Borooah, S., Burr, K., Story, D., McCampbell, A., Shaw, C.E., Kind, P.C., Aitman, T.J., Whitelaw, C.B.A., Wilmut, I., Smith, C., Miles, G.B., Hardingham, G.E., Wyllie, D.J.A., Chandran, S., 2018. C9ORF72 repeat expansion causes vulnerability of motor neurons to Ca2+-permeable AMPA receptor-mediated excitotoxicity. Nat Commun 9, 347. https://doi.org/10.1038/s41467-017-02729-0

Seminary, E.R., Santarriaga, S., Wheeler, L., Mejaki, M., Abrudan, J., Demos, W., Zimmermann, M.T., Urrutia, R.A., Fee, D., Barkhaus, P.E., Ebert, A.D., 2020. Motor Neuron Generation from iPSCs from Identical Twins Discordant for Amyotrophic Lateral Sclerosis. Cells 9. https://doi.org/10.3390/CELLS9030571

Shang, J., Yamashita, T., Nakano, Y., Morihara, R., Li, X., Feng, T., Liu, X., Huang, Y., Fukui, Y., Hishikawa, N., Ohta, Y., Abe, K., 2017. Aberrant distributions of nuclear pore complex proteins in ALS mice and ALS patients. Neuroscience 350, 158–168. https://doi.org/10.1016/J.NEUROSCIENCE.2017.03.024

Shao, Q., Liang, C., Chang, Q., Zhang, W., Yang, M., Chen, J.F., 2019. C9orf72 deficiency promotes motor deficits of a C9ALS/FTD mouse model in a dose-dependent manner. Acta Neuropathol Commun 7, 32. https://doi.org/10.1186/S40478-019-0685-7/FIGURES/1

Shav-Tal, Y., Darzacq, X., Shenoy, S.M., Fusco, D., Janicki, S.M., Spector, D.L., Singer, R.H., 2004. Dynamics of single mRNPs in nuclei of living cells. Science 304, 1797–1800. https://doi.org/10.1126/SCIENCE.1099754

Sheffield, L.G., Miskiewicz, H.B., Tannenbaum, L.B., Mirra, S.S., 2006. Nuclear Pore Complex Proteins in Alzheimer Disease. J Neuropathol Exp Neurol 65, 45–54. https://doi.org/10.1097/01.JNEN.0000195939.40410.08

Sheinberger, J., Shav-Tal, Y., 2013. The dynamic pathway of nuclear RNA in eukaryotes. Nucleus 4, 195. https://doi.org/10.4161/NUCL.24434

Shi, K.Y., Mori, E., Nizami, Z.F., Lin, Y., Kato, M., Xiang, S., Wu, L.C., Ding, M., Yu, Y., Gall, J.G., McKnight, S.L., 2017. Toxic PRn poly-dipeptides encoded by the C9orf72 repeat expansion block nuclear import and export. Proc Natl Acad Sci U S A 114, E1111–E1117. https://doi.org/10.1073/pnas.1620293114

Shi, Y., Lin, S., Staats, K.A., Li, Y., Chang, W.-H., Hung, S.-T., Hendricks, E., Linares, G.R., Wang, Y., Son, E.Y., Wen, X., Kisler, K., Wilkinson, B., Menendez, L., Sugawara, T., Woolwine, P., Huang, M., Cowan, M.J., Ge, B., Koutsodendris, N., Sandor, K.P., Komberg, J., Vangoor, V.R., Senthilkumar, K., Hennes, V., Seah, C., Nelson, A.R., Cheng, T.-Y., Lee, S.-J.J., August, P.R., Chen, J.A., Wisniewski, N., Hanson-Smith, V., Belgard, T.G., Zhang, A., Coba, M., Grunseich, C., Ward, M.E., van den Berg, L.H., Pasterkamp, R.J., Trotti, D., Zlokovic, B. v, Ichida, J.K., 2018. Haploinsufficiency leads to neurodegeneration in C9ORF72 ALS/FTD human induced motor neurons. Nat Med 24, 313–325. https://doi.org/10.1038/nm.4490

Simone, R., Balendra, R., Moens, T.G., Preza, E., Wilson, K.M., Heslegrave, A., Woodling, N.S., Niccoli, T., Gilbert-Jaramillo, J., Abdelkarim, S., Clayton, E.L., Clarke, M., Konrad, M.-T., Nicoll, A.J., Mitchell, J.S., Calvo, A., Chio, A., Houlden, H., Polke, J.M., Ismail, M.A., Stephens, C.E., Vo, T., Farahat, A.A., Wilson, W.D., Boykin, D.W., Zetterberg, H., Partridge, L., Wray, S., Parkinson, G., Neidle, S., Patani, R., Fratta, P., Isaacs, A.M., 2018. G-quadruplex-binding small molecules ameliorate C9orf72 FTD/ALS pathology in vitro and in vivo. EMBO Mol Med 10, 22–31. https://doi.org/10.15252/emmm.201707850

Singam, C., Walterfang, M., Mocellin, R., Evans, A., Velakoulis, D., 2013. Topiramate for Abnormal Eating Behaviour in Frontotemporal Dementia. Behavioural Neurology 27, 285. https://doi.org/10.3233/BEN-120257

Sivasathiaseelan, H., Marshall, C.R., Agustus, J.L., Benhamou, E., Bond, R.L., van Leeuwen, J.E.P., Hardy, C.J.D., Rohrer, J.D., Warren, J.D., 2019. Frontotemporal Dementia: A Clinical Review. Semin Neurol 39, 251–263. https://doi.org/10.1055/S-0039-1683379/ID/JR180080-31

Sloan, K.E., Gleizes, P.E., Bohnsack, M.T., 2016. Nucleocytoplasmic Transport of RNAs and RNA-Protein Complexes. J Mol Biol 428, 2040–2059. https://doi.org/10.1016/J.JMB.2015.09.023

Smeyers, J., Banchi, E.G., Latouche, M., 2021. C9ORF72: What It Is, What It Does, and Why It Matters. Front Cell Neurosci 15, 109. https://doi.org/10.3389/FNCEL.2021.661447/BIBTEX

Smith, A.E., Slepchenko, B.M., Schaff, J.C., Loew, L.M., Macara, I.G., 2002. Systems analysis of ran transport. Science (1979) 295, 488–491. https://doi.org/10.1126/SCIENCE.1064732/SUPPL_FILE/SMITHWEBTABLE3.PDF

Solomon, D.A., Smikle, R., Reid, M.J., Mizielinska, S., 2021. Altered Phase Separation and Cellular Impact in C9orf72-Linked ALS/FTD. Front Cell Neurosci 15. https://doi.org/10.3389/fncel.2021.664151

Solomon, D.A., Stepto, A., Au, W.H., Adachi, Y., Diaper, D.C., Hall, R., Rekhi, A., Boudi, A., Tziortzouda, P., Lee, Y.-B., Smith, B., Bridi, J.C., Spinelli, G., Dearlove, J., Humphrey, D.M., Gallo, J.-M., Troakes, C., Fanto, M., Soller, M., Rogelj, B., Parsons, R.B., Shaw, C.E., Hortobágyi, T., Hirth, F., 2018. A feedback loop between dipeptide-repeat protein, TDP-43 and karyopherin-α mediates C9orf72-related neurodegeneration. Brain 141, 2908–2924. https://doi.org/10.1093/brain/awy241

Soniat, M., Chook, Y.M., 2016. Karyopherin-β2 recognition of a PY-NLS variant that lacks the proline-tyrosine motif. Structure 24, 1802. https://doi.org/10.1016/J.STR.2016.07.018

Soniat, M., Chook, Y.M., 2015. Nuclear localization signals for four distinct karyopherin-β nuclear import systems. Biochem J 468, 353–362. https://doi.org/10.1042/BJ20150368

Sternburg, E.L., Gruijs da Silva, L.A., Dormann, D., 2022. Post-translational modifications on RNA-binding proteins: accelerators, brakes, or passengers in neurodegeneration? Trends Biochem Sci 47, 6–22. https://doi.org/10.1016/J.TIBS.2021.07.004

Stewart, H., Rutherford, N.J., Briemberg, H., Krieger, C., Cashman, N., Fabros, M., Baker, M., Fok, A., DeJesus-Hernandez, M., Eisen, A., Rademakers, R., Mackenzie, I.R.A., 2012. Clinical and pathological features of amyotrophic lateral sclerosis caused by mutation in the C9ORF72 gene on chromosome 9p. Acta Neuropathol 123, 409. https://doi.org/10.1007/S00401-011-0937-5

Stewart, M., 2010. Nuclear export of mRNA. Trends Biochem Sci 35, 609–617. https://doi.org/10.1016/j.tibs.2010.07.001

Stewart, M., 2007. Molecular mechanism of the nuclear protein import cycle. Nat Rev Mol Cell Biol 8, 195–208. https://doi.org/10.1038/nrm2114

Strambio-De-Castillia, C., Niepel, M., Rout, M.P., 2010. The nuclear pore complex: bridging nuclear transport and gene regulation. Nature Reviews Molecular Cell Biology 2010 11:7 11, 490–501. https://doi.org/10.1038/nrm2928

Sträßer, K., Masuda, S., Mason, P., Pfannstiel, J., Oppizzi, M., Rodriguez-Navarro, S., Rondón, A.G., Aguilera, A., Struhl, K., Reed, R., Hurt, E., 2002. TREX is a conserved complex coupling transcription with messenger RNA export. Nature 417, 304–308. https://doi.org/10.1038/NATURE746

Štukovnik, V., Zidar, J., Podnar, S., Repovš, G., 2010. Amyotrophic lateral sclerosis patients show executive impairments on standard neuropsychological measures and an ecologically valid motor-free test of executive functions. http://dx.doi.org/10.1080/13803391003749236 32, 1095–1109. https://doi.org/10.1080/13803391003749236

Su, Z., Zhang, Y., Gendron, T.F., Bauer, P.O., Chew, J., Yang, W.Y., Fostvedt, E., Jansen-West, K., Belzil, V. v., Desaro, P., Johnston, A., Overstreet, K., Oh, S.Y., Todd, P.K., Berry, J.D., Cudkowicz, M.E., Boeve, B.F., Dickson, D., Floeter, M.K., Traynor, B.J., Morelli, C., Ratti, A., Silani, V., Rademakers, R., Brown, R.H., Rothstein, J.D., Boylan, K.B., Petrucelli, L., Disney, M.D., 2014. Discovery of a biomarker and lead small molecules to target r(GGGGCC)-associated defects in c9FTD/ALS. Neuron 83, 1043–1050. https://doi.org/10.1016/J.NEURON.2014.07.041

Suárez-Calvet, M., Neumann, M., Arzberger, T., Abou-Ajram, C., Funk, E., Hartmann, H., Edbauer, D., Kremmer, E., Göbl, C., Resch, M., Bourgeois, B., Madl, T., Reber, S., Jutzi, D., Ruepp, M.D., Mackenzie, I.R.A., Ansorge, O., Dormann, D., Haass, C., 2016. Monomethylated and unmethylated FUS exhibit increased binding to Transportin and distinguish FTLD-FUS from ALS-FUS. Acta Neuropathol 131, 587–604. https://doi.org/10.1007/S00401-016-1544-2/TABLES/2

Sudria-Lopez, E., Koppers, M., de Wit, M., van der Meer, C., Westeneng, H.-J., Zundel, C.A.C., Youssef, S.A., Harkema, L., de Bruin, A., Veldink, J.H., van den Berg, L.H., Pasterkamp, R.J., 2016. Full ablation of C9orf72 in mice causes immune system-related pathology and neoplastic events but no motor neuron

defects. Acta Neuropathol 132, 145–147. https://doi.org/10.1007/s00401-016-1581-x

Süel, K.E., Gu, H., Chook, Y.M., 2008. Modular Organization and Combinatorial Energetics of Proline–Tyrosine Nuclear Localization Signals. PLoS Biol 6, e137. https://doi.org/10.1371/JOURNAL.PBIO.0060137

Sugai, A., Kato, T., Koyama, A., Koike, Y., Konno, T., Ishihara, T., Onodera, O., 2019. Non-genetically modified models exhibit TARDBP mRNA increase due to perturbed TDP-43 autoregulation. Neurobiol Dis 130, 104534. https://doi.org/10.1016/J.NBD.2019.104534

Suh, E.R., Lee, E.B., Neal, D., Wood, E.M., Toledo, J.B., Rennert, L., Irwin, D.J., McMillan, C.T., Krock, B., Elman, L.B., McCluskey, L.F., Grossman, M., Xie, S.X., Trojanowski, J.Q., van Deerlin, V.M., 2015. Semi-automated quantification of C9orf72 expansion size reveals inverse correlation between hexanucleotide repeat number and disease duration in frontotemporal degeneration. Acta Neuropathol 130, 363–372. https://doi.org/10.1007/S00401-015-1445-9/TABLES/4

Suhr, S.T., Senut, M.C., Whitelegge, J.P., Faull, K.F., Cuizon, D.B., Gage, F.H., 2001. Identities of sequestered proteins in aggregates from cells with induced polyglutamine expression. J Cell Biol 153, 283–294. https://doi.org/10.1083/JCB.153.2.283

Sung, H., Lloyd, T.E., 2022. Defective axonal transport of endo-lysosomes and dense core vesicles in a Drosophila model of C9-ALS/FTD. Traffic 23, 430–441. https://doi.org/10.1111/TRA.12861

Suzuki, H., Shibagaki, Y., Hattori, S., Matsuoka, M., 2019. C9-ALS/FTD-linked proline–arginine dipeptide repeat protein associates with paraspeckle components and increases paraspeckle formation. Cell Death Dis 10, 746. https://doi.org/10.1038/s41419-019-1983-5

Swaminathan, A., Bouffard, M., Liao, M., Ryan, S., Callister, J.B., Pickering-Brown, S.M., Armstrong, G.A.B., Drapeau, P., 2018. Expression of C9orf72-related dipeptides impairs motor function in a vertebrate model. Hum Mol Genet 27, 1754–1762. https://doi.org/10.1093/hmg/ddy083

Swartz, J.R., Miller, B.L., Darby, A.L., 1997. Frontotemporal Dementia: Treatment Response to Serotonin Selective Reuptake Inhibitors. J Clin Psychiatry 58, 7480.

Swinnen, B., Bento-Abreu, A., Gendron, T.F., Boeynaems, S., Bogaert, E., Nuyts, R., Timmers, M., Scheveneels, W., Hersmus, N., Wang, J., Mizielinska, S., Isaacs, A.M., Petrucelli, L., Lemmens, R., van Damme, P., van den Bosch, L., Robberecht, W., 2018. A zebrafish model for C9orf72 ALS reveals RNA toxicity as a pathogenic mechanism. Acta Neuropathol 135, 427–443. https://doi.org/10.1007/s00401-017-1796-5

Tabet, R., Schaeffer, L., Freyermuth, F., Jambeau, M., Workman, M., Lee, C.Z., Lin, C.C., Jiang, J., Jansen-West, K., Abou-Hamdan, H., Désaubry, L., Gendron, T., Petrucelli, L., Martin, F., Lagier-Tourenne, C., 2018. CUG initiation and frameshifting enable production of dipeptide repeat proteins from ALS/FTD C9ORF72 transcripts. Nature Communications 2018 9:1 9, 1–14. https://doi.org/10.1038/s41467-017-02643-5

Takanashi, K., Yamaguchi, A., 2014. Aggregation of ALS-linked FUS mutant sequesters RNA binding proteins and impairs RNA granules formation. Biochem Biophys Res Commun 452, 600–607. https://doi.org/10.1016/J.BBRC.2014.08.115

Tan, R.H., Ke, Y.D., Ittner, L.M., Halliday, G.M., 2017. ALS/FTLD: experimental models and reality. Acta Neuropathol 133, 177–196. https://doi.org/10.1007/s00401-016-1666-6

Tao, Z., Wang, H., Xia, Q., Li, Ke, Li, Kai, Jiang, X., Xu, G., Wang, G., Ying, Z., 2015. Nucleolar stress and impaired stress granule formation contribute to C9orf72 RAN translation-induced cytotoxicity. Hum Mol Genet 24, 2426–2441. https://doi.org/10.1093/hmg/ddv005

Taylor, J.P., Brown, R.H., Cleveland, D.W., 2016. Decoding ALS: from genes to mechanism. Nature 2016 539:7628 539, 197–206. https://doi.org/10.1038/nature20413

Taylor, L.J., Brown, R.G., Tsermentseli, S., Al-Chalabi, A., Shaw, C.E., Ellis, C.M., Leigh, P.N., Goldstein, L.H., 2013. Is language impairment more common than executive dysfunction in amyotrophic lateral sclerosis? J Neurol Neurosurg Psychiatry 84, 494–498. https://doi.org/10.1136/JNNP-2012-303526

Timney, B.L., Raveh, B., Mironska, R., Trivedi, J.M., Kim, S.J., Russel, D., Wente, S.R., Sali, A., Rout, M.P., 2016. Simple rules for passive diffusion through the nuclear pore complex. J Cell Biol 215. https://doi.org/10.1083/JCB.201601004

Topple, A., Smith, G., Fifkova, E., Cullen-Dockstader, K., 1990. Nuclear pore complex frequency in CA1 pyramidal cells of the aging rat. Mech Ageing Dev 51, 33–39. https://doi.org/10.1016/0047-6374(90)90159-D

Toyama, B.H., Drigo, R.A., Lev-Ram, V., Ramachandra, R., Deerinck, T.J., Lechene, C., Ellisman, M.H., Hetzer, M.W., 2019. Visualization of long-lived proteins reveals age mosaicism within nuclei of postmitotic cells. Journal of Cell Biology 218, 433–444. https://doi.org/10.1083/JCB.201809123

Toyama, B.H., Savas, J.N., Park, S.K., Harris, M.S., Ingolia, N.T., Yates, J.R., Hetzer, M.W., 2013. Identification of Long-Lived Proteins Reveals Exceptional Stability of Essential Cellular Structures. Cell 154, 971–982. https://doi.org/10.1016/J.CELL.2013.07.037

Tran, H., Almeida, S., Moore, J., Gendron, T.F., Chalasani, U.D., Lu, Y., Du, X., Nickerson, J.A., Petrucelli, L., Weng, Z., Gao, F.B., 2015. Differential Toxicity of Nuclear RNA Foci versus Dipeptide Repeat Proteins in a Drosophila Model of C9ORF72 FTD/ALS. Neuron 87, 1207–1214. https://doi.org/10.1016/J.NEURON.2015.09.015

Trias, E., Ibarburu, S., Barreto-Núñez, R., Babdor, J., Maciel, T.T., Guillo, M., Gros, L., Dubreuil, P., Díaz-Amarilla, P., Cassina, P., Martínez-Palma, L., Moura, I.C., Beckman, J.S., Hermine, O., Barbeito, L., 2016. Post-paralysis tyrosine kinase inhibition with masitinib abrogates neuroinflammation and slows disease progression in inherited amyotrophic lateral sclerosis. J Neuroinflammation 13. https://doi.org/10.1186/S12974-016-0620-9

Trias, E., Ibarburu, S., Barreto-Núñez, R., Varela, V., Moura, I.C., Dubreuil, P., Hermine, O., Beckman, J.S., Barbeito, L., 2017. Evidence for mast cells contributing to neuromuscular pathology in an inherited model of ALS. JCI Insight 2. https://doi.org/10.1172/JCI.INSIGHT.95934

Trias, E., King, P.H., Si, Y., Kwon, Y., Varela, V., Ibarburu, S., Kovacs, M., Moura, I.C., Beckman, J.S., Hermine, O., Barbeito, L., 2018. Mast cells and neutrophils mediate peripheral motor pathway degeneration in ALS. JCI Insight 3. https://doi.org/10.1172/JCI.INSIGHT.123249

Trias, E., Kovacs, M., King, P.H., Si, Y., Kwon, Y., Varela, V., Ibarburu, S., Moura, I.C., Hermine, O., Beckman, J.S., Barbeito, L., 2020. Schwann cells orchestrate peripheral nerve inflammation through the expression of CSF1, IL-34, and SCF

in amyotrophic lateral sclerosis. Glia 68, 1165–1181. https://doi.org/10.1002/GLIA.23768

Tsai, Y.L., Coady, T.H., Lu, L., Zheng, D., Alland, I., Tian, B., Shneider, N.A., Manley, J.L., 2020. ALS/FTD-associated protein FUS induces mitochondrial dysfunction by preferentially sequestering respiratory chain complex mRNAs. Genes Dev 34, 785–805. https://doi.org/10.1101/GAD.335836.119

Turner, M.R., Al-Chalabi, A., Chio, A., Hardiman, O., Kiernan, M.C., Rohrer, J.D., Rowe, J., Seeley, W., Talbot, K., 2017. Genetic screening in sporadic ALS and FTD. J Neurol Neurosurg Psychiatry 88, 1042–1044. https://doi.org/10.1136/JNNP-2017-315995

Twyffels, L., Gueydan, C., Kruys, V., 2014. Transportin-1 and Transportin-2: Protein nuclear import and beyond. FEBS Lett 588, 1857–1868. https://doi.org/10.1016/J.FEBSLET.2014.04.023

Tziortzouda, P., van den Bosch, L., Hirth, F., 2021. Triad of TDP43 control in neurodegeneration: autoregulation, localization and aggregation. Nature Reviews Neuroscience 2021 22:4 22, 197–208. https://doi.org/10.1038/s41583-021-00431-1

Ugolino, J., Ji, Y.J., Conchina, K., Chu, J., Nirujogi, R.S., Pandey, A., Brady, N.R., Hamacher-Brady, A., Wang, J., 2016. Loss of C9orf72 Enhances Autophagic Activity via Deregulated mTOR and TFEB Signaling. PLoS Genet 12. https://doi.org/10.1371/JOURNAL.PGEN.1006443

Umlauf, D., Bonnet, J., Waharte, F., Fournier, M., Stierle, M., Fischer, B., Brino, L., Devys, D., Tora, L., 2013. The human TREX-2 complex is stably associated with the nuclear pore basket. J Cell Sci 126, 2656–2667. https://doi.org/10.1242/JCS.118000

Valkov, E., Dean, J.C., Jani, D., Kuhlmann, S.I., Stewart, M., 2012. Structural basis for the assembly and disassembly of mRNA nuclear export complexes. Biochimica et Biophysica Acta (BBA) - Gene Regulatory Mechanisms 1819, 578–592. https://doi.org/10.1016/J.BBAGRM.2012.02.017

van Blitterswijk, M., DeJesus-Hernandez, M., Niemantsverdriet, E., Murray, M.E., Heckman, M.G., Diehl, N.N., Brown, P.H., Baker, M.C., Finch, N.C.A., Bauer, P.O., Serrano, G., Beach, T.G., Josephs, K.A., Knopman, D.S., Petersen, R.C., Boeve, B.F., Graff-Radford, N.R., Boylan, K.B., Petrucelli, L., Dickson, D.W., Rademakers, R., 2013. Association between repeat sizes and clinical and

pathological characteristics in carriers of C9ORF72 repeat expansions (Xpansize-72): a cross-sectional cohort study. Lancet Neurol 12, 978–988. https://doi.org/10.1016/S1474-4422(13)70210-2

van Blitterswijk, M., Gendron, T.F., Baker, M.C., DeJesus-Hernandez, M., Finch, N.A., Brown, P.H., Daughrity, L.M., Murray, M.E., Heckman, M.G., Jiang, J., Lagier-Tourenne, C., Edbauer, D., Cleveland, D.W., Josephs, K.A., Parisi, J.E., Knopman, D.S., Petersen, R.C., Petrucelli, L., Boeve, B.F., Graff-Radford, N.R., Boylan, K.B., Dickson, D.W., Rademakers, R., 2015. Novel clinical associations with specific C9ORF72 transcripts in patients with repeat expansions in C9ORF72. Acta Neuropathol 130, 863–876. https://doi.org/10.1007/s00401-015-1480-6

van Es, M.A., Hardiman, O., Chio, A., Al-Chalabi, A., Pasterkamp, R.J., Veldink, J.H., van den Berg, L.H., 2017. Amyotrophic lateral sclerosis. The Lancet 390, 2084–2098. https://doi.org/10.1016/S0140-6736(17)31287-4

van Langenhove, T., van der Zee, J., Sleegers, K., Engelborghs, S., Vandenberghe, R., Gijselinck, I., van den Broeck, M., Mattheijssens, M., Peeters, K., de Deyn, P.P., Cruts, M., van Broeckhoven, C., 2010. Genetic contribution of FUS to frontotemporal lobar degeneration. Neurology 74, 366–371. https://doi.org/10.1212/WNL.0B013E3181CCC732

van Mossevelde, S., van der Zee, J., Gijselinck, I., Engelborghs, S., Sieben, A., van Langenhove, T., de Bleecker, J., Baets, J., Vandenbulcke, M., van Laere, K., Ceyssens, S., van den Broeck, M., Peeters, K., Mattheijssens, M., Cras, P., Vandenberghe, R., de Jonghe, P., Martin, J.J., de Deyn, P.P., Cruts, M., van Broeckhoven, C., Nuytten, D., Smets, K., Robberecht, W., van Damme, P., Santens, P., Dermaut, B., Deryck, O., Bergmans, B., Delbeck, J., Versijpt, J., Michotte, A., Willems, C., Ivanoiu, A., Salmon, E., 2016. Clinical features of TBK1 carriers compared with C9orf72, GRN and non-mutation carriers in a Belgian cohort. Brain 139, 452. https://doi.org/10.1093/BRAIN/AWV358

Vanneste, J., Vercruysse, T., Boeynaems, S., Sicart, A., van Damme, P., Daelemans, D., van den Bosch, L., 2019. C9orf72-generated poly-GR and poly-PR do not directly interfere with nucleocytoplasmic transport. Sci Rep 9, 15728. https://doi.org/10.1038/s41598-019-52035-6

Vanneste, J., Vercruysse, T., Boeynaems, S., van Damme, P., Daelemans, D., van den Bosch, L., 2022. Cellular Stress Induces Nucleocytoplasmic Transport

Deficits Independent of Stress Granules. Biomedicines 10. https://doi.org/10.3390/BIOMEDICINES10051057

Vatsavayai, S.C., Nana, A.L., Yokoyama, J.S., Seeley, W.W., 2018. C9orf72-FTD/ALS pathogenesis: evidence from human neuropathological studies. Acta Neuropathologica 2018 137:1 137, 1–26. https://doi.org/10.1007/S00401-018-1921-0

Vetter, I.R., Nowak, C., Nishimoto, T., Kuhlmann, J., Wittinghofer, A., 1999. Structure of a Ran-binding domain complexed with Ran bound to a GTP analogue: implications for nuclear transport. Nature 1999 398:6722 398, 39–46. https://doi.org/10.1038/17969

Vetter, I.R., Wittinghofer, A., 2001. The guanine nucleotide-binding switch in three dimensions. Science 294, 1299–1304. https://doi.org/10.1126/SCIENCE.1062023

Viodé, A., Fournier, C., Camuzat, A., Fenaille, F., Latouche, M., Elahi, F., le Ber, I., Junot, C., Lamari, F., Anquetil, V., Becher, F., 2018. New antibody-free mass spectrometry-based quantification reveals that C9ORF72 long protein isoform is reduced in the frontal cortex of hexanucleotide-repeat expansion carriers. Front Neurosci 12, 589. https://doi.org/10.3389/FNINS.2018.00589/BIBTEX

von Appen, A., Kosinski, J., Sparks, L., Ori, A., DiGuilio, A.L., Vollmer, B., Mackmull, M.T., Banterle, N., Parca, L., Kastritis, P., Buczak, K., Mosalaganti, S., Hagen, W., Andres-Pons, A., Lemke, E.A., Bork, P., Antonin, W., Glavy, J.S., Bui, K.H., Beck, M., 2015. In situ structural analysis of the human nuclear pore complex. Nature 2015 526:7571 526, 140–143. https://doi.org/10.1038/nature15381

von Moeller, H., Basquin, C., Conti, E., 2009. The mRNA export protein DBP5 binds RNA and the cytoplasmic nucleoporin NUP214 in a mutually exclusive manner. Nat Struct Mol Biol 16, 247–254. https://doi.org/10.1038/NSMB.1561

Waegaert, R., Dirrig-Grosch, S., Parisot, F., Keime, C., Henriques, A., Loeffler, J.P., René, F., 2020. Longitudinal transcriptomic analysis of altered pathways in a CHMP2Bintron5-based model of ALS-FTD. Neurobiol Dis 136, 104710. https://doi.org/10.1016/J.NBD.2019.104710

Waite, A.J., Bäumer, D., East, S., Neal, J., Morris, H.R., Ansorge, O., Blake, D.J., 2014. Reduced C9orf72 protein levels in frontal cortex of amyotrophic lateral sclerosis and frontotemporal degeneration brain with the C9ORF72

hexanucleotide repeat expansion. Neurobiol Aging 35, 1779.e5-1779.e13. https://doi.org/10.1016/J.NEUROBIOLAGING.2014.01.016

Walker, C., Herranz-Martin, S., Karyka, E., Liao, C., Lewis, K., Elsayed, W., Lukashchuk, V., Chiang, S.-C., Ray, S., Mulcahy, P.J., Jurga, M., Tsagakis, I., Iannitti, T., Chandran, J., Coldicott, I., de Vos, K.J., Hassan, M.K., Higginbottom, A., Shaw, P.J., Hautbergue, G.M., Azzouz, M., El-Khamisy, S.F., 2017. C9orf72 expansion disrupts ATM-mediated chromosomal break repair. Nat Neurosci 20, 1225–1235. https://doi.org/10.1038/nn.4604

Walther, T.C., Fornerod, M., Pickersgill, H., Goldberg, M., Allen, T.D., Mattaj, I.W., 2001. The nucleoporin Nup153 is required for nuclear pore basket formation, nuclear pore complex anchoring and import of a subset of nuclear proteins. EMBO J 20, 5703–5714. https://doi.org/10.1093/EMBOJ/20.20.5703

Warren, J.D., Hardy, C.J., Fletcher, P.D., Marshall, C.R., Clark, C.N., Rohrer, J.D., Rossor, M.N., 2016. Binary reversals in primary progressive aphasia. Cortex 82, 287–289. https://doi.org/10.1016/J.CORTEX.2016.05.017

Warren, J.D., Rohrer, J.D., Rossor, M.N., 2013. Clinical review. Frontotemporal dementia. BMJ 347, f4827. https://doi.org/10.1136/BMJ.F4827

Watanabe, S., Kaneko, K., Yamanaka, K., 2013. Accelerated Disease Onset with Stabilized Familial Amyotrophic Lateral Sclerosis (ALS)-linked Mutant TDP-43 Proteins. J Biol Chem 288, 3641. https://doi.org/10.1074/JBC.M112.433615

Watanabe, T., Yuki, S., Egawa, M., Nishi, H., 1994. Protective effects of MCI-186 on cerebral ischemia: possible involvement of free radical scavenging and antioxidant actions. Journal of Pharmacology and Experimental Therapeutics 268.

Webster, C.P., Smith, E.F., Bauer, C.S., Moller, A., Hautbergue, G.M., Ferraiuolo, L., Myszczynska, M.A., Higginbottom, A., Walsh, M.J., Whitworth, A.J., Kaspar, B.K., Meyer, K., Shaw, P.J., Grierson, A.J., de Vos, K.J., 2016. The C9orf72 protein interacts with Rab1a and the ULK1 complex to regulate initiation of autophagy. EMBO J 35, 1656–76. https://doi.org/10.15252/embj.201694401

Weirich, C.S., Erzberger, J.P., Flick, J.S., Berger, J.M., Thorner, J., Weis, K., 2006. Activation of the DExD/H-box protein Dbp5 by the nuclear-pore protein Gle1 and its coactivator InsP6 is required for mRNA export. Nat Cell Biol 8, 668–676. https://doi.org/10.1038/NCB1424

Wen, X., Tan, W., Westergard, T., Krishnamurthy, K., Markandaiah, S.S., Shi, Y., Lin, S., Shneider, N.A., Monaghan, J., Pandey, U.B., Pasinelli, P., Ichida, J.K., Trotti, D., 2014. Antisense proline-arginine RAN dipeptides linked to C9ORF72-ALS/FTD form toxic nuclear aggregates that initiate in vitro and in vivo neuronal death. Neuron 84, 1213–25. https://doi.org/10.1016/j.neuron.2014.12.010

Weskamp, K., Tank, E.M., Miguez, R., McBride, J.P., Gómez, N.B., White, M., Lin, Z., Moreno Gonzalez, C., Serio, A., Sreedharan, J., Barmada, S.J., 2019. Shortened TDP43 isoforms upregulated by neuronal hyperactivity drive TDP43 pathology in ALS. Journal of Clinical Investigation. https://doi.org/10.1172/JCI130988

White, M.A., Kim, E., Duffy, A., Adalbert, R., Phillips, B.U., Peters, O.M., Stephenson, J., Yang, S., Massenzio, F., Lin, Z., Andrews, S., Segonds-Pichon, A., Metterville, J., Saksida, L.M., Mead, R., Ribchester, R.R., Barhomi, Y., Serre, T., Coleman, M.P., Fallon, J., Bussey, T.J., Brown, R.H., Sreedharan, J., 2018. TDP-43 gains function due to perturbed autoregulation in a Tardbp knock-in mouse model of ALS-FTD. Nature Neuroscience 2018 21:4 21, 552–563. https://doi.org/10.1038/s41593-018-0113-5

White, M.R., Mitrea, D.M., Zhang, P., Stanley, C.B., Cassidy, D.E., Nourse, A., Phillips, A.H., Tolbert, M., Taylor, J.P., Kriwacki, R.W., 2019. C9orf72 Poly(PR) Dipeptide Repeats Disturb Biomolecular Phase Separation and Disrupt Nucleolar Function. Mol Cell 74, 713-728.e6. https://doi.org/10.1016/J.MOLCEL.2019.03.019

Wickramasinghe, V.O., Andrews, R., Ellis, P., Langford, C., Gurdon, J.B., Stewart, M., Venkitaraman, A.R., Laskey, R.A., 2014. Selective nuclear export of specific classes of mRNA from mammalian nuclei is promoted by GANP. Nucleic Acids Res 42, 5059. https://doi.org/10.1093/NAR/GKU095

Wickramasinghe, V.O., Laskey, R.A., 2015. Control of mammalian gene expression by selective mRNA export. Nature Reviews Molecular Cell Biology 2015 16:7 16, 431–442. https://doi.org/10.1038/nrm4010

Wing, C.E., Fung, H.Y.J., Chook, Y.M., 2022. Karyopherin-mediated nucleocytoplasmic transport. Nature Reviews Molecular Cell Biology 2022 23:5 23, 307–328. https://doi.org/10.1038/s41580-021-00446-7

Winton, M.J., Igaz, L.M., Wong, M.M., Kwong, L.K., Trojanowski, J.Q., Lee, V.M.-Y., 2008. Disturbance of Nuclear and Cytoplasmic TAR DNA-binding Protein (TDP-

43) Induces Disease-like Redistribution, Sequestration, and Aggregate Formation. Journal of Biological Chemistry 283, 13302–13309. https://doi.org/10.1074/jbc.M800342200

Witzel, S., Maier, A., Steinbach, R., Grosskreutz, J., Koch, J.C., Sarikidi, A., Petri, S., Günther, R., Wolf, J., Hermann, A., Prudlo, J., Cordts, I., Lingor, P., Löscher, W.N., Kohl, Z., Hagenacker, T., Ruckes, C., Koch, B., Spittel, S., Günther, K., Michels, S., Dorst, J., Meyer, T., Ludolph, A.C., 2022. Safety and Effectiveness of Long-term Intravenous Administration of Edaravone for Treatment of Patients With Amyotrophic Lateral Sclerosis. JAMA Neurol 79, 121–130. https://doi.org/10.1001/JAMANEUROL.2021.4893

Woollacott, I.O.C., Rohrer, J.D., 2016. The clinical spectrum of sporadic and familial forms of frontotemporal dementia. J Neurochem 138, 6–31. https://doi.org/10.1111/JNC.13654

Wu, L.S., Cheng, W.C., Shen, C.K.J., 2012. Targeted depletion of TDP-43 expression in the spinal cord motor neurons leads to the development of amyotrophic lateral sclerosis-like phenotypes in mice. Journal of Biological Chemistry 287, 27335–27344. https://doi.org/10.1074/jbc.M112.359000

Xi, Z., Rainero, I., Rubino, E., Pinessi, L., Bruni, A.C., Maletta, R.G., Nacmias, B., Sorbi, S., Galimberti, D., Surace, E.I., Zheng, Y., Moreno, D., Sato, C., Liang, Y., Zhou, Y., Robertson, J., Zinman, L., Tartaglia, M.C., st. George-Hyslop, P., Rogaeva, E., 2014. Hypermethylation of the CpG-island near the C9orf72 G4C2-repeat expansion in FTLD patients. Hum Mol Genet 23, 5630–5637. https://doi.org/10.1093/HMG/DDU279

Xi, Z., Zhang, M., Bruni, A.C., Maletta, R.G., Colao, R., Fratta, P., Polke, J.M., Sweeney, M.G., Mudanohwo, E., Nacmias, B., Sorbi, S., Tartaglia, M.C., Rainero, I., Rubino, E., Pinessi, L., Galimberti, D., Surace, E.I., McGoldrick, P., McKeever, P., Moreno, D., Sato, C., Liang, Y., Keith, J., Zinman, L., Robertson, J., Rogaeva, E., 2015. The C9orf72 repeat expansion itself is methylated in ALS and FTLD patients. Acta Neuropathol 129, 715–727. https://doi.org/10.1007/S00401-015-1401-8/FIGURES/5

Xiao, S., MacNair, L., McGoldrick, P., McKeever, P.M., McLean, J.R., Zhang, M., Keith, J., Zinman, L., Rogaeva, E., Robertson, J., 2015. Isoform-specific antibodies reveal distinct subcellular localizations of C9orf72 in amyotrophic lateral sclerosis. Ann Neurol 78, 568–583. https://doi.org/10.1002/ana.24469

Xu, D., Farmer, A., Collett, G., Grishin, N. v., Chook, Y.M., 2012. Sequence and structural analyses of nuclear export signals in the NESdb database. Mol Biol Cell 23, 3677–3693. https://doi.org/10.1091/MBC.E12-01-0046/ASSET/IMAGES/LARGE/3677FIG9.JPEG

Xu, W., Bao, P., Jiang, X., Wang, H., Qin, M., Wang, R., Wang, T., Yang, Y., Lorenzini, I., Liao, L., Sattler, R., Xu, J., 2019. Reactivation of nonsense-mediated mRNA decay protects against C9orf72 dipeptide-repeat neurotoxicity. Brain 142, 1349–1364. https://doi.org/10.1093/brain/awz070

Xu, Z., Poidevin, M., Li, X., Li, Y., Shu, L., Nelson, D.L., Li, H., Hales, C.M., Gearing, M., Wingo, T.S., Jin, P., 2013. Expanded GGGGCC repeat RNA associated with amyotrophic lateral sclerosis and frontotemporal dementia causes neurodegeneration. Proc Natl Acad Sci U S A 110, 7778–83. https://doi.org/10.1073/pnas.1219643110

Yamada, J., Phillips, J.L., Patel, S., Goldfien, G., Calestagne-Morelli, A., Huang, H., Reza, R., Acheson, J., Krishnan, V. v., Newsam, S., Gopinathan, A., Lau, E.Y., Colvin, M.E., Uversky, V.N., Rexacha, M.F., 2010. A bimodal distribution of two distinct categories of intrinsically disordered structures with separate functions in FG nucleoporins. Mol Cell Proteomics 9, 2205–2224. https://doi.org/10.1074/MCP.M000035-MCP201

Yamakawa, M., Ito, D., Honda, T., Kubo, K., Noda, M., Nakajima, K., Suzuki, N., 2015. Characterization of the dipeptide repeat protein in the molecular pathogenesis of c9FTD/ALS. Hum Mol Genet 24, 1630–1645. https://doi.org/10.1093/hmg/ddu576

Yamashita, M., Nonaka, T., Hirai, S., Miwa, A., Okado, H., Arai, T., Hosokawa, M., Akiyama, H., Hasegawa, M., 2014. Distinct pathways leading to TDP-43-induced cellular dysfunctions. Hum Mol Genet 23, 4345–4356. https://doi.org/10.1093/HMG/DDU152

Yamashita, T., Aizawa, H., Teramoto, S., Akamatsu, M., Kwak, S., 2017. Calpain-dependent disruption of nucleo-cytoplasmic transport in ALS motor neurons. Scientific Reports 2017 7:1 7, 1–11. https://doi.org/10.1038/srep39994

Yang, D., Abdallah, A., Li, Z., Lu, Y., Almeida, S., Gao, F.-B., 2015. FTD/ALS-associated poly(GR) protein impairs the Notch pathway and is recruited by poly(GA) into cytoplasmic inclusions. Acta Neuropathol 130, 525–535. https://doi.org/10.1007/s00401-015-1448-6

Yaseen, N.R., Blobel, G., 1999. Two distinct classes of Ran-binding sites on the nucleoporin Nup-358. Proc Natl Acad Sci U S A 96, 5516–5521. https://doi.org/10.1073/PNAS.96.10.5516/ASSET/EE8E966B-AABD-49EF-88EC-FD4B8E29B32B/ASSETS/GRAPHIC/PQ1091104006.JPEG

Yin, S., Lopez-Gonzalez, R., Kunz, R.C., Gangopadhyay, J., Borufka, C., Gygi, S.P., Gao, F.-B., Reed, R., 2017. Evidence that C9ORF72 Dipeptide Repeat Proteins Associate with U2 snRNP to Cause Mis-splicing in ALS/FTD Patients. Cell Rep 19, 2244–2256. https://doi.org/10.1016/J.CELREP.2017.05.056

Yoshizawa, T., Ali, R., Jiou, J., Fung, H.Y.J., Burke, K.A., Kim, S.J., Lin, Y., Peeples, W.B., Saltzberg, D., Soniat, M., Baumhardt, J.M., Oldenbourg, R., Sali, A., Fawzi, N.L., Rosen, M.K., Chook, Y.M., 2018. Nuclear Import Receptor Inhibits Phase Separation of FUS through Binding to Multiple Sites. Cell 173, 693-705.e22. https://doi.org/10.1016/j.cell.2018.03.003

Zee, J. van der, Gijselinck, I., Dillen, L., Langenhove, T. van, Theuns, J., Engelborghs, S., Philtjens, S., Vandenbulcke, M., Sleegers, K., Sieben, A., Bäumer, V., Maes, G., Corsmit, E., Borroni, B., Padovani, A., Archetti, S., Perneczky, R., Diehl-Schmid, J., Mendonça, A. de, Miltenberger-Miltenyi, G., Pereira, S., Pimentel, J., Nacmias, B., Bagnoli, S., Sorbi, S., Graff, C., Chiang, H.-H., Westerlund, M., Sanchez-Valle, R., Llado, A., Gelpi, E., Santana, I., Almeida, M.R., Santiago, B., Frisoni, G., Zanetti, O., Bonvicini, C., Synofzik, M., Maetzler, W., Hagen, J.M. vom, Schöls, L., Heneka, M.T., Jessen, F., Matej, R., Parobkova, E., Kovacs, G.G., Ströbel, T., Sarafov, S., Tournev, I., Jordanova, A., Danek, A., Arzberger, T., Fabrizi, G.M., Testi, S., Salmon, E., Santens, P., Martin, J.-J., Cras, P., Vandenberghe, R., Deyn, Peter Paul de, Cruts, M., Broeckhoven, C. van, Zee, J. van der, Gijselinck, I., Dillen, L., Langenhove, T. van, Theuns, J., Philtjens, S., Sleegers, K., Bäumer, V., Maes, G., Corsmit, E., Cruts, M., Broeckhoven, C. van, Zee, J. van der, Gijselinck, I., Dillen, L., Langenhove, T. van, Philtjens, S., Theuns, J., Sleegers, K., Bäumer, V., Maes, G., Cruts, M., Broeckhoven, C. van, Engelborghs, S., Deyn, Peter P. de, Cras, P., Engelborghs, S., Deyn, Peter P. de, Vandenbulcke, M., Vandenbulcke, M., Borroni, B., Padovani, A., Archetti, S., Perneczky, R., Diehl-Schmid, J., Synofzik, M., Maetzler, W., Hagen, J.M. vom, Schöls, L., Synofzik, M., Maetzler, W., Hagen, J.M. vom, Schöls, L., Heneka, M.T., Jessen, F., Ramirez, A., Kurzwelly, D., Sachtleben, C., Mairer, W., Mendonça, A. de, Miltenberger-

Miltenyi, G., Pereira, S., Firmo, C., Pimentel, J., Sanchez-Valle, R., Llado, A., Antonell, A., Molinuevo, J., Gelpi, E., Graff, C., Chiang, H.-H., Westerlund, M., Graff, C., Ståhlbom, A.K., Thonberg, H., Nennesmo, I., Börjesson-Hanson, A., Nacmias, B., Bagnoli, S., Sorbi, S., Bessi, V., Piaceri, I., Santana, I., Santiago, B., Santana, I., Ribeiro, M.H., Almeida, M.R., Oliveira, C., Massano, J., Garret, C., Pires, P., Frisoni, G., Zanetti, O., Bonvicini, C., Sarafov, S., Tournev, I., Jordanova, A., Tournev, I., Kovacs, G.G., Ströbel, T., Heneka, M.T., Jessen, F., Ramirez, A., Kurzwelly, D., Sachtleben, C., Mairer;, W., Jessen, F., Matej, R., Parobkova, E., Danel, A., Arzberger, T., Fabrizi, G.M., Testi, S., Ferrari, S., Cavallaro, T., Salmon, E., Santens, P., Cras, P., 2013. A Pan-European Study of the C9orf72 Repeat Associated with FTLD: Geographic Prevalence, Genomic Instability, and Intermediate Repeats. Hum Mutat 34, 363–373. https://doi.org/10.1002/HUMU.22244

Zhang, J., Ito, H., Wate, R., Ohnishi, S., Nakano, S., Kusaka, H., 2006. Altered distributions of nucleocytoplasmic transport-related proteins in the spinal cord of a mouse model of amyotrophic lateral sclerosis. Acta Neuropathol 112, 673–680. https://doi.org/10.1007/S00401-006-0130-4/FIGURES/2

Zhang, J., Velmeshev, D., Hashimoto, K., Huang, Y.-H., Hofmann, J.W., Shi, X., Chen, J., Leidal, A.M., Dishart, J.G., Cahill, M.K., Kelley, K.W., Liddelow, S.A., Seeley, W.W., Miller, B.L., Walther, T.C., Farese, R. v, Taylor, J.P., Ullian, E.M., Huang, B., Debnath, J., Wittmann, T., Kriegstein, A.R., Huang, E.J., 2020. Neurotoxic microglia promote TDP-43 proteinopathy in progranulin deficiency. https://doi.org/10.1038/s41586-020-2709-7

Zhang, K., Daigle, J.G., Cunningham, K.M., Coyne, A.N., Ruan, K., Grima, J.C., Bowen, K.E., Wadhwa, H., Yang, P., Rigo, F., Taylor, J.P., Gitler, A.D., Rothstein, J.D., Lloyd, T.E., 2018. Stress Granule Assembly Disrupts Nucleocytoplasmic Transport. Cell 173, 958-971.e17. https://doi.org/10.1016/J.CELL.2018.03.025

Zhang, K., Donnelly, C.J., Haeusler, A.R., Grima, J.C., Machamer, J.B., Steinwald, P., Daley, E.L., Miller, S.J., Cunningham, K.M., Vidensky, S., Gupta, S., Thomas, M.A., Hong, I., Chiu, S.-L., Huganir, R.L., Ostrow, L.W., Matunis, M.J., Wang, J., Sattler, R., Lloyd, T.E., Rothstein, J.D., 2015. The C9orf72 repeat expansion disrupts nucleocytoplasmic transport. Nature 525, 56–61. https://doi.org/10.1038/nature14973

Zhang, P., Fan, B., Yang, P., Temirov, J., Messing, J., Kim, H.J., Taylor, J.P., 2019. Chronic optogenetic induction of stress granules is cytotoxic and reveals the evolution of ALS-FTD pathology. Elife 8. https://doi.org/10.7554/ELIFE.39578

Zhang, Y.J., Gendron, T.F., Ebbert, M.T.W., O'Raw, A.D., Yue, M., Jansen-West, K., Zhang, X., Prudencio, M., Chew, J., Cook, C.N., Daughrity, L.M., Tong, J., Song, Y., Pickles, S.R., Castanedes-Casey, M., Kurti, A., Rademakers, R., Oskarsson, B., Dickson, D.W., Hu, W., Gitler, A.D., Fryer, J.D., Petrucelli, L., 2018. Poly(GR) impairs protein translation and stress granule dynamics in C9orf72-associated frontotemporal dementia and amyotrophic lateral sclerosis. Nat Med 24, 1136–1142. https://doi.org/10.1038/s41591-018-0071-1

Zhang, Y.-J., Gendron, T.F., Grima, J.C., Sasaguri, H., Jansen-West, K., Xu, Y.-F., Katzman, R.B., Gass, J., Murray, M.E., Shinohara, M., Lin, W.-L., Garrett, A., Stankowski, J.N., Daughrity, L., Tong, J., Perkerson, E.A., Yue, M., Chew, J., Castanedes-Casey, M., Kurti, A., Wang, Z.S., Liesinger, A.M., Baker, J.D., Jiang, J., Lagier-Tourenne, C., Edbauer, D., Cleveland, D.W., Rademakers, R., Boylan, K.B., Bu, G., Link, C.D., Dickey, C.A., Rothstein, J.D., Dickson, D.W., Fryer, J.D., Petrucelli, L., 2016. C9ORF72 poly(GA) aggregates sequester and impair HR23 and nucleocytoplasmic transport proteins. Nat Neurosci 19, 668–677. https://doi.org/10.1038/nn.4272

Zhang, Y.J., Guo, L., Gonzales, P.K., Gendron, T.F., Wu, Y., Jansen-West, K., O'Raw, A.D., Pickles, S.R., Prudencio, M., Carlomagno, Y., Gachechiladze, M.A., Ludwig, C., Tian, R., Chew, J., DeTure, M., Lin, W.L., Tong, J., Daughrity, L.M., Yue, M., Song, Y., Andersen, J.W., Castanedes-Casey, M., Kurti, A., Datta, A., Antognetti, G., McCampbell, A., Rademakers, R., Oskarsson, B., Dickson, D.W., Kampmann, M., Ward, M.E., Fryer, J.D., Link, C.D., Shorter, J., Petrucelli, L., 2019. Heterochromatin anomalies and double-stranded RNA accumulation underlie C9orf72 poly(PR) toxicity. Science (1979) 363. https://doi.org/10.1126/SCIENCE.AAV2606/SUPPL_FILE/ZHANG-AAV2606-SM.PDF

Zhang, Y.-J., Jansen-West, K., Xu, Y.-F., Gendron, T.F., Bieniek, K.F., Lin, W.-L., Sasaguri, H., Caulfield, T., Hubbard, J., Daughrity, L., Chew, J., Belzil, V. v., Prudencio, M., Stankowski, J.N., Castanedes-Casey, M., Whitelaw, E., Ash, P.E.A., DeTure, M., Rademakers, R., Boylan, K.B., Dickson, D.W., Petrucelli, L., 2014. Aggregation-prone c9FTD/ALS poly(GA) RAN-translated proteins cause

neurotoxicity by inducing ER stress. Acta Neuropathol 128, 505–524. https://doi.org/10.1007/s00401-014-1336-5

Zhou, B., Geng, Y., Liu, C., Miao, H., Ren, Y., Xu, N., Shi, X., You, Y., Lee, T., Zhu, G., 2018. Characterizations of distinct parallel and antiparallel G-quadruplexes formed by two-repeat ALS and FTD related GGGGCC sequence. Scientific Reports 2018 8:1 8, 1–7. https://doi.org/10.1038/s41598-018-20852-w

Zhou, Z., Luo, M.J., Straesser, K., Katahira, J., Hurt, E., Reed, R., 2000. The protein Aly links pre-messenger-RNA splicing to nuclear export in metazoans. Nature 407, 401–405. https://doi.org/10.1038/35030160

Zhu, Q., Jiang, J., Gendron, T.F., McAlonis-Downes, M., Jiang, L., Taylor, A., Diaz Garcia, S., Ghosh Dastidar, S., Rodriguez, M.J., King, P., Zhang, Y., la Spada, A.R., Xu, H., Petrucelli, L., Ravits, J., da Cruz, S., Lagier-Tourenne, C., Cleveland, D.W., 2020. Reduced C9ORF72 function exacerbates gain of toxicity from ALS/FTD-causing repeat expansion in C9orf72. Nat Neurosci 1–10. https://doi.org/10.1038/s41593-020-0619-5

Zu, T., Liu, Y., Bañez-Coronel, M., Reid, T., Pletnikova, O., Lewis, J., Miller, T.M., Harms, M.B., Falchook, A.E., Subramony, S.H., Ostrow, L.W., Rothstein, J.D., Troncoso, J.C., Ranum, L.P.W., 2013. RAN proteins and RNA foci from antisense transcripts in C9ORF72 ALS and frontotemporal dementia. Proc Natl Acad Sci U S A 110, E4968-77. https://doi.org/10.1073/pnas.1315438110